Directed Evolution of Arginine Deiminase (ADI) for Anti-tumor Application

Von der Fakultät für Mathematik, Informatik und Naturwissenschaften der RWTH Aachen University zur Erlangung des akademischen Grades einer Doktorin der Naturwissenschaften genehmigte Dissertation

vorgelegt von

Master of Biochemistry

Leilei Zhu

aus Weifang China

Berichter: **Universitätsprofessor Dr. Ulrich Schwaneberg**
Universitätsprofessor Dr. Lothar Elling

Tag der mündlichen Prüfung: 14.09.2010

Diese Dissertation ist auf den Internetseiten der Hochschulbibliothek online verfügbar.

Table of contents

Acknowledgement.....I
Abstract.....III
Abbreviations V
List of figures..... VI
List of tables..... IX
Chapter 1 Arginine deiminase (ADI) 1
1.1 Arginine deiminase (ADI).....1
1.2 ADI structure 5
1.3 Catalytic reaction mechanism of ADI.....10
1.4 Anti-tumor application of ADI.....11
1.5 Conclusion.....16
Chapter 2 Directed evolution 17
2.1 Introduction to directed evolution.....17
2.2 Directed enzyme evolution for pH tolerance of enzymes 22
2.3 Directed enzyme evolution for medical application.....24
2.3.1 Prodrug enzymes for tumor chemotherapy.....24
2.3.2 Oncolytic viruses for tumor chemotherapy.....25
2.3.3 Amino acid depriving enzyme for anti-tumor applications.....27
2.3.4 Affibody molecules for cancer prognosis 28
2.3.5 Interferon for anti-tumor applicaiton 29
2.4 Conclusion.....30
Chapter 3. Directed evolution of Arginine deiminase for increased activity at physiological pH.....31
3. 1 Abstract 31
3.2 Introduction.....31
3.3 Materials and methods 33
3.3.1 Materials 33
3.3.2 Methods 34

3.3.2.1 Reagents used in assays 34
3.3.2.2 Cloning of ADI into pET42b(+) 34
3.3.2.3 Site directed mutagenesis of PpADI gene at position H404 35
3.3.2.4 Site sturation mutagenesis of PpADI gene at nine amino acid position 35
3.3.2.5 Construction of PpADI error-prone library 36
3.3.2.6 Expression of PpADI in LB media with IPTG induction 37
3.3.2.7 Expression of PpADI in auto-induction media 37
3.3.2.8 Cultivation and expression of PpADI in 96-well plates 37
3.3.2.9 Screening Procedure 38
3.3.2.10 Expression of ADI in shaking flask and purification 39
3.3.2.11 Characterization of ADI wild type and mutants 40
3.3.2.12 Molecular Modeling 41
3.3.2.13 Stability of PpADI in presence of serum 41
3.3.2.14 Activity of PpADI (wild type, M1, M2) towards arginine derivative dimethylarginine 42
3.4 Results 42
3.4.1 PpADI cloning 42
3.4.2 PpADI expression in LB media with IPTG as inducer 44
3.4.3 PpADI expression in auto-induction media 44
3.4.4 PpADI assay based on citrulline detection 46
3.4.5 PpADI screening system for citrulline production in microtiter plates 47
3.4.6 Focused libraries generated by saturation mutagenesis 50
3.4.7 Validation of variant M1 (H404R) citrulline colorimetric assay in cuvette format 50
3.4.8 epPCR library generation and screening with citrulline detection assay by screening error-prone mutant libraries 50
3.4.9 Characterization of PpADI variants 53
3.4.9.1 Determination of k_{cat} and K_m of ADI wild type and the mutants 53
3.4.9.2 Relative pH profile of wild type and mutant 54
3.4.10 Stability of PpADI in the presence of human serum 55

3.4.11 Activity of PpADI (wild type, M1, M2) towards arginine derivative (N^G, N^G)-dimethylarginine 56
3.5 Discussion 56
3.6 Conclusion 59
Chapter 4. PpADI reengineered for efficient operation under physiological conditions 60
4.1 Abstract 60
4.2 Introduction 60
4.3 Materials and methods 62
4.3.1 Materials 62
4.3.2 Methods 62
4.3.2.1 Site saturation mutagenesis of *PpADI* M2 at position A128 62
4.3.2.2 Construction of PpADI error-prone library 63
4.3.2.3 Site directed mutagenesis at position D38 of *PpADI* M4 63
4.3.2.4 Site saturation mutagenesis at position D38 and E296 of *PpADI* M3 64
4.3.2.5 Cultivation and expression of PpADI in 96-well plates 64
4.3.2.6 Improved screening system in 96-well plate to identify PpADI variants with high activities at low arginine concentration 64
4.3.2.7 Expression of PpADI in shaking flask and purification 65
4.3.2.8 Characterization of PpADI variants 65
4.3.2.9 Native polyacrylamide gel electrophoresis of PpADI variants 66
4.3.2.10 Homology modeling 67
4.4 Results 67
4.4.1 Improved screening system in microtiter plates to identify PpADI variants with high activities at low arginine concentration 67
4.4.2 Genealogic tree of directed PpADI evolution 68
4.4.3 EpPCR library construction and screening for variants with high activities at low arginine concentration 69
4.4.4 Site saturation mutagenesis of *PpADI* at position D38 and E296 70

4.4.5 Determination of kinetic constants (k_{cat} and $S_{0.5}$) of PpADI wild type and variants M3, M4, M5 and M6 72
4.4.6 Native polyacrylamide gel electrophoresis of PpADI variants 73
4.5 Discussion 74
Summary and outlook 95
Publication list 97
Curriculum vitae 98

Acknowledgement

First and foremost I want to thank my supervisor Prof. Dr. Ulrich Schwaneberg for offering me the opportunity to study in Germany, his continuous support of my PhD study and research, for his patience, motivation, enthusiasm, and immense knowledge, which influence my view of science and life. His guidance helped me all the time in research and writing of paper and thesis. I could not have imagined having a better advisor and mentor for my PhD study.

Besides my supervisor, I would like to thank other two committee member Prof. Dr. Lothar Elling and Prof. Dr. Anett Kirschner. I appreciate their taking time to read this thesis and give valuable comments.

My sincere thanks also go to Kang Lan, who became a great friend of mine after I came to Bremen of Germany three years ago. She helped me a lot with my PhD project and she was a great company in my daily life. I will never forget the two months I spent on the first cloning working in my life and how Kang Lan taught me and encouraged me.

I am grateful to Prof. Dr. Danilo Roccatano for spending a lot of time discussing my results. After the first meeting with Prof. Roccatano, I started to know and learn computational tools which are really useful for my PhD study. I also thank Rajni for her contribution of homology modeling to my project.

The members of the Schwaneberg group have contributed immensely to my personal and professional time in Jacobs University Bremen and RWTH Aachen University. The group has been a source of friendships as well as good advice and collaboration. I appreciate the help from Marina, Daniela, Gisela, Wolfgang and Brigitta in lab and Marina, Monika and Anita's patient explanation of the registration regulation RWTH Aachen University. I would like to acknowledge honorary group members. I thank Liqing for her sharing apartment with me and helped me start my life in Germany and also thank Haiyan for her offering me a room later and often cooked nice food for us. Ran shared a lot of lab techniques which are very useful for my experiments. I always admire her professional and

accurate attitude towards work. I thank other labmates who I got to know in Jacobs university: Ronny, Hemu, Chaoning, Amol, Dominik and Amir for the stimulating discussions, little help in lab and all the fun we have had in the last three years; Dragana, Ljubica, Noor, Pravine and Raluca helped me move to Aachen and we finally got through the tough transition period from Bremen to Aachen. I thank our group leaders Marco, Jan and Radivoje, who are not my direct supervisor, but are always helpful when I have questions. I thank my fellow labmates who I got to know in RWTH Aachen University: Tamara, Felix, Alex, Christian, Joelle, André, Joana……, who are always helpful with all the problems (PhD registration, Germany letters from university…….) because of my poor German.

I also want to acknowledge my students, Burcu and Alice, both of whom were hard-working and smart. They were all a great help in the lab and I really enjoyed working with them.

I would like to thank my family because of their love, support and trust. They love me the most in the world. I thank for their efforts that they made over the years to make sure I have a good growth and education environment. I wish them healthy and happy life. I thank my elder sister for her love and understanding and always taking good care of my parents these years when I am not around. I thank my husband, Haifeng, who supports me all the time and always is there for me. I am lucky to have him with me.

The financial support of the Jacobs University Bremen and RWTH Aachen University is gratefully acknowledged.

Abstract

Arginine deiminase (ADI), an arginine-degrading enzyme, is involved in the first step of arginine dihydrolase pathway. It catalyzes the hydrolysis of L-arginine to form citrulline and ammonia. ADI has been studied as a potential cancer therapeutic agent for the arginine-auxotrophic tumors, such as hepatocellular carcinomas (HCC) and melanomas. Furthermore, studies also indicate that ADI is a potential anti-angiogenic agent; therefore it could become a novel anti-cancer drug targeting the neovascularization-related tumors. Studies show ADI is more potent for the treatment of leukemia than L-asparaginase. However, the anti-tumor application of ADI for therapeutic purpose faces considerable challenges, such as, microbial ADI has low activity at physiological pH (7.35~7.45), short circulating half-life (~5 h) and high antigenicity. Pegylation of ADI improved its efficacy as a clinical drug, including its half-life in serum and antigenicity. The aim of the project is to improve ADI catalytic performance at physiological pH by directed evolution.

Protein engineering by rational design and directed evolution offers opportunities to tailor ADI properties to physiological conditions. Directed protein evolution has over the last decades become a versatile and successful approach for tailoring protein properties to industrial demands and for advancing our understanding of structure-function relationships in biocatalysts. Unlike rational design relying on the gathering of extensive structure-function relationships of enzymes, directed evolution is used to reengineer enzyme properties through iterative rounds of diversity generation and function selection for improved variants.

In order to improve the ADI activity at physiological pH, we established a directed evolution protocol for this purpose. A microtiter plate (MTP) format colorimetric screening assay based on citrulline detection with diacetyl monoxime (DAM) was developed. Reaction temperature for color development and DAM concentration

were optimized to ensure sufficient sensitivity, appropriate linear range and throughput. With the optimized assay and PpADI wild type expressed in *E. coli* as a model protein, true standard deviation 12.8 % was obtained, which is appropriate for the library screening.

With the established microtiter plate assay system, for the first time, we reengineered ADI for improved activity at physiological pH (pH 7.4) with higher potency in medical application. After one site directed mutagenesis and one round of epPCR library screening, variant M2 (K5T/D44E/H404R) was obtained. M2 shows 4-fold improved k_{cat} value than the PpADI wild type, a shifted pH optimum at pH 7.0 (by 0.5 pH unit), and however an increased K_m value, 3.6-fold under assay conditions (0.5 M sodium phosphate buffer).

Low K_m ($S_{0.5}$) value for ADI is an important factor for efficient consume of arginine in plasma because of the low arginine concentration in human plasma (100-120 µM). Therefore after our proof of concept of reengineering PpADI by directed evolution, we aim to decrease the K_m value of PpADI towards arginine and improve the k_{cat} furthermore thereby improve the efficiency of arginine depletion by ADI. The established citrulline colorimetric assay in 96-well microtiter plate is improved to reflect application conditions: PBS buffer and 1 mM arginine were used in screening system. After the second round of epPCR library and site directed mutagenesis, variant M5 (K5T/D38H/D44E/A128T/H404R) and M6 (K5T/D38H/D44E/A128T/E296K/H404R) were generated: at pH 7.4 (PBS buffer), the $S_{0.5}$ value decrease from 2.01 mM (parent M3, K5T/D44E/A128T/H404R) to 1.48 mM (M5) and 0.81 mM (M6). Under physiological pH in PBS buffer, the $S_{0.5}$ value of M6 (0.81 mM) is lower than that of PpADI wild type (1.30 mM); the k_{cat} value improved from 0.18 s^{-1} (PpADI wild type) to 17.56 s^{-1} (M5, 97.6-folds) and 11.64 s^{-1} (M6, 64.7-fold).

Abbreviations

ADI	arginine deiminase
ADH	arginine degradation pathway
ASS	argininosuccinate synthetase
ASL	argininosuccinate lyase
CARD	caspase recruitment domain
PCR	polymerase chain reaction
epPCR	error prone PCR
DAM	diacetyl monoxime
Da	dalton
DNA	deoxyribonucleic acid
E. coli	*Escherichia coli*
GMSF	guanidino-group modifying enzyme superfamily
HCC	hepatocellular carcinomas
HUVEC	human umbilical vein endothelial cells
IPTG	isopropyl β-D-1-thiogalactopyranoside
iNOs	inducible nitric oxide synthase
LB	Luria-Bertani-medium
MTP	microtiter plate
OD_{600}	optical density at 600 nm
OTC	ornithine carbamoyl transferase
PEG	polyethylene glycol
PDB	protein data bank
TSC	thiosemicarbazide
WT	wild type

List of tables

Figures Pages

Chapter 1

Scheme 1. Arginine dihydrolase pathway. OTC, ornithine transcarbamylase; CK, carbamate kinase. 1

Figure 1. Structural of ADIs from *P. aeruginosa* and *M. arginini*. 5

Figure 2 (A). stereoscopic view of PaADI key active site residues. 2 (B). stereoscopic view of a modeled arginine substrate (green) docked in the active site of ADI. Atomic colors are red, oxygen; blue, nitrogen; yellow, sulfur; and gray, carbon. Ion pair interactions are shown as dashed lines. 7

Figure 3. Structural characteristics of the PaADI. 9

Figure 4 (A). Stereoscopic view of ADI in the unbound and bound states. 4 (B). Structural relationship between ADI (yellow) and PAD4 (cyan). 10

Figure 5. Mechanism of PaADI catalysis of arginine to citrulline and ammonia. 11

Firgure 6. Urea cycle. 13

Firgure 7. Summary of ADI effects on arginine-related cellular functions. 15

Chapter 2

Figure 1. Procedure of a directed evolution experiment. 18

Figure 2. Overview of screening technologies. 21

Figure 3. Hermiston's "Directed Evolution" process of viruses and derivative viral pools. 26

Chapter 3

Figure 1. DNA electrophoresis of PpADI. 43

Figure 2. PpADI sequencing results. 43

Figure 3. SDS-PAGE of PpADI expression. 44

Figures Pages

Figure 4(A). Activity of PpADI expressed in auto-induction media. 45

Figure 4(B). SDS-PAGE of ADI expressed in auto-induction media 1, LS-5052; 2, P-5052; 3, MD-5052; 4 TYM-5052; 5, TYP-5052. 45

Figure 5. Arginine conversion by ADI and detection of citrulline using DAM/TSC assay. 46

Figure 6. Citrulline colorimetric assay in cuvette format using DAM/TSC assay. 46

Figure 7. Calibration curve of cuvette format citrulline colorimetric assay. 47

Figure 8. Citrulline colorimetric assay in MTP format using DAM assay. 47

Figure 9. Calibration curve of 96-well microtiter plate format citrulline colorimetric screening assay. 48

Figure 10. Activity values in descending order of the ADI wild-type conversion of arginine to citrulline in a 96-well microtiter plate using the optimized assay protocol. 49

Figure 11. PpADI model derived from PaADI crystal structure (PDB code 2a9gD) by SWISS MODEL WORKSPACE. 49

Figure 12 (A). Electrophoresis of epPCR products. Lane 1, 0.01 mM of $MnCl_2$; Lane 2, 0.02 mM of $MnCl_2$; Lane 3, 0.05 mM of $MnCl_2$. 51

Figure 12 (B). Electrophoresis of MEGAWHOP product with epPCR products as megaprimer. 51

Figure 13. Relative activity of ADI variants towards arginine. The relative activity is the ratio of the activity at the pH of each variant relative to the activity at pH 7.4 of wild type ADI. 52

Figure 14. Elution profile of wild type PpADI and improved variants from epPCR library, generated with Protein 230 Kit using a mircofluidic device (Agilent Bioanalyzer). BSA was added as an internal standard. 53

Figure 15. Kinetic parameters of ADI and mutants for conversion of arginine to citrulline. White: ADI wild type, grey: M1 (H404R), black: M2 (K5T D44E H404R). 54

Figure 16. pH profile of wild type ADI, M1(H404R), M2(K5T/D44E /H404R. 55

Figures Pages

Figure 17. Structural alignment of mutant M1 model with corresponding residues of the crystal structures of the PaADI (in orange). 57

Figure 18. Structural alignment of mutant M2 model with corresponding residues of the crystal structures of the PaADI (in orange). 58

Chaper 4

Figure 1. Figure 1. Activity values in descending order of the PpADI variant M3 conversion of arginine to citrulline in a 96-well microtiter plate using the optimized assay protocol. 68

Figure 2. Genealogic tree of PpADI variants (M1 to M6) with generated amino acid substitutions. Novel substitutions are indicated by an asterisk. 69

Figure 3. Native polyacrylamide gel electrophoresis of PpADI variants (M3 to M6) with different dimer/tetramer distribution 73

Figure 4. Kinetic curve of PpADI wild type, M3, M5 and M6. 75

Figure 5. A). The model of WT tetramer after energy minimization in vacuum (GROMOS 43B1). B). The model of M6 tetramer after energy minimization in vacuum (GROMOS 43B1). 77

Figure 6. A). Structure model of variant M6. B). Structure alignment of PpADI WT model and M6 model with four loops 78

List of tables

Tables Page

Chapter 1

Table 1. ADI expression, enzymatic properties and medical applications. 3

Table 2. Crystal structures of ADI in protein data bank (PDB). 6

Table 3. Residues important for catalytic function of PaADI. 8

Chapter 2

Table 1. Improvement obtained from directed evolution or rational design for pH performance. 22

Chapter 3

Table 1. Primer sequences for site saturation mutagenesis. 36

Table 2. Activity of ADI variants towards arginine determined using citrulline colorimetric assay in cuvette format. 52

Table 3. Stability of PpADI variants in the presence of human serum. 55

Chapter 4

Table 1. Nucleotide and amino acid substitutions at position 38 71

Table 2. Nucleotide and amino acid substitutions at position 296 71

Table 3. Kinetic constants of wild type PpADI and variants. 72

Arginine deiminase (ADI)

1.1 Arginine deiminase (ADI)

Arginine deiminase (ADI, EC 3.5.3.6), an arginine-metabolizing hydrolase, catalyzes the hydrolysis of L-arginine to form citrulline and ammonia. This reaction is the first step in the L-arginine degradation pathway (ADH, scheme 1, (1). First, arginine is deiminated by arginine deiminase. The resulting citrulline is converted to carbamoyl phosphate and ornithine by ornithine transcarbamylase (EC 2.1.3.3), and finally the carbamoyl phosphate is used to phosphorylate ADP by carbamate kinase (EC 2.7.2.2), producing one ATP molecule. ADI is absent in humans but present in a wide range of bacterial species such as *Pseudomonas aeruginosa* (2), *Pseudomonas plecoglossicida* (3) and *Mycoplasma arginini* (4) and in parasitic protists such as *Giardia intestinalis* (5), *Trichomonas Vaginalis* (6), *Trichomonas fetus* (7), and *Hexamita inflate* (8). For pathogenic bacteria, ADI is required in arginine dehydrolase pathway for virulence and for energy production under anaerobic conditions (9, 10).

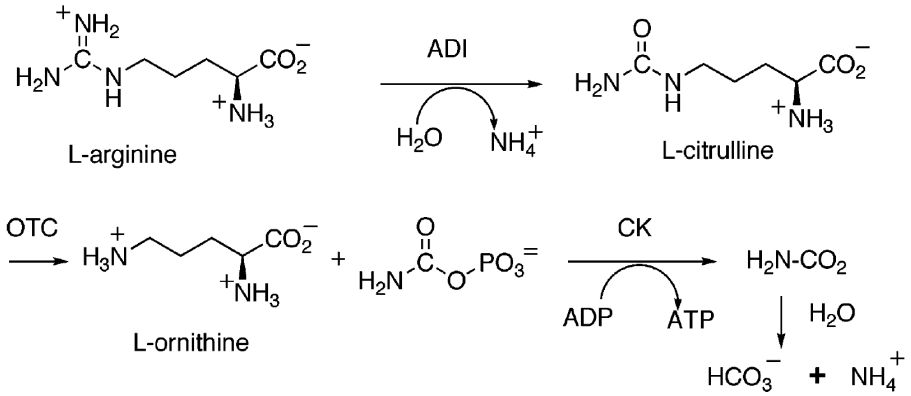

Scheme 1. Arginine dihydrolase pathway. OTC, ornithine transcarbamylase; CK, carbamate kinase.

The establishment of a high-level production system for ADI is an essential step for further research and development of this enzyme. After ADI was discovered from Mycoplasma in 1960s (11), various ADI genes have been cloned, expressed in *E. coli* strains, and the enzyme properties were also studied (Table 1).

Table 1. ADI expression, enzymatic properties and medical applications.

ADIs	Origin	Expression host/vector	Multimeric form	K_m; k_{cat}	Optimum pH	Specific activity	Medical application	References
MhADI (SYN1903)	*Mycoplasma hominis* PG21*	*E.coli* BL21 (DE3)/pET-47b	Dimer			0.618 U/mg (pH 6.5)	Human melanoma (G361), 0.036 U/ml for 50 % IC_{50}	Japan, Harasawa, 2009 (12)
MhADI	*Mycoplasma hominis* (ATCC 23114)	-	Dimer		6.0	35.5 U/mg (pH 6.0) ; 3.9 U/mg (pH 7.4)	Mouse melanoma (MH134) *in vitro*, 100 ng/ml for 50 % IC_{50}	Japan, Takaku, 1995 (13)
MhADI	*Mycoplasma hominis* (ATCC 14027)	-	Dimer	0.17 mM (pH6.6)				USA, Fenske, 1976(14)
MhADI	*Mycoplasma hominis*	*E.coli* BL21 (DE3)/pET25b		0.24 mM; 0.151 s^{-1}				China, Luo, 2007 (15)
MhADI	*Mycoplasma hominis*	*E.coli*				20 U/mg ADI (37℃). [a]	ADI-SS PEG_{20000}, human melanoma, human HCC	USA, Pheonix Pharmacologics, Inc., Clark, 2002 (16)
PaADI (PA5171)	*Pseudomonas aeruginosa* (ATCC 47085D)	*E. coli* BL21(DE3)/pET100	Tetramer	0.14±0.01 mM (pH 5.6)	5.6			USA, Dunaway-Mariano, 2005 (17)
PaADI	*Pseudomonas aeruginosa*	*E. coli* BL21 (DE3)/ pET SUMO				CARD-like domain, no catalytic activity	Human cancer cell line SKOV-3	USA, Chakrabarty, 2006 (18)
PpADI	*Pseudomonas plecoglossicida*	*E. coli* BL21 Gold-(DE3)/ pET42b		0.7 mM; 5.6 s^{-1} (pH 7.4, 0.5 M sodium phosphate buffer)	6.5	31.3 U/mg (pH 7.4, 0.5 M sodium phosphate buffer)		Germany, Schwaneberg, 2010 (3)

MaADI	*Mycoplasma arginini* (ATCC 23838D)	*E. coli* DH5α/PTTQ118				32.7 U/mg. [a]	Human umbilical vein endothelial (HUVE)	USA, Shen, 2002 (19)
MaADI	*Mycoplasma arginini* (ATCC 23838)	*E. coli* JM101/pADTc1	Dimer			33.6 U/mg (37℃, pH 6.5). [a]	Mouse hepatoma, 17 ng/ml for 50 % IC_{50}; mouse fibrosarcoma, 15 ng/ml for 50 % IC_{50}	Japan, Hayashi, 1994 (20)
MaADI	*Mycoplasma arginini* (ATCC 23838)					42 U/mg (37℃, pH 6.5); 29.9 U/mg (37℃, pH 7.4)	Mouse melanoma (MH134) *in vitro*, 10 ng/ml for 50 % IC_{50}	Japan, Takaku, 1995 (13)
MaADI	*Mycoplasma arginini* (ATCC 23838)	-					HUVE, neuroblastoma, retinoblastoma, osteosarcoma, 5~10 ng/ml for 50 % IC_{50}	Germany, Schweigerer, 1999 (21)
MaADI	*Mycoplasma arginini* (ATCC 23838)	-	Dimer	0.2 mM	6.0-7.5	50 U/mg	Mouse tumor carcinoma, fibrosarcoma and melanoma, 5~20 ng/ml for 50 % IC_{50}	Japan, Takaku, 1992 (22)
LlADI	*L. lactis* (ATCC 7962)	*E. coli* BL21Gold(DE3)/pGEM-T Easy	Trimer	8.67 mM	7.2	140.27 U/mg		Korea, Lee, 2007 (23)

[a] ADI was expressed in inclusion body and denaturation-renaturation had to be employed to get soluble protein.

1.2 ADI structure

In 1970s, Kakimoto et al. (24, 25) diffracted the first ADI crystals from *P. putida* through multiple-step chromatography followed by crystallization. Almost three decades later, the X-ray crystal structure of ADI from *P. aeruginosa* (PaADI, Figure 1A) (26) and *M. arginini* (MaADI, Figure 1B) (4) were solved to assist in understanding structure-function relationships. PaADI and MaADI share 27 % sequence identity and belong to guanidino group-modifying enzyme superfamily (GMSF). The catalytic triad (Cys-His-Glu/Asp) is conserved in members of the GMSF. Both crystal structures of PaADI and MaADI show a characteristic 5-fold pseudosymmetrical barrel with ββαβ subunits. Table 2 summarizes the crystal structures of PaADI and MaADI.

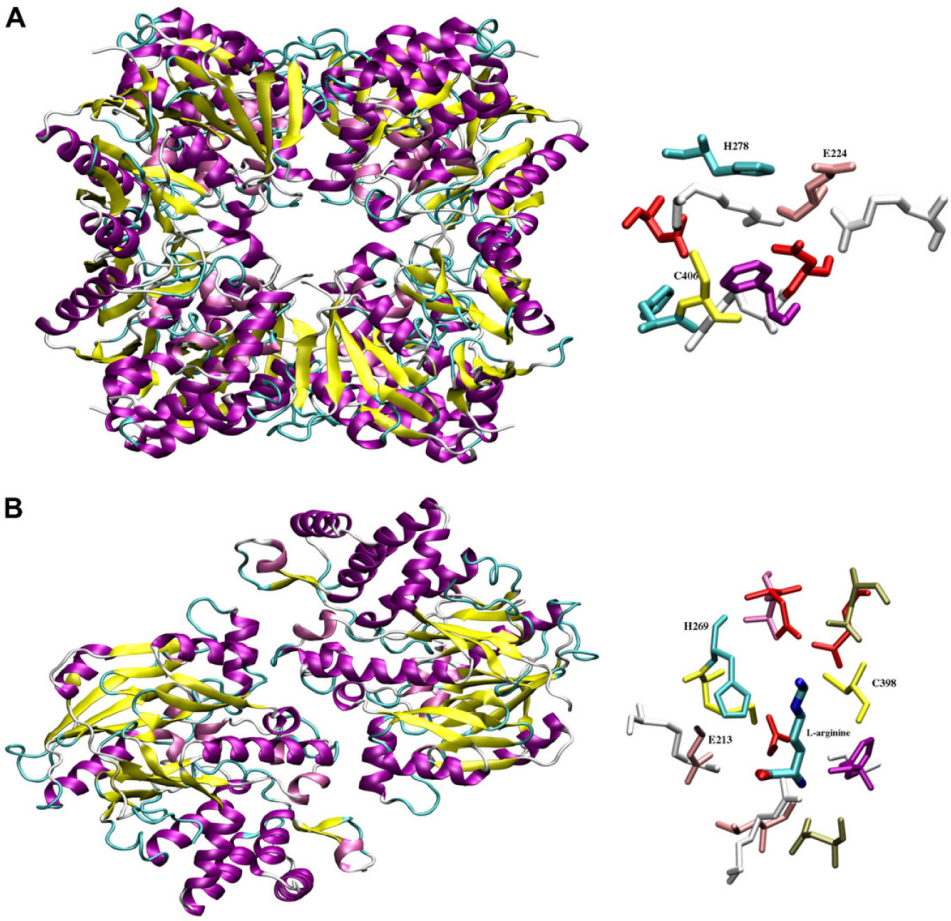

Figure 1. Structural of ADIs from *P. aeruginosa* and *M. arginini*. (A) PaADI (PDB ID: 1RXX) and stereo view of its catalytic triad (C406-H278-E224). (B) MaADI (PDB ID: 1S9R) and stereo view of its catalytic triad (C398-H269-E213) with substrate L-arginine (27).

Table 2. Crystal structures of ADI in protein data bank (PDB).

PDB code	Ligand in crystal structure	Description	Resolution (year)
2A9G	Arginine	Crystal structure of PaADI variant C406A in complex with L-arginine	2.30 Å (2005)
2AAF		Crystal structure of PaADI variant H278A forming a S-alkylthiouronium reaction intermediate	2.30 Å (2005)
2ABR		Crystal structure of PaADI variant D280A with L-arginine forming a S-alkylthiouronium reaction intermediate	2.9 Å (2005)
2ACI		Crystal structure of D166A arginine deiminase	2.50 Å (2005)
1S9R	Arginine	Crystal structure of MaADI covalently linker with a reaction in intermediate	1.60 Å (2004)
1LXY	Citrulline	Crystal Structure of MaADI covalently linked with L-citrulline	2.00 Å (2004)
1RXX		Crystal structure of MaADI	2.45 Å (2004)

MaADI was crystallized as a homodimer and its catalytic triad is formed by Cys398-His269-Glu213. MaADI has a catalytic domain and a five-helix bundle domain (Figure 3). The buried and compact substrate binding pocket is located approximately at the center of the molecule, from which a small solvent channel leads to the surface of the enzyme. The opening to the channel is located adjacent to the dimer interface region, which is at the opposite side of the 5-fold pseudosymmetric moiety of ADI. The shape and size of the channel does not permit transport of the substrate (L-arginine and end product (L-citrulline) in and out of the pocket. Substantial conformational changes in ADI are required to permit entry of the substrate and expulsion of the end product. The occurrence of "closed" and "open" form was suspected to be dependent on binding of substrate.

PaADI has a tetrametric structure with 1630 amino acid residues in total, which makes it the largest enzyme of its structural superfamily. The catalytic triad of PaADI is Cys406-His278-Glu224. Similar to MaADI, the active site of PaADI is

located in a narrow crevice formed by a network of charged residues. Ligand binding energy is derived from ion pair and hydrogen bonding interactions between active site residues and the guanidinium, carboxylate and ammonium groups of the substrate. The proposed substrate-binding model shows that the catalytic center contains abundant charged residues (e.g. Asp280, His405, Glu13 and Arg165). The ion pairing interactions between these residues contribute to the integrity and activity of ADI. In addition, Asp116, Asp227, Arg185, Arg401, His278, Glu118, and Glu224 are part of an extended charged network. The proposed catalytic mechanism suggests that the active site of PaADI is blocked by Arg401, and therefore a conformational transition is taking place upon the substrate binding. Based on the proposed reaction mechanism, Cys406 is as a key residue responsible for the nucleophilic attack on the guanidinium carbon atom of arginine. PaADI contains only one hydrophobic residue, Phe-163 and a Cys-406 with an unknown protonation state. The known functions of important residues are shown in Table 3, and the interactions between important residues and substrate arginine are shown in Figure 2.

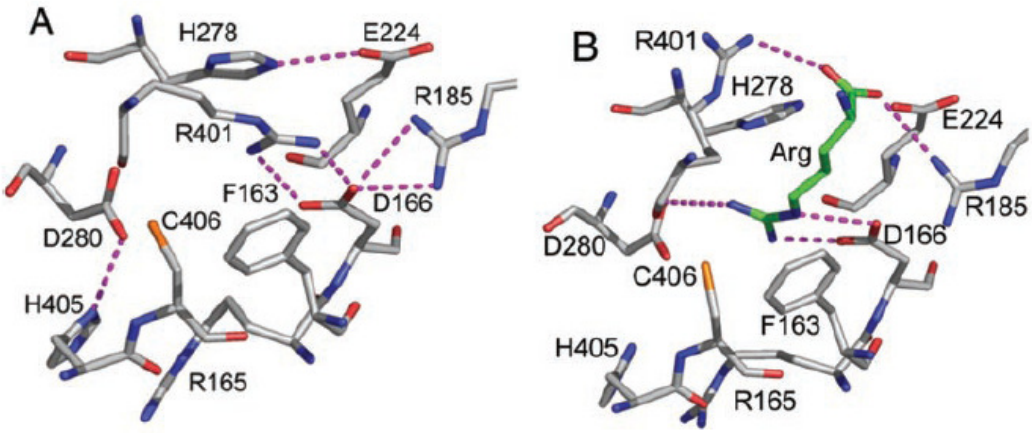

Figure 2. A. stereoscopic view of PaADI key active site residues. B. stereoscopic view of a modeled arginine substrate (green) docked in the active site of ADI. Atomic colors are red, oxygen; blue, nitrogen; yellow, sulfur; and gray, carbon. Ion pair interactions are shown as dashed lines (26).

Table 3. Residues important for catalytic function of PaADI (28, 29).	
Residues	Known/postulated function or comment
Cys406	Mounts the nucleophilic attack on the carbon atom of the guanidinium group of arginine
His278	Serves as a general base and activate the water molecule
Glu224	Modulate the ionization state of His278
Asp280	Interacts with the imidazole group of His405 F via the carboxylate group, which in turn interacts with Glu13. Invariant residue in all known ADIs
Asp280, Asp166	Fix the guanidinium group of the arginine substrate tightly by interactions with the carboxyl groups
Arg401, Arg185	Form ionic interaction with The carboxyl group of the arginine substrate
Phe163	Interacts with the hydrophobic part of arginine substrate
Glu13	Interacts His405 and is invariant in all known ADIs
His405	Sometimes is replaced by an arginine, as in the case of McADI. This may explain the low pH optimum of PaADI (5.6) in contrast to the neutral pH optimum of McADI, the enzyme that contains an arginine residue instead of His405
Arg165	Is fixed by electrostatic interactions with the main chain oxygen atoms of Thr408 and His405 and with the hydroxyl group of Thr-408
Arg401	Blocks the ADI active site via the side chain by forming an ion pair with the carboxyl group of Asp166 and occupies approximately the same position as the guanidinium group of an arginine substrate

The overall fold of MaADI and PaADI consist of five ββαβ modules in cyclical arrangement, generating a pseudo 5-fold symmetrical barrel and an additional 85-residue α-helical domain inserted between the first and the second ββαβ modules giving the typical “Clip-on-fan” moiety. The α-helical domain of PaADI mediates tetramer formation and the α-helical domain of MaADI was speculated to play a role in activating the series of reaction in arginine dehydrolysis pathway (4). Structural alignments by Chakrabarty et al. (18) demonstrated the unique 85 residue 5-α-helical bundle domain exhibiting structural similarity to the mammalian CARD (caspase recruitment domains)-containing proteins and this CARD-like domain is present only in the PaADI and MaADI but not in the other

GMSF members (Figure 3B). Furthermore, PaADI putative CARD-like domain induced apoptosis to cancer cells.

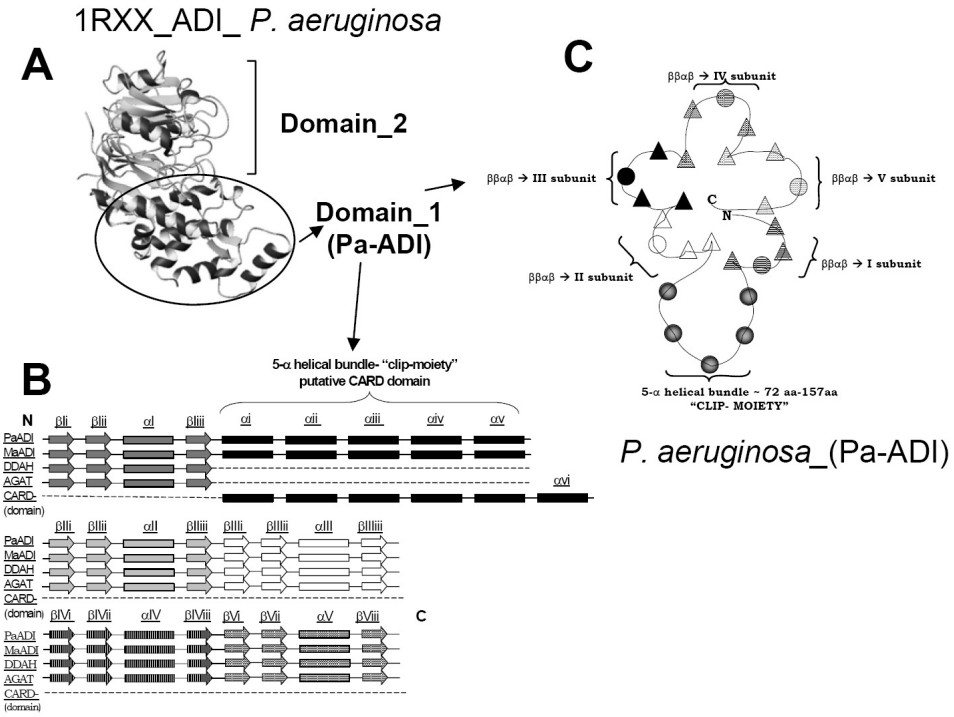

Figure 3. Structural characteristics of the PaADI. A. Ribbon drawing of PaADI (1RXX_A) highlighting the two domains. B. The presence of the CARD domain in PaADI and MaADI but its absence in other members of the GMSF (guanidino-group modifying superfamily) enzymes such as DDAH and AGAT, as shown from the structure-based sequence alignments. The CARD domain represents that of caspase-9. DDAH, dimethylarginine dimethylaminohydrolase; AGAT, arginine: glycine amidinotransferase. The β-strand and α-helices are shown as arrows and strips respectively. Roman numericals I to V are the five ββαβ subunits. The clip moiety (α-helical module) in Figure 3 is seen only in PaADI and MaADI which bears structural homology to the six-α-helical modules that form the CARD domain of the caspase-9 protein molecule. N, N-terminal; C, C-terminal. C. A schematic diagram showing the overall fold and topology of PaADI, as reported (18).

Comparison of substrate free and substrate bound structure of PaADI gives interesting insight into structure changes upon substrate binding (17). Pairwise superposition of the free wild-type PaADI (PDB code: 1rxx) and the mutant enzyme substrate complexes (PDB code: 2a9g) show that the overall fold of the structures remains similar, yet with some local changes. In particular, four loops (Figure 4) associated with the active site undergo conformational transitions not

related to crystal packing: loop 1 (residues 30-46), loop 2 (residues 178-185), loop 3 (residues 271-281, part of this loop is disordered in the apoADI structure), and loop 4 (residues 393-404). Residues adjacent to the substrate exhibit the most significant shifts. For example, the α-carbon atom of Leu41 (loop 1) shifts by 2.7Å and that of Arg185 (loop 2) by 1.8 Å; the α-carbon atom of His278 (loop 3) shifts by 0.9 Å and that of Gly400 (loop 4) by 4.4 Å. These are localized but mechanistically important conformational transitions that tighten the surrounding of the substrate. Simultaneously, substrate binding is accompanied by displacement of the side chain of Arg401 (loop 4) by more than 8 Å to enable access to the active site. The superposition of ADI and PAD4 ADI active site is shielded from the solvent by a long loop (residues 25-48 in PaADI) and the following two turns of α-helix (residues 49-56).

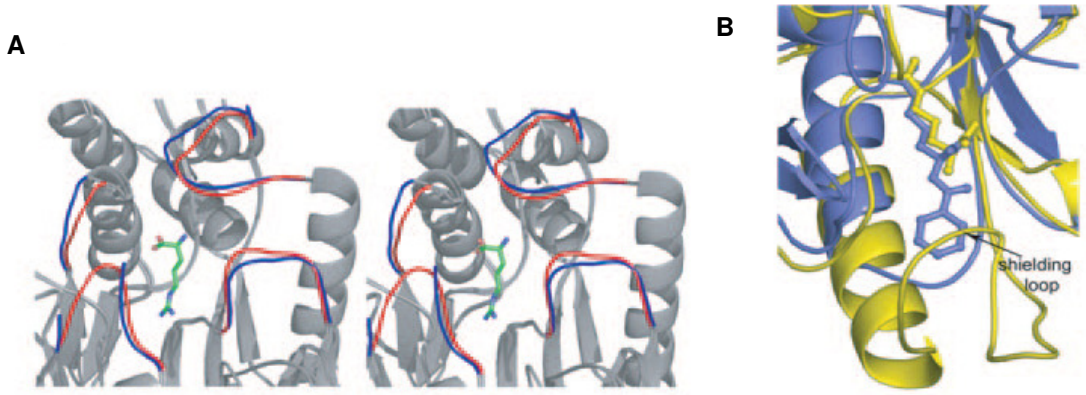

Figure 4 (A). Stereoscopic view of ADI in the unbound and bound states. Superposed molecules are colored gray where the trace of the polypeptide chain is similar in both structures. For regions exhibiting differences, loops of the apoADI structure are highlighted in blue, and loops of the ADI structure complexed with arginine are highlighted in red. 4(B). Structural relationship between ADI (yellow) and PAD4 (cyan) (17).

1.3 Catalytic reaction mechanism of ADI

The overall reaction catalyzed by ADI is the hydrolytic substitution of the ηNH_2 group from the guanidinium group Cζ of L-arginine, leading to citrulline and ammonia (Figure 5). Herzberg (17) and Arnold (4) proposed ADI catalysis mechanism for PaADI (Figure 5) and MaADI, respectively. Basically, both of the proposed mechanisms are composed of three main steps: 1) thiol group of

Cys406 mount a nucleophilic attack on the guanidinium group of arginine and a proton is transferred first to ηNH$_2$ group; 2) water molecule is activated by His278 and followed by attacking the covalent intermediate to replace and release NH$_3$; 3) the C-S covalent bond between enzyme and the resulting citrulline is cleaved and thus end product citrulline is released and free enzyme is generated for next catalytic cycle.

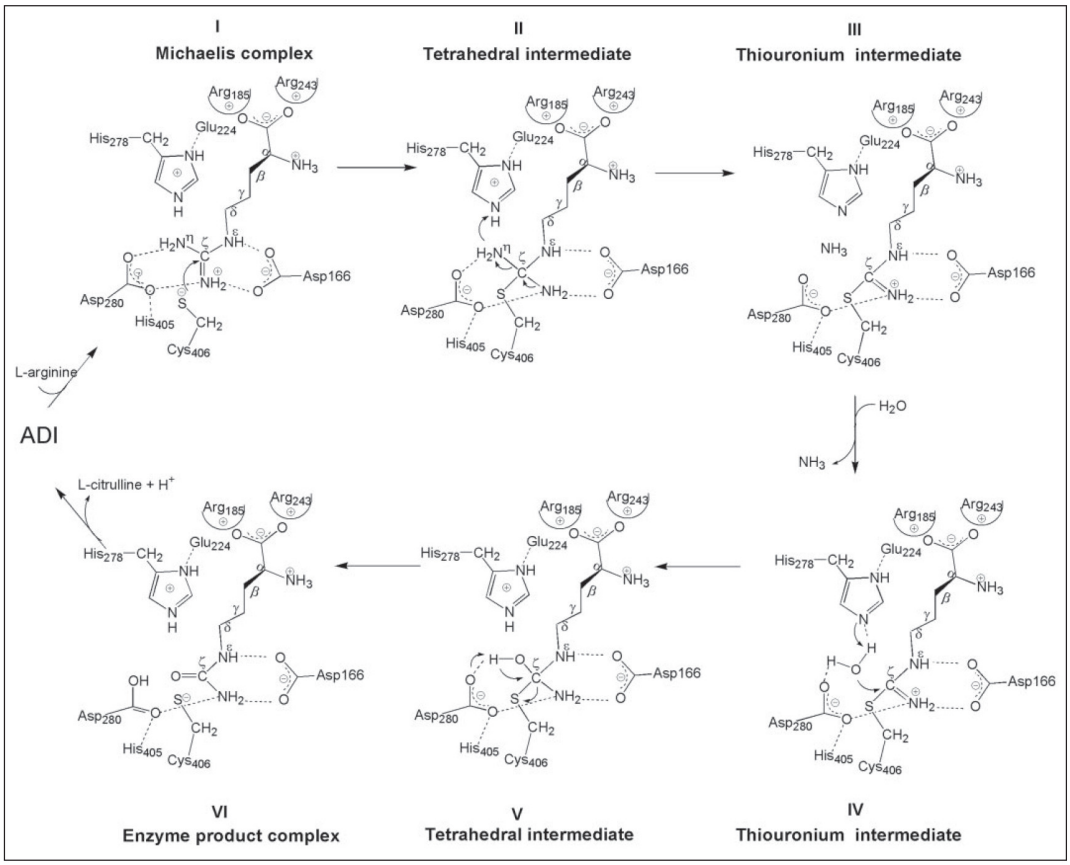

Figure 5. Mechanism of PaADI catalysis of arginine to citrulline and ammonia (17).

1.4 Anti-tumor application of ADI

Amino acids depletion is one type of targeted therapy for human cancers which are auxotrophic for a particular amino acid. Amino acids degrading enzymes, such as asparaginase (30), methioninase (31), arginase (32), arginine deiminase (27), phenylalanine ammonialyase (33) and tryptophanase (34) have been

studied for inhibition of tumor cells *in vitro*. The most representative anticancer enzyme is asparaginase, which is particularly effective in acute lymphoblastic leukaemia. PEG asparaginase is commercialized for acute lymphoblastic leukaemia treatment (Oncaspar®, pegaspargase) (35). However, asparaginase treatment is sometimes accompanied by serous side-effects including anaphylactic shock, coagulapathies as well as liver and pancreatic toxicity (36).

Arginine is an important amino acid involved in the synthesis of a wide range of peptides and proteins, production of creatine and nitric oxide, and a myriad of metabolic pathways and cellular events. It is a precursor of proline, polyamines, glutamine, glutamate, and other neurotransmitters, such as g-aminobutyric acid and also serves as a substrate for two important enzymes, arginase and nitric oxide synthetase (37). Arginine is an indispensable amino acid to children but a semi-essential amino acid in adult humans since many adult somatic cells can synthesize it from citrulline in two steps via urea cycles (Figure 6). The enzyme argininosuccinate synthetase (ASS) catalyzes the conversion of citrulline and aspartic acid to argininosuccinate which is then further converted to arginine and fumaric acid by argininosuccinate lyase (ASL). Arginine can be degraded to ornithine by the urea cycle enzyme arginase. Ornithine is then converted back to citrulline by ornithine carbamoyl transferase (OTC) and then recycles back to arginine from citrulline by ASS/ASL. Thus, the ability to regenerate arginine from citrulline depends on the amount/activity of ASS and ASL, which are tightly coupled. The sensitivity of cells to arginine deprivation depends on the ability of ASS and ASL to regenerate arginine from the alternative intermediate (ornithine, citrulline and argininosuccinate) in the urea cycle.

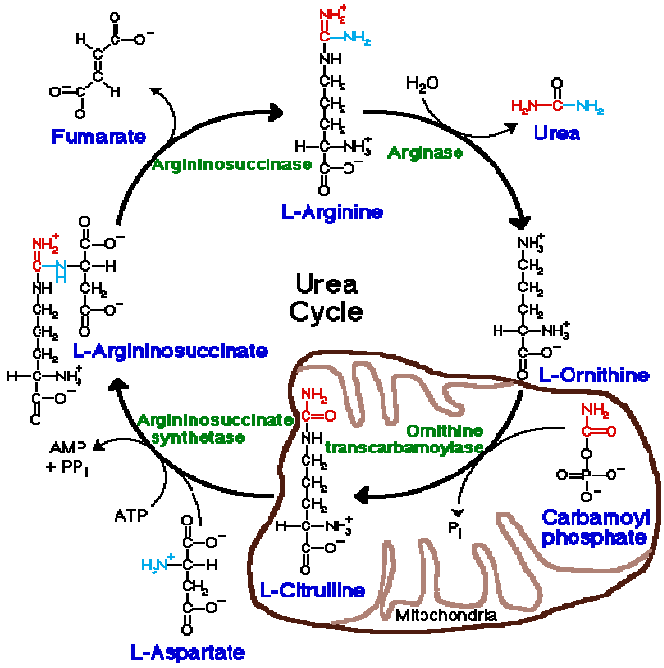

Firgure 6. Urea cycle. Argininosuccinate synthetase (ASS) catalyzes the conversion of citrulline and aspartic acid to argininosuccinate which is then further converted to arginine and fumaric acid by argininosuccinate lyase (ASL). Arginine can be degraded to ornithine by the urea cycle enzyme arginase. Ornithine is then converted back to citrulline by ornithine carbamoyl transferase (OTC) and then recycles back to arginine from citrulline by ASS/ASL.

Arginine begins to become limiting at ~10^{-4} M, whereas other amino acids can sustain growth at 10^{-5}-10^{-6} M. Wheatley et al. showed that most tumour cell lines die considerably more quickly during arginine deprivation than in the absence of any other single (or group of) essential amino acids (38). Since 1930 for the first time arginine known is essential for the growth of some forms of cancer, the potential of arginine degrading enzymes as therapeutic agents was recognized, investigated and employed for arginine auxotrophic tumor treatments. Enzymes capable of depleting arginine *in vitro* include arginase existing in human liver, arginine decarboxylase from bacterial, plant and human, and ADI from microorganism.

Arginine decarboxylase converts arginine to agmatine, which is toxic at high plasma concentration. Furthermore, arginine decarboxylase has a short half-life and it loses virtually all enzymatic activities upon pegylation though pegylation of

arginine decarboxylase is inefficient because not enough lysine residues for polyethylene glycol to attach (39).

Arginase is limited for anti-tumor application because of its low substrate affinity (K_m value 2-4 mM; plasma arginine 100-120 μM), short circulatory half-life (10-15 min) and sub-optimal enzymatic activity at physiological pH (alkaline pH optimum, pH 9.3)(40). Despite these disadvantages of arginase, Lam et al. reported remission of hepatocellular carcinoma induced by systemic release of endogenous hepatic arginase (41) and Leung et al. proved pegylated recombinant human arginase (rhArg-peg 5,000mw) can inhibit ASS-positive HCCs while ADI can not (42).

In addition, ADI, another arginine-degrading microbial enzyme, has various biological activities including anti-proliferation, anti-angiogenesis and inhibition of inducible nitric oxide synthase (iNOs). Figure 7 summarizes how ADI affect many arginine-related cellular functions. ADIs (Table 1) have been shown to have strong *in vitro* and *in vivo* inhibition for arginine auxotrophic tumors (e.g. hepatocellular carcinomas (HCCs), melanomas, retinoblastoma (43), prostate cancer(44)) and ADI from *M. hominis* (MhADI) is currently under clinical trial for HCC (phase II) (45) and melanomas (phase I/II) (46). Studies on human lymphatic leukemia cell lines confirmed ADI's anti-angiogenic activity. Among all the ADIs, MhADI and MaADI were studied most intensively (Table 1).

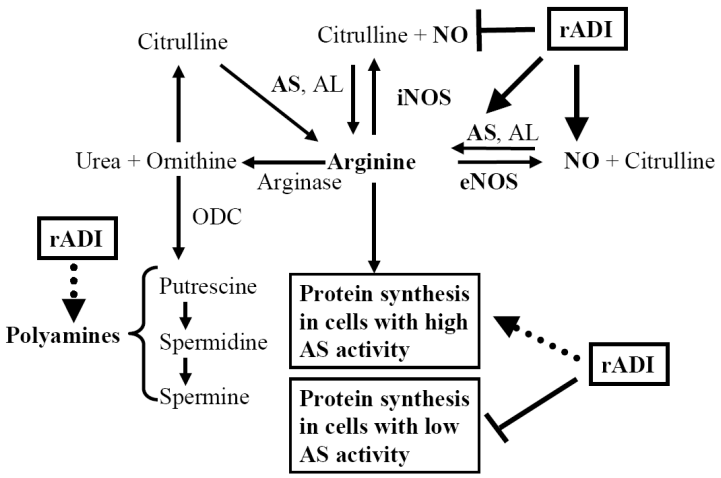

Firgure 7. Summary of ADI effects on arginine-related cellular functions. rADI inhibits NO production via iNOS, but potentiates NO production via eNOS in the cultured endothelial cell model. rADI enhances or inhibits AS activity in different cells. rADI inhibits de novo protein synthesis in cells with low AS activity, but not in cells with high AS activity. Polyamine synthesis was not significantly affected by rADI, even in cells with low AS activity. Arrow representation: solid, potentiates; blocked, inhibits; dotted, no effect (47).

In 1999, US Food and Drug Administration (FDA) designated ADI-PEG-20 orphan drug status for treating HCC and invasive malignant melanomas. In 2005, also the European Agency for the Evaluation of Medicinal Products (EMEA) also granted ADI-PEG-20 orphan drug status for HCC. Phase II trials of ADI-PEG-20 in patients with metastatic hepatocellular carcinomas have shown that the drug is safe, well tolerated, and may benefit patients with unresectable HCC. Izzo and coworker suspected that combination therapies of arginine deprivation and growth inhibition via kinase inhibitors might improve the survival rate further. Additionally, ADI enhances radio sensitivity of human mammary adenocarcinoma (MCF-7 cells) (48), exerts anti-proliferative as well as anti-angiogenic activities and inhibits the growth of viruses such as HIV-1 and hepatitis (49, 50). Current research efforts are focused on ADI's *in vivo* inhibitory effect towards leukemia, melanoma, prostate cancer, renal cell carcinoma, and human umbilical vein endothelial cells (HUVEC) (19, 44, 51-53), clinical trials for HCC (phase II) (45) and melanoma (phase I/II) (46), and tumor inhibitory mechanisms of ADI (54).

The effectiveness of ADIs as anti-tumor agent depends on their enzymatic properties (such as K_m, k_{cat}, optimum pH, stability at neutral pH), selectivity on tumor cells, stability in blood circulation and immunogenicity. Pegylation (35) has been effective in reducing their immunogenicity in animal and increase their stability to various hydrolytic enzymes in plasma. Directed evolution as powerful algorithm to design proteins allows improving all properties that can be reflected in a screening system through iterative rounds of diversity generation and screening. Small libraries of a few thousand variants are often sufficient to find improved variants (55) even without rational understanding of the targeted property. The first example of directed ADI evolution by our group (3) provides a simple and effective screening system to improve activity of PpADI at physiological pH.

1.5 Conclusion

ADI-based arginine deprivation is a novel and promising targeted approach to the treatment arginine auxotrophic tumors, in particular, melanoma, hepatocellular carcinoma and leukemia. Certain mesotheliomas and renal cell cancers were also proved to be sensitive to ADI therapy. Due to its low incidence of major side effects (myelosuppression and gastrointestinal toxicity or other major organ toxicity) arginine deprivation treatment should be combined with other anticancer treatments to increase the response rate. Reengineering of ADI by protein engineering is a promising strayegy to tailor ADI properties for demands in medical applications. Solved ADI crystal structure enables to understand structure function relationships and to guide protein engineering.

Directed evolution

2.1 Introduction to directed evolution

Enzymes are increasingly being used in the generation of products that are traditionally made using chemical synthesis and the field continues to expand its horizons, particularly as applied to the synthesis of the fine chemicals and pharmaceuticals (56, 57). Naturally occurring enzymes are often not designed for the applications of interest, since after all they are evolved in nature for a purpose other than being the catalysts of industrial processes. Directed evolution, rational design and biodiversity screening and combined approches are the main strategies to reengineer enzymes for addressing application demands. Directed evolution has emerged as a powerful enabling method for improving enzyme properties in iterative cycles of diversity generation and screening (Figure 1).

A main advantage of directed evolution compared to rational design is that it does not require structural or mechanistic information for protein optimization. Directed protein evolution has been successfully used for altering and improving protein properties (solubility, expression, enantioselectivity, stability and activity in unusual environment, allosteric interactions, tolerance to pH), as well as for regulating other molecules and systems, including RNA, DNA regulatory elements, biosynthetic pathways and genetic regulatory circuits (58-60).

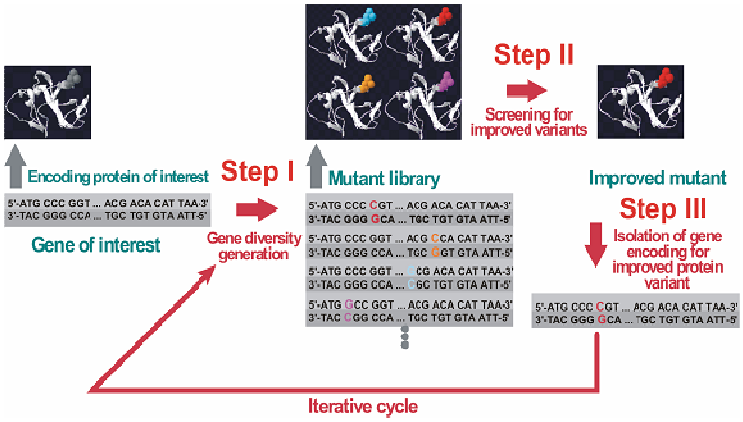

Figure 1. Procedure of a directed evolution experiment. It involves three key steps: 1) selection a good starting sequence and mutating the parent to create a library of variants; 2) identification variants with improved function and 3) isolation of gene encoding for improved variant and repeating the process until the desired function is achieved.

A parent sequence (or sequences) is chosen based on its perceived proximity to the desired function and its evolvability (the ability of a protein to adapt in response to mutation and selective pressure). A parent protein for directed evolution should exhibit enough of the desired function that small improvements can be reliably discerned in a high-throughput screen.

Variants library should be generated with high probability of finding improved variants given the screening capacity. With a high-throughput screening method, a library can be constructed to generate the large potential improvement. Arnold and coworkers(61) showed that very low mutation rates result in many functional sequences but only a small number are unique sequences, however very high mutation rates produce diverse sequences but few retain function. Schwaneberg and coworkers(62) reviewed random mutagenesis methods, focused library generation methods and computational tools for high-quality mutant libraries generation. Schwaneberg and coworkers (63) also summarized criteria for an ideal mutagenesis methods: unbiased mutational spectrum, controllable mutation frequency, consecutive nucleotide substitutions or codon-based substitutions, enable subset mutagenesis (e.g. introduction mainly positively or negatively charged amino acid), independent of gene length, technically simple and reproducible, and economical.

Screening is used to identify library members improved in the targeted property. Identification of improved variants though selection or screening is “analogous” to evolutionary pressure in natural evolution (i.e. only the fittest survive). As the word “directed” in directed evolution implies, laboratory evolutionary pressure is defined and applied by the researcher in screening system. Gradually increasing the selection pressure or evolving against a series of intermediate challenges often accumulates useful single mutations and yields desired variants (64).

Traditional methods for screening employ microtiter plate formats (96-well, 384-well, 1,536-well (65) and even 1,000,000-well (66)) or solid phase assay (agar plate, filter paper and nitrocellulose membrane), which typically enable the screening of no more than 10^6 variants by using robotic automation (67). Sometimes, fast and universal analytic methods like HPLC (68) or GC-MS (69) are utilized for performing an efficient screen of a non-natural substrate. However, the number of screened mutants is limited to 10^4-10^6. In recent years flow cytometry systems (67, 70, 71) have become increasingly attractive, especially after the development of emulsion technology offering compartmentalization and high throughput up to 10^7/h. In addition, Weitz and coworkers (72) recently reported a promising ultrahigh-throughput screening in drop-based microfluidics, by which one can screen a library of 10^8 in about 10 h. Dijkhuizen et al. compared in a review (73) six kinds of library screening strategies (Figure 2). Selection techniques rely on a direct link between cell growth and improved or acquired enzyme function and therefore it is limited to engineering detoxifying enzymes (e.g. b-lactamase) or enzymes that synthesize essential nutrients for cell growth and survival. The traditional microtiter plate screenings are medium-throughput and the most simplistic format of screening. It involves the incubation of colonies with the substrate of targeted enzyme. The crucial factor with this screening technique is that substrate conversion creates a visual signal, such as fluorescence or color, to identify colonies expressing an enzyme with desirable properties. Microtiter plate based screenings are the most commonly applied method in identifying desirable enzyme variants. Microtiter plate based

screenings enable the use of various analytical tools and in the mean while they offer a great dynamic range. Their screening capacity is usually limited to less than 10^4 variants per day. Screening based on microfluidic device and sorting device is a new screening platform for directed evolution, which offers ultra-high-throughput. It allows the discriminate between wild-type and a less active mutant and allows for the addition of substrates and quenchers at desired time thus extending the scope of directed evolution screening strategies. Cell as micro-rector, cell surface display and *in vitro* compartmentalization technology are also FACS (fluorescence-activated cell sorting system) dependent methods for high-throughput screening and allow 10^9-10^{10} screening capacity.

Once improved enzymes are identified, encoding genes are isolated and subjected to further iterative cycles of mutation and screening in order to accumulate beneficial mutations until the targeted improvement is hopefully achieved. The number of iterations required depends on the starting point, the protein fold and the selected properties which determine the possible mutational load and achievable improvement.

Four accepted requirements for successful directed evolution (http://www.che.caltech.edu/groups/fha/) are, 1) the desired function must be physically possible; 2) the function must also be biologically, or evolutionarily, feasible. In practice, this means that there exists a mutational pathway to get from here to there through ever-improving variants (see above). A good experiment will maximize the likelihood; 3) Suitable host (*E. coli* or *S. cerevisiae*) which allows functional expression of more than 10^6 variants per µg of DNA. 4) A rapid screen or selection that reflects the desired function. How rapid the screen must be depends on how rare mutations leading to the desired property are and how many must be accumulated to achieve the desired result.

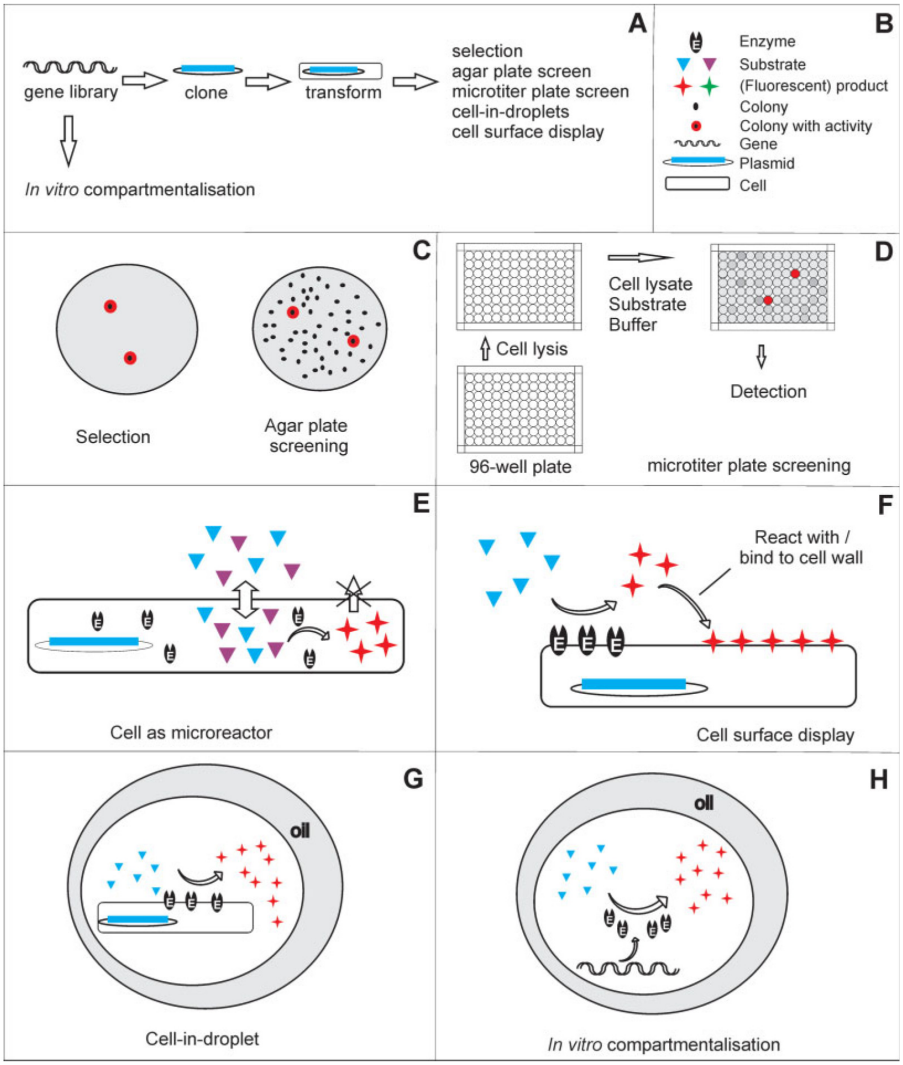

Comparison of screening and selection technologies

Strategy	Library size	Advantage	Disadvantage
Selection	$\sim 10^9$	Yields desirable variants only	Only possible if activity gives growth advantage
Agar plate screen	$\sim 10^5$	Simple to operate	Limited dynamic range
Microtiter plate screen	$\sim 10^4$	All analytical methods possible Excellent dynamic range	Relatively low screening capacity
Cell-in-droplet screen	$\sim 10^9$	Large libraries	Fluorescence detection and DNA modifying enzymes only
Cell as microreactor	$\sim 10^9$	Large libraries	Fluorescence detection only
Cell surface display	$\sim 10^9$	Large libraries	Fluorescence detection only
In vitro compartmentalization	$\sim 10^{10}$	No cloning steps Large libraries	Fluorescence detection and DNA modifying enzymes only

Figure 2. Overview of screening technologies. (A) Experimental steps from obtaining the gene library as PCR product to the actual screen. Note that cloning and transformation efficiency are often limiting library size; (B) Explanation of symbols; (C) Cell growth/survival selection and agar plate screening; (D) Microtiter plate screening; (E) Cell as micro-reactor; (F) Cell surface display; (G) Cell-in-droplet; and (H) *In vitro* compartmentalization (73).

2.2 Directed enzyme evolution for pH tolerance of enzymes

Application of enzymes in processes at a specified pH necessitates protein engineering to change their pH performance. Directed evolution and rational design method were applied to improve enzyme specific activity at certain pH or shift their pH profiles. Some representative success stories of directed protein evolution improving pH performance are summarized in Table 1.

Table 1. Improvement obtained from directed evolution or rational design for pH performance.

Enzymes	Mutagenesis methods	Screening methods	Improvements	References
Human β-glucuronidase	EpPCR and saturation mutagenesis	Flow cytometry	60-fold more active (k_{cat}/K_m) at pH 7.0 and were up to an order of magnitude more effective at catalyzing the conversion of two structurally disparate glucuronide prodrugs to anticancer agents	2008 (74)
Bacterial xylanase	DNA shuffling	Agar plate assay	About 5-fold improvement of specific activity at pH 9.0	2008 (75)
Human pancreatic lipase	EpPCR	Agar plate and microtiter plate assay	1.5-fold of activity improvement at acidic pH	2010 (76)
Bacterial arginine deiminase	EpPCR and site directed mutagenesis	Microtiter plate assay	pH optimum shifted from pH 6.5 to pH 7; 4-fold of activity improvement at pH 7.4	2010 (3)
Bacterial α-amylase	EpPCR	Microtiter plate assay	5-fold higher activity at pH 10 than wild type	2003 (77)
Eukaryote D-pantonohydrolase	EpPCR and DNA shuffling	Agar plate assay	10.5-fold higher specific activity and retain 85% of its original activity after incubation under low pH	2006 (78)
Vanadium chloroperoxidase	EpPCR, site saturation mutagenesis and site directed mutagenesis	Microtiter plate assay	About 100-fold improvement of specific activity at pH 8	2006 (79)
Bacterial class-A non-specific acid phosphatase (PhoN)	Site directed mutagenesis		1.6-fold of activity improvement over broder pH range	2006 (80)
Aspergillus niger PhyA phytase	Site directed mutagenesis		pH shifted from 5.5 to 3.8 (1.7 unit); 2.66 -fold improvement of activity at pH 3.5 than wild type.	2006 (81)
Bacillus cereus β-amylase	Site directed mutagenesis		pH optimum shifted to pH 4.2-4.8 by 2 pH units.	2004 (82)
Phytase	Site directed mutagenesis		pH optimum shifted by 0.5-1 pH unit; a slight increase in maximum specific activity	2002 (83)
Alcohol dehydrogenase	Site directed mutagenesis		pH optimum shifted from 7.8 to 9.0; about 2-fold improvement of maximum activity at pH 9.0 than that of wild type	1991 (84)

Many examples of rational reengineering of an enzyme pH optimum exist (Table 1). For shifting the pH optimum, a deep understanding of molecular dynamics is essential part of understanding enzyme flexibility. Rational design method successfully shifted enzyme pH profile. pH dependence of an enzyme is determined by the ionization of the catalytic groups, which is affected by various interactions involved in their microenvironments. In order to catalyze certain reactions, ionizable residues in active site should act as nucleophile or acid/base catalyst and they need to maintain proper ionization state for proper activities of proteins. The p*K*a value of the proton donor and the catalytic nucleophilic residue are therefore limiting the pH range at which the enzyme can function, and therefore pH-dependent activity can be differed by the p*K*a of the key residues. The p*K*a value of the residue is governed by intrinsic acidity of the functional group and other factors (electrostatic interaction from neighboring and the heterogeneous dielectric environment in the protein solution system). The electrostatic potential generated by the charged titratable residues affects the ground state of the protein, such as stability, binding to ligands and p*K*a values of ionizable groups. The electrostatic potential of proteins can be calculated by using computational procedures (Delphi, UHBD, CHARMM) and can be increased or decreased through mutations. For shifting the pH optimum of enzymes, many researchers have tried to substitute catalytic residue by site-directed mutagenesis (Table 1).

Yoo and coworkers (85) analyzed the relation between the shift of pH optimum and change in electrostatic potential due to mutation using Delphi. They identified key residues of xylanase responsible for electrostatic potential of catalytic residues but not affecting the catalysis directly. The latter hypothesis was proven by site directed mutagenesis in a later report. Wyss and coworkers (83) summarized strategies for enzyme pH profile modification, 1) replacement of ionizable groups that are directly involved in substrate or product binding and/or catalysis by nonionizable ones or by amino acids with different charge or p*K*a values; 2) replacement of residues that are in direct contact with residues

mentioned in 1) by forming hydrogen bonds and/or salt bridges; 3) alteration of longer-range (indirect) charge-charge interactions by modification of the surface charge of the enzyme.

When there is no structure-function relationship information available for an enzyme, directed evolution is the best option to tailor the pH performance of enzyme for application demands (Table 1). Directed evolution allows improving all properties that can be reflected in a screening system through iterative rounds of diversity generation and screening. Small libraries of a few thousand variants are often sufficient to find improved muteins even without rational understanding of the targeted property (76, 86). Using MTP assay, epPCR mutant libraries with a ratio of 50 % active and 50 % inactive clones have often been used successfully in directed evolution, improving enzyme properties by gradual changes (one or two amino acids changes per round of mutagenesis and screening).

2.3 Directed enzyme evolution for medical application

Directed evolution has been very useful for improving enzymes for industrial needs. In recent years, there is also growing number of enzymes applied for therapeutic purpose. For the development of protein therapeutics, directed evolution started to be used to tailor enzyme properties in medical field, for example drug delivery (87, 88) and has proven to be a useful tool for generating protein variants with enhanced therapeutic potential (88), for example, improving the effectiveness of therapeutic enzymes, antibodies, vaccines and viruses. Here, the improvements of therapeutic protein for anti-tumor application by directed evolution are discussed in more details.

2.3.1 Prodrug enzymes for tumor chemotherapy

Prodrug cancer chemotherapy has attracted considerable interest due to the possibilities it provids to overcome various barriers to drug formulation and delivery (such as poor aqueous solubility, chemical instability, insufficient oral

adsorption, rapid pre-systemic metabolism, inadequate brain penetration, toxicity and local irritation) (89). Examples of such drugs currently in use in cancer treatment include 5-fluorocytosine, cyclophosphamide, capecitabine, mitomycin C, and AQ4N (90). However, the side effects of prodrug therapy remain a serious concern which arises from the fact that noncancerous cells also possess the capacity to degrade them. This has triggered the interest to generate more effective prodrug-activating enzymes so that prodrugs can kill tumor cells at concentrations that generate little or no side effects. Further goals are to design more powerful and tumor-specific drugs, and to devise more effective methods for delivering them specifically to tumors.

By applying directed evolution through the technique of error-prone PCR, Martin and coworkers (90) indentified YieF variant exhibiting >5-fold increased capacity to kill HeLa cells. Furthermore, YieF variant was proved to be effectively delivered to tumor cells using a strain of *Salmonella typhimurium* (SL 7838).

Human β-glucuronidase, due to low intrinsic immunogenicity in humans, is an attractive enzyme for tumor-specific prodrug activation. However its utility is limited by low activity at physiological pH. Roffler and coworkers (74) developed a high-throughput screening procedure for enzymatic activity based on the stable retention of fluorescent reaction product in mammalian cells expressing properly folded glycoproteins on their surface. This procedure was utilized to screen error-prone PCR and saturation mutagenesis libraries to isolate β-glucuronidase tetramers that were up to 60-fold more active (k_{cat}/K_m) at pH 7.0 and were up to one order of magnitude more effective at catalyzing the conversion of two structurally disparate glucuronide prodrugs to anticancer agents.

2.3.2 Oncolytic viruses for tumor chemotherapy

Viral-mediated oncolysis is a novel cancer therapeutic approach with the potential to be more effective and less toxic than current therapies due to the agents' selective growth and amplification in tumor cells. To date, these agents

have been regarded as highly safe in patients but have generally fallen short of their expected therapeutic value as monotherapies.

Consequently, new approaches to generate highly potent oncolytic viruses are required. For the latter purpose, Hermiston and coworkers (91) developed a new method and termed it also ‘‘Directed Evolution’’ for creating highly potent oncolytic viruses. Viral serotypes representing Ad subgroups B-F were pooled and passaged twice on sub-confluent cultures of the target tumor cell lines at a particle-per-cell ratio of approximately 200 to invite recombination between serotypes (Figure 3). Supernatants from the second round of the high viral particle-per-cell infection of sub-confluent cultures were then used in a 10-fold dilution series to infect confluent T-75 tissue culture flasks of target tumor cell lines PC-3, HT-29, Panc-1 and MDA-231. Using this ‘‘Directed Evolution’’ methodology, the novel generated chimeric oncolytic virus ColoAd1 demonstrated ~ 2 log increase in both potency and selectivity when compared to ONYX-015 on colon cancer cells. *In vivo* and *ex vivo* studies therefore validated the innovative general approach for deriving clinically-relevant and potent anti-cancer virotherapies.

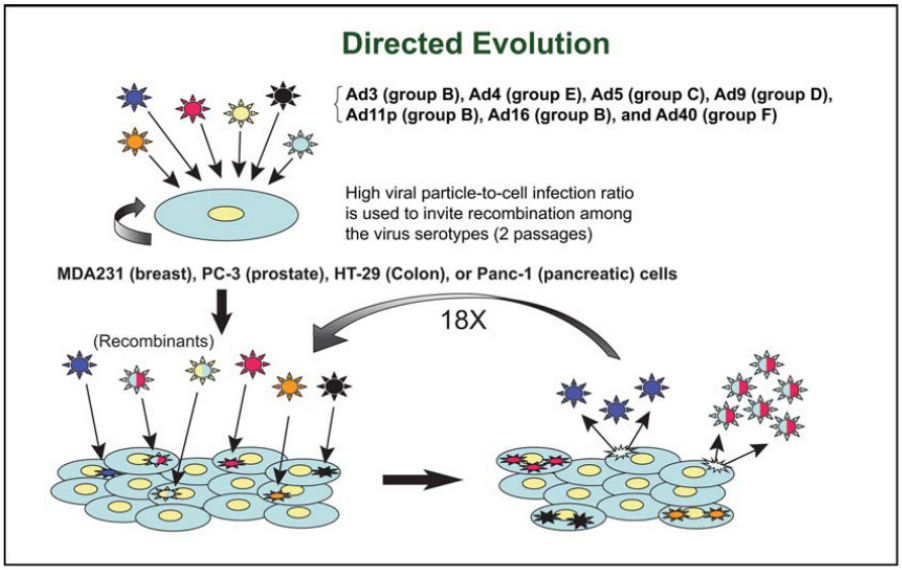

Figure 3. Hermiston’s “Directed Evolution” process of viruses and derivative viral pools (91).

2.3.3 Amino acid depriving enzyme for anti-tumor applications

Naturally available enzymes are usually not optimally suited for therapeutic purposes. This incompatibility often relates to the stability or activity of the enzymes under body conditions.

Despite many successful efforts to broaden the understanding of the structural basis of protein stability, there is still no universal strategy to stabilize protein by a limited number of rationally designed mutations. Well-known and reasonably successful types of rational engineering work include substitutions that increase rigidity (e.g. substitute amino acid Xxx with Pro or substitute Gly with other amino acid Xxx or the introduction of disulfides). These substitutions have effects on the entropy of the unfolded state, improvement of molecular packing (e.g. shortening of loops, improvement of interactions in the hydrophobic core, for example, by the removal of internal cavities), modification of surface charge networks or reinforcement of a higher oligomerization state.

Directed evolution provides a powerful approach for improving thermostability and does not need understanding of structure-function relationship. Most strategies for screening for enzyme stability rely on measuring residual enzyme activity before and after exposure to a denaturing challenge (e.g. high temperature, organic solvents, extreme pH) (92).

Bacterial L-asparaginases have been used as therapeutic agents in the treatment of lymphoblastic leukaemia. The main restrictions to the therapeutic use of L-asparaginase include its premature inactivation. As a result frequent injections are required to maintain therapeutic levels. Repeated injections and high dose can cause several types of side reactions from mild allergies and the development of immune responses to dangerous anaphylactic shocks (93). Enhancing the stability of L-asparaginase by protein engineering improves its body-residence time, and thereby minimizes immunosuppressive effects by lowering the therapeutic dose. Labrou and coworkers (94) obtained a

reengineered L-asparaginase with enhanced thermal stability. Single mutation on the surface of the protein resulted in ~10 degree increased T_m value (half-inactivation temperature). The thermostable variant has to be tested further on animals and/or humans in order to be advanced to a potent therapeutic drug.

Another example of a reengineered amino acid-deprivating enzyme is PpADI. PpADI is a promising anti-tumor enzyme however with a non-physiological optimal pH and relative high K_m value which hindering its medical application. By directed evolution and site saturation mutagenesis, PpADI variants with higher activity at physiological pH and at low arginine concentration of were obtained with improved properties to become a potent anti-tumor drug (see chapter 3 and chapter 4). *In vitro* and *in vivo* test of the improved variants are required to evaluate the anti-tumor effectiveness.

2.3.4 Affibody molecules for cancer prognosis

Affibody molecules represent a new class of affinity proteins that are based on the Z-domain scaffold derived from staphylococcal protein A (95). Among the scaffold proteins, Affibody molecules constitute the smallest non-cysteine-containing protein scaffold. The small size (~ 7 kDa), robust structure, and straightforward production procedures (either by recombinant production in bacteria or by chemical synthesis) make Affibody molecules attractive targeting agents for *in vivo* radionuclide imaging (96) as well as for various biotechnological applications (97, 98). The small size offers a convenient affinity maturation principle. Gene synthesis allows randomizing the whole gene to generate diverse mutant library. The potential use of radiolabeled Affibody molecules for high-contrast radionuclide imaging of biomarkers has been demonstrated in preclinical studies and in pilot clinical studies. Affibody molecules are non-immunoglobulin-derived affinity proteins based on a three-helical bundle protein domain.

Several of affinity proteins have been investigated for both *in vivo* diagnostics and therapy of tumor in radionuclide molecular imaging. Affinity proteins in tumor-targeted therapy can affect tumor progression by altering signal transduction or by delivering a payload of toxin, drug or radionuclide. EGFR (epidermal growth factor receptor), one of the receptor in ErbB family, has been extensively studied as biomarkers in tumor targeting and over expressed in various malignancies, associated with poor patient prognosis and are therefore interesting targets for solid tumors. High affinity and especially slow dissociation rate are important for obtaining high contrast images. Affinity in the low nanomolar range is considered as a prerequisite for successful use of peptide-based tracers.

Ståhl and coworkers (99) described the affinity maturation procedure for the generation of Affibody molecules binding with high affinity and specificity to EGFR. The library for affinity maturation was constructed using a single oligonucleotide for the rerandomization of desired positions. The new binders were selected with phage display technology and the best second-generation binders were characterized *in vitro* using real-time biospecific interaction analysis (BIA) for their binding to recombinant EGFR and with flow cytometry for their binding to native EGFR. Second-generation binders achieved an approximately 30-fold improvement in affinity (K_d = 5-10 nM) for the soluble extracellular domain of EGFR in biospecific interaction analysis using Biacore.

2.3.5 Interferon for anti-tumor applicaiton

Alpha interferons (IFN-as) are members of the diverse helical-bundle superfamily of cytokine genes, which have potent antiviral and antiproliferative activities and therefore can be used as anticancer and antiviral agents. However, doselimiting toxicity, receptor cross-reactivity, and short serum half-lives significantly reduce the clinical use of many of these cytokines.

Patten and coworkers (100) performed a family shuffling experiment with over 20 human interferon-α (Hu-IFN-α) genes. Antiviral assay and proliferation assay

were used to indentify clones with improved activity on Hu-IFN-α receptor. One clone showed 285,000-fold improved activity relative to Hu-IFN-α2a and 185-fold relative to Hu-IFN-α1 (most active native human interferon).

Selective breeding using DNA shuffling has proved to be very effective method to rapidly improve pharmaceutical proteins by which initially have low levels of the desired “activity” (101, 102). Backcrossing of evolved recommbinants with the wild type genes removes functionally neutral changes, which might reduce the immunogenicity of evolved proteins (103).

2.4 Conclusion

Proteins, especially enzymes, have gained a central role in modern chemical, biotechnological, and biopharmaceutical industries. Directed evolution has over the past proved to be a versatile and successful approach for tailoring protein properties to industrial, agricultural and medical demands and for advancing our understanding of structure-function relationships in biocatalysts. Appropriate library generation and screening methods should be employed concerning the target protein and desired property. To set up a sophisticated screening method, complex conditions in human body (pH, ion concentration, proteases, hormones etc.) should be considered. Subsequent *in vivo* or *in vitro* test of improved variants should be carried out to further validate the screening assay. Development of diversity generation and high-throughput screening method will enable evolution to solve problems efficiently. Especially, directed evolution provides a powerful strategy to rapidly advance the development of improved protein-based drugs (enzymes and antibodies, peptide and ligands). Directed evolution promises to play an increasingly important role to generate “desirable” drugs.

Chapter 3. Directed evolution of Arginine deiminase for increased activity at physiological pH

3. 1 Abstract

Arginine deiminase (ADI; EC 3.5.3.6) has been studied as a potential anti-tumor drug for the treatment of arginine-auxotrophic tumors, such as hepatocellular carcinomas (HCCs) and melanomas. Studies with human lymphatic leukemia cell lines confirmed that ADI is a potential anti-angiogenic agent effective in the treatment of leukemia. ADI from *Pseudomonas plecoglossicida* (PpADI) was cloned and expressed in *E.coli*. A main limitation of PpADI lies in its pH-dependent activity profile with a pH optimum at 6.5. A pH shift from 6.5 to 7.5 results in ~80 % activity drop (pH of human plasma is 7.35 to 7.45). For shifting PpADI pH optimum to netrual pH, a directed evolution protocol based on an adapted citrulline screening protocol in microtiter plate (MTP) format was developed and validated. Proof of concept for ADI engineering resulted in a pH optimum of pH 7.0 and increased activity under physiological conditions: at pH 7.4, variant M2 (K5T, D44E and H404R) is 4-fold more active than the wild type PpADI and retains ~30 % of its activity relative to its pH optimum, compared to ~10 % in the case of the wild type PpADI.

3.2 Introduction

Arginine deiminase (ADI) is a potential cancer therapy agent for the treatment of arginine-auxotrophic tumors (e.g. hepatocellular carcinomas and melanomas). The hepatocellular carcinoma (HCC) accounts annually for approximately 1 million new cases worldwide. In the US the incidence rate (per 100,000 persons; 1992-2002) of HCC is 8.6 with a mortality rate of 6.5 due to low responses of hepatoma to chemotherapeutic treatments (27). Current research efforts are

focused on ADI's *in vivo* inhibitory effect towards HCCs, leukemia, melanomas and human umbilical vein endothelial cells (HUVEC) (104-106), clinical trials for HCC (phase III) and melanoma (phase I/II) (105, 107), and PEG formulation of ADI to improve its efficacy as a clinical drug, including serum half-life and antigenicity (16, 108). ADI inhibited the growth of cultured leukemia cells at concentrations of 5-10 ng/ml, which were about 20-100 times lower than those of the L-asparaginase standard resulting in fewer side effects (106, 109). Arginine deprivation is speculated to be the molecular reason for ADI's inhibitory effect on human lymphatic leukemia (106). ADIs catalyze the first step of the arginine deiminase (ADI) pathway by hydrolyzing arginine to citrulline and ammonium. Several ADI genes have been identified, purified, and characterized from bacteria, archaea and some eukaryotes excluding mammalian cells and summarized in a recent review (27). None of these ADIs is from a kinetic point of view ideally suited for *in vivo* applications in humans under physiological conditions.

Protein engineering by rational design and directed evolution offers opportunities to tailor ADI properties to physiological conditions. For the proof of concept, an ADI isolated from *Pseudomonas plecoglossicida* CGMCC2039 (accession number: ABS70718) which can be functionally expressed in *E. coli* has been employed. Directed evolution approaches employ mainly *E. coli* as host due to its fast growth and high transformation efficiency which is a prerequisite for generating complex mutant libraries. Over the last decades, directed protein evolution has become a versatile and successful approach for tailoring protein properties for industrial demands (mainly in chemical synthesis) and for advancing our understanding of structure-function relationships in enzymes. A directed evolution experiment comprises iterative cycles of diversity generation and functional selection for improved variants. Only a few manuscripts for phytases (83), xylanases (110), amylases (77, 82, 111), and an alcohol deyhdrogenase (112) reported a shift of pH optima using directed evolution algorithms. None of these directed evolution campaigns targeted a medical

application and arginine deiminase has to our best knowledge not been altered in its pH activity/resistance by directed evolution.

Comparison of PaADI (*Pseudomonas aeruginosa*, pH optimum 5.6; His405) and MaADI (*Mycoplasma arginini* ADI, pH optimum 6.5, Arg397) led to the speculation that substitution of His by Arg might contribute to MaADI's increased pH optimum (17). A sequence alignment of four ADIs (MaADI, MyADI (*Mycoplasma arthritidis* ADI), PaADI and PpADI) shows that for both Pseudomonas ADIs the synonymous amino acid positions (404 & 405), contain a His whereas both Mycoplasma ADIs contain at corresponding positions an Arg. Interestingly, both Mycoplasma ADIs have an pH optimum approximately one pH unit higher than both Pseudomonas ADIs.

In this study we report the first directed ADI evolution protocol in which the pH profile of PpADI was shifted to higher pH values representing a conceptional proof that ADI properties can be tailored for demands *in vivo* treatment of arginine-auxotrophic tumors. An emphasis is given on detailed description of directed evolution conditions (mutagenic and screening).

3.3 Materials and methods

3.3.1 Materials

All chemicals were of analytical-reagent grade or higher quality and were purchased from Fluka (Neu-Ulm, Germany), Sigma-Aldrich (Steinheim, Germany) and Applichem (Darmstadt, Germany), except the resins for purification (TOSOH, Stuttgart, Germany). All enzymes were purchased from New England Biolabs (Frankfurt, Germany), Fermentas (St. Leon-Rt, Germany), and Sigma-Aldrich Chemie (Taufkirchen, Germany), unless stated otherwise.

Thermal cycler (Mastercyler gradient; Eppendorf, Hamburg, Germany) and thin-wall PCR tubes (Multi-ultra tubes; 0.2 µl; Carl Roth, Germany) were used in all PCRs. The PCR volume was always 50 µl except for Megaprimer PCR of whole

plasmid (MEGAWHOP, 20 µl); larger volumes were prepared in multiple 50-µl PCRs. The amount of DNA in cloning experiments was quantified by using a NanoDrop photometer (NanoDrop Technologies, Germany).

Pseudomonas plecoglossicida CGMCC2039 was provided by Professor Zhihao Sun (Jiangnan University, Wuxi, China).

3.3.2 Methods

3.3.2.1 Reagents used in assays

Acid-ferric solution

To dH_2O (600 ml), concentrated H_3PO_4 (70 ml, 85 %) and concentrated H_2SO_4 (160 ml, 90-91 %) were added slowly. After cooling to room temperature, $FeCl_3 \cdot 6H_2O$ (10 ml, 10 g/L) was added in the above solution, finally the total volume was adjusted to 1 liter with dH_2O.

Diacetyl monoxime -thiosemicarbazide (DAM-TSC) solution

DAM solution (10 g/L) and TSC solution (0.3 g/L) were prepared separately. The two solutions were mixed (volume ratio = 1:1) just prior to use.

3.3.2.2 Cloning of ADI into pET42b(+)

The arginine deiminase (ADI) gene was amplified from *Pseudomonas plecoglossicida* CGMCC2039 by colony PCR (94℃ for 10 min, 1 cycle; 94℃, 30 s/ 54℃, 30 s/ 72℃, 165 s, 29 cycles; 72℃ for 5 min, 1 cycle) using primer (5'-CCGCATTCCGCTGAAAAACAGAAGTACGG-3' and 5'-CTTCTCGAGTTAGTAGTTGATCGGGTCGCGCACG-3'), 1.5 U of Pfu DNA polymerase, 0.20 mM of dNTP mix and a colony of *Pseudomonas plecoglossicida* CGMCC2039. Amplification product was purified by gel extraction, digested using NdeI (20 U) and XhoI (20 U) and purified using QIAquick PCR purification kit (QIAGEN, Hilden, Germany). Cloning vector pET42b(+) was digested with NdeI (20 U) and XhoI (20 U), and purified by gel extraction kit (QIAGEN, Hilden, Germany). Digested ADI gene and pET42b(+)

were ligated using T4 DNA ligase (1 U) to give pET42b(+)-ADI and transformed into *E. coli* BL21-Gold (DE3).

3.3.2.3 Site directed mutagenesis of PpADI gene at position H404

Site directed mutagenesis of ADI gene was performed according to the published method (113) on plasmid pET42b(+)-ADI. The following oligonucleotides were used for mutagenesis of H404R: 5'-GGCCGTGGCGGCGGCCGTTGCATGACCTGCCCG-3' and 5'-CGGGCAGGTCATGCAACGGCCGCCGCCACGGCC-3' (underlining indicated the substituted nucleotide). For the mutagenic PCR (First stage: 95℃ for 30 s, 1 cycle; 95℃, 30 s/ 55℃, 1 min/ 72℃, 130 s, 3 cycles. Second stage: 95℃ for 30 s, 1 cycle; 95℃, 30 s/ 55℃, 1 min/ 72℃, 130 s, 15 cycles; 68℃ for 30 min, 1 cycle), 2 U of Phusion™ Hot Start DNA polymerase (Finnzymes, Keilaranta, Finland), 0.20 mM of dNTP mix, 25 pmol of each primer together with 100 ng of template (pET42b(+) harboring ADI gene) were used. Following the PCR, DpnI (40 U; New England Biolabs) was added, and incubated overnight at 37℃. The PCR products were purified by using a QIAquick PCR Purification Kit (Qiagen) and transformed into *E. coli* BL21-Gold (DE3) for expression.

3.3.2.4 Site sturation mutagenesis of PpADI gene at nine amino acid position

Site saturation mutagenesis of ADI gene was performed according to the published method (113) on plasmid pET42b(+)-ADI. The oligonucleotides were used for mutagenesis were listed in table 1 (underlining indicated the substituted nucleotide). For the mutagenic PCR (First stage: 95℃ for 30 s, 1 cycle; 95℃, 30 s/ 55℃, 1 min/ 72℃, 130 s, 3 cycles. Second stage: 95℃ for 30 s, 1 cycle; 95℃, 30 s/ 55℃, 1 min/ 72℃, 130 s, 15 cycles; 68℃ for 30 min, 1 cycle), 2 U of Phusion™ Hot Start DNA polymerase (Finnzymes, Keilaranta, Finland), 0.20 mM of dNTP mix, 25 pmol of each primer together with 100 ng of template (pET42b(+) harboring ADI gene) were used. Following the PCR, DpnI (40 U; New England Biolabs) was added, and incubated overnight at 37℃. The PCR products were

purified by using a QIAquick PCR Purification Kit (Qiagen) and transformed into *E. coli* BL21-Gold (DE3) for expression.

Table 1. Primer sequences for site saturation mutagenesis.

Primer name	Sequences
Leu 41 FP	AACTGCGACGAGCTGNNNTTCGACGATGTGATC
Leu 41 RP	GATCACATCG TCGAANNNCA GCTCGTCGCAGTT
Asn 360 FP	TGGGATGACGGCAACAACNNNGTGGCGCTGGAG
Asn 360 RP	CTCCAGCGCC ACCACNNNGT TGCCGTCATCCCA
Arg401 FP	GAACTGGGCCGGGGCNNNGGCGGCGGCCACTGC
Arg401 RP	GCAGTGGCCGCCGCCNNNGCCCCGGCCCAGTTC
Phe163 FP	CTGCCCAACACCCAGNNNACCCGCGACACCACC
Phe163 RP	GGTGGTGTCGCGGGTNNNCTGGGTGTTGGGCAG
Asn160 FP	CTGCCGCCGCTGCCCNNNACCCAGTTCACCCGC
Asn160 RP	GCGGGTGAACTGGGTNNNGGGCAGCGGCGGCAG
Arg185 FP	ATGTACTGGCCGGCNNNCGCCAGGAAACCCTG
Arg185 RP	CAGGGTTTCCTGGCGNNNGCCGGCCAGTACAT
Arg243 FP	ATCGGCATGGGTGAGNNNACCTCGCGCCAGGCC
Arg243 RP	GGCCTGGCGCGAGGTNNNCTCACCCATGCCGAT
His405 FP	GGCCGTGGCGGCGGCNNNTGCATGACCTGCCCG
His405 RP	CGGGCAGGTCATGCANNNGCCGCCGCCACGGCC
Gly403 FP	GCCGGGGCCGTGGCNNNGGCCACTGCATGACC
Gly403 RP	GGTCATGCAGTGGCCNNNGCCACGGCCCCGGCC

3.3.2.5 Construction of PpADI error-prone library

The library was generated by the standard error-prone PCR (epPCR) using improved variant H404R as template. For the mutagenic PCR (95℃ for 2 min, 1 cycle; 95℃, 30 s/ 55℃, 30 s/ 72℃, 30 s, 29 cycles; 72℃ for 3 min, 1 cycle), 2.5 U of Taq DNA polymerase, 0.20 mM of dNTP mix, 50 ng of template (pET42b(+) harboring ADI gene H404R), 0.01-0.1 mM of $MnCl_2$ and 10 pmol of each primer (5'-TACATATGTCCGCTGAAAAACAGAAG-3' and 5'- GTGCTCGAGTTAGTAGT TGATCGG-3') were used. The PCR products were purified by using a QIAquick PCR Purification Kit. The purified epPCR products were cloned into expression

plasmid pET42b(+) by MEGAWHOP(114). For MEGAWHOP (68℃ for 5 min, 1 cycle; 95℃ for 5 min, 1 cycle; 95℃, 1 min/ 55℃, 1 min/ 68℃, 13 min 30 s, 24 cycles; 68℃ for 30 min, 1 cycle), 1 U of Taq DNA polymerase, 0.1 U of Pfu DNA polymerase, 0.20 mM of dNTP mix together with 200 ng of template (pET42b(+) harboring ADI gene H404R) were used. Following the PCR, DpnI (40 U; New England Biolabs) was added, and incubated (4 h; 37℃). The MEGAWHOP products were transformed into *E. coli* BL21-Gold (DE3) for expression and screening.

3.3.2.6 Expression of PpADI in LB media with IPTG induction

The strain *E. coli* BL21-Gold (DE3)/ pET42b-PpADI was cultured at 37℃ in 20 ml of LB media that contained 50 μg/ml kanamycine to an absorbance of 0.6 at 578nm. Then, isopropyl β-D-thio-galactopyranoside (IPTG) was added to a final concentration 0.2 mM. The cells were harvested after 9 h induction with IPTG at 37℃. The expressed rADI was analyzed by SDS-PAGE.

3.3.2.7 Expression of PpADI in auto-induction media

A chemically defined auto-induction medium (115) containing salts and trace metals, vitamins including vitamin B12, and glucose, glycerol, and lactose were test for PpADI expression. Five kinds of auto-induction media LS-5052, P-5052, MD-5052, TYM-5052 and TYP-5052 were tested for the ADI expression, under the following conditions: 20 ml LB media in 100 ml flask, 37℃, 250 rpm, 20 h. The expressed rADI was analyzed by SDS-PAGE.

3.3.2.8 Cultivation and expression of PpADI in 96-well plates

Colonies grown on LB_{kan} agar plates were transferred, by using toothpicks, into 96-well microtiter plates (flat bottom, polystyrene plates; Greiner Bio-One GmbH, Frickenhausen, Germany), containing non-inducing medium LSG (150 μL) (115) supplemented with kanamycin (50 μg/ml). After 16 h of cultivation in a microtiter plate shaker (Multitron II, Infors GmbH, Einsbach, Germany; 37℃, 900 rpm, 70 % humidity), each well was replicated using a replicator (EnzyScreen BV, Leiden,

Netherlands) into a second series of 96-well microtiter plates containing 150 µL of auto-induction media LS-5052 (115) supplemented with kanamycin (50 µg/ml). The first set of plates was stored at -80°C after addition of glycerol. The clones in the second set of plates were cultivated for 12 h (Multitron II, Infors GmbH, 37°C, 900 rpm) and used for screening.

3.3.2.9 Screening Procedure

96-well plate format citrulline colorimetric screening assay

A modified protocol of citrulline detection based on carbamido-diacetyl reaction (116) (see Figure 1A for assay mechanism) was used for ADI activity measurement. Screening for increased activity was carried out by measuring the activity at pH 7.4 and 6.4. 20 µl of cell culture was transferred to 96-well microtiter plate. Enzyme reaction was initiated by addition of arginine solution (100 µl, 100 mM) supplemented with cetyltrimethylammoniumbromide (CTAB, 4 mM), and incubated (20 min, 37°C). Subsequently, acid-ferric solution (60 µl) and diacetyl monoxime (DAM, 20 µl, 0.5 M) were added. The reaction mixture was further incubated (15 min, 55°C). Absorbance was measured at 492 nm using a microtiter plate reader (Tecan Sunrise, Tecan Group AG, Zurich, Switzerland).

Standard deviation measurements were performed in 96-well plate format using culture from BL21-Gold (DE3) lacking ADI and in a separate experiment containing ADI. Apparent standard deviation was based on the absolute absorbance values obtained from the ADI wild type plate. The true standard deviation was calculated by subtracting the background absorbance value of the microtiter plate lacking ADI from the apparent values.

Cuvette format citrulline colorimetric assay

ADI activity was routinely measured using a modified protocol of the citrulline detection with DAM and TSC (117) (see Figure 1A for assay mechanism) in Eppendorf tubes. Enzyme reaction was initiated by addition of arginine solution (200 µl, 100 mM) to a 2-ml eppendorf tube containing crude cell lysate (50 µl), and incubated (20 min, 37°C). Subsequently, acid-ferric solution (250 µl) was

added to stop the enzyme reaction. After appropriate dilution with deionized water to ensure the concentration of produced citrulline is within linear detection range, the reaction mixture (400 µl) was mixed with acid-ferric solution (600 µl) and DAM-TSC solution (100 µl). The reaction mixture was further incubated (30 min, 70°C), followed by incubation in ice water to stop color development. Absorbance was measured at 530 nm using a Specord 200 (Analytik Jena AG, Jena, Germany).

Normalization of protein expression for wild type ADI and variants

Agilent Protein 230 Kit (Agilent Protein 230 Kit, Agilent Technologies Deutschland GmbH, Böblingen, Germany) and Agilent 2100 Bioanalyzer (Agilent 2100 Bioanalyzer, Agilent Technologies Deutschland GmbH, Böblingen, Germany) were used for normalization of protein expression in crude cell extract. The protocol used was according to Agilent protein 230 Kit Guide except BSA was used as an internal standard.

3.3.2.10 Expression of ADI in shaking flask and purification

Shaking flasks (1 liter) containing auto induction media LS-5052 (200 ml) supplemented with kanamycin (50 µg/ml) were inoculated with a 1:200 dilution of overnight culture (*E. coli* BL21-Gold(DE3) harboring pET42b-ADI) grown in non-inducing media LSG. After 12 h of expression, *E. coli* cells were harvested by centrifugation (Eppendorf 5810R 4°C, 3220 g, 30 min) and resuspended in phosphate buffer (20 ml, Na_xPO_4, 20 mM, pH 7.0). *E. coli* cells were subsequently lysed by using a high-pressure homogenizer (1500 bar, 2 cycles; Avestin Emulsiflex, Mannheim, Germany). The disrupted cells were centrifuged (Eppendorf 5417R, 4°C, 13000 g, 20 min) and the supernatant was further cleared by filtration through a low protein-binding filter (0.45 µm; Minisart RC 25 single use syringe filter; Sartorius, Hamburg, Germany). ADI wild type and mutants (H404R and K5T D44E H404R) were subsequently purified by a column chromatography procedure: (i) The filtered cell lysates were subjected to a Super-Q anion exchange column, which had been pre-equilibrated with 50 mM

phosphate buffer (Na_xPO_4, pH 7.0). 20 ml of cell lysate was loaded. ADI were eluted by a NaCl step elution in phosphate buffer (Na_xPO_4, 50 mM, pH 7.0) at a rate of 3 ml/min. (ii) The obtained ADI protein from ion exchange chromatography was subjected to a gel filtration column (Matrix: Toyoperl HW-55S, Bed volume: 33 ml, Bed height: 40 cm, Column: Omnifit).

Purified ADI was subsequently concentrated using a Amicon ultra-4 centrifugal filter device (Millipore Corporation, Billerica, U.S.A.) with a 30-kDa cut-off membrane. Total protein concentration was determined by BCA^{TM} assay kit (Pierce, Born, Germany) and homogeneity of the purified sample was controlled by SDS-page electrophoresis using standard molecular biology techniques.

3.3.2.11 Characterization of ADI wild type and mutants

Determination of k_{cat} and K_m of ADI wild type and the mutants

The k_{cat} and K_m values were determined from initial velocity data measured as a function of substrate concentration. Enzyme reaction was carried out at 37°C in a water bath. After 10 min preincubation at 37°C, the enzyme reaction was initiated by addition of purified enzyme (50 µl, 0.2-0.5 µM) to the substrate solution (200 µl, 0.2 mM to 10 mM of arginine, 0.5 M phosphate buffer, pH 7.4) in deep well plates. The reaction mixture was incubated (37°C) and every two minutes reaction mixture (30 µl) of each well was transferred to acid-ferric solution (30 µl) to stop the enzyme reaction. The color development was subsequently performed in 96-well PCR plate. Ferric-acid solution (90 µl) and DAM-TSC solution (15 µl) were added to each well. The 96-well PCR plate was then incubated (70°C, 30 min) in thermal cycler (Eppendorf Mastercyler gradient) for color development, followed by incubation in ice water to stop color development. Absorbance was measured at 530 nm using a microtiter plate reader (SPECTROstar Omega, BMG LABTECH, Offenburg, Germany). The initial velocity data obtained were fitted to the equation $v = V_{max}[S]/([S] + K_m)$ (where v is the initial velocity, V_{max} the maximum velocity, [S] the substrate concentration, and K_m the Michaelis constant) using GraphPad Prism software (GraphPad

software, San Diego, CA, USA). The k_{cat} was calculated from the ratio of V_{max} and enzyme concentration.

Determination of pH profile

Enzyme reaction was carried out at 37°C in a water bath using the following substrate solution: arginine 0.1 M, pH 5-8 phosphate/acetate buffer (0.5 M phosphate, 50 mM acetate). After 10 min preincubation at 37°C, the enzyme reaction was initiated by addition of purified enzyme (50 µl, 0.2-0.5 µM) to the substrate solution (200 µl) in deep well plates. The reaction mixture was incubated (37°C, 10 min) and acid-ferric solution (250 µl) was transferred to each well to stop the enzyme reaction. The color development was subsequently performed in 96-well PCR plate. The reaction mixture (60 µl), ferric-acid solution (90 µl) and DAM-TSC solution (15 µl) were transferred to a 96-well PCR plate. The 96-well PCR plate was then incubated (70°C, 30 min) in thermal cycler (Eppendorf Mastercyler gradient) for color development, followed by incubation in ice water to stop color development. Absorbance was measured at 530 nm using a microtiter plate reader (SPECTROstar Omega, Germany).

3.3.2.12 Molecular Modeling

Two crystal structures of PaADI (PDB codes: 1RXX, 2A9G) were used to model the mutations H405R and D44E. Only one monomeric unit of the tetrameric PaADI was used for the modeling study employing Swiss-PDB viewer (118) (www.expasy.org/spdbv). PaADI variants (H405R; D44E) were generated using the mutate command of Swiss-PDB viewer. The side chain rotamer with the best score was used for subsequent energy optimized with parameter of GROMOS96 force field for in vacuum minimization (119).

3.3.2.13 Stability of PpADI in presence of serum

Purified PpADI (wild type, M1, M2; 20 µl) was incubated (37°C, 60 min) with AB--human serum (80 ul, Invitrogen, Karlsruhe, Germany) and PBS buffer (pH7.4, 80 ul), respectively. Subsequently, the incubated ADI-serum/PBS mix (20 µl) was

added to microtiter plate containing arginine solution (100 µl, 10 mM arginine in PBS buffer, pH 7.4) and incubated (37℃, 30 min). Acid-ferric solution (120 µl) was added to stop the enzyme reaction. The produced citrulline was detected using the assay procedure employed in "Determination of kcat and Km of ADI wild type and the mutants". Before measuring absorbance at 530 nm, centrifugation (Eppendorf, 5810R 4℃, 3000 g, 10 min) was performed to remove the precipitation in the assay solution (likely proteins in serum were precipitated in acidic condition during assay procedure). Meanwhile, a serum control was test for the original citrulline concentration of serum using the same procedure mentioned above except that instead of PpADI, elution buffer of gel filtration (NaxPO4, 50 mM, pH 7.4) was used. All the absorbance values at 530 nm of ADI-serum sample were subtracted the value of serum control to get the citrulline concentration produced by PpADI. The residual activities of PpADI after incubation in serum compared to that in PBS buffer were calculated to show the stability of PpADI after incubated in human serum.

3.3.2.14 Activity of PpADI (wild type, M1, M2) towards arginine derivative dimethylarginine

Purified PpADI (wild type, M1, M2; 15 µl, ~0.2 mg/ml final concentration; >20-fold concentration used for kinetic constant determination) was incubated (37℃, 4 h) with (N^G, N^G)-dimethylarginine solution (20 mM, 100 µl). Acid-ferric solution (120 µl) was added to stop the enzyme reaction. Activity was recorded by citrulline detection using citrulline colorimetric assay (see 3.3.2.11 Characterization of ADI wild type and mutants).

3.4 Results

3.4.1 PpADI cloning

PpADI was cloned into pET42b(+) and expressed in *E.coli* BL21-Gold(DE3) using auto-induction media LS-5052 (see figure 2). The nucleotide sequence of PpADI comprises 1,254 bp nucleotide (figure 1) encoding 417 amino acids which have 85% identity to ADI from *P. aeruginosa* (PaADI). The PpADI cloned into

pET42b(+) was confirmed by nucleotide sequencing. As indicated in Figure 1, sequence analysis of ADI gene showed that there was one synonymous mutation at amino acid position D78 (GAT to GAC) compared to ADI-sequence of *P. plecoglossicida* CGMCC2039 deposited in NCBI (accession number: EU030267). The deduced ADI protein sequence has a calculated molecular weight of 46.5 kDa and shows 85% identity to ADI from *P. aeruginosa*. This clone was used for subsequent directed evolution experiments.

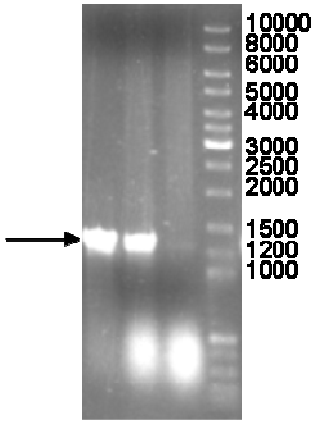

Figure 1. DNA electrophoresis of *PpADI*.

```
1       ATGTCCGCTG AAAAACAGAA GTACGGTGTC CACTCCGAAG CAGGCAAGCT GCGCAAGGTA
61      ATGGTCTGCG CTCCGGGACT GGCGCACAAG CGCCTGACCC CGAGCAACTG CGACGAGCTG
121     CTGTTCGACG ATGTGATCTG GGTCGACCAG GCCAAGCGCG ACCACTTCGA CTTCGTCACC
181     AAGATGCGCG AGCGCGGCGT GGATGTGCTG GAAATGCATA ACCTGCTCAC CGACATCGTG
241     CAGAACCCCG AGGCCCTGAA GTGGATCCTC GACCGCAAGA TCACCCCTGA CACCGTCGGG
301     GTGGGCCTGA CCAACGAAGT GCGCAGCTGG CTGGAGGGCC AGGAGCCACG CCACCTCGCC
361     GAGTTCCTGA TCGGCGGCGT GGCCGGCCAG GACCTGCCGG AGAGCGAAGG TGCCAGCGTG
421     GTCAAGATGT ACAACGACTA CCTGGGCCAC TCCAGCTTCA TCCTGCCGCC GCTGCCCAAC
481     ACCCAGTTCA CCCGCGACAC CACCTGCTGG ATCTACGGCG GCGTGACCCT CAACCCGATG
541     TACTGGCCGG CGCGACGCCA GGAAACCCTG CTGACCACCG CCATCTACAA GTTCCACCCC
601     GAGTTCACCA AGGCCGACTT CCAGGTCTGG TACGGCGACC CGGACCAAGA GCACGGCCAG
661     GCCACCCTCG AAGGCGGCGA CGTCATGCCG ATCGGCAAGG GCATCGTGCT GATCGGCATG
721     GGTGAGCGCA CCTCGCGCCA GGCCATCGGC CAACTGGCAC AGAACCTCTT CGCCAAGGGC
781     GCAGTGGAGC AAGTGATCGT CGCCGGGCTG CCGAAGTCCC GTGCGGCCAT GCACCTGGAC
841     ACCGTGTTCA GCTTCTGCGA CCGCGACCTG GTCACGGTTT TCCCGGAAGT GGTGCGCGAG
901     ATCGTGCCGT TCATCATCCG CCCGGACGAA AGCAAGCCCT ACGGCATGGA CGTACGCCGC
961     GAGAACAAGT CGTTCATCGA GGTGGTCGGC GAGCAGCTGG GCGTCAAGCT GCGTGTGGTC
1021    GAGACCGGCG GCAACAGCTT CGCCGCCGAG CGCGAGCAGT GGGATGACGG CAACAACGTG
1081    GTGGCGCTGG AGCCAGGTGT GGTCATCGGC TACGACCGCA ACACCTACAC CAATACCTTG
1141    CTGCGCAAGG CCGGGATAGA GGTCATCACC ATCAGTGCCG GCGAACTGGG CCGGGGCCGT
1201    GGCGGCGGCC ACTGCATGAC CTGCCCGATC GTGCGCGACC CGATCAACTA CTAA
```

Figure 2. PpADI sequencing results.

3.4.2 PpADI expression in LB media with IPTG as inducer

PpADI was successfully expressed in LB media with IPTG as inducer. Figure 3 (lane 4) shows the expression band of PpADI observed at ~45 kDa, which is similar to the calculated molecular weight of 46 kDa (based on http://expasy.org/tools/pi_tool.html).

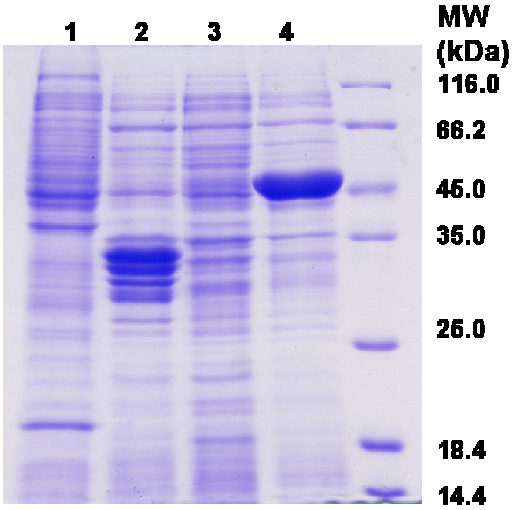

Figure 3. SDS-PAGE of PpADI expression. Lane 1: *P. plecoglossicida*; Lane 2: E. coli BL21-Gold (DE3)/ pET42b; Lane 3: E. coli BL21-Gold (DE3)/ pET42b-PpADI WT, without IPTG; Lane 4: E. coli BL21-Gold (DE3)/ pET42b- PpADI WT.

3.4.3 PpADI expression in auto-induction media

Expressing recombinant protein in auto-induction media is based upon the preferences of bacteria to selectively use different carbon sources during diauxic growth and upon the often-observed negative regulation of gene expression by catabolite repression. Auto-induction is more convenient than IPTG induction because the expression strain is simply inoculated into auto-inducing medium and grown to saturation without the need to follow culture growth and add inducer at the proper time. For high-throughput applications, the auto-induction approach has many advantages over traditional induction methods including avoidance of the strong induction and apparent toxicity associated with chemical inducers such as IPTG.

Five kinds of auto-induction media LS-5052, P-5052, MD-5052, TYM-5052 and TYP-5052 were tested for the ADI expression. Figure 4(A) and 4(B) show ADI

activity and corresponding SDS-PAGE band of the PpADI expression in different auto-induction media. The expression in auto-induction media LS-5052 is shows the highest activity and therefore LS-5052 was used for the following directed evolution experiments.

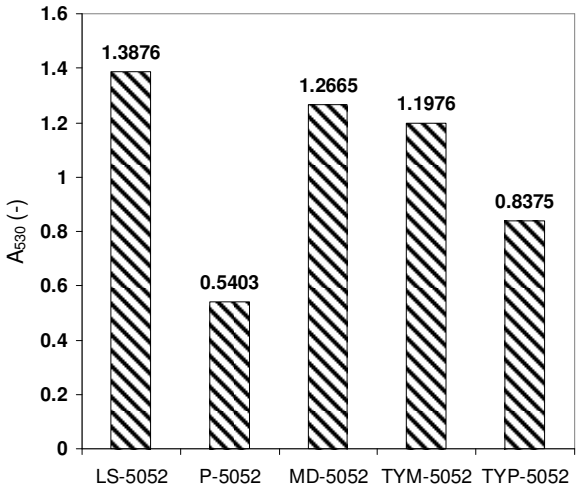

Figure 4(A). Activity of PpADI expressed in auto-induction media.

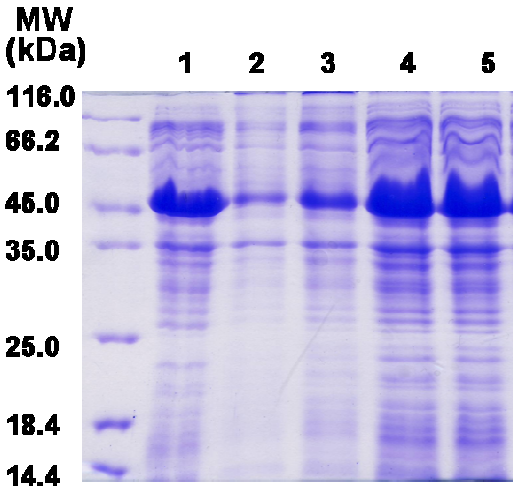

Figure 4(B). SDS-PAGE of ADI expressed in auto-induction media 1, LS-5052; 2, P-5052; 3, MD-5052; 4 TYM-5052; 5, TYP-5052.

3.4.4 PpADI assay based on citrulline detection

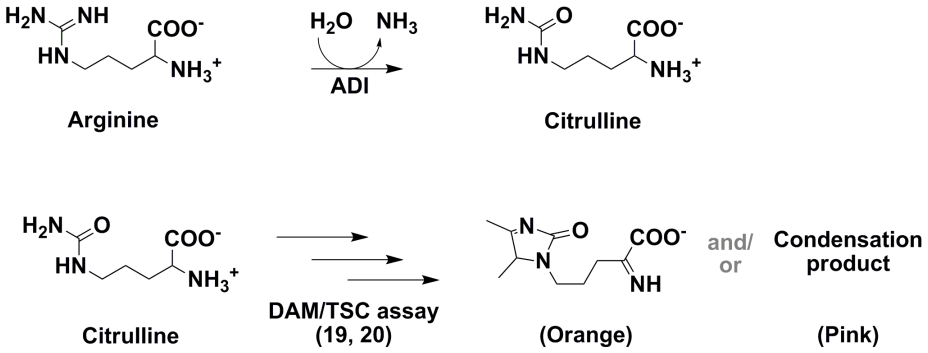

Figure 5. Arginine conversion by ADI and detection of citrulline using DAM/TSC assay.

ADI activity was measured by detecting the production of citrulline from arginine, according to carbamido diacetyl reaction (colorimetric reaction). The conditions of the carbamido diacetyl reaction is as follows： strong acid solution (H_3PO_4, H_2SO_4), oxidizing agent (Fe^{3+}), diacetyl monoxime (DAM), thiosemicarbazide (TSC), and boiling water bath. Figure 5 shows one postulated reaction mechanism for the assay which depicts the reaction between citrulline and DAM. By the addition of TSC to the reaction system, Coulombe and Favreau(120) obtained linearity of response with a more stable pink color which A_{max} was shifted from 490nm to 530nm.

Figure 6 describes the assay procedure for measuring ADI activity in 2 ml eppendorf tube. A calibration curve was prepared using citrulline standard solution (Figure 7) for determining the citrulline production during the assay.

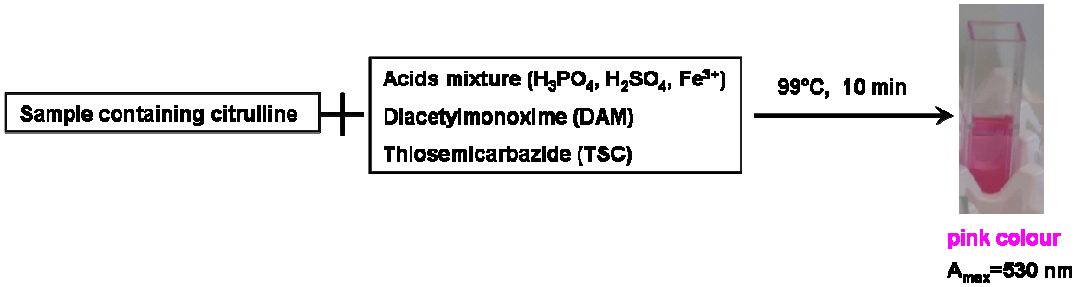

Figure 6. Citrulline colorimetric assay in cuvette format using DAM/TSC assay.

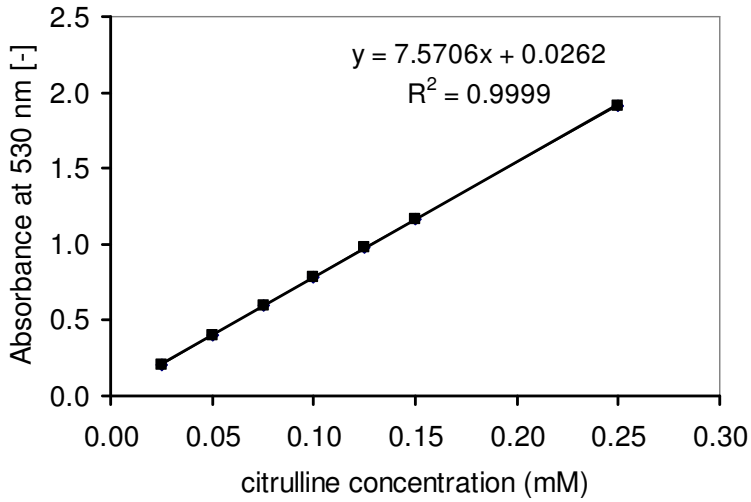

Figure 7. Calibration curve of cuvette format citrulline colorimetric assay.

3.4.5 PpADI screening system for citrulline production in microtiter plates

Two key performance parameters for identifying improved variants in microtiter plate based screening systems are the true standard variation and the linear detection range of the employed assay. Standard deviations have been reduced by optimizing expression and screening conditions (various auto-induction media and assay conditions such as amount of cell, conversion time and color development procedure). A modified version of the DAM-TSC assay for citrulline detection (Scheme 1) was selected for directed evolution of PpADI. The microtiter plate screening format was optimized for simplified handling by lowering the color development temperature (55℃ instead of 100℃), increasing the diacetylmonoxime concentration (~22-fold) and avoiding the use of the sensitizer thiosemicarbazide. Figure 8 shows the procedure of screening assay of citrulline detection.

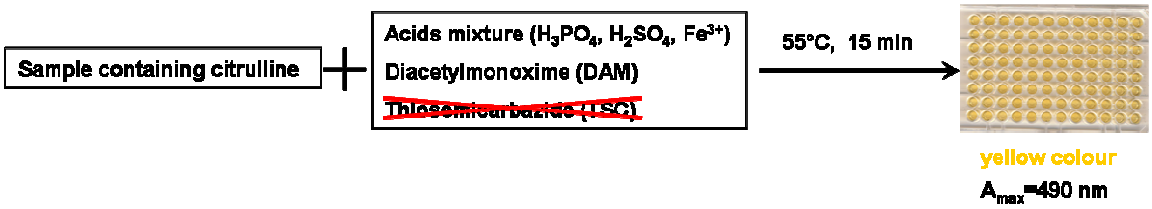

Figure 8. Citrulline colorimetric assay in MTP format using DAM assay.

Standard deviations of the modified citrulline detection assay have been reduced by optimizing expression and screening conditions (various auto-induction media and assay conditions such as amount of cell, conversion time and color development procedure). The preferred combination (150 µl LS5052 auto-induction media and 20 µl cell culture, 20 min conversion time and 15 min color develop time) resulted in a true standard deviation of 12.8 % after subtracting the background (Figure 10). Screening systems with standard deviations around 10 % have successfully been used in directed evolution experiments (121, 122). A wide linear detection window is important for identifying beneficial mutants in directed evolution experiments and screening systems for evolved mutants have to be constantly adapted for hitting the linear detection window. A linear detection range up to 6 mM citrulline could be detected (Figure 9).

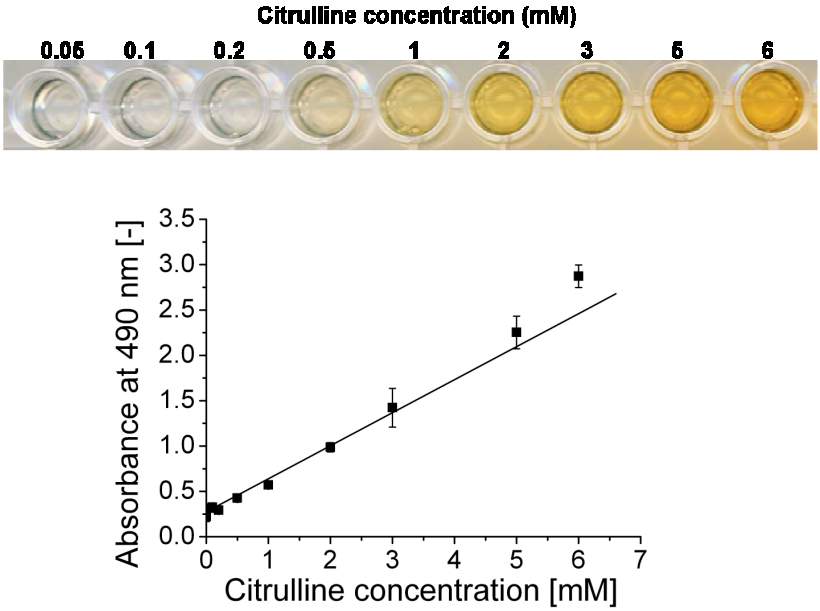

Figure 9. Calibration curve of 96-well microtiter plate format citrulline colorimetric screening assay.

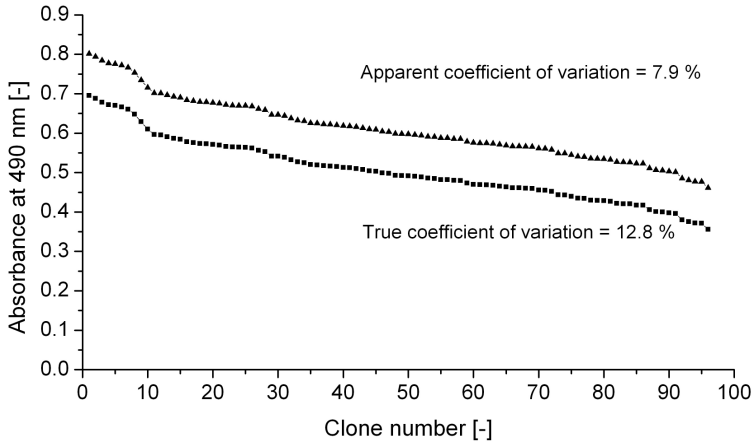

Figure 10. Activity values in descending order of the ADI wild-type conversion of arginine to citrulline in a 96-well microtiter plate using the optimized assay protocol. The apparent coefficients of variation were calculated without subtracting the background and the true coefficients of variation after background subtraction.

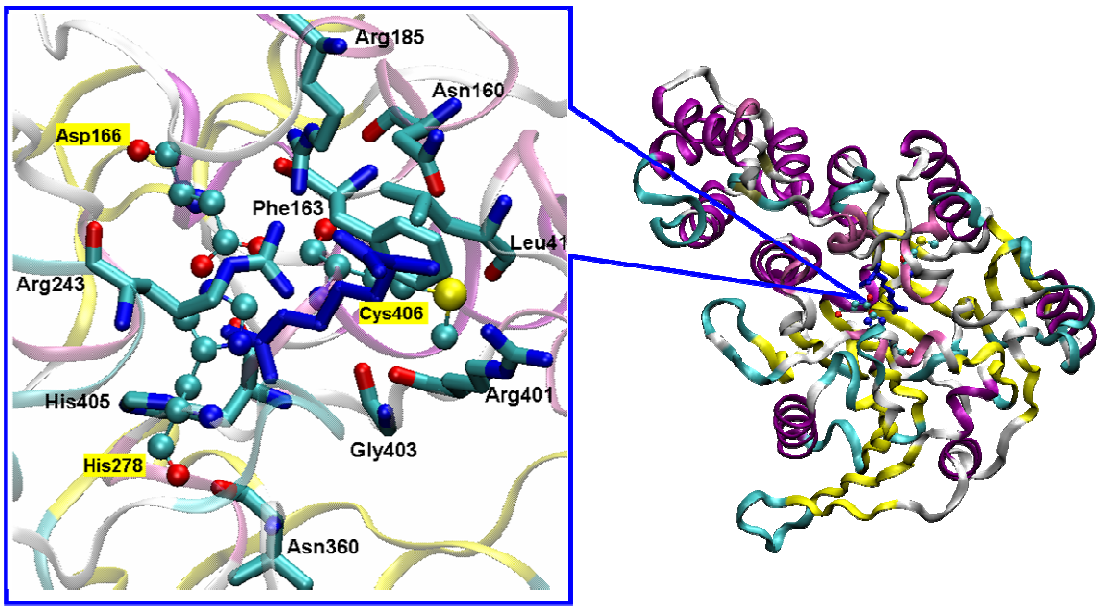

Figure 11. PpADI model derived from PaADI crystal structure (PDB code 2a9gD) by SWISS MODEL WORKSPACE.

3.4.6 Focused libraries generated by saturation mutagenesis

PpADI gene shares 83 % sequence identity with PaADI of which the crystal structure was solved (123). After submitting the ADI sequence to SWISS MODEL WORKSPACE, a proposed ADI model based on the PaADI crystal structure (PDB code 2a9gD) was obtained (Figure 11). According to this model and published literatures, 9 amino acid residues: Leu41, Asn160, Phe163, Arg185, Arg243, Asn360, Arg401, His404, Gly 403 (Figure 11) close to the active center (catalytic triad: Cys406-His278-Glu224) or known to interact with substrate arginine were selected for saturation mutagenesis.

Site saturation mutagenesis at position Leu41, Asn160, Phe163, Arg185, Arg243, Asn360, Arg401, His404 and Gly 403 were performed. 300 clones were screened for each position. However, no improved variant was identified.

3.4.7 Validation of variant M1 (H404R) citrulline colorimetric assay in cuvette format

Position H404 which was suspected to influence ADI pH profile by substitution to R404 (15). Compared to wild type PpADI, variant M1 (H404R) shows higher activity (1.8-fold) and improved activity ratio of pH 7.4 to 6.4 (4.7-fold). Therefore, M1 (H404R) was selected for directed evolution.

3.4.8 epPCR library generation and screening with citrulline detection assay by screening error-prone mutant libraries

Various concentrations of $MnCl_2$ (0.01-0.10 mM) were used in epPCR library generation to adjust the ratio of active to inactive clones. Figure 12 (A) and 12 (B) show the epPCR products and the corresponding MEGAWHOP products. Concentration of 0.01 mM $MnCl_2$ which generated 53 % inactive mutant was selected for library generation. EpPCR mutant libraries with a ratio of 50 % active and 50 % inactive clones have often been used successfully in directed evolution, improving enzyme properties by gradual changes (one or two amino acids changes per round of mutagenesis and screening). A total of 7 variants (listed in

Table 2) were identified from an epPCR library of 2400 mutants and used for further characterization. The most active variant was sequenced and two additional amino acid substitutions (K5T D44E) were identified.

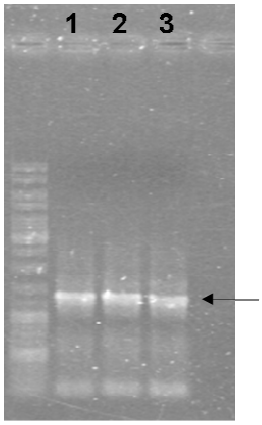

Figure 12 (A). Electrophoresis of epPCR products. Lane 1, 0.01 mM of $MnCl_2$; Lane 2, 0.02 mM of $MnCl_2$; Lane 3, 0.05 mM of $MnCl_2$.

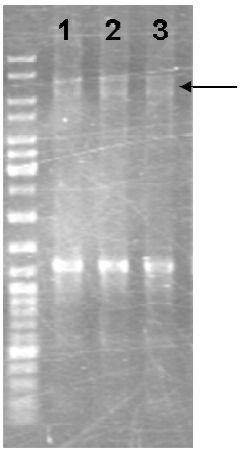

Figure 12 (B). Electrophoresis of MEGAWHOP product with epPCR products as megaprimer. Lane 1, 0.01 mM of $MnCl_2$; Lane 2, 0.02 mM of $MnCl_2$; Lane 3, 0.05 mM of $MnCl_2$.

Table 2. Activity of ADI variants towards arginine determined using citrulline colorimetric assay in cuvette format. Samples were diluted to ensure that detected citrulline concentrations are within the linear detection range of the citrulline colorimetric assay. Wild type, mutant M1 and the "best variant" M2 are in bold and prominent expression mutants (9-B3-1; 21-D5-1) are italized.

	Normalized [ADI][a]				
	Citrulline production (mM/mg)		Relative to activity at pH 7.4 of WT		Activity at pH 7.4/ activity at pH 6.4
ADI variants	pH 7.4	pH 6.4	pH 7.4	pH 6.4	
WT	9.83 (0.74)[b]	124.92 (1.98)	1.00 (0.15)	12.69 (0.01)	0.08 (0.01)
M1 (H404R)	17.80 (0.49)	45.95 (0.87)	1.81 (0.06)	4.67 (0.02)	0.39 (0.02)
M2 (K5T D44E H404R)	38.99 (0.79)	39.20 (0.31)	3.96 (0.02)	3.98 (0.02)	0.99 (0.03)
9-B3-1	24.89 (0.45)	54.50 (1.80)	2.53 (0.03)	5.54 (0.03)	0.46 (0.02)
21-D5-1	25.68 (2.68)	50.95 (2.36)	2.61 (0.07)	5.18 (0.02)	0.50 (0.01)
15-G10-2	13.11 (0.53)	47.02 (0.47)	1.33 (0.09)	4.78 (0.02)	0.28 (0.01)
2-H4-2	12.50 (0.07)	21.58 (0.09)	1.27 (0.06)	2.19 (0.04)	0.58 (0.01)
1-G11-1	24.91 (0.20)	29.12 (0.33)	2.53 (0.03)	2.96 (0.03)	0.85 (0.02)
24-E10-1	14.62 (0.62)	32.82 (0.52)	1.49 (0.08)	3.34 (0.03)	0.45 (0.02)

[a] (Based on quantification employing Agilent 2100 Bioanalyzer (Agilent Protein 230 Kit))
[b] (Standard error of triplicate measurements are given in brackets below each absolute and normalized value.)

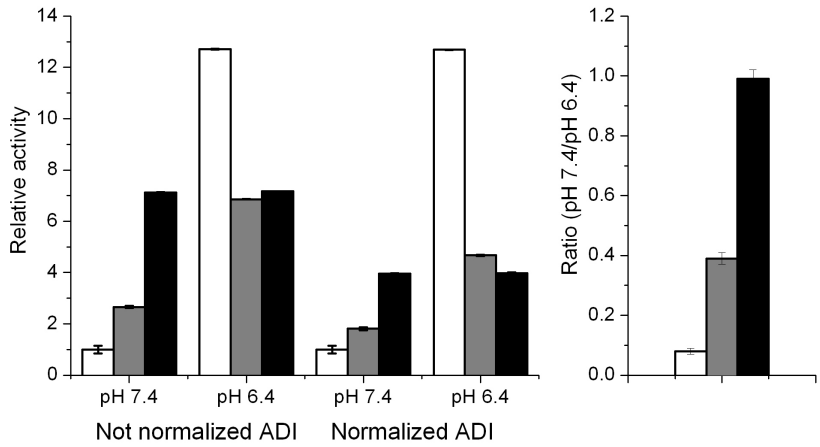

Figure 13. Relative activity of ADI variants towards arginine. The relative activity is the ratio of the activity at the pH of each variant relative to the activity at pH 7.4 of wild type ADI. White: ADI wild type, grey: M1 (H404R), black: M2 (K5T D44E H404R).

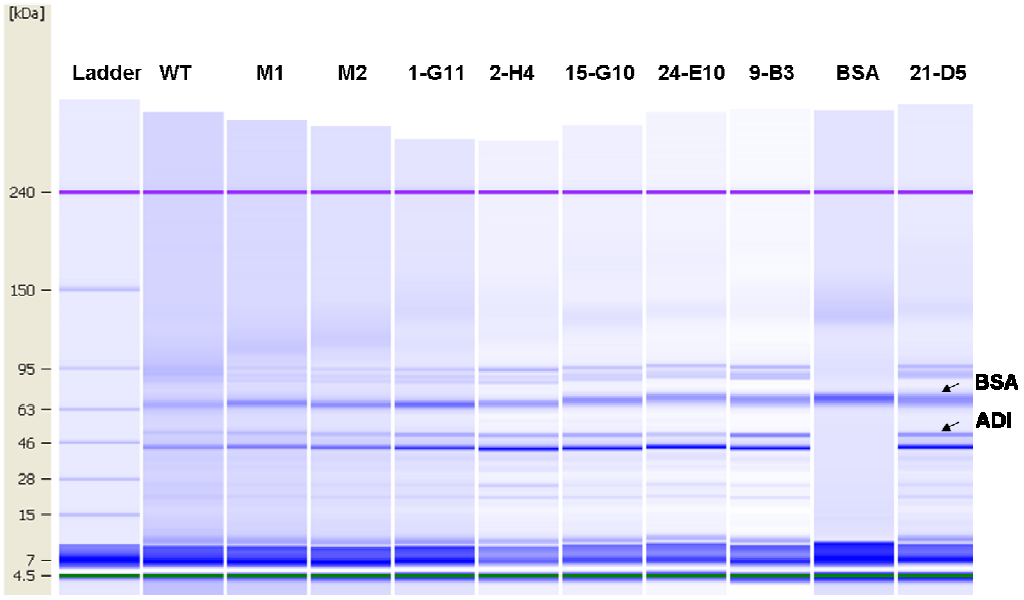

Figure 14. Elution profile of wild type PpADI and improved variants from epPCR library, generated with Protein 230 Kit using a mircofluidic device (Agilent Bioanalyzer). BSA was added as an internal standard.

3.4.9 Characterization of PpADI variants

3.4.9.1 Determination of k_{cat} and K_m of ADI wild type and the mutants

Variants selected from epPCR were first characterized using the crude cell extract to identify the most promising variants (Table 2). Using an activity ratio of pH 7.4 to 6.4 proved to be an effective method to eliminate expression mutants. Additionally ADI concentration in crude cell extract was determined using the Agilent Protein 230 Kit. Microfluidic elution profiles (Figure 14) semi-quantify differences in expression between the wild type PpADI and variants. Normalization of activities against the corresponding ADI concentrations reveals improvements in specific activities of ADI mutants (Table 2). M1, the starting variant for the directed evolution campaign, and M2 were selected for detailed characterization studies. M2 has as “best identified variants” (Figure 13) a more than 2.5-fold higher activity ratio at pH 7.4 to pH 6.4 than M1 and a 12-fold higher activity ratio than wild type in crude cell lysates.

For kinetic characterization of ADI variants the citrulline production was maintained between 0.2-0.8 mM. Calibration curve in Figure 4 shows the linear detection range in the employed 96-well PCR plate format citrulline colorimetric assay system. Figure 15 summarizes the k_{cat} and K_m values of wild type PpADI, identified variants M1 (H404) and M2 (K5T D44E H404R) which were expressed in shaking flasks cultures and purified using a two step procedure (anion exchange followed by gel filtration). Both variants M1 and M2 show an increase in k_{cat} and K_m for citrulline production at pH 7.4. Variant M2 shows a 4-fold higher k_{cat} as also obtained for specific activity in Table 2 using the crude cell extract, validating the characterization procedure with crude cell lysate. Furthermore, an increased K_m from 0.7 mM (wild type PpADI) to 1.2 mM (M1) and 2.5 mM (M2) was found.

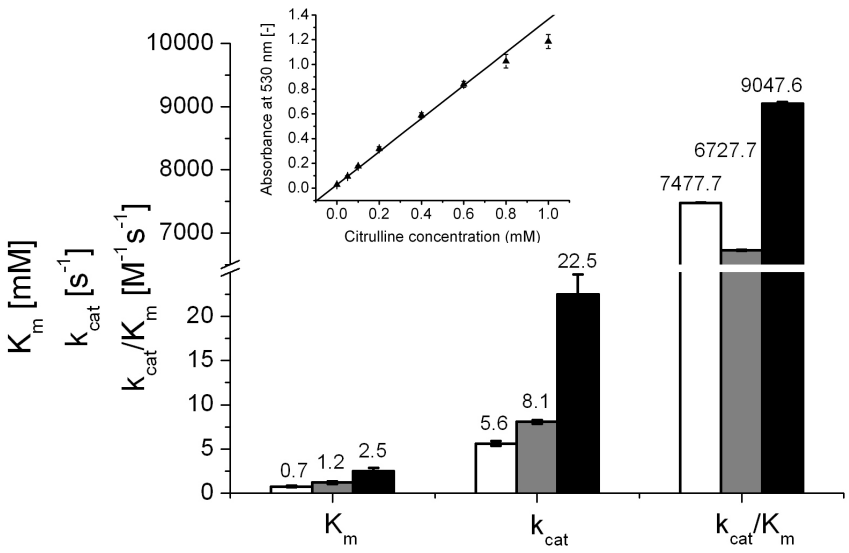

Figure 15. Kinetic parameters of ADI and mutants for conversion of arginine to citrulline. White: ADI wild type, grey: M1 (H404R), black: M2 (K5T D44E H404R). Values reported are the average of three measurements, and average deviations from the mean values are shown. Embedded calibration curve shows linearity of citrulline colorimetric assay in 96-well PCR plate format which was used to determine arginine conversions and kinetic constants.

3.4.9.2 Relative pH profile of wild type and mutant

The relative pH profile (Figure 16) of wild type PpADI and M1 (H404R) shows an identical pH optimum at pH 6.5. Compared to wild type PpADI, variant M2 (K5T

D44E H404R) shows a pH optimum at pH 7.0 which is shifted remarkably (0.5 pH units). Both M1 and M2 show decreased specific activities at pH 6.5, and increased specific activity at pH 7.5. At pH 7.0, the specific activity of M2 exceeds that of wild type PaADI (data not shown).

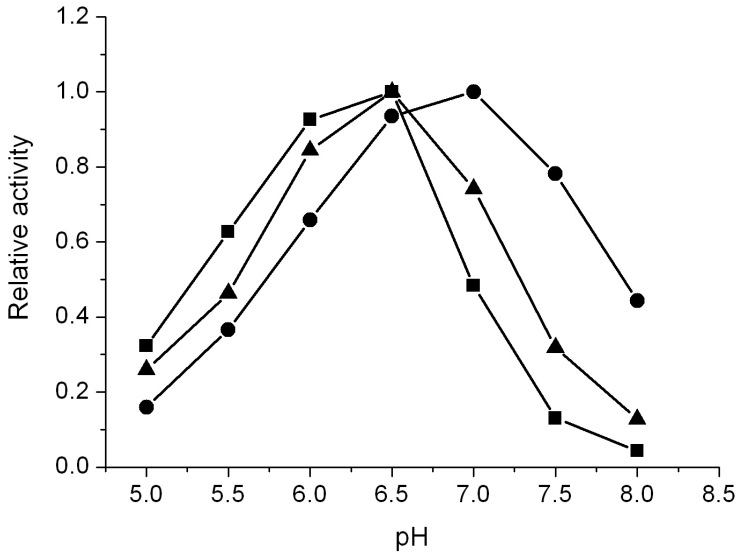

Figure 16. pH profile of wild type ADI, M1(H404R), M2(K5T/D44E/H404R). The relative activity is the ratio of the catalytic activity at the pH relative to the maximum activity of each enzyme. (■) WT, (▲) M1 (H404R), (●) M2 (K5T/D44E/H404R).

3.4.10 Stability of PpADI in the presence of human serum

Table 3 summarizes the stability of PpADI variants in serum (37℃, 60 min; standard deviation of three measurements in brackets). The mutants M1 and M2 have a similar stability in serum when compared to the wild-type PpADI wild type. The substitution D44E and H404R do not destabilize further the PpADI in serum.

Table 3. Stability of PpADI variants in the presence of human serum.

	PpADI WT	M1	M2
No incubation (A_{530})	0.08	0.27	0.98
Incubation with serum (37℃, 60 min) (A_{530})	0.05	0.15	0.69
Residual activity	60 %	55 %	70 %

3.4.11 Activity of PpADI (wild type, M1, M2) towards arginine derivative (N^G, N^G)-dimethylarginine

No detectable conversion of (N^G, N^G)-dimethylarginine could be detected with PpADI variants.

3.5 Discussion

ADI properties have to date not been engineered through directed evolution algorithms despite their often poor performances under physiological conditions and their medical importance as potential anti-tumor drug. Chemically modified of ADI (e.g. through PEGylation) (27) and fusion protein (e. g. Human serum albumin fusion, HSA) (124) have been used for addressing activity and stability demands *in vivo*. Directed evolution offers opportunities to directly improve ADI properties for *in vivo* applications and small libraries of a few thousand variants have often been sufficient to find improved muteins in directed evolution experiments (55, 125).

Our main intention in this report is to provide a validated protocol for directed ADI evolution and improving the activity at the physiological pH 7.4. *Pseudomonas plecoglossicida* CGMCC2039 (PpADI, 7.8 U/mg; pH optimum 6.5) was selected for the directed evolution studies due to its functional expression in *E. coli,* coverage of sequence space in patents and "potential" for activity improvement. PpADI is a relatively slow ADI when compared to Mycoplasma ADIs like MhADI (*Mycoplasma hominus* ADI, 35 U/mg) which would have been good alternatives for directed evolution studies (105). Reported ADI activities range from 0.115 to 140.3 IU/mg. One unit is commonly defined as the ADI amount that converts 1 µmol of L-arginine into 1 µmol of L-citrulline per minute (27).

Screening of PpADI variants yielded three amino acid positions 5, 44 and 404. Positions 44 and 404 resulted in a 4-fold higher k_{cat} at pH 7.4 and a significant shift in the pH optimum (0.5 units) when compared to wild type PpADI (Figure 17 & 8). Position 5 did not show any effect on PpADI activity.

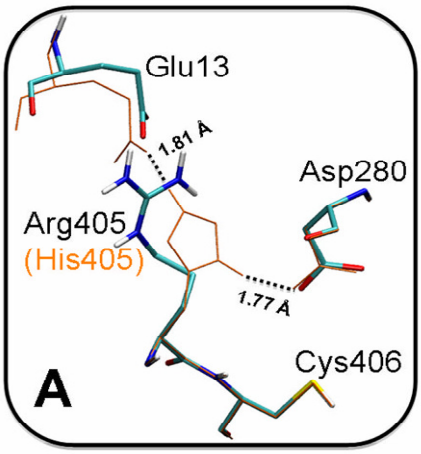

Figure 17. Structural alignment of mutant M1 model with corresponding residues of the crystal structures of the PaADI (in orange). The crystal structure of PaADI which was diffracted in absence of the substrate arginine (1RXX) was used to investigate the substitution of His405 to Arg405. The Arg405 variant shows with respect the Asp280 a different orientation of the guanidinium group when compared to side chain of His405 (in orange).

Galkin and coworkers postulated that the histidine in position 404 (corresponding position in “their” PaADI is 405) is a key residue in controlling activity at acidic and neutral pH. In protonated state of the imidazolium ring a hydrogen bonding interaction can be formed with the oxygen of Asp280 (carboxyl group). This hydrogen bond favors stabilizing interactions between Asp280 and the substrate arginine. His405 in PaADI was reported (17) to share protons with Asp280 and Glu13 and to be important for modulating electrostatic environments of closely located catalytic groups. The same report postulated that H405 is likely to be protonated when the substrate arginine binds to catalytic triad (His278, Glu224, Cys406) [(2)]. Based on these reports the His404 in PpADI was subjected to a site directed mutagenesis to Arg404 and named M1. The M1 variant (H404R) shows 40 % residual activity compared to wild type PpADI at pH 6.4 and a 1.8-fold increase in activity at pH 7.4 (see Table 1). In the M1 (H404R) mutant (see the model in Figure 17; based PaADI 1RXX; residue His404 in PpADI corresponds to His405 in PaADI), the conformational effect due to the extended side chain of Arg likely weakens the hydrogen bond to Asp280 and thus reduces the stabilizing effect on arginine binding. As a result the activity of M1 is reduced, especially at

lower pH values at which His405 is protonated. However at elevated pHs, His405 becomes increasingly deprotonated whereas Arg405 remains protonated and can therefore still stabilize Asp280 for arginine binding. The electrostatic effect suggested by theoretical and experimental studies have evidenced the importance of positively charged residues to modulate the reaction rate of PaADI (126). At pH 6.4, histidine in wild type PpADI and arginine in M1 are both positively charged. At pH 7.4, histidine is only partially positive charged and PpADI's activity is reduced (>90 %) while arginine in M1 remains positively charged preserving M1's activity (Figure 17).

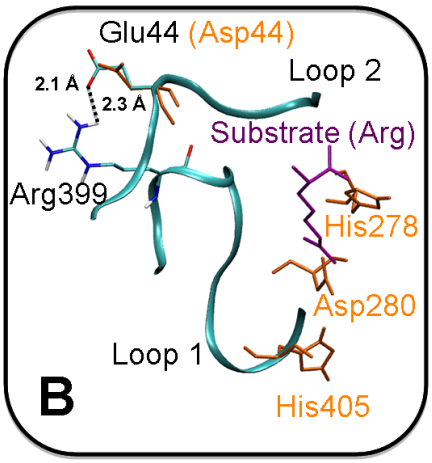

Figure 18. Structural alignment of mutant M2 model with corresponding residues of the crystal structures of the PaADI (in orange). The PaADI crystal structure in presence of substrate arginine was used (2A9G) to investigate the role of the substitution Asp44 to Glu44. The latter was solved for an inactive variant in which Cys406 was replaced by Ala406. The extended side chain of Glu44 might improve the hydrogen bond interaction with the Arg399 inducing a conformational shift of loop 1.

The PpADI H404R was used as starting variant for directed evolution. The amino acid position 44 was identified from a epPCR library (2400 variants screened) resulting in a triple mutant M2 (K5T D44E H404R). For investigating the role of each position the double mutants (K5T H404R) and (D44E H404R) were generated. Only the double mutant (D44E H404R) revealed improvements in k_{cat} (4-fold, pH 7.4; Figure 18). The rationale behind the effects of the mutation D44E on the PpADI activity is more complex to extrapolate from the available ADI crystal structures. Comparative crystallographic studies have shown that the

entrance of the active site is decorated by 4 loops that undergo conformational transitions upon arginine binding (17). The loops exhibit significant shifts that limit the access of water molecules to the active site. The Asp44 is located in loop 1 (residues 30-46) and upon binding of the substrate, Asp44 comes closer to the positively charged Arg399 located on loop 4 (residues 392 to 403). In the D44E mutant, the longer side chain reduces the distance with Arg399 favoring the formation of hydrogen bond (see model in Figure 18). The reinforced interaction between Glu44 and Arg399 might expedite conformational changes in loops, probably confining the arginine substrate in the active site and hence promote arginine conversion. In the future, we plan to further investigate the influence of H404R and D44E using molecular dynamics simulations, further boost the k_{cat} at pH 7.4 and reduce the K_m value of PpADI.

Overall site directed mutagenesis of position H404R and one round of directed evolution (2400 variants screened) resulted in a triple mutant M2 (K5T D44E H404R) with 4-fold higher k_{cat} at pH 7.4 (compared to wild type; Figure 4). The best mutant isolated, M2, has specific activity of 31.3 U/mg at pH 7.4 which is already after one round of evolution close to the specific activity of MhADI (35 U/mg) (127) at its pH optimum. The stability and specificity of improved PpADI variants are furthermore important for cancer treatment *in vivo*. First experiments in AB-human serum (Invitrogen) showed an unaltered stability of M2 compared to the wild type PpADI and (N^G, N^G)-dimethylarginine conversion could not detect with the citrulline colorimetic assay.

3.6 Conclusion

In summary, a directed evolution protocol has been developed for PpADI and validated by increasing the k_{cat} of PpADI at physiological pH (7.4). The reported screening system is the first one employed in directed ADI evolution and can likely be used for other ADIs and other properties such as temperature stability, salt/detergent stability or protease resistance.

Chapter 4. PpADI reengineered for efficient operation under physiological conditions

4.1 Abstract

The proof of concept for ADI engineering by directed evolution resulted in variant M2 (K5T/D44E/H404R). M2 has a pH optimum of pH 7.0 and 4-fold higher k_{cat} value than the wild type PpADI (pH 7.4, 0.5 M phosphate buffer) and an increased K_m value for substrate arginine. In this chapter, in order to improve the catalytic efficiency of PpADI at low concentration of arginine, variant M5 (K5T/D38H/D44E/A128T/H404R) and M6 (K5T/D38H/D44E/A128T/E296K/H404R) were generated from an epPCR library: at pH 7.4 (PBS buffer), the $S_{0.5}$ value decreased from 2.01 mM (parent M3, K5T/D44E/A128T/H404R) to 1.48 mM (M5) and 0.81 mM (M6). The $S_{0.5}$ value of M6 (0.81 mM) is lower than that of PpADI wild type (1.30 mM); the k_{cat} value improved from 0.18 s^{-1} (PpADI wild type) to 17.56 s^{-1} (M5, 97.6-folds) and 11.64 s^{-1} (M6, 64.7-fold).

4.2 Introduction

ADI-based arginine depletion is a target specific therapy for arginine-auxotrophic tumors (e.g. hepatocellular carcinomas and melanomas) and pegylated ADI is currently under clinical trials for HCC with promising results (45). HCC is the third leading cause of cancer mortality world wide with a less than 10 % 5-year survival rate (EU and USA) (128) due to low responses of hepatoma to chemotherapeutic treatments. In 1999, US Food and Drug Administration (FDA) designated ADI-PEG-20 orphan drug status for the treatment of HCC and invasive malignant melanomas, and in 2005 European Agency for the Evaluation of Medicinal Products (EMEA) also granted ADI-PEG-20 orphan drug status for the treatment of HCC. Phase II trials of ADI-PEG-20 in patients with metastatic

hepatocellular carcinomas have shown that the drug is safe, well tolerated, and may benefit patients with unresectable HCC. Izzo and coworker suspected that combination therapies of arginine deprivation and growth inhibition via kinase inhibitors might improve the survival rate further more. Additionally, ADI can enhance radio sensitivity of human mammary adenocarcinoma (MCF-7 cells) (48), exerts anti-proliferative and anti-angiogenic activities and inhibits the growth of viruses such as HIV-1 and hepatitis (49, 50). Current research efforts are focused on ADI's *in vivo* inhibitory effect towards leukemia, melanoma, prostate cancer, renal cell carcinoma, and human umbilical vein endothelial cells (HUVEC) (19, 44, 51-53), clinical trials for HCC (phase II) (45) and melanoma (phase I/II) (46), and inhibitory mechanisms of ADI to tumors (54).

Arginine deprivation is believed to be a main molecular reason for ADI's inhibitory effects on arginine auxotrophic tumors which do not express argininosuccinate synthetase (ASS). ADIs catalyze the first step of the arginine dehydrolase pathway by hydrolyzing arginine to citrulline and ammonium. ADI genes have been identified, purified, and characterized from bacteria, archaea and some eukaryotes excluding mammalian cells (see review (27)). Enzymatic properties of several recombinant ADIs have been examined, such as specific activity, functional expression level, temperature optimum, pH optimum, substrate affinity for arginine, and half-life in human plasma. Only the ADI from *Mycoplasma hominis* has so far been developed as orphan drug by Pheonix Pharmacologics Inc. for HCC and melanoma (129). From enzyme kinetic point of view, none of the ADIs is ideally suited for *in vivo* applications under physiological conditions. Protein engineering by rational design and directed evolution offers opportunities to tailor ADI properties to physiological conditions. PpADI (ADI from *Pseudomonas plecoglossicida*) was functionally expressed in *E. coli* with a simple protocol and has been engineered for the first time by directed evolution for improved activity at physiological pH (3). The variant M2 (K5T/D44E/H404R), by our group reported, showed a 4-fold higher specific activity than the wild type PpADI (0.5 M phosphate buffer, pH 7.4), but a increased K_m value (3.5-fold).

High activity at low arginine concentration is an important prerequisite for ADI's medical application, allowing low ADI dose required per treatment.
In the present work, we improved the directed evolution protocol and identified a PpADI variant with further improved activity and slightly decreased "K_m value" and PpADI variant with lowered K_m value maintaining its high catalytic activity. Those variants were characterized in respect to their kinetic constants.

4.3 Materials and methods

4.3.1 Materials

All chemicals were of analytical-reagent grade or higher quality and were purchased from Fluka (Neu-Ulm, Germany), Sigma-Aldrich (Steinheim, Germany) and Applichem (Darmstadt, Germany), except the resins for purification (TOSOH, Stuttgart, Germany). All enzymes were purchased from New England Biolabs (Frankfurt, Germany), Fermentas (St. Leon-Rt, Germany), and Sigma-Aldrich Chemie (Taufkirchen, Germany), unless stated otherwise.
Thermal cycler (Mastercyler gradient; Eppendorf, Hamburg, Germany) and thin-wall PCR tubes (Multi-ultra tubes; 0.2 µl; Carl Roth, Germany) were used in all PCRs. The PCR volume was always 50 µl except for Megaprimer PCR of whole plasmid (MEGAWHOP, 25 µl); larger volumes were prepared in multiple 50-µl PCRs. The amount of DNA in cloning experiments was quantified by using a NanoDrop photometer (NanoDrop Technologies, Germany).

4.3.2 Methods

4.3.2.1 Site saturation mutagenesis of *PpADI* M2 at position A128

Site directed mutagenesis of *PpADI* M2 (K5T/D44E/H404R) at position A128 was performed according to the published method (130). The following oligonucleotides were used for mutagenesis of A128: 5'-CTGATCGGCGGCGTGNNNGGCCAGGACCTGCCG-3' and 5'-CGGCAGGTCCTGGCCNNNCACGCCGCCGATCAG-3' (underlining indicated the substituted nucleotide). For the mutagenic PCR (First stage: 98°C for 30 s, 1 cycle; 98°C, 30 s/ 55°C, 1 min/ 72°C, 3 min, 3 cycles. Second stage: 98°C for 30

s, 1 cycle; 98℃, 30 s/ 55℃, 1 min/ 72℃, 3 min, 15 cycles; 72℃ for 3 min, 1 cycle), 2 U of PhuS DNA polymerase, 0.20 mM of dNTP mix, 25 pmol of each primer together with 100 ng of template (pET42b(+) harboring PpADI M2 gene) were used. Following the PCR, DpnI (40 U; New England Biolabs) was added, and incubated overnight at 37℃. The PCR products were purified by using a QIAquick PCR Purification Kit (Qiagen) and transformed into *E. coli* BL21-Gold (DE3) for expression.

4.3.2.2 Construction of PpADI error-prone library

EpPCR library was generated by the standard error-prone PCR (epPCR) using improved variant M3 (K5T/D44E/A128T/H404R) as template. For the mutagenic PCR (95℃ for 2 min, 1 cycle; 95℃, 30 s/ 55℃, 30 s/ 72℃, 30 s, 29 cycles; 72℃ for 3 min, 1 cycle), 2.5 U of Taq DNA polymerase, 0.20 mM of dNTP mix, 50 ng of template (pET42b(+) harboring PpADI M3 gene), 0.01-0.1 mM of $MnCl_2$ and 10 pmol of each primer (5'-TACATATGTCCGCTGAAACACAGAAG-3' and 5'-GTGCTCGAGTTAGTAGTTGATCGG-3') were used. The PCR products were purified by using a QIAquick PCR Purification Kit. The purified epPCR products were cloned into expression plasmid pET42b(+) by MEGAWHOP (114). For MEGAWHOP (72℃ for 5 min, 1 cycle; 98℃ for 1 min 30 s, 1 cycle; 98℃, 45 s/ 55℃, 45 s/72℃, 4 min, 24 cycles; 72℃ for 10 min, 1 cycle), 1.2 U of PfuS DNA polymerase, 0.20 mM of dNTP mix, 500 ng of epPCR products together with 50 ng of template (pET42b(+) harboring PpADI gene of variant M3) were used. Following the PCR, DpnI (40 U; New England Biolabs) was added, and incubated (overnight; 37℃). The MEGAWHOP products were transformed into *E. coli* BL21-Gold (DE3) for expression and screening.

4.3.2.3 Site directed mutagenesis at position D38 of *PpADI* M4

Site directed mutagenesis of *PpADI* variant M4 at position D38 was performed according to the published method on plasmid pET42b(+)-ADI-M4 (K5T/D44E/A128T/E296K/H404R). The following oligonucleotides were used for mutagenesis of D38H: 5'-ACCCCGAGCAACTGCCACGAGCTGCTGTTCGAC-3'

and 5'-GTCGAACAGCAGCTCGTGGCAGTTGCTCGGGGT-3' (underlining indicated the substituted nucleotide). Conditions for mutagenic PCR are as described in "Site saturation mutagenesis of *PpADI* M2 at position A128".The PCR products were purified by using a QIAquick PCR Purification Kit (Qiagen) and transformed into *E. coli* BL21-Gold (DE3) for expression.

4.3.2.4 Site saturation mutagenesis at position D38 and E296 of *PpADI* M3

Site saturation mutagenesis library at position D38 and E296 of *PpADI* variant M3 (K5T/D44E/A128T/H404R) were generated according to the published method on plasmid pET42b(+)-ADI-M3 using the following oligonucleotides: D38FP (5'-ACCCCGAGCAACTGCNNNGAGCTGCTGTTCGAC-3'), D38RP (5'-GTCGAACAGCAGCTCNNNGCAGTTGCTCGGGGT-3') and E296FP (5'-GTCACGGTTTTCCCGNNNGTGGTGCGCGAGATC-3'), E296RP (5'-GATCTCGCGCACCACNNNCGGGAAAACCGTGAC-3') (underlining indicated the substituted nucleotide). Conditions for mutagenic PCR are as described in "Site saturation mutagenesis of PpADI M3 gene at position A128".The PCR products were purified by using a QIAquick PCR Purification Kit (Qiagen) and transformed into *E. coli* BL21-Gold (DE3) for expression.

4.3.2.5 Cultivation and expression of PpADI in 96-well plates

Cultivation and expression in 96-well plates (flat bottom, polystyrene plates; Greiner Bio-One GmbH, Frickenhausen, Germany) were performed as previously described in 3.3.2.8.

4.3.2.6 Improved screening system in 96-well plate to identify PpADI variants with high activities at low arginine concentration

As describe previously, the modified protocol of citrulline detection based on carbamido-diacetyl reaction was used for screening for improved ADI affinity to arginine at pH 7.4. 15 µl of cell culture was transferred to 96-well microtiter plate. Enzyme reaction was initiated by addition of arginine solution (105 µl, 1mM arginine in PBS buffer, pH 7.4) supplemented with

cetyltrimethylammoniumbromide (CTAB, 4 mM), and incubated (10 min, 37°C). The following color development procedure was carried out as described previously (3).

Standard deviation measurements were performed in 96-well plate format using culture from BL21-Gold (DE3) lacking PpADI and in a separate experiment containing PpADI variant M3. Apparent standard deviation was based on the absolute absorbance values obtained from the PpADI variant M3 plate. The true standard deviation was calculated by subtracting the background absorbance value of the microtiter plate lacking ADI from the apparent values.

4.3.2.7 Expression of PpADI in shaking flask and purification

Expression of PpADI in shaking flasks and purification (by anion exchange chromatography and gel filtration) was performed as previously described in 3.3.2.10.

4.3.2.8 Characterization of PpADI variants

Preliminary determination of kinetic constants for site saturation mutagenesis variants of position 38 and 296

The k_{cat} and K_m values were determined from initial velocity data measured as a function of substrate concentration. Enzyme reaction was carried out at 37°C in incubator (Heraeus Holding GmbH, Hanau, Germany) using cell crude extract. 2 ml of expression culture was harvested by centrifugation (Eppendorf 5415R 4°C, 13,000 g, 10 min) and then freezed (-20°C, overnight). Cell lysate was prepared by resuspending the cell pellet in lysozyme (91000 U, 50 mM phosphate buffer, pH 7.4, 1.3 ml) followed by incubation (37°C, 40 min) and centrifugation (4°C, 13,000 g, 10 min). 15 µl of diluted (4 times diluted with 50 mM phosphate buffer, pH 7.4) cell lysate was transferred to 96-well microtiter plates. Enzyme reaction was initiated by addition of arginine solution (105 µl, 0.25-10 mM arginine in PBS buffer, pH 7.4) and incubated (7 min, 37°C). Subsequently, ferric-acid solution (120 µl) was added to each well to stop enzyme reaction. 60 µl of terminated

enzyme reaction mixture was transferred to 96-well PCR plate for color development. Ferric-acid solution (90 µl) and DAM-TSC solution (15 µl) were added to each well. The 96-well PCR plate was then incubated (70°C, 30 min) in thermal cycler (Eppendorf Mastercyler gradient) for color development, followed by incubation in ice water to stop color development. Absorbance was measured at 530 nm using a microtiter plate reader (Tecan Sunrise TC reader, Tecan Group AG, Zurich, Switzerland). The initial velocity data obtained were fitted to the equation $v = V_{max}[S]/([S] + K_m)$ (where v is the initial velocity, Vmax the maximum velocity, [S] the substrate concentration, and Km the Michaelis constant) using GraphPad Prism software (GraphPad software, San Diego, CA, USA). The kcat was calculated from the ratio of V_{max} and enzyme concentration.

Determination of kinetic constants of PpADI wild type and variants M3, M4, M5, M6

The k_{cat} and $S_{0.5}$ values were determined from initial velocity data measured as a function of substrate concentration. Enzyme reaction was carried out at 37°C in a water bath as described previously using purified enzyme (50 µl, 0.1-1.8 µM) to and substrate solution (200 µl, 0.5 mM to 10 mM of arginine, PBS buffer, pH 7.4) in deep well plates.

The initial velocity data obtained were fitted to the sigmoidal model of kinetics equation $v = V_{max}^{n}/(S_{0.5}^{n} + K^{n})$ (where v is the initial velocity, V_{max} is the maximum velocity, K is the substrate concentration, and $S_{0.5}$ is the ligand concentration producing half occupation (131)) using GraphPad Prism software (GraphPad software, San Diego, CA, USA). The k_{cat} was calculated from the ratio of V_{max} and enzyme concentration.

4.3.2.9 Native polyacrylamide gel electrophoresis of PpADI variants

10% of polyacrylamide native gels were used for protein electrophoresis to analyze the native form of PpADI variants. Purified protein of PpADI variants (7 µl of protein and 3 µl of loading dye) were loaded into each lane of native gel. The

molecular marker used in the gel is NativeMark™ Unstained Protein Standard (Invitrogen, Darmstadt, Germany). The electrophoresis was performed with tris/glycine buffer (pH 8.3) and electrophoresis chamber was incubated in ice-water bath. Protein bands were stained with Coomassie brilliant blue solution.

4.3.2.10 Homology modeling

Homology modeling approach was used for the structure prediction of PpADI. The model was built by using the automated structure prediction tool, Protein homology/analogy recognition engine (Phyre: http://www.sbg.bio.ic.ac.uk/~phyre/) (132). The crystal structure of PaADI (PDB ID: 2A9G) was used as template by the server and It has 84.9% sequence identity (http://blast.ncbi.nlm.nih.gov/Blast) with PpADI. Procheck program suit (http://www.ebi.ac.uk/thornton-srv/software/PROCHECK/) (133) was used to assess the stereochemical quality of the model. Ramachandran plot which represented that 84.7% residues were present in the most favoured region and 14.7% in additional allowed region (Figure 3). Dfire was used to access non bonded atomic interaction in the model (http://sparks.informatics.iupui.edu/hzhou/dfire.html/) (134), and Qmean (http://swissmodel.expasy.org/qmean/cgi/index.cgi) (135) for the estimation of global protein quality. Swiss-PdbViewer (118) was used to create the tetramer structure by fitting the monomer model on the 4 units of the 2A9G template. The variant M6 (D38H, D44E, A128T, E296K, H404R) were created by using the “mutate” tool of the Swiss-PdbViewer and by selecting rotamers with the best fitness score. All tetramers were energy minimized in vacuum using GROMOS 43B1 force field (119).

4.4 Results

4.4.1 Improved screening system in microtiter plates to identify PpADI variants with high activities at low arginine concentration

Screening assay was based on the validated citrulline colorimetric screening protocol in microtiter plate, as reported previously (3). In order to screen for variants with high activity at low arginine concentration under physiological

condition concerning pH and ion concentrations, 1 mM arginine in PBS buffer (pH 7.4) as substrate solution was employed in screening assay and enzyme reaction time was controlled accordingly (10 min). The coefficient of variation is an important performance criterion of a screening system to determine its accuracy. Optimized assay condition with 1 mM arginine (PBS buffer, pH 7.4) as substrate resulted in true coefficient of variation of 14.9 % (Figure 1). The resulting low absolute absorbance value is a main reason for the high true coefficient of variation (14.9 %). In the previous screening system, 100 mM arginine in 0.5 M sodium phosphate buffer was used and yielded higher activity variants but with higher K_m value.

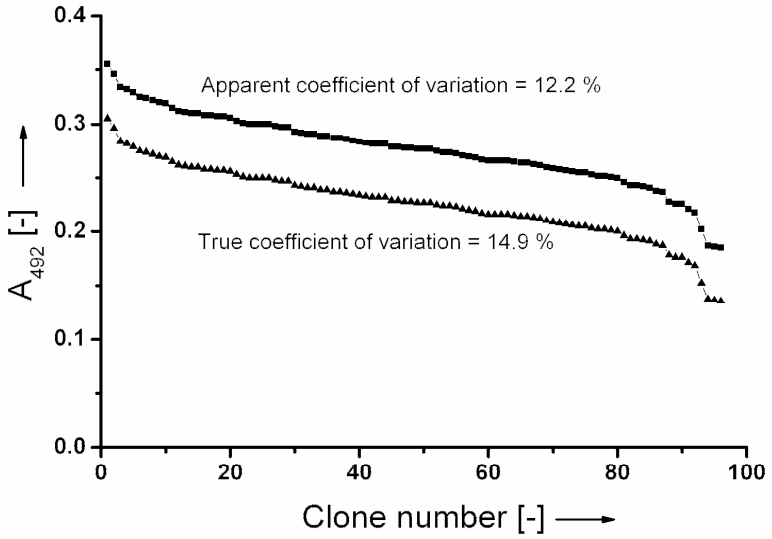

Figure 1. Activity values in descending order of the PpADI variant M3 conversion of arginine to citrulline in a 96-well microtiter plate using the optimized assay protocol. The apparent coefficients of variation were calculated without subtracting the background and the true coefficients of variation after background subtraction.

4.4.2 Genealogic tree of directed PpADI evolution

Figure 2 shows the two rounds of PpADI evolution, generation of saturation mutagenesis libraries and recombination of beneficial positions to finally obtain the PpADI variant M6 with 64.7-fold higher k_{cat} and reduced $S_{0.5}$ (1.3 mM (WT) to 0.81 mM (M6). Based on structure-function analysis of PaADI[16], M1 was generated by substitute His at position 404 with Arg. Position 404 is through

interactions with position Asp280 involved in substrate stabilization during catalysis. M1 was subject to the first round of epPCR library, from which M2 was identified showing a 4-fold improved k_{cat} value and increased K_m value (2.5 mM in 0.5 mM sodium phosphate buffer, pH 7.4)[15]. M3 was generated by a site saturation mutagenesis library at position 128 which increased in another clone the expression level (data not shown). In order to improve PpADI towards medical application demands (high activity at low arginine concentration), a second epPCR mutant library was constructed using M3 as parent. M4 with decreased $S_{0.5}$ value (0.81 mM) and M5 with increased K_{cat} value (17.56 s^{-1}) were identified after screening of ~1400 clones. In M4 the position E296 was identified to be important for lowering $S_{0.5}$ and in M5 position D38 was identified to be important for activity increase. M6 was finally constructed by combining the substations at position D38 and E296. Saturation mutagenesis of these two positions did not yield any further improved $S_{0.5}$ or activity variant.

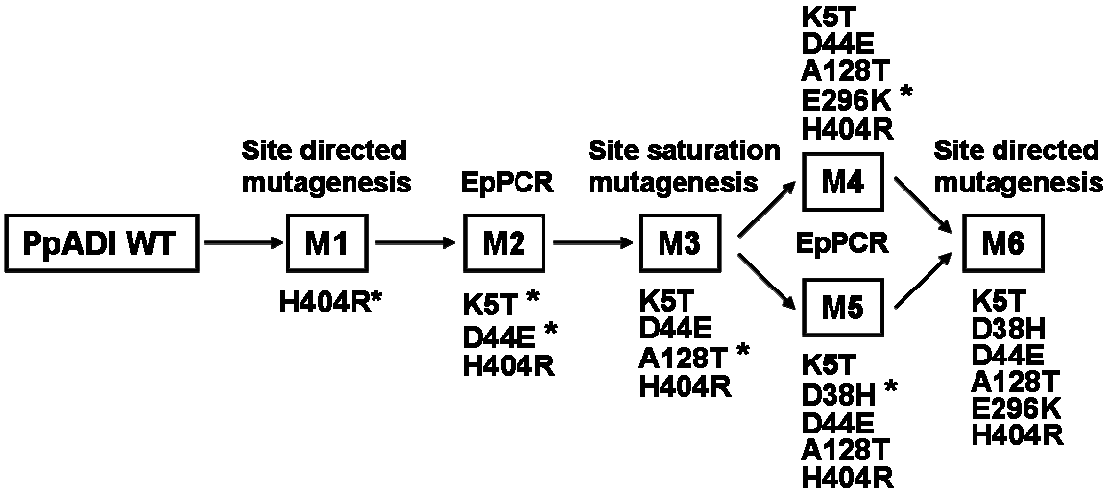

Figure 2. Genealogic tree of PpADI variants (M1 to M6) with generated amino acid substitutions. Novel substitutions are indicated by an asterisk.

4.4.3 EpPCR library construction and screening for variants with high activities at low arginine concentration

Variant M2 was used as a starting template. As described previously, M2 shifts the pH optimum from pH 6.5 to pH 7.0 and has a 4-fold faster k_{cat} than PpADI wild type. In one sequenced mutant, position A128 was identified to be

responsible for higher expression (data not shown). Site saturation mutagenesis on M2 therefore was carried out at position A128. The resulting variant M3 (K5T/D44E/A128T/H404R) showed a ~2-fold improved expression and was subsequently used as parent template for epPCR library.

Three concentrations of $MnCl_2$ (0.01-0.10 mM) were used in epPCR library generation to adjust the ratio of active to inactive clones. Instead of 0.02 mM $MnCl_2$, 0.05 mM $MnCl_2$ which generated 46 % of inactive mutant was selected for library generation. EpPCR mutant libraries with a ratio of ~50 % active and ~50 % inactive clones have often been used successfully in directed evolution, improving enzyme properties by gradual changes (one or two amino acids changes per round of mutagenesis and screening). Two variants M4 and M5 were identified from this epPCR library (~1400 clones) and further characterized. Variant M4 and M5 were sequenced and one additional amino acid substitution was identified for each variant, E296K and D38H, respectively.

4.4.4 Site saturation mutagenesis of *PpADI* at position D38 and E296

To investigate their role in improving of catalytic performance for arginine, site saturation mutagenesis library at position D38 and E296 were generated using PpADI M3 as template. For each position, ~300 clones were screened at low concentration of arginine (1 mM, PBS buffer, pH 7.4), using 96-well plate format citrulline colorimetric screening assay.

After the screening of site saturation mutagenesis libraries of position 38 and 296, variants with higher activity were chosen for preliminary kinetic investigation using crude cell extract. Beneficial mutants were identified and sequenced from both sites (Table 1). At position 38, the following beneficial substitutions were found: D38R (three times, AGA, CGG, CGT) and D38K (twice, AAG, AAA). In all cases, the negatively charged acidic amino Asp had been replaced by positively charged amino acids, Arg or His. Substitution by negatively charged Glu resulted in a clone showing a parent M3-like kinetic behavior. Hydrophobic amino acid

substitution by Pro resulted inactive clone under assay conditions. At position 296, the following substitutions were found to be beneficial: E296K (twice, AAA, AAG), E296N (once, AAC), E296T (once, ACC), E296G (once, GGA). Among these substitutions, variants with substitution to positively charged residue Lys show lowest $S_{0.5}$ value for arginine while substitution by uncharged amino acids (Asn, Thr, Gly) shows relatively marginal improvement compared to E296K. Hydrophobic amino acid substitution by Pro and Trp resulted in very low activity clones.

Table 1. Nucleotide and amino acid substitutions at position 38 in PpADI M3.

PpADI variants	Substitution at position 38	k_m (mM)
M3 (parent)	Asp (GAC)	3.74 ± 0.35
SSM-D38R	Arg (AGA, CGG, CGT)	1.16 ± 0.21
SSM-D38K	Lys (AAG, AAA)	1.01 ± 0.28
SSM-D38E	Glu (GAG)	2.95 ± 0.77
SSM-D38P	Pro (CCA)	n. d.
SSM-D38T	Thr (ACC)	n. d.
M5	His (CAC)	1.26 ± 0.12

Kinetic experiments were performed with crude cell extracts.

Table 2. Nucleotide and amino acid substitutions at position 296 in PpADI M3.

PpADI variants	Substitution at position 296	k_m (mM)
M3 (parent)	Glu (GAA)	3.74 ± 0.35
SSM-E296K	Lys (AAA, AAG)	0.20 ± 0.01
SSM-E296N	Asn (AAC)	0.53 ± 0.04
SSM-E296T	Thr (ACC)	0.61 ± 0.04
SSM-E296Q	Gln (CAA)	0.79 ± 0.06
SSM-E296G	Gly (GGA)	1.29 ± 0.12
SSM-E296W	Trp (TGG)	n. d.
SSM-E296P	Pro (CCT)	n. d.
M4	Lys (AAA)	0.27 ± 0.02

Kinetic experiments were performed with crude cell extracts.
* n. d. activity not detectable under assay conditions.

4.4.5 Determination of kinetic constants (k_{cat} and $S_{0.5}$) of PpADI wild type and variants M3, M4, M5 and M6

Table 3. Kinetic constants of wild type PpADI and variants.

	Wild type	M3 (parent)	M4	M5	M6
k_{cat} (s^{-1})	0.18 ± 0.05	10.13 ± 0.36	5.88 ± 0.09	17.56 ± 1.15	11.64 ± 0.50
$S_{0.5}$ (mM)	1.30 ± 0.25	2.01 ± 0.19	0.81 ± 0.03	1.48 ± 0.17	0.81 ± 0.09

* Kinetic contants of PpADI wild type is different from our previous report because in stead of 0.5 M phosphate buffer, PBS buffer was used for kinetic measurements. K_{cat} value of PpADI wild type dropped from 5.6 s^{-1} to 0.18 s^{-1} and k_{cat} value of M2 is reduced ~2-fold.

M3, the parent of the second round of PpADI epPCR library, M4 with decreased $S_{0.5}$, M5 with increased k_{cat} and best variant M6 with best combination of k_{cat} value and $S_{0.5}$ were selected for detailed characterization studies.

Kinetic characterization of PpADI variants was performed using PBS buffer (pH 7.4), which is commonly used in biological research. PBS buffer helps to maintain a constant pH and its osmolarity and ion concentrations usually match those of the human body. Citrulline production of PpADI variants was maintained between 0.2-0.8 mM. Table 3 summarizes the k_{cat} and $S_{0.5}$ values of parent M3 (K5T/D44E/A128T/H404R), variants M4 (K5T/D44E/A128T/E296K/H404R), M5 (K5T/D44E/A128T/D38H/H404R) and M6 (K5T/D38H/D44E/A128T/E296K/H404R), which were expressed in shaking flasks cultures and purified using a two step procedure (anion exchange follows by gel filtration). Compared to parent M3 ($S_{0.5}$ = 2.01 mM), both variants M4 and M5 have a lower $S_{0.5}$ for arginine conversion at pH 7.4, 0.81 mM and 1.48 mM, respectively. Variant M4 shows a decreased k_{cat} value, 58% of parent M3 while M5 shows a 1.7-fold higher k_{cat} compared to parent M3. Variant M6 with combined mutations (K5T/D38H/D44E/A128T/E296K/H404R) shows decreased $S_{0.5}$ value, 40 % of parent M3 (K5T/D44E/A128T/H404R), 62 % of PpADI wild type, and a 64.7-fold faster k_{cat} value than PpADI wild type. M6 is 42.3-fold faster than PpADI wild type with 0.4 mM arginine (PBS buffer, pH 7.4) as substrate.

After two rounds of epPCR libraries coupled with site directed mutagenesis, a variant M6 with 64.7-fold higher k_{cat} and lower $S_{0.5}$ value (0.81 mM) than PpADI wild type (0.31 mM). At low concentration of arginine, activity of M6 enhanced dramatically than M3 and wild type. For example, M6 is 42.3-fold faster than PpADI wild type in 0.4 mM arginine (PBS buffer, pH 7.4).

4.4.6 Native polyacrylamide gel electrophoresis of PpADI variants

Multimeric form of PpADI variants were investigated by native polyacrylamide gel electrophoresis. As shown in Figure 3, two distinct protein bands representing two multimeric forms tetramer and dimer (molecular weight of a subunit is ~ 46 kDa) were observed, but with different concentration percentage. The major multimeric form of M3 is dimer. Compared to M3, M4 with an additional mutation E296K shows a very different pattern: tetramer is the main form; while M5 with an additional mutation D38H contains more or less equal amount of dimer and tetramer. M6, with both mutations E296K and D38H, contains more tetramer than dimer.

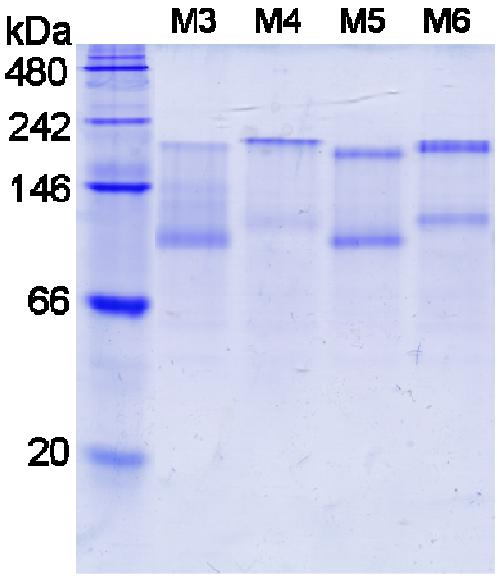

Figure 3. Native polyacrylamide gel electrophoresis of PpADI variants (M3 to M6) with different dimer/tetramer distribution. Single subunit has a molecular weight of ~46 kDa.

4.5 Discussion

Directed evolution allows improving all properties that can be reflected in a screening system through iterative rounds of diversity generation and screening. Small libraries of a few thousand variants are often sufficient to find improved variants [18] even without rational understanding of the targeted property. After establishing a first directed ADI evolution protocol yielding mutant M2, we adjusted the screening system to better reflect ADI's application conditions. Prerequisite for ADI to become an effective anti-tumor agent is that low concentrations of arginine in human plasma can effectively be converted.

Figure 2 shows the genealogic tree of PpADI evolution and before discussing the influence of each substitution individually the effect on kinetics are briefly summarized. Amino acid substitution D44E (M2) increases k_{cat} and $S_{0.5}$, substitution A128T (M3) increases the expression level, and substitution E296K (M4) decreases k_{cat} and $S_{0.5}$ and is responsible for tetramer formation. Substitution D38H (M5) increase largely k_{cat} and reduces slightly $S_{0.5}$. The combination of all mentioned residues in M6 result in a finally 64.7-fold improved PpADI activity and reduced $S_{0.5}$ (1.30 to 0.81 mM).

PpADI M3 was obtained from site saturation mutagenesis library at position A128 using M2 as template (Figure 2). M3 shows improved functional expression level of ADI (data not shown) and was used as parent for generating an epPCR library. Screening of epPCR library yielded two improved variants M4 and M5, carrying an additional mutation, E296K (M4) and D38H (M5). M4 has a decreased $S_{0.5}$ (0.81 mM) and a decreased k_{cat} value (5.88 s^{-1}; see Table 3). M5 has a decreased $S_{0.5}$ (1.48 mM) and an increased k_{cat} value (17.56 s^{-1}) when compared to parent M3 ($S_{0.5}$, 2.01 mM; k_{cat}, 10.03 s^{-1}; see Table 3). M6 which harbors both substitutions (E296K and D38H) has a decreased $S_{0.5}$ value (0.81 mM) compared to the parent M3 (1.30 mM) and the wild type (2.01 mM), and a 64.7-fold higher k_{cat} value than the PpADI wild type.

Despite further enhancing the activity of PpADI, it is crucial for an efficient conversion of the substrate arginine in human plasma (100-120 µM arginine) to reduce PpADI's "K_m" ($S_{0.5}$) value. Figure 4 shows the kinetics of PpADI WT, parent M3, and the variants M4, M5 and M6. M3 has a significantly higher k_{cat} value compared to WT, but its activity at low concentration of arginine (<1.0 mM) is very low ($S_{0.5}$ value 2.01 mM). In contrast, the most efficient variant M6 with a decreased $S_{0.5}$ value (0.81 mM) shows a remarkable activity improvement at low concentrations of arginine (<0.5 mM; see Figure 4). M6 has additional two amino acid substitutions (D38H and E296K) compared to M3 which increases k_{cat} and reduces the $S_{0.5}$ value. The combination of D38H and E296K improves especially the activity of M6 at low arginine concentrations (< 0.5 mM; see Figure 4).

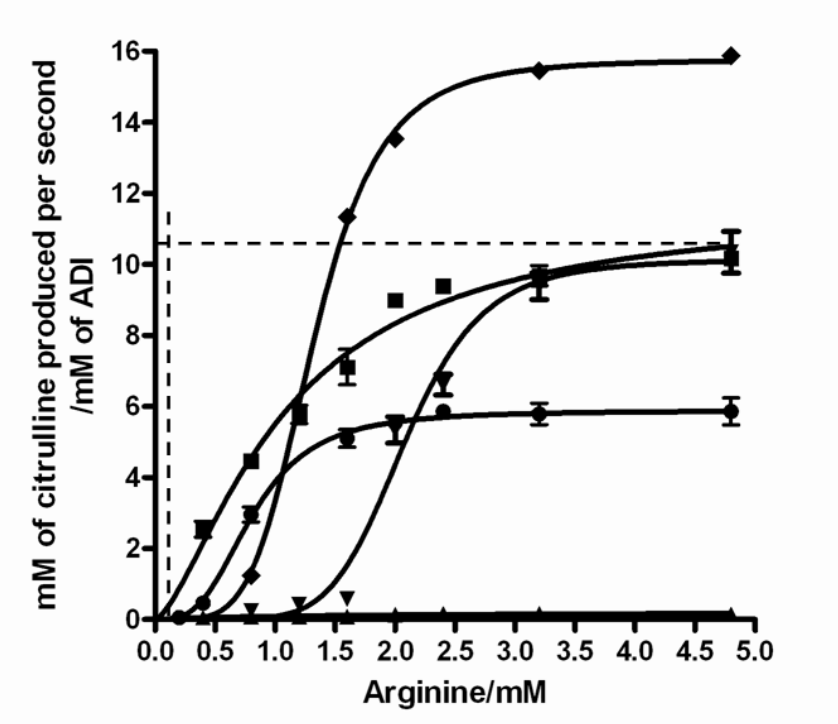

Figure 4. Kinetic curve of PpADI wild type, M3, M5 and M6. (▲) PpADI wild type, (▼) M3, (●) M4, (♦) M5 and (■) M6.

Figure 5 shows the tetrameric model (based on PaADI, PDB code 2A9G) of PpADI WT (Figure 5A) and variant M6 (Figure 5B). Monomeric units are

indicated with the letters a, b, c and d. The access channel to the active sites of each monomer is highlighted in square and faces an internal cavity generated by the assembly of four PpADI monomers. The substitutions D38H (in blue) and D44E (in green) are localized at the interface of monomer pair a-b and c-d. The substitution of Glu by Asp at position 44 provides a longer side chain in close proximity of the also negatively charged residue Asp43 (Figure 6A). The substitution E296K is localized at the border of the entrance to the internal cavity of the PpADI tetramer. E296K promotes the tetramer formation likely by introducing stabilizing interactions with other residues, for example with Thr33 (hydrogen bond). E296K inverts the charge at this position and its increased length of the side chain might promote further interactions to a neighboring monomer (Figure 6A). The combination of D44E and E296K results in a population consisting of mainly tetramers (see Figure 3; mutein M4). Interestingly with the formation of a tetramer (M4) the $S_{0.5}$ value is reduced which indicates that the tetramer complex formation promotes interactions with the substrate arginine at low concentrations. The substitution D38H together with the E296K in the mutein M6 reestablishes an almost equal population of PpADI dimers and tetramers. A hypothesis is that Lys of the E296K has an electrostatic stabilizing interaction with the Glu38 in the M4 but not to the neutral His38.

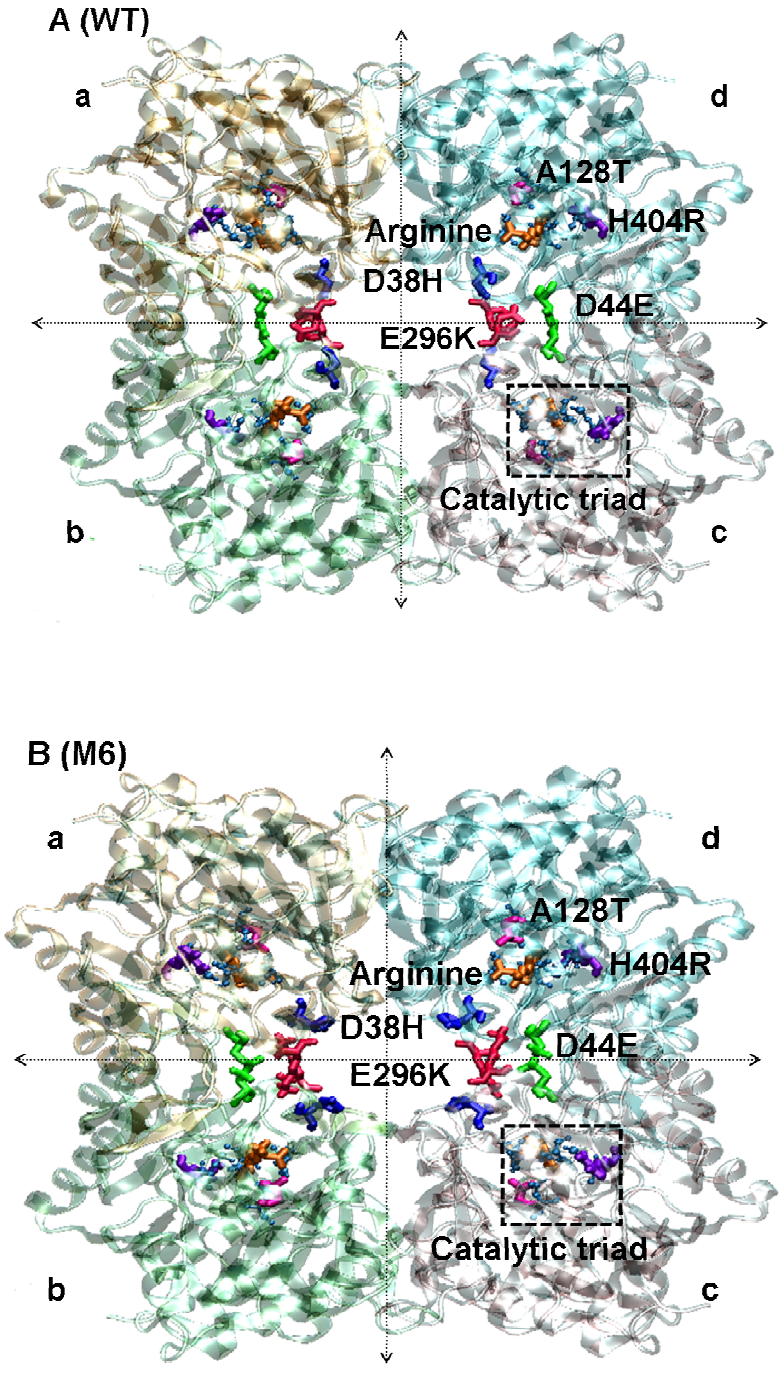

Figure 5. A). The model of WT tetramer after energy minimization in vacuum (GROMOS 43B1). B). The model of M6 tetramer after energy minimization in vacuum (GROMOS 43B1). Active site residues are represented in CRK format in a square (Blue). Mutated residues are shown in licorice format in different colors like D38H (blue), D44E (green), A128T (magenta), E296K (red) and H404R (violet). Substrate arginine is represented in orange color by licorice format.

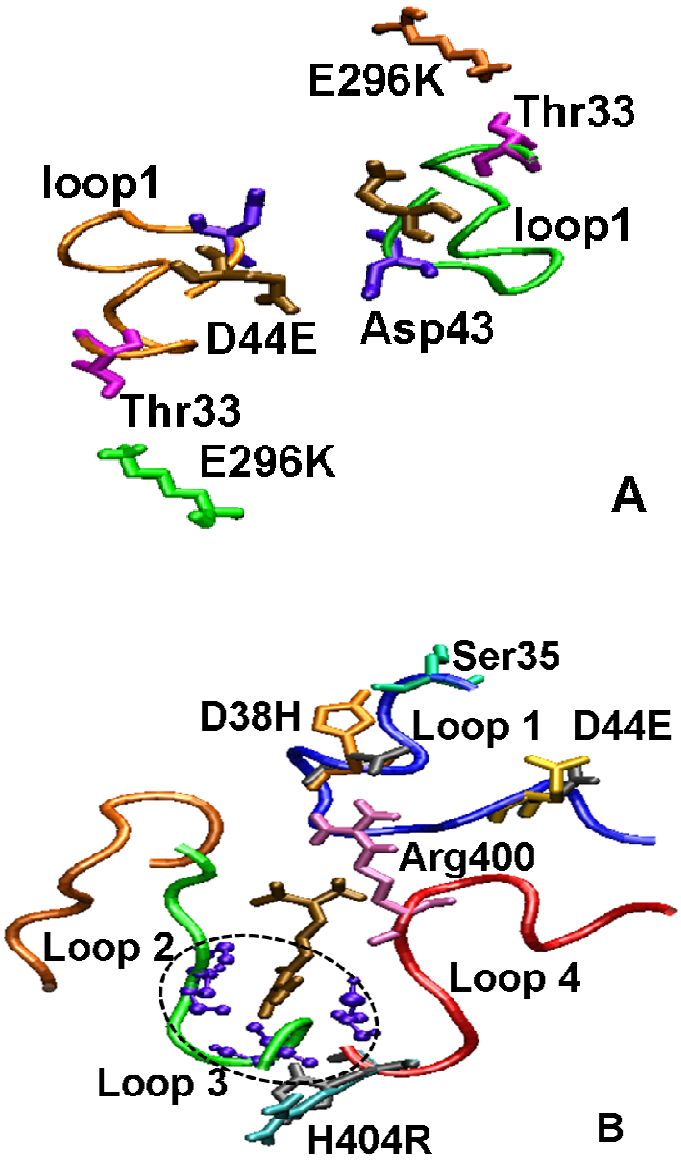

Figure 6. A). Structure model of variant M6. E296K is involved in intermonomer interaction (between chain a (orange) and b (green)) with Thr33. D44E is involved in intermonomer interaction, between chain A (orange) and B (green), with Asp43 (violet). B). Structure alignment of PpADI WT model and M6 model with four loops (loop 1:30-46, loop 2:178-175, loop 3:271-281 and loop 4: 393-404) surrounding the entrance of the active site. The substitutions in these loops and the residues involved in the interaction with those substitutions are representing: D38H (orange), D44E (yellow) and H404R (cyan, in M6; gray, in WT), Ser35 (green), Arg 400 (pink), substrate arginine (ochre), catalytic triad His278, Asp280 and Cys406 (violet, highlighted in an oval)

Figure 6B shows that the active site of the PaADI is surrounded by four loops (loop 1: 30-46, loop 2: 178-185, loop 3: 271-281, and loop 4: 393-404). These four loops undergo a conformational transition upon arginine binding and tighten

the surrounding of the arginine substrate[16]. D38 is located in loop 1 and faces towards the substrate access channel. In PpADI model (Figure 6B), the D38H mutation promotes the formation of a hydrogen bond interaction with the neighboring residues Ser35, contributing to the stability of the entropically unfavorable folded conformation of loop1. The rigidified loop 1 might be beneficial for arginine conversion. According to PaADI structure analysis, the side chain of gating residue Arg401 (Arg400 in PpADI) is located at the active site entrance and fills the substrate-binding site. The structure analysis of the C406A PaADI-L-arginine complex[16] shows that the Arg401 side chain (Arg400 in PpADI) is displaced by the substrate arginine to a position near the active site entrance that allows its hydrocarbon chain to assist shielding the catalytic site from solvent. D38 is involved in an ionic interaction and hydrogen bonding with Arg400. The substitution of Asp to His at position 38 results in a loss of ionic interactions to Arg400 due to the different lengths of the side chains. His38 can form only a hydrogen bond with active site gating residue Arg400. A weakened interaction between position 38 and Arg400 might increase the flexibility of the side chain of Arg400 which then might block less efficiently the access of arginine to the active site. As a result the variant M5 shows an improved k_{cat} value (1.7-fold compared to parent M3) due to the substitution D38H.

For elucidating further the individual role of the five identified amino acid substitutions and their influence on the active site geometry and tetramer formation crystal structures of variant M4 and M6 have to be solved.

4.6 Conclusion

In summary, with the modified screening protocol, PpADI variants with improved k_{cat} and $S_{0.5}$ were identified. The increased k_{cat} value and decreased $S_{0.5}$ value result in significant activity improvement of PpADI at low arginine concentrations. Especially the kinetic constants of PpADI variant M6 demonstrate that PpADI properties can be tailored by directed evolution. The generated PpADI variants match from their kinetic behavior therapeutic application demands much better

than the wild type PpADI. We therefore hope that by directed evolution improved PpADIs will further be investigated *in vivo* for tumor therapy.

References

1. Li L, Li ZM, Chen DQ*, et al.* Inactivation of microbial arginine deiminases by L-canavanine. Journal of the American Chemical Society, 2008; 130(6): 1918-31.

2. Lu XF, Li L, Wu R*, et al.* Kinetic analysis of *Pseudomonas aeruginosa* arginine deiminase mutants and alternate substrates provides insight into structural determinants of function. Biochemistry, 2006; 45(4): 1162-72.

3. Zhu LL, Tee KL, Roccatano D*, et al.* Directed evolution of an antitumor drug (arginine deiminase PpADI) for increased activity at physiological pH. Chembiochem, 2010; 11(5): 691-7.

4. Das K, Butler GH, Kwiatkowski V, Clark AD, Yadav P, Arnold E. Crystal structures of arginine deiminase with covalent reaction intermediates: Implications for catalytic mechanism. Structure, 2004; 12(4): 657-67.

5. Schofield PJ, Edwards MR, Matthews J, Wilson JR. The pathway of arginine catabolism in *Giardia intestinalis*. Molecular and Biochemical Parasitology, 1992; 51(1): 29-36.

6. Linstead D, Cranshaw MA. The pathway of arginine catabolism in the parasitic flagellate *Trichomonas vaginalis*. Molecular and Biochemical Parasitology, 1983; 8(3): 241-52.

7. Yarlett N, Lindmark DG, Goldberg B, Moharrami MA, Bacchi CJ. Subcellular localization of the enzymes of the arginine dihydrolase pathway in Trichomonas vaginalis and Tritrichomonas foetus. J Eukaryot Microbiol, 1994; 41(6): 554-9.

8. Biagini GA, Yarlett N, Ball GE*, et al.* Bacterial-like energy metabolism in the amitochondriate protozoon Hexamita inflata. Mol Biochem Parasitol, 2003; 128(1): 11-9.

9. Makhlin J, Kofman T, Borovok I*, et al.* Staphylococcus aureus ArcR controls expression of the arginine deiminase operon. Journal of Bacteriology, 2007; 189(16): 5976-86.

10. Seggewiss J, Becker K, Kotte O*, et al.* Reporter metabolite analysis of transcriptional profiles of a Staphylococcus aureus strain with normal phenotype

and its isogenic hemB mutant displaying the small-colony-variant phenotype. Journal of Bacteriology, 2006; 188(22): 7765-77.

11. Altucci P, Sapio V, Vitale P, de Vargas F. Mycoplasma in human pathology. Current status of the problem, with special reference to respiratory pathology. Recenti Prog Med, 1966; 41(5): 409-55.

12. Harasawa R, Koshimizu K, Kitagawa M, Asada K, Kato I. Nucleotide sequence of the arginine deiminase gene of *Mycoplasma hominis*. Microbiology and Immunology, 1992; 36(6): 661-5.

13. Takaku H, Matsumoto M, Misawa S, Miyazaki K. Antitumor activity of arginine deiminase from *Mycoplasma arginini* and its growth inhibitory mechanism. Japanese Journal of Cancer Research, 1995; 86(9): 840-6.

14. Fenske JD, Kenny GE. Role of arginine deiminase in growth of *Mycoplasma hominis*. Journal of Bacteriology, 1976; 126(1): 501-10.

15. Wei YZ, Zhou H, Sun Y, He YB, Luo YZ. Insight into the catalytic mechanism of arginine deiminase: Functional studies on the crucial sites. Proteins-Structure Function and Bioinformatics, 2007; 66(3): 740-50.

16. Ensor CM, Holtsberg FW, Bomalaski JS, Clark MA. Pegylated arginine deiminase (ADI-SS PEG(20,000) (mw)) inhibits human melanomas and hepatocellular carcinomas in vitro and in vivo. Cancer Research, 2002; 62(19): 5443-50.

17. Galkin A, Lu XF, Dunaway-Mariano D, Herzberg O. Crystal structures representing the Michaelis complex and the thiouronium reaction intermediate of Pseudomonas aeruginosa arginine deiminase. Journal of Biological Chemistry, 2005; 280(40): 34080-7.

18. Kundu M, Thomas J, Fialho AM*, et al.* The anticancer activity of the N-terminal CARD-Like domain of arginine deiminase (ADI) from *Pseudomonas aeruginosa*. Letters in Drug Design & Discovery, 2009; 6(6): 403-12.

19. Beloussow K, Wang L, Wu J, Ann D, Shen WC. Recombinant arginine deiminase as a potential anti-angiogenic agent. Cancer Letters, 2002; 183(2): 155-62.

20. Misawa S, Aoshima M, Takaku H, Matsumoto M, Hayashi H. High-Level expression of Mycoplasma arginine deiminase in *Escherichia coli* and Its efficient renaturation as an antitumor enzyme. Journal of Biotechnology, 1994; 36(2): 145-55.
21. Gong H, Zolzer F, von Recklinghausen G*, et al.* Arginine deiminase inhibits cell proliferation by arresting cell cycle and inducing apoptosis. Biochemical and Biophysical Research Communications, 1999; 261(1): 10-4.
22. Takaku H, Takase M, Abe S, Hayashi H, Miyazaki K. *In vivo* antitumor activity of arginine deiminase purified from *Mycoplasma arginini*. International Journal of Cancer, 1992; 51(2): 244-9.
23. Kim JE, Jeong DW, Lee HJ. Expression, purification, and characterization of arginine deiminase from Lactococcus lactis ssp lactis ATCC 7962 in Escherichia coli BL21. Protein Expression and Purification, 2007; 53(1): 9-15.
24. Kakimoto T, Shibatan.T, Chibata I. Crystallization of L-arginine deiminase from *Pseudomonas putida*. Febs Letters, 1971; 19(2): 166-8.
25. Shibatani T, Kakimoto T, Chibata I. Crystallization and properties of L-arginine deiminase of *Pseudomonas Putida* 2. Journal of Biological Chemistry, 1975; 250(12): 4580-3.
26. Galkin A, Kulakova L, Sarikaya E, Lim K, Howard A, Herzberg O. Structural insight into arginine degradation by arginine deiminase, an antibacterial and parasite drug target. Journal of Biological Chemistry, 2004; 279(14): 14001-8.
27. Ni Y, Schwaneberg U, Sun ZH. Arginine deiminase, a potential anti-tumor drug. Cancer Lett, 2008; 261(1): 1-11.
28. Galkin A, Kulakova L, Sarikaya E, Lim K, Howard A, Herzberg O. J Biol Chem, 2004; 279: 14001.
29. Galkin A, Lu XF, Dunaway-Mariano D, Herzberg O. J Biol Chem, 2005; 280: 34080.
30. Holle LM. Pegaspargase: an alternative? Annals of Pharmacotherapy, 1997; 31(5): 616-24.

31. Yoshioka T, Wada T, Uchida N*, et al.* Anticancer efficacy in vivo and in vitro, synergy with 5-fluorouracil, and safety of recombinant methioninase. Cancer Research, 1998; 58(12): 2583-7.
32. Lam TL, Wong GKY, Chong HC*, et al.* Recombinant human arginase inhibits proliferation of human hepatocellular carcinoma by inducing cell cycle arrest. Cancer Letters, 2009; 277(1): 91-100.
33. Shen RS, Fritz RR, Abell CW. Biochemical-Properties and Immunogenicity of L-Phenylalanine Ammonia-Lyase - Effects on Tumor-Bearing Mice. Cancer Treatment Reports, 1979; 63(6): 1063-8.
34. Yoshimoto T, Chao SG, Saito Y, Imamura I, Wada H, Inada Y. Chemical modification of tryptophanase from E. coli with polyethylene glycol to reduce its immunoreactivity towards anti-tryptophanase antibodies. Enzyme, 1986; 36(4): 261-5.
35. Feun LG, Savaraj N, Marini A*, et al.* Phase II study of pegylated arginine deiminase (ADI-PEG20), a novel targeted therapy for melanoma. Journal of Clinical Oncology, 2006; 24(18): 464s-s.
36. Gong H, Zolzer F, von Recklinghausen G, Havers W, Schweigerer L. Arginine deiminase inhibits proliferation of human leukemia cells more potently than asparaginase by inducing cell cycle arrest and apoptosis. Leukemia, 2000; 14(5): 826-9.
37. Morris SM, Jr. Regulation of enzymes of the urea cycle and arginine metabolism. Annu Rev Nutr, 2002; 22: 87-105.
38. Scott L, Lamb J, Smith S, Wheatley DN. Single amino acid (arginine) deprivation: rapid and selective death of cultured transformed and malignant cells. British Journal of Cancer, 2000; 83(6): 800-10.
39. Wheatley DN, Campbell E. Arginine catabolism, liver extracts and cancer. Pathol Oncol Res, 2002; 8(1): 18-25.
40. Thomas JB, Holtsberg FW, Ensor CM, Bomalaski JS, Clark MA. Enzymatic degradation of plasma arginine using arginine deiminase inhibits nitric oxide production and protects mice from the lethal effects of tumor necrosis factor and endotoxin. Molecular Biology of the Cell, 2001; 12: 404a-a.

41. Cheng PNM, Leung YC, Lo WH, Tsui SM, Lam KC. Remission of hepatocellular carcinoma with arginine depletion induced by systemic release of endogenous hepatic arginase due to transhepatic arterial embolisation, augmented by high-dose insulin: arginase as a potential drug candidate for hepatocellular carcinoma. Cancer Letters, 2005; 224(1): 67-80.
42. Cheng PNM, Lam TL, Lam WM*, et al.* Pegylated recombinant human arginase (rhArg-peg(5,000mw)) inhibits the in vitro and in vivo proliferation of human hepatocellular carcinoma through arginine depletion. Cancer Research, 2007; 67(1): 309-17.
43. Kim JH, Yu YS, Kim DH, Min BH, Kim KW. Anti-tumor activity of arginine deiminase via arginine deprivation in retinoblastoma. Oncol Rep, 2007; 18(6): 1373-7.
44. Kim RH, Coates JM, Bowles TL*, et al.* Arginine deiminase as a novel therapy for prostate cancer induces autophagy and caspase-independent apoptosis. Cancer Research, 2009; 69(2): 700-8.
45. Glazer ES, Piccirillo M, Albino V*, et al.* Phase II study of pegylated arginine deiminase for nonresectable and metastatic hepatocellular carcinoma. Journal of Clinical Oncology, 2010; 28(13): 2220-6.
46. Ascierto PA, Scala S, Castello G*, et al.* Pegylated arginine deiminase treatment of patients with metastatic melanoma: Results from phase I and II studies. Journal of Clinical Oncology, 2005; 23(30): 7660-8.
47. Shen LJ, Beloussow K, Shen WC. Accessibility of endothelial and inducible nitric oxide synthase to the intracellular citrulline-arginine regeneration pathway. Biochemical Pharmacology, 2005; 69(1): 97-104.
48. Park H, Lee JB, Shim YJ*, et al.* Arginine deiminase enhances MCF-7 cell radiosensitivity by inducing changes in the expression of cell cycle-related proteins. Molecules and Cells, 2008; 25(2): 305-11.
49. Kubo M, Nishitsuji H, Kurihara K, Hayashi T, Masuda T, Kannagi M. Suppression of human immunodeficiency virus type 1 replication by arginine deiminase of *Mycoplasma arginini*. Journal of General Virology, 2006; 87: 1589-93.

50. Izzo F, Montella M, Orlando AP*, et al.* Pegylated arginine deiminase lowers hepatitis C viral titers and inhibits nitric oxide synthesis. Journal of Gastroenterology and Hepatology, 2007; 22(1): 86-91.
51. Kwan JM, Fialho AM, Kundu M*, et al.* Bacterial proteins as potential drugs in the treatment of leukemia. Leukemia Research, 2009; 33(10): 1392-9.
52. Tsai WB, Aiba I, Lee SY, Feun L, Savaraj N, Kuo MT. Resistance to arginine deiminase treatment in melanoma cells is associated with induced argininosuccinate synthetase expression involving c-Myc/HIF-1 alpha/Sp4. Molecular Cancer Therapeutics, 2009; 8(12): 3223-33.
53. Yoon CY, Shim YJ, Kim EH*, et al.* Renal cell carcinoma does not express argininosuccinate synthetase and is highly sensitive to arginine deprivation via arginine deiminase. International Journal of Cancer, 2007; 120(4): 897-905.
54. Feun L, You M, Wu CJ*, et al.* Arginine deprivation as a targeted therapy for cancer. Current Pharmaceutical Design, 2008; 14(11): 1049-57.
55. Zhu ZW, Momeu C, Zakhartsev M, Schwaneberg U. Making glucose oxidase fit for biofuel cell applications by directed protein evolution. Biosens Bioelectron, 2006; 21(11): 2046-51.
56. Panke S, Held M, Wubbolts M. Trends and innovations in industrial biocatalysis for the production of fine chemicals. Current Opinion in Biotechnology, 2004; 15(4): 272-9.
57. Patel RN. Chemo-enzymatic synthesis of pharmaceutical intermediates. Expert Opinion on Drug Discovery, 2008; 3(2): 187-245.
58. Yokobayashi Y, Weiss R, Arnold FH. Directed evolution of a genetic circuit. Proc Natl Acad Sci U S A, 2002; 99(26): 16587-91.
59. Ellington AD, Chen X, Robertson M, Syrett A. Evolutionary origins and directed evolution of RNA. International Journal of Biochemistry & Cell Biology, 2009; 41(2): 254-65.
60. Alper H, Fischer C, Nevoigt E, Stephanopoulos G. Tuning genetic control through promoter engineering. Proceedings of the National Academy of Sciences of the United States of America, 2005; 102(36): 12678-83.

61. Drummond DA, Iverson BL, Georgiou G, Arnold FH. Why high-error-rate random mutagenesis libraries are enriched in functional and improved proteins. J Mol Biol, 2005; 350(4): 806-16.
62. Wong TS, Roccatano D, Schwaneberg U. Steering directed protein evolution: strategies to manage combinatorial complexity of mutant libraries. Environmental Microbiology, 2007; 9(11): 2645-59.
63. Wong TS, Zhurina D, Schwaneberg U. The diversity challenge in directed protein evolution. Combinatorial Chemistry & High Throughput Screening, 2006; 9(4): 271-88.
64. Fasan R, Chen MM, Crook NC, Arnold FH. Engineered alkane-hydroxylating cytochrome P450(BM3) exhibiting nativelike catalytic properties. Angewandte Chemie-International Edition, 2007; 46(44): 8414-8.
65. Titus SA, Xiao L, Southall N*, et al.* Cell-based PDE4 assay in 1536-well plate format for high-throughput screening. Journal of Biomolecular Screening, 2008; 13(7): 609-18.
66. Lafferty M, Dycaico MJ. GigaMatrix^{TM}: an ultra highthroughput tool for accessing biodiversity. JALA, 2009; 9: 200-8.
67. Yang GY, Withers SG. Ultrahigh-throughput FACS-based screening for directed enzyme evolution. Chembiochem, 2009; 10(17): 2704-15.
68. Miller OJ, Hibbert EG, Ingram CU, Lye GJ, Dalby PA. Optimisation and evaluation of a generic microplate-based HPLC screen for transketolase activity. Biotechnology Letters, 2007; 29(11): 1759-70.
69. Yoshikuni Y, Ferrin TE, Keasling JD. Designed divergent evolution of enzyme function. Nature, 2006; 440(7087): 1078-82.
70. Becker S, Schmoldt HU, Adams TM, Wilhelm S, Kolmar H. Ultra-high-throughput screening based on cell-surface display and fluorescence-activated cell sorting for the identification of novel biocatalysts. Current Opinion in Biotechnology, 2004; 15(4): 323-9.
71. Farinas ET. Fluorescence activated cell sorting for enzymatic activity. Combinatorial Chemistry & High Throughput Screening, 2006; 9(4): 321-8.

72. Agresti JJ, Antipov E, Abate AR*, et al.* Ultrahigh-throughput screening in drop-based microfluidics for directed evolution. Proceedings of the National Academy of Sciences of the United States of America, 2010; 107(9): 4004-9.
73. Leemhuis H, Kelly RM, Dijkhuizen L. Directed evolution of enzymes: library screening strategies. Iubmb Life, 2009; 61(3): 222-8.
74. Chen KC, Wu CH, Chang CY*, et al.* Directed evolution of a lysosomal enzyme with enhanced activity at neutral pH by mammalian cell-surface display. Chem Biol, 2008; 15(12): 1277-86.
75. Wang Q, Xia T. Enhancement of the activity and alkaline pH stability of Thermobifida fusca xylanase A by directed evolution. Biotechnology Letters, 2008; 30(5): 937-44.
76. Colin DY, Deprez-Beauclair P, Silva N, Infantes L, Kerfelec B. Modification of pancreatic lipase properties by directed molecular evolution. Protein Engineering Design & Selection, 2010; 23(5): 365-73.
77. Bessler C, Schmitt J, Maurer KH, Schmid RD. Directed evolution of a bacterial alpha-araylase: Toward enhanced pH-performance and higher specific activity. Protein Sci, 2003; 12(10): 2141-9.
78. Liu ZQ, Sun ZH, Leng Y. Directed evolution and characterization of a novel D-pantonohydrolase from Fusarium moniliforme. Journal of Agricultural and Food Chemistry, 2006; 54(16): 5823-30.
79. Hasan Z, Renirie R, Kerkman R, Ruijssenaars HJ, Hartog AF, Wever R. Laboratory-evolved vanadium chloroperoxidase exhibits 100-fold higher halogenating activity at alkaline pH - Catalytic effects from first and second coordination sphere mutations. Journal of Biological Chemistry, 2006; 281(14): 9738-44.
80. Makde RD, Dikshit K, Kumar V. Protein engineering of class-A non-specific acid phosphatase (PhoN) of Salmonella typhimurium: Modulation of the pH-activity profile. Biomolecular Engineering, 2006; 23(5): 247-51.
81. Kim T, Mullaney EJ, Porres JM*, et al.* Shifting the pH profile of *Aspergillus niger* PhyA phytase to match the stomach pH enhances its effectiveness as an

animal feed additive. Applied and Environmental Microbiology, 2006; 72(6): 4397-403.
82. Hirata A, Adachi M, Utsumi S, Mikami B. Engineering of the pH optimum of Bacillus cereus beta-amylase: Conversion of the pH optimum from a bacterial type to a higher-plant type. Biochemistry, 2004; 43(39): 12523-31.
83. Tomschy A, Brugger R, Lehmann M*, et al.* Engineering of phytase for improved activity at low pH. Appl Environ Microbiol, 2002; 68(4): 1907-13.
84. Sakoda H, Imanaka T. Cloning and sequencing of the gene coding for alcohol dehydrogenase of Bacillus stearothermophilus and rational shift of the optimum pH. J Bacteriol, 1992; 174(4): 1397-402.
85. Yang JH, Park JY, Kim SH, Yoo YJ. Shifting pH optimum of Bacillus circulans xylanase based on molecular modeling. Journal of Biotechnology, 2008; 133(3): 294-300.
86. MacPherson IS, Rosell FI, Scofield M, Mauk AG, Murphy MEP. Directed evolution of copper nitrite reductase to a chromogenic reductant. Protein Engineering Design & Selection, 2010; 23(3): 137-45.
87. Hida K, Hanes J, Ostermeier M. Directed evolution for drug and nucleic acid delivery. Adv Drug Deliv Rev, 2007; 59(15): 1562-78.
88. Yuan L, Kurek I, English J, Keenan R. Laboratory-directed protein evolution. Microbiology and Molecular Biology Reviews, 2005; 69(3): 373-92.
89. Rautio J, Kumpulainen H, Heimbach T*, et al.* Prodrugs: design and clinical applications. Nat Rev Drug Discov, 2008; 7(3): 255-70.
90. Barak Y, Thorne SH, Ackerley DF, Lynch SV, Contag CH, Matin A. New enzyme for reductive cancer chemotherapy, YieF, and its improvement by directed evolution. Molecular Cancer Therapeutics, 2006; 5(1): 97-103.
91. Kuhn I, Harden P, Bauzon M*, et al.* Directed evolution generates a novel oncolytic virus for the treatment of colon cancer. PLoS One, 2008; 3(6): e2409.
92. Robertson DE, Steer BA. Recent progress in biocatalyst discovery and optimization. Current Opinion in Chemical Biology, 2004; 8(2): 141-9.
93. Soares AL, Guirmaraes GM, Polakiewicz B, Pitombo RND, Abrahao-Neto J. Effects of polyethylene glycol attachment on physicochemical and biological

stability of E-coli L-asparaginase. International Journal of Pharmaceutics, 2002; 237(1-2): 163-70.
94. Kotzia GA, Labrou NE. Engineering thermal stability of L-asparaginase by in vitro directed evolution. Febs Journal, 2009; 276(6): 1750-61.
95. Orlova A, Feldwisch J, Abrahmsen L, Tolmachev V. Affibody molecules for molecular imaging and therapy for cancer. Cancer Biotherapy and Radiopharmaceuticals, 2007; 22(5): 573-84.
96. Nilsson FY, Tolmachev V. Affibody (R) molecules: New protein domains for molecular imaging and targeted tumor therapy. Current Opinion in Drug Discovery & Development, 2007; 10(2): 167-75.
97. Gronwall C, Sjoberg A, Ramstrom M*, et al.* Affibody-mediated transferrin depletion for proteomics applications. Biotechnol J, 2007; 2(11): 1389-98.
98. Renberg B, Shiroyama I, Engfeldt T, Nygren PA, Karlstrom AE. Affibody protein capture microarrays: Synthesis and evaluation of random and directed immobilization of affibody molecules. Analytical Biochemistry, 2005; 341(2): 334-43.
99. Friedman M, Orlova A, Johansson E*, et al.* Directed evolution to low nanomolar affinity of a tumor-targeting epidermal growth factor receptor-binding affibody molecule. Journal of Molecular Biology, 2008; 376(5): 1388-402.
100. Chang CCJ, Chen TT, Cox BW*, et al.* Evolution of a cytokine using DNA family shuffling. Nature Biotechnology, 1999; 17(8): 793-7.
101. Zhang JH, Dawes G, Stemmer WPC. Directed evolution of a fucosidase from a galactosidase by DNA shuffling and screening. Proceedings of the National Academy of Sciences of the United States of America, 1997; 94(9): 4504-9.
102. Crameri A, Cwirla S, Stemmer WPC. Construction and evolution of antibody-phage libraries by DNA shuffling. Nature Medicine, 1996; 2(1): 100-2.
103. Patten PA, Howard RJ, Stemmer WP. Applications of DNA shuffling to pharmaceuticals and vaccines. Curr Opin Biotechnol, 1997; 8(6): 724-33.
104. Park IS, Kang SW, Shin YJ*, et al.* Arginine deiminase: a potential inhibitor of angiogenesis and tumour growth. Br J Cancer, 2003; 89(5): 907-14.

105. Izzo F, Marra P, Beneduce G*, et al.* Pegylated arginine deiminase treatment of patients with unresectable hepatocellular carcinoma: Results from phase I/II studies. J Clin Oncol, 2004; 22(10): 1815-22.
106. Gong H, Zölzer F, von Recklinghausen G, Havers W, Schweigerer L. Arginine deiminase inhibits proliferation of human leukemia cells more potently than asparaginase by inducing cell cycle arrest and apoptosis. Leukemia, 2000; 14(5): 826-9.
107. Shen LJ, Shen WC. Drug evaluation: ADI-PEG-20 - a PEGylated arginine deiminase for arginine-auxotrophic cancers. Curr Opin in Mol Ther, 2006; 8(3): 240-8.
108. Holtsberg FW, Ensor CM, Steiner MR, Bomalaski JS, Clark MA. Poly(ethylene glycol) (PEG) conjugated arginine deiminase: effects of PEG formulations on its pharmacological properties. J Controlled Release, 2002; 80(1-3): 259-71.
109. Mûller HJ, Boos J. Use of L-asparaginase in childhood all. Crit Rev Oncol Hematol, 1998; 28(2): 97-113.
110. Turunen O, Janis J, Fenel F, Leisola M. Engineering the thermotolerance and pH optimum of family 11 xylanases by site-directed mutagenesis. Methods Enzymol, 2004; 388: 156-67.
111. Fang TY, Ford C. Protein engineering of *Aspergillus awamori* glucoamylase to increase its pH optimum. Protein Eng, 1998; 11(5): 383-8.
112. Sakoda H, Imanaka T. Cloning and sequencing of the gene coding for alcohol-dehydrogenase of *Bacillus stearothermophilus* and rational shift of the optimum pH. J Bacteriol, 1992; 174(4): 1397-402.
113. Wang WY, Malcolm BA. Two-stage PCR protocol allowing introduction of multiple mutations, deletions and insertions using QuikChange™ site-directed mutagenesis. BioTechniques, 1999; 26(4): 680-2.
114. Miyazaki K, Takenouchi M. Creating random mutagenesis libraries using megaprimer PCR of whole plasmid. Biotechniques, 2002; 33(5): 1033-8.
115. Studier FW. Protein production by auto-induction in high-density shaking cultures. Protein Expression and Purification, 2005; 41(1): 207-34.

116. Archibald RM. Deternination of citrulline and allantoin and demonstration of citrulline in blood plasma. J Biol Chem, 1944; 156(1): 121-42.
117. Boyde TRC, Rahmatullah M. Optimization of conditions for the colorimetric determination of citrulline, using diacetyl monoxime. Anal Biochem, 1980; 107(2): 424-31.
118. Guex N, Peitsch MC. SWISS-MODEL and the Swiss-PdbViewer: an environment for comparative protein modeling. Electrophoresis, 1997; 18(15): 2714-23.
119. van Gunsteren WF, Billeter SR, Eising AA*, et al.* Biomolecular simulation: the gromos 96 manual and user guide ETH Zürich; 1996.
120. Mather A, Roland D. Automated thiosemicarbazide-diacetyl monoxime method for plasma urea. Clinical Chemistry, 1969; 15(5): 393-6.
121. Wong TS, Arnold FH, Schwaneberg U. Laboratory evolution of cytochrome P450BM-3 monooxygenase for organic cosolvents. Biotechnol Bioeng, 2004; 85(3): 351-8.
122. Glieder A, Farinas ET, Arnold FH. Laboratory evolution of a soluble, self-sufficient, highly active alkane hydroxylase. Nat Biotechnol, 2002; 20(11): 1135-9.
123. Galkin A, Lu X, Dunaway-Mariano D, Herzberg O. Crystal structures representing the Michaelis complex and the thiouronium reaction intermediate of Pseudomonas aeruginosa arginine deiminase. Journal of biological chemistry, 2005; 280(40): 34080-7.
124. Chuang VTG, Kragh-Hansen U, Otagiri M. Pharmaceutical strategies utilizing recombinant human serum albumin. Pharm Res, 2002; 19(5): 569-77.
125. Tee KL, Dmytrenko O, Otto K, Schmid A, Schwaneberg U. A p-nitrothiophenolate screening system for the directed evolution of a two-component epoxygenase (StyAB). J Mol Catal B: Enzym, 2008; 50(2-4): 121-7.
126. Li L, Li ZM, Wang CH*, et al.* The electrostatic driving force for nucleophilic catalysis in L-arginine deiminase: a combined experimental and theoretical study. Biochemistry (Mosc), 2008; 47(16): 4721-32.

127. Takaku H, Matsumoto M, Misawa S, Miyazaki K. Antitumor-activity of arginine deiminase from *Mycoplasma arginini* and its growth-Inhibitory mechanism. Jap J Cancer Res, 1995; 86(9): 840-6.
128. Capocaccia R, Sant M, Berrino F, Simonetti A, Santi V, Trevisani F. Hepatocellular carcinoma: trends of incidence and survival in Europe and the United States at the end of the 20th century. American Journal of Gastroenterol, 2007; 102(8): 1661-70.
129. Shen LJ, Shen WC. Drug evaluation: ADI-PEG-20 - a PEGylated arginine deiminase for arginine-auxotrophic cancers. Current Opinion in Molecular Therapeutics, 2006; 8(3): 240-8.
130. Wang WY, Malcolm BA. Two-stage PCR protocol allowing introduction of multiple mutations, deletions and insertions using QuikChange (TM) site-directed mutagenesis. Biotechniques, 1999; 26(4): 680-2.
131. Vaughn WK, Neal RA, Anderson AJ. Computer estimation of the parameters of the sigmoidal kinetic model. Computers in Biology and Medicine, 1976; 6(1): 1-7.
132. Kelley LA, Sternberg MJE. Protein structure prediction on the web: a case study using the Phyre server. Nature Protocols, 2009; 4(3): 363-71.
133. Laskowski RA, Macarthur MW, Moss DS, Thornton JM. Procheck - a program to check the stereochemical quality of protein structures. Journal of Applied Crystallography, 1993; 26: 283-91.
134. Zhou HY, Zhou YQ. Distance-scaled, finite ideal-gas reference state improves structure-derived potentials of mean force for structure selection and stability prediction. Protein Science, 2002; 11(11): 2714-26.
135. Benkert P, Tosatto SCE, Schomburg D. QMEAN: A comprehensive scoring function for model quality assessment. Proteins-Structure Function and Bioinformatics, 2008; 71(1): 261-77.
136. Berendsen HJC, Postman JPM, van Gunsteren WF, Hermans J. Interaction models for water in relation to protein hydration. Intermolecular Forces, 1981: 331-42.

137. Hess B, Bekker H, Berendsen HJC, Fraaije JGEM. LINCS: A linear constraint solver for molecular simulations. Journal of Computational Chemistry, 1997; 18(12): 1463-72.
138. Miyamoto S, Kollman PA. Settle - an analytical version of the shake and rattle algorithm for rigid water models. Journal of Computational Chemistry, 1992; 13(8): 952-62.
139. Darden T, York D, Pedersen L. Particle mesh ewald - an N.Log(N) method for ewald sums in large systems. Journal of Chemical Physics, 1993; 98(12): 10089-92.
140. Berendsen HJC, Postma JPM, Vangunsteren WF, Dinola A, Haak JR. Molecular dynamics with coupling to an external bath. Journal of Chemical Physics, 1984; 81(8): 3684-90.
141. Hess B, Kutzner C, van der Spoel D, Lindahl E. GROMACS 4: algorithms for highly efficient, load-balanced, and scalable molecular simulation. Journal of Chemical Theory and Computation, 2008; 4(3): 435-47.

Summary and outlook

Arginine depletion based on ADI is an emerging strategy for anti-tumor treatment. ADIs have been studied for the therapy of HCCs and melanomas and were approved as an orphan drug for both kinds of tumors. ADI is proved to be effective in the treatment of leukemia. The effectiveness of ADIs as anti-tumor agent depends on their enzymatic properties (such as K_m, k_{cat}, optimum pH, stability at neutral pH). Directed evolution, without rational understanding of the targeted property, allows improving all properties that can be reflected in a screening system through iterative rounds of diversity generation and screening.

In order to improve PpADI activity at physiological pH by directed evolution, a colorimetric screening assay based on citrulline detection has been developed in 96-well microtiter plate format. Single mutation H404R was identified according to PpADI homology model (based on PaADI crystal structure), introduced to PpADI wild type and eventually resulted in 1.4-fold of increase in k_{cat}. M1 (H404R) was used as template for the first round of epPCR library generation. M2 (K5T/D44E/H404R) obtained from the first round of epPCR library showed 4-fold improved k_{cat} value when compared to the PpADI wild type. Furthermore, a shift of pH optimum from pH 6.5 to pH 7.0 was observed, combined with an increased K_m value (2.5 mM) under assay conditions (0.5 M sodium phosphate buffer, pH 7.4), compared to PpADI wild type (0.7 mM).

Arginine concentration in human plasma is however relatively low (100-120 µM). Therefore the second round of epPCR library was performed to decrease K_m value and further improve k_{cat} value. The validated screening assay was modified to reflect more close physiological condition (1 mM arginine in PBS buffer, pH 7.4). Two important variants with one additional mutation, M4 (K5T/D44E/A128T/E296K/H404R) with decreased $S_{0.5}$ vaule, and M5 (K5T/D38H/D44E/A128T/H404R) with improved k_{cat} were obtained. Their two mutations were combined and resulted in variants M6

(K5T/D38H/D44E/A128T/E296K/H404R). Under physiological pH in PBS buffer, the $S_{0.5}$ value of M6 (0.81 mM) is lower than that of PpADI wild type (1.30 mM); the k_{cat} value improved from 0.18 s^{-1} (PpADI wild type) to 17.56 s^{-1} (M5, 97.6-folds) and 11.64 s^{-1} (M6, 64.7-fold).

A reamaining challenge facing PpADI's anti-tumor application is to decrease the K_m ($S_{0.5}$) value further close to arginine concentration level in human plasma. A more sensitive assay for screening has to be developed with the addition of sensitizer like thiosemicarbazide (TSC), optimized temperature and incubation time. Improved variants should be tested tested in human plasma or with human plasma composition. *In vitro* testing of ADI variants with arginine auxotrophic tumor cell lines is the first step towards *in vivo* in human.

In summary, directed evolution has been very useful algorithim for improving ADI's k_{cat} and K_m at physiological pH (pH 7.4) for its medical application. Hope that directed evolution will be become a standard method for therapeutic protein like its use in industry.

Publications

1. **Leilei Zhu**, Kang Lan Tee, Danilo Roccatano, Burcu Sonmez, Ye Ni, Zhi-Hao Sun, and Ulrich Schwaneberg. Directed evolution of an antitumor drug (Arginine Deiminase PpADI) for increased activity at physiological pH. ChemBioChem. 2010, 11, 691-697.

2. **Leilei Zhu**, Rajni Verma, Danilo Roccatano, Ye Ni, Zhi-Hao Sun, and Ulrich Schwaneberg. A potential anti-tumor drug (arginine deiminase) reengineered for efficient operation under physiological conditions. ChemBioChem. *In press*.

3. Ye Ni, Zhenwei Li, Zhihao Sun, Pu Zheng, Yongmei Liu and **Leilei Zhu**, Ulrich Schwaneberg. Expression of arginine deiminase from *Pseudomonas plecoglossicida* CGMCC2039 in *Escherichia coli* and its anti-tumor activity. Current Microbiology. 2009, 58(6):593-598.

Patent

1. Directed evolution of arginine deiminase for increased activity at physiological pH. Application number: PCT/EP2010/061884.

Curriculum vitae

Personal data

Name:	Leilei Zhu
Gender:	Female
Date of Birth:	27th April, 1982
Place of Birth:	Weifang, China
Marital Status:	Married
Nationality:	Chinese

Education

2009-	PhD fellow of biotechnology, RWTH Aachen University, Aachen, Germany
2007-2009	PhD fellow of engineering and science, Jacobs University Bremen, Bremen, Germany
2005-2007	Master of biochemical engineering, Jiangnan University (Southern Yantze University), Wuxi, China
2001-2005	Bachelor of biotechnology, Jiangnan University (Southern Yantze University), Wuxi, China

2001-1998	The first high school of Hanting, Weifang, China
1998-1994	The sixth middle school of Hanting, Weifang, China
1989-1994	Primary school of Liuhe, Weifang, China

Directed Evolution of Arginine Deiminase (ADI) for Anti-tumor Application

Von der Fakultät für Mathematik, Informatik und Naturwissenschaften der RWTH Aachen University zur Erlangung des akademischen Grades eines(r) Doktors(in) der Naturwissenschaften oder eines(r) Doktors(in) der Ingenieurwissenschaften genehmigte Dissertation

vorgelegt von

Master of Biochemistry

Leilei Zhu

Aus Weifang China

Berichter: **Universitätsprofessor Dr. Ulrich Schwaneberg**
Universitätsprofessor Dr. Lothar Elling

Tag der mündlichen Prüfung: 14.09.2010

Diese Dissertation ist auf den Internetseiten der Hochschulbibliothek online verfügbar.

Table of contents

Acknowledgement.....I
Abstract.....III
Abbreviations V
List of figures..... VI
List of tables..... IX
Chapter 1 Arginine deiminase (ADI) 1
1.1 Arginine deiminase (ADI).....1
1.2 ADI structure 5
1.3 Catalytic reaction mechanism of ADI.....10
1.4 Anti-tumor application of ADI.....11
1.5 Conclusion.....16
Chapter 2 Directed evolution 17
2.1 Introduction to directed evolution.....17
2.2 Directed enzyme evolution for pH tolerance of enzymes 22
2.3 Directed enzyme evolution for medical application.....24
2.3.1 Prodrug enzymes for tumor chemotherapy.....24
2.3.2 Oncolytic viruses for tumor chemotherapy.....25
2.3.3 Amino acid depriving enzyme for anti-tumor applications.....27
2.3.4 Affibody molecules for cancer prognosis 28
2.3.5 Interferon for anti-tumor applicaiton 29
2.4 Conclusion.....30
Chapter 3. Directed evolution of Arginine deiminase for increased activity at physiological pH.....31
3. 1 Abstract 31
3.2 Introduction.....31
3.3 Materials and methods 33
3.3.1 Materials 33
3.3.2 Methods 34

3.3.2.1 Reagents used in assays 34
3.3.2.2 Cloning of ADI into pET42b(+) 34
3.3.2.3 Site directed mutagenesis of PpADI gene at position H404 35
3.3.2.4 Site sturation mutagenesis of PpADI gene at nine amino acid position 35
3.3.2.5 Construction of PpADI error-prone library 36
3.3.2.6 Expression of PpADI in LB media with IPTG induction 37
3.3.2.7 Expression of PpADI in auto-induction media 37
3.3.2.8 Cultivation and expression of PpADI in 96-well plates 37
3.3.2.9 Screening Procedure 38
3.3.2.10 Expression of ADI in shaking flask and purification 39
3.3.2.11 Characterization of ADI wild type and mutants 40
3.3.2.12 Molecular Modeling 41
3.3.2.13 Stability of PpADI in presence of serum 41
3.3.2.14 Activity of PpADI (wild type, M1, M2) towards arginine derivative dimethylarginine 42
3.4 Results 42
3.4.1 PpADI cloning 42
3.4.2 PpADI expression in LB media with IPTG as inducer 44
3.4.3 PpADI expression in auto-induction media 44
3.4.4 PpADI assay based on citrulline detection 46
3.4.5 PpADI screening system for citrulline production in microtiter plates 47
3.4.6 Focused libraries generated by saturation mutagenesis 50
3.4.7 Validation of variant M1 (H404R) citrulline colorimetric assay in cuvette format 50
3.4.8 epPCR library generation and screening with citrulline detection assay by screening error-prone mutant libraries 50
3.4.9 Characterization of PpADI variants 53
3.4.9.1 Determination of k_{cat} and K_m of ADI wild type and the mutants 53
3.4.9.2 Relative pH profile of wild type and mutant 54
3.4.10 Stability of PpADI in the presence of human serum 55

3.4.11 Activity of PpADI (wild type, M1, M2) towards arginine derivative (N^G, N^G)-dimethylarginine 56
3.5 Discussion 56
3.6 Conclusion 59
Chapter 4. PpADI reengineered for efficient operation under physiological conditions 60
4.1 Abstract 60
4.2 Introduction 60
4.3 Materials and methods 62
4.3.1 Materials 62
4.3.2 Methods 62
4.3.2.1 Site saturation mutagenesis of *PpADI* M2 at position A128 62
4.3.2.2 Construction of PpADI error-prone library 63
4.3.2.3 Site directed mutagenesis at position D38 of *PpADI* M4 63
4.3.2.4 Site saturation mutagenesis at position D38 and E296 of *PpADI* M3 64
4.3.2.5 Cultivation and expression of PpADI in 96-well plates 64
4.3.2.6 Improved screening system in 96-well plate to identify PpADI variants with high activities at low arginine concentration 64
4.3.2.7 Expression of PpADI in shaking flask and purification 65
4.3.2.8 Characterization of PpADI variants 65
4.3.2.9 Native polyacrylamide gel electrophoresis of PpADI variants 66
4.3.2.10 Homology modeling 67
4.4 Results 67
4.4.1 Improved screening system in microtiter plates to identify PpADI variants with high activities at low arginine concentration 67
4.4.2 Genealogic tree of directed PpADI evolution 68
4.4.3 EpPCR library construction and screening for variants with high activities at low arginine concentration 69
4.4.4 Site saturation mutagenesis of *PpADI* at position D38 and E296 70

4.4.5 Determination of kinetic constants (k_{cat} and $S_{0.5}$) of PpADI wild type and variants M3, M4, M5 and M6 72
4.4.6 Native polyacrylamide gel electrophoresis of PpADI variants 73
4.5 Discussion 74
Summary and outlook 95
Publication list 97
Curriculum vitae 98

Acknowledgement

First and foremost I want to thank my supervisor Prof. Dr. Ulrich Schwaneberg for offering me the opportunity to study in Germany, his continuous support of my PhD study and research, for his patience, motivation, enthusiasm, and immense knowledge, which influence my view of science and life. His guidance helped me all the time in research and writing of paper and thesis. I could not have imagined having a better advisor and mentor for my PhD study.

Besides my supervisor, I would like to thank other two committee member Prof. Dr. Lothar Elling and Prof. Dr. Anett Kirschner. I appreciate their taking time to read this thesis and give valuable comments.

My sincere thanks also go to Kang Lan, who became a great friend of mine after I came to Bremen of Germany three years ago. She helped me a lot with my PhD project and she was a great company in my daily life. I will never forget the two months I spent on the first cloning working in my life and how Kang Lan taught me and encouraged me.

I am grateful to Prof. Dr. Danilo Roccatano for spending a lot of time discussing my results. After the first meeting with Prof. Roccatano, I started to know and learn computational tools which are really useful for my PhD study. I also thank Rajni for her contribution of homology modeling to my project.

The members of the Schwaneberg group have contributed immensely to my personal and professional time in Jacobs University Bremen and RWTH Aachen University. The group has been a source of friendships as well as good advice and collaboration. I appreciate the help from Marina, Daniela, Gisela, Wolfgang and Brigitta in lab and Marina, Monika and Anita's patient explanation of the registration regulation RWTH Aachen University. I would like to acknowledge honorary group members. I thank Liqing for her sharing apartment with me and helped me start my life in Germany and also thank Haiyan for her offering me a room later and often cooked nice food for us. Ran shared a lot of lab techniques which are very useful for my experiments. I always admire her professional and

accurate attitude towards work. I thank other labmates who I got to know in Jacobs university: Ronny, Hemu, Chaoning, Amol, Dominik and Amir for the stimulating discussions, little help in lab and all the fun we have had in the last three years; Dragana, Ljubica, Noor, Pravine and Raluca helped me move to Aachen and we finally got through the tough transition period from Bremen to Aachen. I thank our group leaders Marco, Jan and Radivoje, who are not my direct supervisor, but are always helpful when I have questions. I thank my fellow labmates who I got to know in RWTH Aachen University: Tamara, Felix, Alex, Christian, Joelle, André, Joana……, who are always helpful with all the problems (PhD registration, Germany letters from university…….) because of my poor German.

I also want to acknowledge my students, Burcu and Alice, both of whom were hard-working and smart. They were all a great help in the lab and I really enjoyed working with them.

I would like to thank my family because of their love, support and trust. They love me the most in the world. I thank for their efforts that they made over the years to make sure I have a good growth and education environment. I wish them healthy and happy life. I thank my elder sister for her love and understanding and always taking good care of my parents these years when I am not around. I thank my husband, Haifeng, who supports me all the time and always is there for me. I am lucky to have him with me.

The financial support of the Jacobs University Bremen and RWTH Aachen University is gratefully acknowledged.

Abstract

Arginine deiminase (ADI), an arginine-degrading enzyme, is involved in the first step of arginine dihydrolase pathway. It catalyzes the hydrolysis of L-arginine to form citrulline and ammonia. ADI has been studied as a potential cancer therapeutic agent for the arginine-auxotrophic tumors, such as hepatocellular carcinomas (HCC) and melanomas. Furthermore, studies also indicate that ADI is a potential anti-angiogenic agent; therefore it could become a novel anti-cancer drug targeting the neovascularization-related tumors. Studies show ADI is more potent for the treatment of leukemia than L-asparaginase. However, the anti-tumor application of ADI for therapeutic purpose faces considerable challenges, such as, microbial ADI has low activity at physiological pH (7.35~7.45), short circulating half-life (~5 h) and high antigenicity. Pegylation of ADI improved its efficacy as a clinical drug, including its half-life in serum and antigenicity. The aim of the project is to improve ADI catalytic performance at physiological pH by directed evolution.

Protein engineering by rational design and directed evolution offers opportunities to tailor ADI properties to physiological conditions. Directed protein evolution has over the last decades become a versatile and successful approach for tailoring protein properties to industrial demands and for advancing our understanding of structure-function relationships in biocatalysts. Unlike rational design relying on the gathering of extensive structure-function relationships of enzymes, directed evolution is used to reengineer enzyme properties through iterative rounds of diversity generation and function selection for improved variants.

In order to improve the ADI activity at physiological pH, we established a directed evolution protocol for this purpose. A microtiter plate (MTP) format colorimetric screening assay based on citrulline detection with diacetyl monoxime (DAM) was developed. Reaction temperature for color development and DAM concentration

were optimized to ensure sufficient sensitivity, appropriate linear range and throughput. With the optimized assay and PpADI wild type expressed in *E. coli* as a model protein, true standard deviation 12.8 % was obtained, which is appropriate for the library screening.

With the established microtiter plate assay system, for the first time, we reengineered ADI for improved activity at physiological pH (pH 7.4) with higher potency in medical application. After one site directed mutagenesis and one round of epPCR library screening, variant M2 (K5T/D44E/H404R) was obtained. M2 shows 4-fold improved k_{cat} value than the PpADI wild type, a shifted pH optimum at pH 7.0 (by 0.5 pH unit), and however an increased K_m value, 3.6-fold under assay conditions (0.5 M sodium phosphate buffer).

Low K_m ($S_{0.5}$) value for ADI is an important factor for efficient consume of arginine in plasma because of the low arginine concentration in human plasma (100-120 µM). Therefore after our proof of concept of reengineering PpADI by directed evolution, we aim to decrease the K_m value of PpADI towards arginine and improve the k_{cat} furthermore thereby improve the efficiency of arginine depletion by ADI. The established citrulline colorimetric assay in 96-well microtiter plate is improved to reflect application conditions: PBS buffer and 1 mM arginine were used in screening system. After the second round of epPCR library and site directed mutagenesis, variant M5 (K5T/D38H/D44E/A128T/H404R) and M6 (K5T/D38H/D44E/A128T/E296K/H404R) were generated: at pH 7.4 (PBS buffer), the $S_{0.5}$ value decrease from 2.01 mM (parent M3, K5T/D44E/A128T/H404R) to 1.48 mM (M5) and 0.81 mM (M6). Under physiological pH in PBS buffer, the $S_{0.5}$ value of M6 (0.81 mM) is lower than that of PpADI wild type (1.30 mM); the k_{cat} value improved from 0.18 s^{-1} (PpADI wild type) to 17.56 s^{-1} (M5, 97.6-folds) and 11.64 s^{-1} (M6, 64.7-fold).

Abbreviations

ADI	arginine deiminase
ADH	arginine degradation pathway
ASS	argininosuccinate synthetase
ASL	argininosuccinate lyase
CARD	caspase recruitment domain
PCR	polymerase chain reaction
epPCR	error prone PCR
DAM	diacetyl monoxime
Da	dalton
DNA	deoxyribonucleic acid
E. coli	*Escherichia coli*
GMSF	guanidino-group modifying enzyme superfamily
HCC	hepatocellular carcinomas
HUVEC	human umbilical vein endothelial cells
IPTG	isopropyl β-D-1-thiogalactopyranoside
iNOs	inducible nitric oxide synthase
LB	Luria-Bertani-medium
MTP	microtiter plate
OD_{600}	optical density at 600 nm
OTC	ornithine carbamoyl transferase
PEG	polyethylene glycol
PDB	protein data bank
TSC	thiosemicarbazide
WT	wild type

List of tables

Figures	Pages
Chapter 1	
Scheme 1. Arginine dihydrolase pathway. OTC, ornithine transcarbamylase; CK, carbamate kinase.	1
Figure 1. Structural of ADIs from *P. aeruginosa* and *M. arginini*.	5
Figure 2 (A). stereoscopic view of PaADI key active site residues. 2 (B). stereoscopic view of a modeled arginine substrate (green) docked in the active site of ADI. Atomic colors are red, oxygen; blue, nitrogen; yellow, sulfur; and gray, carbon. Ion pair interactions are shown as dashed lines.	7
Figure 3. Structural characteristics of the PaADI.	9
Figure 4 (A). Stereoscopic view of ADI in the unbound and bound states. 4 (B). Structural relationship between ADI (yellow) and PAD4 (cyan).	10
Figure 5. Mechanism of PaADI catalysis of arginine to citrulline and ammonia.	11
Firgure 6. Urea cycle.	13
Firgure 7. Summary of ADI effects on arginine-related cellular functions.	15
Chapter 2	
Figure 1. Procedure of a directed evolution experiment.	18
Figure 2. Overview of screening technologies.	21
Figure 3. Hermiston's "Directed Evolution" process of viruses and derivative viral pools.	26
Chapter 3	
Figure 1. DNA electrophoresis of PpADI.	43
Figure 2. PpADI sequencing results.	43
Figure 3. SDS-PAGE of PpADI expression.	44

Figures Pages

Figure 4(A). Activity of PpADI expressed in auto-induction media. 45

Figure 4(B). SDS-PAGE of ADI expressed in auto-induction media 1, LS-5052; 2, P-5052; 3, MD-5052; 4 TYM-5052; 5, TYP-5052. 45

Figure 5. Arginine conversion by ADI and detection of citrulline using DAM/TSC assay. 46

Figure 6. Citrulline colorimetric assay in cuvette format using DAM/TSC assay. 46

Figure 7. Calibration curve of cuvette format citrulline colorimetric assay. 47

Figure 8. Citrulline colorimetric assay in MTP format using DAM assay. 47

Figure 9. Calibration curve of 96-well microtiter plate format citrulline colorimetric screening assay. 48

Figure 10. Activity values in descending order of the ADI wild-type conversion of arginine to citrulline in a 96-well microtiter plate using the optimized assay protocol. 49

Figure 11. PpADI model derived from PaADI crystal structure (PDB code 2a9gD) by SWISS MODEL WORKSPACE. 49

Figure 12 (A). Electrophoresis of epPCR products. Lane 1, 0.01 mM of $MnCl_2$; Lane 2, 0.02 mM of $MnCl_2$; Lane 3, 0.05 mM of $MnCl_2$. 51

Figure 12 (B). Electrophoresis of MEGAWHOP product with epPCR products as megaprimer. 51

Figure 13. Relative activity of ADI variants towards arginine. The relative activity is the ratio of the activity at the pH of each variant relative to the activity at pH 7.4 of wild type ADI. 52

Figure 14. Elution profile of wild type PpADI and improved variants from epPCR library, generated with Protein 230 Kit using a mircofluidic device (Agilent Bioanalyzer). BSA was added as an internal standard. 53

Figure 15. Kinetic parameters of ADI and mutants for conversion of arginine to citrulline. White: ADI wild type, grey: M1 (H404R), black: M2 (K5T D44E H404R). 54

Figure 16. pH profile of wild type ADI, M1(H404R), M2(K5T/D44E /H404R. 55

Figures Pages

Figure 17. Structural alignment of mutant M1 model with corresponding residues of the crystal structures of the PaADI (in orange). 57

Figure 18. Structural alignment of mutant M2 model with corresponding residues of the crystal structures of the PaADI (in orange). 58

Chaper 4

Figure 1. Figure 1. Activity values in descending order of the PpADI variant M3 conversion of arginine to citrulline in a 96-well microtiter plate using the optimized assay protocol. 68

Figure 2. Genealogic tree of PpADI variants (M1 to M6) with generated amino acid substitutions. Novel substitutions are indicated by an asterisk. 69

Figure 3. Native polyacrylamide gel electrophoresis of PpADI variants (M3 to M6) with different dimer/tetramer distribution 73

Figure 4. Kinetic curve of PpADI wild type, M3, M5 and M6. 75

Figure 5. A). The model of WT tetramer after energy minimization in vacuum (GROMOS 43B1). B). The model of M6 tetramer after energy minimization in vacuum (GROMOS 43B1). 77

Figure 6. A). Structure model of variant M6. B). Structure alignment of PpADI WT model and M6 model with four loops 78

List of tables

Tables Page

Chapter 1

Table 1. ADI expression, enzymatic properties and medical applications. 3

Table 2. Crystal structures of ADI in protein data bank (PDB). 6

Table 3. Residues important for catalytic function of PaADI. 8

Chapter 2

Table 1. Improvement obtained from directed evolution or rational design for pH performance. 22

Chapter 3

Table 1. Primer sequences for site saturation mutagenesis. 36

Table 2. Activity of ADI variants towards arginine determined using citrulline colorimetric assay in cuvette format. 52

Table 3. Stability of PpADI variants in the presence of human serum. 55

Chapter 4

Table 1. Nucleotide and amino acid substitutions at position 38 71

Table 2. Nucleotide and amino acid substitutions at position 296 71

Table 3. Kinetic constants of wild type PpADI and variants. 72

Arginine deiminase (ADI)

1.1 Arginine deiminase (ADI)

Arginine deiminase (ADI, EC 3.5.3.6), an arginine-metabolizing hydrolase, catalyzes the hydrolysis of L-arginine to form citrulline and ammonia. This reaction is the first step in the L-arginine degradation pathway (ADH, scheme 1, (1). First, arginine is deiminated by arginine deiminase. The resulting citrulline is converted to carbamoyl phosphate and ornithine by ornithine transcarbamylase (EC 2.1.3.3), and finally the carbamoyl phosphate is used to phosphorylate ADP by carbamate kinase (EC 2.7.2.2), producing one ATP molecule. ADI is absent in humans but present in a wide range of bacterial species such as *Pseudomonas aeruginosa* (2), *Pseudomonas plecoglossicida* (3) and *Mycoplasma arginini* (4) and in parasitic protists such as *Giardia intestinalis* (5), *Trichomonas Vaginalis* (6), *Trichomonas fetus* (7), and *Hexamita inflate* (8). For pathogenic bacteria, ADI is required in arginine dehydrolase pathway for virulence and for energy production under anaerobic conditions (9, 10).

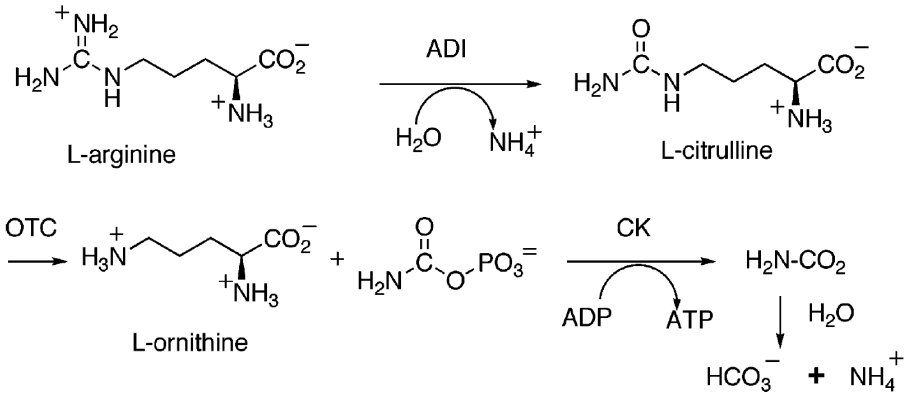

Scheme 1. Arginine dihydrolase pathway. OTC, ornithine transcarbamylase; CK, carbamate kinase.

The establishment of a high-level production system for ADI is an essential step for further research and development of this enzyme. After ADI was discovered from Mycoplasma in 1960s (11), various ADI genes have been cloned, expressed in *E. coli* strains, and the enzyme properties were also studied (Table 1).

Table 1. ADI expression, enzymatic properties and medical applications.

ADIs	Origin	Expression host/vector	Multimeric form	K_m; k_{cat}	Optimum pH	Specific activity	Medical application	References
MhADI (SYN1903)	*Mycoplasma hominis* PG21*	*E.coli* BL21 (DE3)/pET-47b	Dimer			0.618 U/mg (pH 6.5)	Human melanoma (G361), 0.036 U/ml for 50 % IC_{50}	Japan, Harasawa, 2009 (12)
MhADI	*Mycoplasma hominis* (ATCC 23114)	-	Dimer		6.0	35.5 U/mg (pH 6.0) ; 3.9 U/mg (pH 7.4)	Mouse melanoma (MH134) *in vitro*, 100 ng/ml for 50 % IC_{50}	Japan, Takaku, 1995 (13)
MhADI	*Mycoplasma hominis* (ATCC 14027)	-	Dimer	0.17 mM (pH6.6)				USA, Fenske, 1976(14)
MhADI	*Mycoplasma hominis*	*E.coli* BL21 (DE3)/pET25b		0.24 mM; 0.151 s^{-1}				China, Luo, 2007 (15)
MhADI	*Mycoplasma hominis*	*E.coli*				20 U/mg ADI (37℃). [a]	ADI-SS PEG_{20000}, human melanoma, human HCC	USA, Pheonix Pharmacologics, Inc., Clark, 2002 (16)
PaADI (PA5171)	*Pseudomonas aeruginosa* (ATCC 47085D)	*E. coli* BL21(DE3)/pET100	Tetramer	0.14±0.01 mM (pH 5.6)	5.6			USA, Dunaway-Mariano, 2005 (17)
PaADI	*Pseudomonas aeruginosa*	*E. coli* BL21 (DE3)/ pET SUMO				CARD-like domain, no catalytic activity	Human cancer cell line SKOV-3	USA, Chakrabarty, 2006 (18)
PpADI	*Pseudomonas plecoglossicida*	*E. coli* BL21 Gold-(DE3)/ pET42b		0.7 mM; 5.6 s^{-1} (pH 7.4, 0.5 M sodium phosphate buffer)	6.5	31.3 U/mg (pH 7.4, 0.5 M sodium phosphate buffer)		Germany, Schwaneberg, 2010 (3)

MaADI	*Mycoplasma arginini* (ATCC 23838D)	*E. coli* DH5α/PTTQ118				32.7 U/mg. [a]	Human umbilical vein endothelial (HUVE)	USA, Shen, 2002 (19)
MaADI	*Mycoplasma arginini* (ATCC 23838)	*E. coli* JM101/pADTc1	Dimer			33.6 U/mg (37℃, pH 6.5). [a]	Mouse hepatoma, 17 ng/ml for 50 % IC_{50}; mouse fibrosarcoma, 15 ng/ml for 50 % IC_{50}	Japan, Hayashi, 1994 (20)
MaADI	*Mycoplasma arginini* (ATCC 23838)					42 U/mg (37℃, pH 6.5); 29.9 U/mg (37℃, pH 7.4)	Mouse melanoma (MH134) *in vitro*, 10 ng/ml for 50 % IC_{50}	Japan, Takaku, 1995 (13)
MaADI	*Mycoplasma arginini* (ATCC 23838)	-					HUVE, neuroblastoma, retinoblastoma, osteosarcoma, 5~10 ng/ml for 50 % IC_{50}	Germany, Schweigerer, 1999 (21)
MaADI	*Mycoplasma arginini* (ATCC 23838)	-	Dimer	0.2 mM	6.0-7.5	50 U/mg	Mouse tumor carcinoma, fibrosarcoma and melanoma, 5~20 ng/ml for 50 % IC_{50}	Japan, Takaku, 1992 (22)
LlADI	*L. lactis* (ATCC 7962)	*E. coli* BL21Gold(DE3)/pGEM-T Easy	Trimer	8.67 mM	7.2	140.27 U/mg		Korea, Lee, 2007 (23)

[a] ADI was expressed in inclusion body and denaturation-renaturation had to be employed to get soluble protein.

1.2 ADI structure

In 1970s, Kakimoto et al. (24, 25) diffracted the first ADI crystals from *P. putida* through multiple-step chromatography followed by crystallization. Almost three decades later, the X-ray crystal structure of ADI from *P. aeruginosa* (PaADI, Figure 1A) (26) and *M. arginini* (MaADI, Figure 1B) (4) were solved to assist in understanding structure-function relationships. PaADI and MaADI share 27 % sequence identity and belong to guanidino group-modifying enzyme superfamily (GMSF). The catalytic triad (Cys-His-Glu/Asp) is conserved in members of the GMSF. Both crystal structures of PaADI and MaADI show a characteristic 5-fold pseudosymmetrical barrel with ββαβ subunits. Table 2 summarizes the crystal structures of PaADI and MaADI.

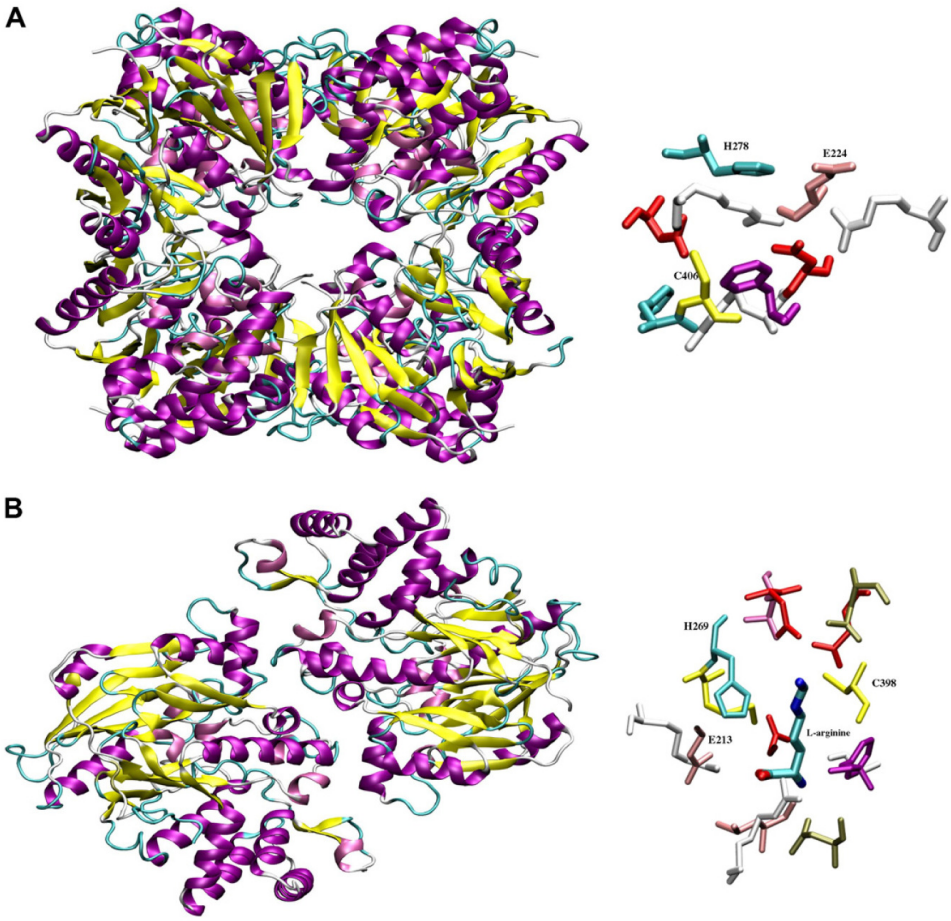

Figure 1. Structural of ADIs from *P. aeruginosa* and *M. arginini*. (A) PaADI (PDB ID: 1RXX) and stereo view of its catalytic triad (C406-H278-E224). (B) MaADI (PDB ID: 1S9R) and stereo view of its catalytic triad (C398-H269-E213) with substrate L-arginine (27).

Table 2. Crystal structures of ADI in protein data bank (PDB).

PDB code	Ligand in crystal structure	Description	Resolution (year)
2A9G	Arginine	Crystal structure of PaADI variant C406A in complex with L-arginine	2.30 Å (2005)
2AAF		Crystal structure of PaADI variant H278A forming a S-alkylthiouronium reaction intermediate	2.30 Å (2005)
2ABR		Crystal structure of PaADI variant D280A with L-arginine forming a S-alkylthiouronium reaction intermediate	2.9 Å (2005)
2ACI		Crystal structure of D166A arginine deiminase	2.50 Å (2005)
1S9R	Arginine	Crystal structure of MaADI covalently linker with a reaction in intermediate	1.60 Å (2004)
1LXY	Citrulline	Crystal Structure of MaADI covalently linked with L-citrulline	2.00 Å (2004)
1RXX		Crystal structure of MaADI	2.45 Å (2004)

MaADI was crystallized as a homodimer and its catalytic triad is formed by Cys398-His269-Glu213. MaADI has a catalytic domain and a five-helix bundle domain (Figure 3). The buried and compact substrate binding pocket is located approximately at the center of the molecule, from which a small solvent channel leads to the surface of the enzyme. The opening to the channel is located adjacent to the dimer interface region, which is at the opposite side of the 5-fold pseudosymmetric moiety of ADI. The shape and size of the channel does not permit transport of the substrate (L-arginine and end product (L-citrulline) in and out of the pocket. Substantial conformational changes in ADI are required to permit entry of the substrate and expulsion of the end product. The occurrence of "closed" and "open" form was suspected to be dependent on binding of substrate.

PaADI has a tetrametric structure with 1630 amino acid residues in total, which makes it the largest enzyme of its structural superfamily. The catalytic triad of PaADI is Cys406-His278-Glu224. Similar to MaADI, the active site of PaADI is

located in a narrow crevice formed by a network of charged residues. Ligand binding energy is derived from ion pair and hydrogen bonding interactions between active site residues and the guanidinium, carboxylate and ammonium groups of the substrate. The proposed substrate-binding model shows that the catalytic center contains abundant charged residues (e.g. Asp280, His405, Glu13 and Arg165). The ion pairing interactions between these residues contribute to the integrity and activity of ADI. In addition, Asp116, Asp227, Arg185, Arg401, His278, Glu118, and Glu224 are part of an extended charged network. The proposed catalytic mechanism suggests that the active site of PaADI is blocked by Arg401, and therefore a conformational transition is taking place upon the substrate binding. Based on the proposed reaction mechanism, Cys406 is as a key residue responsible for the nucleophilic attack on the guanidinium carbon atom of arginine. PaADI contains only one hydrophobic residue, Phe-163 and a Cys-406 with an unknown protonation state. The known functions of important residues are shown in Table 3, and the interactions between important residues and substrate arginine are shown in Figure 2.

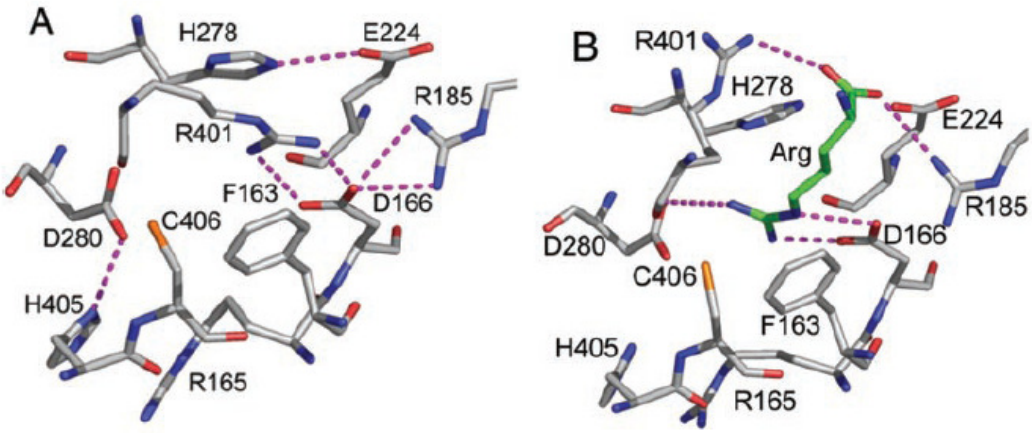

Figure 2. A. stereoscopic view of PaADI key active site residues. B. stereoscopic view of a modeled arginine substrate (green) docked in the active site of ADI. Atomic colors are red, oxygen; blue, nitrogen; yellow, sulfur; and gray, carbon. Ion pair interactions are shown as dashed lines (26).

Table 3. Residues important for catalytic function of PaADI (28, 29).	
Residues	Known/postulated function or comment
Cys406	Mounts the nucleophilic attack on the carbon atom of the guanidinium group of arginine
His278	Serves as a general base and activate the water molecule
Glu224	Modulate the ionization state of His278
Asp280	Interacts with the imidazole group of His405 F via the carboxylate group, which in turn interacts with Glu13. Invariant residue in all known ADIs
Asp280, Asp166	Fix the guanidinium group of the arginine substrate tightly by interactions with the carboxyl groups
Arg401, Arg185	Form ionic interaction with The carboxyl group of the arginine substrate
Phe163	Interacts with the hydrophobic part of arginine substrate
Glu13	Interacts His405 and is invariant in all known ADIs
His405	Sometimes is replaced by an arginine, as in the case of McADI. This may explain the low pH optimum of PaADI (5.6) in contrast to the neutral pH optimum of McADI, the enzyme that contains an arginine residue instead of His405
Arg165	Is fixed by electrostatic interactions with the main chain oxygen atoms of Thr408 and His405 and with the hydroxyl group of Thr-408
Arg401	Blocks the ADI active site via the side chain by forming an ion pair with the carboxyl group of Asp166 and occupies approximately the same position as the guanidinium group of an arginine substrate

The overall fold of MaADI and PaADI consist of five ββαβ modules in cyclical arrangement, generating a pseudo 5-fold symmetrical barrel and an additional 85-residue α-helical domain inserted between the first and the second ββαβ modules giving the typical “Clip-on-fan” moiety. The α-helical domain of PaADI mediates tetramer formation and the α-helical domain of MaADI was speculated to play a role in activating the series of reaction in arginine dehydrolysis pathway (4). Structural alignments by Chakrabarty et al. (18) demonstrated the unique 85 residue 5-α-helical bundle domain exhibiting structural similarity to the mammalian CARD (caspase recruitment domains)-containing proteins and this CARD-like domain is present only in the PaADI and MaADI but not in the other

GMSF members (Figure 3B). Furthermore, PaADI putative CARD-like domain induced apoptosis to cancer cells.

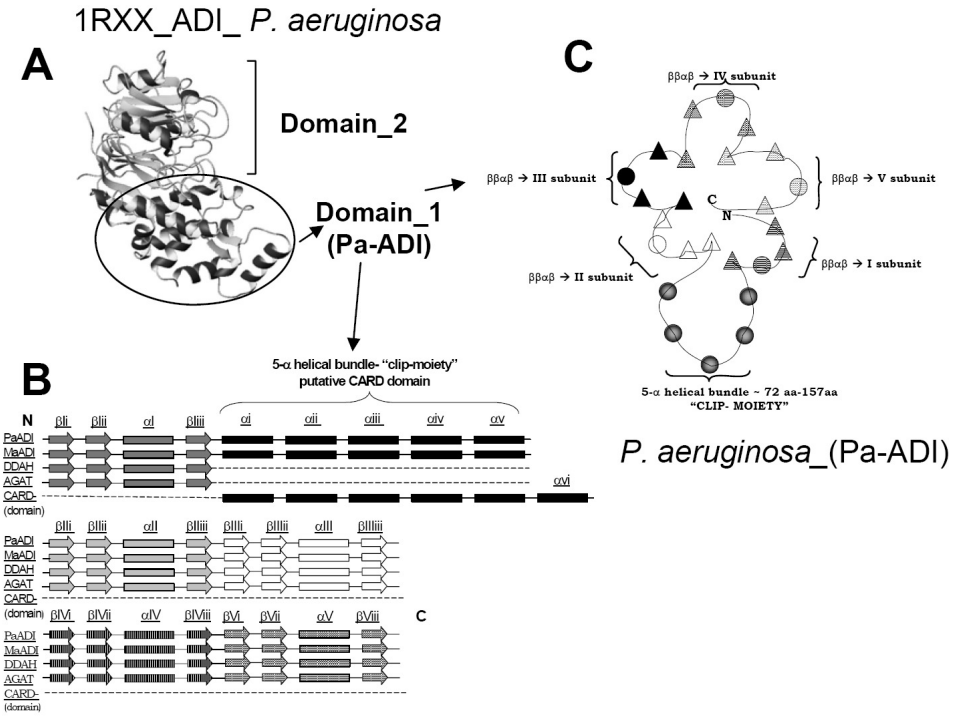

Figure 3. Structural characteristics of the PaADI. A. Ribbon drawing of PaADI (1RXX_A) highlighting the two domains. B. The presence of the CARD domain in PaADI and MaADI but its absence in other members of the GMSF (guanidino-group modifying superfamily) enzymes such as DDAH and AGAT, as shown from the structure-based sequence alignments. The CARD domain represents that of caspase-9. DDAH, dimethylarginine dimethylaminohydrolase; AGAT, arginine: glycine amidinotransferase. The β-strand and α-helices are shown as arrows and strips respectively. Roman numericals I to V are the five ββαβ subunits. The clip moiety (α-helical module) in Figure 3 is seen only in PaADI and MaADI which bears structural homology to the six-α-helical modules that form the CARD domain of the caspase-9 protein molecule. N, N-terminal; C, C-terminal. C. A schematic diagram showing the overall fold and topology of PaADI, as reported (18).

Comparison of substrate free and substrate bound structure of PaADI gives interesting insight into structure changes upon substrate binding (17). Pairwise superposition of the free wild-type PaADI (PDB code: 1rxx) and the mutant enzyme substrate complexes (PDB code: 2a9g) show that the overall fold of the structures remains similar, yet with some local changes. In particular, four loops (Figure 4) associated with the active site undergo conformational transitions not

related to crystal packing: loop 1 (residues 30-46), loop 2 (residues 178-185), loop 3 (residues 271-281, part of this loop is disordered in the apoADI structure), and loop 4 (residues 393-404). Residues adjacent to the substrate exhibit the most significant shifts. For example, the α-carbon atom of Leu41 (loop 1) shifts by 2.7Å and that of Arg185 (loop 2) by 1.8 Å; the α-carbon atom of His278 (loop 3) shifts by 0.9 Å and that of Gly400 (loop 4) by 4.4 Å. These are localized but mechanistically important conformational transitions that tighten the surrounding of the substrate. Simultaneously, substrate binding is accompanied by displacement of the side chain of Arg401 (loop 4) by more than 8 Å to enable access to the active site. The superposition of ADI and PAD4 ADI active site is shielded from the solvent by a long loop (residues 25-48 in PaADI) and the following two turns of α-helix (residues 49-56).

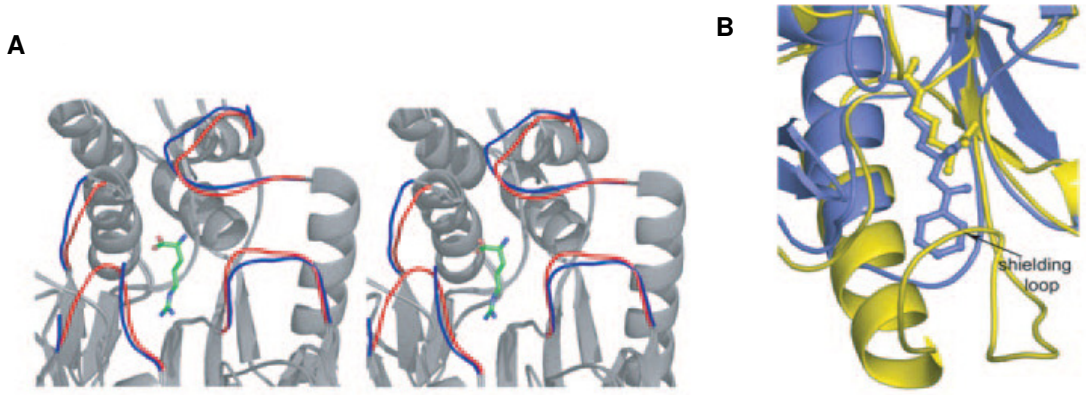

Figure 4 (A). Stereoscopic view of ADI in the unbound and bound states. Superposed molecules are colored gray where the trace of the polypeptide chain is similar in both structures. For regions exhibiting differences, loops of the apoADI structure are highlighted in blue, and loops of the ADI structure complexed with arginine are highlighted in red. 4(B). Structural relationship between ADI (yellow) and PAD4 (cyan) (17).

1.3 Catalytic reaction mechanism of ADI

The overall reaction catalyzed by ADI is the hydrolytic substitution of the ηNH_2 group from the guanidinium group Cζ of L-arginine, leading to citrulline and ammonia (Figure 5). Herzberg (17) and Arnold (4) proposed ADI catalysis mechanism for PaADI (Figure 5) and MaADI, respectively. Basically, both of the proposed mechanisms are composed of three main steps: 1) thiol group of

Cys406 mount a nucleophilic attack on the guanidinium group of arginine and a proton is transferred first to ηNH$_2$ group; 2) water molecule is activated by His278 and followed by attacking the covalent intermediate to replace and release NH$_3$; 3) the C-S covalent bond between enzyme and the resulting citrulline is cleaved and thus end product citrulline is released and free enzyme is generated for next catalytic cycle.

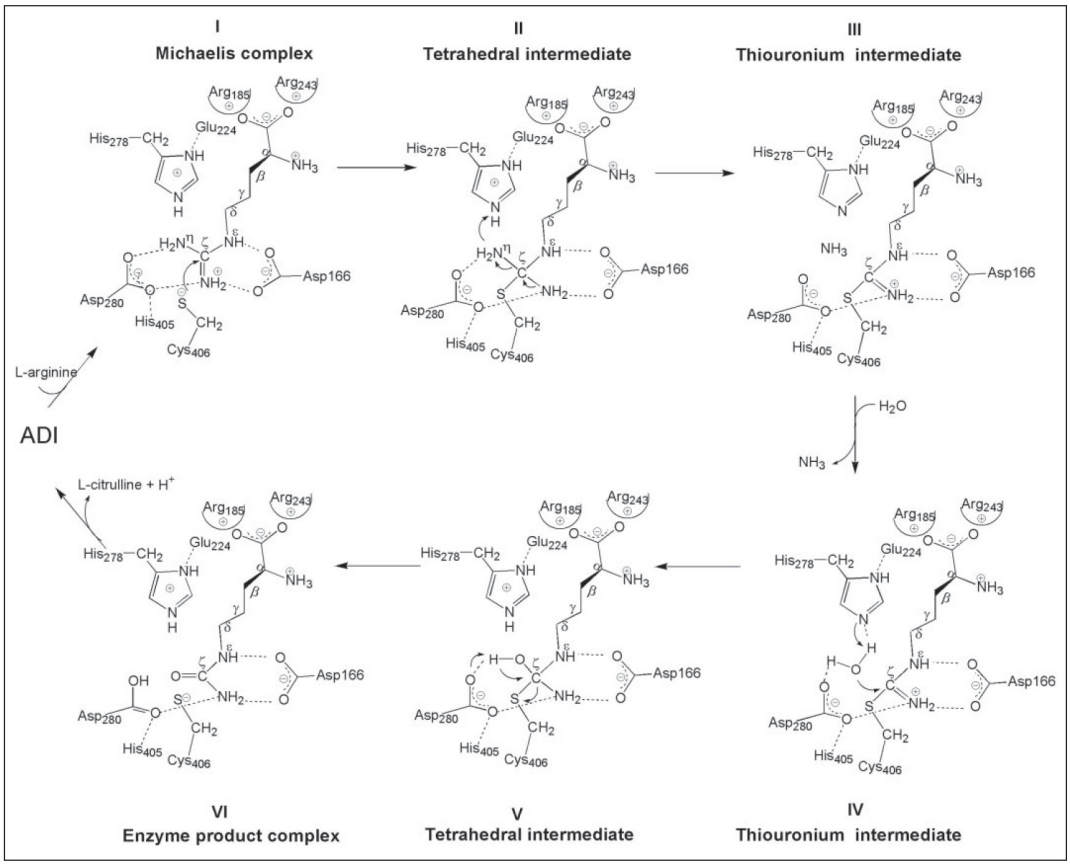

Figure 5. Mechanism of PaADI catalysis of arginine to citrulline and ammonia (17).

1.4 Anti-tumor application of ADI

Amino acids depletion is one type of targeted therapy for human cancers which are auxotrophic for a particular amino acid. Amino acids degrading enzymes, such as asparaginase (30), methioninase (31), arginase (32), arginine deiminase (27), phenylalanine ammonialyase (33) and tryptophanase (34) have been

studied for inhibition of tumor cells *in vitro*. The most representative anticancer enzyme is asparaginase, which is particularly effective in acute lymphoblastic leukaemia. PEG asparaginase is commercialized for acute lymphoblastic leukaemia treatment (Oncaspar®, pegaspargase) (35). However, asparaginase treatment is sometimes accompanied by serous side-effects including anaphylactic shock, coagulapathies as well as liver and pancreatic toxicity (36).

Arginine is an important amino acid involved in the synthesis of a wide range of peptides and proteins, production of creatine and nitric oxide, and a myriad of metabolic pathways and cellular events. It is a precursor of proline, polyamines, glutamine, glutamate, and other neurotransmitters, such as g-aminobutyric acid and also serves as a substrate for two important enzymes, arginase and nitric oxide synthetase (37). Arginine is an indispensable amino acid to children but a semi-essential amino acid in adult humans since many adult somatic cells can synthesize it from citrulline in two steps via urea cycles (Figure 6). The enzyme argininosuccinate synthetase (ASS) catalyzes the conversion of citrulline and aspartic acid to argininosuccinate which is then further converted to arginine and fumaric acid by argininosuccinate lyase (ASL). Arginine can be degraded to ornithine by the urea cycle enzyme arginase. Ornithine is then converted back to citrulline by ornithine carbamoyl transferase (OTC) and then recycles back to arginine from citrulline by ASS/ASL. Thus, the ability to regenerate arginine from citrulline depends on the amount/activity of ASS and ASL, which are tightly coupled. The sensitivity of cells to arginine deprivation depends on the ability of ASS and ASL to regenerate arginine from the alternative intermediate (ornithine, citrulline and argininosuccinate) in the urea cycle.

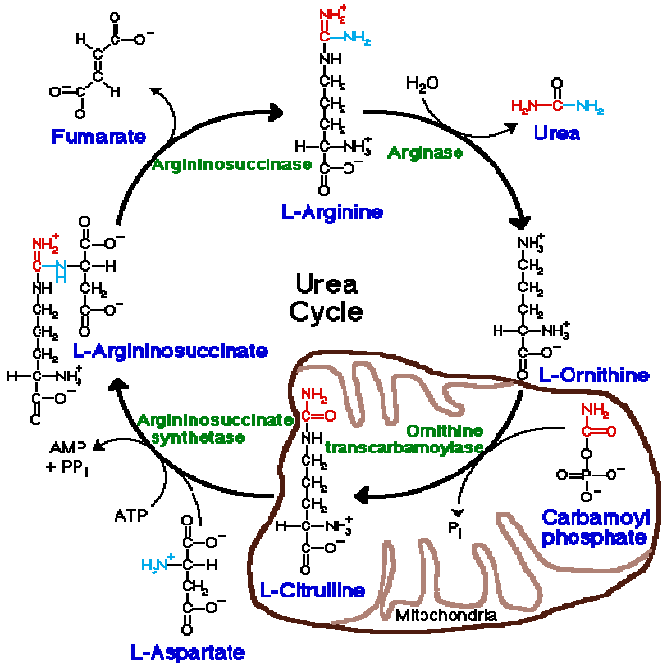

Firgure 6. Urea cycle. Argininosuccinate synthetase (ASS) catalyzes the conversion of citrulline and aspartic acid to argininosuccinate which is then further converted to arginine and fumaric acid by argininosuccinate lyase (ASL). Arginine can be degraded to ornithine by the urea cycle enzyme arginase. Ornithine is then converted back to citrulline by ornithine carbamoyl transferase (OTC) and then recycles back to arginine from citrulline by ASS/ASL.

Arginine begins to become limiting at ~10^{-4} M, whereas other amino acids can sustain growth at 10^{-5}-10^{-6} M. Wheatley et al. showed that most tumour cell lines die considerably more quickly during arginine deprivation than in the absence of any other single (or group of) essential amino acids (38). Since 1930 for the first time arginine known is essential for the growth of some forms of cancer, the potential of arginine degrading enzymes as therapeutic agents was recognized, investigated and employed for arginine auxotrophic tumor treatments. Enzymes capable of depleting arginine *in vitro* include arginase existing in human liver, arginine decarboxylase from bacterial, plant and human, and ADI from microorganism.

Arginine decarboxylase converts arginine to agmatine, which is toxic at high plasma concentration. Furthermore, arginine decarboxylase has a short half-life and it loses virtually all enzymatic activities upon pegylation though pegylation of

arginine decarboxylase is inefficient because not enough lysine residues for polyethylene glycol to attach (39).

Arginase is limited for anti-tumor application because of its low substrate affinity (K_m value 2-4 mM; plasma arginine 100-120 μM), short circulatory half-life (10-15 min) and sub-optimal enzymatic activity at physiological pH (alkaline pH optimum, pH 9.3)(40). Despite these disadvantages of arginase, Lam et al. reported remission of hepatocellular carcinoma induced by systemic release of endogenous hepatic arginase (41) and Leung et al. proved pegylated recombinant human arginase (rhArg-peg 5,000mw) can inhibit ASS-positive HCCs while ADI can not (42).

In addition, ADI, another arginine-degrading microbial enzyme, has various biological activities including anti-proliferation, anti-angiogenesis and inhibition of inducible nitric oxide synthase (iNOs). Figure 7 summarizes how ADI affect many arginine-related cellular functions. ADIs (Table 1) have been shown to have strong *in vitro* and *in vivo* inhibition for arginine auxotrophic tumors (e.g. hepatocellular carcinomas (HCCs), melanomas, retinoblastoma (43), prostate cancer(44)) and ADI from *M. hominis* (MhADI) is currently under clinical trial for HCC (phase II) (45) and melanomas (phase I/II) (46). Studies on human lymphatic leukemia cell lines confirmed ADI's anti-angiogenic activity. Among all the ADIs, MhADI and MaADI were studied most intensively (Table 1).

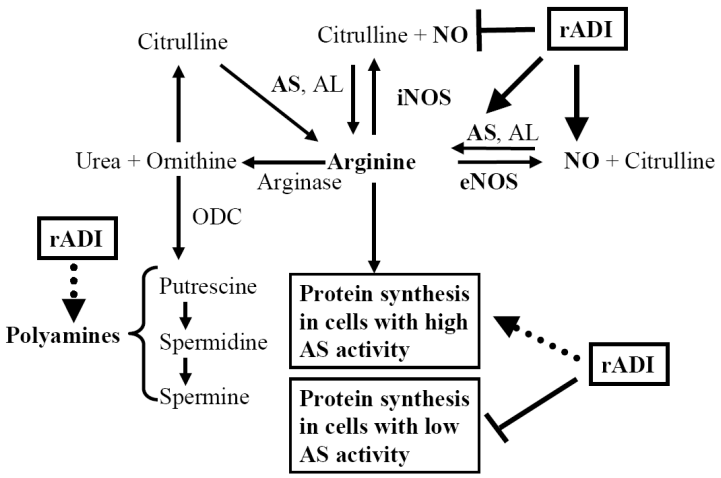

Firgure 7. Summary of ADI effects on arginine-related cellular functions. rADI inhibits NO production via iNOS, but potentiates NO production via eNOS in the cultured endothelial cell model. rADI enhances or inhibits AS activity in different cells. rADI inhibits de novo protein synthesis in cells with low AS activity, but not in cells with high AS activity. Polyamine synthesis was not significantly affected by rADI, even in cells with low AS activity. Arrow representation: solid, potentiates; blocked, inhibits; dotted, no effect (47).

In 1999, US Food and Drug Administration (FDA) designated ADI-PEG-20 orphan drug status for treating HCC and invasive malignant melanomas. In 2005, also the European Agency for the Evaluation of Medicinal Products (EMEA) also granted ADI-PEG-20 orphan drug status for HCC. Phase II trials of ADI-PEG-20 in patients with metastatic hepatocellular carcinomas have shown that the drug is safe, well tolerated, and may benefit patients with unresectable HCC. Izzo and coworker suspected that combination therapies of arginine deprivation and growth inhibition via kinase inhibitors might improve the survival rate further. Additionally, ADI enhances radio sensitivity of human mammary adenocarcinoma (MCF-7 cells) (48), exerts anti-proliferative as well as anti-angiogenic activities and inhibits the growth of viruses such as HIV-1 and hepatitis (49, 50). Current research efforts are focused on ADI's *in vivo* inhibitory effect towards leukemia, melanoma, prostate cancer, renal cell carcinoma, and human umbilical vein endothelial cells (HUVEC) (19, 44, 51-53), clinical trials for HCC (phase II) (45) and melanoma (phase I/II) (46), and tumor inhibitory mechanisms of ADI (54).

The effectiveness of ADIs as anti-tumor agent depends on their enzymatic properties (such as K_m, k_{cat}, optimum pH, stability at neutral pH), selectivity on tumor cells, stability in blood circulation and immunogenicity. Pegylation (35) has been effective in reducing their immunogenicity in animal and increase their stability to various hydrolytic enzymes in plasma. Directed evolution as powerful algorithm to design proteins allows improving all properties that can be reflected in a screening system through iterative rounds of diversity generation and screening. Small libraries of a few thousand variants are often sufficient to find improved variants (55) even without rational understanding of the targeted property. The first example of directed ADI evolution by our group (3) provides a simple and effective screening system to improve activity of PpADI at physiological pH.

1.5 Conclusion

ADI-based arginine deprivation is a novel and promising targeted approach to the treatment arginine auxotrophic tumors, in particular, melanoma, hepatocellular carcinoma and leukemia. Certain mesotheliomas and renal cell cancers were also proved to be sensitive to ADI therapy. Due to its low incidence of major side effects (myelosuppression and gastrointestinal toxicity or other major organ toxicity) arginine deprivation treatment should be combined with other anticancer treatments to increase the response rate. Reengineering of ADI by protein engineering is a promising strayegy to tailor ADI properties for demands in medical applications. Solved ADI crystal structure enables to understand structure function relationships and to guide protein engineering.

Directed evolution

2.1 Introduction to directed evolution

Enzymes are increasingly being used in the generation of products that are traditionally made using chemical synthesis and the field continues to expand its horizons, particularly as applied to the synthesis of the fine chemicals and pharmaceuticals (56, 57). Naturally occurring enzymes are often not designed for the applications of interest, since after all they are evolved in nature for a purpose other than being the catalysts of industrial processes. Directed evolution, rational design and biodiversity screening and combined approches are the main strategies to reengineer enzymes for addressing application demands. Directed evolution has emerged as a powerful enabling method for improving enzyme properties in iterative cycles of diversity generation and screening (Figure 1).

A main advantage of directed evolution compared to rational design is that it does not require structural or mechanistic information for protein optimization. Directed protein evolution has been successfully used for altering and improving protein properties (solubility, expression, enantioselectivity, stability and activity in unusual environment, allosteric interactions, tolerance to pH), as well as for regulating other molecules and systems, including RNA, DNA regulatory elements, biosynthetic pathways and genetic regulatory circuits (58-60).

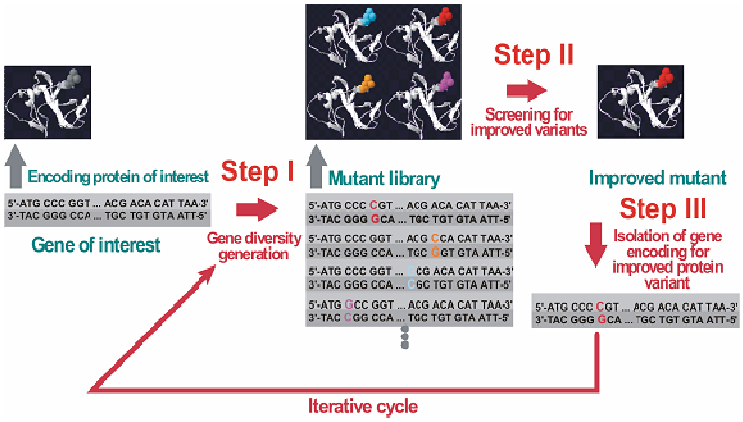

Figure 1. Procedure of a directed evolution experiment. It involves three key steps: 1) selection a good starting sequence and mutating the parent to create a library of variants; 2) identification variants with improved function and 3) isolation of gene encoding for improved variant and repeating the process until the desired function is achieved.

A parent sequence (or sequences) is chosen based on its perceived proximity to the desired function and its evolvability (the ability of a protein to adapt in response to mutation and selective pressure). A parent protein for directed evolution should exhibit enough of the desired function that small improvements can be reliably discerned in a high-throughput screen.

Variants library should be generated with high probability of finding improved variants given the screening capacity. With a high-throughput screening method, a library can be constructed to generate the large potential improvement. Arnold and coworkers(61) showed that very low mutation rates result in many functional sequences but only a small number are unique sequences, however very high mutation rates produce diverse sequences but few retain function. Schwaneberg and coworkers(62) reviewed random mutagenesis methods, focused library generation methods and computational tools for high-quality mutant libraries generation. Schwaneberg and coworkers (63) also summarized criteria for an ideal mutagenesis methods: unbiased mutational spectrum, controllable mutation frequency, consecutive nucleotide substitutions or codon-based substitutions, enable subset mutagenesis (e.g. introduction mainly positively or negatively charged amino acid), independent of gene length, technically simple and reproducible, and economical.

Screening is used to identify library members improved in the targeted property. Identification of improved variants though selection or screening is “analogous” to evolutionary pressure in natural evolution (i.e. only the fittest survive). As the word “directed” in directed evolution implies, laboratory evolutionary pressure is defined and applied by the researcher in screening system. Gradually increasing the selection pressure or evolving against a series of intermediate challenges often accumulates useful single mutations and yields desired variants (64).

Traditional methods for screening employ microtiter plate formats (96-well, 384-well, 1,536-well (65) and even 1,000,000-well (66)) or solid phase assay (agar plate, filter paper and nitrocellulose membrane), which typically enable the screening of no more than 10^6 variants by using robotic automation (67). Sometimes, fast and universal analytic methods like HPLC (68) or GC-MS (69) are utilized for performing an efficient screen of a non-natural substrate. However, the number of screened mutants is limited to 10^4-10^6. In recent years flow cytometry systems (67, 70, 71) have become increasingly attractive, especially after the development of emulsion technology offering compartmentalization and high throughput up to 10^7/h. In addition, Weitz and coworkers (72) recently reported a promising ultrahigh-throughput screening in drop-based microfluidics, by which one can screen a library of 10^8 in about 10 h. Dijkhuizen et al. compared in a review (73) six kinds of library screening strategies (Figure 2). Selection techniques rely on a direct link between cell growth and improved or acquired enzyme function and therefore it is limited to engineering detoxifying enzymes (e.g. b-lactamase) or enzymes that synthesize essential nutrients for cell growth and survival. The traditional microtiter plate screenings are medium-throughput and the most simplistic format of screening. It involves the incubation of colonies with the substrate of targeted enzyme. The crucial factor with this screening technique is that substrate conversion creates a visual signal, such as fluorescence or color, to identify colonies expressing an enzyme with desirable properties. Microtiter plate based screenings are the most commonly applied method in identifying desirable enzyme variants. Microtiter plate based

screenings enable the use of various analytical tools and in the mean while they offer a great dynamic range. Their screening capacity is usually limited to less than 10^4 variants per day. Screening based on microfluidic device and sorting device is a new screening platform for directed evolution, which offers ultra-high-throughput. It allows the discriminate between wild-type and a less active mutant and allows for the addition of substrates and quenchers at desired time thus extending the scope of directed evolution screening strategies. Cell as micro-rector, cell surface display and *in vitro* compartmentalization technology are also FACS (fluorescence-activated cell sorting system) dependent methods for high-throughput screening and allow 10^9-10^{10} screening capacity.

Once improved enzymes are identified, encoding genes are isolated and subjected to further iterative cycles of mutation and screening in order to accumulate beneficial mutations until the targeted improvement is hopefully achieved. The number of iterations required depends on the starting point, the protein fold and the selected properties which determine the possible mutational load and achievable improvement.

Four accepted requirements for successful directed evolution (http://www.che.caltech.edu/groups/fha/) are, 1) the desired function must be physically possible; 2) the function must also be biologically, or evolutionarily, feasible. In practice, this means that there exists a mutational pathway to get from here to there through ever-improving variants (see above). A good experiment will maximize the likelihood; 3) Suitable host (*E. coli* or *S. cerevisiae*) which allows functional expression of more than 10^6 variants per µg of DNA. 4) A rapid screen or selection that reflects the desired function. How rapid the screen must be depends on how rare mutations leading to the desired property are and how many must be accumulated to achieve the desired result.

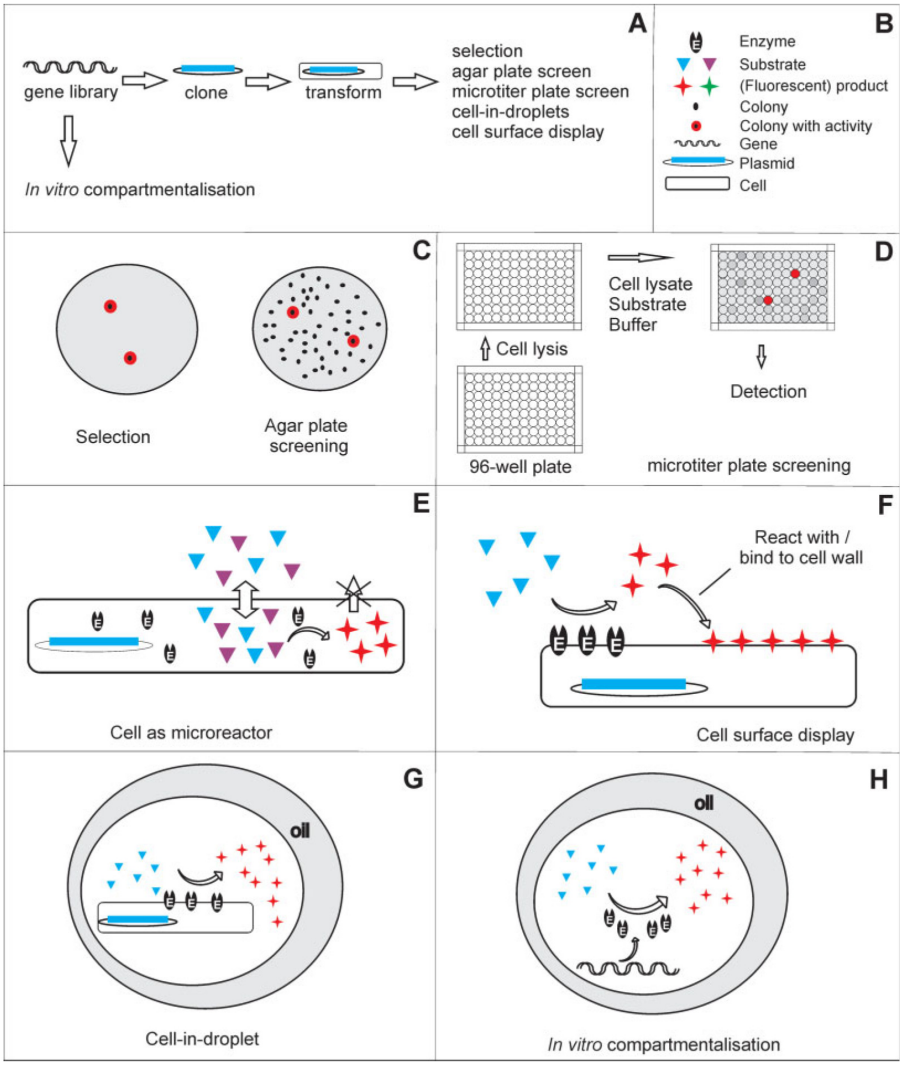

Comparison of screening and selection technologies

Strategy	Library size	Advantage	Disadvantage
Selection	$\sim 10^9$	Yields desirable variants only	Only possible if activity gives growth advantage
Agar plate screen	$\sim 10^5$	Simple to operate	Limited dynamic range
Microtiter plate screen	$\sim 10^4$	All analytical methods possible Excellent dynamic range	Relatively low screening capacity
Cell-in-droplet screen	$\sim 10^9$	Large libraries	Fluorescence detection and DNA modifying enzymes only
Cell as microreactor	$\sim 10^9$	Large libraries	Fluorescence detection only
Cell surface display	$\sim 10^9$	Large libraries	Fluorescence detection only
In vitro compartmentalization	$\sim 10^{10}$	No cloning steps Large libraries	Fluorescence detection and DNA modifying enzymes only

Figure 2. Overview of screening technologies. (A) Experimental steps from obtaining the gene library as PCR product to the actual screen. Note that cloning and transformation efficiency are often limiting library size; (B) Explanation of symbols; (C) Cell growth/survival selection and agar plate screening; (D) Microtiter plate screening; (E) Cell as micro-reactor; (F) Cell surface display; (G) Cell-in-droplet; and (H) *In vitro* compartmentalization (73).

2.2 Directed enzyme evolution for pH tolerance of enzymes

Application of enzymes in processes at a specified pH necessitates protein engineering to change their pH performance. Directed evolution and rational design method were applied to improve enzyme specific activity at certain pH or shift their pH profiles. Some representative success stories of directed protein evolution improving pH performance are summarized in Table 1.

Table 1. Improvement obtained from directed evolution or rational design for pH performance.

Enzymes	Mutagenesis methods	Screening methods	Improvements	References
Human β-glucuronidase	EpPCR and saturation mutagenesis	Flow cytometry	60-fold more active (k_{cat}/K_m) at pH 7.0 and were up to an order of magnitude more effective at catalyzing the conversion of two structurally disparate glucuronide prodrugs to anticancer agents	2008 (74)
Bacterial xylanase	DNA shuffling	Agar plate assay	About 5-fold improvement of specific activity at pH 9.0	2008 (75)
Human pancreatic lipase	EpPCR	Agar plate and microtiter plate assay	1.5-fold of activity improvement at acidic pH	2010 (76)
Bacterial arginine deiminase	EpPCR and site directed mutagenesis	Microtiter plate assay	pH optimum shifted from pH 6.5 to pH 7; 4-fold of activity improvement at pH 7.4	2010 (3)
Bacterial α-amylase	EpPCR	Microtiter plate assay	5-fold higher activity at pH 10 than wild type	2003 (77)
Eukaryote D-pantonohydrolase	EpPCR and DNA shuffling	Agar plate assay	10.5-fold higher specific activity and retain 85% of its original activity after incubation under low pH	2006 (78)
Vanadium chloroperoxidase	EpPCR, site saturation mutagenesis and site directed mutagenesis	Microtiter plate assay	About 100-fold improvement of specific activity at pH 8	2006 (79)
Bacterial class-A non-specific acid phosphatase (PhoN)	Site directed mutagenesis		1.6-fold of activity improvement over broder pH range	2006 (80)
Aspergillus niger PhyA phytase	Site directed mutagenesis		pH shifted from 5.5 to 3.8 (1.7 unit); 2.66 -fold improvement of activity at pH 3.5 than wild type.	2006 (81)
Bacillus cereus β-amylase	Site directed mutagenesis		pH optimum shifted to pH 4.2-4.8 by 2 pH units.	2004 (82)
Phytase	Site directed mutagenesis		pH optimum shifted by 0.5-1 pH unit; a slight increase in maximum specific activity	2002 (83)
Alcohol dehydrogenase	Site directed mutagenesis		pH optimum shifted from 7.8 to 9.0; about 2-fold improvement of maximum activity at pH 9.0 than that of wild type	1991 (84)

Many examples of rational reengineering of an enzyme pH optimum exist (Table 1). For shifting the pH optimum, a deep understanding of molecular dynamics is essential part of understanding enzyme flexibility. Rational design method successfully shifted enzyme pH profile. pH dependence of an enzyme is determined by the ionization of the catalytic groups, which is affected by various interactions involved in their microenvironments. In order to catalyze certain reactions, ionizable residues in active site should act as nucleophile or acid/base catalyst and they need to maintain proper ionization state for proper activities of proteins. The p*K*a value of the proton donor and the catalytic nucleophilic residue are therefore limiting the pH range at which the enzyme can function, and therefore pH-dependent activity can be differed by the p*K*a of the key residues. The p*K*a value of the residue is governed by intrinsic acidity of the functional group and other factors (electrostatic interaction from neighboring and the heterogeneous dielectric environment in the protein solution system). The electrostatic potential generated by the charged titratable residues affects the ground state of the protein, such as stability, binding to ligands and p*K*a values of ionizable groups. The electrostatic potential of proteins can be calculated by using computational procedures (Delphi, UHBD, CHARMM) and can be increased or decreased through mutations. For shifting the pH optimum of enzymes, many researchers have tried to substitute catalytic residue by site-directed mutagenesis (Table 1).

Yoo and coworkers (85) analyzed the relation between the shift of pH optimum and change in electrostatic potential due to mutation using Delphi. They identified key residues of xylanase responsible for electrostatic potential of catalytic residues but not affecting the catalysis directly. The latter hypothesis was proven by site directed mutagenesis in a later report. Wyss and coworkers (83) summarized strategies for enzyme pH profile modification, 1) replacement of ionizable groups that are directly involved in substrate or product binding and/or catalysis by nonionizable ones or by amino acids with different charge or p*K*a values; 2) replacement of residues that are in direct contact with residues

mentioned in 1) by forming hydrogen bonds and/or salt bridges; 3) alteration of longer-range (indirect) charge-charge interactions by modification of the surface charge of the enzyme.

When there is no structure-function relationship information available for an enzyme, directed evolution is the best option to tailor the pH performance of enzyme for application demands (Table 1). Directed evolution allows improving all properties that can be reflected in a screening system through iterative rounds of diversity generation and screening. Small libraries of a few thousand variants are often sufficient to find improved muteins even without rational understanding of the targeted property (76, 86). Using MTP assay, epPCR mutant libraries with a ratio of 50 % active and 50 % inactive clones have often been used successfully in directed evolution, improving enzyme properties by gradual changes (one or two amino acids changes per round of mutagenesis and screening).

2.3 Directed enzyme evolution for medical application

Directed evolution has been very useful for improving enzymes for industrial needs. In recent years, there is also growing number of enzymes applied for therapeutic purpose. For the development of protein therapeutics, directed evolution started to be used to tailor enzyme properties in medical field, for example drug delivery (87, 88) and has proven to be a useful tool for generating protein variants with enhanced therapeutic potential (88), for example, improving the effectiveness of therapeutic enzymes, antibodies, vaccines and viruses. Here, the improvements of therapeutic protein for anti-tumor application by directed evolution are discussed in more details.

2.3.1 Prodrug enzymes for tumor chemotherapy

Prodrug cancer chemotherapy has attracted considerable interest due to the possibilities it provids to overcome various barriers to drug formulation and delivery (such as poor aqueous solubility, chemical instability, insufficient oral

adsorption, rapid pre-systemic metabolism, inadequate brain penetration, toxicity and local irritation) (89). Examples of such drugs currently in use in cancer treatment include 5-fluorocytosine, cyclophosphamide, capecitabine, mitomycin C, and AQ4N (90). However, the side effects of prodrug therapy remain a serious concern which arises from the fact that noncancerous cells also possess the capacity to degrade them. This has triggered the interest to generate more effective prodrug-activating enzymes so that prodrugs can kill tumor cells at concentrations that generate little or no side effects. Further goals are to design more powerful and tumor-specific drugs, and to devise more effective methods for delivering them specifically to tumors.

By applying directed evolution through the technique of error-prone PCR, Martin and coworkers (90) indentified YieF variant exhibiting >5-fold increased capacity to kill HeLa cells. Furthermore, YieF variant was proved to be effectively delivered to tumor cells using a strain of *Salmonella typhimurium* (SL 7838).

Human β-glucuronidase, due to low intrinsic immunogenicity in humans, is an attractive enzyme for tumor-specific prodrug activation. However its utility is limited by low activity at physiological pH. Roffler and coworkers (74) developed a high-throughput screening procedure for enzymatic activity based on the stable retention of fluorescent reaction product in mammalian cells expressing properly folded glycoproteins on their surface. This procedure was utilized to screen error-prone PCR and saturation mutagenesis libraries to isolate β-glucuronidase tetramers that were up to 60-fold more active (k_{cat}/K_m) at pH 7.0 and were up to one order of magnitude more effective at catalyzing the conversion of two structurally disparate glucuronide prodrugs to anticancer agents.

2.3.2 Oncolytic viruses for tumor chemotherapy

Viral-mediated oncolysis is a novel cancer therapeutic approach with the potential to be more effective and less toxic than current therapies due to the agents' selective growth and amplification in tumor cells. To date, these agents

have been regarded as highly safe in patients but have generally fallen short of their expected therapeutic value as monotherapies.

Consequently, new approaches to generate highly potent oncolytic viruses are required. For the latter purpose, Hermiston and coworkers (91) developed a new method and termed it also ‘‘Directed Evolution’’ for creating highly potent oncolytic viruses. Viral serotypes representing Ad subgroups B-F were pooled and passaged twice on sub-confluent cultures of the target tumor cell lines at a particle-per-cell ratio of approximately 200 to invite recombination between serotypes (Figure 3). Supernatants from the second round of the high viral particle-per-cell infection of sub-confluent cultures were then used in a 10-fold dilution series to infect confluent T-75 tissue culture flasks of target tumor cell lines PC-3, HT-29, Panc-1 and MDA-231. Using this ‘‘Directed Evolution’’ methodology, the novel generated chimeric oncolytic virus ColoAd1 demonstrated ~ 2 log increase in both potency and selectivity when compared to ONYX-015 on colon cancer cells. *In vivo* and *ex vivo* studies therefore validated the innovative general approach for deriving clinically-relevant and potent anti-cancer virotherapies.

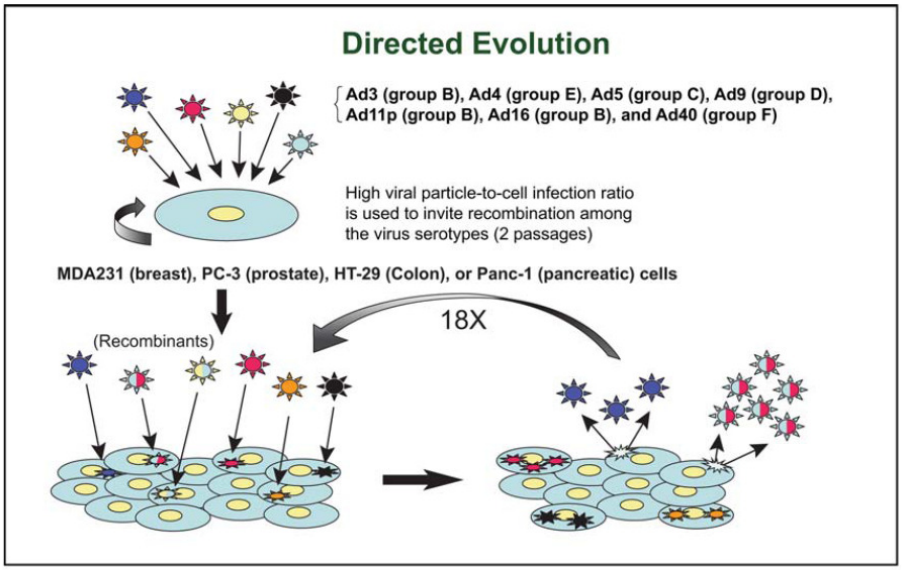

Figure 3. Hermiston’s “Directed Evolution” process of viruses and derivative viral pools (91).

2.3.3 Amino acid depriving enzyme for anti-tumor applications

Naturally available enzymes are usually not optimally suited for therapeutic purposes. This incompatibility often relates to the stability or activity of the enzymes under body conditions.

Despite many successful efforts to broaden the understanding of the structural basis of protein stability, there is still no universal strategy to stabilize protein by a limited number of rationally designed mutations. Well-known and reasonably successful types of rational engineering work include substitutions that increase rigidity (e.g. substitute amino acid Xxx with Pro or substitute Gly with other amino acid Xxx or the introduction of disulfides). These substitutions have effects on the entropy of the unfolded state, improvement of molecular packing (e.g. shortening of loops, improvement of interactions in the hydrophobic core, for example, by the removal of internal cavities), modification of surface charge networks or reinforcement of a higher oligomerization state.

Directed evolution provides a powerful approach for improving thermostability and does not need understanding of structure-function relationship. Most strategies for screening for enzyme stability rely on measuring residual enzyme activity before and after exposure to a denaturing challenge (e.g. high temperature, organic solvents, extreme pH) (92).

Bacterial L-asparaginases have been used as therapeutic agents in the treatment of lymphoblastic leukaemia. The main restrictions to the therapeutic use of L-asparaginase include its premature inactivation. As a result frequent injections are required to maintain therapeutic levels. Repeated injections and high dose can cause several types of side reactions from mild allergies and the development of immune responses to dangerous anaphylactic shocks (93). Enhancing the stability of L-asparaginase by protein engineering improves its body-residence time, and thereby minimizes immunosuppressive effects by lowering the therapeutic dose. Labrou and coworkers (94) obtained a

reengineered L-asparaginase with enhanced thermal stability. Single mutation on the surface of the protein resulted in ~10 degree increased T_m value (half-inactivation temperature). The thermostable variant has to be tested further on animals and/or humans in order to be advanced to a potent therapeutic drug.

Another example of a reengineered amino acid-deprivating enzyme is PpADI. PpADI is a promising anti-tumor enzyme however with a non-physiological optimal pH and relative high K_m value which hindering its medical application. By directed evolution and site saturation mutagenesis, PpADI variants with higher activity at physiological pH and at low arginine concentration of were obtained with improved properties to become a potent anti-tumor drug (see chapter 3 and chapter 4). *In vitro* and *in vivo* test of the improved variants are required to evaluate the anti-tumor effectiveness.

2.3.4 Affibody molecules for cancer prognosis

Affibody molecules represent a new class of affinity proteins that are based on the Z-domain scaffold derived from staphylococcal protein A (95). Among the scaffold proteins, Affibody molecules constitute the smallest non-cysteine-containing protein scaffold. The small size (~ 7 kDa), robust structure, and straightforward production procedures (either by recombinant production in bacteria or by chemical synthesis) make Affibody molecules attractive targeting agents for *in vivo* radionuclide imaging (96) as well as for various biotechnological applications (97, 98). The small size offers a convenient affinity maturation principle. Gene synthesis allows randomizing the whole gene to generate diverse mutant library. The potential use of radiolabeled Affibody molecules for high-contrast radionuclide imaging of biomarkers has been demonstrated in preclinical studies and in pilot clinical studies. Affibody molecules are non-immunoglobulin-derived affinity proteins based on a three-helical bundle protein domain.

Several of affinity proteins have been investigated for both *in vivo* diagnostics and therapy of tumor in radionuclide molecular imaging. Affinity proteins in tumor-targeted therapy can affect tumor progression by altering signal transduction or by delivering a payload of toxin, drug or radionuclide. EGFR (epidermal growth factor receptor), one of the receptor in ErbB family, has been extensively studied as biomarkers in tumor targeting and over expressed in various malignancies, associated with poor patient prognosis and are therefore interesting targets for solid tumors. High affinity and especially slow dissociation rate are important for obtaining high contrast images. Affinity in the low nanomolar range is considered as a prerequisite for successful use of peptide-based tracers.

Ståhl and coworkers (99) described the affinity maturation procedure for the generation of Affibody molecules binding with high affinity and specificity to EGFR. The library for affinity maturation was constructed using a single oligonucleotide for the rerandomization of desired positions. The new binders were selected with phage display technology and the best second-generation binders were characterized *in vitro* using real-time biospecific interaction analysis (BIA) for their binding to recombinant EGFR and with flow cytometry for their binding to native EGFR. Second-generation binders achieved an approximately 30-fold improvement in affinity (K_d = 5-10 nM) for the soluble extracellular domain of EGFR in biospecific interaction analysis using Biacore.

2.3.5 Interferon for anti-tumor applicaiton

Alpha interferons (IFN-as) are members of the diverse helical-bundle superfamily of cytokine genes, which have potent antiviral and antiproliferative activities and therefore can be used as anticancer and antiviral agents. However, doselimiting toxicity, receptor cross-reactivity, and short serum half-lives significantly reduce the clinical use of many of these cytokines.

Patten and coworkers (100) performed a family shuffling experiment with over 20 human interferon-α (Hu-IFN-α) genes. Antiviral assay and proliferation assay

were used to indentify clones with improved activity on Hu-IFN-α receptor. One clone showed 285,000-fold improved activity relative to Hu-IFN-α2a and 185-fold relative to Hu-IFN-α1 (most active native human interferon).

Selective breeding using DNA shuffling has proved to be very effective method to rapidly improve pharmaceutical proteins by which initially have low levels of the desired “activity” (101, 102). Backcrossing of evolved recommbinants with the wild type genes removes functionally neutral changes, which might reduce the immunogenicity of evolved proteins (103).

2.4 Conclusion

Proteins, especially enzymes, have gained a central role in modern chemical, biotechnological, and biopharmaceutical industries. Directed evolution has over the past proved to be a versatile and successful approach for tailoring protein properties to industrial, agricultural and medical demands and for advancing our understanding of structure-function relationships in biocatalysts. Appropriate library generation and screening methods should be employed concerning the target protein and desired property. To set up a sophisticated screening method, complex conditions in human body (pH, ion concentration, proteases, hormones etc.) should be considered. Subsequent *in vivo* or *in vitro* test of improved variants should be carried out to further validate the screening assay. Development of diversity generation and high-throughput screening method will enable evolution to solve problems efficiently. Especially, directed evolution provides a powerful strategy to rapidly advance the development of improved protein-based drugs (enzymes and antibodies, peptide and ligands). Directed evolution promises to play an increasingly important role to generate “desirable” drugs.

Chapter 3. Directed evolution of Arginine deiminase for increased activity at physiological pH

3. 1 Abstract

Arginine deiminase (ADI; EC 3.5.3.6) has been studied as a potential anti-tumor drug for the treatment of arginine-auxotrophic tumors, such as hepatocellular carcinomas (HCCs) and melanomas. Studies with human lymphatic leukemia cell lines confirmed that ADI is a potential anti-angiogenic agent effective in the treatment of leukemia. ADI from *Pseudomonas plecoglossicida* (PpADI) was cloned and expressed in *E.coli*. A main limitation of PpADI lies in its pH-dependent activity profile with a pH optimum at 6.5. A pH shift from 6.5 to 7.5 results in ~80 % activity drop (pH of human plasma is 7.35 to 7.45). For shifting PpADI pH optimum to netrual pH, a directed evolution protocol based on an adapted citrulline screening protocol in microtiter plate (MTP) format was developed and validated. Proof of concept for ADI engineering resulted in a pH optimum of pH 7.0 and increased activity under physiological conditions: at pH 7.4, variant M2 (K5T, D44E and H404R) is 4-fold more active than the wild type PpADI and retains ~30 % of its activity relative to its pH optimum, compared to ~10 % in the case of the wild type PpADI.

3.2 Introduction

Arginine deiminase (ADI) is a potential cancer therapy agent for the treatment of arginine-auxotrophic tumors (e.g. hepatocellular carcinomas and melanomas). The hepatocellular carcinoma (HCC) accounts annually for approximately 1 million new cases worldwide. In the US the incidence rate (per 100,000 persons; 1992-2002) of HCC is 8.6 with a mortality rate of 6.5 due to low responses of hepatoma to chemotherapeutic treatments (27). Current research efforts are

focused on ADI's *in vivo* inhibitory effect towards HCCs, leukemia, melanomas and human umbilical vein endothelial cells (HUVEC) (104-106), clinical trials for HCC (phase III) and melanoma (phase I/II) (105, 107), and PEG formulation of ADI to improve its efficacy as a clinical drug, including serum half-life and antigenicity (16, 108). ADI inhibited the growth of cultured leukemia cells at concentrations of 5-10 ng/ml, which were about 20-100 times lower than those of the L-asparaginase standard resulting in fewer side effects (106, 109). Arginine deprivation is speculated to be the molecular reason for ADI's inhibitory effect on human lymphatic leukemia (106). ADIs catalyze the first step of the arginine deiminase (ADI) pathway by hydrolyzing arginine to citrulline and ammonium. Several ADI genes have been identified, purified, and characterized from bacteria, archaea and some eukaryotes excluding mammalian cells and summarized in a recent review (27). None of these ADIs is from a kinetic point of view ideally suited for *in vivo* applications in humans under physiological conditions.

Protein engineering by rational design and directed evolution offers opportunities to tailor ADI properties to physiological conditions. For the proof of concept, an ADI isolated from *Pseudomonas plecoglossicida* CGMCC2039 (accession number: ABS70718) which can be functionally expressed in *E. coli* has been employed. Directed evolution approaches employ mainly *E. coli* as host due to its fast growth and high transformation efficiency which is a prerequisite for generating complex mutant libraries. Over the last decades, directed protein evolution has become a versatile and successful approach for tailoring protein properties for industrial demands (mainly in chemical synthesis) and for advancing our understanding of structure-function relationships in enzymes. A directed evolution experiment comprises iterative cycles of diversity generation and functional selection for improved variants. Only a few manuscripts for phytases (83), xylanases (110), amylases (77, 82, 111), and an alcohol deyhdrogenase (112) reported a shift of pH optima using directed evolution algorithms. None of these directed evolution campaigns targeted a medical

application and arginine deiminase has to our best knowledge not been altered in its pH activity/resistance by directed evolution.

Comparison of PaADI (*Pseudomonas aeruginosa*, pH optimum 5.6; His405) and MaADI (*Mycoplasma arginini* ADI, pH optimum 6.5, Arg397) led to the speculation that substitution of His by Arg might contribute to MaADI's increased pH optimum (17). A sequence alignment of four ADIs (MaADI, MyADI (*Mycoplasma arthritidis* ADI), PaADI and PpADI) shows that for both Pseudomonas ADIs the synonymous amino acid positions (404 & 405), contain a His whereas both Mycoplasma ADIs contain at corresponding positions an Arg. Interestingly, both Mycoplasma ADIs have an pH optimum approximately one pH unit higher than both Pseudomonas ADIs.

In this study we report the first directed ADI evolution protocol in which the pH profile of PpADI was shifted to higher pH values representing a conceptional proof that ADI properties can be tailored for demands *in vivo* treatment of arginine-auxotrophic tumors. An emphasis is given on detailed description of directed evolution conditions (mutagenic and screening).

3.3 Materials and methods

3.3.1 Materials

All chemicals were of analytical-reagent grade or higher quality and were purchased from Fluka (Neu-Ulm, Germany), Sigma-Aldrich (Steinheim, Germany) and Applichem (Darmstadt, Germany), except the resins for purification (TOSOH, Stuttgart, Germany). All enzymes were purchased from New England Biolabs (Frankfurt, Germany), Fermentas (St. Leon-Rt, Germany), and Sigma-Aldrich Chemie (Taufkirchen, Germany), unless stated otherwise.

Thermal cycler (Mastercyler gradient; Eppendorf, Hamburg, Germany) and thin-wall PCR tubes (Multi-ultra tubes; 0.2 µl; Carl Roth, Germany) were used in all PCRs. The PCR volume was always 50 µl except for Megaprimer PCR of whole

plasmid (MEGAWHOP, 20 µl); larger volumes were prepared in multiple 50-µl PCRs. The amount of DNA in cloning experiments was quantified by using a NanoDrop photometer (NanoDrop Technologies, Germany).

Pseudomonas plecoglossicida CGMCC2039 was provided by Professor Zhihao Sun (Jiangnan University, Wuxi, China).

3.3.2 Methods

3.3.2.1 Reagents used in assays

Acid-ferric solution

To dH_2O (600 ml), concentrated H_3PO_4 (70 ml, 85 %) and concentrated H_2SO_4 (160 ml, 90-91 %) were added slowly. After cooling to room temperature, $FeCl_3 \cdot 6H_2O$ (10 ml, 10 g/L) was added in the above solution, finally the total volume was adjusted to 1 liter with dH_2O.

Diacetyl monoxime -thiosemicarbazide (DAM-TSC) solution

DAM solution (10 g/L) and TSC solution (0.3 g/L) were prepared separately. The two solutions were mixed (volume ratio = 1:1) just prior to use.

3.3.2.2 Cloning of ADI into pET42b(+)

The arginine deiminase (ADI) gene was amplified from *Pseudomonas plecoglossicida* CGMCC2039 by colony PCR (94℃ for 10 min, 1 cycle; 94℃, 30 s/ 54℃, 30 s/ 72℃, 165 s, 29 cycles; 72℃ for 5 min, 1 cycle) using primer (5'-CCGCATTCCGCTGAAAAACAGAAGTACGG-3' and 5'-CTTCTCGAGTTAGTAGTTGATCGGGTCGCGCACG-3'), 1.5 U of Pfu DNA polymerase, 0.20 mM of dNTP mix and a colony of *Pseudomonas plecoglossicida* CGMCC2039. Amplification product was purified by gel extraction, digested using NdeI (20 U) and XhoI (20 U) and purified using QIAquick PCR purification kit (QIAGEN, Hilden, Germany). Cloning vector pET42b(+) was digested with NdeI (20 U) and XhoI (20 U), and purified by gel extraction kit (QIAGEN, Hilden, Germany). Digested ADI gene and pET42b(+)

were ligated using T4 DNA ligase (1 U) to give pET42b(+)-ADI and transformed into *E. coli* BL21-Gold (DE3).

3.3.2.3 Site directed mutagenesis of PpADI gene at position H404

Site directed mutagenesis of ADI gene was performed according to the published method (113) on plasmid pET42b(+)-ADI. The following oligonucleotides were used for mutagenesis of H404R: 5'-GGCCGTGGCGGCGGCCGTTGCATGACCTGCCCG-3' and 5'-CGGGCAGGTCATGCAACGGCCGCCGCCACGGCC-3' (underlining indicated the substituted nucleotide). For the mutagenic PCR (First stage: 95℃ for 30 s, 1 cycle; 95℃, 30 s/ 55℃, 1 min/ 72℃, 130 s, 3 cycles. Second stage: 95℃ for 30 s, 1 cycle; 95℃, 30 s/ 55℃, 1 min/ 72℃, 130 s, 15 cycles; 68℃ for 30 min, 1 cycle), 2 U of Phusion™ Hot Start DNA polymerase (Finnzymes, Keilaranta, Finland), 0.20 mM of dNTP mix, 25 pmol of each primer together with 100 ng of template (pET42b(+) harboring ADI gene) were used. Following the PCR, DpnI (40 U; New England Biolabs) was added, and incubated overnight at 37℃. The PCR products were purified by using a QIAquick PCR Purification Kit (Qiagen) and transformed into *E. coli* BL21-Gold (DE3) for expression.

3.3.2.4 Site sturation mutagenesis of PpADI gene at nine amino acid position

Site saturation mutagenesis of ADI gene was performed according to the published method (113) on plasmid pET42b(+)-ADI. The oligonucleotides were used for mutagenesis were listed in table 1 (underlining indicated the substituted nucleotide). For the mutagenic PCR (First stage: 95℃ for 30 s, 1 cycle; 95℃, 30 s/ 55℃, 1 min/ 72℃, 130 s, 3 cycles. Second stage: 95℃ for 30 s, 1 cycle; 95℃, 30 s/ 55℃, 1 min/ 72℃, 130 s, 15 cycles; 68℃ for 30 min, 1 cycle), 2 U of Phusion™ Hot Start DNA polymerase (Finnzymes, Keilaranta, Finland), 0.20 mM of dNTP mix, 25 pmol of each primer together with 100 ng of template (pET42b(+) harboring ADI gene) were used. Following the PCR, DpnI (40 U; New England Biolabs) was added, and incubated overnight at 37℃. The PCR products were

purified by using a QIAquick PCR Purification Kit (Qiagen) and transformed into *E. coli* BL21-Gold (DE3) for expression.

Table 1. Primer sequences for site saturation mutagenesis.

Primer name	Sequences
Leu 41 FP	AACTGCGACGAGCTGNNNTTCGACGATGTGATC
Leu 41 RP	GATCACATCG TCGAANNNCA GCTCGTCGCAGTT
Asn 360 FP	TGGGATGACGGCAACAACNNNGTGGCGCTGGAG
Asn 360 RP	CTCCAGCGCC ACCACNNNGT TGCCGTCATCCCA
Arg401 FP	GAACTGGGCCGGGGCNNNGGCGGCGGCCACTGC
Arg401 RP	GCAGTGGCCGCCGCCNNNGCCCCGGCCCAGTTC
Phe163 FP	CTGCCCAACACCCAGNNNACCCGCGACACCACC
Phe163 RP	GGTGGTGTCGCGGGTNNNCTGGGTGTTGGGCAG
Asn160 FP	CTGCCGCCGCTGCCCNNNACCCAGTTCACCCGC
Asn160 RP	GCGGGTGAACTGGGTNNNGGGCAGCGGCGGCAG
Arg185 FP	ATGTACTGGCCGGCNNNCGCCAGGAAACCCTG
Arg185 RP	CAGGGTTTCCTGGCGNNNGCCGGCCAGTACAT
Arg243 FP	ATCGGCATGGGTGAGNNNACCTCGCGCCAGGCC
Arg243 RP	GGCCTGGCGCGAGGTNNNCTCACCCATGCCGAT
His405 FP	GGCCGTGGCGGCGGCNNNTGCATGACCTGCCCG
His405 RP	CGGGCAGGTCATGCANNNGCCGCCGCCACGGCC
Gly403 FP	GCCGGGGCCGTGGCNNNGGCCACTGCATGACC
Gly403 RP	GGTCATGCAGTGGCCNNNGCCACGGCCCCGGCC

3.3.2.5 Construction of PpADI error-prone library

The library was generated by the standard error-prone PCR (epPCR) using improved variant H404R as template. For the mutagenic PCR (95℃ for 2 min, 1 cycle; 95℃, 30 s/ 55℃, 30 s/ 72℃, 30 s, 29 cycles; 72℃ for 3 min, 1 cycle), 2.5 U of Taq DNA polymerase, 0.20 mM of dNTP mix, 50 ng of template (pET42b(+) harboring ADI gene H404R), 0.01-0.1 mM of $MnCl_2$ and 10 pmol of each primer (5'-TACATATGTCCGCTGAAAAACAGAAG-3' and 5'- GTGCTCGAGTTAGTAGT TGATCGG-3') were used. The PCR products were purified by using a QIAquick PCR Purification Kit. The purified epPCR products were cloned into expression

plasmid pET42b(+) by MEGAWHOP(114). For MEGAWHOP (68℃ for 5 min, 1 cycle; 95℃ for 5 min, 1 cycle; 95℃, 1 min/ 55℃, 1 min/ 68℃, 13 min 30 s, 24 cycles; 68℃ for 30 min, 1 cycle), 1 U of Taq DNA polymerase, 0.1 U of Pfu DNA polymerase, 0.20 mM of dNTP mix together with 200 ng of template (pET42b(+) harboring ADI gene H404R) were used. Following the PCR, DpnI (40 U; New England Biolabs) was added, and incubated (4 h; 37℃). The MEGAWHOP products were transformed into *E. coli* BL21-Gold (DE3) for expression and screening.

3.3.2.6 Expression of PpADI in LB media with IPTG induction

The strain *E. coli* BL21-Gold (DE3)/ pET42b-PpADI was cultured at 37℃ in 20 ml of LB media that contained 50 μg/ml kanamycine to an absorbance of 0.6 at 578nm. Then, isopropyl β-D-thio-galactopyranoside (IPTG) was added to a final concentration 0.2 mM. The cells were harvested after 9 h induction with IPTG at 37℃. The expressed rADI was analyzed by SDS-PAGE.

3.3.2.7 Expression of PpADI in auto-induction media

A chemically defined auto-induction medium (115) containing salts and trace metals, vitamins including vitamin B12, and glucose, glycerol, and lactose were test for PpADI expression. Five kinds of auto-induction media LS-5052, P-5052, MD-5052, TYM-5052 and TYP-5052 were tested for the ADI expression, under the following conditions: 20 ml LB media in 100 ml flask, 37℃, 250 rpm, 20 h. The expressed rADI was analyzed by SDS-PAGE.

3.3.2.8 Cultivation and expression of PpADI in 96-well plates

Colonies grown on LB_{kan} agar plates were transferred, by using toothpicks, into 96-well microtiter plates (flat bottom, polystyrene plates; Greiner Bio-One GmbH, Frickenhausen, Germany), containing non-inducing medium LSG (150 μL) (115) supplemented with kanamycin (50 μg/ml). After 16 h of cultivation in a microtiter plate shaker (Multitron II, Infors GmbH, Einsbach, Germany; 37℃, 900 rpm, 70 % humidity), each well was replicated using a replicator (EnzyScreen BV, Leiden,

Netherlands) into a second series of 96-well microtiter plates containing 150 µL of auto-induction media LS-5052 (115) supplemented with kanamycin (50 µg/ml). The first set of plates was stored at -80°C after addition of glycerol. The clones in the second set of plates were cultivated for 12 h (Multitron II, Infors GmbH, 37°C, 900 rpm) and used for screening.

3.3.2.9 Screening Procedure

96-well plate format citrulline colorimetric screening assay

A modified protocol of citrulline detection based on carbamido-diacetyl reaction (116) (see Figure 1A for assay mechanism) was used for ADI activity measurement. Screening for increased activity was carried out by measuring the activity at pH 7.4 and 6.4. 20 µl of cell culture was transferred to 96-well microtiter plate. Enzyme reaction was initiated by addition of arginine solution (100 µl, 100 mM) supplemented with cetyltrimethylammoniumbromide (CTAB, 4 mM), and incubated (20 min, 37°C). Subsequently, acid-ferric solution (60 µl) and diacetyl monoxime (DAM, 20 µl, 0.5 M) were added. The reaction mixture was further incubated (15 min, 55°C). Absorbance was measured at 492 nm using a microtiter plate reader (Tecan Sunrise, Tecan Group AG, Zurich, Switzerland).

Standard deviation measurements were performed in 96-well plate format using culture from BL21-Gold (DE3) lacking ADI and in a separate experiment containing ADI. Apparent standard deviation was based on the absolute absorbance values obtained from the ADI wild type plate. The true standard deviation was calculated by subtracting the background absorbance value of the microtiter plate lacking ADI from the apparent values.

Cuvette format citrulline colorimetric assay

ADI activity was routinely measured using a modified protocol of the citrulline detection with DAM and TSC (117) (see Figure 1A for assay mechanism) in Eppendorf tubes. Enzyme reaction was initiated by addition of arginine solution (200 µl, 100 mM) to a 2-ml eppendorf tube containing crude cell lysate (50 µl), and incubated (20 min, 37°C). Subsequently, acid-ferric solution (250 µl) was

added to stop the enzyme reaction. After appropriate dilution with deionized water to ensure the concentration of produced citrulline is within linear detection range, the reaction mixture (400 µl) was mixed with acid-ferric solution (600 µl) and DAM-TSC solution (100 µl). The reaction mixture was further incubated (30 min, 70°C), followed by incubation in ice water to stop color development. Absorbance was measured at 530 nm using a Specord 200 (Analytik Jena AG, Jena, Germany).

Normalization of protein expression for wild type ADI and variants

Agilent Protein 230 Kit (Agilent Protein 230 Kit, Agilent Technologies Deutschland GmbH, Böblingen, Germany) and Agilent 2100 Bioanalyzer (Agilent 2100 Bioanalyzer, Agilent Technologies Deutschland GmbH, Böblingen, Germany) were used for normalization of protein expression in crude cell extract. The protocol used was according to Agilent protein 230 Kit Guide except BSA was used as an internal standard.

3.3.2.10 Expression of ADI in shaking flask and purification

Shaking flasks (1 liter) containing auto induction media LS-5052 (200 ml) supplemented with kanamycin (50 µg/ml) were inoculated with a 1:200 dilution of overnight culture (*E. coli* BL21-Gold(DE3) harboring pET42b-ADI) grown in non-inducing media LSG. After 12 h of expression, *E. coli* cells were harvested by centrifugation (Eppendorf 5810R 4°C, 3220 g, 30 min) and resuspended in phosphate buffer (20 ml, Na_xPO_4, 20 mM, pH 7.0). *E. coli* cells were subsequently lysed by using a high-pressure homogenizer (1500 bar, 2 cycles; Avestin Emulsiflex, Mannheim, Germany). The disrupted cells were centrifuged (Eppendorf 5417R, 4°C, 13000 g, 20 min) and the supernatant was further cleared by filtration through a low protein-binding filter (0.45 µm; Minisart RC 25 single use syringe filter; Sartorius, Hamburg, Germany). ADI wild type and mutants (H404R and K5T D44E H404R) were subsequently purified by a column chromatography procedure: (i) The filtered cell lysates were subjected to a Super-Q anion exchange column, which had been pre-equilibrated with 50 mM

phosphate buffer (Na_xPO_4, pH 7.0). 20 ml of cell lysate was loaded. ADI were eluted by a NaCl step elution in phosphate buffer (Na_xPO_4, 50 mM, pH 7.0) at a rate of 3 ml/min. (ii) The obtained ADI protein from ion exchange chromatography was subjected to a gel filtration column (Matrix: Toyoperl HW-55S, Bed volume: 33 ml, Bed height: 40 cm, Column: Omnifit).

Purified ADI was subsequently concentrated using a Amicon ultra-4 centrifugal filter device (Millipore Corporation, Billerica, U.S.A.) with a 30-kDa cut-off membrane. Total protein concentration was determined by BCA^{TM} assay kit (Pierce, Born, Germany) and homogeneity of the purified sample was controlled by SDS-page electrophoresis using standard molecular biology techniques.

3.3.2.11 Characterization of ADI wild type and mutants

Determination of k_{cat} and K_m of ADI wild type and the mutants

The k_{cat} and K_m values were determined from initial velocity data measured as a function of substrate concentration. Enzyme reaction was carried out at 37°C in a water bath. After 10 min preincubation at 37°C, the enzyme reaction was initiated by addition of purified enzyme (50 µl, 0.2-0.5 µM) to the substrate solution (200 µl, 0.2 mM to 10 mM of arginine, 0.5 M phosphate buffer, pH 7.4) in deep well plates. The reaction mixture was incubated (37°C) and every two minutes reaction mixture (30 µl) of each well was transferred to acid-ferric solution (30 µl) to stop the enzyme reaction. The color development was subsequently performed in 96-well PCR plate. Ferric-acid solution (90 µl) and DAM-TSC solution (15 µl) were added to each well. The 96-well PCR plate was then incubated (70°C, 30 min) in thermal cycler (Eppendorf Mastercyler gradient) for color development, followed by incubation in ice water to stop color development. Absorbance was measured at 530 nm using a microtiter plate reader (SPECTROstar Omega, BMG LABTECH, Offenburg, Germany). The initial velocity data obtained were fitted to the equation $v = V_{max}[S]/([S] + K_m)$ (where v is the initial velocity, V_{max} the maximum velocity, [S] the substrate concentration, and K_m the Michaelis constant) using GraphPad Prism software (GraphPad

software, San Diego, CA, USA). The k_{cat} was calculated from the ratio of V_{max} and enzyme concentration.

Determination of pH profile

Enzyme reaction was carried out at 37°C in a water bath using the following substrate solution: arginine 0.1 M, pH 5-8 phosphate/acetate buffer (0.5 M phosphate, 50 mM acetate). After 10 min preincubation at 37°C, the enzyme reaction was initiated by addition of purified enzyme (50 µl, 0.2-0.5 µM) to the substrate solution (200 µl) in deep well plates. The reaction mixture was incubated (37°C, 10 min) and acid-ferric solution (250 µl) was transferred to each well to stop the enzyme reaction. The color development was subsequently performed in 96-well PCR plate. The reaction mixture (60 µl), ferric-acid solution (90 µl) and DAM-TSC solution (15 µl) were transferred to a 96-well PCR plate. The 96-well PCR plate was then incubated (70°C, 30 min) in thermal cycler (Eppendorf Mastercyler gradient) for color development, followed by incubation in ice water to stop color development. Absorbance was measured at 530 nm using a microtiter plate reader (SPECTROstar Omega, Germany).

3.3.2.12 Molecular Modeling

Two crystal structures of PaADI (PDB codes: 1RXX, 2A9G) were used to model the mutations H405R and D44E. Only one monomeric unit of the tetrameric PaADI was used for the modeling study employing Swiss-PDB viewer (118) (www.expasy.org/spdbv). PaADI variants (H405R; D44E) were generated using the mutate command of Swiss-PDB viewer. The side chain rotamer with the best score was used for subsequent energy optimized with parameter of GROMOS96 force field for in vacuum minimization (119).

3.3.2.13 Stability of PpADI in presence of serum

Purified PpADI (wild type, M1, M2; 20 µl) was incubated (37°C, 60 min) with AB--human serum (80 ul, Invitrogen, Karlsruhe, Germany) and PBS buffer (pH7.4, 80 ul), respectively. Subsequently, the incubated ADI-serum/PBS mix (20 µl) was

added to microtiter plate containing arginine solution (100 µl, 10 mM arginine in PBS buffer, pH 7.4) and incubated (37℃, 30 min). Acid-ferric solution (120 µl) was added to stop the enzyme reaction. The produced citrulline was detected using the assay procedure employed in "Determination of kcat and Km of ADI wild type and the mutants". Before measuring absorbance at 530 nm, centrifugation (Eppendorf, 5810R 4℃, 3000 g, 10 min) was performed to remove the precipitation in the assay solution (likely proteins in serum were precipitated in acidic condition during assay procedure). Meanwhile, a serum control was test for the original citrulline concentration of serum using the same procedure mentioned above except that instead of PpADI, elution buffer of gel filtration (NaxPO4, 50 mM, pH 7.4) was used. All the absorbance values at 530 nm of ADI-serum sample were subtracted the value of serum control to get the citrulline concentration produced by PpADI. The residual activities of PpADI after incubation in serum compared to that in PBS buffer were calculated to show the stability of PpADI after incubated in human serum.

3.3.2.14 Activity of PpADI (wild type, M1, M2) towards arginine derivative dimethylarginine

Purified PpADI (wild type, M1, M2; 15 µl, ~0.2 mg/ml final concentration; >20-fold concentration used for kinetic constant determination) was incubated (37℃, 4 h) with (N^G, N^G)-dimethylarginine solution (20 mM, 100 µl). Acid-ferric solution (120 µl) was added to stop the enzyme reaction. Activity was recorded by citrulline detection using citrulline colorimetric assay (see 3.3.2.11 Characterization of ADI wild type and mutants).

3.4 Results

3.4.1 PpADI cloning

PpADI was cloned into pET42b(+) and expressed in *E.coli* BL21-Gold(DE3) using auto-induction media LS-5052 (see figure 2). The nucleotide sequence of PpADI comprises 1,254 bp nucleotide (figure 1) encoding 417 amino acids which have 85% identity to ADI from *P. aeruginosa* (PaADI). The PpADI cloned into

pET42b(+) was confirmed by nucleotide sequencing. As indicated in Figure 1, sequence analysis of ADI gene showed that there was one synonymous mutation at amino acid position D78 (GAT to GAC) compared to ADI-sequence of *P. plecoglossicida* CGMCC2039 deposited in NCBI (accession number: EU030267). The deduced ADI protein sequence has a calculated molecular weight of 46.5 kDa and shows 85% identity to ADI from *P. aeruginosa*. This clone was used for subsequent directed evolution experiments.

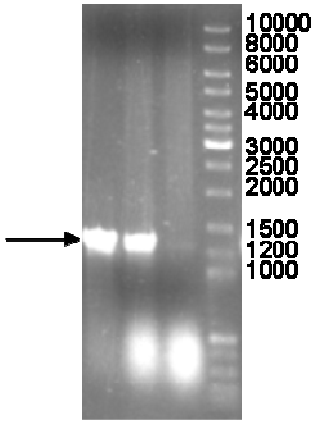

Figure 1. DNA electrophoresis of *PpADI*.

```
1       ATGTCCGCTG AAAAACAGAA GTACGGTGTC CACTCCGAAG CAGGCAAGCT GCGCAAGGTA
61      ATGGTCTGCG CTCCGGGACT GGCGCACAAG CGCCTGACCC CGAGCAACTG CGACGAGCTG
121     CTGTTCGACG ATGTGATCTG GGTCGACCAG GCCAAGCGCG ACCACTTCGA CTTCGTCACC
181     AAGATGCGCG AGCGCGGCGT GGATGTGCTG GAAATGCATA ACCTGCTCAC CGACATCGTG
241     CAGAACCCCG AGGCCCTGAA GTGGATCCTC GACCGCAAGA TCACCCCTGA CACCGTCGGG
301     GTGGGCCTGA CCAACGAAGT GCGCAGCTGG CTGGAGGGCC AGGAGCCACG CCACCTCGCC
361     GAGTTCCTGA TCGGCGGCGT GGCCGGCCAG GACCTGCCGG AGAGCGAAGG TGCCAGCGTG
421     GTCAAGATGT ACAACGACTA CCTGGGCCAC TCCAGCTTCA TCCTGCCGCC GCTGCCCAAC
481     ACCCAGTTCA CCCGCGACAC CACCTGCTGG ATCTACGGCG GCGTGACCCT CAACCCGATG
541     TACTGGCCGG CGCGACGCCA GGAAACCCTG CTGACCACCG CCATCTACAA GTTCCACCCC
601     GAGTTCACCA AGGCCGACTT CCAGGTCTGG TACGGCGACC CGGACCAAGA GCACGGCCAG
661     GCCACCCTCG AAGGCGGCGA CGTCATGCCG ATCGGCAAGG GCATCGTGCT GATCGGCATG
721     GGTGAGCGCA CCTCGCGCCA GGCCATCGGC CAACTGGCAC AGAACCTCTT CGCCAAGGGC
781     GCAGTGGAGC AAGTGATCGT CGCCGGGCTG CCGAAGTCCC GTGCGGCCAT GCACCTGGAC
841     ACCGTGTTCA GCTTCTGCGA CCGCGACCTG GTCACGGTTT TCCCGGAAGT GGTGCGCGAG
901     ATCGTGCCGT TCATCATCCG CCCGGACGAA AGCAAGCCCT ACGGCATGGA CGTACGCCGC
961     GAGAACAAGT CGTTCATCGA GGTGGTCGGC GAGCAGCTGG GCGTCAAGCT GCGTGTGGTC
1021    GAGACCGGCG GCAACAGCTT CGCCGCCGAG CGCGAGCAGT GGGATGACGG CAACAACGTG
1081    GTGGCGCTGG AGCCAGGTGT GGTCATCGGC TACGACCGCA ACACCTACAC CAATACCTTG
1141    CTGCGCAAGG CCGGGATAGA GGTCATCACC ATCAGTGCCG GCGAACTGGG CCGGGGCCGT
1201    GGCGGCGGCC ACTGCATGAC CTGCCCGATC GTGCGCGACC CGATCAACTA CTAA
```

Figure 2. PpADI sequencing results.

3.4.2 PpADI expression in LB media with IPTG as inducer

PpADI was successfully expressed in LB media with IPTG as inducer. Figure 3 (lane 4) shows the expression band of PpADI observed at ~45 kDa, which is similar to the calculated molecular weight of 46 kDa (based on http://expasy.org/tools/pi_tool.html).

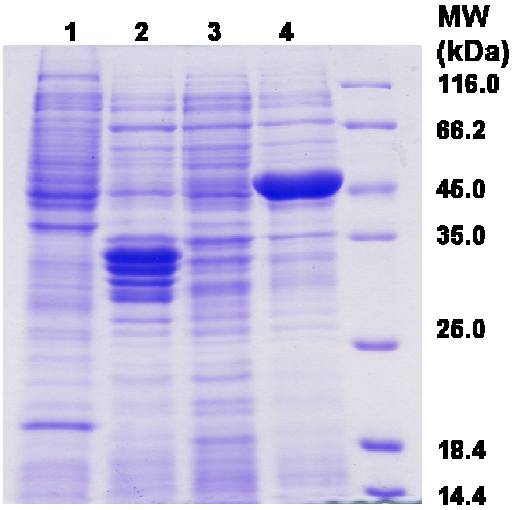

Figure 3. SDS-PAGE of PpADI expression. Lane 1: *P. plecoglossicida*; Lane 2: E. coli BL21-Gold (DE3)/ pET42b; Lane 3: E. coli BL21-Gold (DE3)/ pET42b-PpADI WT, without IPTG; Lane 4: E. coli BL21-Gold (DE3)/ pET42b- PpADI WT.

3.4.3 PpADI expression in auto-induction media

Expressing recombinant protein in auto-induction media is based upon the preferences of bacteria to selectively use different carbon sources during diauxic growth and upon the often-observed negative regulation of gene expression by catabolite repression. Auto-induction is more convenient than IPTG induction because the expression strain is simply inoculated into auto-inducing medium and grown to saturation without the need to follow culture growth and add inducer at the proper time. For high-throughput applications, the auto-induction approach has many advantages over traditional induction methods including avoidance of the strong induction and apparent toxicity associated with chemical inducers such as IPTG.

Five kinds of auto-induction media LS-5052, P-5052, MD-5052, TYM-5052 and TYP-5052 were tested for the ADI expression. Figure 4(A) and 4(B) show ADI

activity and corresponding SDS-PAGE band of the PpADI expression in different auto-induction media. The expression in auto-induction media LS-5052 is shows the highest activity and therefore LS-5052 was used for the following directed evolution experiments.

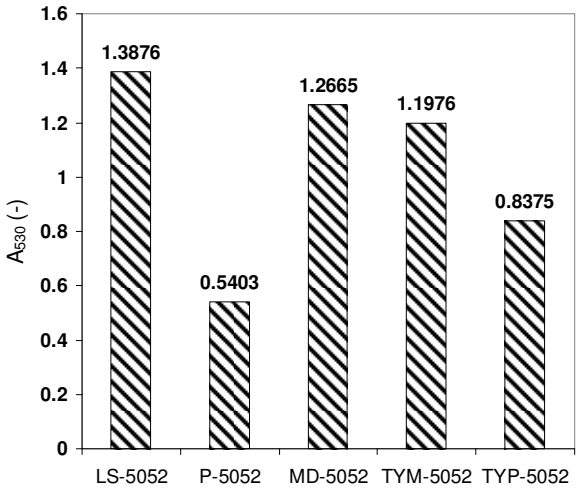

Figure 4(A). Activity of PpADI expressed in auto-induction media.

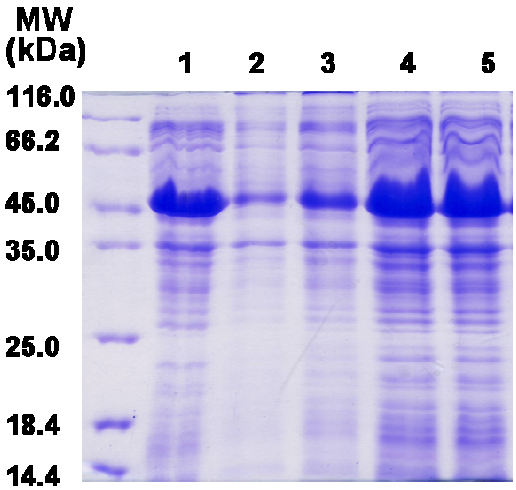

Figure 4(B). SDS-PAGE of ADI expressed in auto-induction media 1, LS-5052; 2, P-5052; 3, MD-5052; 4 TYM-5052; 5, TYP-5052.

3.4.4 PpADI assay based on citrulline detection

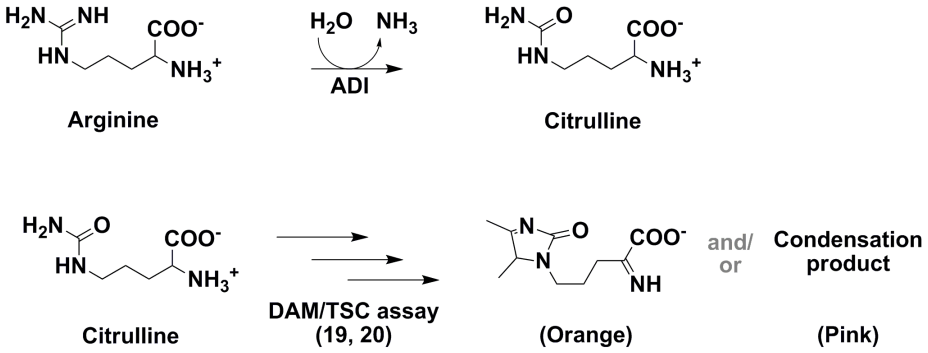

Figure 5. Arginine conversion by ADI and detection of citrulline using DAM/TSC assay.

ADI activity was measured by detecting the production of citrulline from arginine, according to carbamido diacetyl reaction (colorimetric reaction). The conditions of the carbamido diacetyl reaction is as follows： strong acid solution (H_3PO_4, H_2SO_4), oxidizing agent (Fe^{3+}), diacetyl monoxime (DAM), thiosemicarbazide (TSC), and boiling water bath. Figure 5 shows one postulated reaction mechanism for the assay which depicts the reaction between citrulline and DAM. By the addition of TSC to the reaction system, Coulombe and Favreau(120) obtained linearity of response with a more stable pink color which A_{max} was shifted from 490nm to 530nm.

Figure 6 describes the assay procedure for measuring ADI activity in 2 ml eppendorf tube. A calibration curve was prepared using citrulline standard solution (Figure 7) for determining the citrulline production during the assay.

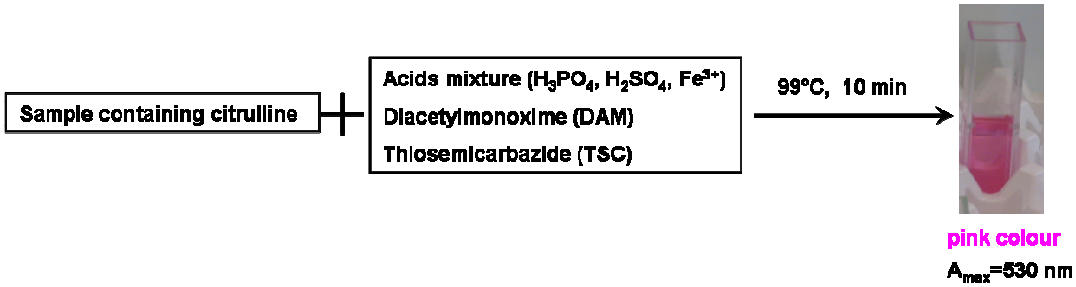

Figure 6. Citrulline colorimetric assay in cuvette format using DAM/TSC assay.

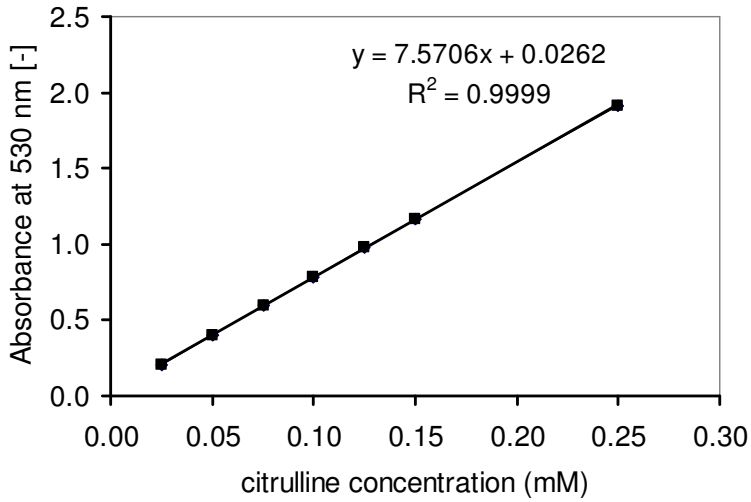

Figure 7. Calibration curve of cuvette format citrulline colorimetric assay.

3.4.5 PpADI screening system for citrulline production in microtiter plates

Two key performance parameters for identifying improved variants in microtiter plate based screening systems are the true standard variation and the linear detection range of the employed assay. Standard deviations have been reduced by optimizing expression and screening conditions (various auto-induction media and assay conditions such as amount of cell, conversion time and color development procedure). A modified version of the DAM-TSC assay for citrulline detection (Scheme 1) was selected for directed evolution of PpADI. The microtiter plate screening format was optimized for simplified handling by lowering the color development temperature (55℃ instead of 100℃), increasing the diacetylmonoxime concentration (~22-fold) and avoiding the use of the sensitizer thiosemicarbazide. Figure 8 shows the procedure of screening assay of citrulline detection.

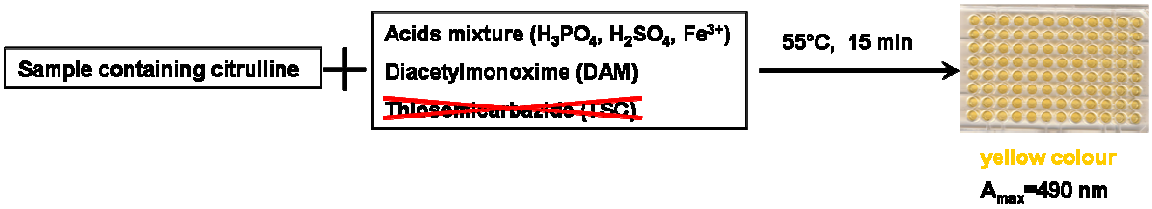

Figure 8. Citrulline colorimetric assay in MTP format using DAM assay.

Standard deviations of the modified citrulline detection assay have been reduced by optimizing expression and screening conditions (various auto-induction media and assay conditions such as amount of cell, conversion time and color development procedure). The preferred combination (150 µl LS5052 auto-induction media and 20 µl cell culture, 20 min conversion time and 15 min color develop time) resulted in a true standard deviation of 12.8 % after subtracting the background (Figure 10). Screening systems with standard deviations around 10 % have successfully been used in directed evolution experiments (121, 122). A wide linear detection window is important for identifying beneficial mutants in directed evolution experiments and screening systems for evolved mutants have to be constantly adapted for hitting the linear detection window. A linear detection range up to 6 mM citrulline could be detected (Figure 9).

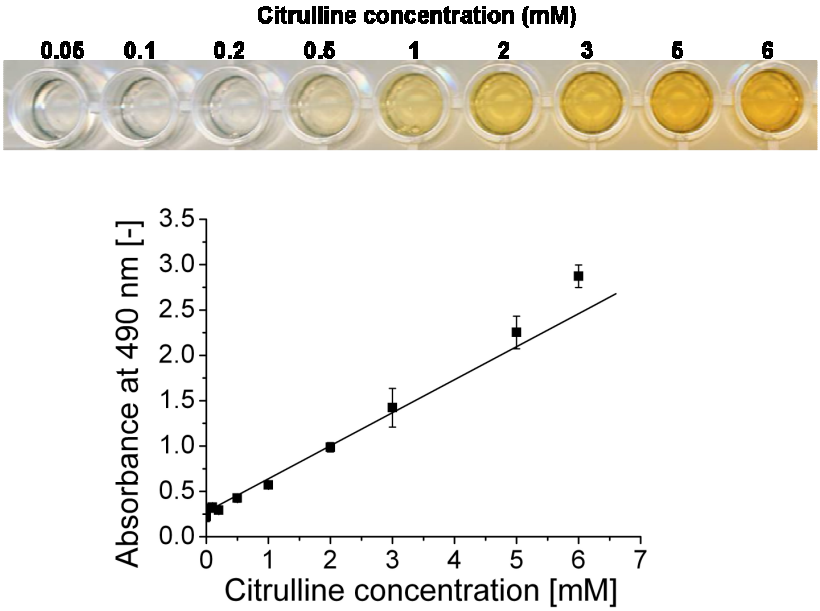

Figure 9. Calibration curve of 96-well microtiter plate format citrulline colorimetric screening assay.

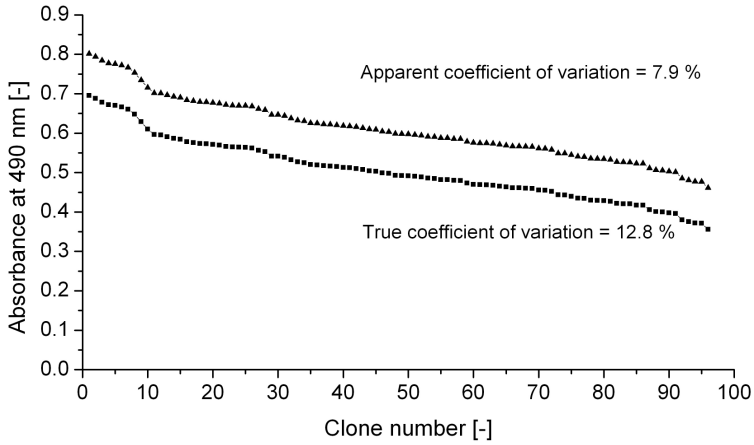

Figure 10. Activity values in descending order of the ADI wild-type conversion of arginine to citrulline in a 96-well microtiter plate using the optimized assay protocol. The apparent coefficients of variation were calculated without subtracting the background and the true coefficients of variation after background subtraction.

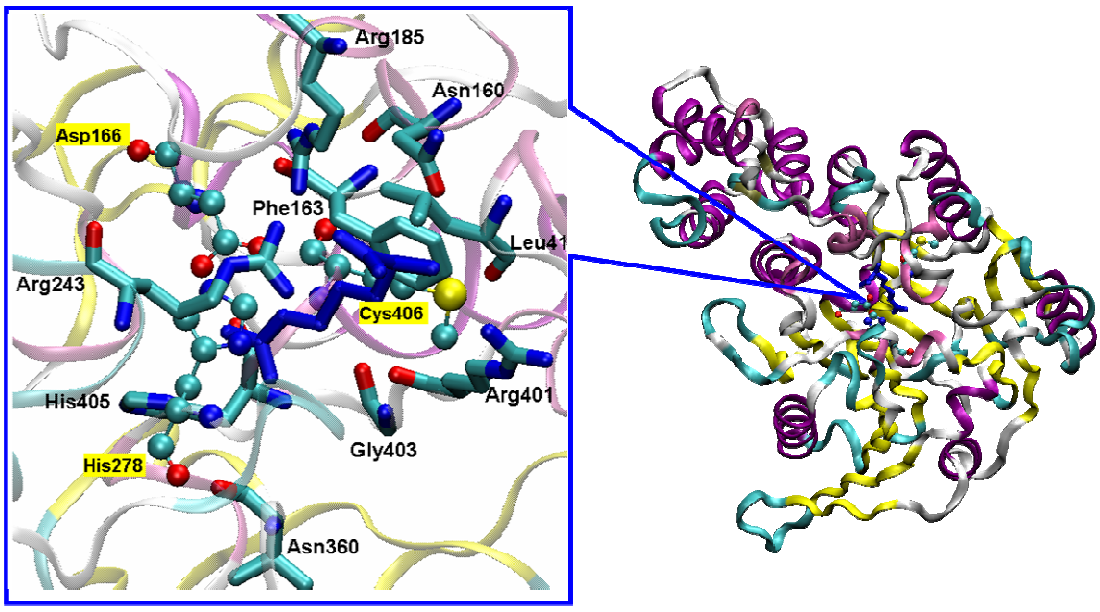

Figure 11. PpADI model derived from PaADI crystal structure (PDB code 2a9gD) by SWISS MODEL WORKSPACE.

3.4.6 Focused libraries generated by saturation mutagenesis

PpADI gene shares 83 % sequence identity with PaADI of which the crystal structure was solved (123). After submitting the ADI sequence to SWISS MODEL WORKSPACE, a proposed ADI model based on the PaADI crystal structure (PDB code 2a9gD) was obtained (Figure 11). According to this model and published literatures, 9 amino acid residues: Leu41, Asn160, Phe163, Arg185, Arg243, Asn360, Arg401, His404, Gly 403 (Figure 11) close to the active center (catalytic triad: Cys406-His278-Glu224) or known to interact with substrate arginine were selected for saturation mutagenesis.

Site saturation mutagenesis at position Leu41, Asn160, Phe163, Arg185, Arg243, Asn360, Arg401, His404 and Gly 403 were performed. 300 clones were screened for each position. However, no improved variant was identified.

3.4.7 Validation of variant M1 (H404R) citrulline colorimetric assay in cuvette format

Position H404 which was suspected to influence ADI pH profile by substitution to R404 (15). Compared to wild type PpADI, variant M1 (H404R) shows higher activity (1.8-fold) and improved activity ratio of pH 7.4 to 6.4 (4.7-fold). Therefore, M1 (H404R) was selected for directed evolution.

3.4.8 epPCR library generation and screening with citrulline detection assay by screening error-prone mutant libraries

Various concentrations of $MnCl_2$ (0.01-0.10 mM) were used in epPCR library generation to adjust the ratio of active to inactive clones. Figure 12 (A) and 12 (B) show the epPCR products and the corresponding MEGAWHOP products. Concentration of 0.01 mM $MnCl_2$ which generated 53 % inactive mutant was selected for library generation. EpPCR mutant libraries with a ratio of 50 % active and 50 % inactive clones have often been used successfully in directed evolution, improving enzyme properties by gradual changes (one or two amino acids changes per round of mutagenesis and screening). A total of 7 variants (listed in

Table 2) were identified from an epPCR library of 2400 mutants and used for further characterization. The most active variant was sequenced and two additional amino acid substitutions (K5T D44E) were identified.

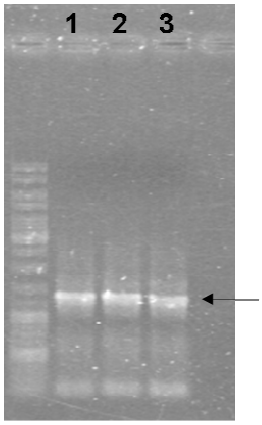

Figure 12 (A). Electrophoresis of epPCR products. Lane 1, 0.01 mM of $MnCl_2$; Lane 2, 0.02 mM of $MnCl_2$; Lane 3, 0.05 mM of $MnCl_2$.

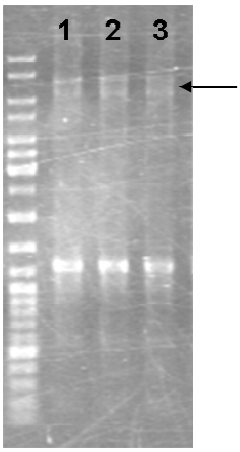

Figure 12 (B). Electrophoresis of MEGAWHOP product with epPCR products as megaprimer. Lane 1, 0.01 mM of $MnCl_2$; Lane 2, 0.02 mM of $MnCl_2$; Lane 3, 0.05 mM of $MnCl_2$.

Table 2. Activity of ADI variants towards arginine determined using citrulline colorimetric assay in cuvette format. Samples were diluted to ensure that detected citrulline concentrations are within the linear detection range of the citrulline colorimetric assay. Wild type, mutant M1 and the "best variant" M2 are in bold and prominent expression mutants (9-B3-1; 21-D5-1) are italized.

	Normalized [ADI][a]				
	Citrulline production (mM/mg)		Relative to activity at pH 7.4 of WT		Activity at pH 7.4/ activity at pH 6.4
ADI variants	pH 7.4	pH 6.4	pH 7.4	pH 6.4	
WT	9.83 (0.74)[b]	124.92 (1.98)	1.00 (0.15)	12.69 (0.01)	0.08 (0.01)
M1 (H404R)	17.80 (0.49)	45.95 (0.87)	1.81 (0.06)	4.67 (0.02)	0.39 (0.02)
M2 (K5T D44E H404R)	38.99 (0.79)	39.20 (0.31)	3.96 (0.02)	3.98 (0.02)	0.99 (0.03)
9-B3-1	24.89 (0.45)	54.50 (1.80)	2.53 (0.03)	5.54 (0.03)	0.46 (0.02)
21-D5-1	25.68 (2.68)	50.95 (2.36)	2.61 (0.07)	5.18 (0.02)	0.50 (0.01)
15-G10-2	13.11 (0.53)	47.02 (0.47)	1.33 (0.09)	4.78 (0.02)	0.28 (0.01)
2-H4-2	12.50 (0.07)	21.58 (0.09)	1.27 (0.06)	2.19 (0.04)	0.58 (0.01)
1-G11-1	24.91 (0.20)	29.12 (0.33)	2.53 (0.03)	2.96 (0.03)	0.85 (0.02)
24-E10-1	14.62 (0.62)	32.82 (0.52)	1.49 (0.08)	3.34 (0.03)	0.45 (0.02)

[a] (Based on quantification employing Agilent 2100 Bioanalyzer (Agilent Protein 230 Kit))
[b] (Standard error of triplicate measurements are given in brackets below each absolute and normalized value.)

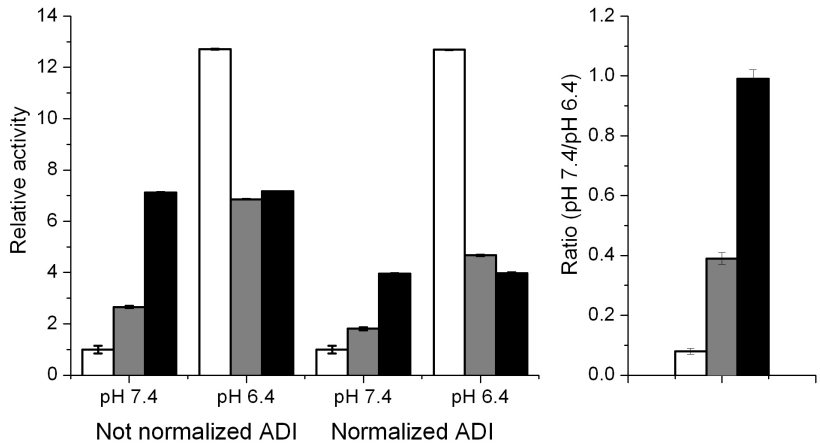

Figure 13. Relative activity of ADI variants towards arginine. The relative activity is the ratio of the activity at the pH of each variant relative to the activity at pH 7.4 of wild type ADI. White: ADI wild type, grey: M1 (H404R), black: M2 (K5T D44E H404R).

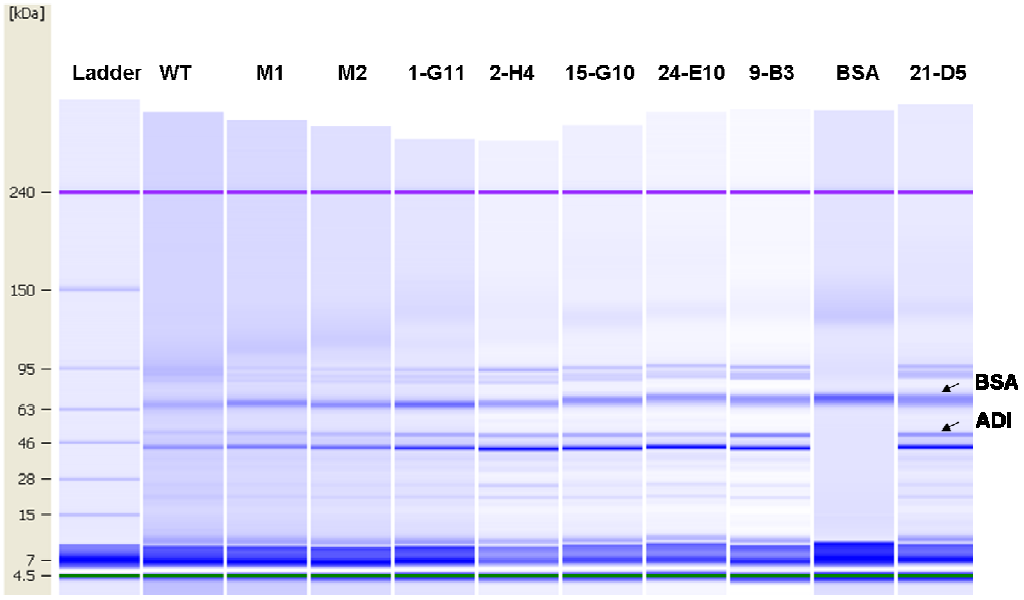

Figure 14. Elution profile of wild type PpADI and improved variants from epPCR library, generated with Protein 230 Kit using a mircofluidic device (Agilent Bioanalyzer). BSA was added as an internal standard.

3.4.9 Characterization of PpADI variants

3.4.9.1 Determination of k_{cat} and K_m of ADI wild type and the mutants

Variants selected from epPCR were first characterized using the crude cell extract to identify the most promising variants (Table 2). Using an activity ratio of pH 7.4 to 6.4 proved to be an effective method to eliminate expression mutants. Additionally ADI concentration in crude cell extract was determined using the Agilent Protein 230 Kit. Microfluidic elution profiles (Figure 14) semi-quantify differences in expression between the wild type PpADI and variants. Normalization of activities against the corresponding ADI concentrations reveals improvements in specific activities of ADI mutants (Table 2). M1, the starting variant for the directed evolution campaign, and M2 were selected for detailed characterization studies. M2 has as “best identified variants” (Figure 13) a more than 2.5-fold higher activity ratio at pH 7.4 to pH 6.4 than M1 and a 12-fold higher activity ratio than wild type in crude cell lysates.

For kinetic characterization of ADI variants the citrulline production was maintained between 0.2-0.8 mM. Calibration curve in Figure 4 shows the linear detection range in the employed 96-well PCR plate format citrulline colorimetric assay system. Figure 15 summarizes the k_{cat} and K_m values of wild type PpADI, identified variants M1 (H404) and M2 (K5T D44E H404R) which were expressed in shaking flasks cultures and purified using a two step procedure (anion exchange followed by gel filtration). Both variants M1 and M2 show an increase in k_{cat} and K_m for citrulline production at pH 7.4. Variant M2 shows a 4-fold higher k_{cat} as also obtained for specific activity in Table 2 using the crude cell extract, validating the characterization procedure with crude cell lysate. Furthermore, an increased K_m from 0.7 mM (wild type PpADI) to 1.2 mM (M1) and 2.5 mM (M2) was found.

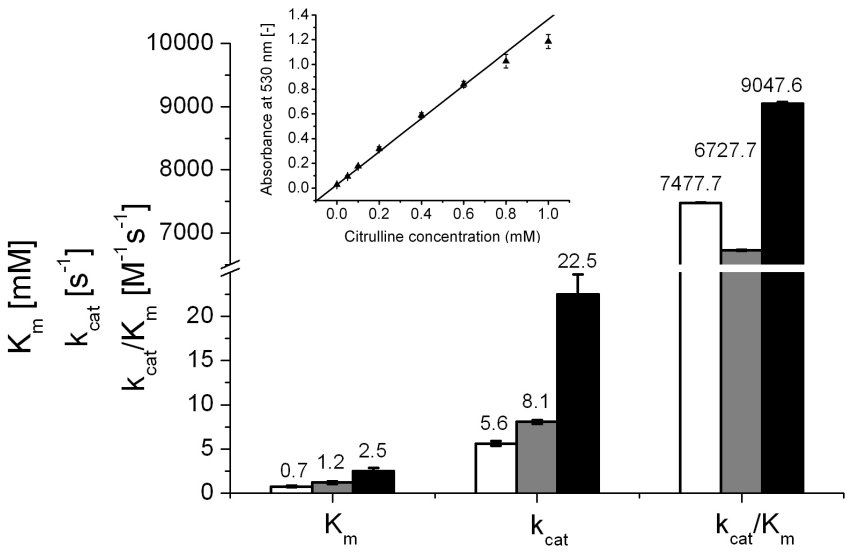

Figure 15. Kinetic parameters of ADI and mutants for conversion of arginine to citrulline. White: ADI wild type, grey: M1 (H404R), black: M2 (K5T D44E H404R). Values reported are the average of three measurements, and average deviations from the mean values are shown. Embedded calibration curve shows linearity of citrulline colorimetric assay in 96-well PCR plate format which was used to determine arginine conversions and kinetic constants.

3.4.9.2 Relative pH profile of wild type and mutant

The relative pH profile (Figure 16) of wild type PpADI and M1 (H404R) shows an identical pH optimum at pH 6.5. Compared to wild type PpADI, variant M2 (K5T

D44E H404R) shows a pH optimum at pH 7.0 which is shifted remarkably (0.5 pH units). Both M1 and M2 show decreased specific activities at pH 6.5, and increased specific activity at pH 7.5. At pH 7.0, the specific activity of M2 exceeds that of wild type PaADI (data not shown).

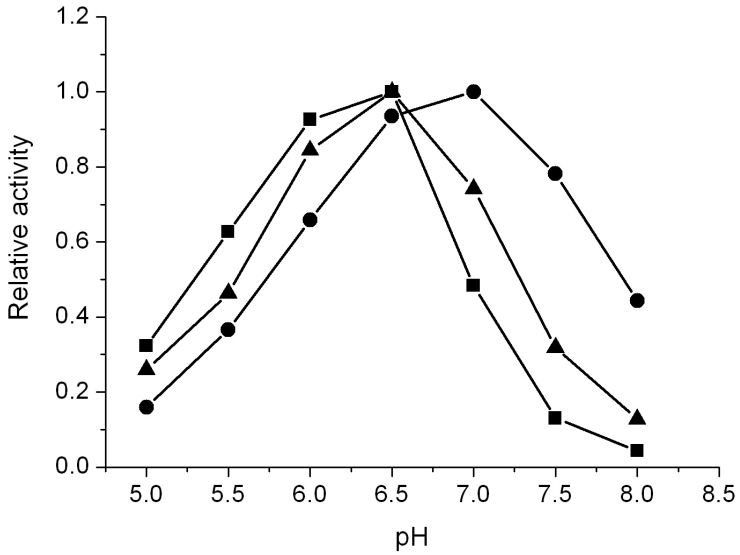

Figure 16. pH profile of wild type ADI, M1(H404R), M2(K5T/D44E/H404R). The relative activity is the ratio of the catalytic activity at the pH relative to the maximum activity of each enzyme. (■) WT, (▲) M1 (H404R), (●) M2 (K5T/D44E/H404R).

3.4.10 Stability of PpADI in the presence of human serum

Table 3 summarizes the stability of PpADI variants in serum (37℃, 60 min; standard deviation of three measurements in brackets). The mutants M1 and M2 have a similar stability in serum when compared to the wild-type PpADI wild type. The substitution D44E and H404R do not destabilize further the PpADI in serum.

Table 3. Stability of PpADI variants in the presence of human serum.

	PpADI WT	M1	M2
No incubation (A_{530})	0.08	0.27	0.98
Incubation with serum (37℃, 60 min) (A_{530})	0.05	0.15	0.69
Residual activity	60 %	55 %	70 %

3.4.11 Activity of PpADI (wild type, M1, M2) towards arginine derivative (N^G, N^G)-dimethylarginine

No detectable conversion of (N^G, N^G)-dimethylarginine could be detected with PpADI variants.

3.5 Discussion

ADI properties have to date not been engineered through directed evolution algorithms despite their often poor performances under physiological conditions and their medical importance as potential anti-tumor drug. Chemically modified of ADI (e.g. through PEGylation) (27) and fusion protein (e. g. Human serum albumin fusion, HSA) (124) have been used for addressing activity and stability demands *in vivo*. Directed evolution offers opportunities to directly improve ADI properties for *in vivo* applications and small libraries of a few thousand variants have often been sufficient to find improved muteins in directed evolution experiments (55, 125).

Our main intention in this report is to provide a validated protocol for directed ADI evolution and improving the activity at the physiological pH 7.4. *Pseudomonas plecoglossicida* CGMCC2039 (PpADI, 7.8 U/mg; pH optimum 6.5) was selected for the directed evolution studies due to its functional expression in *E. coli,* coverage of sequence space in patents and "potential" for activity improvement. PpADI is a relatively slow ADI when compared to Mycoplasma ADIs like MhADI (*Mycoplasma hominus* ADI, 35 U/mg) which would have been good alternatives for directed evolution studies (105). Reported ADI activities range from 0.115 to 140.3 IU/mg. One unit is commonly defined as the ADI amount that converts 1 µmol of L-arginine into 1 µmol of L-citrulline per minute (27).

Screening of PpADI variants yielded three amino acid positions 5, 44 and 404. Positions 44 and 404 resulted in a 4-fold higher k_{cat} at pH 7.4 and a significant shift in the pH optimum (0.5 units) when compared to wild type PpADI (Figure 17 & 8). Position 5 did not show any effect on PpADI activity.

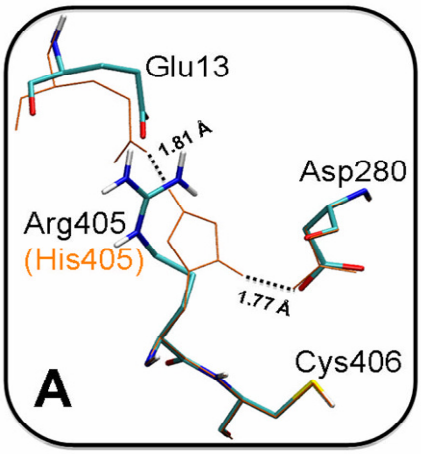

Figure 17. Structural alignment of mutant M1 model with corresponding residues of the crystal structures of the PaADI (in orange). The crystal structure of PaADI which was diffracted in absence of the substrate arginine (1RXX) was used to investigate the substitution of His405 to Arg405. The Arg405 variant shows with respect the Asp280 a different orientation of the guanidinium group when compared to side chain of His405 (in orange).

Galkin and coworkers postulated that the histidine in position 404 (corresponding position in “their” PaADI is 405) is a key residue in controlling activity at acidic and neutral pH. In protonated state of the imidazolium ring a hydrogen bonding interaction can be formed with the oxygen of Asp280 (carboxyl group). This hydrogen bond favors stabilizing interactions between Asp280 and the substrate arginine. His405 in PaADI was reported (17) to share protons with Asp280 and Glu13 and to be important for modulating electrostatic environments of closely located catalytic groups. The same report postulated that H405 is likely to be protonated when the substrate arginine binds to catalytic triad (His278, Glu224, Cys406) [(2)]. Based on these reports the His404 in PpADI was subjected to a site directed mutagenesis to Arg404 and named M1. The M1 variant (H404R) shows 40 % residual activity compared to wild type PpADI at pH 6.4 and a 1.8-fold increase in activity at pH 7.4 (see Table 1). In the M1 (H404R) mutant (see the model in Figure 17; based PaADI 1RXX; residue His404 in PpADI corresponds to His405 in PaADI), the conformational effect due to the extended side chain of Arg likely weakens the hydrogen bond to Asp280 and thus reduces the stabilizing effect on arginine binding. As a result the activity of M1 is reduced, especially at

lower pH values at which His405 is protonated. However at elevated pHs, His405 becomes increasingly deprotonated whereas Arg405 remains protonated and can therefore still stabilize Asp280 for arginine binding. The electrostatic effect suggested by theoretical and experimental studies have evidenced the importance of positively charged residues to modulate the reaction rate of PaADI (126). At pH 6.4, histidine in wild type PpADI and arginine in M1 are both positively charged. At pH 7.4, histidine is only partially positive charged and PpADI's activity is reduced (>90 %) while arginine in M1 remains positively charged preserving M1's activity (Figure 17).

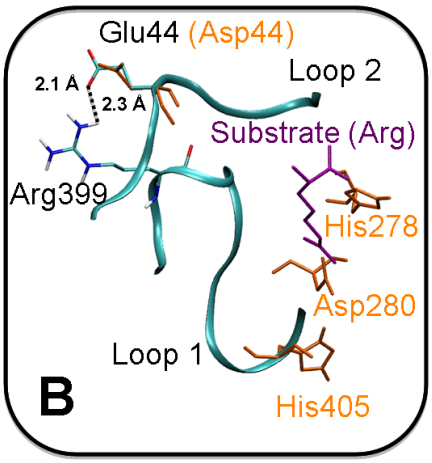

Figure 18. Structural alignment of mutant M2 model with corresponding residues of the crystal structures of the PaADI (in orange). The PaADI crystal structure in presence of substrate arginine was used (2A9G) to investigate the role of the substitution Asp44 to Glu44. The latter was solved for an inactive variant in which Cys406 was replaced by Ala406. The extended side chain of Glu44 might improve the hydrogen bond interaction with the Arg399 inducing a conformational shift of loop 1.

The PpADI H404R was used as starting variant for directed evolution. The amino acid position 44 was identified from a epPCR library (2400 variants screened) resulting in a triple mutant M2 (K5T D44E H404R). For investigating the role of each position the double mutants (K5T H404R) and (D44E H404R) were generated. Only the double mutant (D44E H404R) revealed improvements in k_{cat} (4-fold, pH 7.4; Figure 18). The rationale behind the effects of the mutation D44E on the PpADI activity is more complex to extrapolate from the available ADI crystal structures. Comparative crystallographic studies have shown that the

entrance of the active site is decorated by 4 loops that undergo conformational transitions upon arginine binding (17). The loops exhibit significant shifts that limit the access of water molecules to the active site. The Asp44 is located in loop 1 (residues 30-46) and upon binding of the substrate, Asp44 comes closer to the positively charged Arg399 located on loop 4 (residues 392 to 403). In the D44E mutant, the longer side chain reduces the distance with Arg399 favoring the formation of hydrogen bond (see model in Figure 18). The reinforced interaction between Glu44 and Arg399 might expedite conformational changes in loops, probably confining the arginine substrate in the active site and hence promote arginine conversion. In the future, we plan to further investigate the influence of H404R and D44E using molecular dynamics simulations, further boost the k_{cat} at pH 7.4 and reduce the K_m value of PpADI.

Overall site directed mutagenesis of position H404R and one round of directed evolution (2400 variants screened) resulted in a triple mutant M2 (K5T D44E H404R) with 4-fold higher k_{cat} at pH 7.4 (compared to wild type; Figure 4). The best mutant isolated, M2, has specific activity of 31.3 U/mg at pH 7.4 which is already after one round of evolution close to the specific activity of MhADI (35 U/mg) (127) at its pH optimum. The stability and specificity of improved PpADI variants are furthermore important for cancer treatment *in vivo*. First experiments in AB-human serum (Invitrogen) showed an unaltered stability of M2 compared to the wild type PpADI and (N^G, N^G)-dimethylarginine conversion could not detect with the citrulline colorimetic assay.

3.6 Conclusion

In summary, a directed evolution protocol has been developed for PpADI and validated by increasing the k_{cat} of PpADI at physiological pH (7.4). The reported screening system is the first one employed in directed ADI evolution and can likely be used for other ADIs and other properties such as temperature stability, salt/detergent stability or protease resistance.

Chapter 4. PpADI reengineered for efficient operation under physiological conditions

4.1 Abstract

The proof of concept for ADI engineering by directed evolution resulted in variant M2 (K5T/D44E/H404R). M2 has a pH optimum of pH 7.0 and 4-fold higher k_{cat} value than the wild type PpADI (pH 7.4, 0.5 M phosphate buffer) and an increased K_m value for substrate arginine. In this chapter, in order to improve the catalytic efficiency of PpADI at low concentration of arginine, variant M5 (K5T/D38H/D44E/A128T/H404R) and M6 (K5T/D38H/D44E/A128T/E296K/H404R) were generated from an epPCR library: at pH 7.4 (PBS buffer), the $S_{0.5}$ value decreased from 2.01 mM (parent M3, K5T/D44E/A128T/H404R) to 1.48 mM (M5) and 0.81 mM (M6). The $S_{0.5}$ value of M6 (0.81 mM) is lower than that of PpADI wild type (1.30 mM); the k_{cat} value improved from 0.18 s^{-1} (PpADI wild type) to 17.56 s^{-1} (M5, 97.6-folds) and 11.64 s^{-1} (M6, 64.7-fold).

4.2 Introduction

ADI-based arginine depletion is a target specific therapy for arginine-auxotrophic tumors (e.g. hepatocellular carcinomas and melanomas) and pegylated ADI is currently under clinical trials for HCC with promising results (45). HCC is the third leading cause of cancer mortality world wide with a less than 10 % 5-year survival rate (EU and USA) (128) due to low responses of hepatoma to chemotherapeutic treatments. In 1999, US Food and Drug Administration (FDA) designated ADI-PEG-20 orphan drug status for the treatment of HCC and invasive malignant melanomas, and in 2005 European Agency for the Evaluation of Medicinal Products (EMEA) also granted ADI-PEG-20 orphan drug status for the treatment of HCC. Phase II trials of ADI-PEG-20 in patients with metastatic

hepatocellular carcinomas have shown that the drug is safe, well tolerated, and may benefit patients with unresectable HCC. Izzo and coworker suspected that combination therapies of arginine deprivation and growth inhibition via kinase inhibitors might improve the survival rate further more. Additionally, ADI can enhance radio sensitivity of human mammary adenocarcinoma (MCF-7 cells) (48), exerts anti-proliferative and anti-angiogenic activities and inhibits the growth of viruses such as HIV-1 and hepatitis (49, 50). Current research efforts are focused on ADI's *in vivo* inhibitory effect towards leukemia, melanoma, prostate cancer, renal cell carcinoma, and human umbilical vein endothelial cells (HUVEC) (19, 44, 51-53), clinical trials for HCC (phase II) (45) and melanoma (phase I/II) (46), and inhibitory mechanisms of ADI to tumors (54).

Arginine deprivation is believed to be a main molecular reason for ADI's inhibitory effects on arginine auxotrophic tumors which do not express argininosuccinate synthetase (ASS). ADIs catalyze the first step of the arginine dehydrolase pathway by hydrolyzing arginine to citrulline and ammonium. ADI genes have been identified, purified, and characterized from bacteria, archaea and some eukaryotes excluding mammalian cells (see review (27)). Enzymatic properties of several recombinant ADIs have been examined, such as specific activity, functional expression level, temperature optimum, pH optimum, substrate affinity for arginine, and half-life in human plasma. Only the ADI from *Mycoplasma hominis* has so far been developed as orphan drug by Pheonix Pharmacologics Inc. for HCC and melanoma (129). From enzyme kinetic point of view, none of the ADIs is ideally suited for *in vivo* applications under physiological conditions. Protein engineering by rational design and directed evolution offers opportunities to tailor ADI properties to physiological conditions. PpADI (ADI from *Pseudomonas plecoglossicida*) was functionally expressed in *E. coli* with a simple protocol and has been engineered for the first time by directed evolution for improved activity at physiological pH (3). The variant M2 (K5T/D44E/H404R), by our group reported, showed a 4-fold higher specific activity than the wild type PpADI (0.5 M phosphate buffer, pH 7.4), but a increased K_m value (3.5-fold).

High activity at low arginine concentration is an important prerequisite for ADI's medical application, allowing low ADI dose required per treatment.
In the present work, we improved the directed evolution protocol and identified a PpADI variant with further improved activity and slightly decreased "K_m value" and PpADI variant with lowered K_m value maintaining its high catalytic activity. Those variants were characterized in respect to their kinetic constants.

4.3 Materials and methods

4.3.1 Materials

All chemicals were of analytical-reagent grade or higher quality and were purchased from Fluka (Neu-Ulm, Germany), Sigma-Aldrich (Steinheim, Germany) and Applichem (Darmstadt, Germany), except the resins for purification (TOSOH, Stuttgart, Germany). All enzymes were purchased from New England Biolabs (Frankfurt, Germany), Fermentas (St. Leon-Rt, Germany), and Sigma-Aldrich Chemie (Taufkirchen, Germany), unless stated otherwise.
Thermal cycler (Mastercyler gradient; Eppendorf, Hamburg, Germany) and thin-wall PCR tubes (Multi-ultra tubes; 0.2 µl; Carl Roth, Germany) were used in all PCRs. The PCR volume was always 50 µl except for Megaprimer PCR of whole plasmid (MEGAWHOP, 25 µl); larger volumes were prepared in multiple 50-µl PCRs. The amount of DNA in cloning experiments was quantified by using a NanoDrop photometer (NanoDrop Technologies, Germany).

4.3.2 Methods

4.3.2.1 Site saturation mutagenesis of *PpADI* M2 at position A128

Site directed mutagenesis of *PpADI* M2 (K5T/D44E/H404R) at position A128 was performed according to the published method (130). The following oligonucleotides were used for mutagenesis of A128: 5'-CTGATCGGCGGCGTGNNNGGCCAGGACCTGCCG-3' and 5'-CGGCAGGTCCTGGCCNNNCACGCCGCCGATCAG-3' (underlining indicated the substituted nucleotide). For the mutagenic PCR (First stage: 98°C for 30 s, 1 cycle; 98°C, 30 s/ 55°C, 1 min/ 72°C, 3 min, 3 cycles. Second stage: 98°C for 30

s, 1 cycle; 98℃, 30 s/ 55℃, 1 min/ 72℃, 3 min, 15 cycles; 72℃ for 3 min, 1 cycle), 2 U of PhuS DNA polymerase, 0.20 mM of dNTP mix, 25 pmol of each primer together with 100 ng of template (pET42b(+) harboring PpADI M2 gene) were used. Following the PCR, DpnI (40 U; New England Biolabs) was added, and incubated overnight at 37℃. The PCR products were purified by using a QIAquick PCR Purification Kit (Qiagen) and transformed into *E. coli* BL21-Gold (DE3) for expression.

4.3.2.2 Construction of PpADI error-prone library

EpPCR library was generated by the standard error-prone PCR (epPCR) using improved variant M3 (K5T/D44E/A128T/H404R) as template. For the mutagenic PCR (95℃ for 2 min, 1 cycle; 95℃, 30 s/ 55℃, 30 s/ 72℃, 30 s, 29 cycles; 72℃ for 3 min, 1 cycle), 2.5 U of Taq DNA polymerase, 0.20 mM of dNTP mix, 50 ng of template (pET42b(+) harboring PpADI M3 gene), 0.01-0.1 mM of $MnCl_2$ and 10 pmol of each primer (5'-TACATATGTCCGCTGAAACACAGAAG-3' and 5'-GTGCTCGAGTTAGTAGTTGATCGG-3') were used. The PCR products were purified by using a QIAquick PCR Purification Kit. The purified epPCR products were cloned into expression plasmid pET42b(+) by MEGAWHOP (114). For MEGAWHOP (72℃ for 5 min, 1 cycle; 98℃ for 1 min 30 s, 1 cycle; 98℃, 45 s/ 55℃, 45 s/72℃, 4 min, 24 cycles; 72℃ for 10 min, 1 cycle), 1.2 U of PfuS DNA polymerase, 0.20 mM of dNTP mix, 500 ng of epPCR products together with 50 ng of template (pET42b(+) harboring PpADI gene of variant M3) were used. Following the PCR, DpnI (40 U; New England Biolabs) was added, and incubated (overnight; 37℃). The MEGAWHOP products were transformed into *E. coli* BL21-Gold (DE3) for expression and screening.

4.3.2.3 Site directed mutagenesis at position D38 of *PpADI* M4

Site directed mutagenesis of *PpADI* variant M4 at position D38 was performed according to the published method on plasmid pET42b(+)-ADI-M4 (K5T/D44E/A128T/E296K/H404R). The following oligonucleotides were used for mutagenesis of D38H: 5'-ACCCCGAGCAACTGCCACGAGCTGCTGTTCGAC-3'

and 5'-GTCGAACAGCAGCTCGTGGCAGTTGCTCGGGGT-3' (underlining indicated the substituted nucleotide). Conditions for mutagenic PCR are as described in "Site saturation mutagenesis of *PpADI* M2 at position A128".The PCR products were purified by using a QIAquick PCR Purification Kit (Qiagen) and transformed into *E. coli* BL21-Gold (DE3) for expression.

4.3.2.4 Site saturation mutagenesis at position D38 and E296 of *PpADI* M3

Site saturation mutagenesis library at position D38 and E296 of *PpADI* variant M3 (K5T/D44E/A128T/H404R) were generated according to the published method on plasmid pET42b(+)-ADI-M3 using the following oligonucleotides: D38FP (5'-ACCCCGAGCAACTGCNNNGAGCTGCTGTTCGAC-3'), D38RP (5'-GTCGAACAGCAGCTCNNNGCAGTTGCTCGGGGT-3') and E296FP (5'-GTCACGGTTTTCCCGNNNGTGGTGCGCGAGATC-3'), E296RP (5'-GATCTCGCGCACCACNNNCGGGAAAACCGTGAC-3') (underlining indicated the substituted nucleotide). Conditions for mutagenic PCR are as described in "Site saturation mutagenesis of PpADI M3 gene at position A128".The PCR products were purified by using a QIAquick PCR Purification Kit (Qiagen) and transformed into *E. coli* BL21-Gold (DE3) for expression.

4.3.2.5 Cultivation and expression of PpADI in 96-well plates

Cultivation and expression in 96-well plates (flat bottom, polystyrene plates; Greiner Bio-One GmbH, Frickenhausen, Germany) were performed as previously described in 3.3.2.8.

4.3.2.6 Improved screening system in 96-well plate to identify PpADI variants with high activities at low arginine concentration

As describe previously, the modified protocol of citrulline detection based on carbamido-diacetyl reaction was used for screening for improved ADI affinity to arginine at pH 7.4. 15 µl of cell culture was transferred to 96-well microtiter plate. Enzyme reaction was initiated by addition of arginine solution (105 µl, 1mM arginine in PBS buffer, pH 7.4) supplemented with

cetyltrimethylammoniumbromide (CTAB, 4 mM), and incubated (10 min, 37°C). The following color development procedure was carried out as described previously (3).

Standard deviation measurements were performed in 96-well plate format using culture from BL21-Gold (DE3) lacking PpADI and in a separate experiment containing PpADI variant M3. Apparent standard deviation was based on the absolute absorbance values obtained from the PpADI variant M3 plate. The true standard deviation was calculated by subtracting the background absorbance value of the microtiter plate lacking ADI from the apparent values.

4.3.2.7 Expression of PpADI in shaking flask and purification

Expression of PpADI in shaking flasks and purification (by anion exchange chromatography and gel filtration) was performed as previously described in 3.3.2.10.

4.3.2.8 Characterization of PpADI variants

Preliminary determination of kinetic constants for site saturation mutagenesis variants of position 38 and 296

The k_{cat} and K_m values were determined from initial velocity data measured as a function of substrate concentration. Enzyme reaction was carried out at 37°C in incubator (Heraeus Holding GmbH, Hanau, Germany) using cell crude extract. 2 ml of expression culture was harvested by centrifugation (Eppendorf 5415R 4°C, 13,000 g, 10 min) and then freezed (-20°C, overnight). Cell lysate was prepared by resuspending the cell pellet in lysozyme (91000 U, 50 mM phosphate buffer, pH 7.4, 1.3 ml) followed by incubation (37°C, 40 min) and centrifugation (4°C, 13,000 g, 10 min). 15 µl of diluted (4 times diluted with 50 mM phosphate buffer, pH 7.4) cell lysate was transferred to 96-well microtiter plates. Enzyme reaction was initiated by addition of arginine solution (105 µl, 0.25-10 mM arginine in PBS buffer, pH 7.4) and incubated (7 min, 37°C). Subsequently, ferric-acid solution (120 µl) was added to each well to stop enzyme reaction. 60 µl of terminated

enzyme reaction mixture was transferred to 96-well PCR plate for color development. Ferric-acid solution (90 µl) and DAM-TSC solution (15 µl) were added to each well. The 96-well PCR plate was then incubated (70°C, 30 min) in thermal cycler (Eppendorf Mastercyler gradient) for color development, followed by incubation in ice water to stop color development. Absorbance was measured at 530 nm using a microtiter plate reader (Tecan Sunrise TC reader, Tecan Group AG, Zurich, Switzerland). The initial velocity data obtained were fitted to the equation $v = V_{max}[S]/([S] + K_m)$ (where v is the initial velocity, Vmax the maximum velocity, [S] the substrate concentration, and Km the Michaelis constant) using GraphPad Prism software (GraphPad software, San Diego, CA, USA). The kcat was calculated from the ratio of V_{max} and enzyme concentration.

Determination of kinetic constants of PpADI wild type and variants M3, M4, M5, M6

The k_{cat} and $S_{0.5}$ values were determined from initial velocity data measured as a function of substrate concentration. Enzyme reaction was carried out at 37°C in a water bath as described previously using purified enzyme (50 µl, 0.1-1.8 µM) to and substrate solution (200 µl, 0.5 mM to 10 mM of arginine, PBS buffer, pH 7.4) in deep well plates.

The initial velocity data obtained were fitted to the sigmoidal model of kinetics equation $v = V_{max}^{n}/(S_{0.5}^{n} + K^{n})$ (where v is the initial velocity, V_{max} is the maximum velocity, K is the substrate concentration, and $S_{0.5}$ is the ligand concentration producing half occupation (131)) using GraphPad Prism software (GraphPad software, San Diego, CA, USA). The k_{cat} was calculated from the ratio of V_{max} and enzyme concentration.

4.3.2.9 Native polyacrylamide gel electrophoresis of PpADI variants

10% of polyacrylamide native gels were used for protein electrophoresis to analyze the native form of PpADI variants. Purified protein of PpADI variants (7 µl of protein and 3 µl of loading dye) were loaded into each lane of native gel. The

molecular marker used in the gel is NativeMark™ Unstained Protein Standard (Invitrogen, Darmstadt, Germany). The electrophoresis was performed with tris/glycine buffer (pH 8.3) and electrophoresis chamber was incubated in ice-water bath. Protein bands were stained with Coomassie brilliant blue solution.

4.3.2.10 Homology modeling

Homology modeling approach was used for the structure prediction of PpADI. The model was built by using the automated structure prediction tool, Protein homology/analogy recognition engine (Phyre: http://www.sbg.bio.ic.ac.uk/~phyre/) (132). The crystal structure of PaADI (PDB ID: 2A9G) was used as template by the server and It has 84.9% sequence identity (http://blast.ncbi.nlm.nih.gov/Blast) with PpADI. Procheck program suit (http://www.ebi.ac.uk/thornton-srv/software/PROCHECK/) (133) was used to assess the stereochemical quality of the model. Ramachandran plot which represented that 84.7% residues were present in the most favoured region and 14.7% in additional allowed region (Figure 3). Dfire was used to access non bonded atomic interaction in the model (http://sparks.informatics.iupui.edu/hzhou/dfire.html/) (134), and Qmean (http://swissmodel.expasy.org/qmean/cgi/index.cgi) (135) for the estimation of global protein quality. Swiss-PdbViewer (118) was used to create the tetramer structure by fitting the monomer model on the 4 units of the 2A9G template. The variant M6 (D38H, D44E, A128T, E296K, H404R) were created by using the “mutate” tool of the Swiss-PdbViewer and by selecting rotamers with the best fitness score. All tetramers were energy minimized in vacuum using GROMOS 43B1 force field (119).

4.4 Results

4.4.1 Improved screening system in microtiter plates to identify PpADI variants with high activities at low arginine concentration

Screening assay was based on the validated citrulline colorimetric screening protocol in microtiter plate, as reported previously (3). In order to screen for variants with high activity at low arginine concentration under physiological

condition concerning pH and ion concentrations, 1 mM arginine in PBS buffer (pH 7.4) as substrate solution was employed in screening assay and enzyme reaction time was controlled accordingly (10 min). The coefficient of variation is an important performance criterion of a screening system to determine its accuracy. Optimized assay condition with 1 mM arginine (PBS buffer, pH 7.4) as substrate resulted in true coefficient of variation of 14.9 % (Figure 1). The resulting low absolute absorbance value is a main reason for the high true coefficient of variation (14.9 %). In the previous screening system, 100 mM arginine in 0.5 M sodium phosphate buffer was used and yielded higher activity variants but with higher K_m value.

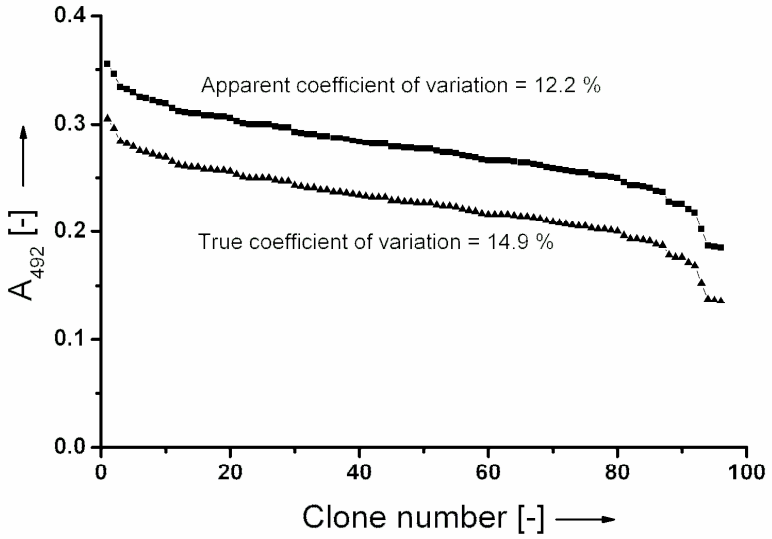

Figure 1. Activity values in descending order of the PpADI variant M3 conversion of arginine to citrulline in a 96-well microtiter plate using the optimized assay protocol. The apparent coefficients of variation were calculated without subtracting the background and the true coefficients of variation after background subtraction.

4.4.2 Genealogic tree of directed PpADI evolution

Figure 2 shows the two rounds of PpADI evolution, generation of saturation mutagenesis libraries and recombination of beneficial positions to finally obtain the PpADI variant M6 with 64.7-fold higher k_{cat} and reduced $S_{0.5}$ (1.3 mM (WT) to 0.81 mM (M6). Based on structure-function analysis of PaADI[16], M1 was generated by substitute His at position 404 with Arg. Position 404 is through

interactions with position Asp280 involved in substrate stabilization during catalysis. M1 was subject to the first round of epPCR library, from which M2 was identified showing a 4-fold improved k_{cat} value and increased K_m value (2.5 mM in 0.5 mM sodium phosphate buffer, pH 7.4)[15]. M3 was generated by a site saturation mutagenesis library at position 128 which increased in another clone the expression level (data not shown). In order to improve PpADI towards medical application demands (high activity at low arginine concentration), a second epPCR mutant library was constructed using M3 as parent. M4 with decreased $S_{0.5}$ value (0.81 mM) and M5 with increased K_{cat} value (17.56 s^{-1}) were identified after screening of ~1400 clones. In M4 the position E296 was identified to be important for lowering $S_{0.5}$ and in M5 position D38 was identified to be important for activity increase. M6 was finally constructed by combining the substations at position D38 and E296. Saturation mutagenesis of these two positions did not yield any further improved $S_{0.5}$ or activity variant.

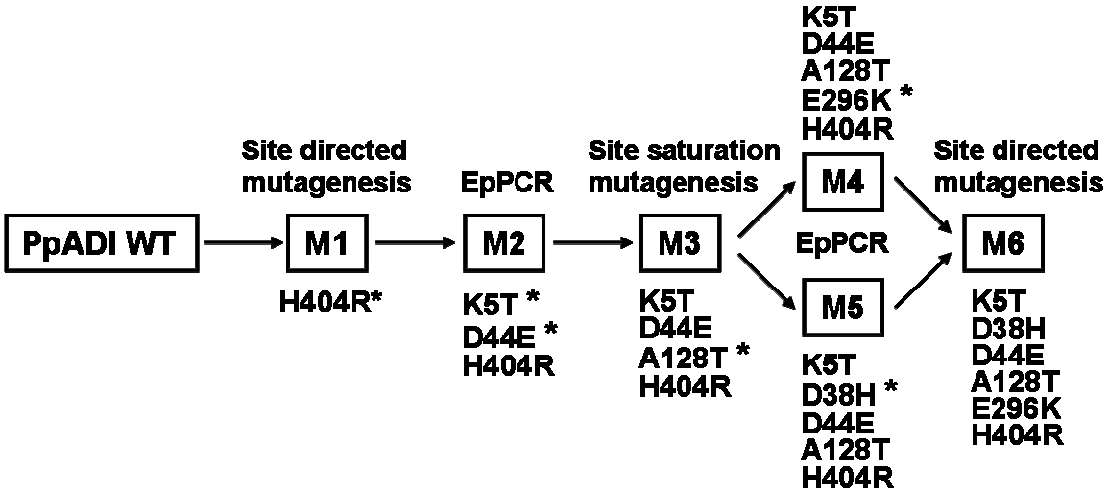

Figure 2. Genealogic tree of PpADI variants (M1 to M6) with generated amino acid substitutions. Novel substitutions are indicated by an asterisk.

4.4.3 EpPCR library construction and screening for variants with high activities at low arginine concentration

Variant M2 was used as a starting template. As described previously, M2 shifts the pH optimum from pH 6.5 to pH 7.0 and has a 4-fold faster k_{cat} than PpADI wild type. In one sequenced mutant, position A128 was identified to be

responsible for higher expression (data not shown). Site saturation mutagenesis on M2 therefore was carried out at position A128. The resulting variant M3 (K5T/D44E/A128T/H404R) showed a ~2-fold improved expression and was subsequently used as parent template for epPCR library.

Three concentrations of $MnCl_2$ (0.01-0.10 mM) were used in epPCR library generation to adjust the ratio of active to inactive clones. Instead of 0.02 mM $MnCl_2$, 0.05 mM $MnCl_2$ which generated 46 % of inactive mutant was selected for library generation. EpPCR mutant libraries with a ratio of ~50 % active and ~50 % inactive clones have often been used successfully in directed evolution, improving enzyme properties by gradual changes (one or two amino acids changes per round of mutagenesis and screening). Two variants M4 and M5 were identified from this epPCR library (~1400 clones) and further characterized. Variant M4 and M5 were sequenced and one additional amino acid substitution was identified for each variant, E296K and D38H, respectively.

4.4.4 Site saturation mutagenesis of *PpADI* at position D38 and E296

To investigate their role in improving of catalytic performance for arginine, site saturation mutagenesis library at position D38 and E296 were generated using PpADI M3 as template. For each position, ~300 clones were screened at low concentration of arginine (1 mM, PBS buffer, pH 7.4), using 96-well plate format citrulline colorimetric screening assay.

After the screening of site saturation mutagenesis libraries of position 38 and 296, variants with higher activity were chosen for preliminary kinetic investigation using crude cell extract. Beneficial mutants were identified and sequenced from both sites (Table 1). At position 38, the following beneficial substitutions were found: D38R (three times, AGA, CGG, CGT) and D38K (twice, AAG, AAA). In all cases, the negatively charged acidic amino Asp had been replaced by positively charged amino acids, Arg or His. Substitution by negatively charged Glu resulted in a clone showing a parent M3-like kinetic behavior. Hydrophobic amino acid

substitution by Pro resulted inactive clone under assay conditions. At position 296, the following substitutions were found to be beneficial: E296K (twice, AAA, AAG), E296N (once, AAC), E296T (once, ACC), E296G (once, GGA). Among these substitutions, variants with substitution to positively charged residue Lys show lowest $S_{0.5}$ value for arginine while substitution by uncharged amino acids (Asn, Thr, Gly) shows relatively marginal improvement compared to E296K. Hydrophobic amino acid substitution by Pro and Trp resulted in very low activity clones.

Table 1. Nucleotide and amino acid substitutions at position 38 in PpADI M3.

PpADI variants	Substitution at position 38	k_m (mM)
M3 (parent)	Asp (GAC)	3.74 ± 0.35
SSM-D38R	Arg (AGA, CGG, CGT)	1.16 ± 0.21
SSM-D38K	Lys (AAG, AAA)	1.01 ± 0.28
SSM-D38E	Glu (GAG)	2.95 ± 0.77
SSM-D38P	Pro (CCA)	n. d.
SSM-D38T	Thr (ACC)	n. d.
M5	His (CAC)	1.26 ± 0.12

Kinetic experiments were performed with crude cell extracts.

Table 2. Nucleotide and amino acid substitutions at position 296 in PpADI M3.

PpADI variants	Substitution at position 296	k_m (mM)
M3 (parent)	Glu (GAA)	3.74 ± 0.35
SSM-E296K	Lys (AAA, AAG)	0.20 ± 0.01
SSM-E296N	Asn (AAC)	0.53 ± 0.04
SSM-E296T	Thr (ACC)	0.61 ± 0.04
SSM-E296Q	Gln (CAA)	0.79 ± 0.06
SSM-E296G	Gly (GGA)	1.29 ± 0.12
SSM-E296W	Trp (TGG)	n. d.
SSM-E296P	Pro (CCT)	n. d.
M4	Lys (AAA)	0.27 ± 0.02

Kinetic experiments were performed with crude cell extracts.
* n. d. activity not detectable under assay conditions.

4.4.5 Determination of kinetic constants (k_{cat} and $S_{0.5}$) of PpADI wild type and variants M3, M4, M5 and M6

Table 3. Kinetic constants of wild type PpADI and variants.

	Wild type	M3 (parent)	M4	M5	M6
k_{cat} (s^{-1})	0.18 ± 0.05	10.13 ± 0.36	5.88 ± 0.09	17.56 ± 1.15	11.64 ± 0.50
$S_{0.5}$ (mM)	1.30 ± 0.25	2.01 ± 0.19	0.81 ± 0.03	1.48 ± 0.17	0.81 ± 0.09

* Kinetic contants of PpADI wild type is different from our previous report because in stead of 0.5 M phosphate buffer, PBS buffer was used for kinetic measurements. K_{cat} value of PpADI wild type dropped from 5.6 s^{-1} to 0.18 s^{-1} and k_{cat} value of M2 is reduced ~2-fold.

M3, the parent of the second round of PpADI epPCR library, M4 with decreased $S_{0.5}$, M5 with increased k_{cat} and best variant M6 with best combination of k_{cat} value and $S_{0.5}$ were selected for detailed characterization studies.

Kinetic characterization of PpADI variants was performed using PBS buffer (pH 7.4), which is commonly used in biological research. PBS buffer helps to maintain a constant pH and its osmolarity and ion concentrations usually match those of the human body. Citrulline production of PpADI variants was maintained between 0.2-0.8 mM. Table 3 summarizes the k_{cat} and $S_{0.5}$ values of parent M3 (K5T/D44E/A128T/H404R), variants M4 (K5T/D44E/A128T/E296K/H404R), M5 (K5T/D44E/A128T/D38H/H404R) and M6 (K5T/D38H/D44E/A128T/E296K/H404R), which were expressed in shaking flasks cultures and purified using a two step procedure (anion exchange follows by gel filtration). Compared to parent M3 ($S_{0.5}$ = 2.01 mM), both variants M4 and M5 have a lower $S_{0.5}$ for arginine conversion at pH 7.4, 0.81 mM and 1.48 mM, respectively. Variant M4 shows a decreased k_{cat} value, 58% of parent M3 while M5 shows a 1.7-fold higher k_{cat} compared to parent M3. Variant M6 with combined mutations (K5T/D38H/D44E/A128T/E296K/H404R) shows decreased $S_{0.5}$ value, 40 % of parent M3 (K5T/D44E/A128T/H404R), 62 % of PpADI wild type, and a 64.7-fold faster k_{cat} value than PpADI wild type. M6 is 42.3-fold faster than PpADI wild type with 0.4 mM arginine (PBS buffer, pH 7.4) as substrate.

After two rounds of epPCR libraries coupled with site directed mutagenesis, a variant M6 with 64.7-fold higher k_{cat} and lower $S_{0.5}$ value (0.81 mM) than PpADI wild type (0.31 mM). At low concentration of arginine, activity of M6 enhanced dramatically than M3 and wild type. For example, M6 is 42.3-fold faster than PpADI wild type in 0.4 mM arginine (PBS buffer, pH 7.4).

4.4.6 Native polyacrylamide gel electrophoresis of PpADI variants

Multimeric form of PpADI variants were investigated by native polyacrylamide gel electrophoresis. As shown in Figure 3, two distinct protein bands representing two multimeric forms tetramer and dimer (molecular weight of a subunit is ~ 46 kDa) were observed, but with different concentration percentage. The major multimeric form of M3 is dimer. Compared to M3, M4 with an additional mutation E296K shows a very different pattern: tetramer is the main form; while M5 with an additional mutation D38H contains more or less equal amount of dimer and tetramer. M6, with both mutations E296K and D38H, contains more tetramer than dimer.

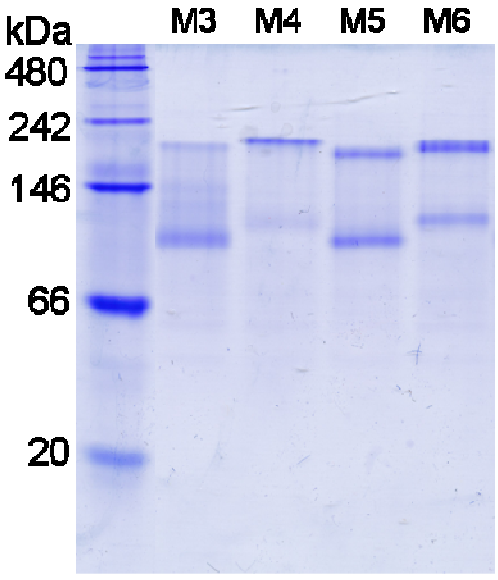

Figure 3. Native polyacrylamide gel electrophoresis of PpADI variants (M3 to M6) with different dimer/tetramer distribution. Single subunit has a molecular weight of ~46 kDa.

4.5 Discussion

Directed evolution allows improving all properties that can be reflected in a screening system through iterative rounds of diversity generation and screening. Small libraries of a few thousand variants are often sufficient to find improved variants [18] even without rational understanding of the targeted property. After establishing a first directed ADI evolution protocol yielding mutant M2, we adjusted the screening system to better reflect ADI's application conditions. Prerequisite for ADI to become an effective anti-tumor agent is that low concentrations of arginine in human plasma can effectively be converted.

Figure 2 shows the genealogic tree of PpADI evolution and before discussing the influence of each substitution individually the effect on kinetics are briefly summarized. Amino acid substitution D44E (M2) increases k_{cat} and $S_{0.5}$, substitution A128T (M3) increases the expression level, and substitution E296K (M4) decreases k_{cat} and $S_{0.5}$ and is responsible for tetramer formation. Substitution D38H (M5) increase largely k_{cat} and reduces slightly $S_{0.5}$. The combination of all mentioned residues in M6 result in a finally 64.7-fold improved PpADI activity and reduced $S_{0.5}$ (1.30 to 0.81 mM).

PpADI M3 was obtained from site saturation mutagenesis library at position A128 using M2 as template (Figure 2). M3 shows improved functional expression level of ADI (data not shown) and was used as parent for generating an epPCR library. Screening of epPCR library yielded two improved variants M4 and M5, carrying an additional mutation, E296K (M4) and D38H (M5). M4 has a decreased $S_{0.5}$ (0.81 mM) and a decreased k_{cat} value (5.88 s^{-1}; see Table 3). M5 has a decreased $S_{0.5}$ (1.48 mM) and an increased k_{cat} value (17.56 s^{-1}) when compared to parent M3 ($S_{0.5}$, 2.01 mM; k_{cat}, 10.03 s^{-1}; see Table 3). M6 which harbors both substitutions (E296K and D38H) has a decreased $S_{0.5}$ value (0.81 mM) compared to the parent M3 (1.30 mM) and the wild type (2.01 mM), and a 64.7-fold higher k_{cat} value than the PpADI wild type.

Despite further enhancing the activity of PpADI, it is crucial for an efficient conversion of the substrate arginine in human plasma (100-120 µM arginine) to reduce PpADI's "K_m" ($S_{0.5}$) value. Figure 4 shows the kinetics of PpADI WT, parent M3, and the variants M4, M5 and M6. M3 has a significantly higher k_{cat} value compared to WT, but its activity at low concentration of arginine (<1.0 mM) is very low ($S_{0.5}$ value 2.01 mM). In contrast, the most efficient variant M6 with a decreased $S_{0.5}$ value (0.81 mM) shows a remarkable activity improvement at low concentrations of arginine (<0.5 mM; see Figure 4). M6 has additional two amino acid substitutions (D38H and E296K) compared to M3 which increases k_{cat} and reduces the $S_{0.5}$ value. The combination of D38H and E296K improves especially the activity of M6 at low arginine concentrations (< 0.5 mM; see Figure 4).

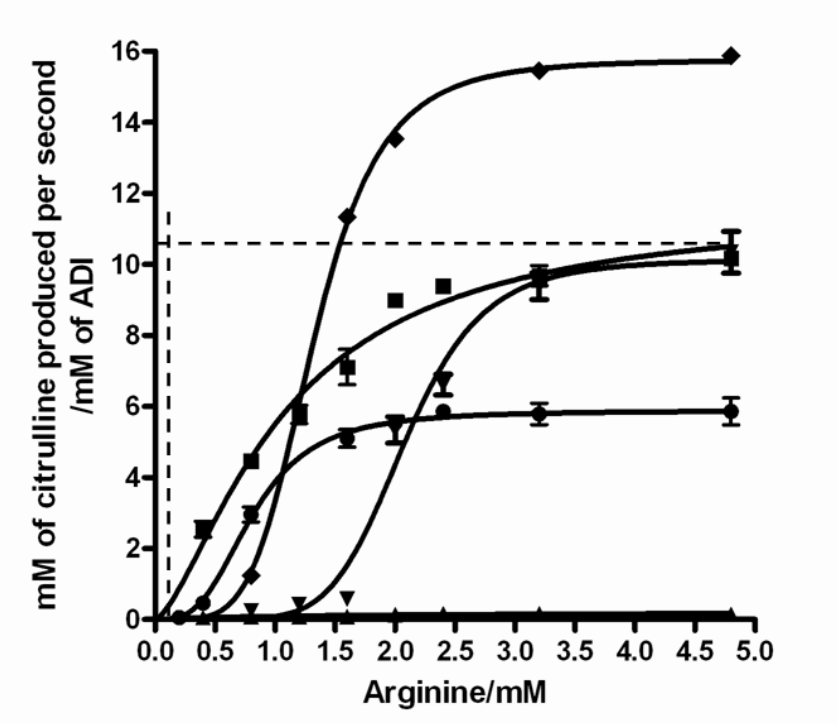

Figure 4. Kinetic curve of PpADI wild type, M3, M5 and M6. (▲) PpADI wild type, (▼) M3, (●) M4, (♦) M5 and (■) M6.

Figure 5 shows the tetrameric model (based on PaADI, PDB code 2A9G) of PpADI WT (Figure 5A) and variant M6 (Figure 5B). Monomeric units are

indicated with the letters a, b, c and d. The access channel to the active sites of each monomer is highlighted in square and faces an internal cavity generated by the assembly of four PpADI monomers. The substitutions D38H (in blue) and D44E (in green) are localized at the interface of monomer pair a-b and c-d. The substitution of Glu by Asp at position 44 provides a longer side chain in close proximity of the also negatively charged residue Asp43 (Figure 6A). The substitution E296K is localized at the border of the entrance to the internal cavity of the PpADI tetramer. E296K promotes the tetramer formation likely by introducing stabilizing interactions with other residues, for example with Thr33 (hydrogen bond). E296K inverts the charge at this position and its increased length of the side chain might promote further interactions to a neighboring monomer (Figure 6A). The combination of D44E and E296K results in a population consisting of mainly tetramers (see Figure 3; mutein M4). Interestingly with the formation of a tetramer (M4) the $S_{0.5}$ value is reduced which indicates that the tetramer complex formation promotes interactions with the substrate arginine at low concentrations. The substitution D38H together with the E296K in the mutein M6 reestablishes an almost equal population of PpADI dimers and tetramers. A hypothesis is that Lys of the E296K has an electrostatic stabilizing interaction with the Glu38 in the M4 but not to the neutral His38.

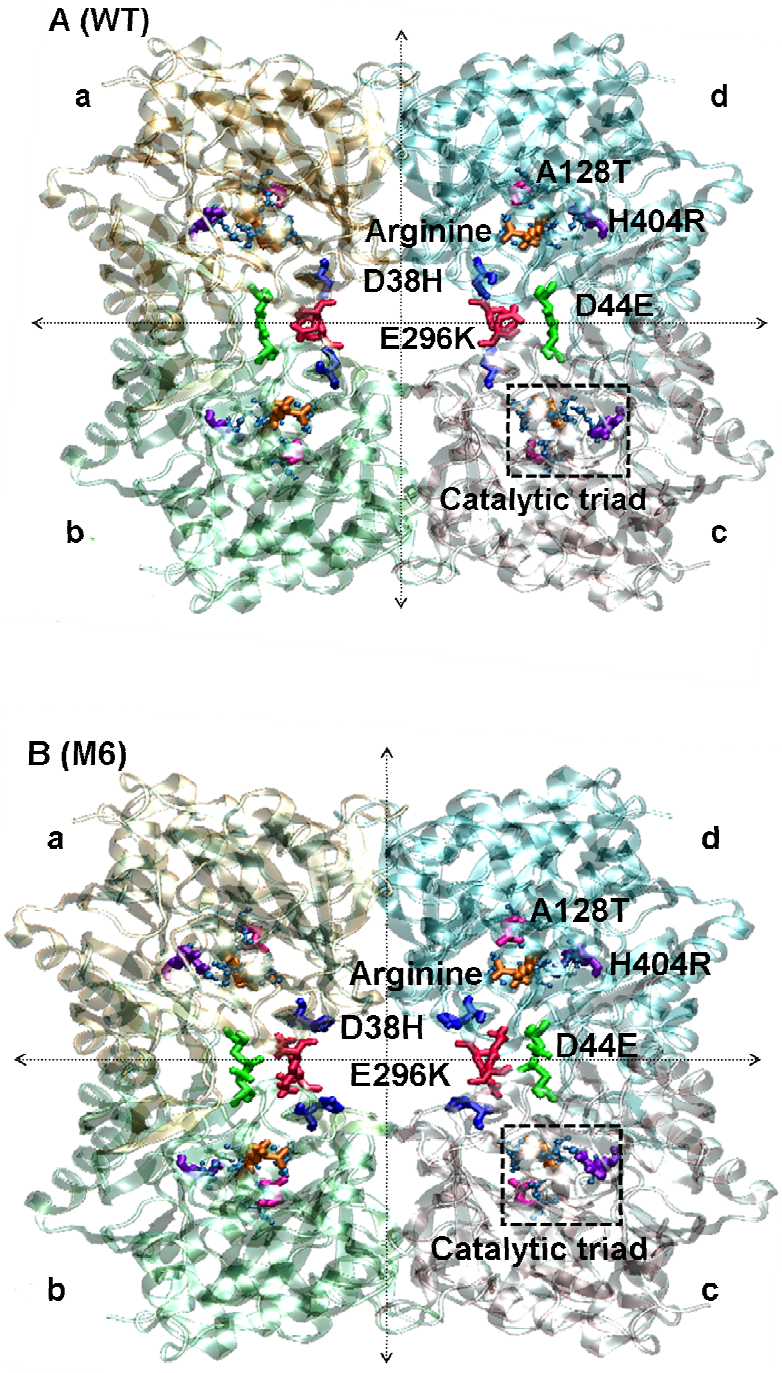

Figure 5. A). The model of WT tetramer after energy minimization in vacuum (GROMOS 43B1). B). The model of M6 tetramer after energy minimization in vacuum (GROMOS 43B1). Active site residues are represented in CRK format in a square (Blue). Mutated residues are shown in licorice format in different colors like D38H (blue), D44E (green), A128T (magenta), E296K (red) and H404R (violet). Substrate arginine is represented in orange color by licorice format.

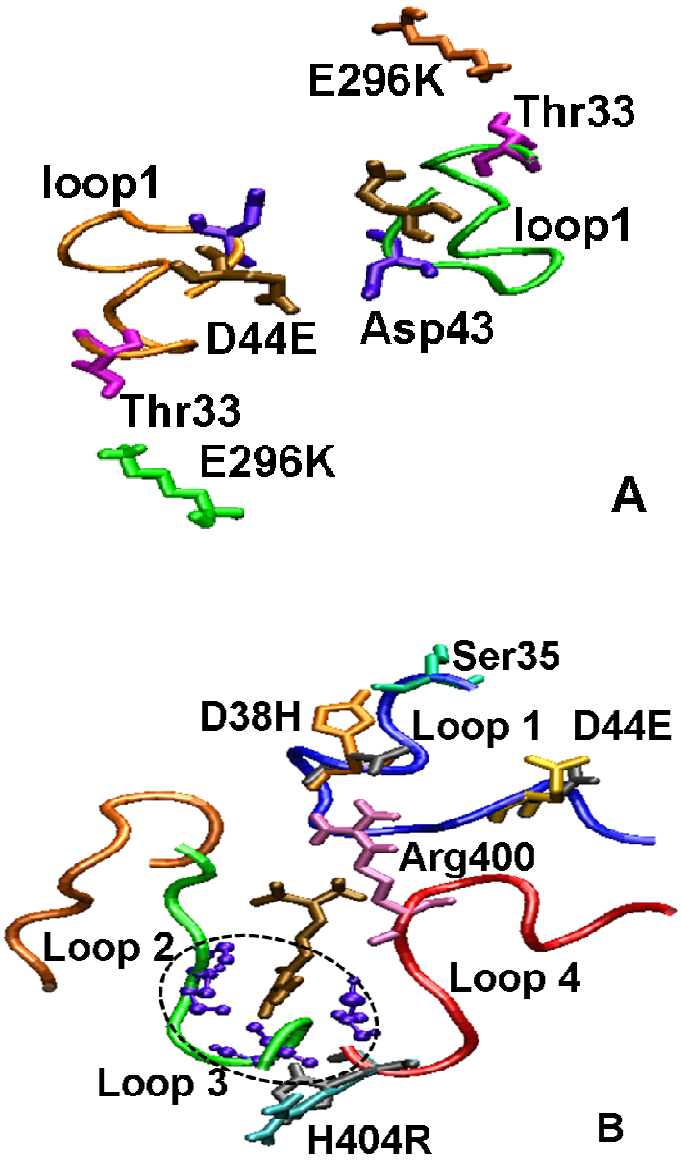

Figure 6. A). Structure model of variant M6. E296K is involved in intermonomer interaction (between chain a (orange) and b (green)) with Thr33. D44E is involved in intermonomer interaction, between chain A (orange) and B (green), with Asp43 (violet). B). Structure alignment of PpADI WT model and M6 model with four loops (loop 1:30-46, loop 2:178-175, loop 3:271-281 and loop 4: 393-404) surrounding the entrance of the active site. The substitutions in these loops and the residues involved in the interaction with those substitutions are representing: D38H (orange), D44E (yellow) and H404R (cyan, in M6; gray, in WT), Ser35 (green), Arg 400 (pink), substrate arginine (ochre), catalytic triad His278, Asp280 and Cys406 (violet, highlighted in an oval)

Figure 6B shows that the active site of the PaADI is surrounded by four loops (loop 1: 30-46, loop 2: 178-185, loop 3: 271-281, and loop 4: 393-404). These four loops undergo a conformational transition upon arginine binding and tighten

the surrounding of the arginine substrate[16]. D38 is located in loop 1 and faces towards the substrate access channel. In PpADI model (Figure 6B), the D38H mutation promotes the formation of a hydrogen bond interaction with the neighboring residues Ser35, contributing to the stability of the entropically unfavorable folded conformation of loop1. The rigidified loop 1 might be beneficial for arginine conversion. According to PaADI structure analysis, the side chain of gating residue Arg401 (Arg400 in PpADI) is located at the active site entrance and fills the substrate-binding site. The structure analysis of the C406A PaADI-L-arginine complex[16] shows that the Arg401 side chain (Arg400 in PpADI) is displaced by the substrate arginine to a position near the active site entrance that allows its hydrocarbon chain to assist shielding the catalytic site from solvent. D38 is involved in an ionic interaction and hydrogen bonding with Arg400. The substitution of Asp to His at position 38 results in a loss of ionic interactions to Arg400 due to the different lengths of the side chains. His38 can form only a hydrogen bond with active site gating residue Arg400. A weakened interaction between position 38 and Arg400 might increase the flexibility of the side chain of Arg400 which then might block less efficiently the access of arginine to the active site. As a result the variant M5 shows an improved k_{cat} value (1.7-fold compared to parent M3) due to the substitution D38H.

For elucidating further the individual role of the five identified amino acid substitutions and their influence on the active site geometry and tetramer formation crystal structures of variant M4 and M6 have to be solved.

4.6 Conclusion

In summary, with the modified screening protocol, PpADI variants with improved k_{cat} and $S_{0.5}$ were identified. The increased k_{cat} value and decreased $S_{0.5}$ value result in significant activity improvement of PpADI at low arginine concentrations. Especially the kinetic constants of PpADI variant M6 demonstrate that PpADI properties can be tailored by directed evolution. The generated PpADI variants match from their kinetic behavior therapeutic application demands much better

than the wild type PpADI. We therefore hope that by directed evolution improved PpADIs will further be investigated *in vivo* for tumor therapy.

References

1. Li L, Li ZM, Chen DQ*, et al.* Inactivation of microbial arginine deiminases by L-canavanine. Journal of the American Chemical Society, 2008; 130(6): 1918-31.

2. Lu XF, Li L, Wu R*, et al.* Kinetic analysis of *Pseudomonas aeruginosa* arginine deiminase mutants and alternate substrates provides insight into structural determinants of function. Biochemistry, 2006; 45(4): 1162-72.

3. Zhu LL, Tee KL, Roccatano D*, et al.* Directed evolution of an antitumor drug (arginine deiminase PpADI) for increased activity at physiological pH. Chembiochem, 2010; 11(5): 691-7.

4. Das K, Butler GH, Kwiatkowski V, Clark AD, Yadav P, Arnold E. Crystal structures of arginine deiminase with covalent reaction intermediates: Implications for catalytic mechanism. Structure, 2004; 12(4): 657-67.

5. Schofield PJ, Edwards MR, Matthews J, Wilson JR. The pathway of arginine catabolism in *Giardia intestinalis*. Molecular and Biochemical Parasitology, 1992; 51(1): 29-36.

6. Linstead D, Cranshaw MA. The pathway of arginine catabolism in the parasitic flagellate *Trichomonas vaginalis*. Molecular and Biochemical Parasitology, 1983; 8(3): 241-52.

7. Yarlett N, Lindmark DG, Goldberg B, Moharrami MA, Bacchi CJ. Subcellular localization of the enzymes of the arginine dihydrolase pathway in Trichomonas vaginalis and Tritrichomonas foetus. J Eukaryot Microbiol, 1994; 41(6): 554-9.

8. Biagini GA, Yarlett N, Ball GE*, et al.* Bacterial-like energy metabolism in the amitochondriate protozoon Hexamita inflata. Mol Biochem Parasitol, 2003; 128(1): 11-9.

9. Makhlin J, Kofman T, Borovok I*, et al.* Staphylococcus aureus ArcR controls expression of the arginine deiminase operon. Journal of Bacteriology, 2007; 189(16): 5976-86.

10. Seggewiss J, Becker K, Kotte O*, et al.* Reporter metabolite analysis of transcriptional profiles of a Staphylococcus aureus strain with normal phenotype

and its isogenic hemB mutant displaying the small-colony-variant phenotype. Journal of Bacteriology, 2006; 188(22): 7765-77.

11. Altucci P, Sapio V, Vitale P, de Vargas F. Mycoplasma in human pathology. Current status of the problem, with special reference to respiratory pathology. Recenti Prog Med, 1966; 41(5): 409-55.

12. Harasawa R, Koshimizu K, Kitagawa M, Asada K, Kato I. Nucleotide sequence of the arginine deiminase gene of *Mycoplasma hominis*. Microbiology and Immunology, 1992; 36(6): 661-5.

13. Takaku H, Matsumoto M, Misawa S, Miyazaki K. Antitumor activity of arginine deiminase from *Mycoplasma arginini* and its growth inhibitory mechanism. Japanese Journal of Cancer Research, 1995; 86(9): 840-6.

14. Fenske JD, Kenny GE. Role of arginine deiminase in growth of *Mycoplasma hominis*. Journal of Bacteriology, 1976; 126(1): 501-10.

15. Wei YZ, Zhou H, Sun Y, He YB, Luo YZ. Insight into the catalytic mechanism of arginine deiminase: Functional studies on the crucial sites. Proteins-Structure Function and Bioinformatics, 2007; 66(3): 740-50.

16. Ensor CM, Holtsberg FW, Bomalaski JS, Clark MA. Pegylated arginine deiminase (ADI-SS PEG(20,000) (mw)) inhibits human melanomas and hepatocellular carcinomas in vitro and in vivo. Cancer Research, 2002; 62(19): 5443-50.

17. Galkin A, Lu XF, Dunaway-Mariano D, Herzberg O. Crystal structures representing the Michaelis complex and the thiouronium reaction intermediate of Pseudomonas aeruginosa arginine deiminase. Journal of Biological Chemistry, 2005; 280(40): 34080-7.

18. Kundu M, Thomas J, Fialho AM*, et al.* The anticancer activity of the N-terminal CARD-Like domain of arginine deiminase (ADI) from *Pseudomonas aeruginosa*. Letters in Drug Design & Discovery, 2009; 6(6): 403-12.

19. Beloussow K, Wang L, Wu J, Ann D, Shen WC. Recombinant arginine deiminase as a potential anti-angiogenic agent. Cancer Letters, 2002; 183(2): 155-62.

20. Misawa S, Aoshima M, Takaku H, Matsumoto M, Hayashi H. High-Level expression of Mycoplasma arginine deiminase in *Escherichia coli* and Its efficient renaturation as an antitumor enzyme. Journal of Biotechnology, 1994; 36(2): 145-55.
21. Gong H, Zolzer F, von Recklinghausen G*, et al.* Arginine deiminase inhibits cell proliferation by arresting cell cycle and inducing apoptosis. Biochemical and Biophysical Research Communications, 1999; 261(1): 10-4.
22. Takaku H, Takase M, Abe S, Hayashi H, Miyazaki K. *In vivo* antitumor activity of arginine deiminase purified from *Mycoplasma arginini*. International Journal of Cancer, 1992; 51(2): 244-9.
23. Kim JE, Jeong DW, Lee HJ. Expression, purification, and characterization of arginine deiminase from Lactococcus lactis ssp lactis ATCC 7962 in Escherichia coli BL21. Protein Expression and Purification, 2007; 53(1): 9-15.
24. Kakimoto T, Shibatan.T, Chibata I. Crystallization of L-arginine deiminase from *Pseudomonas putida*. Febs Letters, 1971; 19(2): 166-8.
25. Shibatani T, Kakimoto T, Chibata I. Crystallization and properties of L-arginine deiminase of *Pseudomonas Putida* 2. Journal of Biological Chemistry, 1975; 250(12): 4580-3.
26. Galkin A, Kulakova L, Sarikaya E, Lim K, Howard A, Herzberg O. Structural insight into arginine degradation by arginine deiminase, an antibacterial and parasite drug target. Journal of Biological Chemistry, 2004; 279(14): 14001-8.
27. Ni Y, Schwaneberg U, Sun ZH. Arginine deiminase, a potential anti-tumor drug. Cancer Lett, 2008; 261(1): 1-11.
28. Galkin A, Kulakova L, Sarikaya E, Lim K, Howard A, Herzberg O. J Biol Chem, 2004; 279: 14001.
29. Galkin A, Lu XF, Dunaway-Mariano D, Herzberg O. J Biol Chem, 2005; 280: 34080.
30. Holle LM. Pegaspargase: an alternative? Annals of Pharmacotherapy, 1997; 31(5): 616-24.

31. Yoshioka T, Wada T, Uchida N*, et al.* Anticancer efficacy in vivo and in vitro, synergy with 5-fluorouracil, and safety of recombinant methioninase. Cancer Research, 1998; 58(12): 2583-7.
32. Lam TL, Wong GKY, Chong HC*, et al.* Recombinant human arginase inhibits proliferation of human hepatocellular carcinoma by inducing cell cycle arrest. Cancer Letters, 2009; 277(1): 91-100.
33. Shen RS, Fritz RR, Abell CW. Biochemical-Properties and Immunogenicity of L-Phenylalanine Ammonia-Lyase - Effects on Tumor-Bearing Mice. Cancer Treatment Reports, 1979; 63(6): 1063-8.
34. Yoshimoto T, Chao SG, Saito Y, Imamura I, Wada H, Inada Y. Chemical modification of tryptophanase from E. coli with polyethylene glycol to reduce its immunoreactivity towards anti-tryptophanase antibodies. Enzyme, 1986; 36(4): 261-5.
35. Feun LG, Savaraj N, Marini A*, et al.* Phase II study of pegylated arginine deiminase (ADI-PEG20), a novel targeted therapy for melanoma. Journal of Clinical Oncology, 2006; 24(18): 464s-s.
36. Gong H, Zolzer F, von Recklinghausen G, Havers W, Schweigerer L. Arginine deiminase inhibits proliferation of human leukemia cells more potently than asparaginase by inducing cell cycle arrest and apoptosis. Leukemia, 2000; 14(5): 826-9.
37. Morris SM, Jr. Regulation of enzymes of the urea cycle and arginine metabolism. Annu Rev Nutr, 2002; 22: 87-105.
38. Scott L, Lamb J, Smith S, Wheatley DN. Single amino acid (arginine) deprivation: rapid and selective death of cultured transformed and malignant cells. British Journal of Cancer, 2000; 83(6): 800-10.
39. Wheatley DN, Campbell E. Arginine catabolism, liver extracts and cancer. Pathol Oncol Res, 2002; 8(1): 18-25.
40. Thomas JB, Holtsberg FW, Ensor CM, Bomalaski JS, Clark MA. Enzymatic degradation of plasma arginine using arginine deiminase inhibits nitric oxide production and protects mice from the lethal effects of tumor necrosis factor and endotoxin. Molecular Biology of the Cell, 2001; 12: 404a-a.

41. Cheng PNM, Leung YC, Lo WH, Tsui SM, Lam KC. Remission of hepatocellular carcinoma with arginine depletion induced by systemic release of endogenous hepatic arginase due to transhepatic arterial embolisation, augmented by high-dose insulin: arginase as a potential drug candidate for hepatocellular carcinoma. Cancer Letters, 2005; 224(1): 67-80.
42. Cheng PNM, Lam TL, Lam WM*, et al.* Pegylated recombinant human arginase (rhArg-peg(5,000mw)) inhibits the in vitro and in vivo proliferation of human hepatocellular carcinoma through arginine depletion. Cancer Research, 2007; 67(1): 309-17.
43. Kim JH, Yu YS, Kim DH, Min BH, Kim KW. Anti-tumor activity of arginine deiminase via arginine deprivation in retinoblastoma. Oncol Rep, 2007; 18(6): 1373-7.
44. Kim RH, Coates JM, Bowles TL*, et al.* Arginine deiminase as a novel therapy for prostate cancer induces autophagy and caspase-independent apoptosis. Cancer Research, 2009; 69(2): 700-8.
45. Glazer ES, Piccirillo M, Albino V*, et al.* Phase II study of pegylated arginine deiminase for nonresectable and metastatic hepatocellular carcinoma. Journal of Clinical Oncology, 2010; 28(13): 2220-6.
46. Ascierto PA, Scala S, Castello G*, et al.* Pegylated arginine deiminase treatment of patients with metastatic melanoma: Results from phase I and II studies. Journal of Clinical Oncology, 2005; 23(30): 7660-8.
47. Shen LJ, Beloussow K, Shen WC. Accessibility of endothelial and inducible nitric oxide synthase to the intracellular citrulline-arginine regeneration pathway. Biochemical Pharmacology, 2005; 69(1): 97-104.
48. Park H, Lee JB, Shim YJ*, et al.* Arginine deiminase enhances MCF-7 cell radiosensitivity by inducing changes in the expression of cell cycle-related proteins. Molecules and Cells, 2008; 25(2): 305-11.
49. Kubo M, Nishitsuji H, Kurihara K, Hayashi T, Masuda T, Kannagi M. Suppression of human immunodeficiency virus type 1 replication by arginine deiminase of *Mycoplasma arginini*. Journal of General Virology, 2006; 87: 1589-93.

50. Izzo F, Montella M, Orlando AP*, et al.* Pegylated arginine deiminase lowers hepatitis C viral titers and inhibits nitric oxide synthesis. Journal of Gastroenterology and Hepatology, 2007; 22(1): 86-91.
51. Kwan JM, Fialho AM, Kundu M*, et al.* Bacterial proteins as potential drugs in the treatment of leukemia. Leukemia Research, 2009; 33(10): 1392-9.
52. Tsai WB, Aiba I, Lee SY, Feun L, Savaraj N, Kuo MT. Resistance to arginine deiminase treatment in melanoma cells is associated with induced argininosuccinate synthetase expression involving c-Myc/HIF-1 alpha/Sp4. Molecular Cancer Therapeutics, 2009; 8(12): 3223-33.
53. Yoon CY, Shim YJ, Kim EH*, et al.* Renal cell carcinoma does not express argininosuccinate synthetase and is highly sensitive to arginine deprivation via arginine deiminase. International Journal of Cancer, 2007; 120(4): 897-905.
54. Feun L, You M, Wu CJ*, et al.* Arginine deprivation as a targeted therapy for cancer. Current Pharmaceutical Design, 2008; 14(11): 1049-57.
55. Zhu ZW, Momeu C, Zakhartsev M, Schwaneberg U. Making glucose oxidase fit for biofuel cell applications by directed protein evolution. Biosens Bioelectron, 2006; 21(11): 2046-51.
56. Panke S, Held M, Wubbolts M. Trends and innovations in industrial biocatalysis for the production of fine chemicals. Current Opinion in Biotechnology, 2004; 15(4): 272-9.
57. Patel RN. Chemo-enzymatic synthesis of pharmaceutical intermediates. Expert Opinion on Drug Discovery, 2008; 3(2): 187-245.
58. Yokobayashi Y, Weiss R, Arnold FH. Directed evolution of a genetic circuit. Proc Natl Acad Sci U S A, 2002; 99(26): 16587-91.
59. Ellington AD, Chen X, Robertson M, Syrett A. Evolutionary origins and directed evolution of RNA. International Journal of Biochemistry & Cell Biology, 2009; 41(2): 254-65.
60. Alper H, Fischer C, Nevoigt E, Stephanopoulos G. Tuning genetic control through promoter engineering. Proceedings of the National Academy of Sciences of the United States of America, 2005; 102(36): 12678-83.

61. Drummond DA, Iverson BL, Georgiou G, Arnold FH. Why high-error-rate random mutagenesis libraries are enriched in functional and improved proteins. J Mol Biol, 2005; 350(4): 806-16.
62. Wong TS, Roccatano D, Schwaneberg U. Steering directed protein evolution: strategies to manage combinatorial complexity of mutant libraries. Environmental Microbiology, 2007; 9(11): 2645-59.
63. Wong TS, Zhurina D, Schwaneberg U. The diversity challenge in directed protein evolution. Combinatorial Chemistry & High Throughput Screening, 2006; 9(4): 271-88.
64. Fasan R, Chen MM, Crook NC, Arnold FH. Engineered alkane-hydroxylating cytochrome P450(BM3) exhibiting nativelike catalytic properties. Angewandte Chemie-International Edition, 2007; 46(44): 8414-8.
65. Titus SA, Xiao L, Southall N*, et al.* Cell-based PDE4 assay in 1536-well plate format for high-throughput screening. Journal of Biomolecular Screening, 2008; 13(7): 609-18.
66. Lafferty M, Dycaico MJ. GigaMatrix^{TM}: an ultra highthroughput tool for accessing biodiversity. JALA, 2009; 9: 200-8.
67. Yang GY, Withers SG. Ultrahigh-throughput FACS-based screening for directed enzyme evolution. Chembiochem, 2009; 10(17): 2704-15.
68. Miller OJ, Hibbert EG, Ingram CU, Lye GJ, Dalby PA. Optimisation and evaluation of a generic microplate-based HPLC screen for transketolase activity. Biotechnology Letters, 2007; 29(11): 1759-70.
69. Yoshikuni Y, Ferrin TE, Keasling JD. Designed divergent evolution of enzyme function. Nature, 2006; 440(7087): 1078-82.
70. Becker S, Schmoldt HU, Adams TM, Wilhelm S, Kolmar H. Ultra-high-throughput screening based on cell-surface display and fluorescence-activated cell sorting for the identification of novel biocatalysts. Current Opinion in Biotechnology, 2004; 15(4): 323-9.
71. Farinas ET. Fluorescence activated cell sorting for enzymatic activity. Combinatorial Chemistry & High Throughput Screening, 2006; 9(4): 321-8.

72. Agresti JJ, Antipov E, Abate AR*, et al.* Ultrahigh-throughput screening in drop-based microfluidics for directed evolution. Proceedings of the National Academy of Sciences of the United States of America, 2010; 107(9): 4004-9.
73. Leemhuis H, Kelly RM, Dijkhuizen L. Directed evolution of enzymes: library screening strategies. Iubmb Life, 2009; 61(3): 222-8.
74. Chen KC, Wu CH, Chang CY*, et al.* Directed evolution of a lysosomal enzyme with enhanced activity at neutral pH by mammalian cell-surface display. Chem Biol, 2008; 15(12): 1277-86.
75. Wang Q, Xia T. Enhancement of the activity and alkaline pH stability of Thermobifida fusca xylanase A by directed evolution. Biotechnology Letters, 2008; 30(5): 937-44.
76. Colin DY, Deprez-Beauclair P, Silva N, Infantes L, Kerfelec B. Modification of pancreatic lipase properties by directed molecular evolution. Protein Engineering Design & Selection, 2010; 23(5): 365-73.
77. Bessler C, Schmitt J, Maurer KH, Schmid RD. Directed evolution of a bacterial alpha-araylase: Toward enhanced pH-performance and higher specific activity. Protein Sci, 2003; 12(10): 2141-9.
78. Liu ZQ, Sun ZH, Leng Y. Directed evolution and characterization of a novel D-pantonohydrolase from Fusarium moniliforme. Journal of Agricultural and Food Chemistry, 2006; 54(16): 5823-30.
79. Hasan Z, Renirie R, Kerkman R, Ruijssenaars HJ, Hartog AF, Wever R. Laboratory-evolved vanadium chloroperoxidase exhibits 100-fold higher halogenating activity at alkaline pH - Catalytic effects from first and second coordination sphere mutations. Journal of Biological Chemistry, 2006; 281(14): 9738-44.
80. Makde RD, Dikshit K, Kumar V. Protein engineering of class-A non-specific acid phosphatase (PhoN) of Salmonella typhimurium: Modulation of the pH-activity profile. Biomolecular Engineering, 2006; 23(5): 247-51.
81. Kim T, Mullaney EJ, Porres JM*, et al.* Shifting the pH profile of *Aspergillus niger* PhyA phytase to match the stomach pH enhances its effectiveness as an

animal feed additive. Applied and Environmental Microbiology, 2006; 72(6): 4397-403.
82. Hirata A, Adachi M, Utsumi S, Mikami B. Engineering of the pH optimum of Bacillus cereus beta-amylase: Conversion of the pH optimum from a bacterial type to a higher-plant type. Biochemistry, 2004; 43(39): 12523-31.
83. Tomschy A, Brugger R, Lehmann M*, et al.* Engineering of phytase for improved activity at low pH. Appl Environ Microbiol, 2002; 68(4): 1907-13.
84. Sakoda H, Imanaka T. Cloning and sequencing of the gene coding for alcohol dehydrogenase of Bacillus stearothermophilus and rational shift of the optimum pH. J Bacteriol, 1992; 174(4): 1397-402.
85. Yang JH, Park JY, Kim SH, Yoo YJ. Shifting pH optimum of Bacillus circulans xylanase based on molecular modeling. Journal of Biotechnology, 2008; 133(3): 294-300.
86. MacPherson IS, Rosell FI, Scofield M, Mauk AG, Murphy MEP. Directed evolution of copper nitrite reductase to a chromogenic reductant. Protein Engineering Design & Selection, 2010; 23(3): 137-45.
87. Hida K, Hanes J, Ostermeier M. Directed evolution for drug and nucleic acid delivery. Adv Drug Deliv Rev, 2007; 59(15): 1562-78.
88. Yuan L, Kurek I, English J, Keenan R. Laboratory-directed protein evolution. Microbiology and Molecular Biology Reviews, 2005; 69(3): 373-92.
89. Rautio J, Kumpulainen H, Heimbach T*, et al.* Prodrugs: design and clinical applications. Nat Rev Drug Discov, 2008; 7(3): 255-70.
90. Barak Y, Thorne SH, Ackerley DF, Lynch SV, Contag CH, Matin A. New enzyme for reductive cancer chemotherapy, YieF, and its improvement by directed evolution. Molecular Cancer Therapeutics, 2006; 5(1): 97-103.
91. Kuhn I, Harden P, Bauzon M*, et al.* Directed evolution generates a novel oncolytic virus for the treatment of colon cancer. PLoS One, 2008; 3(6): e2409.
92. Robertson DE, Steer BA. Recent progress in biocatalyst discovery and optimization. Current Opinion in Chemical Biology, 2004; 8(2): 141-9.
93. Soares AL, Guirmaraes GM, Polakiewicz B, Pitombo RND, Abrahao-Neto J. Effects of polyethylene glycol attachment on physicochemical and biological

stability of E-coli L-asparaginase. International Journal of Pharmaceutics, 2002; 237(1-2): 163-70.
94. Kotzia GA, Labrou NE. Engineering thermal stability of L-asparaginase by in vitro directed evolution. Febs Journal, 2009; 276(6): 1750-61.
95. Orlova A, Feldwisch J, Abrahmsen L, Tolmachev V. Affibody molecules for molecular imaging and therapy for cancer. Cancer Biotherapy and Radiopharmaceuticals, 2007; 22(5): 573-84.
96. Nilsson FY, Tolmachev V. Affibody (R) molecules: New protein domains for molecular imaging and targeted tumor therapy. Current Opinion in Drug Discovery & Development, 2007; 10(2): 167-75.
97. Gronwall C, Sjoberg A, Ramstrom M*, et al.* Affibody-mediated transferrin depletion for proteomics applications. Biotechnol J, 2007; 2(11): 1389-98.
98. Renberg B, Shiroyama I, Engfeldt T, Nygren PA, Karlstrom AE. Affibody protein capture microarrays: Synthesis and evaluation of random and directed immobilization of affibody molecules. Analytical Biochemistry, 2005; 341(2): 334-43.
99. Friedman M, Orlova A, Johansson E*, et al.* Directed evolution to low nanomolar affinity of a tumor-targeting epidermal growth factor receptor-binding affibody molecule. Journal of Molecular Biology, 2008; 376(5): 1388-402.
100. Chang CCJ, Chen TT, Cox BW*, et al.* Evolution of a cytokine using DNA family shuffling. Nature Biotechnology, 1999; 17(8): 793-7.
101. Zhang JH, Dawes G, Stemmer WPC. Directed evolution of a fucosidase from a galactosidase by DNA shuffling and screening. Proceedings of the National Academy of Sciences of the United States of America, 1997; 94(9): 4504-9.
102. Crameri A, Cwirla S, Stemmer WPC. Construction and evolution of antibody-phage libraries by DNA shuffling. Nature Medicine, 1996; 2(1): 100-2.
103. Patten PA, Howard RJ, Stemmer WP. Applications of DNA shuffling to pharmaceuticals and vaccines. Curr Opin Biotechnol, 1997; 8(6): 724-33.
104. Park IS, Kang SW, Shin YJ*, et al.* Arginine deiminase: a potential inhibitor of angiogenesis and tumour growth. Br J Cancer, 2003; 89(5): 907-14.

105. Izzo F, Marra P, Beneduce G*, et al.* Pegylated arginine deiminase treatment of patients with unresectable hepatocellular carcinoma: Results from phase I/II studies. J Clin Oncol, 2004; 22(10): 1815-22.
106. Gong H, Zölzer F, von Recklinghausen G, Havers W, Schweigerer L. Arginine deiminase inhibits proliferation of human leukemia cells more potently than asparaginase by inducing cell cycle arrest and apoptosis. Leukemia, 2000; 14(5): 826-9.
107. Shen LJ, Shen WC. Drug evaluation: ADI-PEG-20 - a PEGylated arginine deiminase for arginine-auxotrophic cancers. Curr Opin in Mol Ther, 2006; 8(3): 240-8.
108. Holtsberg FW, Ensor CM, Steiner MR, Bomalaski JS, Clark MA. Poly(ethylene glycol) (PEG) conjugated arginine deiminase: effects of PEG formulations on its pharmacological properties. J Controlled Release, 2002; 80(1-3): 259-71.
109. Mûller HJ, Boos J. Use of L-asparaginase in childhood all. Crit Rev Oncol Hematol, 1998; 28(2): 97-113.
110. Turunen O, Janis J, Fenel F, Leisola M. Engineering the thermotolerance and pH optimum of family 11 xylanases by site-directed mutagenesis. Methods Enzymol, 2004; 388: 156-67.
111. Fang TY, Ford C. Protein engineering of *Aspergillus awamori* glucoamylase to increase its pH optimum. Protein Eng, 1998; 11(5): 383-8.
112. Sakoda H, Imanaka T. Cloning and sequencing of the gene coding for alcohol-dehydrogenase of *Bacillus stearothermophilus* and rational shift of the optimum pH. J Bacteriol, 1992; 174(4): 1397-402.
113. Wang WY, Malcolm BA. Two-stage PCR protocol allowing introduction of multiple mutations, deletions and insertions using QuikChange™ site-directed mutagenesis. BioTechniques, 1999; 26(4): 680-2.
114. Miyazaki K, Takenouchi M. Creating random mutagenesis libraries using megaprimer PCR of whole plasmid. Biotechniques, 2002; 33(5): 1033-8.
115. Studier FW. Protein production by auto-induction in high-density shaking cultures. Protein Expression and Purification, 2005; 41(1): 207-34.

116. Archibald RM. Deternination of citrulline and allantoin and demonstration of citrulline in blood plasma. J Biol Chem, 1944; 156(1): 121-42.
117. Boyde TRC, Rahmatullah M. Optimization of conditions for the colorimetric determination of citrulline, using diacetyl monoxime. Anal Biochem, 1980; 107(2): 424-31.
118. Guex N, Peitsch MC. SWISS-MODEL and the Swiss-PdbViewer: an environment for comparative protein modeling. Electrophoresis, 1997; 18(15): 2714-23.
119. van Gunsteren WF, Billeter SR, Eising AA*, et al.* Biomolecular simulation: the gromos 96 manual and user guide ETH Zürich; 1996.
120. Mather A, Roland D. Automated thiosemicarbazide-diacetyl monoxime method for plasma urea. Clinical Chemistry, 1969; 15(5): 393-6.
121. Wong TS, Arnold FH, Schwaneberg U. Laboratory evolution of cytochrome P450BM-3 monooxygenase for organic cosolvents. Biotechnol Bioeng, 2004; 85(3): 351-8.
122. Glieder A, Farinas ET, Arnold FH. Laboratory evolution of a soluble, self-sufficient, highly active alkane hydroxylase. Nat Biotechnol, 2002; 20(11): 1135-9.
123. Galkin A, Lu X, Dunaway-Mariano D, Herzberg O. Crystal structures representing the Michaelis complex and the thiouronium reaction intermediate of Pseudomonas aeruginosa arginine deiminase. Journal of biological chemistry, 2005; 280(40): 34080-7.
124. Chuang VTG, Kragh-Hansen U, Otagiri M. Pharmaceutical strategies utilizing recombinant human serum albumin. Pharm Res, 2002; 19(5): 569-77.
125. Tee KL, Dmytrenko O, Otto K, Schmid A, Schwaneberg U. A p-nitrothiophenolate screening system for the directed evolution of a two-component epoxygenase (StyAB). J Mol Catal B: Enzym, 2008; 50(2-4): 121-7.
126. Li L, Li ZM, Wang CH*, et al.* The electrostatic driving force for nucleophilic catalysis in L-arginine deiminase: a combined experimental and theoretical study. Biochemistry (Mosc), 2008; 47(16): 4721-32.

127. Takaku H, Matsumoto M, Misawa S, Miyazaki K. Antitumor-activity of arginine deiminase from *Mycoplasma arginini* and its growth-Inhibitory mechanism. Jap J Cancer Res, 1995; 86(9): 840-6.
128. Capocaccia R, Sant M, Berrino F, Simonetti A, Santi V, Trevisani F. Hepatocellular carcinoma: trends of incidence and survival in Europe and the United States at the end of the 20th century. American Journal of Gastroenterol, 2007; 102(8): 1661-70.
129. Shen LJ, Shen WC. Drug evaluation: ADI-PEG-20 - a PEGylated arginine deiminase for arginine-auxotrophic cancers. Current Opinion in Molecular Therapeutics, 2006; 8(3): 240-8.
130. Wang WY, Malcolm BA. Two-stage PCR protocol allowing introduction of multiple mutations, deletions and insertions using QuikChange (TM) site-directed mutagenesis. Biotechniques, 1999; 26(4): 680-2.
131. Vaughn WK, Neal RA, Anderson AJ. Computer estimation of the parameters of the sigmoidal kinetic model. Computers in Biology and Medicine, 1976; 6(1): 1-7.
132. Kelley LA, Sternberg MJE. Protein structure prediction on the web: a case study using the Phyre server. Nature Protocols, 2009; 4(3): 363-71.
133. Laskowski RA, Macarthur MW, Moss DS, Thornton JM. Procheck - a program to check the stereochemical quality of protein structures. Journal of Applied Crystallography, 1993; 26: 283-91.
134. Zhou HY, Zhou YQ. Distance-scaled, finite ideal-gas reference state improves structure-derived potentials of mean force for structure selection and stability prediction. Protein Science, 2002; 11(11): 2714-26.
135. Benkert P, Tosatto SCE, Schomburg D. QMEAN: A comprehensive scoring function for model quality assessment. Proteins-Structure Function and Bioinformatics, 2008; 71(1): 261-77.
136. Berendsen HJC, Postman JPM, van Gunsteren WF, Hermans J. Interaction models for water in relation to protein hydration. Intermolecular Forces, 1981: 331-42.

137. Hess B, Bekker H, Berendsen HJC, Fraaije JGEM. LINCS: A linear constraint solver for molecular simulations. Journal of Computational Chemistry, 1997; 18(12): 1463-72.
138. Miyamoto S, Kollman PA. Settle - an analytical version of the shake and rattle algorithm for rigid water models. Journal of Computational Chemistry, 1992; 13(8): 952-62.
139. Darden T, York D, Pedersen L. Particle mesh ewald - an N.Log(N) method for ewald sums in large systems. Journal of Chemical Physics, 1993; 98(12): 10089-92.
140. Berendsen HJC, Postma JPM, Vangunsteren WF, Dinola A, Haak JR. Molecular dynamics with coupling to an external bath. Journal of Chemical Physics, 1984; 81(8): 3684-90.
141. Hess B, Kutzner C, van der Spoel D, Lindahl E. GROMACS 4: algorithms for highly efficient, load-balanced, and scalable molecular simulation. Journal of Chemical Theory and Computation, 2008; 4(3): 435-47.

Summary and outlook

Arginine depletion based on ADI is an emerging strategy for anti-tumor treatment. ADIs have been studied for the therapy of HCCs and melanomas and were approved as an orphan drug for both kinds of tumors. ADI is proved to be effective in the treatment of leukemia. The effectiveness of ADIs as anti-tumor agent depends on their enzymatic properties (such as K_m, k_{cat}, optimum pH, stability at neutral pH). Directed evolution, without rational understanding of the targeted property, allows improving all properties that can be reflected in a screening system through iterative rounds of diversity generation and screening.

In order to improve PpADI activity at physiological pH by directed evolution, a colorimetric screening assay based on citrulline detection has been developed in 96-well microtiter plate format. Single mutation H404R was identified according to PpADI homology model (based on PaADI crystal structure), introduced to PpADI wild type and eventually resulted in 1.4-fold of increase in k_{cat}. M1 (H404R) was used as template for the first round of epPCR library generation. M2 (K5T/D44E/H404R) obtained from the first round of epPCR library showed 4-fold improved k_{cat} value when compared to the PpADI wild type. Furthermore, a shift of pH optimum from pH 6.5 to pH 7.0 was observed, combined with an increased K_m value (2.5 mM) under assay conditions (0.5 M sodium phosphate buffer, pH 7.4), compared to PpADI wild type (0.7 mM).

Arginine concentration in human plasma is however relatively low (100-120 µM). Therefore the second round of epPCR library was performed to decrease K_m value and further improve k_{cat} value. The validated screening assay was modified to reflect more close physiological condition (1 mM arginine in PBS buffer, pH 7.4). Two important variants with one additional mutation, M4 (K5T/D44E/A128T/E296K/H404R) with decreased $S_{0.5}$ vaule, and M5 (K5T/D38H/D44E/A128T/H404R) with improved k_{cat} were obtained. Their two mutations were combined and resulted in variants M6

(K5T/D38H/D44E/A128T/E296K/H404R). Under physiological pH in PBS buffer, the $S_{0.5}$ value of M6 (0.81 mM) is lower than that of PpADI wild type (1.30 mM); the k_{cat} value improved from 0.18 s^{-1} (PpADI wild type) to 17.56 s^{-1} (M5, 97.6-folds) and 11.64 s^{-1} (M6, 64.7-fold).

A reamaining challenge facing PpADI's anti-tumor application is to decrease the K_m ($S_{0.5}$) value further close to arginine concentration level in human plasma. A more sensitive assay for screening has to be developed with the addition of sensitizer like thiosemicarbazide (TSC), optimized temperature and incubation time. Improved variants should be tested tested in human plasma or with human plasma composition. *In vitro* testing of ADI variants with arginine auxotrophic tumor cell lines is the first step towards *in vivo* in human.

In summary, directed evolution has been very useful algorithim for improving ADI's k_{cat} and K_m at physiological pH (pH 7.4) for its medical application. Hope that directed evolution will be become a standard method for therapeutic protein like its use in industry.

Publications

1. **Leilei Zhu**, Kang Lan Tee, Danilo Roccatano, Burcu Sonmez, Ye Ni, Zhi-Hao Sun, and Ulrich Schwaneberg. Directed evolution of an antitumor drug (Arginine Deiminase PpADI) for increased activity at physiological pH. ChemBioChem. 2010, 11, 691-697.

2. **Leilei Zhu**, Rajni Verma, Danilo Roccatano, Ye Ni, Zhi-Hao Sun, and Ulrich Schwaneberg. A potential anti-tumor drug (arginine deiminase) reengineered for efficient operation under physiological conditions. ChemBioChem. *In press*.

3. Ye Ni, Zhenwei Li, Zhihao Sun, Pu Zheng, Yongmei Liu and **Leilei Zhu**, Ulrich Schwaneberg. Expression of arginine deiminase from *Pseudomonas plecoglossicida* CGMCC2039 in *Escherichia coli* and its anti-tumor activity. Current Microbiology. 2009, 58(6):593-598.

Patent

1. Directed evolution of arginine deiminase for increased activity at physiological pH. Application number: PCT/EP2010/061884.

Curriculum vitae

Personal data

Name:	Leilei Zhu
Gender:	Female
Date of Birth:	27th April, 1982
Place of Birth:	Weifang, China
Marital Status:	Married
Nationality:	Chinese

Education

2009-	PhD fellow of biotechnology, RWTH Aachen University, Aachen, Germany
2007-2009	PhD fellow of engineering and science, Jacobs University Bremen, Bremen, Germany
2005-2007	Master of biochemical engineering, Jiangnan University (Southern Yantze University), Wuxi, China
2001-2005	Bachelor of biotechnology, Jiangnan University (Southern Yantze University), Wuxi, China

2001-1998	The first high school of Hanting, Weifang, China
1998-1994	The sixth middle school of Hanting, Weifang, China
1989-1994	Primary school of Liuhe, Weifang, China

Directed Evolution of Arginine Deiminase (ADI) for Anti-tumor Application

Von der Fakultät für Mathematik, Informatik und Naturwissenschaften der RWTH Aachen University zur Erlangung des akademischen Grades eines(r) Doktors(in) der Naturwissenschaften oder eines(r) Doktors(in) der Ingenieurwissenschaften genehmigte Dissertation

vorgelegt von

Master of Biochemistry

Leilei Zhu

Aus Weifang China

Berichter: **Universitätsprofessor Dr. Ulrich Schwaneberg**
Universitätsprofessor Dr. Lothar Elling

Tag der mündlichen Prüfung: 14.09.2010

Diese Dissertation ist auf den Internetseiten der Hochschulbibliothek online verfügbar.

Table of contents

Acknowledgement.....I
Abstract.....III
Abbreviations V
List of figures..... VI
List of tables..... IX
Chapter 1 Arginine deiminase (ADI) 1
1.1 Arginine deiminase (ADI).....1
1.2 ADI structure 5
1.3 Catalytic reaction mechanism of ADI.....10
1.4 Anti-tumor application of ADI.....11
1.5 Conclusion.....16
Chapter 2 Directed evolution 17
2.1 Introduction to directed evolution.....17
2.2 Directed enzyme evolution for pH tolerance of enzymes 22
2.3 Directed enzyme evolution for medical application.....24
2.3.1 Prodrug enzymes for tumor chemotherapy.....24
2.3.2 Oncolytic viruses for tumor chemotherapy.....25
2.3.3 Amino acid depriving enzyme for anti-tumor applications.....27
2.3.4 Affibody molecules for cancer prognosis 28
2.3.5 Interferon for anti-tumor applicaiton 29
2.4 Conclusion.....30
Chapter 3. Directed evolution of Arginine deiminase for increased activity at physiological pH.....31
3. 1 Abstract 31
3.2 Introduction.....31
3.3 Materials and methods 33
3.3.1 Materials 33
3.3.2 Methods 34

3.3.2.1 Reagents used in assays 34
3.3.2.2 Cloning of ADI into pET42b(+) 34
3.3.2.3 Site directed mutagenesis of PpADI gene at position H404 35
3.3.2.4 Site sturation mutagenesis of PpADI gene at nine amino acid position 35
3.3.2.5 Construction of PpADI error-prone library 36
3.3.2.6 Expression of PpADI in LB media with IPTG induction 37
3.3.2.7 Expression of PpADI in auto-induction media 37
3.3.2.8 Cultivation and expression of PpADI in 96-well plates 37
3.3.2.9 Screening Procedure 38
3.3.2.10 Expression of ADI in shaking flask and purification 39
3.3.2.11 Characterization of ADI wild type and mutants 40
3.3.2.12 Molecular Modeling 41
3.3.2.13 Stability of PpADI in presence of serum 41
3.3.2.14 Activity of PpADI (wild type, M1, M2) towards arginine derivative dimethylarginine 42
3.4 Results 42
3.4.1 PpADI cloning 42
3.4.2 PpADI expression in LB media with IPTG as inducer 44
3.4.3 PpADI expression in auto-induction media 44
3.4.4 PpADI assay based on citrulline detection 46
3.4.5 PpADI screening system for citrulline production in microtiter plates 47
3.4.6 Focused libraries generated by saturation mutagenesis 50
3.4.7 Validation of variant M1 (H404R) citrulline colorimetric assay in cuvette format 50
3.4.8 epPCR library generation and screening with citrulline detection assay by screening error-prone mutant libraries 50
3.4.9 Characterization of PpADI variants 53
3.4.9.1 Determination of k_{cat} and K_m of ADI wild type and the mutants 53
3.4.9.2 Relative pH profile of wild type and mutant 54
3.4.10 Stability of PpADI in the presence of human serum 55

3.4.11 Activity of PpADI (wild type, M1, M2) towards arginine derivative (N^G, N^G)-dimethylarginine 56
3.5 Discussion 56
3.6 Conclusion 59
Chapter 4. PpADI reengineered for efficient operation under physiological conditions 60
4.1 Abstract 60
4.2 Introduction 60
4.3 Materials and methods 62
4.3.1 Materials 62
4.3.2 Methods 62
4.3.2.1 Site saturation mutagenesis of *PpADI* M2 at position A128 62
4.3.2.2 Construction of PpADI error-prone library 63
4.3.2.3 Site directed mutagenesis at position D38 of *PpADI* M4 63
4.3.2.4 Site saturation mutagenesis at position D38 and E296 of *PpADI* M3 64
4.3.2.5 Cultivation and expression of PpADI in 96-well plates 64
4.3.2.6 Improved screening system in 96-well plate to identify PpADI variants with high activities at low arginine concentration 64
4.3.2.7 Expression of PpADI in shaking flask and purification 65
4.3.2.8 Characterization of PpADI variants 65
4.3.2.9 Native polyacrylamide gel electrophoresis of PpADI variants 66
4.3.2.10 Homology modeling 67
4.4 Results 67
4.4.1 Improved screening system in microtiter plates to identify PpADI variants with high activities at low arginine concentration 67
4.4.2 Genealogic tree of directed PpADI evolution 68
4.4.3 EpPCR library construction and screening for variants with high activities at low arginine concentration 69
4.4.4 Site saturation mutagenesis of *PpADI* at position D38 and E296 70

4.4.5 Determination of kinetic constants (k_{cat} and $S_{0.5}$) of PpADI wild type and variants M3, M4, M5 and M6 72
4.4.6 Native polyacrylamide gel electrophoresis of PpADI variants 73
4.5 Discussion 74
Summary and outlook 95
Publication list 97
Curriculum vitae 98

Acknowledgement

First and foremost I want to thank my supervisor Prof. Dr. Ulrich Schwaneberg for offering me the opportunity to study in Germany, his continuous support of my PhD study and research, for his patience, motivation, enthusiasm, and immense knowledge, which influence my view of science and life. His guidance helped me all the time in research and writing of paper and thesis. I could not have imagined having a better advisor and mentor for my PhD study.

Besides my supervisor, I would like to thank other two committee member Prof. Dr. Lothar Elling and Prof. Dr. Anett Kirschner. I appreciate their taking time to read this thesis and give valuable comments.

My sincere thanks also go to Kang Lan, who became a great friend of mine after I came to Bremen of Germany three years ago. She helped me a lot with my PhD project and she was a great company in my daily life. I will never forget the two months I spent on the first cloning working in my life and how Kang Lan taught me and encouraged me.

I am grateful to Prof. Dr. Danilo Roccatano for spending a lot of time discussing my results. After the first meeting with Prof. Roccatano, I started to know and learn computational tools which are really useful for my PhD study. I also thank Rajni for her contribution of homology modeling to my project.

The members of the Schwaneberg group have contributed immensely to my personal and professional time in Jacobs University Bremen and RWTH Aachen University. The group has been a source of friendships as well as good advice and collaboration. I appreciate the help from Marina, Daniela, Gisela, Wolfgang and Brigitta in lab and Marina, Monika and Anita's patient explanation of the registration regulation RWTH Aachen University. I would like to acknowledge honorary group members. I thank Liqing for her sharing apartment with me and helped me start my life in Germany and also thank Haiyan for her offering me a room later and often cooked nice food for us. Ran shared a lot of lab techniques which are very useful for my experiments. I always admire her professional and

accurate attitude towards work. I thank other labmates who I got to know in Jacobs university: Ronny, Hemu, Chaoning, Amol, Dominik and Amir for the stimulating discussions, little help in lab and all the fun we have had in the last three years; Dragana, Ljubica, Noor, Pravine and Raluca helped me move to Aachen and we finally got through the tough transition period from Bremen to Aachen. I thank our group leaders Marco, Jan and Radivoje, who are not my direct supervisor, but are always helpful when I have questions. I thank my fellow labmates who I got to know in RWTH Aachen University: Tamara, Felix, Alex, Christian, Joelle, André, Joana……, who are always helpful with all the problems (PhD registration, Germany letters from university…….) because of my poor German.

I also want to acknowledge my students, Burcu and Alice, both of whom were hard-working and smart. They were all a great help in the lab and I really enjoyed working with them.

I would like to thank my family because of their love, support and trust. They love me the most in the world. I thank for their efforts that they made over the years to make sure I have a good growth and education environment. I wish them healthy and happy life. I thank my elder sister for her love and understanding and always taking good care of my parents these years when I am not around. I thank my husband, Haifeng, who supports me all the time and always is there for me. I am lucky to have him with me.

The financial support of the Jacobs University Bremen and RWTH Aachen University is gratefully acknowledged.

Abstract

Arginine deiminase (ADI), an arginine-degrading enzyme, is involved in the first step of arginine dihydrolase pathway. It catalyzes the hydrolysis of L-arginine to form citrulline and ammonia. ADI has been studied as a potential cancer therapeutic agent for the arginine-auxotrophic tumors, such as hepatocellular carcinomas (HCC) and melanomas. Furthermore, studies also indicate that ADI is a potential anti-angiogenic agent; therefore it could become a novel anti-cancer drug targeting the neovascularization-related tumors. Studies show ADI is more potent for the treatment of leukemia than L-asparaginase. However, the anti-tumor application of ADI for therapeutic purpose faces considerable challenges, such as, microbial ADI has low activity at physiological pH (7.35~7.45), short circulating half-life (~5 h) and high antigenicity. Pegylation of ADI improved its efficacy as a clinical drug, including its half-life in serum and antigenicity. The aim of the project is to improve ADI catalytic performance at physiological pH by directed evolution.

Protein engineering by rational design and directed evolution offers opportunities to tailor ADI properties to physiological conditions. Directed protein evolution has over the last decades become a versatile and successful approach for tailoring protein properties to industrial demands and for advancing our understanding of structure-function relationships in biocatalysts. Unlike rational design relying on the gathering of extensive structure-function relationships of enzymes, directed evolution is used to reengineer enzyme properties through iterative rounds of diversity generation and function selection for improved variants.

In order to improve the ADI activity at physiological pH, we established a directed evolution protocol for this purpose. A microtiter plate (MTP) format colorimetric screening assay based on citrulline detection with diacetyl monoxime (DAM) was developed. Reaction temperature for color development and DAM concentration

were optimized to ensure sufficient sensitivity, appropriate linear range and throughput. With the optimized assay and PpADI wild type expressed in *E. coli* as a model protein, true standard deviation 12.8 % was obtained, which is appropriate for the library screening.

With the established microtiter plate assay system, for the first time, we reengineered ADI for improved activity at physiological pH (pH 7.4) with higher potency in medical application. After one site directed mutagenesis and one round of epPCR library screening, variant M2 (K5T/D44E/H404R) was obtained. M2 shows 4-fold improved k_{cat} value than the PpADI wild type, a shifted pH optimum at pH 7.0 (by 0.5 pH unit), and however an increased K_m value, 3.6-fold under assay conditions (0.5 M sodium phosphate buffer).

Low K_m ($S_{0.5}$) value for ADI is an important factor for efficient consume of arginine in plasma because of the low arginine concentration in human plasma (100-120 µM). Therefore after our proof of concept of reengineering PpADI by directed evolution, we aim to decrease the K_m value of PpADI towards arginine and improve the k_{cat} furthermore thereby improve the efficiency of arginine depletion by ADI. The established citrulline colorimetric assay in 96-well microtiter plate is improved to reflect application conditions: PBS buffer and 1 mM arginine were used in screening system. After the second round of epPCR library and site directed mutagenesis, variant M5 (K5T/D38H/D44E/A128T/H404R) and M6 (K5T/D38H/D44E/A128T/E296K/H404R) were generated: at pH 7.4 (PBS buffer), the $S_{0.5}$ value decrease from 2.01 mM (parent M3, K5T/D44E/A128T/H404R) to 1.48 mM (M5) and 0.81 mM (M6). Under physiological pH in PBS buffer, the $S_{0.5}$ value of M6 (0.81 mM) is lower than that of PpADI wild type (1.30 mM); the k_{cat} value improved from 0.18 s^{-1} (PpADI wild type) to 17.56 s^{-1} (M5, 97.6-folds) and 11.64 s^{-1} (M6, 64.7-fold).

Abbreviations

ADI	arginine deiminase
ADH	arginine degradation pathway
ASS	argininosuccinate synthetase
ASL	argininosuccinate lyase
CARD	caspase recruitment domain
PCR	polymerase chain reaction
epPCR	error prone PCR
DAM	diacetyl monoxime
Da	dalton
DNA	deoxyribonucleic acid
E. coli	*Escherichia coli*
GMSF	guanidino-group modifying enzyme superfamily
HCC	hepatocellular carcinomas
HUVEC	human umbilical vein endothelial cells
IPTG	isopropyl β-D-1-thiogalactopyranoside
iNOs	inducible nitric oxide synthase
LB	Luria-Bertani-medium
MTP	microtiter plate
OD_{600}	optical density at 600 nm
OTC	ornithine carbamoyl transferase
PEG	polyethylene glycol
PDB	protein data bank
TSC	thiosemicarbazide
WT	wild type

List of tables

Figures	Pages
Chapter 1	
Scheme 1. Arginine dihydrolase pathway. OTC, ornithine transcarbamylase; CK, carbamate kinase.	1
Figure 1. Structural of ADIs from *P. aeruginosa* and *M. arginini*.	5
Figure 2 (A). stereoscopic view of PaADI key active site residues. 2 (B). stereoscopic view of a modeled arginine substrate (green) docked in the active site of ADI. Atomic colors are red, oxygen; blue, nitrogen; yellow, sulfur; and gray, carbon. Ion pair interactions are shown as dashed lines.	7
Figure 3. Structural characteristics of the PaADI.	9
Figure 4 (A). Stereoscopic view of ADI in the unbound and bound states. 4 (B). Structural relationship between ADI (yellow) and PAD4 (cyan).	10
Figure 5. Mechanism of PaADI catalysis of arginine to citrulline and ammonia.	11
Firgure 6. Urea cycle.	13
Firgure 7. Summary of ADI effects on arginine-related cellular functions.	15
Chapter 2	
Figure 1. Procedure of a directed evolution experiment.	18
Figure 2. Overview of screening technologies.	21
Figure 3. Hermiston's "Directed Evolution" process of viruses and derivative viral pools.	26
Chapter 3	
Figure 1. DNA electrophoresis of PpADI.	43
Figure 2. PpADI sequencing results.	43
Figure 3. SDS-PAGE of PpADI expression.	44

Figures Pages

Figure 4(A). Activity of PpADI expressed in auto-induction media. 45

Figure 4(B). SDS-PAGE of ADI expressed in auto-induction media 1, LS-5052; 2, P-5052; 3, MD-5052; 4 TYM-5052; 5, TYP-5052. 45

Figure 5. Arginine conversion by ADI and detection of citrulline using DAM/TSC assay. 46

Figure 6. Citrulline colorimetric assay in cuvette format using DAM/TSC assay. 46

Figure 7. Calibration curve of cuvette format citrulline colorimetric assay. 47

Figure 8. Citrulline colorimetric assay in MTP format using DAM assay. 47

Figure 9. Calibration curve of 96-well microtiter plate format citrulline colorimetric screening assay. 48

Figure 10. Activity values in descending order of the ADI wild-type conversion of arginine to citrulline in a 96-well microtiter plate using the optimized assay protocol. 49

Figure 11. PpADI model derived from PaADI crystal structure (PDB code 2a9gD) by SWISS MODEL WORKSPACE. 49

Figure 12 (A). Electrophoresis of epPCR products. Lane 1, 0.01 mM of $MnCl_2$; Lane 2, 0.02 mM of $MnCl_2$; Lane 3, 0.05 mM of $MnCl_2$. 51

Figure 12 (B). Electrophoresis of MEGAWHOP product with epPCR products as megaprimer. 51

Figure 13. Relative activity of ADI variants towards arginine. The relative activity is the ratio of the activity at the pH of each variant relative to the activity at pH 7.4 of wild type ADI. 52

Figure 14. Elution profile of wild type PpADI and improved variants from epPCR library, generated with Protein 230 Kit using a mircofluidic device (Agilent Bioanalyzer). BSA was added as an internal standard. 53

Figure 15. Kinetic parameters of ADI and mutants for conversion of arginine to citrulline. White: ADI wild type, grey: M1 (H404R), black: M2 (K5T D44E H404R). 54

Figure 16. pH profile of wild type ADI, M1(H404R), M2(K5T/D44E /H404R. 55

Figures Pages

Figure 17. Structural alignment of mutant M1 model with corresponding residues of the crystal structures of the PaADI (in orange). 57

Figure 18. Structural alignment of mutant M2 model with corresponding residues of the crystal structures of the PaADI (in orange). 58

Chaper 4

Figure 1. Figure 1. Activity values in descending order of the PpADI variant M3 conversion of arginine to citrulline in a 96-well microtiter plate using the optimized assay protocol. 68

Figure 2. Genealogic tree of PpADI variants (M1 to M6) with generated amino acid substitutions. Novel substitutions are indicated by an asterisk. 69

Figure 3. Native polyacrylamide gel electrophoresis of PpADI variants (M3 to M6) with different dimer/tetramer distribution 73

Figure 4. Kinetic curve of PpADI wild type, M3, M5 and M6. 75

Figure 5. A). The model of WT tetramer after energy minimization in vacuum (GROMOS 43B1). B). The model of M6 tetramer after energy minimization in vacuum (GROMOS 43B1). 77

Figure 6. A). Structure model of variant M6. B). Structure alignment of PpADI WT model and M6 model with four loops 78

List of tables

Tables Page

Chapter 1

Table 1. ADI expression, enzymatic properties and medical applications. 3

Table 2. Crystal structures of ADI in protein data bank (PDB). 6

Table 3. Residues important for catalytic function of PaADI. 8

Chapter 2

Table 1. Improvement obtained from directed evolution or rational design for pH performance. 22

Chapter 3

Table 1. Primer sequences for site saturation mutagenesis. 36

Table 2. Activity of ADI variants towards arginine determined using citrulline colorimetric assay in cuvette format. 52

Table 3. Stability of PpADI variants in the presence of human serum. 55

Chapter 4

Table 1. Nucleotide and amino acid substitutions at position 38 71

Table 2. Nucleotide and amino acid substitutions at position 296 71

Table 3. Kinetic constants of wild type PpADI and variants. 72

Arginine deiminase (ADI)

1.1 Arginine deiminase (ADI)

Arginine deiminase (ADI, EC 3.5.3.6), an arginine-metabolizing hydrolase, catalyzes the hydrolysis of L-arginine to form citrulline and ammonia. This reaction is the first step in the L-arginine degradation pathway (ADH, scheme 1, (1). First, arginine is deiminated by arginine deiminase. The resulting citrulline is converted to carbamoyl phosphate and ornithine by ornithine transcarbamylase (EC 2.1.3.3), and finally the carbamoyl phosphate is used to phosphorylate ADP by carbamate kinase (EC 2.7.2.2), producing one ATP molecule. ADI is absent in humans but present in a wide range of bacterial species such as *Pseudomonas aeruginosa* (2), *Pseudomonas plecoglossicida* (3) and *Mycoplasma arginini* (4) and in parasitic protists such as *Giardia intestinalis* (5), *Trichomonas Vaginalis* (6), *Trichomonas fetus* (7), and *Hexamita inflate* (8). For pathogenic bacteria, ADI is required in arginine dehydrolase pathway for virulence and for energy production under anaerobic conditions (9, 10).

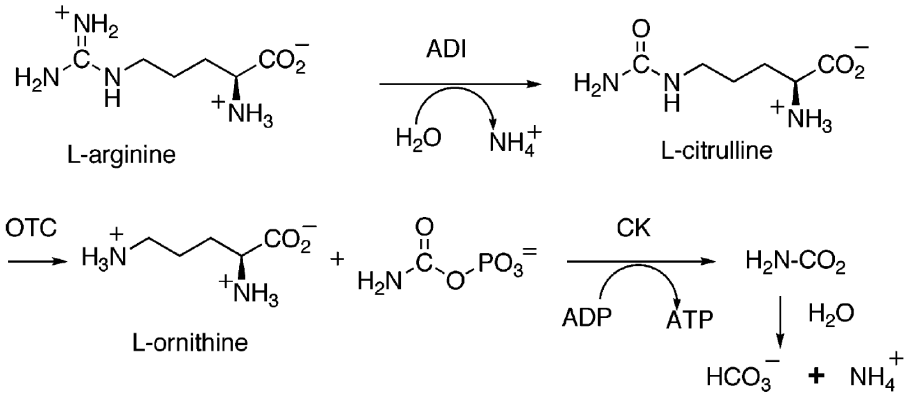

Scheme 1. Arginine dihydrolase pathway. OTC, ornithine transcarbamylase; CK, carbamate kinase.

The establishment of a high-level production system for ADI is an essential step for further research and development of this enzyme. After ADI was discovered from Mycoplasma in 1960s (11), various ADI genes have been cloned, expressed in *E. coli* strains, and the enzyme properties were also studied (Table 1).

Table 1. ADI expression, enzymatic properties and medical applications.

ADIs	Origin	Expression host/vector	Multimeric form	K_m; k_{cat}	Optimum pH	Specific activity	Medical application	References
MhADI (SYN1903)	*Mycoplasma hominis* PG21*	*E.coli* BL21 (DE3)/pET-47b	Dimer			0.618 U/mg (pH 6.5)	Human melanoma (G361), 0.036 U/ml for 50 % IC_{50}	Japan, Harasawa, 2009 (12)
MhADI	*Mycoplasma hominis* (ATCC 23114)	-	Dimer		6.0	35.5 U/mg (pH 6.0) ; 3.9 U/mg (pH 7.4)	Mouse melanoma (MH134) *in vitro*, 100 ng/ml for 50 % IC_{50}	Japan, Takaku, 1995 (13)
MhADI	*Mycoplasma hominis* (ATCC 14027)	-	Dimer	0.17 mM (pH6.6)				USA, Fenske, 1976(14)
MhADI	*Mycoplasma hominis*	*E.coli* BL21 (DE3)/pET25b		0.24 mM; 0.151 s^{-1}				China, Luo, 2007 (15)
MhADI	*Mycoplasma hominis*	*E.coli*				20 U/mg ADI (37℃). [a]	ADI-SS PEG_{20000}, human melanoma, human HCC	USA, Pheonix Pharmacologics, Inc., Clark, 2002 (16)
PaADI (PA5171)	*Pseudomonas aeruginosa* (ATCC 47085D)	*E. coli* BL21(DE3)/pET100	Tetramer	0.14±0.01 mM (pH 5.6)	5.6			USA, Dunaway-Mariano, 2005 (17)
PaADI	*Pseudomonas aeruginosa*	*E. coli* BL21 (DE3)/ pET SUMO				CARD-like domain, no catalytic activity	Human cancer cell line SKOV-3	USA, Chakrabarty, 2006 (18)
PpADI	*Pseudomonas plecoglossicida*	*E. coli* BL21 Gold-(DE3)/ pET42b		0.7 mM; 5.6 s^{-1} (pH 7.4, 0.5 M sodium phosphate buffer)	6.5	31.3 U/mg (pH 7.4, 0.5 M sodium phosphate buffer)		Germany, Schwaneberg, 2010 (3)

MaADI	*Mycoplasma arginini* (ATCC 23838D)	*E. coli* DH5α/PTTQ118				32.7 U/mg. [a]	Human umbilical vein endothelial (HUVE)	USA, Shen, 2002 (19)
MaADI	*Mycoplasma arginini* (ATCC 23838)	*E. coli* JM101/pADTc1	Dimer			33.6 U/mg (37℃, pH 6.5). [a]	Mouse hepatoma, 17 ng/ml for 50 % IC_{50}; mouse fibrosarcoma, 15 ng/ml for 50 % IC_{50}	Japan, Hayashi, 1994 (20)
MaADI	*Mycoplasma arginini* (ATCC 23838)					42 U/mg (37℃, pH 6.5); 29.9 U/mg (37℃, pH 7.4)	Mouse melanoma (MH134) *in vitro*, 10 ng/ml for 50 % IC_{50}	Japan, Takaku, 1995 (13)
MaADI	*Mycoplasma arginini* (ATCC 23838)	-					HUVE, neuroblastoma, retinoblastoma, osteosarcoma, 5~10 ng/ml for 50 % IC_{50}	Germany, Schweigerer, 1999 (21)
MaADI	*Mycoplasma arginini* (ATCC 23838)	-	Dimer	0.2 mM	6.0-7.5	50 U/mg	Mouse tumor carcinoma, fibrosarcoma and melanoma, 5~20 ng/ml for 50 % IC_{50}	Japan, Takaku, 1992 (22)
LlADI	*L. lactis* (ATCC 7962)	*E. coli* BL21Gold(DE3)/pGEM-T Easy	Trimer	8.67 mM	7.2	140.27 U/mg		Korea, Lee, 2007 (23)

[a] ADI was expressed in inclusion body and denaturation-renaturation had to be employed to get soluble protein.

1.2 ADI structure

In 1970s, Kakimoto et al. (24, 25) diffracted the first ADI crystals from *P. putida* through multiple-step chromatography followed by crystallization. Almost three decades later, the X-ray crystal structure of ADI from *P. aeruginosa* (PaADI, Figure 1A) (26) and *M. arginini* (MaADI, Figure 1B) (4) were solved to assist in understanding structure-function relationships. PaADI and MaADI share 27 % sequence identity and belong to guanidino group-modifying enzyme superfamily (GMSF). The catalytic triad (Cys-His-Glu/Asp) is conserved in members of the GMSF. Both crystal structures of PaADI and MaADI show a characteristic 5-fold pseudosymmetrical barrel with ββαβ subunits. Table 2 summarizes the crystal structures of PaADI and MaADI.

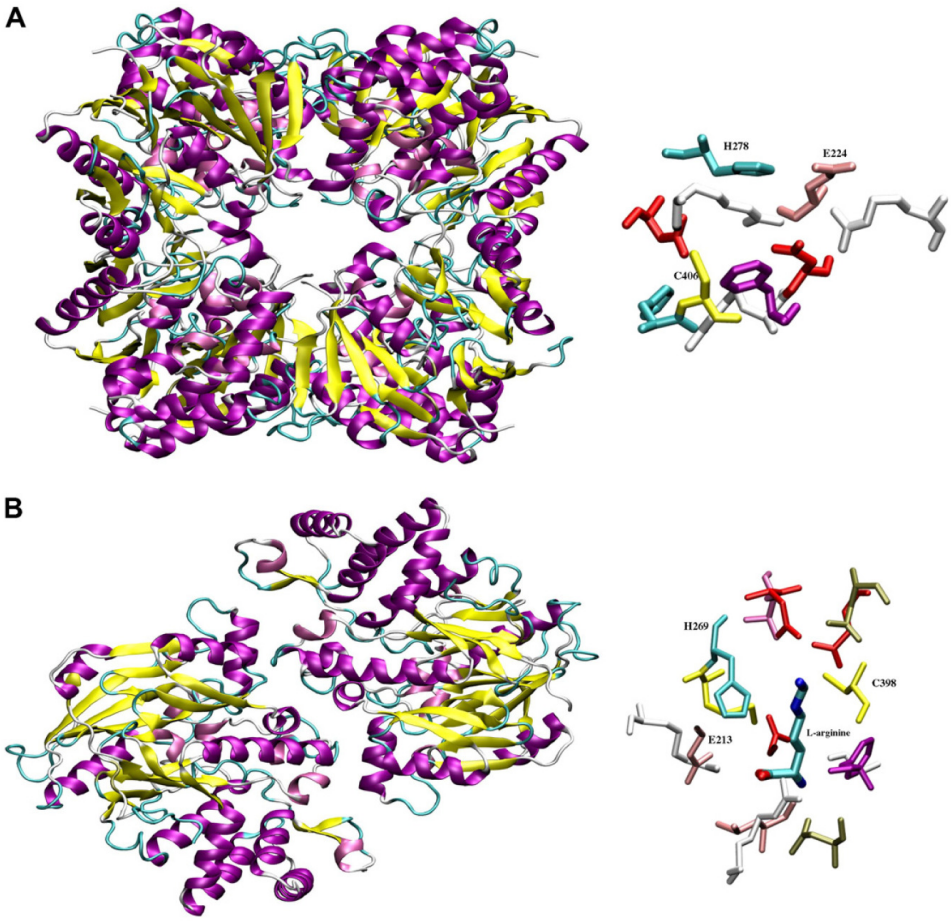

Figure 1. Structural of ADIs from *P. aeruginosa* and *M. arginini*. (A) PaADI (PDB ID: 1RXX) and stereo view of its catalytic triad (C406-H278-E224). (B) MaADI (PDB ID: 1S9R) and stereo view of its catalytic triad (C398-H269-E213) with substrate L-arginine (27).

Table 2. Crystal structures of ADI in protein data bank (PDB).

PDB code	Ligand in crystal structure	Description	Resolution (year)
2A9G	Arginine	Crystal structure of PaADI variant C406A in complex with L-arginine	2.30 Å (2005)
2AAF		Crystal structure of PaADI variant H278A forming a S-alkylthiouronium reaction intermediate	2.30 Å (2005)
2ABR		Crystal structure of PaADI variant D280A with L-arginine forming a S-alkylthiouronium reaction intermediate	2.9 Å (2005)
2ACI		Crystal structure of D166A arginine deiminase	2.50 Å (2005)
1S9R	Arginine	Crystal structure of MaADI covalently linker with a reaction in intermediate	1.60 Å (2004)
1LXY	Citrulline	Crystal Structure of MaADI covalently linked with L-citrulline	2.00 Å (2004)
1RXX		Crystal structure of MaADI	2.45 Å (2004)

MaADI was crystallized as a homodimer and its catalytic triad is formed by Cys398-His269-Glu213. MaADI has a catalytic domain and a five-helix bundle domain (Figure 3). The buried and compact substrate binding pocket is located approximately at the center of the molecule, from which a small solvent channel leads to the surface of the enzyme. The opening to the channel is located adjacent to the dimer interface region, which is at the opposite side of the 5-fold pseudosymmetric moiety of ADI. The shape and size of the channel does not permit transport of the substrate (L-arginine and end product (L-citrulline) in and out of the pocket. Substantial conformational changes in ADI are required to permit entry of the substrate and expulsion of the end product. The occurrence of "closed" and "open" form was suspected to be dependent on binding of substrate.

PaADI has a tetrametric structure with 1630 amino acid residues in total, which makes it the largest enzyme of its structural superfamily. The catalytic triad of PaADI is Cys406-His278-Glu224. Similar to MaADI, the active site of PaADI is

located in a narrow crevice formed by a network of charged residues. Ligand binding energy is derived from ion pair and hydrogen bonding interactions between active site residues and the guanidinium, carboxylate and ammonium groups of the substrate. The proposed substrate-binding model shows that the catalytic center contains abundant charged residues (e.g. Asp280, His405, Glu13 and Arg165). The ion pairing interactions between these residues contribute to the integrity and activity of ADI. In addition, Asp116, Asp227, Arg185, Arg401, His278, Glu118, and Glu224 are part of an extended charged network. The proposed catalytic mechanism suggests that the active site of PaADI is blocked by Arg401, and therefore a conformational transition is taking place upon the substrate binding. Based on the proposed reaction mechanism, Cys406 is as a key residue responsible for the nucleophilic attack on the guanidinium carbon atom of arginine. PaADI contains only one hydrophobic residue, Phe-163 and a Cys-406 with an unknown protonation state. The known functions of important residues are shown in Table 3, and the interactions between important residues and substrate arginine are shown in Figure 2.

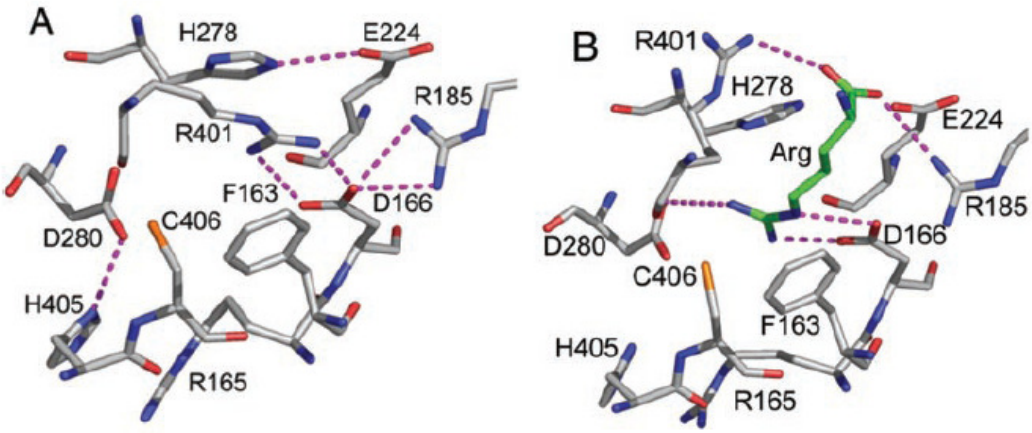

Figure 2. A. stereoscopic view of PaADI key active site residues. B. stereoscopic view of a modeled arginine substrate (green) docked in the active site of ADI. Atomic colors are red, oxygen; blue, nitrogen; yellow, sulfur; and gray, carbon. Ion pair interactions are shown as dashed lines (26).

Table 3. Residues important for catalytic function of PaADI (28, 29).	
Residues	Known/postulated function or comment
Cys406	Mounts the nucleophilic attack on the carbon atom of the guanidinium group of arginine
His278	Serves as a general base and activate the water molecule
Glu224	Modulate the ionization state of His278
Asp280	Interacts with the imidazole group of His405 F via the carboxylate group, which in turn interacts with Glu13. Invariant residue in all known ADIs
Asp280, Asp166	Fix the guanidinium group of the arginine substrate tightly by interactions with the carboxyl groups
Arg401, Arg185	Form ionic interaction with The carboxyl group of the arginine substrate
Phe163	Interacts with the hydrophobic part of arginine substrate
Glu13	Interacts His405 and is invariant in all known ADIs
His405	Sometimes is replaced by an arginine, as in the case of McADI. This may explain the low pH optimum of PaADI (5.6) in contrast to the neutral pH optimum of McADI, the enzyme that contains an arginine residue instead of His405
Arg165	Is fixed by electrostatic interactions with the main chain oxygen atoms of Thr408 and His405 and with the hydroxyl group of Thr-408
Arg401	Blocks the ADI active site via the side chain by forming an ion pair with the carboxyl group of Asp166 and occupies approximately the same position as the guanidinium group of an arginine substrate

The overall fold of MaADI and PaADI consist of five ββαβ modules in cyclical arrangement, generating a pseudo 5-fold symmetrical barrel and an additional 85-residue α-helical domain inserted between the first and the second ββαβ modules giving the typical “Clip-on-fan” moiety. The α-helical domain of PaADI mediates tetramer formation and the α-helical domain of MaADI was speculated to play a role in activating the series of reaction in arginine dehydrolysis pathway (4). Structural alignments by Chakrabarty et al. (18) demonstrated the unique 85 residue 5-α-helical bundle domain exhibiting structural similarity to the mammalian CARD (caspase recruitment domains)-containing proteins and this CARD-like domain is present only in the PaADI and MaADI but not in the other

GMSF members (Figure 3B). Furthermore, PaADI putative CARD-like domain induced apoptosis to cancer cells.

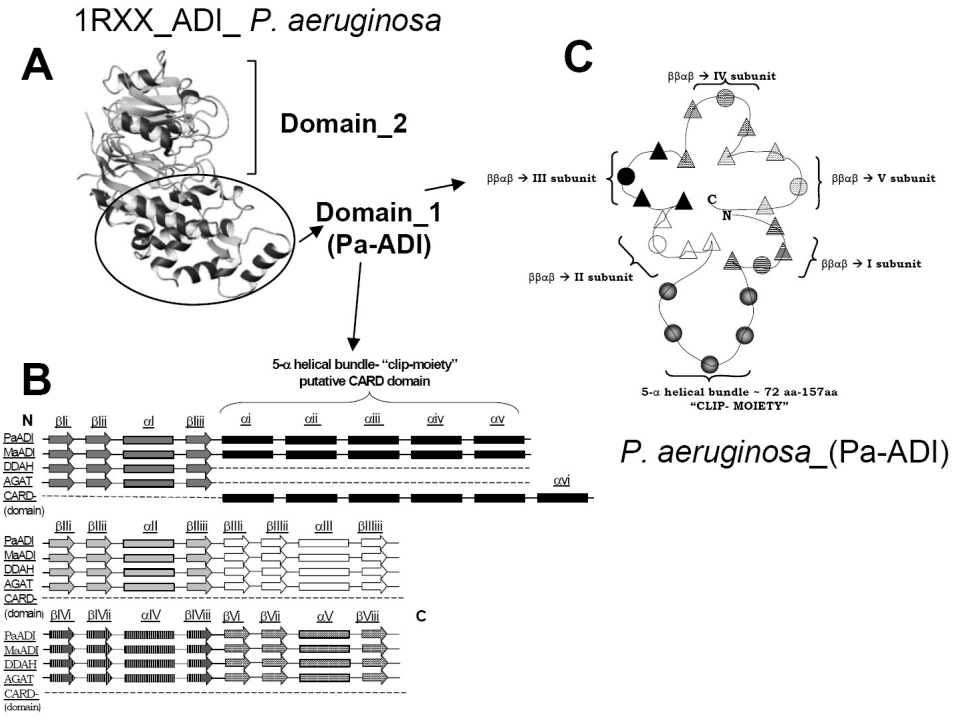

Figure 3. Structural characteristics of the PaADI. A. Ribbon drawing of PaADI (1RXX_A) highlighting the two domains. B. The presence of the CARD domain in PaADI and MaADI but its absence in other members of the GMSF (guanidino-group modifying superfamily) enzymes such as DDAH and AGAT, as shown from the structure-based sequence alignments. The CARD domain represents that of caspase-9. DDAH, dimethylarginine dimethylaminohydrolase; AGAT, arginine: glycine amidinotransferase. The β-strand and α-helices are shown as arrows and strips respectively. Roman numericals I to V are the five ββαβ subunits. The clip moiety (α-helical module) in Figure 3 is seen only in PaADI and MaADI which bears structural homology to the six-α-helical modules that form the CARD domain of the caspase-9 protein molecule. N, N-terminal; C, C-terminal. C. A schematic diagram showing the overall fold and topology of PaADI, as reported (18).

Comparison of substrate free and substrate bound structure of PaADI gives interesting insight into structure changes upon substrate binding (17). Pairwise superposition of the free wild-type PaADI (PDB code: 1rxx) and the mutant enzyme substrate complexes (PDB code: 2a9g) show that the overall fold of the structures remains similar, yet with some local changes. In particular, four loops (Figure 4) associated with the active site undergo conformational transitions not

related to crystal packing: loop 1 (residues 30-46), loop 2 (residues 178-185), loop 3 (residues 271-281, part of this loop is disordered in the apoADI structure), and loop 4 (residues 393-404). Residues adjacent to the substrate exhibit the most significant shifts. For example, the α-carbon atom of Leu41 (loop 1) shifts by 2.7Å and that of Arg185 (loop 2) by 1.8 Å; the α-carbon atom of His278 (loop 3) shifts by 0.9 Å and that of Gly400 (loop 4) by 4.4 Å. These are localized but mechanistically important conformational transitions that tighten the surrounding of the substrate. Simultaneously, substrate binding is accompanied by displacement of the side chain of Arg401 (loop 4) by more than 8 Å to enable access to the active site. The superposition of ADI and PAD4 ADI active site is shielded from the solvent by a long loop (residues 25-48 in PaADI) and the following two turns of α-helix (residues 49-56).

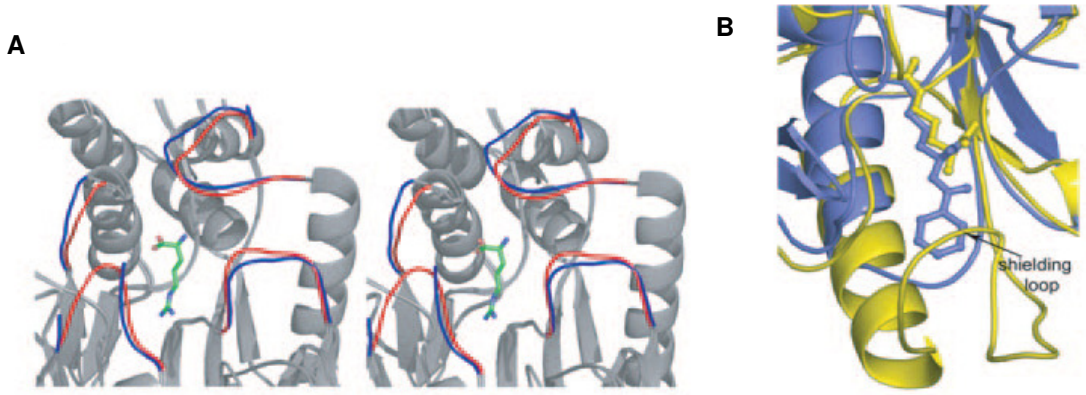

Figure 4 (A). Stereoscopic view of ADI in the unbound and bound states. Superposed molecules are colored gray where the trace of the polypeptide chain is similar in both structures. For regions exhibiting differences, loops of the apoADI structure are highlighted in blue, and loops of the ADI structure complexed with arginine are highlighted in red. 4(B). Structural relationship between ADI (yellow) and PAD4 (cyan) (17).

1.3 Catalytic reaction mechanism of ADI

The overall reaction catalyzed by ADI is the hydrolytic substitution of the ηNH_2 group from the guanidinium group Cζ of L-arginine, leading to citrulline and ammonia (Figure 5). Herzberg (17) and Arnold (4) proposed ADI catalysis mechanism for PaADI (Figure 5) and MaADI, respectively. Basically, both of the proposed mechanisms are composed of three main steps: 1) thiol group of

Cys406 mount a nucleophilic attack on the guanidinium group of arginine and a proton is transferred first to ηNH$_2$ group; 2) water molecule is activated by His278 and followed by attacking the covalent intermediate to replace and release NH$_3$; 3) the C-S covalent bond between enzyme and the resulting citrulline is cleaved and thus end product citrulline is released and free enzyme is generated for next catalytic cycle.

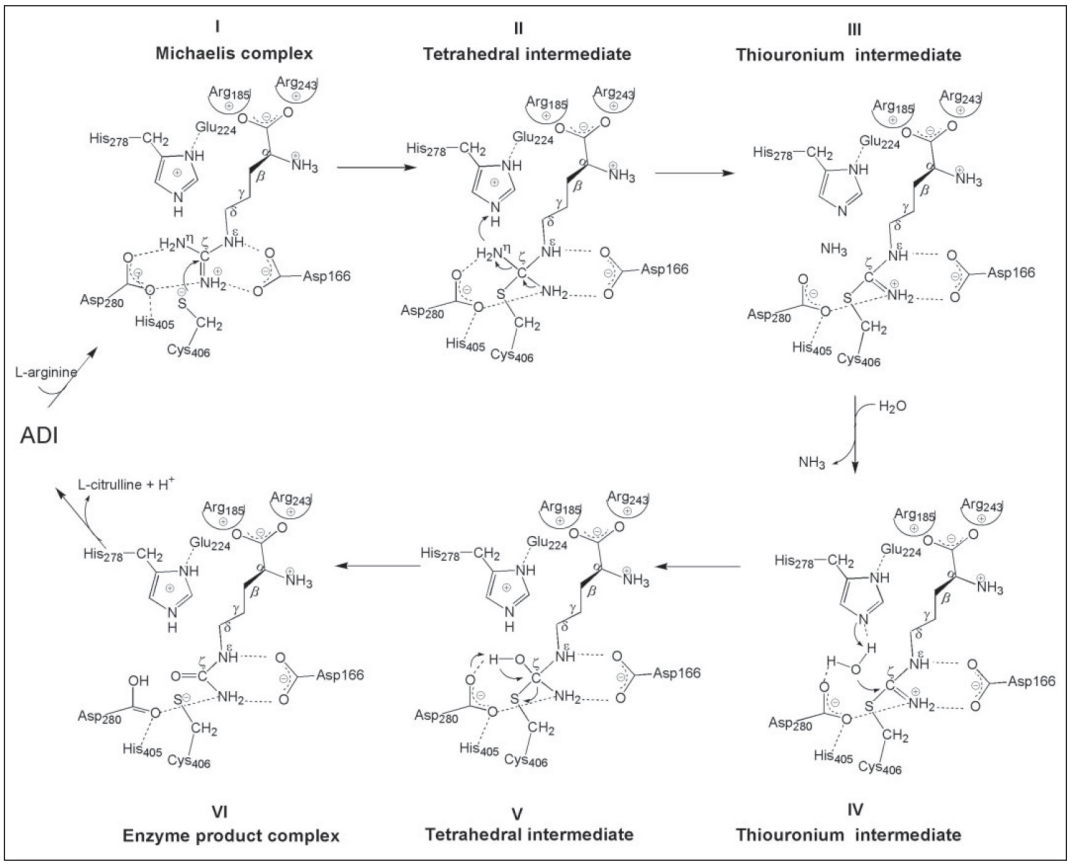

Figure 5. Mechanism of PaADI catalysis of arginine to citrulline and ammonia (17).

1.4 Anti-tumor application of ADI

Amino acids depletion is one type of targeted therapy for human cancers which are auxotrophic for a particular amino acid. Amino acids degrading enzymes, such as asparaginase (30), methioninase (31), arginase (32), arginine deiminase (27), phenylalanine ammonialyase (33) and tryptophanase (34) have been

studied for inhibition of tumor cells *in vitro*. The most representative anticancer enzyme is asparaginase, which is particularly effective in acute lymphoblastic leukaemia. PEG asparaginase is commercialized for acute lymphoblastic leukaemia treatment (Oncaspar®, pegaspargase) (35). However, asparaginase treatment is sometimes accompanied by serous side-effects including anaphylactic shock, coagulapathies as well as liver and pancreatic toxicity (36).

Arginine is an important amino acid involved in the synthesis of a wide range of peptides and proteins, production of creatine and nitric oxide, and a myriad of metabolic pathways and cellular events. It is a precursor of proline, polyamines, glutamine, glutamate, and other neurotransmitters, such as g-aminobutyric acid and also serves as a substrate for two important enzymes, arginase and nitric oxide synthetase (37). Arginine is an indispensable amino acid to children but a semi-essential amino acid in adult humans since many adult somatic cells can synthesize it from citrulline in two steps via urea cycles (Figure 6). The enzyme argininosuccinate synthetase (ASS) catalyzes the conversion of citrulline and aspartic acid to argininosuccinate which is then further converted to arginine and fumaric acid by argininosuccinate lyase (ASL). Arginine can be degraded to ornithine by the urea cycle enzyme arginase. Ornithine is then converted back to citrulline by ornithine carbamoyl transferase (OTC) and then recycles back to arginine from citrulline by ASS/ASL. Thus, the ability to regenerate arginine from citrulline depends on the amount/activity of ASS and ASL, which are tightly coupled. The sensitivity of cells to arginine deprivation depends on the ability of ASS and ASL to regenerate arginine from the alternative intermediate (ornithine, citrulline and argininosuccinate) in the urea cycle.

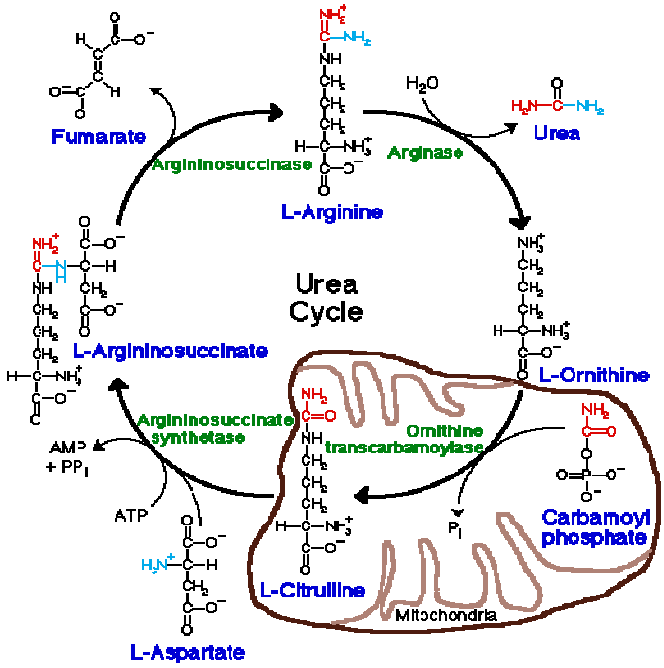

Firgure 6. Urea cycle. Argininosuccinate synthetase (ASS) catalyzes the conversion of citrulline and aspartic acid to argininosuccinate which is then further converted to arginine and fumaric acid by argininosuccinate lyase (ASL). Arginine can be degraded to ornithine by the urea cycle enzyme arginase. Ornithine is then converted back to citrulline by ornithine carbamoyl transferase (OTC) and then recycles back to arginine from citrulline by ASS/ASL.

Arginine begins to become limiting at ~10^{-4} M, whereas other amino acids can sustain growth at 10^{-5}-10^{-6} M. Wheatley et al. showed that most tumour cell lines die considerably more quickly during arginine deprivation than in the absence of any other single (or group of) essential amino acids (38). Since 1930 for the first time arginine known is essential for the growth of some forms of cancer, the potential of arginine degrading enzymes as therapeutic agents was recognized, investigated and employed for arginine auxotrophic tumor treatments. Enzymes capable of depleting arginine *in vitro* include arginase existing in human liver, arginine decarboxylase from bacterial, plant and human, and ADI from microorganism.

Arginine decarboxylase converts arginine to agmatine, which is toxic at high plasma concentration. Furthermore, arginine decarboxylase has a short half-life and it loses virtually all enzymatic activities upon pegylation though pegylation of

arginine decarboxylase is inefficient because not enough lysine residues for polyethylene glycol to attach (39).

Arginase is limited for anti-tumor application because of its low substrate affinity (K_m value 2-4 mM; plasma arginine 100-120 μM), short circulatory half-life (10-15 min) and sub-optimal enzymatic activity at physiological pH (alkaline pH optimum, pH 9.3)(40). Despite these disadvantages of arginase, Lam et al. reported remission of hepatocellular carcinoma induced by systemic release of endogenous hepatic arginase (41) and Leung et al. proved pegylated recombinant human arginase (rhArg-peg 5,000mw) can inhibit ASS-positive HCCs while ADI can not (42).

In addition, ADI, another arginine-degrading microbial enzyme, has various biological activities including anti-proliferation, anti-angiogenesis and inhibition of inducible nitric oxide synthase (iNOs). Figure 7 summarizes how ADI affect many arginine-related cellular functions. ADIs (Table 1) have been shown to have strong *in vitro* and *in vivo* inhibition for arginine auxotrophic tumors (e.g. hepatocellular carcinomas (HCCs), melanomas, retinoblastoma (43), prostate cancer(44)) and ADI from *M. hominis* (MhADI) is currently under clinical trial for HCC (phase II) (45) and melanomas (phase I/II) (46). Studies on human lymphatic leukemia cell lines confirmed ADI's anti-angiogenic activity. Among all the ADIs, MhADI and MaADI were studied most intensively (Table 1).

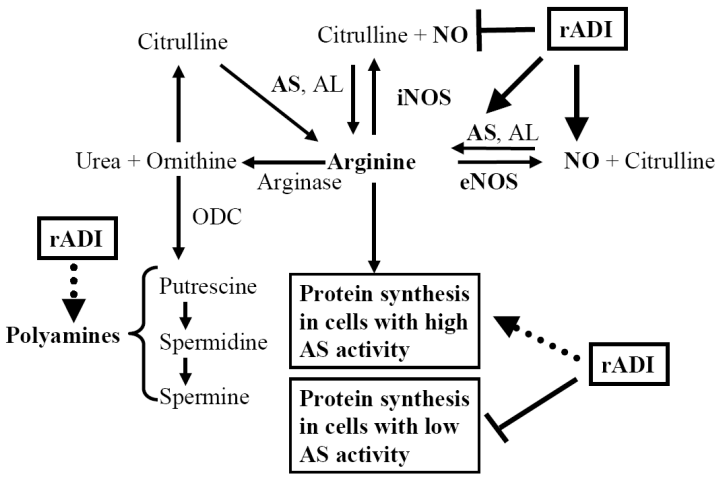

Firgure 7. Summary of ADI effects on arginine-related cellular functions. rADI inhibits NO production via iNOS, but potentiates NO production via eNOS in the cultured endothelial cell model. rADI enhances or inhibits AS activity in different cells. rADI inhibits de novo protein synthesis in cells with low AS activity, but not in cells with high AS activity. Polyamine synthesis was not significantly affected by rADI, even in cells with low AS activity. Arrow representation: solid, potentiates; blocked, inhibits; dotted, no effect (47).

In 1999, US Food and Drug Administration (FDA) designated ADI-PEG-20 orphan drug status for treating HCC and invasive malignant melanomas. In 2005, also the European Agency for the Evaluation of Medicinal Products (EMEA) also granted ADI-PEG-20 orphan drug status for HCC. Phase II trials of ADI-PEG-20 in patients with metastatic hepatocellular carcinomas have shown that the drug is safe, well tolerated, and may benefit patients with unresectable HCC. Izzo and coworker suspected that combination therapies of arginine deprivation and growth inhibition via kinase inhibitors might improve the survival rate further. Additionally, ADI enhances radio sensitivity of human mammary adenocarcinoma (MCF-7 cells) (48), exerts anti-proliferative as well as anti-angiogenic activities and inhibits the growth of viruses such as HIV-1 and hepatitis (49, 50). Current research efforts are focused on ADI's *in vivo* inhibitory effect towards leukemia, melanoma, prostate cancer, renal cell carcinoma, and human umbilical vein endothelial cells (HUVEC) (19, 44, 51-53), clinical trials for HCC (phase II) (45) and melanoma (phase I/II) (46), and tumor inhibitory mechanisms of ADI (54).

The effectiveness of ADIs as anti-tumor agent depends on their enzymatic properties (such as K_m, k_{cat}, optimum pH, stability at neutral pH), selectivity on tumor cells, stability in blood circulation and immunogenicity. Pegylation (35) has been effective in reducing their immunogenicity in animal and increase their stability to various hydrolytic enzymes in plasma. Directed evolution as powerful algorithm to design proteins allows improving all properties that can be reflected in a screening system through iterative rounds of diversity generation and screening. Small libraries of a few thousand variants are often sufficient to find improved variants (55) even without rational understanding of the targeted property. The first example of directed ADI evolution by our group (3) provides a simple and effective screening system to improve activity of PpADI at physiological pH.

1.5 Conclusion

ADI-based arginine deprivation is a novel and promising targeted approach to the treatment arginine auxotrophic tumors, in particular, melanoma, hepatocellular carcinoma and leukemia. Certain mesotheliomas and renal cell cancers were also proved to be sensitive to ADI therapy. Due to its low incidence of major side effects (myelosuppression and gastrointestinal toxicity or other major organ toxicity) arginine deprivation treatment should be combined with other anticancer treatments to increase the response rate. Reengineering of ADI by protein engineering is a promising strayegy to tailor ADI properties for demands in medical applications. Solved ADI crystal structure enables to understand structure function relationships and to guide protein engineering.

Directed evolution

2.1 Introduction to directed evolution

Enzymes are increasingly being used in the generation of products that are traditionally made using chemical synthesis and the field continues to expand its horizons, particularly as applied to the synthesis of the fine chemicals and pharmaceuticals (56, 57). Naturally occurring enzymes are often not designed for the applications of interest, since after all they are evolved in nature for a purpose other than being the catalysts of industrial processes. Directed evolution, rational design and biodiversity screening and combined approches are the main strategies to reengineer enzymes for addressing application demands. Directed evolution has emerged as a powerful enabling method for improving enzyme properties in iterative cycles of diversity generation and screening (Figure 1).

A main advantage of directed evolution compared to rational design is that it does not require structural or mechanistic information for protein optimization. Directed protein evolution has been successfully used for altering and improving protein properties (solubility, expression, enantioselectivity, stability and activity in unusual environment, allosteric interactions, tolerance to pH), as well as for regulating other molecules and systems, including RNA, DNA regulatory elements, biosynthetic pathways and genetic regulatory circuits (58-60).

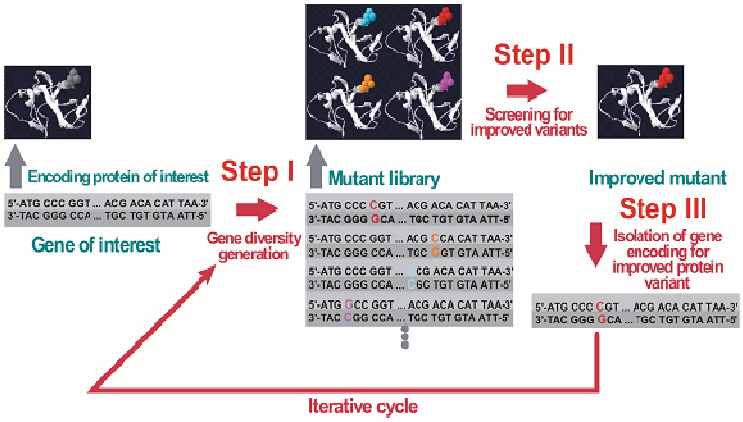

Figure 1. Procedure of a directed evolution experiment. It involves three key steps: 1) selection a good starting sequence and mutating the parent to create a library of variants; 2) identification variants with improved function and 3) isolation of gene encoding for improved variant and repeating the process until the desired function is achieved.

A parent sequence (or sequences) is chosen based on its perceived proximity to the desired function and its evolvability (the ability of a protein to adapt in response to mutation and selective pressure). A parent protein for directed evolution should exhibit enough of the desired function that small improvements can be reliably discerned in a high-throughput screen.

Variants library should be generated with high probability of finding improved variants given the screening capacity. With a high-throughput screening method, a library can be constructed to generate the large potential improvement. Arnold and coworkers(61) showed that very low mutation rates result in many functional sequences but only a small number are unique sequences, however very high mutation rates produce diverse sequences but few retain function. Schwaneberg and coworkers(62) reviewed random mutagenesis methods, focused library generation methods and computational tools for high-quality mutant libraries generation. Schwaneberg and coworkers (63) also summarized criteria for an ideal mutagenesis methods: unbiased mutational spectrum, controllable mutation frequency, consecutive nucleotide substitutions or codon-based substitutions, enable subset mutagenesis (e.g. introduction mainly positively or negatively charged amino acid), independent of gene length, technically simple and reproducible, and economical.

Screening is used to identify library members improved in the targeted property. Identification of improved variants though selection or screening is “analogous” to evolutionary pressure in natural evolution (i.e. only the fittest survive). As the word “directed” in directed evolution implies, laboratory evolutionary pressure is defined and applied by the researcher in screening system. Gradually increasing the selection pressure or evolving against a series of intermediate challenges often accumulates useful single mutations and yields desired variants (64).

Traditional methods for screening employ microtiter plate formats (96-well, 384-well, 1,536-well (65) and even 1,000,000-well (66)) or solid phase assay (agar plate, filter paper and nitrocellulose membrane), which typically enable the screening of no more than 10^6 variants by using robotic automation (67). Sometimes, fast and universal analytic methods like HPLC (68) or GC-MS (69) are utilized for performing an efficient screen of a non-natural substrate. However, the number of screened mutants is limited to 10^4-10^6. In recent years flow cytometry systems (67, 70, 71) have become increasingly attractive, especially after the development of emulsion technology offering compartmentalization and high throughput up to 10^7/h. In addition, Weitz and coworkers (72) recently reported a promising ultrahigh-throughput screening in drop-based microfluidics, by which one can screen a library of 10^8 in about 10 h. Dijkhuizen et al. compared in a review (73) six kinds of library screening strategies (Figure 2). Selection techniques rely on a direct link between cell growth and improved or acquired enzyme function and therefore it is limited to engineering detoxifying enzymes (e.g. b-lactamase) or enzymes that synthesize essential nutrients for cell growth and survival. The traditional microtiter plate screenings are medium-throughput and the most simplistic format of screening. It involves the incubation of colonies with the substrate of targeted enzyme. The crucial factor with this screening technique is that substrate conversion creates a visual signal, such as fluorescence or color, to identify colonies expressing an enzyme with desirable properties. Microtiter plate based screenings are the most commonly applied method in identifying desirable enzyme variants. Microtiter plate based

screenings enable the use of various analytical tools and in the mean while they offer a great dynamic range. Their screening capacity is usually limited to less than 10^4 variants per day. Screening based on microfluidic device and sorting device is a new screening platform for directed evolution, which offers ultra-high-throughput. It allows the discriminate between wild-type and a less active mutant and allows for the addition of substrates and quenchers at desired time thus extending the scope of directed evolution screening strategies. Cell as micro-rector, cell surface display and *in vitro* compartmentalization technology are also FACS (fluorescence-activated cell sorting system) dependent methods for high-throughput screening and allow 10^9-10^{10} screening capacity.

Once improved enzymes are identified, encoding genes are isolated and subjected to further iterative cycles of mutation and screening in order to accumulate beneficial mutations until the targeted improvement is hopefully achieved. The number of iterations required depends on the starting point, the protein fold and the selected properties which determine the possible mutational load and achievable improvement.

Four accepted requirements for successful directed evolution (http://www.che.caltech.edu/groups/fha/) are, 1) the desired function must be physically possible; 2) the function must also be biologically, or evolutionarily, feasible. In practice, this means that there exists a mutational pathway to get from here to there through ever-improving variants (see above). A good experiment will maximize the likelihood; 3) Suitable host (*E. coli* or *S. cerevisiae*) which allows functional expression of more than 10^6 variants per µg of DNA. 4) A rapid screen or selection that reflects the desired function. How rapid the screen must be depends on how rare mutations leading to the desired property are and how many must be accumulated to achieve the desired result.

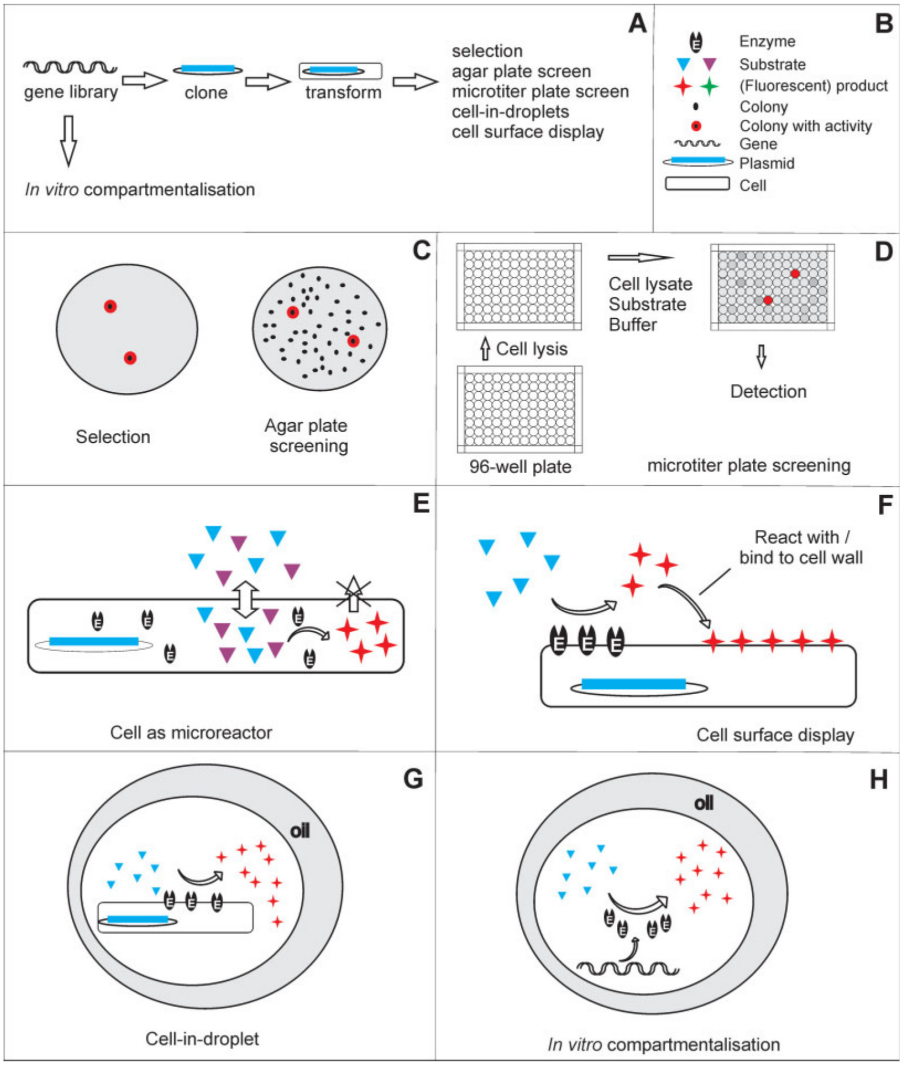

Comparison of screening and selection technologies

Strategy	Library size	Advantage	Disadvantage
Selection	$\sim 10^9$	Yields desirable variants only	Only possible if activity gives growth advantage
Agar plate screen	$\sim 10^5$	Simple to operate	Limited dynamic range
Microtiter plate screen	$\sim 10^4$	All analytical methods possible Excellent dynamic range	Relatively low screening capacity
Cell-in-droplet screen	$\sim 10^9$	Large libraries	Fluorescence detection and DNA modifying enzymes only
Cell as microreactor	$\sim 10^9$	Large libraries	Fluorescence detection only
Cell surface display	$\sim 10^9$	Large libraries	Fluorescence detection only
In vitro compartmentalization	$\sim 10^{10}$	No cloning steps Large libraries	Fluorescence detection and DNA modifying enzymes only

Figure 2. Overview of screening technologies. (A) Experimental steps from obtaining the gene library as PCR product to the actual screen. Note that cloning and transformation efficiency are often limiting library size; (B) Explanation of symbols; (C) Cell growth/survival selection and agar plate screening; (D) Microtiter plate screening; (E) Cell as micro-reactor; (F) Cell surface display; (G) Cell-in-droplet; and (H) *In vitro* compartmentalization (73).

2.2 Directed enzyme evolution for pH tolerance of enzymes

Application of enzymes in processes at a specified pH necessitates protein engineering to change their pH performance. Directed evolution and rational design method were applied to improve enzyme specific activity at certain pH or shift their pH profiles. Some representative success stories of directed protein evolution improving pH performance are summarized in Table 1.

Table 1. Improvement obtained from directed evolution or rational design for pH performance.

Enzymes	Mutagenesis methods	Screening methods	Improvements	References
Human β-glucuronidase	EpPCR and saturation mutagenesis	Flow cytometry	60-fold more active (k_{cat}/K_m) at pH 7.0 and were up to an order of magnitude more effective at catalyzing the conversion of two structurally disparate glucuronide prodrugs to anticancer agents	2008 (74)
Bacterial xylanase	DNA shuffling	Agar plate assay	About 5-fold improvement of specific activity at pH 9.0	2008 (75)
Human pancreatic lipase	EpPCR	Agar plate and microtiter plate assay	1.5-fold of activity improvement at acidic pH	2010 (76)
Bacterial arginine deiminase	EpPCR and site directed mutagenesis	Microtiter plate assay	pH optimum shifted from pH 6.5 to pH 7; 4-fold of activity improvement at pH 7.4	2010 (3)
Bacterial α-amylase	EpPCR	Microtiter plate assay	5-fold higher activity at pH 10 than wild type	2003 (77)
Eukaryote D-pantonohydrolase	EpPCR and DNA shuffling	Agar plate assay	10.5-fold higher specific activity and retain 85% of its original activity after incubation under low pH	2006 (78)
Vanadium chloroperoxidase	EpPCR, site saturation mutagenesis and site directed mutagenesis	Microtiter plate assay	About 100-fold improvement of specific activity at pH 8	2006 (79)
Bacterial class-A non-specific acid phosphatase (PhoN)	Site directed mutagenesis		1.6-fold of activity improvement over broder pH range	2006 (80)
Aspergillus niger PhyA phytase	Site directed mutagenesis		pH shifted from 5.5 to 3.8 (1.7 unit); 2.66 -fold improvement of activity at pH 3.5 than wild type.	2006 (81)
Bacillus cereus β-amylase	Site directed mutagenesis		pH optimum shifted to pH 4.2-4.8 by 2 pH units.	2004 (82)
Phytase	Site directed mutagenesis		pH optimum shifted by 0.5-1 pH unit; a slight increase in maximum specific activity	2002 (83)
Alcohol dehydrogenase	Site directed mutagenesis		pH optimum shifted from 7.8 to 9.0; about 2-fold improvement of maximum activity at pH 9.0 than that of wild type	1991 (84)

Many examples of rational reengineering of an enzyme pH optimum exist (Table 1). For shifting the pH optimum, a deep understanding of molecular dynamics is essential part of understanding enzyme flexibility. Rational design method successfully shifted enzyme pH profile. pH dependence of an enzyme is determined by the ionization of the catalytic groups, which is affected by various interactions involved in their microenvironments. In order to catalyze certain reactions, ionizable residues in active site should act as nucleophile or acid/base catalyst and they need to maintain proper ionization state for proper activities of proteins. The p*K*a value of the proton donor and the catalytic nucleophilic residue are therefore limiting the pH range at which the enzyme can function, and therefore pH-dependent activity can be differed by the p*K*a of the key residues. The p*K*a value of the residue is governed by intrinsic acidity of the functional group and other factors (electrostatic interaction from neighboring and the heterogeneous dielectric environment in the protein solution system). The electrostatic potential generated by the charged titratable residues affects the ground state of the protein, such as stability, binding to ligands and p*K*a values of ionizable groups. The electrostatic potential of proteins can be calculated by using computational procedures (Delphi, UHBD, CHARMM) and can be increased or decreased through mutations. For shifting the pH optimum of enzymes, many researchers have tried to substitute catalytic residue by site-directed mutagenesis (Table 1).

Yoo and coworkers (85) analyzed the relation between the shift of pH optimum and change in electrostatic potential due to mutation using Delphi. They identified key residues of xylanase responsible for electrostatic potential of catalytic residues but not affecting the catalysis directly. The latter hypothesis was proven by site directed mutagenesis in a later report. Wyss and coworkers (83) summarized strategies for enzyme pH profile modification, 1) replacement of ionizable groups that are directly involved in substrate or product binding and/or catalysis by nonionizable ones or by amino acids with different charge or p*K*a values; 2) replacement of residues that are in direct contact with residues

mentioned in 1) by forming hydrogen bonds and/or salt bridges; 3) alteration of longer-range (indirect) charge-charge interactions by modification of the surface charge of the enzyme.

When there is no structure-function relationship information available for an enzyme, directed evolution is the best option to tailor the pH performance of enzyme for application demands (Table 1). Directed evolution allows improving all properties that can be reflected in a screening system through iterative rounds of diversity generation and screening. Small libraries of a few thousand variants are often sufficient to find improved muteins even without rational understanding of the targeted property (76, 86). Using MTP assay, epPCR mutant libraries with a ratio of 50 % active and 50 % inactive clones have often been used successfully in directed evolution, improving enzyme properties by gradual changes (one or two amino acids changes per round of mutagenesis and screening).

2.3 Directed enzyme evolution for medical application

Directed evolution has been very useful for improving enzymes for industrial needs. In recent years, there is also growing number of enzymes applied for therapeutic purpose. For the development of protein therapeutics, directed evolution started to be used to tailor enzyme properties in medical field, for example drug delivery (87, 88) and has proven to be a useful tool for generating protein variants with enhanced therapeutic potential (88), for example, improving the effectiveness of therapeutic enzymes, antibodies, vaccines and viruses. Here, the improvements of therapeutic protein for anti-tumor application by directed evolution are discussed in more details.

2.3.1 Prodrug enzymes for tumor chemotherapy

Prodrug cancer chemotherapy has attracted considerable interest due to the possibilities it provids to overcome various barriers to drug formulation and delivery (such as poor aqueous solubility, chemical instability, insufficient oral

adsorption, rapid pre-systemic metabolism, inadequate brain penetration, toxicity and local irritation) (89). Examples of such drugs currently in use in cancer treatment include 5-fluorocytosine, cyclophosphamide, capecitabine, mitomycin C, and AQ4N (90). However, the side effects of prodrug therapy remain a serious concern which arises from the fact that noncancerous cells also possess the capacity to degrade them. This has triggered the interest to generate more effective prodrug-activating enzymes so that prodrugs can kill tumor cells at concentrations that generate little or no side effects. Further goals are to design more powerful and tumor-specific drugs, and to devise more effective methods for delivering them specifically to tumors.

By applying directed evolution through the technique of error-prone PCR, Martin and coworkers (90) indentified YieF variant exhibiting >5-fold increased capacity to kill HeLa cells. Furthermore, YieF variant was proved to be effectively delivered to tumor cells using a strain of *Salmonella typhimurium* (SL 7838).

Human β-glucuronidase, due to low intrinsic immunogenicity in humans, is an attractive enzyme for tumor-specific prodrug activation. However its utility is limited by low activity at physiological pH. Roffler and coworkers (74) developed a high-throughput screening procedure for enzymatic activity based on the stable retention of fluorescent reaction product in mammalian cells expressing properly folded glycoproteins on their surface. This procedure was utilized to screen error-prone PCR and saturation mutagenesis libraries to isolate β-glucuronidase tetramers that were up to 60-fold more active (k_{cat}/K_m) at pH 7.0 and were up to one order of magnitude more effective at catalyzing the conversion of two structurally disparate glucuronide prodrugs to anticancer agents.

2.3.2 Oncolytic viruses for tumor chemotherapy

Viral-mediated oncolysis is a novel cancer therapeutic approach with the potential to be more effective and less toxic than current therapies due to the agents' selective growth and amplification in tumor cells. To date, these agents

have been regarded as highly safe in patients but have generally fallen short of their expected therapeutic value as monotherapies.

Consequently, new approaches to generate highly potent oncolytic viruses are required. For the latter purpose, Hermiston and coworkers (91) developed a new method and termed it also ‘‘Directed Evolution’’ for creating highly potent oncolytic viruses. Viral serotypes representing Ad subgroups B-F were pooled and passaged twice on sub-confluent cultures of the target tumor cell lines at a particle-per-cell ratio of approximately 200 to invite recombination between serotypes (Figure 3). Supernatants from the second round of the high viral particle-per-cell infection of sub-confluent cultures were then used in a 10-fold dilution series to infect confluent T-75 tissue culture flasks of target tumor cell lines PC-3, HT-29, Panc-1 and MDA-231. Using this ‘‘Directed Evolution’’ methodology, the novel generated chimeric oncolytic virus ColoAd1 demonstrated ~ 2 log increase in both potency and selectivity when compared to ONYX-015 on colon cancer cells. *In vivo* and *ex vivo* studies therefore validated the innovative general approach for deriving clinically-relevant and potent anti-cancer virotherapies.

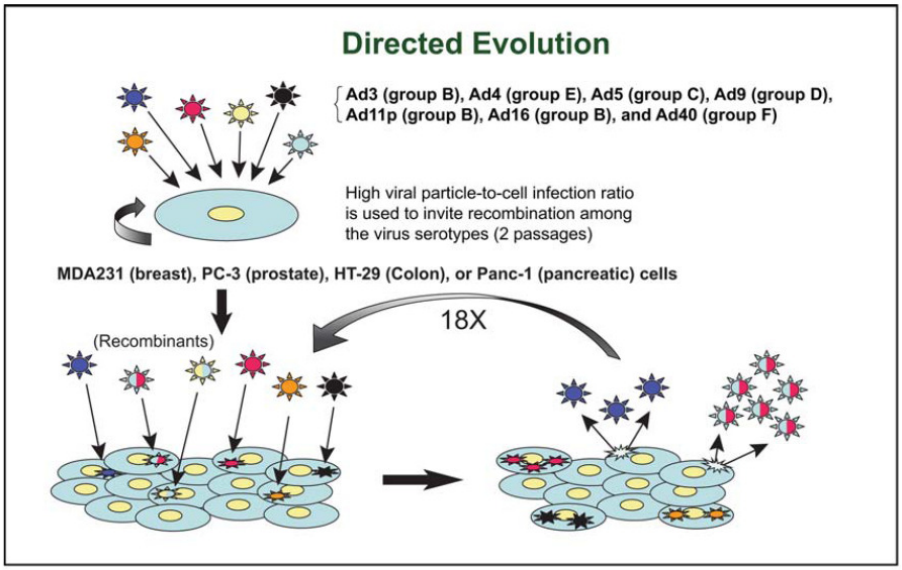

Figure 3. Hermiston’s “Directed Evolution” process of viruses and derivative viral pools (91).

2.3.3 Amino acid depriving enzyme for anti-tumor applications

Naturally available enzymes are usually not optimally suited for therapeutic purposes. This incompatibility often relates to the stability or activity of the enzymes under body conditions.

Despite many successful efforts to broaden the understanding of the structural basis of protein stability, there is still no universal strategy to stabilize protein by a limited number of rationally designed mutations. Well-known and reasonably successful types of rational engineering work include substitutions that increase rigidity (e.g. substitute amino acid Xxx with Pro or substitute Gly with other amino acid Xxx or the introduction of disulfides). These substitutions have effects on the entropy of the unfolded state, improvement of molecular packing (e.g. shortening of loops, improvement of interactions in the hydrophobic core, for example, by the removal of internal cavities), modification of surface charge networks or reinforcement of a higher oligomerization state.

Directed evolution provides a powerful approach for improving thermostability and does not need understanding of structure-function relationship. Most strategies for screening for enzyme stability rely on measuring residual enzyme activity before and after exposure to a denaturing challenge (e.g. high temperature, organic solvents, extreme pH) (92).

Bacterial L-asparaginases have been used as therapeutic agents in the treatment of lymphoblastic leukaemia. The main restrictions to the therapeutic use of L-asparaginase include its premature inactivation. As a result frequent injections are required to maintain therapeutic levels. Repeated injections and high dose can cause several types of side reactions from mild allergies and the development of immune responses to dangerous anaphylactic shocks (93). Enhancing the stability of L-asparaginase by protein engineering improves its body-residence time, and thereby minimizes immunosuppressive effects by lowering the therapeutic dose. Labrou and coworkers (94) obtained a

reengineered L-asparaginase with enhanced thermal stability. Single mutation on the surface of the protein resulted in ~10 degree increased T_m value (half-inactivation temperature). The thermostable variant has to be tested further on animals and/or humans in order to be advanced to a potent therapeutic drug.

Another example of a reengineered amino acid-deprivating enzyme is PpADI. PpADI is a promising anti-tumor enzyme however with a non-physiological optimal pH and relative high K_m value which hindering its medical application. By directed evolution and site saturation mutagenesis, PpADI variants with higher activity at physiological pH and at low arginine concentration of were obtained with improved properties to become a potent anti-tumor drug (see chapter 3 and chapter 4). *In vitro* and *in vivo* test of the improved variants are required to evaluate the anti-tumor effectiveness.

2.3.4 Affibody molecules for cancer prognosis

Affibody molecules represent a new class of affinity proteins that are based on the Z-domain scaffold derived from staphylococcal protein A (95). Among the scaffold proteins, Affibody molecules constitute the smallest non-cysteine-containing protein scaffold. The small size (~ 7 kDa), robust structure, and straightforward production procedures (either by recombinant production in bacteria or by chemical synthesis) make Affibody molecules attractive targeting agents for *in vivo* radionuclide imaging (96) as well as for various biotechnological applications (97, 98). The small size offers a convenient affinity maturation principle. Gene synthesis allows randomizing the whole gene to generate diverse mutant library. The potential use of radiolabeled Affibody molecules for high-contrast radionuclide imaging of biomarkers has been demonstrated in preclinical studies and in pilot clinical studies. Affibody molecules are non-immunoglobulin-derived affinity proteins based on a three-helical bundle protein domain.

Several of affinity proteins have been investigated for both *in vivo* diagnostics and therapy of tumor in radionuclide molecular imaging. Affinity proteins in tumor-targeted therapy can affect tumor progression by altering signal transduction or by delivering a payload of toxin, drug or radionuclide. EGFR (epidermal growth factor receptor), one of the receptor in ErbB family, has been extensively studied as biomarkers in tumor targeting and over expressed in various malignancies, associated with poor patient prognosis and are therefore interesting targets for solid tumors. High affinity and especially slow dissociation rate are important for obtaining high contrast images. Affinity in the low nanomolar range is considered as a prerequisite for successful use of peptide-based tracers.

Ståhl and coworkers (99) described the affinity maturation procedure for the generation of Affibody molecules binding with high affinity and specificity to EGFR. The library for affinity maturation was constructed using a single oligonucleotide for the rerandomization of desired positions. The new binders were selected with phage display technology and the best second-generation binders were characterized *in vitro* using real-time biospecific interaction analysis (BIA) for their binding to recombinant EGFR and with flow cytometry for their binding to native EGFR. Second-generation binders achieved an approximately 30-fold improvement in affinity (K_d = 5-10 nM) for the soluble extracellular domain of EGFR in biospecific interaction analysis using Biacore.

2.3.5 Interferon for anti-tumor applicaiton

Alpha interferons (IFN-as) are members of the diverse helical-bundle superfamily of cytokine genes, which have potent antiviral and antiproliferative activities and therefore can be used as anticancer and antiviral agents. However, doselimiting toxicity, receptor cross-reactivity, and short serum half-lives significantly reduce the clinical use of many of these cytokines.

Patten and coworkers (100) performed a family shuffling experiment with over 20 human interferon-α (Hu-IFN-α) genes. Antiviral assay and proliferation assay

were used to indentify clones with improved activity on Hu-IFN-α receptor. One clone showed 285,000-fold improved activity relative to Hu-IFN-α2a and 185-fold relative to Hu-IFN-α1 (most active native human interferon).

Selective breeding using DNA shuffling has proved to be very effective method to rapidly improve pharmaceutical proteins by which initially have low levels of the desired “activity” (101, 102). Backcrossing of evolved recommbinants with the wild type genes removes functionally neutral changes, which might reduce the immunogenicity of evolved proteins (103).

2.4 Conclusion

Proteins, especially enzymes, have gained a central role in modern chemical, biotechnological, and biopharmaceutical industries. Directed evolution has over the past proved to be a versatile and successful approach for tailoring protein properties to industrial, agricultural and medical demands and for advancing our understanding of structure-function relationships in biocatalysts. Appropriate library generation and screening methods should be employed concerning the target protein and desired property. To set up a sophisticated screening method, complex conditions in human body (pH, ion concentration, proteases, hormones etc.) should be considered. Subsequent *in vivo* or *in vitro* test of improved variants should be carried out to further validate the screening assay. Development of diversity generation and high-throughput screening method will enable evolution to solve problems efficiently. Especially, directed evolution provides a powerful strategy to rapidly advance the development of improved protein-based drugs (enzymes and antibodies, peptide and ligands). Directed evolution promises to play an increasingly important role to generate “desirable” drugs.

Chapter 3. Directed evolution of Arginine deiminase for increased activity at physiological pH

3. 1 Abstract

Arginine deiminase (ADI; EC 3.5.3.6) has been studied as a potential anti-tumor drug for the treatment of arginine-auxotrophic tumors, such as hepatocellular carcinomas (HCCs) and melanomas. Studies with human lymphatic leukemia cell lines confirmed that ADI is a potential anti-angiogenic agent effective in the treatment of leukemia. ADI from *Pseudomonas plecoglossicida* (PpADI) was cloned and expressed in *E.coli*. A main limitation of PpADI lies in its pH-dependent activity profile with a pH optimum at 6.5. A pH shift from 6.5 to 7.5 results in ~80 % activity drop (pH of human plasma is 7.35 to 7.45). For shifting PpADI pH optimum to netrual pH, a directed evolution protocol based on an adapted citrulline screening protocol in microtiter plate (MTP) format was developed and validated. Proof of concept for ADI engineering resulted in a pH optimum of pH 7.0 and increased activity under physiological conditions: at pH 7.4, variant M2 (K5T, D44E and H404R) is 4-fold more active than the wild type PpADI and retains ~30 % of its activity relative to its pH optimum, compared to ~10 % in the case of the wild type PpADI.

3.2 Introduction

Arginine deiminase (ADI) is a potential cancer therapy agent for the treatment of arginine-auxotrophic tumors (e.g. hepatocellular carcinomas and melanomas). The hepatocellular carcinoma (HCC) accounts annually for approximately 1 million new cases worldwide. In the US the incidence rate (per 100,000 persons; 1992-2002) of HCC is 8.6 with a mortality rate of 6.5 due to low responses of hepatoma to chemotherapeutic treatments (27). Current research efforts are

focused on ADI's *in vivo* inhibitory effect towards HCCs, leukemia, melanomas and human umbilical vein endothelial cells (HUVEC) (104-106), clinical trials for HCC (phase III) and melanoma (phase I/II) (105, 107), and PEG formulation of ADI to improve its efficacy as a clinical drug, including serum half-life and antigenicity (16, 108). ADI inhibited the growth of cultured leukemia cells at concentrations of 5-10 ng/ml, which were about 20-100 times lower than those of the L-asparaginase standard resulting in fewer side effects (106, 109). Arginine deprivation is speculated to be the molecular reason for ADI's inhibitory effect on human lymphatic leukemia (106). ADIs catalyze the first step of the arginine deiminase (ADI) pathway by hydrolyzing arginine to citrulline and ammonium. Several ADI genes have been identified, purified, and characterized from bacteria, archaea and some eukaryotes excluding mammalian cells and summarized in a recent review (27). None of these ADIs is from a kinetic point of view ideally suited for *in vivo* applications in humans under physiological conditions.

Protein engineering by rational design and directed evolution offers opportunities to tailor ADI properties to physiological conditions. For the proof of concept, an ADI isolated from *Pseudomonas plecoglossicida* CGMCC2039 (accession number: ABS70718) which can be functionally expressed in *E. coli* has been employed. Directed evolution approaches employ mainly *E. coli* as host due to its fast growth and high transformation efficiency which is a prerequisite for generating complex mutant libraries. Over the last decades, directed protein evolution has become a versatile and successful approach for tailoring protein properties for industrial demands (mainly in chemical synthesis) and for advancing our understanding of structure-function relationships in enzymes. A directed evolution experiment comprises iterative cycles of diversity generation and functional selection for improved variants. Only a few manuscripts for phytases (83), xylanases (110), amylases (77, 82, 111), and an alcohol deyhdrogenase (112) reported a shift of pH optima using directed evolution algorithms. None of these directed evolution campaigns targeted a medical

application and arginine deiminase has to our best knowledge not been altered in its pH activity/resistance by directed evolution.

Comparison of PaADI (*Pseudomonas aeruginosa*, pH optimum 5.6; His405) and MaADI (*Mycoplasma arginini* ADI, pH optimum 6.5, Arg397) led to the speculation that substitution of His by Arg might contribute to MaADI's increased pH optimum (17). A sequence alignment of four ADIs (MaADI, MyADI (*Mycoplasma arthritidis* ADI), PaADI and PpADI) shows that for both Pseudomonas ADIs the synonymous amino acid positions (404 & 405), contain a His whereas both Mycoplasma ADIs contain at corresponding positions an Arg. Interestingly, both Mycoplasma ADIs have an pH optimum approximately one pH unit higher than both Pseudomonas ADIs.

In this study we report the first directed ADI evolution protocol in which the pH profile of PpADI was shifted to higher pH values representing a conceptional proof that ADI properties can be tailored for demands *in vivo* treatment of arginine-auxotrophic tumors. An emphasis is given on detailed description of directed evolution conditions (mutagenic and screening).

3.3 Materials and methods

3.3.1 Materials

All chemicals were of analytical-reagent grade or higher quality and were purchased from Fluka (Neu-Ulm, Germany), Sigma-Aldrich (Steinheim, Germany) and Applichem (Darmstadt, Germany), except the resins for purification (TOSOH, Stuttgart, Germany). All enzymes were purchased from New England Biolabs (Frankfurt, Germany), Fermentas (St. Leon-Rt, Germany), and Sigma-Aldrich Chemie (Taufkirchen, Germany), unless stated otherwise.

Thermal cycler (Mastercyler gradient; Eppendorf, Hamburg, Germany) and thin-wall PCR tubes (Multi-ultra tubes; 0.2 µl; Carl Roth, Germany) were used in all PCRs. The PCR volume was always 50 µl except for Megaprimer PCR of whole

plasmid (MEGAWHOP, 20 µl); larger volumes were prepared in multiple 50-µl PCRs. The amount of DNA in cloning experiments was quantified by using a NanoDrop photometer (NanoDrop Technologies, Germany).

Pseudomonas plecoglossicida CGMCC2039 was provided by Professor Zhihao Sun (Jiangnan University, Wuxi, China).

3.3.2 Methods

3.3.2.1 Reagents used in assays

Acid-ferric solution

To dH_2O (600 ml), concentrated H_3PO_4 (70 ml, 85 %) and concentrated H_2SO_4 (160 ml, 90-91 %) were added slowly. After cooling to room temperature, $FeCl_3 \cdot 6H_2O$ (10 ml, 10 g/L) was added in the above solution, finally the total volume was adjusted to 1 liter with dH_2O.

Diacetyl monoxime -thiosemicarbazide (DAM-TSC) solution

DAM solution (10 g/L) and TSC solution (0.3 g/L) were prepared separately. The two solutions were mixed (volume ratio = 1:1) just prior to use.

3.3.2.2 Cloning of ADI into pET42b(+)

The arginine deiminase (ADI) gene was amplified from *Pseudomonas plecoglossicida* CGMCC2039 by colony PCR (94℃ for 10 min, 1 cycle; 94℃, 30 s/ 54℃, 30 s/ 72℃, 165 s, 29 cycles; 72℃ for 5 min, 1 cycle) using primer (5'-CCGCATTCCGCTGAAAAACAGAAGTACGG-3' and 5'-CTTCTCGAGTTAGTAGTTGATCGGGTCGCGCACG-3'), 1.5 U of Pfu DNA polymerase, 0.20 mM of dNTP mix and a colony of *Pseudomonas plecoglossicida* CGMCC2039. Amplification product was purified by gel extraction, digested using NdeI (20 U) and XhoI (20 U) and purified using QIAquick PCR purification kit (QIAGEN, Hilden, Germany). Cloning vector pET42b(+) was digested with NdeI (20 U) and XhoI (20 U), and purified by gel extraction kit (QIAGEN, Hilden, Germany). Digested ADI gene and pET42b(+)

were ligated using T4 DNA ligase (1 U) to give pET42b(+)-ADI and transformed into *E. coli* BL21-Gold (DE3).

3.3.2.3 Site directed mutagenesis of PpADI gene at position H404

Site directed mutagenesis of ADI gene was performed according to the published method (113) on plasmid pET42b(+)-ADI. The following oligonucleotides were used for mutagenesis of H404R: 5'-GGCCGTGGCGGCGGCCGTTGCATGACCTGCCCG-3' and 5'-CGGGCAGGTCATGCAACGGCCGCCGCCACGGCC-3' (underlining indicated the substituted nucleotide). For the mutagenic PCR (First stage: 95℃ for 30 s, 1 cycle; 95℃, 30 s/ 55℃, 1 min/ 72℃, 130 s, 3 cycles. Second stage: 95℃ for 30 s, 1 cycle; 95℃, 30 s/ 55℃, 1 min/ 72℃, 130 s, 15 cycles; 68℃ for 30 min, 1 cycle), 2 U of Phusion™ Hot Start DNA polymerase (Finnzymes, Keilaranta, Finland), 0.20 mM of dNTP mix, 25 pmol of each primer together with 100 ng of template (pET42b(+) harboring ADI gene) were used. Following the PCR, DpnI (40 U; New England Biolabs) was added, and incubated overnight at 37℃. The PCR products were purified by using a QIAquick PCR Purification Kit (Qiagen) and transformed into *E. coli* BL21-Gold (DE3) for expression.

3.3.2.4 Site sturation mutagenesis of PpADI gene at nine amino acid position

Site saturation mutagenesis of ADI gene was performed according to the published method (113) on plasmid pET42b(+)-ADI. The oligonucleotides were used for mutagenesis were listed in table 1 (underlining indicated the substituted nucleotide). For the mutagenic PCR (First stage: 95℃ for 30 s, 1 cycle; 95℃, 30 s/ 55℃, 1 min/ 72℃, 130 s, 3 cycles. Second stage: 95℃ for 30 s, 1 cycle; 95℃, 30 s/ 55℃, 1 min/ 72℃, 130 s, 15 cycles; 68℃ for 30 min, 1 cycle), 2 U of Phusion™ Hot Start DNA polymerase (Finnzymes, Keilaranta, Finland), 0.20 mM of dNTP mix, 25 pmol of each primer together with 100 ng of template (pET42b(+) harboring ADI gene) were used. Following the PCR, DpnI (40 U; New England Biolabs) was added, and incubated overnight at 37℃. The PCR products were

purified by using a QIAquick PCR Purification Kit (Qiagen) and transformed into *E. coli* BL21-Gold (DE3) for expression.

Table 1. Primer sequences for site saturation mutagenesis.

Primer name	Sequences
Leu 41 FP	AACTGCGACGAGCTGNNNTTCGACGATGTGATC
Leu 41 RP	GATCACATCG TCGAANNNCA GCTCGTCGCAGTT
Asn 360 FP	TGGGATGACGGCAACAACNNNGTGGCGCTGGAG
Asn 360 RP	CTCCAGCGCC ACCACNNNGT TGCCGTCATCCCA
Arg401 FP	GAACTGGGCCGGGGCNNNGGCGGCGGCCACTGC
Arg401 RP	GCAGTGGCCGCCGCCNNNGCCCCGGCCCAGTTC
Phe163 FP	CTGCCCAACACCCAGNNNACCCGCGACACCACC
Phe163 RP	GGTGGTGTCGCGGGTNNNCTGGGTGTTGGGCAG
Asn160 FP	CTGCCGCCGCTGCCCNNNACCCAGTTCACCCGC
Asn160 RP	GCGGGTGAACTGGGTNNNGGGCAGCGGCGGCAG
Arg185 FP	ATGTACTGGCCGGCNNNCGCCAGGAAACCCTG
Arg185 RP	CAGGGTTTCCTGGCGNNNGCCGGCCAGTACAT
Arg243 FP	ATCGGCATGGGTGAGNNNACCTCGCGCCAGGCC
Arg243 RP	GGCCTGGCGCGAGGTNNNCTCACCCATGCCGAT
His405 FP	GGCCGTGGCGGCGGCNNNTGCATGACCTGCCCG
His405 RP	CGGGCAGGTCATGCANNNGCCGCCGCCACGGCC
Gly403 FP	GCCGGGGCCGTGGCNNNGGCCACTGCATGACC
Gly403 RP	GGTCATGCAGTGGCCNNNGCCACGGCCCCGGCC

3.3.2.5 Construction of PpADI error-prone library

The library was generated by the standard error-prone PCR (epPCR) using improved variant H404R as template. For the mutagenic PCR (95℃ for 2 min, 1 cycle; 95℃, 30 s/ 55℃, 30 s/ 72℃, 30 s, 29 cycles; 72℃ for 3 min, 1 cycle), 2.5 U of Taq DNA polymerase, 0.20 mM of dNTP mix, 50 ng of template (pET42b(+) harboring ADI gene H404R), 0.01-0.1 mM of $MnCl_2$ and 10 pmol of each primer (5'-TACATATGTCCGCTGAAAAACAGAAG-3' and 5'- GTGCTCGAGTTAGTAGT TGATCGG-3') were used. The PCR products were purified by using a QIAquick PCR Purification Kit. The purified epPCR products were cloned into expression

plasmid pET42b(+) by MEGAWHOP(114). For MEGAWHOP (68℃ for 5 min, 1 cycle; 95℃ for 5 min, 1 cycle; 95℃, 1 min/ 55℃, 1 min/ 68℃, 13 min 30 s, 24 cycles; 68℃ for 30 min, 1 cycle), 1 U of Taq DNA polymerase, 0.1 U of Pfu DNA polymerase, 0.20 mM of dNTP mix together with 200 ng of template (pET42b(+) harboring ADI gene H404R) were used. Following the PCR, DpnI (40 U; New England Biolabs) was added, and incubated (4 h; 37℃). The MEGAWHOP products were transformed into *E. coli* BL21-Gold (DE3) for expression and screening.

3.3.2.6 Expression of PpADI in LB media with IPTG induction

The strain *E. coli* BL21-Gold (DE3)/ pET42b-PpADI was cultured at 37℃ in 20 ml of LB media that contained 50 μg/ml kanamycine to an absorbance of 0.6 at 578nm. Then, isopropyl β-D-thio-galactopyranoside (IPTG) was added to a final concentration 0.2 mM. The cells were harvested after 9 h induction with IPTG at 37℃. The expressed rADI was analyzed by SDS-PAGE.

3.3.2.7 Expression of PpADI in auto-induction media

A chemically defined auto-induction medium (115) containing salts and trace metals, vitamins including vitamin B12, and glucose, glycerol, and lactose were test for PpADI expression. Five kinds of auto-induction media LS-5052, P-5052, MD-5052, TYM-5052 and TYP-5052 were tested for the ADI expression, under the following conditions: 20 ml LB media in 100 ml flask, 37℃, 250 rpm, 20 h. The expressed rADI was analyzed by SDS-PAGE.

3.3.2.8 Cultivation and expression of PpADI in 96-well plates

Colonies grown on LB_{kan} agar plates were transferred, by using toothpicks, into 96-well microtiter plates (flat bottom, polystyrene plates; Greiner Bio-One GmbH, Frickenhausen, Germany), containing non-inducing medium LSG (150 μL) (115) supplemented with kanamycin (50 μg/ml). After 16 h of cultivation in a microtiter plate shaker (Multitron II, Infors GmbH, Einsbach, Germany; 37℃, 900 rpm, 70 % humidity), each well was replicated using a replicator (EnzyScreen BV, Leiden,

Netherlands) into a second series of 96-well microtiter plates containing 150 µL of auto-induction media LS-5052 (115) supplemented with kanamycin (50 µg/ml). The first set of plates was stored at -80°C after addition of glycerol. The clones in the second set of plates were cultivated for 12 h (Multitron II, Infors GmbH, 37°C, 900 rpm) and used for screening.

3.3.2.9 Screening Procedure

96-well plate format citrulline colorimetric screening assay

A modified protocol of citrulline detection based on carbamido-diacetyl reaction (116) (see Figure 1A for assay mechanism) was used for ADI activity measurement. Screening for increased activity was carried out by measuring the activity at pH 7.4 and 6.4. 20 µl of cell culture was transferred to 96-well microtiter plate. Enzyme reaction was initiated by addition of arginine solution (100 µl, 100 mM) supplemented with cetyltrimethylammoniumbromide (CTAB, 4 mM), and incubated (20 min, 37°C). Subsequently, acid-ferric solution (60 µl) and diacetyl monoxime (DAM, 20 µl, 0.5 M) were added. The reaction mixture was further incubated (15 min, 55°C). Absorbance was measured at 492 nm using a microtiter plate reader (Tecan Sunrise, Tecan Group AG, Zurich, Switzerland).

Standard deviation measurements were performed in 96-well plate format using culture from BL21-Gold (DE3) lacking ADI and in a separate experiment containing ADI. Apparent standard deviation was based on the absolute absorbance values obtained from the ADI wild type plate. The true standard deviation was calculated by subtracting the background absorbance value of the microtiter plate lacking ADI from the apparent values.

Cuvette format citrulline colorimetric assay

ADI activity was routinely measured using a modified protocol of the citrulline detection with DAM and TSC (117) (see Figure 1A for assay mechanism) in Eppendorf tubes. Enzyme reaction was initiated by addition of arginine solution (200 µl, 100 mM) to a 2-ml eppendorf tube containing crude cell lysate (50 µl), and incubated (20 min, 37°C). Subsequently, acid-ferric solution (250 µl) was

added to stop the enzyme reaction. After appropriate dilution with deionized water to ensure the concentration of produced citrulline is within linear detection range, the reaction mixture (400 µl) was mixed with acid-ferric solution (600 µl) and DAM-TSC solution (100 µl). The reaction mixture was further incubated (30 min, 70°C), followed by incubation in ice water to stop color development. Absorbance was measured at 530 nm using a Specord 200 (Analytik Jena AG, Jena, Germany).

Normalization of protein expression for wild type ADI and variants

Agilent Protein 230 Kit (Agilent Protein 230 Kit, Agilent Technologies Deutschland GmbH, Böblingen, Germany) and Agilent 2100 Bioanalyzer (Agilent 2100 Bioanalyzer, Agilent Technologies Deutschland GmbH, Böblingen, Germany) were used for normalization of protein expression in crude cell extract. The protocol used was according to Agilent protein 230 Kit Guide except BSA was used as an internal standard.

3.3.2.10 Expression of ADI in shaking flask and purification

Shaking flasks (1 liter) containing auto induction media LS-5052 (200 ml) supplemented with kanamycin (50 µg/ml) were inoculated with a 1:200 dilution of overnight culture (*E. coli* BL21-Gold(DE3) harboring pET42b-ADI) grown in non-inducing media LSG. After 12 h of expression, *E. coli* cells were harvested by centrifugation (Eppendorf 5810R 4°C, 3220 g, 30 min) and resuspended in phosphate buffer (20 ml, Na_xPO_4, 20 mM, pH 7.0). *E. coli* cells were subsequently lysed by using a high-pressure homogenizer (1500 bar, 2 cycles; Avestin Emulsiflex, Mannheim, Germany). The disrupted cells were centrifuged (Eppendorf 5417R, 4°C, 13000 g, 20 min) and the supernatant was further cleared by filtration through a low protein-binding filter (0.45 µm; Minisart RC 25 single use syringe filter; Sartorius, Hamburg, Germany). ADI wild type and mutants (H404R and K5T D44E H404R) were subsequently purified by a column chromatography procedure: (i) The filtered cell lysates were subjected to a Super-Q anion exchange column, which had been pre-equilibrated with 50 mM

phosphate buffer (Na_xPO_4, pH 7.0). 20 ml of cell lysate was loaded. ADI were eluted by a NaCl step elution in phosphate buffer (Na_xPO_4, 50 mM, pH 7.0) at a rate of 3 ml/min. (ii) The obtained ADI protein from ion exchange chromatography was subjected to a gel filtration column (Matrix: Toyoperl HW-55S, Bed volume: 33 ml, Bed height: 40 cm, Column: Omnifit).

Purified ADI was subsequently concentrated using a Amicon ultra-4 centrifugal filter device (Millipore Corporation, Billerica, U.S.A.) with a 30-kDa cut-off membrane. Total protein concentration was determined by BCA^{TM} assay kit (Pierce, Born, Germany) and homogeneity of the purified sample was controlled by SDS-page electrophoresis using standard molecular biology techniques.

3.3.2.11 Characterization of ADI wild type and mutants

Determination of k_{cat} and K_m of ADI wild type and the mutants

The k_{cat} and K_m values were determined from initial velocity data measured as a function of substrate concentration. Enzyme reaction was carried out at 37°C in a water bath. After 10 min preincubation at 37°C, the enzyme reaction was initiated by addition of purified enzyme (50 µl, 0.2-0.5 µM) to the substrate solution (200 µl, 0.2 mM to 10 mM of arginine, 0.5 M phosphate buffer, pH 7.4) in deep well plates. The reaction mixture was incubated (37°C) and every two minutes reaction mixture (30 µl) of each well was transferred to acid-ferric solution (30 µl) to stop the enzyme reaction. The color development was subsequently performed in 96-well PCR plate. Ferric-acid solution (90 µl) and DAM-TSC solution (15 µl) were added to each well. The 96-well PCR plate was then incubated (70°C, 30 min) in thermal cycler (Eppendorf Mastercyler gradient) for color development, followed by incubation in ice water to stop color development. Absorbance was measured at 530 nm using a microtiter plate reader (SPECTROstar Omega, BMG LABTECH, Offenburg, Germany). The initial velocity data obtained were fitted to the equation $v = V_{max}[S]/([S] + K_m)$ (where v is the initial velocity, V_{max} the maximum velocity, [S] the substrate concentration, and K_m the Michaelis constant) using GraphPad Prism software (GraphPad

software, San Diego, CA, USA). The k_{cat} was calculated from the ratio of V_{max} and enzyme concentration.

Determination of pH profile

Enzyme reaction was carried out at 37°C in a water bath using the following substrate solution: arginine 0.1 M, pH 5-8 phosphate/acetate buffer (0.5 M phosphate, 50 mM acetate). After 10 min preincubation at 37°C, the enzyme reaction was initiated by addition of purified enzyme (50 µl, 0.2-0.5 µM) to the substrate solution (200 µl) in deep well plates. The reaction mixture was incubated (37°C, 10 min) and acid-ferric solution (250 µl) was transferred to each well to stop the enzyme reaction. The color development was subsequently performed in 96-well PCR plate. The reaction mixture (60 µl), ferric-acid solution (90 µl) and DAM-TSC solution (15 µl) were transferred to a 96-well PCR plate. The 96-well PCR plate was then incubated (70°C, 30 min) in thermal cycler (Eppendorf Mastercyler gradient) for color development, followed by incubation in ice water to stop color development. Absorbance was measured at 530 nm using a microtiter plate reader (SPECTROstar Omega, Germany).

3.3.2.12 Molecular Modeling

Two crystal structures of PaADI (PDB codes: 1RXX, 2A9G) were used to model the mutations H405R and D44E. Only one monomeric unit of the tetrameric PaADI was used for the modeling study employing Swiss-PDB viewer (118) (www.expasy.org/spdbv). PaADI variants (H405R; D44E) were generated using the mutate command of Swiss-PDB viewer. The side chain rotamer with the best score was used for subsequent energy optimized with parameter of GROMOS96 force field for in vacuum minimization (119).

3.3.2.13 Stability of PpADI in presence of serum

Purified PpADI (wild type, M1, M2; 20 µl) was incubated (37°C, 60 min) with AB--human serum (80 ul, Invitrogen, Karlsruhe, Germany) and PBS buffer (pH7.4, 80 ul), respectively. Subsequently, the incubated ADI-serum/PBS mix (20 µl) was

added to microtiter plate containing arginine solution (100 µl, 10 mM arginine in PBS buffer, pH 7.4) and incubated (37℃, 30 min). Acid-ferric solution (120 µl) was added to stop the enzyme reaction. The produced citrulline was detected using the assay procedure employed in "Determination of kcat and Km of ADI wild type and the mutants". Before measuring absorbance at 530 nm, centrifugation (Eppendorf, 5810R 4℃, 3000 g, 10 min) was performed to remove the precipitation in the assay solution (likely proteins in serum were precipitated in acidic condition during assay procedure). Meanwhile, a serum control was test for the original citrulline concentration of serum using the same procedure mentioned above except that instead of PpADI, elution buffer of gel filtration (NaxPO4, 50 mM, pH 7.4) was used. All the absorbance values at 530 nm of ADI-serum sample were subtracted the value of serum control to get the citrulline concentration produced by PpADI. The residual activities of PpADI after incubation in serum compared to that in PBS buffer were calculated to show the stability of PpADI after incubated in human serum.

3.3.2.14 Activity of PpADI (wild type, M1, M2) towards arginine derivative dimethylarginine

Purified PpADI (wild type, M1, M2; 15 µl, ~0.2 mg/ml final concentration; >20-fold concentration used for kinetic constant determination) was incubated (37℃, 4 h) with (N^G, N^G)-dimethylarginine solution (20 mM, 100 µl). Acid-ferric solution (120 µl) was added to stop the enzyme reaction. Activity was recorded by citrulline detection using citrulline colorimetric assay (see 3.3.2.11 Characterization of ADI wild type and mutants).

3.4 Results

3.4.1 PpADI cloning

PpADI was cloned into pET42b(+) and expressed in *E.coli* BL21-Gold(DE3) using auto-induction media LS-5052 (see figure 2). The nucleotide sequence of PpADI comprises 1,254 bp nucleotide (figure 1) encoding 417 amino acids which have 85% identity to ADI from *P. aeruginosa* (PaADI). The PpADI cloned into

pET42b(+) was confirmed by nucleotide sequencing. As indicated in Figure 1, sequence analysis of ADI gene showed that there was one synonymous mutation at amino acid position D78 (GAT to GAC) compared to ADI-sequence of *P. plecoglossicida* CGMCC2039 deposited in NCBI (accession number: EU030267). The deduced ADI protein sequence has a calculated molecular weight of 46.5 kDa and shows 85% identity to ADI from *P. aeruginosa*. This clone was used for subsequent directed evolution experiments.

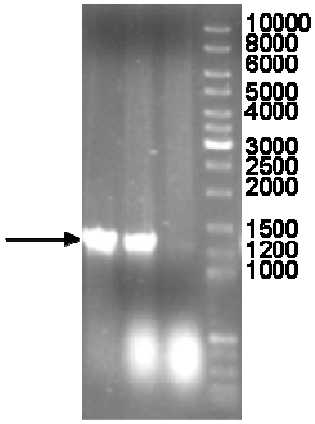

Figure 1. DNA electrophoresis of *PpADI*.

```
1       ATGTCCGCTG AAAAACAGAA GTACGGTGTC CACTCCGAAG CAGGCAAGCT GCGCAAGGTA
61      ATGGTCTGCG CTCCGGGACT GGCGCACAAG CGCCTGACCC CGAGCAACTG CGACGAGCTG
121     CTGTTCGACG ATGTGATCTG GGTCGACCAG GCCAAGCGCG ACCACTTCGA CTTCGTCACC
181     AAGATGCGCG AGCGCGGCGT GGATGTGCTG GAAATGCATA ACCTGCTCAC CGACATCGTG
241     CAGAACCCCG AGGCCCTGAA GTGGATCCTC GACCGCAAGA TCACCCCTGA CACCGTCGGG
301     GTGGGCCTGA CCAACGAAGT GCGCAGCTGG CTGGAGGGCC AGGAGCCACG CCACCTCGCC
361     GAGTTCCTGA TCGGCGGCGT GGCCGGCCAG GACCTGCCGG AGAGCGAAGG TGCCAGCGTG
421     GTCAAGATGT ACAACGACTA CCTGGGCCAC TCCAGCTTCA TCCTGCCGCC GCTGCCCAAC
481     ACCCAGTTCA CCCGCGACAC CACCTGCTGG ATCTACGGCG GCGTGACCCT CAACCCGATG
541     TACTGGCCGG CGCGACGCCA GGAAACCCTG CTGACCACCG CCATCTACAA GTTCCACCCC
601     GAGTTCACCA AGGCCGACTT CCAGGTCTGG TACGGCGACC CGGACCAAGA GCACGGCCAG
661     GCCACCCTCG AAGGCGGCGA CGTCATGCCG ATCGGCAAGG GCATCGTGCT GATCGGCATG
721     GGTGAGCGCA CCTCGCGCCA GGCCATCGGC CAACTGGCAC AGAACCTCTT CGCCAAGGGC
781     GCAGTGGAGC AAGTGATCGT CGCCGGGCTG CCGAAGTCCC GTGCGGCCAT GCACCTGGAC
841     ACCGTGTTCA GCTTCTGCGA CCGCGACCTG GTCACGGTTT TCCCGGAAGT GGTGCGCGAG
901     ATCGTGCCGT TCATCATCCG CCCGGACGAA AGCAAGCCCT ACGGCATGGA CGTACGCCGC
961     GAGAACAAGT CGTTCATCGA GGTGGTCGGC GAGCAGCTGG GCGTCAAGCT GCGTGTGGTC
1021    GAGACCGGCG GCAACAGCTT CGCCGCCGAG CGCGAGCAGT GGGATGACGG CAACAACGTG
1081    GTGGCGCTGG AGCCAGGTGT GGTCATCGGC TACGACCGCA ACACCTACAC CAATACCTTG
1141    CTGCGCAAGG CCGGGATAGA GGTCATCACC ATCAGTGCCG GCGAACTGGG CCGGGGCCGT
1201    GGCGGCGGCC ACTGCATGAC CTGCCCGATC GTGCGCGACC CGATCAACTA CTAA
```

Figure 2. PpADI sequencing results.

3.4.2 PpADI expression in LB media with IPTG as inducer

PpADI was successfully expressed in LB media with IPTG as inducer. Figure 3 (lane 4) shows the expression band of PpADI observed at ~45 kDa, which is similar to the calculated molecular weight of 46 kDa (based on http://expasy.org/tools/pi_tool.html).

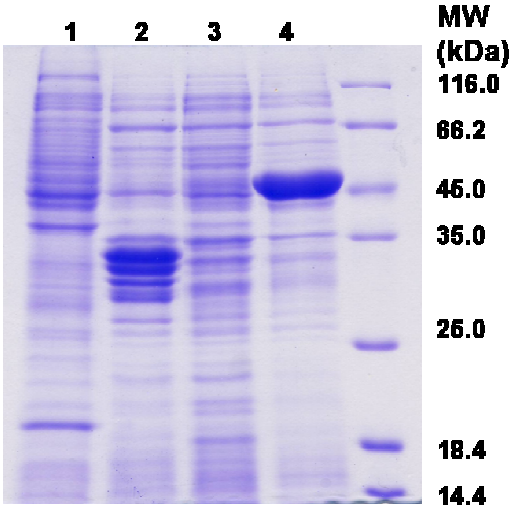

Figure 3. SDS-PAGE of PpADI expression. Lane 1: *P. plecoglossicida*; Lane 2: E. coli BL21-Gold (DE3)/ pET42b; Lane 3: E. coli BL21-Gold (DE3)/ pET42b-PpADI WT, without IPTG; Lane 4: E. coli BL21-Gold (DE3)/ pET42b- PpADI WT.

3.4.3 PpADI expression in auto-induction media

Expressing recombinant protein in auto-induction media is based upon the preferences of bacteria to selectively use different carbon sources during diauxic growth and upon the often-observed negative regulation of gene expression by catabolite repression. Auto-induction is more convenient than IPTG induction because the expression strain is simply inoculated into auto-inducing medium and grown to saturation without the need to follow culture growth and add inducer at the proper time. For high-throughput applications, the auto-induction approach has many advantages over traditional induction methods including avoidance of the strong induction and apparent toxicity associated with chemical inducers such as IPTG.

Five kinds of auto-induction media LS-5052, P-5052, MD-5052, TYM-5052 and TYP-5052 were tested for the ADI expression. Figure 4(A) and 4(B) show ADI

activity and corresponding SDS-PAGE band of the PpADI expression in different auto-induction media. The expression in auto-induction media LS-5052 is shows the highest activity and therefore LS-5052 was used for the following directed evolution experiments.

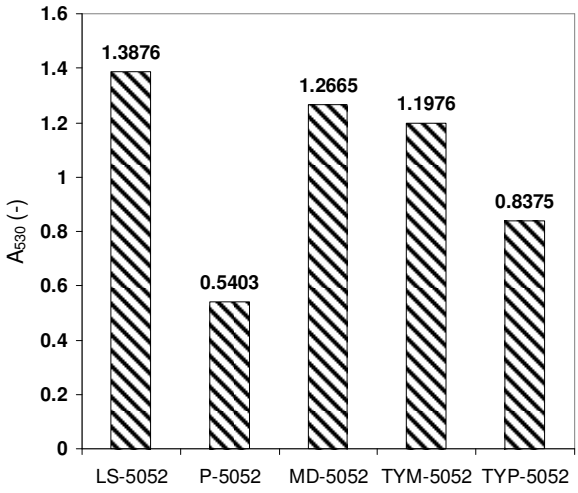

Figure 4(A). Activity of PpADI expressed in auto-induction media.

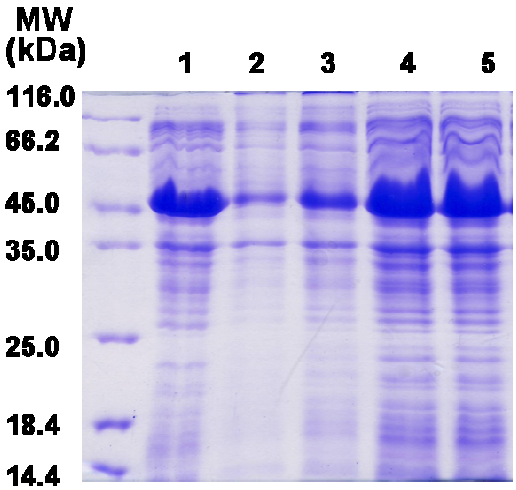

Figure 4(B). SDS-PAGE of ADI expressed in auto-induction media 1, LS-5052; 2, P-5052; 3, MD-5052; 4 TYM-5052; 5, TYP-5052.

3.4.4 PpADI assay based on citrulline detection

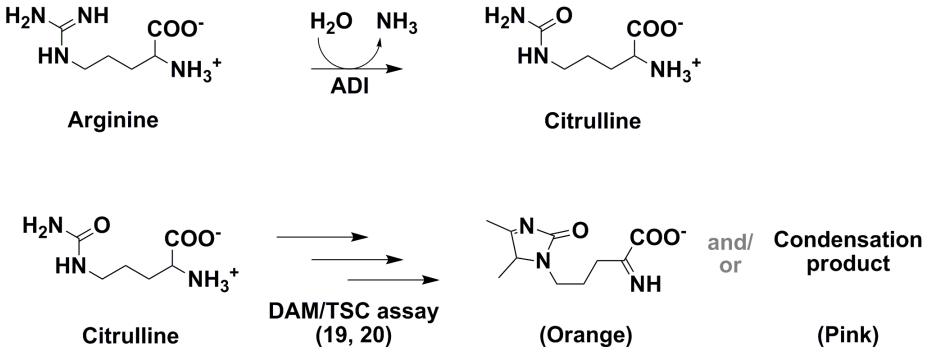

Figure 5. Arginine conversion by ADI and detection of citrulline using DAM/TSC assay.

ADI activity was measured by detecting the production of citrulline from arginine, according to carbamido diacetyl reaction (colorimetric reaction). The conditions of the carbamido diacetyl reaction is as follows： strong acid solution (H_3PO_4, H_2SO_4), oxidizing agent (Fe^{3+}), diacetyl monoxime (DAM), thiosemicarbazide (TSC), and boiling water bath. Figure 5 shows one postulated reaction mechanism for the assay which depicts the reaction between citrulline and DAM. By the addition of TSC to the reaction system, Coulombe and Favreau(120) obtained linearity of response with a more stable pink color which A_{max} was shifted from 490nm to 530nm.

Figure 6 describes the assay procedure for measuring ADI activity in 2 ml eppendorf tube. A calibration curve was prepared using citrulline standard solution (Figure 7) for determining the citrulline production during the assay.

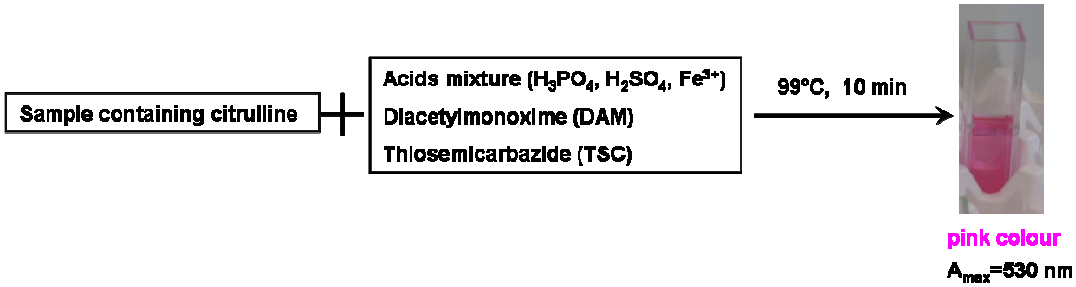

Figure 6. Citrulline colorimetric assay in cuvette format using DAM/TSC assay.

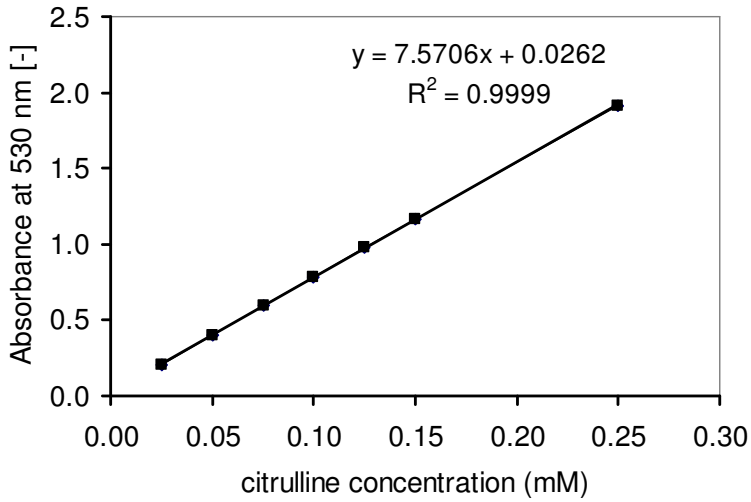

Figure 7. Calibration curve of cuvette format citrulline colorimetric assay.

3.4.5 PpADI screening system for citrulline production in microtiter plates

Two key performance parameters for identifying improved variants in microtiter plate based screening systems are the true standard variation and the linear detection range of the employed assay. Standard deviations have been reduced by optimizing expression and screening conditions (various auto-induction media and assay conditions such as amount of cell, conversion time and color development procedure). A modified version of the DAM-TSC assay for citrulline detection (Scheme 1) was selected for directed evolution of PpADI. The microtiter plate screening format was optimized for simplified handling by lowering the color development temperature (55℃ instead of 100℃), increasing the diacetylmonoxime concentration (~22-fold) and avoiding the use of the sensitizer thiosemicarbazide. Figure 8 shows the procedure of screening assay of citrulline detection.

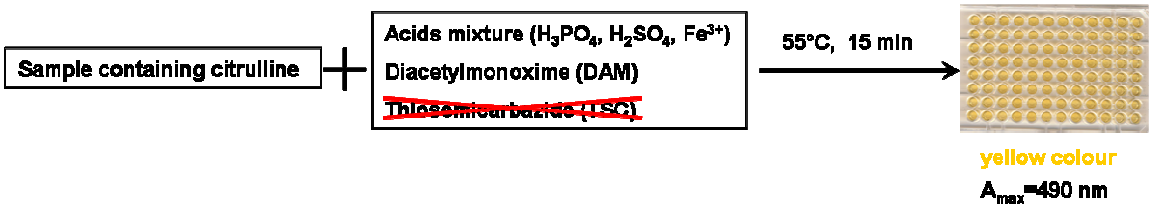

Figure 8. Citrulline colorimetric assay in MTP format using DAM assay.

Standard deviations of the modified citrulline detection assay have been reduced by optimizing expression and screening conditions (various auto-induction media and assay conditions such as amount of cell, conversion time and color development procedure). The preferred combination (150 µl LS5052 auto-induction media and 20 µl cell culture, 20 min conversion time and 15 min color develop time) resulted in a true standard deviation of 12.8 % after subtracting the background (Figure 10). Screening systems with standard deviations around 10 % have successfully been used in directed evolution experiments (121, 122). A wide linear detection window is important for identifying beneficial mutants in directed evolution experiments and screening systems for evolved mutants have to be constantly adapted for hitting the linear detection window. A linear detection range up to 6 mM citrulline could be detected (Figure 9).

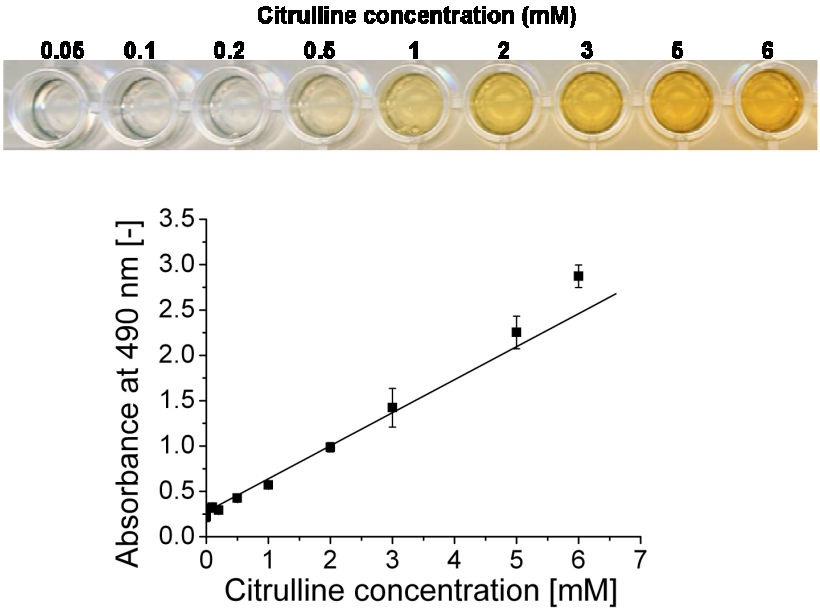

Figure 9. Calibration curve of 96-well microtiter plate format citrulline colorimetric screening assay.

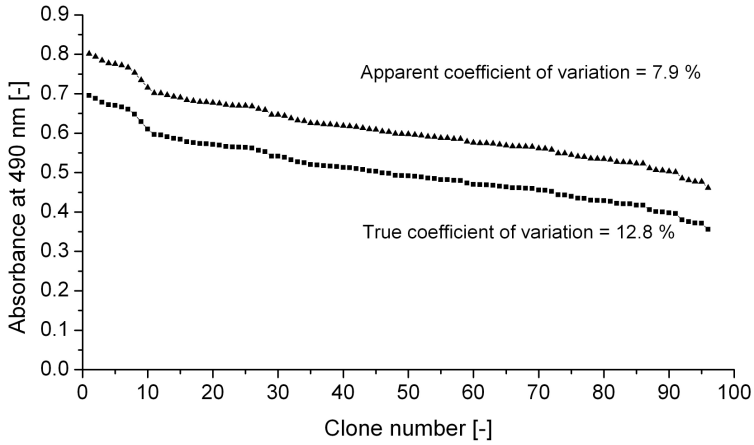

Figure 10. Activity values in descending order of the ADI wild-type conversion of arginine to citrulline in a 96-well microtiter plate using the optimized assay protocol. The apparent coefficients of variation were calculated without subtracting the background and the true coefficients of variation after background subtraction.

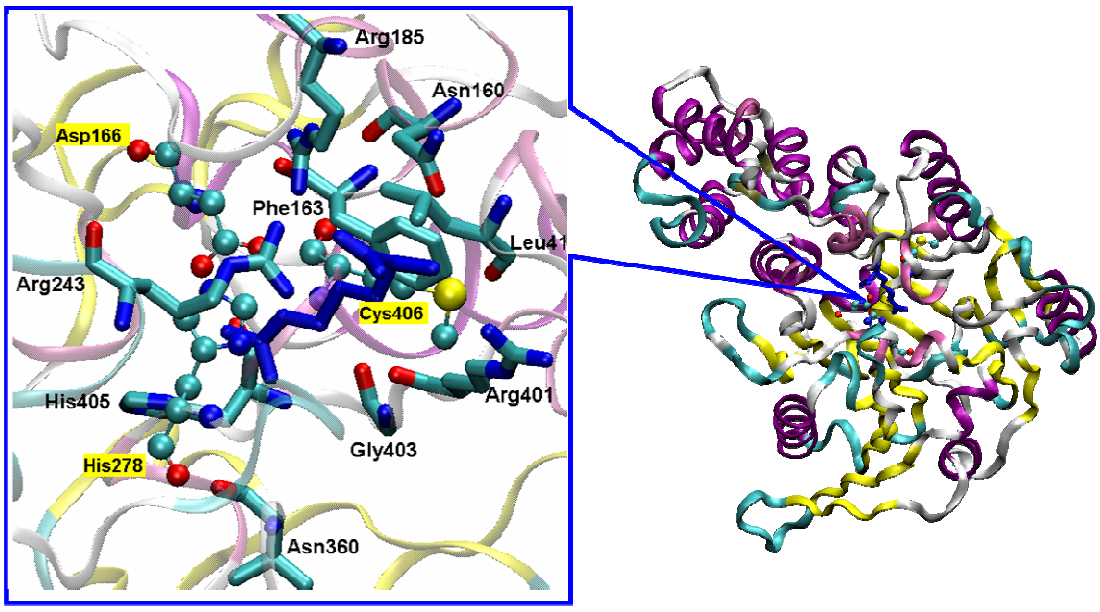

Figure 11. PpADI model derived from PaADI crystal structure (PDB code 2a9gD) by SWISS MODEL WORKSPACE.

3.4.6 Focused libraries generated by saturation mutagenesis

PpADI gene shares 83 % sequence identity with PaADI of which the crystal structure was solved (123). After submitting the ADI sequence to SWISS MODEL WORKSPACE, a proposed ADI model based on the PaADI crystal structure (PDB code 2a9gD) was obtained (Figure 11). According to this model and published literatures, 9 amino acid residues: Leu41, Asn160, Phe163, Arg185, Arg243, Asn360, Arg401, His404, Gly 403 (Figure 11) close to the active center (catalytic triad: Cys406-His278-Glu224) or known to interact with substrate arginine were selected for saturation mutagenesis.

Site saturation mutagenesis at position Leu41, Asn160, Phe163, Arg185, Arg243, Asn360, Arg401, His404 and Gly 403 were performed. 300 clones were screened for each position. However, no improved variant was identified.

3.4.7 Validation of variant M1 (H404R) citrulline colorimetric assay in cuvette format

Position H404 which was suspected to influence ADI pH profile by substitution to R404 (15). Compared to wild type PpADI, variant M1 (H404R) shows higher activity (1.8-fold) and improved activity ratio of pH 7.4 to 6.4 (4.7-fold). Therefore, M1 (H404R) was selected for directed evolution.

3.4.8 epPCR library generation and screening with citrulline detection assay by screening error-prone mutant libraries

Various concentrations of $MnCl_2$ (0.01-0.10 mM) were used in epPCR library generation to adjust the ratio of active to inactive clones. Figure 12 (A) and 12 (B) show the epPCR products and the corresponding MEGAWHOP products. Concentration of 0.01 mM $MnCl_2$ which generated 53 % inactive mutant was selected for library generation. EpPCR mutant libraries with a ratio of 50 % active and 50 % inactive clones have often been used successfully in directed evolution, improving enzyme properties by gradual changes (one or two amino acids changes per round of mutagenesis and screening). A total of 7 variants (listed in

Table 2) were identified from an epPCR library of 2400 mutants and used for further characterization. The most active variant was sequenced and two additional amino acid substitutions (K5T D44E) were identified.

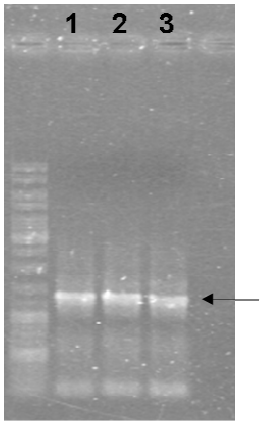

Figure 12 (A). Electrophoresis of epPCR products. Lane 1, 0.01 mM of $MnCl_2$; Lane 2, 0.02 mM of $MnCl_2$; Lane 3, 0.05 mM of $MnCl_2$.

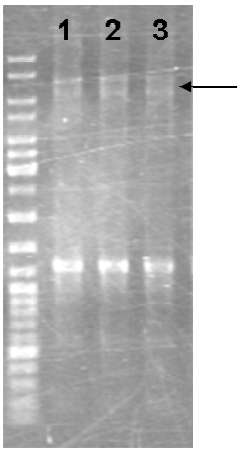

Figure 12 (B). Electrophoresis of MEGAWHOP product with epPCR products as megaprimer. Lane 1, 0.01 mM of $MnCl_2$; Lane 2, 0.02 mM of $MnCl_2$; Lane 3, 0.05 mM of $MnCl_2$.

Table 2. Activity of ADI variants towards arginine determined using citrulline colorimetric assay in cuvette format. Samples were diluted to ensure that detected citrulline concentrations are within the linear detection range of the citrulline colorimetric assay. Wild type, mutant M1 and the "best variant" M2 are in bold and prominent expression mutants (9-B3-1; 21-D5-1) are italized.

	Normalized [ADI][a]				
	Citrulline production (mM/mg)		Relative to activity at pH 7.4 of WT		Activity at pH 7.4/ activity at pH 6.4
ADI variants	pH 7.4	pH 6.4	pH 7.4	pH 6.4	
WT	9.83 (0.74)[b]	124.92 (1.98)	1.00 (0.15)	12.69 (0.01)	0.08 (0.01)
M1 (H404R)	17.80 (0.49)	45.95 (0.87)	1.81 (0.06)	4.67 (0.02)	0.39 (0.02)
M2 (K5T D44E H404R)	38.99 (0.79)	39.20 (0.31)	3.96 (0.02)	3.98 (0.02)	0.99 (0.03)
9-B3-1	24.89 (0.45)	54.50 (1.80)	2.53 (0.03)	5.54 (0.03)	0.46 (0.02)
21-D5-1	25.68 (2.68)	50.95 (2.36)	2.61 (0.07)	5.18 (0.02)	0.50 (0.01)
15-G10-2	13.11 (0.53)	47.02 (0.47)	1.33 (0.09)	4.78 (0.02)	0.28 (0.01)
2-H4-2	12.50 (0.07)	21.58 (0.09)	1.27 (0.06)	2.19 (0.04)	0.58 (0.01)
1-G11-1	24.91 (0.20)	29.12 (0.33)	2.53 (0.03)	2.96 (0.03)	0.85 (0.02)
24-E10-1	14.62 (0.62)	32.82 (0.52)	1.49 (0.08)	3.34 (0.03)	0.45 (0.02)

[a] (Based on quantification employing Agilent 2100 Bioanalyzer (Agilent Protein 230 Kit))
[b] (Standard error of triplicate measurements are given in brackets below each absolute and normalized value.)

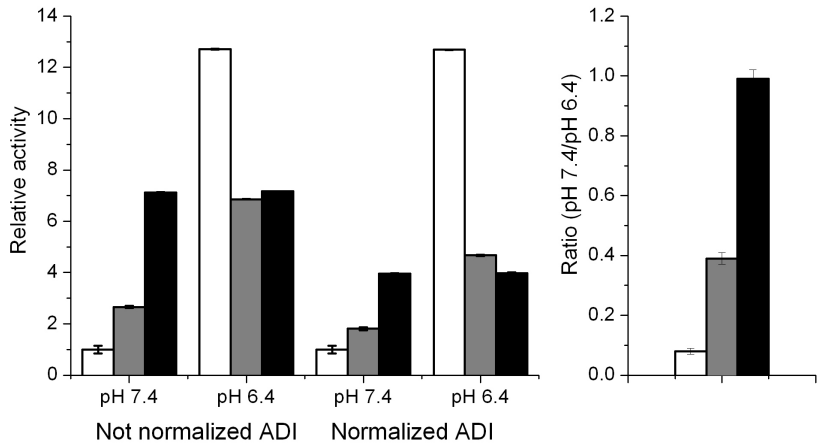

Figure 13. Relative activity of ADI variants towards arginine. The relative activity is the ratio of the activity at the pH of each variant relative to the activity at pH 7.4 of wild type ADI. White: ADI wild type, grey: M1 (H404R), black: M2 (K5T D44E H404R).

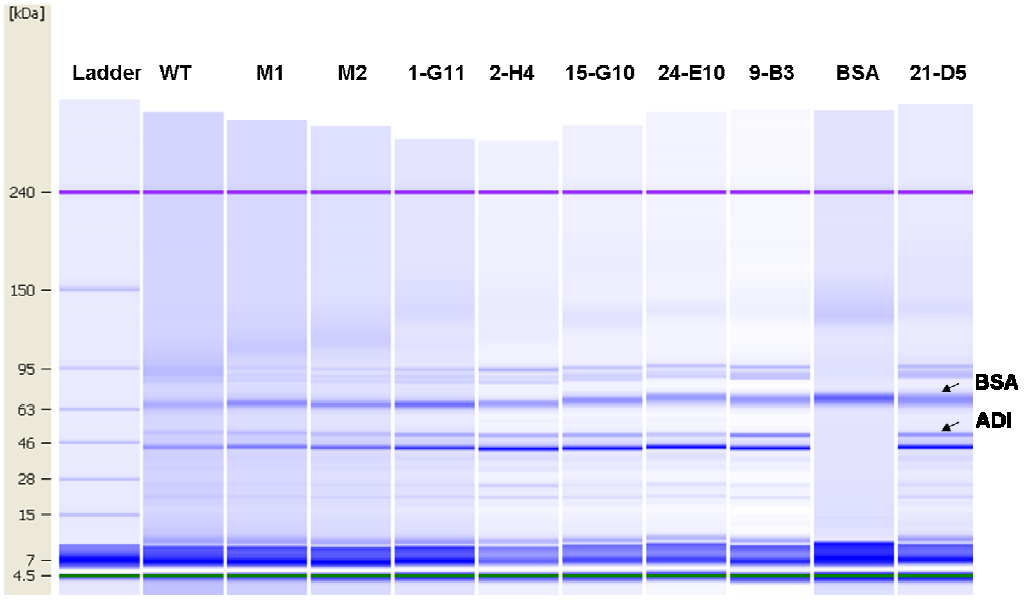

Figure 14. Elution profile of wild type PpADI and improved variants from epPCR library, generated with Protein 230 Kit using a mircofluidic device (Agilent Bioanalyzer). BSA was added as an internal standard.

3.4.9 Characterization of PpADI variants

3.4.9.1 Determination of k_{cat} and K_m of ADI wild type and the mutants

Variants selected from epPCR were first characterized using the crude cell extract to identify the most promising variants (Table 2). Using an activity ratio of pH 7.4 to 6.4 proved to be an effective method to eliminate expression mutants. Additionally ADI concentration in crude cell extract was determined using the Agilent Protein 230 Kit. Microfluidic elution profiles (Figure 14) semi-quantify differences in expression between the wild type PpADI and variants. Normalization of activities against the corresponding ADI concentrations reveals improvements in specific activities of ADI mutants (Table 2). M1, the starting variant for the directed evolution campaign, and M2 were selected for detailed characterization studies. M2 has as “best identified variants” (Figure 13) a more than 2.5-fold higher activity ratio at pH 7.4 to pH 6.4 than M1 and a 12-fold higher activity ratio than wild type in crude cell lysates.

For kinetic characterization of ADI variants the citrulline production was maintained between 0.2-0.8 mM. Calibration curve in Figure 4 shows the linear detection range in the employed 96-well PCR plate format citrulline colorimetric assay system. Figure 15 summarizes the k_{cat} and K_m values of wild type PpADI, identified variants M1 (H404) and M2 (K5T D44E H404R) which were expressed in shaking flasks cultures and purified using a two step procedure (anion exchange followed by gel filtration). Both variants M1 and M2 show an increase in k_{cat} and K_m for citrulline production at pH 7.4. Variant M2 shows a 4-fold higher k_{cat} as also obtained for specific activity in Table 2 using the crude cell extract, validating the characterization procedure with crude cell lysate. Furthermore, an increased K_m from 0.7 mM (wild type PpADI) to 1.2 mM (M1) and 2.5 mM (M2) was found.

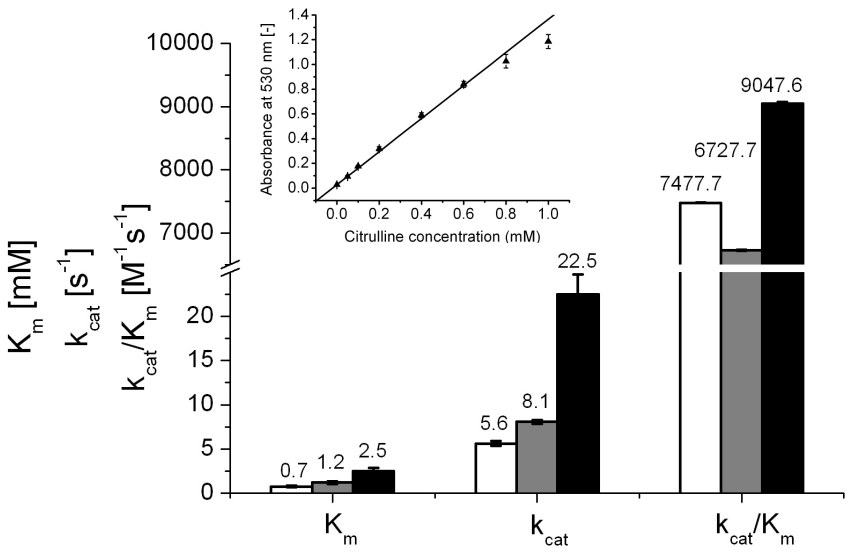

Figure 15. Kinetic parameters of ADI and mutants for conversion of arginine to citrulline. White: ADI wild type, grey: M1 (H404R), black: M2 (K5T D44E H404R). Values reported are the average of three measurements, and average deviations from the mean values are shown. Embedded calibration curve shows linearity of citrulline colorimetric assay in 96-well PCR plate format which was used to determine arginine conversions and kinetic constants.

3.4.9.2 Relative pH profile of wild type and mutant

The relative pH profile (Figure 16) of wild type PpADI and M1 (H404R) shows an identical pH optimum at pH 6.5. Compared to wild type PpADI, variant M2 (K5T

D44E H404R) shows a pH optimum at pH 7.0 which is shifted remarkably (0.5 pH units). Both M1 and M2 show decreased specific activities at pH 6.5, and increased specific activity at pH 7.5. At pH 7.0, the specific activity of M2 exceeds that of wild type PaADI (data not shown).

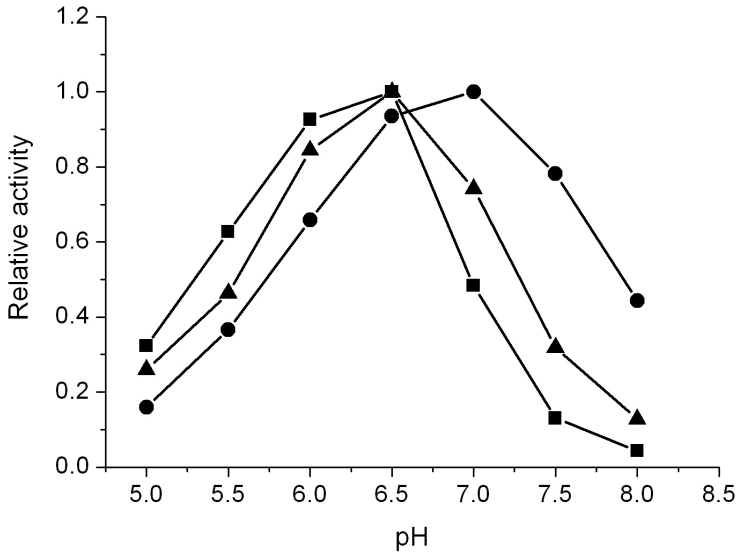

Figure 16. pH profile of wild type ADI, M1(H404R), M2(K5T/D44E/H404R). The relative activity is the ratio of the catalytic activity at the pH relative to the maximum activity of each enzyme. (■) WT, (▲) M1 (H404R), (●) M2 (K5T/D44E/H404R).

3.4.10 Stability of PpADI in the presence of human serum

Table 3 summarizes the stability of PpADI variants in serum (37℃, 60 min; standard deviation of three measurements in brackets). The mutants M1 and M2 have a similar stability in serum when compared to the wild-type PpADI wild type. The substitution D44E and H404R do not destabilize further the PpADI in serum.

Table 3. Stability of PpADI variants in the presence of human serum.

	PpADI WT	M1	M2
No incubation (A_{530})	0.08	0.27	0.98
Incubation with serum (37℃, 60 min) (A_{530})	0.05	0.15	0.69
Residual activity	60 %	55 %	70 %

3.4.11 Activity of PpADI (wild type, M1, M2) towards arginine derivative (N^G, N^G)-dimethylarginine

No detectable conversion of (N^G, N^G)-dimethylarginine could be detected with PpADI variants.

3.5 Discussion

ADI properties have to date not been engineered through directed evolution algorithms despite their often poor performances under physiological conditions and their medical importance as potential anti-tumor drug. Chemically modified of ADI (e.g. through PEGylation) (27) and fusion protein (e. g. Human serum albumin fusion, HSA) (124) have been used for addressing activity and stability demands *in vivo*. Directed evolution offers opportunities to directly improve ADI properties for *in vivo* applications and small libraries of a few thousand variants have often been sufficient to find improved muteins in directed evolution experiments (55, 125).

Our main intention in this report is to provide a validated protocol for directed ADI evolution and improving the activity at the physiological pH 7.4. *Pseudomonas plecoglossicida* CGMCC2039 (PpADI, 7.8 U/mg; pH optimum 6.5) was selected for the directed evolution studies due to its functional expression in *E. coli,* coverage of sequence space in patents and "potential" for activity improvement. PpADI is a relatively slow ADI when compared to Mycoplasma ADIs like MhADI (*Mycoplasma hominus* ADI, 35 U/mg) which would have been good alternatives for directed evolution studies (105). Reported ADI activities range from 0.115 to 140.3 IU/mg. One unit is commonly defined as the ADI amount that converts 1 µmol of L-arginine into 1 µmol of L-citrulline per minute (27).

Screening of PpADI variants yielded three amino acid positions 5, 44 and 404. Positions 44 and 404 resulted in a 4-fold higher k_{cat} at pH 7.4 and a significant shift in the pH optimum (0.5 units) when compared to wild type PpADI (Figure 17 & 8). Position 5 did not show any effect on PpADI activity.

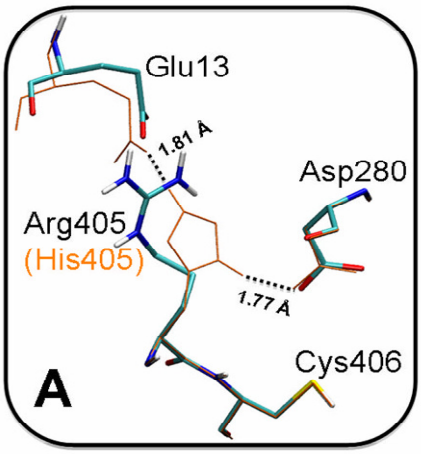

Figure 17. Structural alignment of mutant M1 model with corresponding residues of the crystal structures of the PaADI (in orange). The crystal structure of PaADI which was diffracted in absence of the substrate arginine (1RXX) was used to investigate the substitution of His405 to Arg405. The Arg405 variant shows with respect the Asp280 a different orientation of the guanidinium group when compared to side chain of His405 (in orange).

Galkin and coworkers postulated that the histidine in position 404 (corresponding position in “their” PaADI is 405) is a key residue in controlling activity at acidic and neutral pH. In protonated state of the imidazolium ring a hydrogen bonding interaction can be formed with the oxygen of Asp280 (carboxyl group). This hydrogen bond favors stabilizing interactions between Asp280 and the substrate arginine. His405 in PaADI was reported (17) to share protons with Asp280 and Glu13 and to be important for modulating electrostatic environments of closely located catalytic groups. The same report postulated that H405 is likely to be protonated when the substrate arginine binds to catalytic triad (His278, Glu224, Cys406) [(2)]. Based on these reports the His404 in PpADI was subjected to a site directed mutagenesis to Arg404 and named M1. The M1 variant (H404R) shows 40 % residual activity compared to wild type PpADI at pH 6.4 and a 1.8-fold increase in activity at pH 7.4 (see Table 1). In the M1 (H404R) mutant (see the model in Figure 17; based PaADI 1RXX; residue His404 in PpADI corresponds to His405 in PaADI), the conformational effect due to the extended side chain of Arg likely weakens the hydrogen bond to Asp280 and thus reduces the stabilizing effect on arginine binding. As a result the activity of M1 is reduced, especially at

lower pH values at which His405 is protonated. However at elevated pHs, His405 becomes increasingly deprotonated whereas Arg405 remains protonated and can therefore still stabilize Asp280 for arginine binding. The electrostatic effect suggested by theoretical and experimental studies have evidenced the importance of positively charged residues to modulate the reaction rate of PaADI (126). At pH 6.4, histidine in wild type PpADI and arginine in M1 are both positively charged. At pH 7.4, histidine is only partially positive charged and PpADI's activity is reduced (>90 %) while arginine in M1 remains positively charged preserving M1's activity (Figure 17).

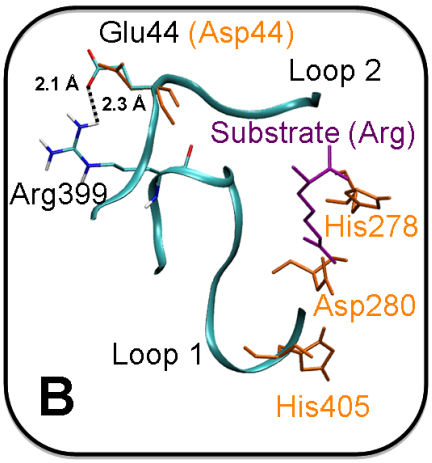

Figure 18. Structural alignment of mutant M2 model with corresponding residues of the crystal structures of the PaADI (in orange). The PaADI crystal structure in presence of substrate arginine was used (2A9G) to investigate the role of the substitution Asp44 to Glu44. The latter was solved for an inactive variant in which Cys406 was replaced by Ala406. The extended side chain of Glu44 might improve the hydrogen bond interaction with the Arg399 inducing a conformational shift of loop 1.

The PpADI H404R was used as starting variant for directed evolution. The amino acid position 44 was identified from a epPCR library (2400 variants screened) resulting in a triple mutant M2 (K5T D44E H404R). For investigating the role of each position the double mutants (K5T H404R) and (D44E H404R) were generated. Only the double mutant (D44E H404R) revealed improvements in k_{cat} (4-fold, pH 7.4; Figure 18). The rationale behind the effects of the mutation D44E on the PpADI activity is more complex to extrapolate from the available ADI crystal structures. Comparative crystallographic studies have shown that the

entrance of the active site is decorated by 4 loops that undergo conformational transitions upon arginine binding (17). The loops exhibit significant shifts that limit the access of water molecules to the active site. The Asp44 is located in loop 1 (residues 30-46) and upon binding of the substrate, Asp44 comes closer to the positively charged Arg399 located on loop 4 (residues 392 to 403). In the D44E mutant, the longer side chain reduces the distance with Arg399 favoring the formation of hydrogen bond (see model in Figure 18). The reinforced interaction between Glu44 and Arg399 might expedite conformational changes in loops, probably confining the arginine substrate in the active site and hence promote arginine conversion. In the future, we plan to further investigate the influence of H404R and D44E using molecular dynamics simulations, further boost the k_{cat} at pH 7.4 and reduce the K_m value of PpADI.

Overall site directed mutagenesis of position H404R and one round of directed evolution (2400 variants screened) resulted in a triple mutant M2 (K5T D44E H404R) with 4-fold higher k_{cat} at pH 7.4 (compared to wild type; Figure 4). The best mutant isolated, M2, has specific activity of 31.3 U/mg at pH 7.4 which is already after one round of evolution close to the specific activity of MhADI (35 U/mg) (127) at its pH optimum. The stability and specificity of improved PpADI variants are furthermore important for cancer treatment *in vivo*. First experiments in AB-human serum (Invitrogen) showed an unaltered stability of M2 compared to the wild type PpADI and (N^G, N^G)-dimethylarginine conversion could not detect with the citrulline colorimetic assay.

3.6 Conclusion

In summary, a directed evolution protocol has been developed for PpADI and validated by increasing the k_{cat} of PpADI at physiological pH (7.4). The reported screening system is the first one employed in directed ADI evolution and can likely be used for other ADIs and other properties such as temperature stability, salt/detergent stability or protease resistance.

Chapter 4. PpADI reengineered for efficient operation under physiological conditions

4.1 Abstract

The proof of concept for ADI engineering by directed evolution resulted in variant M2 (K5T/D44E/H404R). M2 has a pH optimum of pH 7.0 and 4-fold higher k_{cat} value than the wild type PpADI (pH 7.4, 0.5 M phosphate buffer) and an increased K_m value for substrate arginine. In this chapter, in order to improve the catalytic efficiency of PpADI at low concentration of arginine, variant M5 (K5T/D38H/D44E/A128T/H404R) and M6 (K5T/D38H/D44E/A128T/E296K/H404R) were generated from an epPCR library: at pH 7.4 (PBS buffer), the $S_{0.5}$ value decreased from 2.01 mM (parent M3, K5T/D44E/A128T/H404R) to 1.48 mM (M5) and 0.81 mM (M6). The $S_{0.5}$ value of M6 (0.81 mM) is lower than that of PpADI wild type (1.30 mM); the k_{cat} value improved from 0.18 s^{-1} (PpADI wild type) to 17.56 s^{-1} (M5, 97.6-folds) and 11.64 s^{-1} (M6, 64.7-fold).

4.2 Introduction

ADI-based arginine depletion is a target specific therapy for arginine-auxotrophic tumors (e.g. hepatocellular carcinomas and melanomas) and pegylated ADI is currently under clinical trials for HCC with promising results (45). HCC is the third leading cause of cancer mortality world wide with a less than 10 % 5-year survival rate (EU and USA) (128) due to low responses of hepatoma to chemotherapeutic treatments. In 1999, US Food and Drug Administration (FDA) designated ADI-PEG-20 orphan drug status for the treatment of HCC and invasive malignant melanomas, and in 2005 European Agency for the Evaluation of Medicinal Products (EMEA) also granted ADI-PEG-20 orphan drug status for the treatment of HCC. Phase II trials of ADI-PEG-20 in patients with metastatic

hepatocellular carcinomas have shown that the drug is safe, well tolerated, and may benefit patients with unresectable HCC. Izzo and coworker suspected that combination therapies of arginine deprivation and growth inhibition via kinase inhibitors might improve the survival rate further more. Additionally, ADI can enhance radio sensitivity of human mammary adenocarcinoma (MCF-7 cells) (48), exerts anti-proliferative and anti-angiogenic activities and inhibits the growth of viruses such as HIV-1 and hepatitis (49, 50). Current research efforts are focused on ADI's *in vivo* inhibitory effect towards leukemia, melanoma, prostate cancer, renal cell carcinoma, and human umbilical vein endothelial cells (HUVEC) (19, 44, 51-53), clinical trials for HCC (phase II) (45) and melanoma (phase I/II) (46), and inhibitory mechanisms of ADI to tumors (54).

Arginine deprivation is believed to be a main molecular reason for ADI's inhibitory effects on arginine auxotrophic tumors which do not express argininosuccinate synthetase (ASS). ADIs catalyze the first step of the arginine dehydrolase pathway by hydrolyzing arginine to citrulline and ammonium. ADI genes have been identified, purified, and characterized from bacteria, archaea and some eukaryotes excluding mammalian cells (see review (27)). Enzymatic properties of several recombinant ADIs have been examined, such as specific activity, functional expression level, temperature optimum, pH optimum, substrate affinity for arginine, and half-life in human plasma. Only the ADI from *Mycoplasma hominis* has so far been developed as orphan drug by Pheonix Pharmacologics Inc. for HCC and melanoma (129). From enzyme kinetic point of view, none of the ADIs is ideally suited for *in vivo* applications under physiological conditions. Protein engineering by rational design and directed evolution offers opportunities to tailor ADI properties to physiological conditions. PpADI (ADI from *Pseudomonas plecoglossicida*) was functionally expressed in *E. coli* with a simple protocol and has been engineered for the first time by directed evolution for improved activity at physiological pH (3). The variant M2 (K5T/D44E/H404R), by our group reported, showed a 4-fold higher specific activity than the wild type PpADI (0.5 M phosphate buffer, pH 7.4), but a increased K_m value (3.5-fold).

High activity at low arginine concentration is an important prerequisite for ADI's medical application, allowing low ADI dose required per treatment.
In the present work, we improved the directed evolution protocol and identified a PpADI variant with further improved activity and slightly decreased "K_m value" and PpADI variant with lowered K_m value maintaining its high catalytic activity. Those variants were characterized in respect to their kinetic constants.

4.3 Materials and methods

4.3.1 Materials

All chemicals were of analytical-reagent grade or higher quality and were purchased from Fluka (Neu-Ulm, Germany), Sigma-Aldrich (Steinheim, Germany) and Applichem (Darmstadt, Germany), except the resins for purification (TOSOH, Stuttgart, Germany). All enzymes were purchased from New England Biolabs (Frankfurt, Germany), Fermentas (St. Leon-Rt, Germany), and Sigma-Aldrich Chemie (Taufkirchen, Germany), unless stated otherwise.
Thermal cycler (Mastercyler gradient; Eppendorf, Hamburg, Germany) and thin-wall PCR tubes (Multi-ultra tubes; 0.2 µl; Carl Roth, Germany) were used in all PCRs. The PCR volume was always 50 µl except for Megaprimer PCR of whole plasmid (MEGAWHOP, 25 µl); larger volumes were prepared in multiple 50-µl PCRs. The amount of DNA in cloning experiments was quantified by using a NanoDrop photometer (NanoDrop Technologies, Germany).

4.3.2 Methods

4.3.2.1 Site saturation mutagenesis of *PpADI* M2 at position A128

Site directed mutagenesis of *PpADI* M2 (K5T/D44E/H404R) at position A128 was performed according to the published method (130). The following oligonucleotides were used for mutagenesis of A128: 5'-CTGATCGGCGGCGTGNNNGGCCAGGACCTGCCG-3' and 5'-CGGCAGGTCCTGGCCNNNCACGCCGCCGATCAG-3' (underlining indicated the substituted nucleotide). For the mutagenic PCR (First stage: 98°C for 30 s, 1 cycle; 98°C, 30 s/ 55°C, 1 min/ 72°C, 3 min, 3 cycles. Second stage: 98°C for 30

s, 1 cycle; 98℃, 30 s/ 55℃, 1 min/ 72℃, 3 min, 15 cycles; 72℃ for 3 min, 1 cycle), 2 U of PhuS DNA polymerase, 0.20 mM of dNTP mix, 25 pmol of each primer together with 100 ng of template (pET42b(+) harboring PpADI M2 gene) were used. Following the PCR, DpnI (40 U; New England Biolabs) was added, and incubated overnight at 37℃. The PCR products were purified by using a QIAquick PCR Purification Kit (Qiagen) and transformed into *E. coli* BL21-Gold (DE3) for expression.

4.3.2.2 Construction of PpADI error-prone library

EpPCR library was generated by the standard error-prone PCR (epPCR) using improved variant M3 (K5T/D44E/A128T/H404R) as template. For the mutagenic PCR (95℃ for 2 min, 1 cycle; 95℃, 30 s/ 55℃, 30 s/ 72℃, 30 s, 29 cycles; 72℃ for 3 min, 1 cycle), 2.5 U of Taq DNA polymerase, 0.20 mM of dNTP mix, 50 ng of template (pET42b(+) harboring PpADI M3 gene), 0.01-0.1 mM of $MnCl_2$ and 10 pmol of each primer (5'-TACATATGTCCGCTGAAACACAGAAG-3' and 5'-GTGCTCGAGTTAGTAGTTGATCGG-3') were used. The PCR products were purified by using a QIAquick PCR Purification Kit. The purified epPCR products were cloned into expression plasmid pET42b(+) by MEGAWHOP (114). For MEGAWHOP (72℃ for 5 min, 1 cycle; 98℃ for 1 min 30 s, 1 cycle; 98℃, 45 s/ 55℃, 45 s/72℃, 4 min, 24 cycles; 72℃ for 10 min, 1 cycle), 1.2 U of PfuS DNA polymerase, 0.20 mM of dNTP mix, 500 ng of epPCR products together with 50 ng of template (pET42b(+) harboring PpADI gene of variant M3) were used. Following the PCR, DpnI (40 U; New England Biolabs) was added, and incubated (overnight; 37℃). The MEGAWHOP products were transformed into *E. coli* BL21-Gold (DE3) for expression and screening.

4.3.2.3 Site directed mutagenesis at position D38 of *PpADI* M4

Site directed mutagenesis of *PpADI* variant M4 at position D38 was performed according to the published method on plasmid pET42b(+)-ADI-M4 (K5T/D44E/A128T/E296K/H404R). The following oligonucleotides were used for mutagenesis of D38H: 5'-ACCCCGAGCAACTGCCACGAGCTGCTGTTCGAC-3'

and 5'-GTCGAACAGCAGCTCGTGGCAGTTGCTCGGGGT-3' (underlining indicated the substituted nucleotide). Conditions for mutagenic PCR are as described in "Site saturation mutagenesis of *PpADI* M2 at position A128".The PCR products were purified by using a QIAquick PCR Purification Kit (Qiagen) and transformed into *E. coli* BL21-Gold (DE3) for expression.

4.3.2.4 Site saturation mutagenesis at position D38 and E296 of *PpADI* M3

Site saturation mutagenesis library at position D38 and E296 of *PpADI* variant M3 (K5T/D44E/A128T/H404R) were generated according to the published method on plasmid pET42b(+)-ADI-M3 using the following oligonucleotides: D38FP (5'-ACCCCGAGCAACTGCNNNGAGCTGCTGTTCGAC-3'), D38RP (5'-GTCGAACAGCAGCTCNNNGCAGTTGCTCGGGGT-3') and E296FP (5'-GTCACGGTTTTCCCGNNNGTGGTGCGCGAGATC-3'), E296RP (5'-GATCTCGCGCACCACNNNCGGGAAAACCGTGAC-3') (underlining indicated the substituted nucleotide). Conditions for mutagenic PCR are as described in "Site saturation mutagenesis of PpADI M3 gene at position A128".The PCR products were purified by using a QIAquick PCR Purification Kit (Qiagen) and transformed into *E. coli* BL21-Gold (DE3) for expression.

4.3.2.5 Cultivation and expression of PpADI in 96-well plates

Cultivation and expression in 96-well plates (flat bottom, polystyrene plates; Greiner Bio-One GmbH, Frickenhausen, Germany) were performed as previously described in 3.3.2.8.

4.3.2.6 Improved screening system in 96-well plate to identify PpADI variants with high activities at low arginine concentration

As describe previously, the modified protocol of citrulline detection based on carbamido-diacetyl reaction was used for screening for improved ADI affinity to arginine at pH 7.4. 15 µl of cell culture was transferred to 96-well microtiter plate. Enzyme reaction was initiated by addition of arginine solution (105 µl, 1mM arginine in PBS buffer, pH 7.4) supplemented with

cetyltrimethylammoniumbromide (CTAB, 4 mM), and incubated (10 min, 37°C). The following color development procedure was carried out as described previously (3).

Standard deviation measurements were performed in 96-well plate format using culture from BL21-Gold (DE3) lacking PpADI and in a separate experiment containing PpADI variant M3. Apparent standard deviation was based on the absolute absorbance values obtained from the PpADI variant M3 plate. The true standard deviation was calculated by subtracting the background absorbance value of the microtiter plate lacking ADI from the apparent values.

4.3.2.7 Expression of PpADI in shaking flask and purification

Expression of PpADI in shaking flasks and purification (by anion exchange chromatography and gel filtration) was performed as previously described in 3.3.2.10.

4.3.2.8 Characterization of PpADI variants

Preliminary determination of kinetic constants for site saturation mutagenesis variants of position 38 and 296

The k_{cat} and K_m values were determined from initial velocity data measured as a function of substrate concentration. Enzyme reaction was carried out at 37°C in incubator (Heraeus Holding GmbH, Hanau, Germany) using cell crude extract. 2 ml of expression culture was harvested by centrifugation (Eppendorf 5415R 4°C, 13,000 g, 10 min) and then freezed (-20°C, overnight). Cell lysate was prepared by resuspending the cell pellet in lysozyme (91000 U, 50 mM phosphate buffer, pH 7.4, 1.3 ml) followed by incubation (37°C, 40 min) and centrifugation (4°C, 13,000 g, 10 min). 15 µl of diluted (4 times diluted with 50 mM phosphate buffer, pH 7.4) cell lysate was transferred to 96-well microtiter plates. Enzyme reaction was initiated by addition of arginine solution (105 µl, 0.25-10 mM arginine in PBS buffer, pH 7.4) and incubated (7 min, 37°C). Subsequently, ferric-acid solution (120 µl) was added to each well to stop enzyme reaction. 60 µl of terminated

enzyme reaction mixture was transferred to 96-well PCR plate for color development. Ferric-acid solution (90 µl) and DAM-TSC solution (15 µl) were added to each well. The 96-well PCR plate was then incubated (70°C, 30 min) in thermal cycler (Eppendorf Mastercyler gradient) for color development, followed by incubation in ice water to stop color development. Absorbance was measured at 530 nm using a microtiter plate reader (Tecan Sunrise TC reader, Tecan Group AG, Zurich, Switzerland). The initial velocity data obtained were fitted to the equation $v = V_{max}[S]/([S] + K_m)$ (where v is the initial velocity, Vmax the maximum velocity, [S] the substrate concentration, and Km the Michaelis constant) using GraphPad Prism software (GraphPad software, San Diego, CA, USA). The kcat was calculated from the ratio of V_{max} and enzyme concentration.

Determination of kinetic constants of PpADI wild type and variants M3, M4, M5, M6

The k_{cat} and $S_{0.5}$ values were determined from initial velocity data measured as a function of substrate concentration. Enzyme reaction was carried out at 37°C in a water bath as described previously using purified enzyme (50 µl, 0.1-1.8 µM) to and substrate solution (200 µl, 0.5 mM to 10 mM of arginine, PBS buffer, pH 7.4) in deep well plates.

The initial velocity data obtained were fitted to the sigmoidal model of kinetics equation $v = V_{max}^{n}/(S_{0.5}^{n} + K^{n})$ (where v is the initial velocity, V_{max} is the maximum velocity, K is the substrate concentration, and $S_{0.5}$ is the ligand concentration producing half occupation (131)) using GraphPad Prism software (GraphPad software, San Diego, CA, USA). The k_{cat} was calculated from the ratio of V_{max} and enzyme concentration.

4.3.2.9 Native polyacrylamide gel electrophoresis of PpADI variants

10% of polyacrylamide native gels were used for protein electrophoresis to analyze the native form of PpADI variants. Purified protein of PpADI variants (7 µl of protein and 3 µl of loading dye) were loaded into each lane of native gel. The

molecular marker used in the gel is NativeMark™ Unstained Protein Standard (Invitrogen, Darmstadt, Germany). The electrophoresis was performed with tris/glycine buffer (pH 8.3) and electrophoresis chamber was incubated in ice-water bath. Protein bands were stained with Coomassie brilliant blue solution.

4.3.2.10 Homology modeling

Homology modeling approach was used for the structure prediction of PpADI. The model was built by using the automated structure prediction tool, Protein homology/analogy recognition engine (Phyre: http://www.sbg.bio.ic.ac.uk/~phyre/) (132). The crystal structure of PaADI (PDB ID: 2A9G) was used as template by the server and It has 84.9% sequence identity (http://blast.ncbi.nlm.nih.gov/Blast) with PpADI. Procheck program suit (http://www.ebi.ac.uk/thornton-srv/software/PROCHECK/) (133) was used to assess the stereochemical quality of the model. Ramachandran plot which represented that 84.7% residues were present in the most favoured region and 14.7% in additional allowed region (Figure 3). Dfire was used to access non bonded atomic interaction in the model (http://sparks.informatics.iupui.edu/hzhou/dfire.html/) (134), and Qmean (http://swissmodel.expasy.org/qmean/cgi/index.cgi) (135) for the estimation of global protein quality. Swiss-PdbViewer (118) was used to create the tetramer structure by fitting the monomer model on the 4 units of the 2A9G template. The variant M6 (D38H, D44E, A128T, E296K, H404R) were created by using the “mutate” tool of the Swiss-PdbViewer and by selecting rotamers with the best fitness score. All tetramers were energy minimized in vacuum using GROMOS 43B1 force field (119).

4.4 Results

4.4.1 Improved screening system in microtiter plates to identify PpADI variants with high activities at low arginine concentration

Screening assay was based on the validated citrulline colorimetric screening protocol in microtiter plate, as reported previously (3). In order to screen for variants with high activity at low arginine concentration under physiological

condition concerning pH and ion concentrations, 1 mM arginine in PBS buffer (pH 7.4) as substrate solution was employed in screening assay and enzyme reaction time was controlled accordingly (10 min). The coefficient of variation is an important performance criterion of a screening system to determine its accuracy. Optimized assay condition with 1 mM arginine (PBS buffer, pH 7.4) as substrate resulted in true coefficient of variation of 14.9 % (Figure 1). The resulting low absolute absorbance value is a main reason for the high true coefficient of variation (14.9 %). In the previous screening system, 100 mM arginine in 0.5 M sodium phosphate buffer was used and yielded higher activity variants but with higher K_m value.

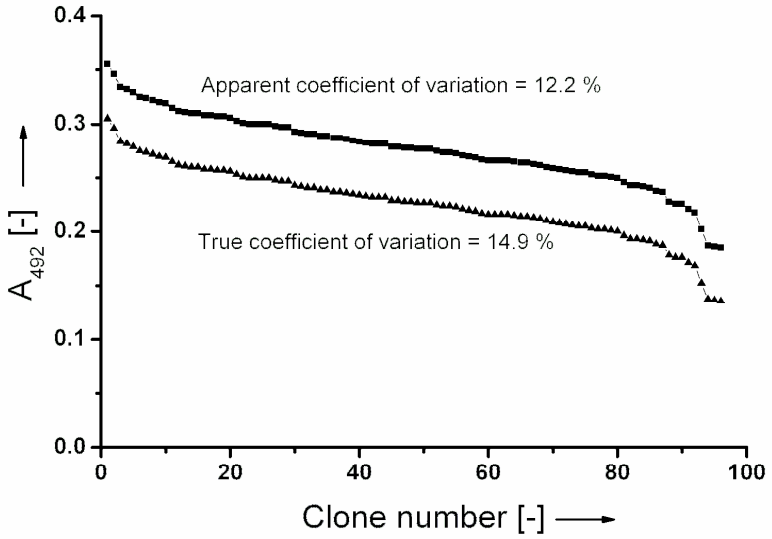

Figure 1. Activity values in descending order of the PpADI variant M3 conversion of arginine to citrulline in a 96-well microtiter plate using the optimized assay protocol. The apparent coefficients of variation were calculated without subtracting the background and the true coefficients of variation after background subtraction.

4.4.2 Genealogic tree of directed PpADI evolution

Figure 2 shows the two rounds of PpADI evolution, generation of saturation mutagenesis libraries and recombination of beneficial positions to finally obtain the PpADI variant M6 with 64.7-fold higher k_{cat} and reduced $S_{0.5}$ (1.3 mM (WT) to 0.81 mM (M6). Based on structure-function analysis of PaADI[16], M1 was generated by substitute His at position 404 with Arg. Position 404 is through

interactions with position Asp280 involved in substrate stabilization during catalysis. M1 was subject to the first round of epPCR library, from which M2 was identified showing a 4-fold improved k_{cat} value and increased K_m value (2.5 mM in 0.5 mM sodium phosphate buffer, pH 7.4)[15]. M3 was generated by a site saturation mutagenesis library at position 128 which increased in another clone the expression level (data not shown). In order to improve PpADI towards medical application demands (high activity at low arginine concentration), a second epPCR mutant library was constructed using M3 as parent. M4 with decreased $S_{0.5}$ value (0.81 mM) and M5 with increased K_{cat} value (17.56 s^{-1}) were identified after screening of ~1400 clones. In M4 the position E296 was identified to be important for lowering $S_{0.5}$ and in M5 position D38 was identified to be important for activity increase. M6 was finally constructed by combining the substations at position D38 and E296. Saturation mutagenesis of these two positions did not yield any further improved $S_{0.5}$ or activity variant.

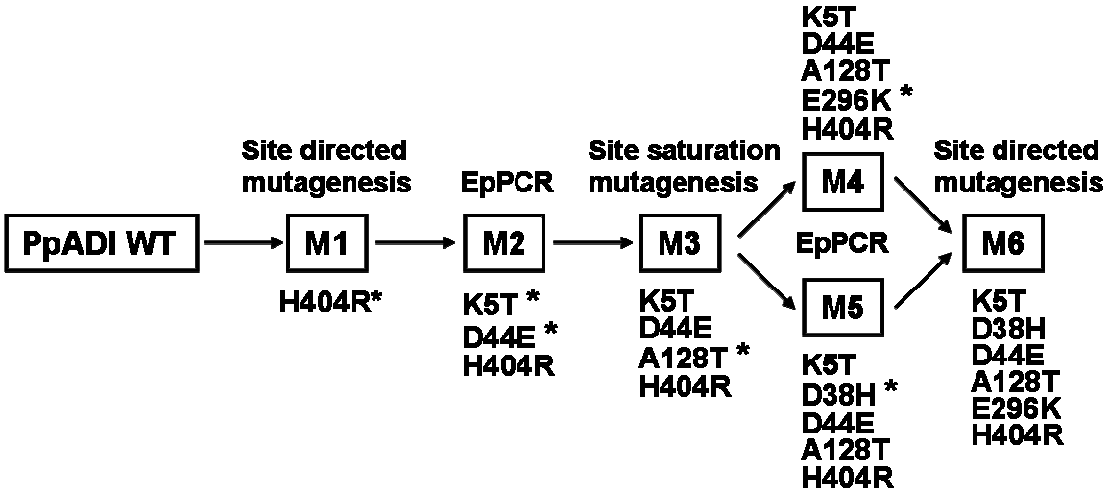

Figure 2. Genealogic tree of PpADI variants (M1 to M6) with generated amino acid substitutions. Novel substitutions are indicated by an asterisk.

4.4.3 EpPCR library construction and screening for variants with high activities at low arginine concentration

Variant M2 was used as a starting template. As described previously, M2 shifts the pH optimum from pH 6.5 to pH 7.0 and has a 4-fold faster k_{cat} than PpADI wild type. In one sequenced mutant, position A128 was identified to be

responsible for higher expression (data not shown). Site saturation mutagenesis on M2 therefore was carried out at position A128. The resulting variant M3 (K5T/D44E/A128T/H404R) showed a ~2-fold improved expression and was subsequently used as parent template for epPCR library.

Three concentrations of $MnCl_2$ (0.01-0.10 mM) were used in epPCR library generation to adjust the ratio of active to inactive clones. Instead of 0.02 mM $MnCl_2$, 0.05 mM $MnCl_2$ which generated 46 % of inactive mutant was selected for library generation. EpPCR mutant libraries with a ratio of ~50 % active and ~50 % inactive clones have often been used successfully in directed evolution, improving enzyme properties by gradual changes (one or two amino acids changes per round of mutagenesis and screening). Two variants M4 and M5 were identified from this epPCR library (~1400 clones) and further characterized. Variant M4 and M5 were sequenced and one additional amino acid substitution was identified for each variant, E296K and D38H, respectively.

4.4.4 Site saturation mutagenesis of *PpADI* at position D38 and E296

To investigate their role in improving of catalytic performance for arginine, site saturation mutagenesis library at position D38 and E296 were generated using PpADI M3 as template. For each position, ~300 clones were screened at low concentration of arginine (1 mM, PBS buffer, pH 7.4), using 96-well plate format citrulline colorimetric screening assay.

After the screening of site saturation mutagenesis libraries of position 38 and 296, variants with higher activity were chosen for preliminary kinetic investigation using crude cell extract. Beneficial mutants were identified and sequenced from both sites (Table 1). At position 38, the following beneficial substitutions were found: D38R (three times, AGA, CGG, CGT) and D38K (twice, AAG, AAA). In all cases, the negatively charged acidic amino Asp had been replaced by positively charged amino acids, Arg or His. Substitution by negatively charged Glu resulted in a clone showing a parent M3-like kinetic behavior. Hydrophobic amino acid

substitution by Pro resulted inactive clone under assay conditions. At position 296, the following substitutions were found to be beneficial: E296K (twice, AAA, AAG), E296N (once, AAC), E296T (once, ACC), E296G (once, GGA). Among these substitutions, variants with substitution to positively charged residue Lys show lowest $S_{0.5}$ value for arginine while substitution by uncharged amino acids (Asn, Thr, Gly) shows relatively marginal improvement compared to E296K. Hydrophobic amino acid substitution by Pro and Trp resulted in very low activity clones.

Table 1. Nucleotide and amino acid substitutions at position 38 in PpADI M3.

PpADI variants	Substitution at position 38	k_m (mM)
M3 (parent)	Asp (GAC)	3.74 ± 0.35
SSM-D38R	Arg (AGA, CGG, CGT)	1.16 ± 0.21
SSM-D38K	Lys (AAG, AAA)	1.01 ± 0.28
SSM-D38E	Glu (GAG)	2.95 ± 0.77
SSM-D38P	Pro (CCA)	n. d.
SSM-D38T	Thr (ACC)	n. d.
M5	His (CAC)	1.26 ± 0.12

Kinetic experiments were performed with crude cell extracts.

Table 2. Nucleotide and amino acid substitutions at position 296 in PpADI M3.

PpADI variants	Substitution at position 296	k_m (mM)
M3 (parent)	Glu (GAA)	3.74 ± 0.35
SSM-E296K	Lys (AAA, AAG)	0.20 ± 0.01
SSM-E296N	Asn (AAC)	0.53 ± 0.04
SSM-E296T	Thr (ACC)	0.61 ± 0.04
SSM-E296Q	Gln (CAA)	0.79 ± 0.06
SSM-E296G	Gly (GGA)	1.29 ± 0.12
SSM-E296W	Trp (TGG)	n. d.
SSM-E296P	Pro (CCT)	n. d.
M4	Lys (AAA)	0.27 ± 0.02

Kinetic experiments were performed with crude cell extracts.
* n. d. activity not detectable under assay conditions.

4.4.5 Determination of kinetic constants (k_{cat} and $S_{0.5}$) of PpADI wild type and variants M3, M4, M5 and M6

Table 3. Kinetic constants of wild type PpADI and variants.

	Wild type	M3 (parent)	M4	M5	M6
k_{cat} (s^{-1})	0.18 ± 0.05	10.13 ± 0.36	5.88 ± 0.09	17.56 ± 1.15	11.64 ± 0.50
$S_{0.5}$ (mM)	1.30 ± 0.25	2.01 ± 0.19	0.81 ± 0.03	1.48 ± 0.17	0.81 ± 0.09

* Kinetic contants of PpADI wild type is different from our previous report because in stead of 0.5 M phosphate buffer, PBS buffer was used for kinetic measurements. K_{cat} value of PpADI wild type dropped from 5.6 s^{-1} to 0.18 s^{-1} and k_{cat} value of M2 is reduced ~2-fold.

M3, the parent of the second round of PpADI epPCR library, M4 with decreased $S_{0.5}$, M5 with increased k_{cat} and best variant M6 with best combination of k_{cat} value and $S_{0.5}$ were selected for detailed characterization studies.

Kinetic characterization of PpADI variants was performed using PBS buffer (pH 7.4), which is commonly used in biological research. PBS buffer helps to maintain a constant pH and its osmolarity and ion concentrations usually match those of the human body. Citrulline production of PpADI variants was maintained between 0.2-0.8 mM. Table 3 summarizes the k_{cat} and $S_{0.5}$ values of parent M3 (K5T/D44E/A128T/H404R), variants M4 (K5T/D44E/A128T/E296K/H404R), M5 (K5T/D44E/A128T/D38H/H404R) and M6 (K5T/D38H/D44E/A128T/E296K/H404R), which were expressed in shaking flasks cultures and purified using a two step procedure (anion exchange follows by gel filtration). Compared to parent M3 ($S_{0.5}$ = 2.01 mM), both variants M4 and M5 have a lower $S_{0.5}$ for arginine conversion at pH 7.4, 0.81 mM and 1.48 mM, respectively. Variant M4 shows a decreased k_{cat} value, 58% of parent M3 while M5 shows a 1.7-fold higher k_{cat} compared to parent M3. Variant M6 with combined mutations (K5T/D38H/D44E/A128T/E296K/H404R) shows decreased $S_{0.5}$ value, 40 % of parent M3 (K5T/D44E/A128T/H404R), 62 % of PpADI wild type, and a 64.7-fold faster k_{cat} value than PpADI wild type. M6 is 42.3-fold faster than PpADI wild type with 0.4 mM arginine (PBS buffer, pH 7.4) as substrate.

After two rounds of epPCR libraries coupled with site directed mutagenesis, a variant M6 with 64.7-fold higher k_{cat} and lower $S_{0.5}$ value (0.81 mM) than PpADI wild type (0.31 mM). At low concentration of arginine, activity of M6 enhanced dramatically than M3 and wild type. For example, M6 is 42.3-fold faster than PpADI wild type in 0.4 mM arginine (PBS buffer, pH 7.4).

4.4.6 Native polyacrylamide gel electrophoresis of PpADI variants

Multimeric form of PpADI variants were investigated by native polyacrylamide gel electrophoresis. As shown in Figure 3, two distinct protein bands representing two multimeric forms tetramer and dimer (molecular weight of a subunit is ~ 46 kDa) were observed, but with different concentration percentage. The major multimeric form of M3 is dimer. Compared to M3, M4 with an additional mutation E296K shows a very different pattern: tetramer is the main form; while M5 with an additional mutation D38H contains more or less equal amount of dimer and tetramer. M6, with both mutations E296K and D38H, contains more tetramer than dimer.

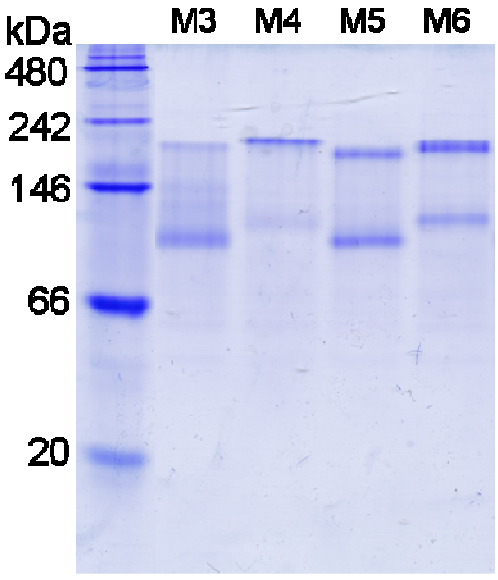

Figure 3. Native polyacrylamide gel electrophoresis of PpADI variants (M3 to M6) with different dimer/tetramer distribution. Single subunit has a molecular weight of ~46 kDa.

4.5 Discussion

Directed evolution allows improving all properties that can be reflected in a screening system through iterative rounds of diversity generation and screening. Small libraries of a few thousand variants are often sufficient to find improved variants [18] even without rational understanding of the targeted property. After establishing a first directed ADI evolution protocol yielding mutant M2, we adjusted the screening system to better reflect ADI's application conditions. Prerequisite for ADI to become an effective anti-tumor agent is that low concentrations of arginine in human plasma can effectively be converted.

Figure 2 shows the genealogic tree of PpADI evolution and before discussing the influence of each substitution individually the effect on kinetics are briefly summarized. Amino acid substitution D44E (M2) increases k_{cat} and $S_{0.5}$, substitution A128T (M3) increases the expression level, and substitution E296K (M4) decreases k_{cat} and $S_{0.5}$ and is responsible for tetramer formation. Substitution D38H (M5) increase largely k_{cat} and reduces slightly $S_{0.5}$. The combination of all mentioned residues in M6 result in a finally 64.7-fold improved PpADI activity and reduced $S_{0.5}$ (1.30 to 0.81 mM).

PpADI M3 was obtained from site saturation mutagenesis library at position A128 using M2 as template (Figure 2). M3 shows improved functional expression level of ADI (data not shown) and was used as parent for generating an epPCR library. Screening of epPCR library yielded two improved variants M4 and M5, carrying an additional mutation, E296K (M4) and D38H (M5). M4 has a decreased $S_{0.5}$ (0.81 mM) and a decreased k_{cat} value (5.88 s^{-1}; see Table 3). M5 has a decreased $S_{0.5}$ (1.48 mM) and an increased k_{cat} value (17.56 s^{-1}) when compared to parent M3 ($S_{0.5}$, 2.01 mM; k_{cat}, 10.03 s^{-1}; see Table 3). M6 which harbors both substitutions (E296K and D38H) has a decreased $S_{0.5}$ value (0.81 mM) compared to the parent M3 (1.30 mM) and the wild type (2.01 mM), and a 64.7-fold higher k_{cat} value than the PpADI wild type.

Despite further enhancing the activity of PpADI, it is crucial for an efficient conversion of the substrate arginine in human plasma (100-120 µM arginine) to reduce PpADI's "K_m" ($S_{0.5}$) value. Figure 4 shows the kinetics of PpADI WT, parent M3, and the variants M4, M5 and M6. M3 has a significantly higher k_{cat} value compared to WT, but its activity at low concentration of arginine (<1.0 mM) is very low ($S_{0.5}$ value 2.01 mM). In contrast, the most efficient variant M6 with a decreased $S_{0.5}$ value (0.81 mM) shows a remarkable activity improvement at low concentrations of arginine (<0.5 mM; see Figure 4). M6 has additional two amino acid substitutions (D38H and E296K) compared to M3 which increases k_{cat} and reduces the $S_{0.5}$ value. The combination of D38H and E296K improves especially the activity of M6 at low arginine concentrations (< 0.5 mM; see Figure 4).

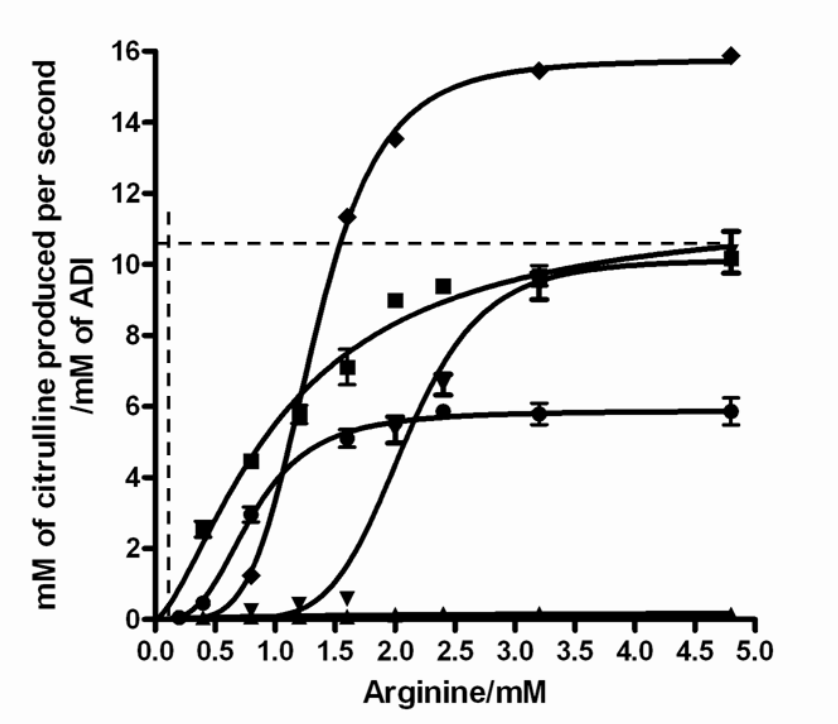

Figure 4. Kinetic curve of PpADI wild type, M3, M5 and M6. (▲) PpADI wild type, (▼) M3, (●) M4, (♦) M5 and (■) M6.

Figure 5 shows the tetrameric model (based on PaADI, PDB code 2A9G) of PpADI WT (Figure 5A) and variant M6 (Figure 5B). Monomeric units are

indicated with the letters a, b, c and d. The access channel to the active sites of each monomer is highlighted in square and faces an internal cavity generated by the assembly of four PpADI monomers. The substitutions D38H (in blue) and D44E (in green) are localized at the interface of monomer pair a-b and c-d. The substitution of Glu by Asp at position 44 provides a longer side chain in close proximity of the also negatively charged residue Asp43 (Figure 6A). The substitution E296K is localized at the border of the entrance to the internal cavity of the PpADI tetramer. E296K promotes the tetramer formation likely by introducing stabilizing interactions with other residues, for example with Thr33 (hydrogen bond). E296K inverts the charge at this position and its increased length of the side chain might promote further interactions to a neighboring monomer (Figure 6A). The combination of D44E and E296K results in a population consisting of mainly tetramers (see Figure 3; mutein M4). Interestingly with the formation of a tetramer (M4) the $S_{0.5}$ value is reduced which indicates that the tetramer complex formation promotes interactions with the substrate arginine at low concentrations. The substitution D38H together with the E296K in the mutein M6 reestablishes an almost equal population of PpADI dimers and tetramers. A hypothesis is that Lys of the E296K has an electrostatic stabilizing interaction with the Glu38 in the M4 but not to the neutral His38.

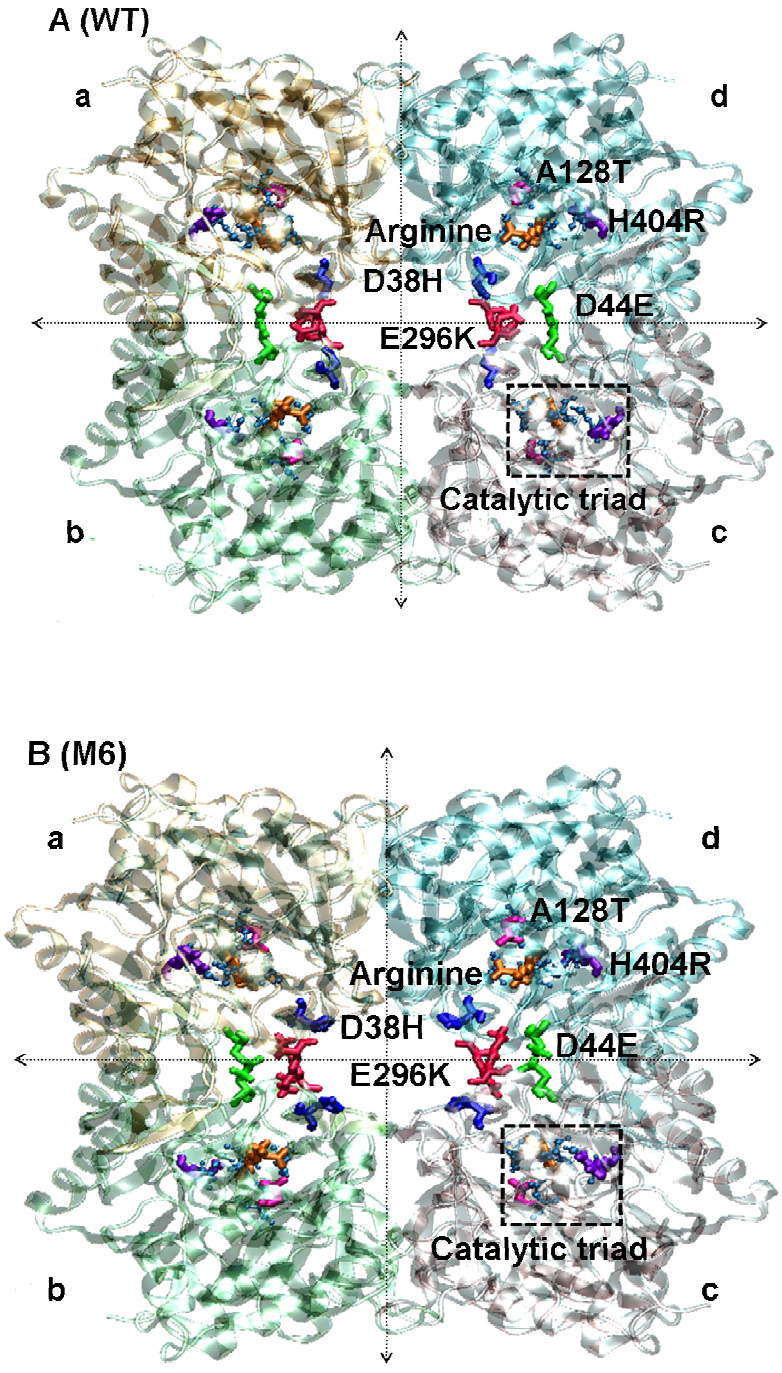

Figure 5. A). The model of WT tetramer after energy minimization in vacuum (GROMOS 43B1). B). The model of M6 tetramer after energy minimization in vacuum (GROMOS 43B1). Active site residues are represented in CRK format in a square (Blue). Mutated residues are shown in licorice format in different colors like D38H (blue), D44E (green), A128T (magenta), E296K (red) and H404R (violet). Substrate arginine is represented in orange color by licorice format.

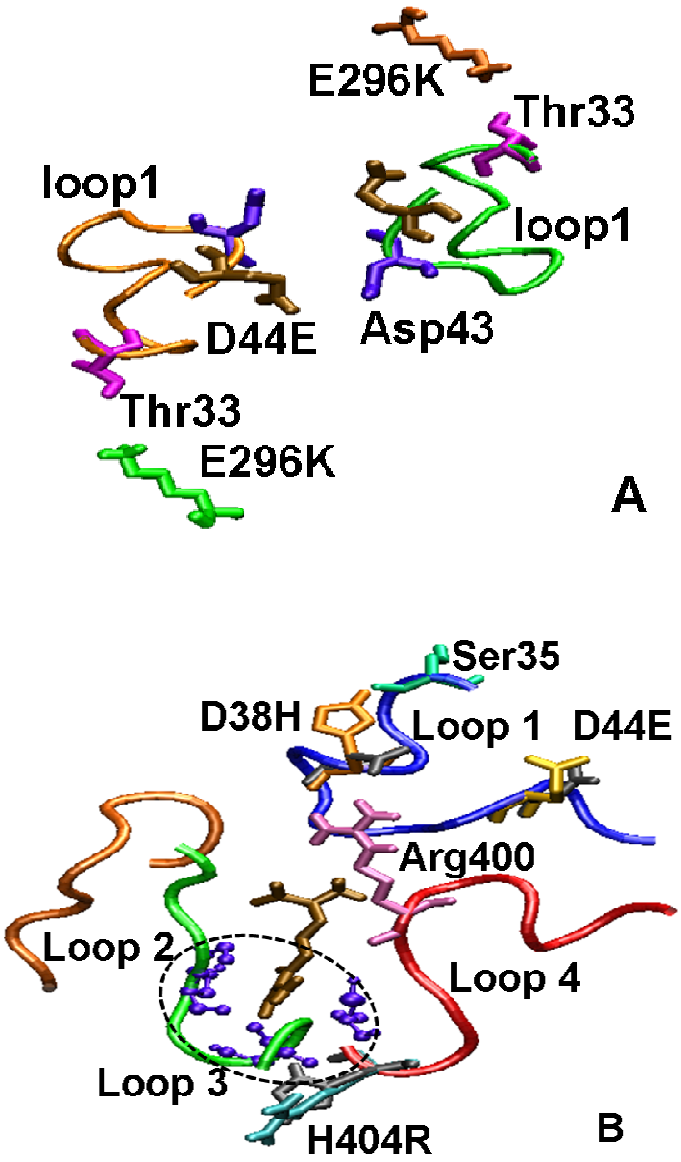

Figure 6. A). Structure model of variant M6. E296K is involved in intermonomer interaction (between chain a (orange) and b (green)) with Thr33. D44E is involved in intermonomer interaction, between chain A (orange) and B (green), with Asp43 (violet). B). Structure alignment of PpADI WT model and M6 model with four loops (loop 1:30-46, loop 2:178-175, loop 3:271-281 and loop 4: 393-404) surrounding the entrance of the active site. The substitutions in these loops and the residues involved in the interaction with those substitutions are representing: D38H (orange), D44E (yellow) and H404R (cyan, in M6; gray, in WT), Ser35 (green), Arg 400 (pink), substrate arginine (ochre), catalytic triad His278, Asp280 and Cys406 (violet, highlighted in an oval)

Figure 6B shows that the active site of the PaADI is surrounded by four loops (loop 1: 30-46, loop 2: 178-185, loop 3: 271-281, and loop 4: 393-404). These four loops undergo a conformational transition upon arginine binding and tighten

the surrounding of the arginine substrate[16]. D38 is located in loop 1 and faces towards the substrate access channel. In PpADI model (Figure 6B), the D38H mutation promotes the formation of a hydrogen bond interaction with the neighboring residues Ser35, contributing to the stability of the entropically unfavorable folded conformation of loop1. The rigidified loop 1 might be beneficial for arginine conversion. According to PaADI structure analysis, the side chain of gating residue Arg401 (Arg400 in PpADI) is located at the active site entrance and fills the substrate-binding site. The structure analysis of the C406A PaADI-L-arginine complex[16] shows that the Arg401 side chain (Arg400 in PpADI) is displaced by the substrate arginine to a position near the active site entrance that allows its hydrocarbon chain to assist shielding the catalytic site from solvent. D38 is involved in an ionic interaction and hydrogen bonding with Arg400. The substitution of Asp to His at position 38 results in a loss of ionic interactions to Arg400 due to the different lengths of the side chains. His38 can form only a hydrogen bond with active site gating residue Arg400. A weakened interaction between position 38 and Arg400 might increase the flexibility of the side chain of Arg400 which then might block less efficiently the access of arginine to the active site. As a result the variant M5 shows an improved k_{cat} value (1.7-fold compared to parent M3) due to the substitution D38H.

For elucidating further the individual role of the five identified amino acid substitutions and their influence on the active site geometry and tetramer formation crystal structures of variant M4 and M6 have to be solved.

4.6 Conclusion

In summary, with the modified screening protocol, PpADI variants with improved k_{cat} and $S_{0.5}$ were identified. The increased k_{cat} value and decreased $S_{0.5}$ value result in significant activity improvement of PpADI at low arginine concentrations. Especially the kinetic constants of PpADI variant M6 demonstrate that PpADI properties can be tailored by directed evolution. The generated PpADI variants match from their kinetic behavior therapeutic application demands much better

than the wild type PpADI. We therefore hope that by directed evolution improved PpADIs will further be investigated *in vivo* for tumor therapy.

References

1. Li L, Li ZM, Chen DQ*, et al.* Inactivation of microbial arginine deiminases by L-canavanine. Journal of the American Chemical Society, 2008; 130(6): 1918-31.

2. Lu XF, Li L, Wu R*, et al.* Kinetic analysis of *Pseudomonas aeruginosa* arginine deiminase mutants and alternate substrates provides insight into structural determinants of function. Biochemistry, 2006; 45(4): 1162-72.

3. Zhu LL, Tee KL, Roccatano D*, et al.* Directed evolution of an antitumor drug (arginine deiminase PpADI) for increased activity at physiological pH. Chembiochem, 2010; 11(5): 691-7.

4. Das K, Butler GH, Kwiatkowski V, Clark AD, Yadav P, Arnold E. Crystal structures of arginine deiminase with covalent reaction intermediates: Implications for catalytic mechanism. Structure, 2004; 12(4): 657-67.

5. Schofield PJ, Edwards MR, Matthews J, Wilson JR. The pathway of arginine catabolism in *Giardia intestinalis*. Molecular and Biochemical Parasitology, 1992; 51(1): 29-36.

6. Linstead D, Cranshaw MA. The pathway of arginine catabolism in the parasitic flagellate *Trichomonas vaginalis*. Molecular and Biochemical Parasitology, 1983; 8(3): 241-52.

7. Yarlett N, Lindmark DG, Goldberg B, Moharrami MA, Bacchi CJ. Subcellular localization of the enzymes of the arginine dihydrolase pathway in Trichomonas vaginalis and Tritrichomonas foetus. J Eukaryot Microbiol, 1994; 41(6): 554-9.

8. Biagini GA, Yarlett N, Ball GE*, et al.* Bacterial-like energy metabolism in the amitochondriate protozoon Hexamita inflata. Mol Biochem Parasitol, 2003; 128(1): 11-9.

9. Makhlin J, Kofman T, Borovok I*, et al.* Staphylococcus aureus ArcR controls expression of the arginine deiminase operon. Journal of Bacteriology, 2007; 189(16): 5976-86.

10. Seggewiss J, Becker K, Kotte O*, et al.* Reporter metabolite analysis of transcriptional profiles of a Staphylococcus aureus strain with normal phenotype

and its isogenic hemB mutant displaying the small-colony-variant phenotype. Journal of Bacteriology, 2006; 188(22): 7765-77.

11. Altucci P, Sapio V, Vitale P, de Vargas F. Mycoplasma in human pathology. Current status of the problem, with special reference to respiratory pathology. Recenti Prog Med, 1966; 41(5): 409-55.

12. Harasawa R, Koshimizu K, Kitagawa M, Asada K, Kato I. Nucleotide sequence of the arginine deiminase gene of *Mycoplasma hominis*. Microbiology and Immunology, 1992; 36(6): 661-5.

13. Takaku H, Matsumoto M, Misawa S, Miyazaki K. Antitumor activity of arginine deiminase from *Mycoplasma arginini* and its growth inhibitory mechanism. Japanese Journal of Cancer Research, 1995; 86(9): 840-6.

14. Fenske JD, Kenny GE. Role of arginine deiminase in growth of *Mycoplasma hominis*. Journal of Bacteriology, 1976; 126(1): 501-10.

15. Wei YZ, Zhou H, Sun Y, He YB, Luo YZ. Insight into the catalytic mechanism of arginine deiminase: Functional studies on the crucial sites. Proteins-Structure Function and Bioinformatics, 2007; 66(3): 740-50.

16. Ensor CM, Holtsberg FW, Bomalaski JS, Clark MA. Pegylated arginine deiminase (ADI-SS PEG(20,000) (mw)) inhibits human melanomas and hepatocellular carcinomas in vitro and in vivo. Cancer Research, 2002; 62(19): 5443-50.

17. Galkin A, Lu XF, Dunaway-Mariano D, Herzberg O. Crystal structures representing the Michaelis complex and the thiouronium reaction intermediate of Pseudomonas aeruginosa arginine deiminase. Journal of Biological Chemistry, 2005; 280(40): 34080-7.

18. Kundu M, Thomas J, Fialho AM*, et al.* The anticancer activity of the N-terminal CARD-Like domain of arginine deiminase (ADI) from *Pseudomonas aeruginosa*. Letters in Drug Design & Discovery, 2009; 6(6): 403-12.

19. Beloussow K, Wang L, Wu J, Ann D, Shen WC. Recombinant arginine deiminase as a potential anti-angiogenic agent. Cancer Letters, 2002; 183(2): 155-62.

20. Misawa S, Aoshima M, Takaku H, Matsumoto M, Hayashi H. High-Level expression of Mycoplasma arginine deiminase in *Escherichia coli* and Its efficient renaturation as an antitumor enzyme. Journal of Biotechnology, 1994; 36(2): 145-55.
21. Gong H, Zolzer F, von Recklinghausen G*, et al.* Arginine deiminase inhibits cell proliferation by arresting cell cycle and inducing apoptosis. Biochemical and Biophysical Research Communications, 1999; 261(1): 10-4.
22. Takaku H, Takase M, Abe S, Hayashi H, Miyazaki K. *In vivo* antitumor activity of arginine deiminase purified from *Mycoplasma arginini*. International Journal of Cancer, 1992; 51(2): 244-9.
23. Kim JE, Jeong DW, Lee HJ. Expression, purification, and characterization of arginine deiminase from Lactococcus lactis ssp lactis ATCC 7962 in Escherichia coli BL21. Protein Expression and Purification, 2007; 53(1): 9-15.
24. Kakimoto T, Shibatan.T, Chibata I. Crystallization of L-arginine deiminase from *Pseudomonas putida*. Febs Letters, 1971; 19(2): 166-8.
25. Shibatani T, Kakimoto T, Chibata I. Crystallization and properties of L-arginine deiminase of *Pseudomonas Putida* 2. Journal of Biological Chemistry, 1975; 250(12): 4580-3.
26. Galkin A, Kulakova L, Sarikaya E, Lim K, Howard A, Herzberg O. Structural insight into arginine degradation by arginine deiminase, an antibacterial and parasite drug target. Journal of Biological Chemistry, 2004; 279(14): 14001-8.
27. Ni Y, Schwaneberg U, Sun ZH. Arginine deiminase, a potential anti-tumor drug. Cancer Lett, 2008; 261(1): 1-11.
28. Galkin A, Kulakova L, Sarikaya E, Lim K, Howard A, Herzberg O. J Biol Chem, 2004; 279: 14001.
29. Galkin A, Lu XF, Dunaway-Mariano D, Herzberg O. J Biol Chem, 2005; 280: 34080.
30. Holle LM. Pegaspargase: an alternative? Annals of Pharmacotherapy, 1997; 31(5): 616-24.

31. Yoshioka T, Wada T, Uchida N*, et al.* Anticancer efficacy in vivo and in vitro, synergy with 5-fluorouracil, and safety of recombinant methioninase. Cancer Research, 1998; 58(12): 2583-7.
32. Lam TL, Wong GKY, Chong HC*, et al.* Recombinant human arginase inhibits proliferation of human hepatocellular carcinoma by inducing cell cycle arrest. Cancer Letters, 2009; 277(1): 91-100.
33. Shen RS, Fritz RR, Abell CW. Biochemical-Properties and Immunogenicity of L-Phenylalanine Ammonia-Lyase - Effects on Tumor-Bearing Mice. Cancer Treatment Reports, 1979; 63(6): 1063-8.
34. Yoshimoto T, Chao SG, Saito Y, Imamura I, Wada H, Inada Y. Chemical modification of tryptophanase from E. coli with polyethylene glycol to reduce its immunoreactivity towards anti-tryptophanase antibodies. Enzyme, 1986; 36(4): 261-5.
35. Feun LG, Savaraj N, Marini A*, et al.* Phase II study of pegylated arginine deiminase (ADI-PEG20), a novel targeted therapy for melanoma. Journal of Clinical Oncology, 2006; 24(18): 464s-s.
36. Gong H, Zolzer F, von Recklinghausen G, Havers W, Schweigerer L. Arginine deiminase inhibits proliferation of human leukemia cells more potently than asparaginase by inducing cell cycle arrest and apoptosis. Leukemia, 2000; 14(5): 826-9.
37. Morris SM, Jr. Regulation of enzymes of the urea cycle and arginine metabolism. Annu Rev Nutr, 2002; 22: 87-105.
38. Scott L, Lamb J, Smith S, Wheatley DN. Single amino acid (arginine) deprivation: rapid and selective death of cultured transformed and malignant cells. British Journal of Cancer, 2000; 83(6): 800-10.
39. Wheatley DN, Campbell E. Arginine catabolism, liver extracts and cancer. Pathol Oncol Res, 2002; 8(1): 18-25.
40. Thomas JB, Holtsberg FW, Ensor CM, Bomalaski JS, Clark MA. Enzymatic degradation of plasma arginine using arginine deiminase inhibits nitric oxide production and protects mice from the lethal effects of tumor necrosis factor and endotoxin. Molecular Biology of the Cell, 2001; 12: 404a-a.

41. Cheng PNM, Leung YC, Lo WH, Tsui SM, Lam KC. Remission of hepatocellular carcinoma with arginine depletion induced by systemic release of endogenous hepatic arginase due to transhepatic arterial embolisation, augmented by high-dose insulin: arginase as a potential drug candidate for hepatocellular carcinoma. Cancer Letters, 2005; 224(1): 67-80.
42. Cheng PNM, Lam TL, Lam WM*, et al.* Pegylated recombinant human arginase (rhArg-peg(5,000mw)) inhibits the in vitro and in vivo proliferation of human hepatocellular carcinoma through arginine depletion. Cancer Research, 2007; 67(1): 309-17.
43. Kim JH, Yu YS, Kim DH, Min BH, Kim KW. Anti-tumor activity of arginine deiminase via arginine deprivation in retinoblastoma. Oncol Rep, 2007; 18(6): 1373-7.
44. Kim RH, Coates JM, Bowles TL*, et al.* Arginine deiminase as a novel therapy for prostate cancer induces autophagy and caspase-independent apoptosis. Cancer Research, 2009; 69(2): 700-8.
45. Glazer ES, Piccirillo M, Albino V*, et al.* Phase II study of pegylated arginine deiminase for nonresectable and metastatic hepatocellular carcinoma. Journal of Clinical Oncology, 2010; 28(13): 2220-6.
46. Ascierto PA, Scala S, Castello G*, et al.* Pegylated arginine deiminase treatment of patients with metastatic melanoma: Results from phase I and II studies. Journal of Clinical Oncology, 2005; 23(30): 7660-8.
47. Shen LJ, Beloussow K, Shen WC. Accessibility of endothelial and inducible nitric oxide synthase to the intracellular citrulline-arginine regeneration pathway. Biochemical Pharmacology, 2005; 69(1): 97-104.
48. Park H, Lee JB, Shim YJ*, et al.* Arginine deiminase enhances MCF-7 cell radiosensitivity by inducing changes in the expression of cell cycle-related proteins. Molecules and Cells, 2008; 25(2): 305-11.
49. Kubo M, Nishitsuji H, Kurihara K, Hayashi T, Masuda T, Kannagi M. Suppression of human immunodeficiency virus type 1 replication by arginine deiminase of *Mycoplasma arginini*. Journal of General Virology, 2006; 87: 1589-93.

50. Izzo F, Montella M, Orlando AP*, et al.* Pegylated arginine deiminase lowers hepatitis C viral titers and inhibits nitric oxide synthesis. Journal of Gastroenterology and Hepatology, 2007; 22(1): 86-91.
51. Kwan JM, Fialho AM, Kundu M*, et al.* Bacterial proteins as potential drugs in the treatment of leukemia. Leukemia Research, 2009; 33(10): 1392-9.
52. Tsai WB, Aiba I, Lee SY, Feun L, Savaraj N, Kuo MT. Resistance to arginine deiminase treatment in melanoma cells is associated with induced argininosuccinate synthetase expression involving c-Myc/HIF-1 alpha/Sp4. Molecular Cancer Therapeutics, 2009; 8(12): 3223-33.
53. Yoon CY, Shim YJ, Kim EH*, et al.* Renal cell carcinoma does not express argininosuccinate synthetase and is highly sensitive to arginine deprivation via arginine deiminase. International Journal of Cancer, 2007; 120(4): 897-905.
54. Feun L, You M, Wu CJ*, et al.* Arginine deprivation as a targeted therapy for cancer. Current Pharmaceutical Design, 2008; 14(11): 1049-57.
55. Zhu ZW, Momeu C, Zakhartsev M, Schwaneberg U. Making glucose oxidase fit for biofuel cell applications by directed protein evolution. Biosens Bioelectron, 2006; 21(11): 2046-51.
56. Panke S, Held M, Wubbolts M. Trends and innovations in industrial biocatalysis for the production of fine chemicals. Current Opinion in Biotechnology, 2004; 15(4): 272-9.
57. Patel RN. Chemo-enzymatic synthesis of pharmaceutical intermediates. Expert Opinion on Drug Discovery, 2008; 3(2): 187-245.
58. Yokobayashi Y, Weiss R, Arnold FH. Directed evolution of a genetic circuit. Proc Natl Acad Sci U S A, 2002; 99(26): 16587-91.
59. Ellington AD, Chen X, Robertson M, Syrett A. Evolutionary origins and directed evolution of RNA. International Journal of Biochemistry & Cell Biology, 2009; 41(2): 254-65.
60. Alper H, Fischer C, Nevoigt E, Stephanopoulos G. Tuning genetic control through promoter engineering. Proceedings of the National Academy of Sciences of the United States of America, 2005; 102(36): 12678-83.

61. Drummond DA, Iverson BL, Georgiou G, Arnold FH. Why high-error-rate random mutagenesis libraries are enriched in functional and improved proteins. J Mol Biol, 2005; 350(4): 806-16.
62. Wong TS, Roccatano D, Schwaneberg U. Steering directed protein evolution: strategies to manage combinatorial complexity of mutant libraries. Environmental Microbiology, 2007; 9(11): 2645-59.
63. Wong TS, Zhurina D, Schwaneberg U. The diversity challenge in directed protein evolution. Combinatorial Chemistry & High Throughput Screening, 2006; 9(4): 271-88.
64. Fasan R, Chen MM, Crook NC, Arnold FH. Engineered alkane-hydroxylating cytochrome P450(BM3) exhibiting nativelike catalytic properties. Angewandte Chemie-International Edition, 2007; 46(44): 8414-8.
65. Titus SA, Xiao L, Southall N*, et al.* Cell-based PDE4 assay in 1536-well plate format for high-throughput screening. Journal of Biomolecular Screening, 2008; 13(7): 609-18.
66. Lafferty M, Dycaico MJ. GigaMatrix^{TM}: an ultra highthroughput tool for accessing biodiversity. JALA, 2009; 9: 200-8.
67. Yang GY, Withers SG. Ultrahigh-throughput FACS-based screening for directed enzyme evolution. Chembiochem, 2009; 10(17): 2704-15.
68. Miller OJ, Hibbert EG, Ingram CU, Lye GJ, Dalby PA. Optimisation and evaluation of a generic microplate-based HPLC screen for transketolase activity. Biotechnology Letters, 2007; 29(11): 1759-70.
69. Yoshikuni Y, Ferrin TE, Keasling JD. Designed divergent evolution of enzyme function. Nature, 2006; 440(7087): 1078-82.
70. Becker S, Schmoldt HU, Adams TM, Wilhelm S, Kolmar H. Ultra-high-throughput screening based on cell-surface display and fluorescence-activated cell sorting for the identification of novel biocatalysts. Current Opinion in Biotechnology, 2004; 15(4): 323-9.
71. Farinas ET. Fluorescence activated cell sorting for enzymatic activity. Combinatorial Chemistry & High Throughput Screening, 2006; 9(4): 321-8.

72. Agresti JJ, Antipov E, Abate AR*, et al.* Ultrahigh-throughput screening in drop-based microfluidics for directed evolution. Proceedings of the National Academy of Sciences of the United States of America, 2010; 107(9): 4004-9.
73. Leemhuis H, Kelly RM, Dijkhuizen L. Directed evolution of enzymes: library screening strategies. Iubmb Life, 2009; 61(3): 222-8.
74. Chen KC, Wu CH, Chang CY*, et al.* Directed evolution of a lysosomal enzyme with enhanced activity at neutral pH by mammalian cell-surface display. Chem Biol, 2008; 15(12): 1277-86.
75. Wang Q, Xia T. Enhancement of the activity and alkaline pH stability of Thermobifida fusca xylanase A by directed evolution. Biotechnology Letters, 2008; 30(5): 937-44.
76. Colin DY, Deprez-Beauclair P, Silva N, Infantes L, Kerfelec B. Modification of pancreatic lipase properties by directed molecular evolution. Protein Engineering Design & Selection, 2010; 23(5): 365-73.
77. Bessler C, Schmitt J, Maurer KH, Schmid RD. Directed evolution of a bacterial alpha-araylase: Toward enhanced pH-performance and higher specific activity. Protein Sci, 2003; 12(10): 2141-9.
78. Liu ZQ, Sun ZH, Leng Y. Directed evolution and characterization of a novel D-pantonohydrolase from Fusarium moniliforme. Journal of Agricultural and Food Chemistry, 2006; 54(16): 5823-30.
79. Hasan Z, Renirie R, Kerkman R, Ruijssenaars HJ, Hartog AF, Wever R. Laboratory-evolved vanadium chloroperoxidase exhibits 100-fold higher halogenating activity at alkaline pH - Catalytic effects from first and second coordination sphere mutations. Journal of Biological Chemistry, 2006; 281(14): 9738-44.
80. Makde RD, Dikshit K, Kumar V. Protein engineering of class-A non-specific acid phosphatase (PhoN) of Salmonella typhimurium: Modulation of the pH-activity profile. Biomolecular Engineering, 2006; 23(5): 247-51.
81. Kim T, Mullaney EJ, Porres JM*, et al.* Shifting the pH profile of *Aspergillus niger* PhyA phytase to match the stomach pH enhances its effectiveness as an

animal feed additive. Applied and Environmental Microbiology, 2006; 72(6): 4397-403.
82. Hirata A, Adachi M, Utsumi S, Mikami B. Engineering of the pH optimum of Bacillus cereus beta-amylase: Conversion of the pH optimum from a bacterial type to a higher-plant type. Biochemistry, 2004; 43(39): 12523-31.
83. Tomschy A, Brugger R, Lehmann M*, et al.* Engineering of phytase for improved activity at low pH. Appl Environ Microbiol, 2002; 68(4): 1907-13.
84. Sakoda H, Imanaka T. Cloning and sequencing of the gene coding for alcohol dehydrogenase of Bacillus stearothermophilus and rational shift of the optimum pH. J Bacteriol, 1992; 174(4): 1397-402.
85. Yang JH, Park JY, Kim SH, Yoo YJ. Shifting pH optimum of Bacillus circulans xylanase based on molecular modeling. Journal of Biotechnology, 2008; 133(3): 294-300.
86. MacPherson IS, Rosell FI, Scofield M, Mauk AG, Murphy MEP. Directed evolution of copper nitrite reductase to a chromogenic reductant. Protein Engineering Design & Selection, 2010; 23(3): 137-45.
87. Hida K, Hanes J, Ostermeier M. Directed evolution for drug and nucleic acid delivery. Adv Drug Deliv Rev, 2007; 59(15): 1562-78.
88. Yuan L, Kurek I, English J, Keenan R. Laboratory-directed protein evolution. Microbiology and Molecular Biology Reviews, 2005; 69(3): 373-92.
89. Rautio J, Kumpulainen H, Heimbach T*, et al.* Prodrugs: design and clinical applications. Nat Rev Drug Discov, 2008; 7(3): 255-70.
90. Barak Y, Thorne SH, Ackerley DF, Lynch SV, Contag CH, Matin A. New enzyme for reductive cancer chemotherapy, YieF, and its improvement by directed evolution. Molecular Cancer Therapeutics, 2006; 5(1): 97-103.
91. Kuhn I, Harden P, Bauzon M*, et al.* Directed evolution generates a novel oncolytic virus for the treatment of colon cancer. PLoS One, 2008; 3(6): e2409.
92. Robertson DE, Steer BA. Recent progress in biocatalyst discovery and optimization. Current Opinion in Chemical Biology, 2004; 8(2): 141-9.
93. Soares AL, Guirmaraes GM, Polakiewicz B, Pitombo RND, Abrahao-Neto J. Effects of polyethylene glycol attachment on physicochemical and biological

stability of E-coli L-asparaginase. International Journal of Pharmaceutics, 2002; 237(1-2): 163-70.
94. Kotzia GA, Labrou NE. Engineering thermal stability of L-asparaginase by in vitro directed evolution. Febs Journal, 2009; 276(6): 1750-61.
95. Orlova A, Feldwisch J, Abrahmsen L, Tolmachev V. Affibody molecules for molecular imaging and therapy for cancer. Cancer Biotherapy and Radiopharmaceuticals, 2007; 22(5): 573-84.
96. Nilsson FY, Tolmachev V. Affibody (R) molecules: New protein domains for molecular imaging and targeted tumor therapy. Current Opinion in Drug Discovery & Development, 2007; 10(2): 167-75.
97. Gronwall C, Sjoberg A, Ramstrom M*, et al.* Affibody-mediated transferrin depletion for proteomics applications. Biotechnol J, 2007; 2(11): 1389-98.
98. Renberg B, Shiroyama I, Engfeldt T, Nygren PA, Karlstrom AE. Affibody protein capture microarrays: Synthesis and evaluation of random and directed immobilization of affibody molecules. Analytical Biochemistry, 2005; 341(2): 334-43.
99. Friedman M, Orlova A, Johansson E*, et al.* Directed evolution to low nanomolar affinity of a tumor-targeting epidermal growth factor receptor-binding affibody molecule. Journal of Molecular Biology, 2008; 376(5): 1388-402.
100. Chang CCJ, Chen TT, Cox BW*, et al.* Evolution of a cytokine using DNA family shuffling. Nature Biotechnology, 1999; 17(8): 793-7.
101. Zhang JH, Dawes G, Stemmer WPC. Directed evolution of a fucosidase from a galactosidase by DNA shuffling and screening. Proceedings of the National Academy of Sciences of the United States of America, 1997; 94(9): 4504-9.
102. Crameri A, Cwirla S, Stemmer WPC. Construction and evolution of antibody-phage libraries by DNA shuffling. Nature Medicine, 1996; 2(1): 100-2.
103. Patten PA, Howard RJ, Stemmer WP. Applications of DNA shuffling to pharmaceuticals and vaccines. Curr Opin Biotechnol, 1997; 8(6): 724-33.
104. Park IS, Kang SW, Shin YJ*, et al.* Arginine deiminase: a potential inhibitor of angiogenesis and tumour growth. Br J Cancer, 2003; 89(5): 907-14.

105. Izzo F, Marra P, Beneduce G*, et al.* Pegylated arginine deiminase treatment of patients with unresectable hepatocellular carcinoma: Results from phase I/II studies. J Clin Oncol, 2004; 22(10): 1815-22.
106. Gong H, Zölzer F, von Recklinghausen G, Havers W, Schweigerer L. Arginine deiminase inhibits proliferation of human leukemia cells more potently than asparaginase by inducing cell cycle arrest and apoptosis. Leukemia, 2000; 14(5): 826-9.
107. Shen LJ, Shen WC. Drug evaluation: ADI-PEG-20 - a PEGylated arginine deiminase for arginine-auxotrophic cancers. Curr Opin in Mol Ther, 2006; 8(3): 240-8.
108. Holtsberg FW, Ensor CM, Steiner MR, Bomalaski JS, Clark MA. Poly(ethylene glycol) (PEG) conjugated arginine deiminase: effects of PEG formulations on its pharmacological properties. J Controlled Release, 2002; 80(1-3): 259-71.
109. Mûller HJ, Boos J. Use of L-asparaginase in childhood all. Crit Rev Oncol Hematol, 1998; 28(2): 97-113.
110. Turunen O, Janis J, Fenel F, Leisola M. Engineering the thermotolerance and pH optimum of family 11 xylanases by site-directed mutagenesis. Methods Enzymol, 2004; 388: 156-67.
111. Fang TY, Ford C. Protein engineering of *Aspergillus awamori* glucoamylase to increase its pH optimum. Protein Eng, 1998; 11(5): 383-8.
112. Sakoda H, Imanaka T. Cloning and sequencing of the gene coding for alcohol-dehydrogenase of *Bacillus stearothermophilus* and rational shift of the optimum pH. J Bacteriol, 1992; 174(4): 1397-402.
113. Wang WY, Malcolm BA. Two-stage PCR protocol allowing introduction of multiple mutations, deletions and insertions using QuikChange™ site-directed mutagenesis. BioTechniques, 1999; 26(4): 680-2.
114. Miyazaki K, Takenouchi M. Creating random mutagenesis libraries using megaprimer PCR of whole plasmid. Biotechniques, 2002; 33(5): 1033-8.
115. Studier FW. Protein production by auto-induction in high-density shaking cultures. Protein Expression and Purification, 2005; 41(1): 207-34.

116. Archibald RM. Deternination of citrulline and allantoin and demonstration of citrulline in blood plasma. J Biol Chem, 1944; 156(1): 121-42.
117. Boyde TRC, Rahmatullah M. Optimization of conditions for the colorimetric determination of citrulline, using diacetyl monoxime. Anal Biochem, 1980; 107(2): 424-31.
118. Guex N, Peitsch MC. SWISS-MODEL and the Swiss-PdbViewer: an environment for comparative protein modeling. Electrophoresis, 1997; 18(15): 2714-23.
119. van Gunsteren WF, Billeter SR, Eising AA*, et al.* Biomolecular simulation: the gromos 96 manual and user guide ETH Zürich; 1996.
120. Mather A, Roland D. Automated thiosemicarbazide-diacetyl monoxime method for plasma urea. Clinical Chemistry, 1969; 15(5): 393-6.
121. Wong TS, Arnold FH, Schwaneberg U. Laboratory evolution of cytochrome P450BM-3 monooxygenase for organic cosolvents. Biotechnol Bioeng, 2004; 85(3): 351-8.
122. Glieder A, Farinas ET, Arnold FH. Laboratory evolution of a soluble, self-sufficient, highly active alkane hydroxylase. Nat Biotechnol, 2002; 20(11): 1135-9.
123. Galkin A, Lu X, Dunaway-Mariano D, Herzberg O. Crystal structures representing the Michaelis complex and the thiouronium reaction intermediate of Pseudomonas aeruginosa arginine deiminase. Journal of biological chemistry, 2005; 280(40): 34080-7.
124. Chuang VTG, Kragh-Hansen U, Otagiri M. Pharmaceutical strategies utilizing recombinant human serum albumin. Pharm Res, 2002; 19(5): 569-77.
125. Tee KL, Dmytrenko O, Otto K, Schmid A, Schwaneberg U. A p-nitrothiophenolate screening system for the directed evolution of a two-component epoxygenase (StyAB). J Mol Catal B: Enzym, 2008; 50(2-4): 121-7.
126. Li L, Li ZM, Wang CH*, et al.* The electrostatic driving force for nucleophilic catalysis in L-arginine deiminase: a combined experimental and theoretical study. Biochemistry (Mosc), 2008; 47(16): 4721-32.

127. Takaku H, Matsumoto M, Misawa S, Miyazaki K. Antitumor-activity of arginine deiminase from *Mycoplasma arginini* and its growth-Inhibitory mechanism. Jap J Cancer Res, 1995; 86(9): 840-6.
128. Capocaccia R, Sant M, Berrino F, Simonetti A, Santi V, Trevisani F. Hepatocellular carcinoma: trends of incidence and survival in Europe and the United States at the end of the 20th century. American Journal of Gastroenterol, 2007; 102(8): 1661-70.
129. Shen LJ, Shen WC. Drug evaluation: ADI-PEG-20 - a PEGylated arginine deiminase for arginine-auxotrophic cancers. Current Opinion in Molecular Therapeutics, 2006; 8(3): 240-8.
130. Wang WY, Malcolm BA. Two-stage PCR protocol allowing introduction of multiple mutations, deletions and insertions using QuikChange (TM) site-directed mutagenesis. Biotechniques, 1999; 26(4): 680-2.
131. Vaughn WK, Neal RA, Anderson AJ. Computer estimation of the parameters of the sigmoidal kinetic model. Computers in Biology and Medicine, 1976; 6(1): 1-7.
132. Kelley LA, Sternberg MJE. Protein structure prediction on the web: a case study using the Phyre server. Nature Protocols, 2009; 4(3): 363-71.
133. Laskowski RA, Macarthur MW, Moss DS, Thornton JM. Procheck - a program to check the stereochemical quality of protein structures. Journal of Applied Crystallography, 1993; 26: 283-91.
134. Zhou HY, Zhou YQ. Distance-scaled, finite ideal-gas reference state improves structure-derived potentials of mean force for structure selection and stability prediction. Protein Science, 2002; 11(11): 2714-26.
135. Benkert P, Tosatto SCE, Schomburg D. QMEAN: A comprehensive scoring function for model quality assessment. Proteins-Structure Function and Bioinformatics, 2008; 71(1): 261-77.
136. Berendsen HJC, Postman JPM, van Gunsteren WF, Hermans J. Interaction models for water in relation to protein hydration. Intermolecular Forces, 1981: 331-42.

137. Hess B, Bekker H, Berendsen HJC, Fraaije JGEM. LINCS: A linear constraint solver for molecular simulations. Journal of Computational Chemistry, 1997; 18(12): 1463-72.
138. Miyamoto S, Kollman PA. Settle - an analytical version of the shake and rattle algorithm for rigid water models. Journal of Computational Chemistry, 1992; 13(8): 952-62.
139. Darden T, York D, Pedersen L. Particle mesh ewald - an N.Log(N) method for ewald sums in large systems. Journal of Chemical Physics, 1993; 98(12): 10089-92.
140. Berendsen HJC, Postma JPM, Vangunsteren WF, Dinola A, Haak JR. Molecular dynamics with coupling to an external bath. Journal of Chemical Physics, 1984; 81(8): 3684-90.
141. Hess B, Kutzner C, van der Spoel D, Lindahl E. GROMACS 4: algorithms for highly efficient, load-balanced, and scalable molecular simulation. Journal of Chemical Theory and Computation, 2008; 4(3): 435-47.

Summary and outlook

Arginine depletion based on ADI is an emerging strategy for anti-tumor treatment. ADIs have been studied for the therapy of HCCs and melanomas and were approved as an orphan drug for both kinds of tumors. ADI is proved to be effective in the treatment of leukemia. The effectiveness of ADIs as anti-tumor agent depends on their enzymatic properties (such as K_m, k_{cat}, optimum pH, stability at neutral pH). Directed evolution, without rational understanding of the targeted property, allows improving all properties that can be reflected in a screening system through iterative rounds of diversity generation and screening.

In order to improve PpADI activity at physiological pH by directed evolution, a colorimetric screening assay based on citrulline detection has been developed in 96-well microtiter plate format. Single mutation H404R was identified according to PpADI homology model (based on PaADI crystal structure), introduced to PpADI wild type and eventually resulted in 1.4-fold of increase in k_{cat}. M1 (H404R) was used as template for the first round of epPCR library generation. M2 (K5T/D44E/H404R) obtained from the first round of epPCR library showed 4-fold improved k_{cat} value when compared to the PpADI wild type. Furthermore, a shift of pH optimum from pH 6.5 to pH 7.0 was observed, combined with an increased K_m value (2.5 mM) under assay conditions (0.5 M sodium phosphate buffer, pH 7.4), compared to PpADI wild type (0.7 mM).

Arginine concentration in human plasma is however relatively low (100-120 µM). Therefore the second round of epPCR library was performed to decrease K_m value and further improve k_{cat} value. The validated screening assay was modified to reflect more close physiological condition (1 mM arginine in PBS buffer, pH 7.4). Two important variants with one additional mutation, M4 (K5T/D44E/A128T/E296K/H404R) with decreased $S_{0.5}$ vaule, and M5 (K5T/D38H/D44E/A128T/H404R) with improved k_{cat} were obtained. Their two mutations were combined and resulted in variants M6

(K5T/D38H/D44E/A128T/E296K/H404R). Under physiological pH in PBS buffer, the $S_{0.5}$ value of M6 (0.81 mM) is lower than that of PpADI wild type (1.30 mM); the k_{cat} value improved from 0.18 s^{-1} (PpADI wild type) to 17.56 s^{-1} (M5, 97.6-folds) and 11.64 s^{-1} (M6, 64.7-fold).

A reamaining challenge facing PpADI's anti-tumor application is to decrease the K_m ($S_{0.5}$) value further close to arginine concentration level in human plasma. A more sensitive assay for screening has to be developed with the addition of sensitizer like thiosemicarbazide (TSC), optimized temperature and incubation time. Improved variants should be tested tested in human plasma or with human plasma composition. *In vitro* testing of ADI variants with arginine auxotrophic tumor cell lines is the first step towards *in vivo* in human.

In summary, directed evolution has been very useful algorithim for improving ADI's k_{cat} and K_m at physiological pH (pH 7.4) for its medical application. Hope that directed evolution will be become a standard method for therapeutic protein like its use in industry.

Publications

1. **Leilei Zhu**, Kang Lan Tee, Danilo Roccatano, Burcu Sonmez, Ye Ni, Zhi-Hao Sun, and Ulrich Schwaneberg. Directed evolution of an antitumor drug (Arginine Deiminase PpADI) for increased activity at physiological pH. ChemBioChem. 2010, 11, 691-697.

2. **Leilei Zhu**, Rajni Verma, Danilo Roccatano, Ye Ni, Zhi-Hao Sun, and Ulrich Schwaneberg. A potential anti-tumor drug (arginine deiminase) reengineered for efficient operation under physiological conditions. ChemBioChem. *In press*.

3. Ye Ni, Zhenwei Li, Zhihao Sun, Pu Zheng, Yongmei Liu and **Leilei Zhu**, Ulrich Schwaneberg. Expression of arginine deiminase from *Pseudomonas plecoglossicida* CGMCC2039 in *Escherichia coli* and its anti-tumor activity. Current Microbiology. 2009, 58(6):593-598.

Patent

1. Directed evolution of arginine deiminase for increased activity at physiological pH. Application number: PCT/EP2010/061884.

Curriculum vitae

Personal data

Name:	Leilei Zhu
Gender:	Female
Date of Birth:	27th April, 1982
Place of Birth:	Weifang, China
Marital Status:	Married
Nationality:	Chinese

Education

2009-	PhD fellow of biotechnology, RWTH Aachen University, Aachen, Germany
2007-2009	PhD fellow of engineering and science, Jacobs University Bremen, Bremen, Germany
2005-2007	Master of biochemical engineering, Jiangnan University (Southern Yantze University), Wuxi, China
2001-2005	Bachelor of biotechnology, Jiangnan University (Southern Yantze University), Wuxi, China

2001-1998	The first high school of Hanting, Weifang, China
1998-1994	The sixth middle school of Hanting, Weifang, China
1989-1994	Primary school of Liuhe, Weifang, China

Directed Evolution of Arginine Deiminase (ADI) for Anti-tumor Application

Von der Fakultät für Mathematik, Informatik und Naturwissenschaften der RWTH Aachen University zur Erlangung des akademischen Grades eines(r) Doktors(in) der Naturwissenschaften oder eines(r) Doktors(in) der Ingenieurwissenschaften genehmigte Dissertation

vorgelegt von

Master of Biochemistry

Leilei Zhu

Aus Weifang China

Berichter: **Universitätsprofessor Dr. Ulrich Schwaneberg**
Universitätsprofessor Dr. Lothar Elling

Tag der mündlichen Prüfung: 14.09.2010

Diese Dissertation ist auf den Internetseiten der Hochschulbibliothek online verfügbar.

Table of contents

Acknowledgement.....I
Abstract.....III
Abbreviations V
List of figures..... VI
List of tables..... IX
Chapter 1 Arginine deiminase (ADI) 1
1.1 Arginine deiminase (ADI).....1
1.2 ADI structure 5
1.3 Catalytic reaction mechanism of ADI.....10
1.4 Anti-tumor application of ADI.....11
1.5 Conclusion.....16
Chapter 2 Directed evolution 17
2.1 Introduction to directed evolution.....17
2.2 Directed enzyme evolution for pH tolerance of enzymes 22
2.3 Directed enzyme evolution for medical application.....24
2.3.1 Prodrug enzymes for tumor chemotherapy.....24
2.3.2 Oncolytic viruses for tumor chemotherapy.....25
2.3.3 Amino acid depriving enzyme for anti-tumor applications.....27
2.3.4 Affibody molecules for cancer prognosis 28
2.3.5 Interferon for anti-tumor applicaiton 29
2.4 Conclusion.....30
Chapter 3. Directed evolution of Arginine deiminase for increased activity at physiological pH.....31
3. 1 Abstract 31
3.2 Introduction.....31
3.3 Materials and methods 33
3.3.1 Materials 33
3.3.2 Methods 34

3.3.2.1 Reagents used in assays 34
3.3.2.2 Cloning of ADI into pET42b(+) 34
3.3.2.3 Site directed mutagenesis of PpADI gene at position H404 35
3.3.2.4 Site sturation mutagenesis of PpADI gene at nine amino acid position 35
3.3.2.5 Construction of PpADI error-prone library 36
3.3.2.6 Expression of PpADI in LB media with IPTG induction 37
3.3.2.7 Expression of PpADI in auto-induction media 37
3.3.2.8 Cultivation and expression of PpADI in 96-well plates 37
3.3.2.9 Screening Procedure 38
3.3.2.10 Expression of ADI in shaking flask and purification 39
3.3.2.11 Characterization of ADI wild type and mutants 40
3.3.2.12 Molecular Modeling 41
3.3.2.13 Stability of PpADI in presence of serum 41
3.3.2.14 Activity of PpADI (wild type, M1, M2) towards arginine derivative dimethylarginine 42
3.4 Results 42
3.4.1 PpADI cloning 42
3.4.2 PpADI expression in LB media with IPTG as inducer 44
3.4.3 PpADI expression in auto-induction media 44
3.4.4 PpADI assay based on citrulline detection 46
3.4.5 PpADI screening system for citrulline production in microtiter plates 47
3.4.6 Focused libraries generated by saturation mutagenesis 50
3.4.7 Validation of variant M1 (H404R) citrulline colorimetric assay in cuvette format 50
3.4.8 epPCR library generation and screening with citrulline detection assay by screening error-prone mutant libraries 50
3.4.9 Characterization of PpADI variants 53
3.4.9.1 Determination of k_{cat} and K_m of ADI wild type and the mutants 53
3.4.9.2 Relative pH profile of wild type and mutant 54
3.4.10 Stability of PpADI in the presence of human serum 55

3.4.11 Activity of PpADI (wild type, M1, M2) towards arginine derivative (N^G, N^G)-dimethylarginine 56
3.5 Discussion 56
3.6 Conclusion 59
Chapter 4. PpADI reengineered for efficient operation under physiological conditions 60
4.1 Abstract 60
4.2 Introduction 60
4.3 Materials and methods 62
4.3.1 Materials 62
4.3.2 Methods 62
4.3.2.1 Site saturation mutagenesis of *PpADI* M2 at position A128 62
4.3.2.2 Construction of PpADI error-prone library 63
4.3.2.3 Site directed mutagenesis at position D38 of *PpADI* M4 63
4.3.2.4 Site saturation mutagenesis at position D38 and E296 of *PpADI* M3 64
4.3.2.5 Cultivation and expression of PpADI in 96-well plates 64
4.3.2.6 Improved screening system in 96-well plate to identify PpADI variants with high activities at low arginine concentration 64
4.3.2.7 Expression of PpADI in shaking flask and purification 65
4.3.2.8 Characterization of PpADI variants 65
4.3.2.9 Native polyacrylamide gel electrophoresis of PpADI variants 66
4.3.2.10 Homology modeling 67
4.4 Results 67
4.4.1 Improved screening system in microtiter plates to identify PpADI variants with high activities at low arginine concentration 67
4.4.2 Genealogic tree of directed PpADI evolution 68
4.4.3 EpPCR library construction and screening for variants with high activities at low arginine concentration 69
4.4.4 Site saturation mutagenesis of *PpADI* at position D38 and E296 70

4.4.5 Determination of kinetic constants (k_{cat} and $S_{0.5}$) of PpADI wild type and variants M3, M4, M5 and M6 72
4.4.6 Native polyacrylamide gel electrophoresis of PpADI variants 73
4.5 Discussion 74
Summary and outlook 95
Publication list 97
Curriculum vitae 98

Acknowledgement

First and foremost I want to thank my supervisor Prof. Dr. Ulrich Schwaneberg for offering me the opportunity to study in Germany, his continuous support of my PhD study and research, for his patience, motivation, enthusiasm, and immense knowledge, which influence my view of science and life. His guidance helped me all the time in research and writing of paper and thesis. I could not have imagined having a better advisor and mentor for my PhD study.

Besides my supervisor, I would like to thank other two committee member Prof. Dr. Lothar Elling and Prof. Dr. Anett Kirschner. I appreciate their taking time to read this thesis and give valuable comments.

My sincere thanks also go to Kang Lan, who became a great friend of mine after I came to Bremen of Germany three years ago. She helped me a lot with my PhD project and she was a great company in my daily life. I will never forget the two months I spent on the first cloning working in my life and how Kang Lan taught me and encouraged me.

I am grateful to Prof. Dr. Danilo Roccatano for spending a lot of time discussing my results. After the first meeting with Prof. Roccatano, I started to know and learn computational tools which are really useful for my PhD study. I also thank Rajni for her contribution of homology modeling to my project.

The members of the Schwaneberg group have contributed immensely to my personal and professional time in Jacobs University Bremen and RWTH Aachen University. The group has been a source of friendships as well as good advice and collaboration. I appreciate the help from Marina, Daniela, Gisela, Wolfgang and Brigitta in lab and Marina, Monika and Anita's patient explanation of the registration regulation RWTH Aachen University. I would like to acknowledge honorary group members. I thank Liqing for her sharing apartment with me and helped me start my life in Germany and also thank Haiyan for her offering me a room later and often cooked nice food for us. Ran shared a lot of lab techniques which are very useful for my experiments. I always admire her professional and

accurate attitude towards work. I thank other labmates who I got to know in Jacobs university: Ronny, Hemu, Chaoning, Amol, Dominik and Amir for the stimulating discussions, little help in lab and all the fun we have had in the last three years; Dragana, Ljubica, Noor, Pravine and Raluca helped me move to Aachen and we finally got through the tough transition period from Bremen to Aachen. I thank our group leaders Marco, Jan and Radivoje, who are not my direct supervisor, but are always helpful when I have questions. I thank my fellow labmates who I got to know in RWTH Aachen University: Tamara, Felix, Alex, Christian, Joelle, André, Joana……, who are always helpful with all the problems (PhD registration, Germany letters from university…….) because of my poor German.

I also want to acknowledge my students, Burcu and Alice, both of whom were hard-working and smart. They were all a great help in the lab and I really enjoyed working with them.

I would like to thank my family because of their love, support and trust. They love me the most in the world. I thank for their efforts that they made over the years to make sure I have a good growth and education environment. I wish them healthy and happy life. I thank my elder sister for her love and understanding and always taking good care of my parents these years when I am not around. I thank my husband, Haifeng, who supports me all the time and always is there for me. I am lucky to have him with me.

The financial support of the Jacobs University Bremen and RWTH Aachen University is gratefully acknowledged.

Abstract

Arginine deiminase (ADI), an arginine-degrading enzyme, is involved in the first step of arginine dihydrolase pathway. It catalyzes the hydrolysis of L-arginine to form citrulline and ammonia. ADI has been studied as a potential cancer therapeutic agent for the arginine-auxotrophic tumors, such as hepatocellular carcinomas (HCC) and melanomas. Furthermore, studies also indicate that ADI is a potential anti-angiogenic agent; therefore it could become a novel anti-cancer drug targeting the neovascularization-related tumors. Studies show ADI is more potent for the treatment of leukemia than L-asparaginase. However, the anti-tumor application of ADI for therapeutic purpose faces considerable challenges, such as, microbial ADI has low activity at physiological pH (7.35~7.45), short circulating half-life (~5 h) and high antigenicity. Pegylation of ADI improved its efficacy as a clinical drug, including its half-life in serum and antigenicity. The aim of the project is to improve ADI catalytic performance at physiological pH by directed evolution.

Protein engineering by rational design and directed evolution offers opportunities to tailor ADI properties to physiological conditions. Directed protein evolution has over the last decades become a versatile and successful approach for tailoring protein properties to industrial demands and for advancing our understanding of structure-function relationships in biocatalysts. Unlike rational design relying on the gathering of extensive structure-function relationships of enzymes, directed evolution is used to reengineer enzyme properties through iterative rounds of diversity generation and function selection for improved variants.

In order to improve the ADI activity at physiological pH, we established a directed evolution protocol for this purpose. A microtiter plate (MTP) format colorimetric screening assay based on citrulline detection with diacetyl monoxime (DAM) was developed. Reaction temperature for color development and DAM concentration

were optimized to ensure sufficient sensitivity, appropriate linear range and throughput. With the optimized assay and PpADI wild type expressed in *E. coli* as a model protein, true standard deviation 12.8 % was obtained, which is appropriate for the library screening.

With the established microtiter plate assay system, for the first time, we reengineered ADI for improved activity at physiological pH (pH 7.4) with higher potency in medical application. After one site directed mutagenesis and one round of epPCR library screening, variant M2 (K5T/D44E/H404R) was obtained. M2 shows 4-fold improved k_{cat} value than the PpADI wild type, a shifted pH optimum at pH 7.0 (by 0.5 pH unit), and however an increased K_m value, 3.6-fold under assay conditions (0.5 M sodium phosphate buffer).

Low K_m ($S_{0.5}$) value for ADI is an important factor for efficient consume of arginine in plasma because of the low arginine concentration in human plasma (100-120 µM). Therefore after our proof of concept of reengineering PpADI by directed evolution, we aim to decrease the K_m value of PpADI towards arginine and improve the k_{cat} furthermore thereby improve the efficiency of arginine depletion by ADI. The established citrulline colorimetric assay in 96-well microtiter plate is improved to reflect application conditions: PBS buffer and 1 mM arginine were used in screening system. After the second round of epPCR library and site directed mutagenesis, variant M5 (K5T/D38H/D44E/A128T/H404R) and M6 (K5T/D38H/D44E/A128T/E296K/H404R) were generated: at pH 7.4 (PBS buffer), the $S_{0.5}$ value decrease from 2.01 mM (parent M3, K5T/D44E/A128T/H404R) to 1.48 mM (M5) and 0.81 mM (M6). Under physiological pH in PBS buffer, the $S_{0.5}$ value of M6 (0.81 mM) is lower than that of PpADI wild type (1.30 mM); the k_{cat} value improved from 0.18 s^{-1} (PpADI wild type) to 17.56 s^{-1} (M5, 97.6-folds) and 11.64 s^{-1} (M6, 64.7-fold).

Abbreviations

ADI	arginine deiminase
ADH	arginine degradation pathway
ASS	argininosuccinate synthetase
ASL	argininosuccinate lyase
CARD	caspase recruitment domain
PCR	polymerase chain reaction
epPCR	error prone PCR
DAM	diacetyl monoxime
Da	dalton
DNA	deoxyribonucleic acid
E. coli	*Escherichia coli*
GMSF	guanidino-group modifying enzyme superfamily
HCC	hepatocellular carcinomas
HUVEC	human umbilical vein endothelial cells
IPTG	isopropyl β-D-1-thiogalactopyranoside
iNOs	inducible nitric oxide synthase
LB	Luria-Bertani-medium
MTP	microtiter plate
OD_{600}	optical density at 600 nm
OTC	ornithine carbamoyl transferase
PEG	polyethylene glycol
PDB	protein data bank
TSC	thiosemicarbazide
WT	wild type

List of tables

Figures	Pages
Chapter 1	
Scheme 1. Arginine dihydrolase pathway. OTC, ornithine transcarbamylase; CK, carbamate kinase.	1
Figure 1. Structural of ADIs from *P. aeruginosa* and *M. arginini*.	5
Figure 2 (A). stereoscopic view of PaADI key active site residues. 2 (B). stereoscopic view of a modeled arginine substrate (green) docked in the active site of ADI. Atomic colors are red, oxygen; blue, nitrogen; yellow, sulfur; and gray, carbon. Ion pair interactions are shown as dashed lines.	7
Figure 3. Structural characteristics of the PaADI.	9
Figure 4 (A). Stereoscopic view of ADI in the unbound and bound states. 4 (B). Structural relationship between ADI (yellow) and PAD4 (cyan).	10
Figure 5. Mechanism of PaADI catalysis of arginine to citrulline and ammonia.	11
Firgure 6. Urea cycle.	13
Firgure 7. Summary of ADI effects on arginine-related cellular functions.	15
Chapter 2	
Figure 1. Procedure of a directed evolution experiment.	18
Figure 2. Overview of screening technologies.	21
Figure 3. Hermiston's "Directed Evolution" process of viruses and derivative viral pools.	26
Chapter 3	
Figure 1. DNA electrophoresis of PpADI.	43
Figure 2. PpADI sequencing results.	43
Figure 3. SDS-PAGE of PpADI expression.	44

Figures Pages

Figure 4(A). Activity of PpADI expressed in auto-induction media. 45

Figure 4(B). SDS-PAGE of ADI expressed in auto-induction media 1, LS-5052; 2, P-5052; 3, MD-5052; 4 TYM-5052; 5, TYP-5052. 45

Figure 5. Arginine conversion by ADI and detection of citrulline using DAM/TSC assay. 46

Figure 6. Citrulline colorimetric assay in cuvette format using DAM/TSC assay. 46

Figure 7. Calibration curve of cuvette format citrulline colorimetric assay. 47

Figure 8. Citrulline colorimetric assay in MTP format using DAM assay. 47

Figure 9. Calibration curve of 96-well microtiter plate format citrulline colorimetric screening assay. 48

Figure 10. Activity values in descending order of the ADI wild-type conversion of arginine to citrulline in a 96-well microtiter plate using the optimized assay protocol. 49

Figure 11. PpADI model derived from PaADI crystal structure (PDB code 2a9gD) by SWISS MODEL WORKSPACE. 49

Figure 12 (A). Electrophoresis of epPCR products. Lane 1, 0.01 mM of $MnCl_2$; Lane 2, 0.02 mM of $MnCl_2$; Lane 3, 0.05 mM of $MnCl_2$. 51

Figure 12 (B). Electrophoresis of MEGAWHOP product with epPCR products as megaprimer. 51

Figure 13. Relative activity of ADI variants towards arginine. The relative activity is the ratio of the activity at the pH of each variant relative to the activity at pH 7.4 of wild type ADI. 52

Figure 14. Elution profile of wild type PpADI and improved variants from epPCR library, generated with Protein 230 Kit using a mircofluidic device (Agilent Bioanalyzer). BSA was added as an internal standard. 53

Figure 15. Kinetic parameters of ADI and mutants for conversion of arginine to citrulline. White: ADI wild type, grey: M1 (H404R), black: M2 (K5T D44E H404R). 54

Figure 16. pH profile of wild type ADI, M1(H404R), M2(K5T/D44E /H404R. 55

Figures Pages

Figure 17. Structural alignment of mutant M1 model with corresponding residues of the crystal structures of the PaADI (in orange). 57

Figure 18. Structural alignment of mutant M2 model with corresponding residues of the crystal structures of the PaADI (in orange). 58

Chaper 4

Figure 1. Figure 1. Activity values in descending order of the PpADI variant M3 conversion of arginine to citrulline in a 96-well microtiter plate using the optimized assay protocol. 68

Figure 2. Genealogic tree of PpADI variants (M1 to M6) with generated amino acid substitutions. Novel substitutions are indicated by an asterisk. 69

Figure 3. Native polyacrylamide gel electrophoresis of PpADI variants (M3 to M6) with different dimer/tetramer distribution 73

Figure 4. Kinetic curve of PpADI wild type, M3, M5 and M6. 75

Figure 5. A). The model of WT tetramer after energy minimization in vacuum (GROMOS 43B1). B). The model of M6 tetramer after energy minimization in vacuum (GROMOS 43B1). 77

Figure 6. A). Structure model of variant M6. B). Structure alignment of PpADI WT model and M6 model with four loops 78

List of tables

Tables Page

Chapter 1

Table 1. ADI expression, enzymatic properties and medical applications. 3

Table 2. Crystal structures of ADI in protein data bank (PDB). 6

Table 3. Residues important for catalytic function of PaADI. 8

Chapter 2

Table 1. Improvement obtained from directed evolution or rational design for pH performance. 22

Chapter 3

Table 1. Primer sequences for site saturation mutagenesis. 36

Table 2. Activity of ADI variants towards arginine determined using citrulline colorimetric assay in cuvette format. 52

Table 3. Stability of PpADI variants in the presence of human serum. 55

Chapter 4

Table 1. Nucleotide and amino acid substitutions at position 38 71

Table 2. Nucleotide and amino acid substitutions at position 296 71

Table 3. Kinetic constants of wild type PpADI and variants. 72

Arginine deiminase (ADI)

1.1 Arginine deiminase (ADI)

Arginine deiminase (ADI, EC 3.5.3.6), an arginine-metabolizing hydrolase, catalyzes the hydrolysis of L-arginine to form citrulline and ammonia. This reaction is the first step in the L-arginine degradation pathway (ADH, scheme 1, (1). First, arginine is deiminated by arginine deiminase. The resulting citrulline is converted to carbamoyl phosphate and ornithine by ornithine transcarbamylase (EC 2.1.3.3), and finally the carbamoyl phosphate is used to phosphorylate ADP by carbamate kinase (EC 2.7.2.2), producing one ATP molecule. ADI is absent in humans but present in a wide range of bacterial species such as *Pseudomonas aeruginosa* (2), *Pseudomonas plecoglossicida* (3) and *Mycoplasma arginini* (4) and in parasitic protists such as *Giardia intestinalis* (5), *Trichomonas Vaginalis* (6), *Trichomonas fetus* (7), and *Hexamita inflate* (8). For pathogenic bacteria, ADI is required in arginine dehydrolase pathway for virulence and for energy production under anaerobic conditions (9, 10).

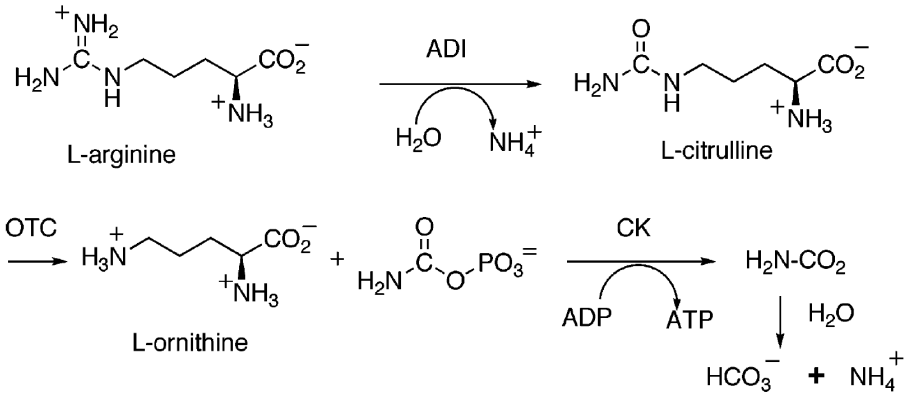

Scheme 1. Arginine dihydrolase pathway. OTC, ornithine transcarbamylase; CK, carbamate kinase.

The establishment of a high-level production system for ADI is an essential step for further research and development of this enzyme. After ADI was discovered from Mycoplasma in 1960s (11), various ADI genes have been cloned, expressed in *E. coli* strains, and the enzyme properties were also studied (Table 1).

Table 1. ADI expression, enzymatic properties and medical applications.

ADIs	Origin	Expression host/vector	Multimeric form	K_m; k_{cat}	Optimum pH	Specific activity	Medical application	References
MhADI (SYN1903)	*Mycoplasma hominis* PG21*	*E.coli* BL21 (DE3)/pET-47b	Dimer			0.618 U/mg (pH 6.5)	Human melanoma (G361), 0.036 U/ml for 50 % IC_{50}	Japan, Harasawa, 2009 (12)
MhADI	*Mycoplasma hominis* (ATCC 23114)	-	Dimer		6.0	35.5 U/mg (pH 6.0) ; 3.9 U/mg (pH 7.4)	Mouse melanoma (MH134) *in vitro*, 100 ng/ml for 50 % IC_{50}	Japan, Takaku, 1995 (13)
MhADI	*Mycoplasma hominis* (ATCC 14027)	-	Dimer	0.17 mM (pH6.6)				USA, Fenske, 1976(14)
MhADI	*Mycoplasma hominis*	*E.coli* BL21 (DE3)/pET25b		0.24 mM; 0.151 s^{-1}				China, Luo, 2007 (15)
MhADI	*Mycoplasma hominis*	*E.coli*				20 U/mg ADI (37℃). [a]	ADI-SS PEG_{20000}, human melanoma, human HCC	USA, Pheonix Pharmacologics, Inc., Clark, 2002 (16)
PaADI (PA5171)	*Pseudomonas aeruginosa* (ATCC 47085D)	*E. coli* BL21(DE3)/pET100	Tetramer	0.14±0.01 mM (pH 5.6)	5.6			USA, Dunaway-Mariano, 2005 (17)
PaADI	*Pseudomonas aeruginosa*	*E. coli* BL21 (DE3)/ pET SUMO				CARD-like domain, no catalytic activity	Human cancer cell line SKOV-3	USA, Chakrabarty, 2006 (18)
PpADI	*Pseudomonas plecoglossicida*	*E. coli* BL21 Gold-(DE3)/ pET42b		0.7 mM; 5.6 s^{-1} (pH 7.4, 0.5 M sodium phosphate buffer)	6.5	31.3 U/mg (pH 7.4, 0.5 M sodium phosphate buffer)		Germany, Schwaneberg, 2010 (3)

MaADI	*Mycoplasma arginini* (ATCC 23838D)	*E. coli* DH5α/PTTQ118				32.7 U/mg. [a]	Human umbilical vein endothelial (HUVE)	USA, Shen, 2002 (19)
MaADI	*Mycoplasma arginini* (ATCC 23838)	*E. coli* JM101/pADTc1	Dimer			33.6 U/mg (37℃, pH 6.5). [a]	Mouse hepatoma, 17 ng/ml for 50 % IC_{50}; mouse fibrosarcoma, 15 ng/ml for 50 % IC_{50}	Japan, Hayashi, 1994 (20)
MaADI	*Mycoplasma arginini* (ATCC 23838)					42 U/mg (37℃, pH 6.5); 29.9 U/mg (37℃, pH 7.4)	Mouse melanoma (MH134) *in vitro*, 10 ng/ml for 50 % IC_{50}	Japan, Takaku, 1995 (13)
MaADI	*Mycoplasma arginini* (ATCC 23838)	-					HUVE, neuroblastoma, retinoblastoma, osteosarcoma, 5~10 ng/ml for 50 % IC_{50}	Germany, Schweigerer, 1999 (21)
MaADI	*Mycoplasma arginini* (ATCC 23838)	-	Dimer	0.2 mM	6.0-7.5	50 U/mg	Mouse tumor carcinoma, fibrosarcoma and melanoma, 5~20 ng/ml for 50 % IC_{50}	Japan, Takaku, 1992 (22)
LlADI	*L. lactis* (ATCC 7962)	*E. coli* BL21Gold(DE3)/pGEM-T Easy	Trimer	8.67 mM	7.2	140.27 U/mg		Korea, Lee, 2007 (23)

[a] ADI was expressed in inclusion body and denaturation-renaturation had to be employed to get soluble protein.

1.2 ADI structure

In 1970s, Kakimoto et al. (24, 25) diffracted the first ADI crystals from *P. putida* through multiple-step chromatography followed by crystallization. Almost three decades later, the X-ray crystal structure of ADI from *P. aeruginosa* (PaADI, Figure 1A) (26) and *M. arginini* (MaADI, Figure 1B) (4) were solved to assist in understanding structure-function relationships. PaADI and MaADI share 27 % sequence identity and belong to guanidino group-modifying enzyme superfamily (GMSF). The catalytic triad (Cys-His-Glu/Asp) is conserved in members of the GMSF. Both crystal structures of PaADI and MaADI show a characteristic 5-fold pseudosymmetrical barrel with ββαβ subunits. Table 2 summarizes the crystal structures of PaADI and MaADI.

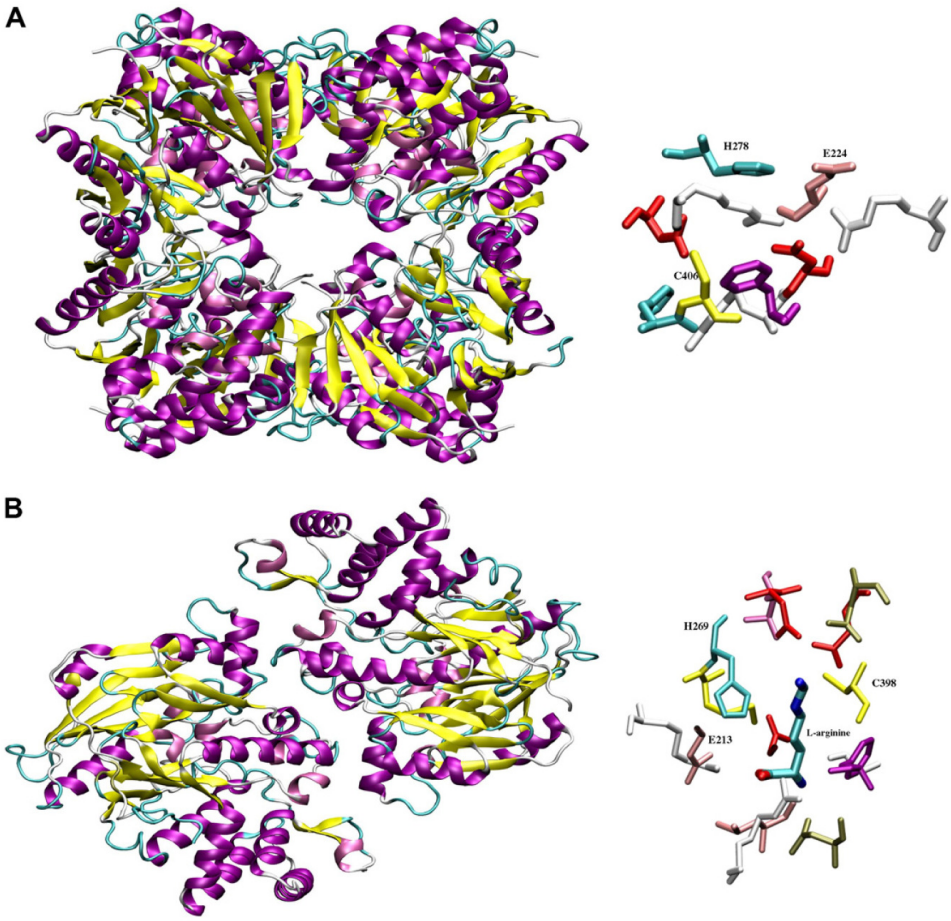

Figure 1. Structural of ADIs from *P. aeruginosa* and *M. arginini*. (A) PaADI (PDB ID: 1RXX) and stereo view of its catalytic triad (C406-H278-E224). (B) MaADI (PDB ID: 1S9R) and stereo view of its catalytic triad (C398-H269-E213) with substrate L-arginine (27).

Table 2. Crystal structures of ADI in protein data bank (PDB).

PDB code	Ligand in crystal structure	Description	Resolution (year)
2A9G	Arginine	Crystal structure of PaADI variant C406A in complex with L-arginine	2.30 Å (2005)
2AAF		Crystal structure of PaADI variant H278A forming a S-alkylthiouronium reaction intermediate	2.30 Å (2005)
2ABR		Crystal structure of PaADI variant D280A with L-arginine forming a S-alkylthiouronium reaction intermediate	2.9 Å (2005)
2ACI		Crystal structure of D166A arginine deiminase	2.50 Å (2005)
1S9R	Arginine	Crystal structure of MaADI covalently linker with a reaction in intermediate	1.60 Å (2004)
1LXY	Citrulline	Crystal Structure of MaADI covalently linked with L-citrulline	2.00 Å (2004)
1RXX		Crystal structure of MaADI	2.45 Å (2004)

MaADI was crystallized as a homodimer and its catalytic triad is formed by Cys398-His269-Glu213. MaADI has a catalytic domain and a five-helix bundle domain (Figure 3). The buried and compact substrate binding pocket is located approximately at the center of the molecule, from which a small solvent channel leads to the surface of the enzyme. The opening to the channel is located adjacent to the dimer interface region, which is at the opposite side of the 5-fold pseudosymmetric moiety of ADI. The shape and size of the channel does not permit transport of the substrate (L-arginine and end product (L-citrulline) in and out of the pocket. Substantial conformational changes in ADI are required to permit entry of the substrate and expulsion of the end product. The occurrence of "closed" and "open" form was suspected to be dependent on binding of substrate.

PaADI has a tetrametric structure with 1630 amino acid residues in total, which makes it the largest enzyme of its structural superfamily. The catalytic triad of PaADI is Cys406-His278-Glu224. Similar to MaADI, the active site of PaADI is

located in a narrow crevice formed by a network of charged residues. Ligand binding energy is derived from ion pair and hydrogen bonding interactions between active site residues and the guanidinium, carboxylate and ammonium groups of the substrate. The proposed substrate-binding model shows that the catalytic center contains abundant charged residues (e.g. Asp280, His405, Glu13 and Arg165). The ion pairing interactions between these residues contribute to the integrity and activity of ADI. In addition, Asp116, Asp227, Arg185, Arg401, His278, Glu118, and Glu224 are part of an extended charged network. The proposed catalytic mechanism suggests that the active site of PaADI is blocked by Arg401, and therefore a conformational transition is taking place upon the substrate binding. Based on the proposed reaction mechanism, Cys406 is as a key residue responsible for the nucleophilic attack on the guanidinium carbon atom of arginine. PaADI contains only one hydrophobic residue, Phe-163 and a Cys-406 with an unknown protonation state. The known functions of important residues are shown in Table 3, and the interactions between important residues and substrate arginine are shown in Figure 2.

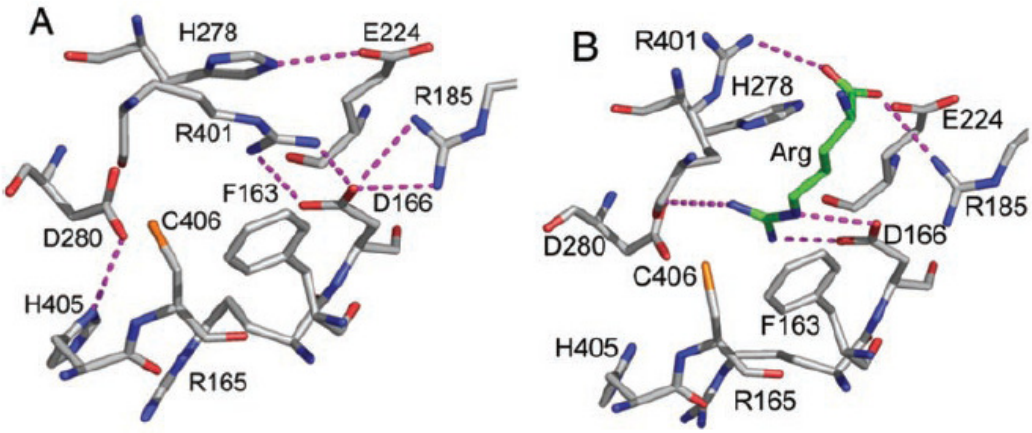

Figure 2. A. stereoscopic view of PaADI key active site residues. B. stereoscopic view of a modeled arginine substrate (green) docked in the active site of ADI. Atomic colors are red, oxygen; blue, nitrogen; yellow, sulfur; and gray, carbon. Ion pair interactions are shown as dashed lines (26).

Table 3. Residues important for catalytic function of PaADI (28, 29).	
Residues	Known/postulated function or comment
Cys406	Mounts the nucleophilic attack on the carbon atom of the guanidinium group of arginine
His278	Serves as a general base and activate the water molecule
Glu224	Modulate the ionization state of His278
Asp280	Interacts with the imidazole group of His405 F via the carboxylate group, which in turn interacts with Glu13. Invariant residue in all known ADIs
Asp280, Asp166	Fix the guanidinium group of the arginine substrate tightly by interactions with the carboxyl groups
Arg401, Arg185	Form ionic interaction with The carboxyl group of the arginine substrate
Phe163	Interacts with the hydrophobic part of arginine substrate
Glu13	Interacts His405 and is invariant in all known ADIs
His405	Sometimes is replaced by an arginine, as in the case of McADI. This may explain the low pH optimum of PaADI (5.6) in contrast to the neutral pH optimum of McADI, the enzyme that contains an arginine residue instead of His405
Arg165	Is fixed by electrostatic interactions with the main chain oxygen atoms of Thr408 and His405 and with the hydroxyl group of Thr-408
Arg401	Blocks the ADI active site via the side chain by forming an ion pair with the carboxyl group of Asp166 and occupies approximately the same position as the guanidinium group of an arginine substrate

The overall fold of MaADI and PaADI consist of five ββαβ modules in cyclical arrangement, generating a pseudo 5-fold symmetrical barrel and an additional 85-residue α-helical domain inserted between the first and the second ββαβ modules giving the typical “Clip-on-fan” moiety. The α-helical domain of PaADI mediates tetramer formation and the α-helical domain of MaADI was speculated to play a role in activating the series of reaction in arginine dehydrolysis pathway (4). Structural alignments by Chakrabarty et al. (18) demonstrated the unique 85 residue 5-α-helical bundle domain exhibiting structural similarity to the mammalian CARD (caspase recruitment domains)-containing proteins and this CARD-like domain is present only in the PaADI and MaADI but not in the other

GMSF members (Figure 3B). Furthermore, PaADI putative CARD-like domain induced apoptosis to cancer cells.

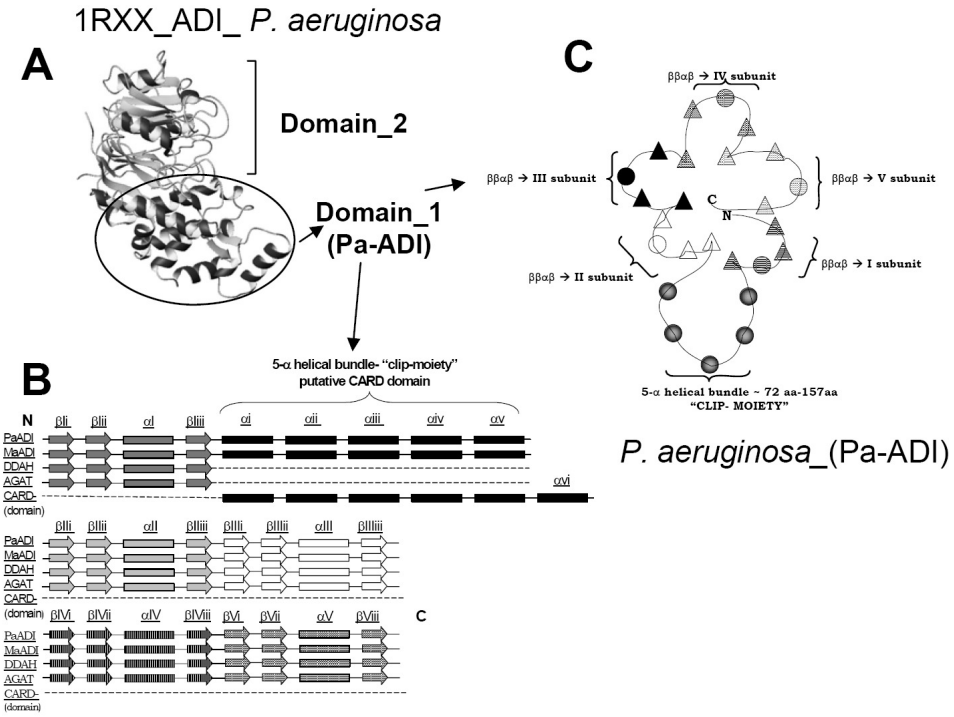

Figure 3. Structural characteristics of the PaADI. A. Ribbon drawing of PaADI (1RXX_A) highlighting the two domains. B. The presence of the CARD domain in PaADI and MaADI but its absence in other members of the GMSF (guanidino-group modifying superfamily) enzymes such as DDAH and AGAT, as shown from the structure-based sequence alignments. The CARD domain represents that of caspase-9. DDAH, dimethylarginine dimethylaminohydrolase; AGAT, arginine: glycine amidinotransferase. The β-strand and α-helices are shown as arrows and strips respectively. Roman numericals I to V are the five ββαβ subunits. The clip moiety (α-helical module) in Figure 3 is seen only in PaADI and MaADI which bears structural homology to the six-α-helical modules that form the CARD domain of the caspase-9 protein molecule. N, N-terminal; C, C-terminal. C. A schematic diagram showing the overall fold and topology of PaADI, as reported (18).

Comparison of substrate free and substrate bound structure of PaADI gives interesting insight into structure changes upon substrate binding (17). Pairwise superposition of the free wild-type PaADI (PDB code: 1rxx) and the mutant enzyme substrate complexes (PDB code: 2a9g) show that the overall fold of the structures remains similar, yet with some local changes. In particular, four loops (Figure 4) associated with the active site undergo conformational transitions not

related to crystal packing: loop 1 (residues 30-46), loop 2 (residues 178-185), loop 3 (residues 271-281, part of this loop is disordered in the apoADI structure), and loop 4 (residues 393-404). Residues adjacent to the substrate exhibit the most significant shifts. For example, the α-carbon atom of Leu41 (loop 1) shifts by 2.7Å and that of Arg185 (loop 2) by 1.8 Å; the α-carbon atom of His278 (loop 3) shifts by 0.9 Å and that of Gly400 (loop 4) by 4.4 Å. These are localized but mechanistically important conformational transitions that tighten the surrounding of the substrate. Simultaneously, substrate binding is accompanied by displacement of the side chain of Arg401 (loop 4) by more than 8 Å to enable access to the active site. The superposition of ADI and PAD4 ADI active site is shielded from the solvent by a long loop (residues 25-48 in PaADI) and the following two turns of α-helix (residues 49-56).

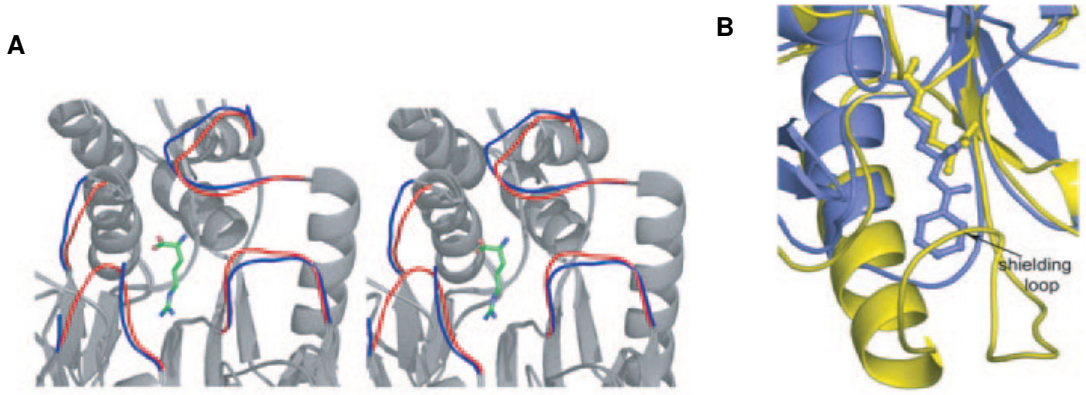

Figure 4 (A). Stereoscopic view of ADI in the unbound and bound states. Superposed molecules are colored gray where the trace of the polypeptide chain is similar in both structures. For regions exhibiting differences, loops of the apoADI structure are highlighted in blue, and loops of the ADI structure complexed with arginine are highlighted in red. 4(B). Structural relationship between ADI (yellow) and PAD4 (cyan) (17).

1.3 Catalytic reaction mechanism of ADI

The overall reaction catalyzed by ADI is the hydrolytic substitution of the ηNH_2 group from the guanidinium group Cζ of L-arginine, leading to citrulline and ammonia (Figure 5). Herzberg (17) and Arnold (4) proposed ADI catalysis mechanism for PaADI (Figure 5) and MaADI, respectively. Basically, both of the proposed mechanisms are composed of three main steps: 1) thiol group of

Cys406 mount a nucleophilic attack on the guanidinium group of arginine and a proton is transferred first to ηNH$_2$ group; 2) water molecule is activated by His278 and followed by attacking the covalent intermediate to replace and release NH$_3$; 3) the C-S covalent bond between enzyme and the resulting citrulline is cleaved and thus end product citrulline is released and free enzyme is generated for next catalytic cycle.

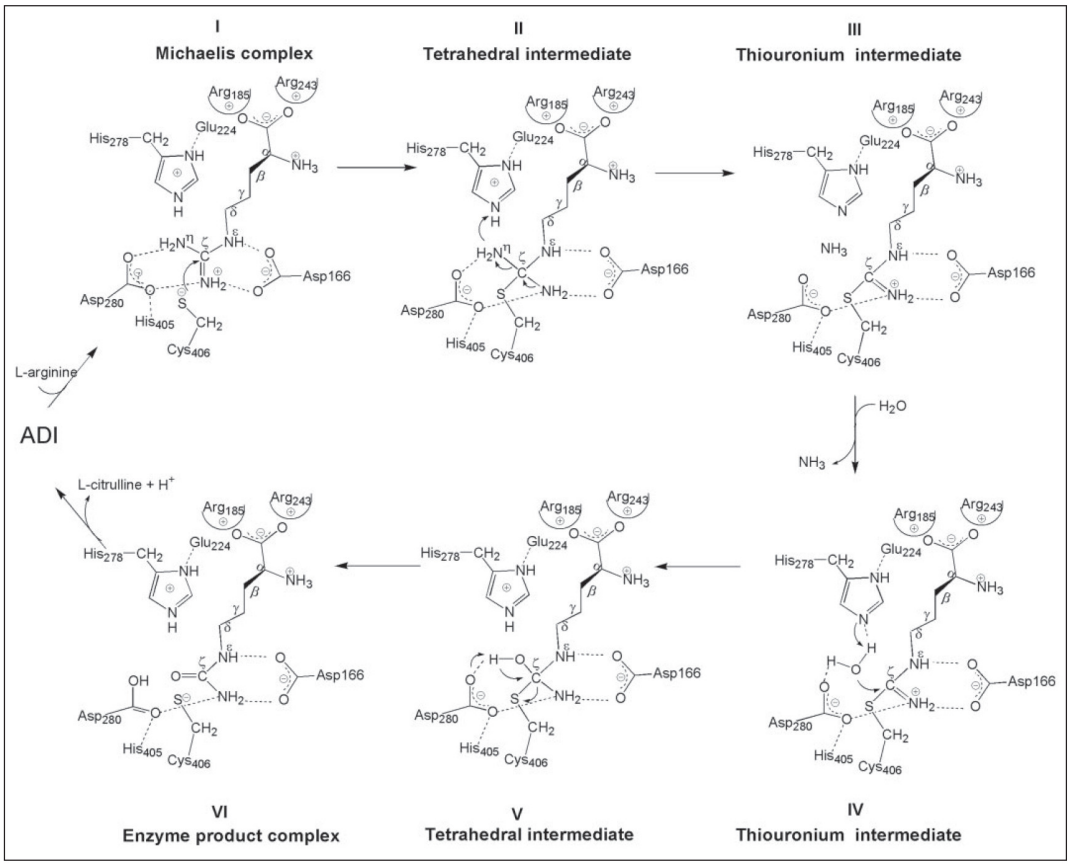

Figure 5. Mechanism of PaADI catalysis of arginine to citrulline and ammonia (17).

1.4 Anti-tumor application of ADI

Amino acids depletion is one type of targeted therapy for human cancers which are auxotrophic for a particular amino acid. Amino acids degrading enzymes, such as asparaginase (30), methioninase (31), arginase (32), arginine deiminase (27), phenylalanine ammonialyase (33) and tryptophanase (34) have been

studied for inhibition of tumor cells *in vitro*. The most representative anticancer enzyme is asparaginase, which is particularly effective in acute lymphoblastic leukaemia. PEG asparaginase is commercialized for acute lymphoblastic leukaemia treatment (Oncaspar®, pegaspargase) (35). However, asparaginase treatment is sometimes accompanied by serous side-effects including anaphylactic shock, coagulapathies as well as liver and pancreatic toxicity (36).

Arginine is an important amino acid involved in the synthesis of a wide range of peptides and proteins, production of creatine and nitric oxide, and a myriad of metabolic pathways and cellular events. It is a precursor of proline, polyamines, glutamine, glutamate, and other neurotransmitters, such as g-aminobutyric acid and also serves as a substrate for two important enzymes, arginase and nitric oxide synthetase (37). Arginine is an indispensable amino acid to children but a semi-essential amino acid in adult humans since many adult somatic cells can synthesize it from citrulline in two steps via urea cycles (Figure 6). The enzyme argininosuccinate synthetase (ASS) catalyzes the conversion of citrulline and aspartic acid to argininosuccinate which is then further converted to arginine and fumaric acid by argininosuccinate lyase (ASL). Arginine can be degraded to ornithine by the urea cycle enzyme arginase. Ornithine is then converted back to citrulline by ornithine carbamoyl transferase (OTC) and then recycles back to arginine from citrulline by ASS/ASL. Thus, the ability to regenerate arginine from citrulline depends on the amount/activity of ASS and ASL, which are tightly coupled. The sensitivity of cells to arginine deprivation depends on the ability of ASS and ASL to regenerate arginine from the alternative intermediate (ornithine, citrulline and argininosuccinate) in the urea cycle.

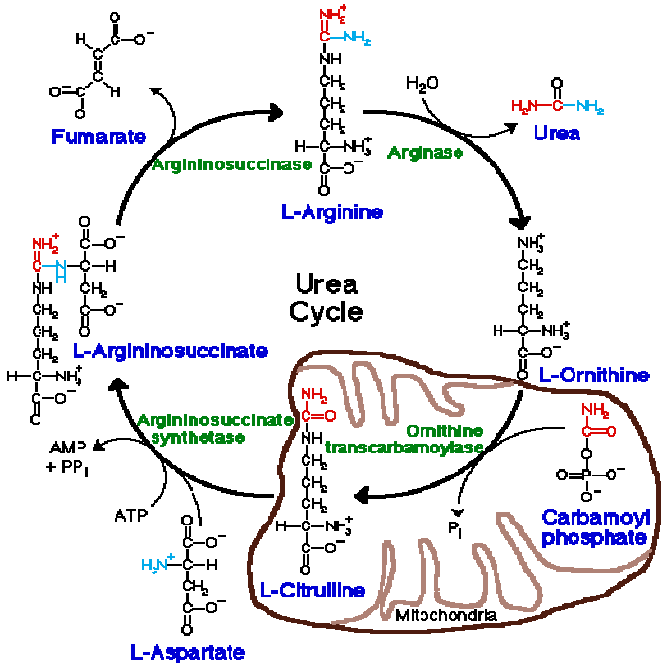

Firgure 6. Urea cycle. Argininosuccinate synthetase (ASS) catalyzes the conversion of citrulline and aspartic acid to argininosuccinate which is then further converted to arginine and fumaric acid by argininosuccinate lyase (ASL). Arginine can be degraded to ornithine by the urea cycle enzyme arginase. Ornithine is then converted back to citrulline by ornithine carbamoyl transferase (OTC) and then recycles back to arginine from citrulline by ASS/ASL.

Arginine begins to become limiting at ~10^{-4} M, whereas other amino acids can sustain growth at 10^{-5}-10^{-6} M. Wheatley et al. showed that most tumour cell lines die considerably more quickly during arginine deprivation than in the absence of any other single (or group of) essential amino acids (38). Since 1930 for the first time arginine known is essential for the growth of some forms of cancer, the potential of arginine degrading enzymes as therapeutic agents was recognized, investigated and employed for arginine auxotrophic tumor treatments. Enzymes capable of depleting arginine *in vitro* include arginase existing in human liver, arginine decarboxylase from bacterial, plant and human, and ADI from microorganism.

Arginine decarboxylase converts arginine to agmatine, which is toxic at high plasma concentration. Furthermore, arginine decarboxylase has a short half-life and it loses virtually all enzymatic activities upon pegylation though pegylation of

arginine decarboxylase is inefficient because not enough lysine residues for polyethylene glycol to attach (39).

Arginase is limited for anti-tumor application because of its low substrate affinity (K_m value 2-4 mM; plasma arginine 100-120 μM), short circulatory half-life (10-15 min) and sub-optimal enzymatic activity at physiological pH (alkaline pH optimum, pH 9.3)(40). Despite these disadvantages of arginase, Lam et al. reported remission of hepatocellular carcinoma induced by systemic release of endogenous hepatic arginase (41) and Leung et al. proved pegylated recombinant human arginase (rhArg-peg 5,000mw) can inhibit ASS-positive HCCs while ADI can not (42).

In addition, ADI, another arginine-degrading microbial enzyme, has various biological activities including anti-proliferation, anti-angiogenesis and inhibition of inducible nitric oxide synthase (iNOs). Figure 7 summarizes how ADI affect many arginine-related cellular functions. ADIs (Table 1) have been shown to have strong *in vitro* and *in vivo* inhibition for arginine auxotrophic tumors (e.g. hepatocellular carcinomas (HCCs), melanomas, retinoblastoma (43), prostate cancer(44)) and ADI from *M. hominis* (MhADI) is currently under clinical trial for HCC (phase II) (45) and melanomas (phase I/II) (46). Studies on human lymphatic leukemia cell lines confirmed ADI's anti-angiogenic activity. Among all the ADIs, MhADI and MaADI were studied most intensively (Table 1).

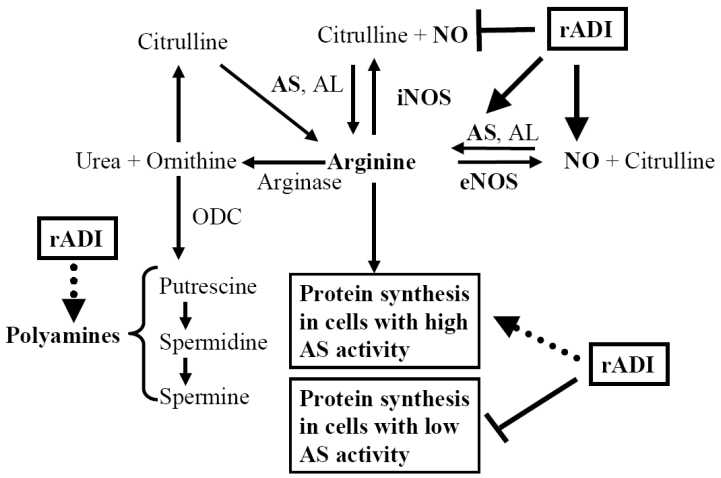

Firgure 7. Summary of ADI effects on arginine-related cellular functions. rADI inhibits NO production via iNOS, but potentiates NO production via eNOS in the cultured endothelial cell model. rADI enhances or inhibits AS activity in different cells. rADI inhibits de novo protein synthesis in cells with low AS activity, but not in cells with high AS activity. Polyamine synthesis was not significantly affected by rADI, even in cells with low AS activity. Arrow representation: solid, potentiates; blocked, inhibits; dotted, no effect (47).

In 1999, US Food and Drug Administration (FDA) designated ADI-PEG-20 orphan drug status for treating HCC and invasive malignant melanomas. In 2005, also the European Agency for the Evaluation of Medicinal Products (EMEA) also granted ADI-PEG-20 orphan drug status for HCC. Phase II trials of ADI-PEG-20 in patients with metastatic hepatocellular carcinomas have shown that the drug is safe, well tolerated, and may benefit patients with unresectable HCC. Izzo and coworker suspected that combination therapies of arginine deprivation and growth inhibition via kinase inhibitors might improve the survival rate further. Additionally, ADI enhances radio sensitivity of human mammary adenocarcinoma (MCF-7 cells) (48), exerts anti-proliferative as well as anti-angiogenic activities and inhibits the growth of viruses such as HIV-1 and hepatitis (49, 50). Current research efforts are focused on ADI's *in vivo* inhibitory effect towards leukemia, melanoma, prostate cancer, renal cell carcinoma, and human umbilical vein endothelial cells (HUVEC) (19, 44, 51-53), clinical trials for HCC (phase II) (45) and melanoma (phase I/II) (46), and tumor inhibitory mechanisms of ADI (54).

The effectiveness of ADIs as anti-tumor agent depends on their enzymatic properties (such as K_m, k_{cat}, optimum pH, stability at neutral pH), selectivity on tumor cells, stability in blood circulation and immunogenicity. Pegylation (35) has been effective in reducing their immunogenicity in animal and increase their stability to various hydrolytic enzymes in plasma. Directed evolution as powerful algorithm to design proteins allows improving all properties that can be reflected in a screening system through iterative rounds of diversity generation and screening. Small libraries of a few thousand variants are often sufficient to find improved variants (55) even without rational understanding of the targeted property. The first example of directed ADI evolution by our group (3) provides a simple and effective screening system to improve activity of PpADI at physiological pH.

1.5 Conclusion

ADI-based arginine deprivation is a novel and promising targeted approach to the treatment arginine auxotrophic tumors, in particular, melanoma, hepatocellular carcinoma and leukemia. Certain mesotheliomas and renal cell cancers were also proved to be sensitive to ADI therapy. Due to its low incidence of major side effects (myelosuppression and gastrointestinal toxicity or other major organ toxicity) arginine deprivation treatment should be combined with other anticancer treatments to increase the response rate. Reengineering of ADI by protein engineering is a promising strayegy to tailor ADI properties for demands in medical applications. Solved ADI crystal structure enables to understand structure function relationships and to guide protein engineering.

Directed evolution

2.1 Introduction to directed evolution

Enzymes are increasingly being used in the generation of products that are traditionally made using chemical synthesis and the field continues to expand its horizons, particularly as applied to the synthesis of the fine chemicals and pharmaceuticals (56, 57). Naturally occurring enzymes are often not designed for the applications of interest, since after all they are evolved in nature for a purpose other than being the catalysts of industrial processes. Directed evolution, rational design and biodiversity screening and combined approches are the main strategies to reengineer enzymes for addressing application demands. Directed evolution has emerged as a powerful enabling method for improving enzyme properties in iterative cycles of diversity generation and screening (Figure 1).

A main advantage of directed evolution compared to rational design is that it does not require structural or mechanistic information for protein optimization. Directed protein evolution has been successfully used for altering and improving protein properties (solubility, expression, enantioselectivity, stability and activity in unusual environment, allosteric interactions, tolerance to pH), as well as for regulating other molecules and systems, including RNA, DNA regulatory elements, biosynthetic pathways and genetic regulatory circuits (58-60).

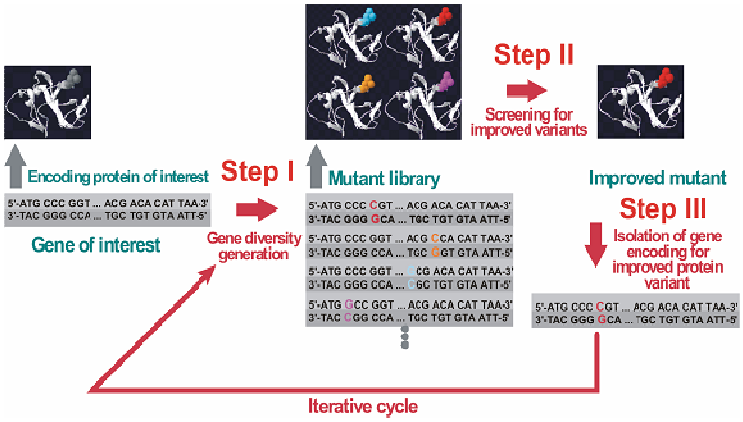

Figure 1. Procedure of a directed evolution experiment. It involves three key steps: 1) selection a good starting sequence and mutating the parent to create a library of variants; 2) identification variants with improved function and 3) isolation of gene encoding for improved variant and repeating the process until the desired function is achieved.

A parent sequence (or sequences) is chosen based on its perceived proximity to the desired function and its evolvability (the ability of a protein to adapt in response to mutation and selective pressure). A parent protein for directed evolution should exhibit enough of the desired function that small improvements can be reliably discerned in a high-throughput screen.

Variants library should be generated with high probability of finding improved variants given the screening capacity. With a high-throughput screening method, a library can be constructed to generate the large potential improvement. Arnold and coworkers(61) showed that very low mutation rates result in many functional sequences but only a small number are unique sequences, however very high mutation rates produce diverse sequences but few retain function. Schwaneberg and coworkers(62) reviewed random mutagenesis methods, focused library generation methods and computational tools for high-quality mutant libraries generation. Schwaneberg and coworkers (63) also summarized criteria for an ideal mutagenesis methods: unbiased mutational spectrum, controllable mutation frequency, consecutive nucleotide substitutions or codon-based substitutions, enable subset mutagenesis (e.g. introduction mainly positively or negatively charged amino acid), independent of gene length, technically simple and reproducible, and economical.

Screening is used to identify library members improved in the targeted property. Identification of improved variants though selection or screening is “analogous” to evolutionary pressure in natural evolution (i.e. only the fittest survive). As the word “directed” in directed evolution implies, laboratory evolutionary pressure is defined and applied by the researcher in screening system. Gradually increasing the selection pressure or evolving against a series of intermediate challenges often accumulates useful single mutations and yields desired variants (64).

Traditional methods for screening employ microtiter plate formats (96-well, 384-well, 1,536-well (65) and even 1,000,000-well (66)) or solid phase assay (agar plate, filter paper and nitrocellulose membrane), which typically enable the screening of no more than 10^6 variants by using robotic automation (67). Sometimes, fast and universal analytic methods like HPLC (68) or GC-MS (69) are utilized for performing an efficient screen of a non-natural substrate. However, the number of screened mutants is limited to 10^4-10^6. In recent years flow cytometry systems (67, 70, 71) have become increasingly attractive, especially after the development of emulsion technology offering compartmentalization and high throughput up to 10^7/h. In addition, Weitz and coworkers (72) recently reported a promising ultrahigh-throughput screening in drop-based microfluidics, by which one can screen a library of 10^8 in about 10 h. Dijkhuizen et al. compared in a review (73) six kinds of library screening strategies (Figure 2). Selection techniques rely on a direct link between cell growth and improved or acquired enzyme function and therefore it is limited to engineering detoxifying enzymes (e.g. b-lactamase) or enzymes that synthesize essential nutrients for cell growth and survival. The traditional microtiter plate screenings are medium-throughput and the most simplistic format of screening. It involves the incubation of colonies with the substrate of targeted enzyme. The crucial factor with this screening technique is that substrate conversion creates a visual signal, such as fluorescence or color, to identify colonies expressing an enzyme with desirable properties. Microtiter plate based screenings are the most commonly applied method in identifying desirable enzyme variants. Microtiter plate based

screenings enable the use of various analytical tools and in the mean while they offer a great dynamic range. Their screening capacity is usually limited to less than 10^4 variants per day. Screening based on microfluidic device and sorting device is a new screening platform for directed evolution, which offers ultra-high-throughput. It allows the discriminate between wild-type and a less active mutant and allows for the addition of substrates and quenchers at desired time thus extending the scope of directed evolution screening strategies. Cell as micro-rector, cell surface display and *in vitro* compartmentalization technology are also FACS (fluorescence-activated cell sorting system) dependent methods for high-throughput screening and allow 10^9-10^{10} screening capacity.

Once improved enzymes are identified, encoding genes are isolated and subjected to further iterative cycles of mutation and screening in order to accumulate beneficial mutations until the targeted improvement is hopefully achieved. The number of iterations required depends on the starting point, the protein fold and the selected properties which determine the possible mutational load and achievable improvement.

Four accepted requirements for successful directed evolution (http://www.che.caltech.edu/groups/fha/) are, 1) the desired function must be physically possible; 2) the function must also be biologically, or evolutionarily, feasible. In practice, this means that there exists a mutational pathway to get from here to there through ever-improving variants (see above). A good experiment will maximize the likelihood; 3) Suitable host (*E. coli* or *S. cerevisiae*) which allows functional expression of more than 10^6 variants per µg of DNA. 4) A rapid screen or selection that reflects the desired function. How rapid the screen must be depends on how rare mutations leading to the desired property are and how many must be accumulated to achieve the desired result.

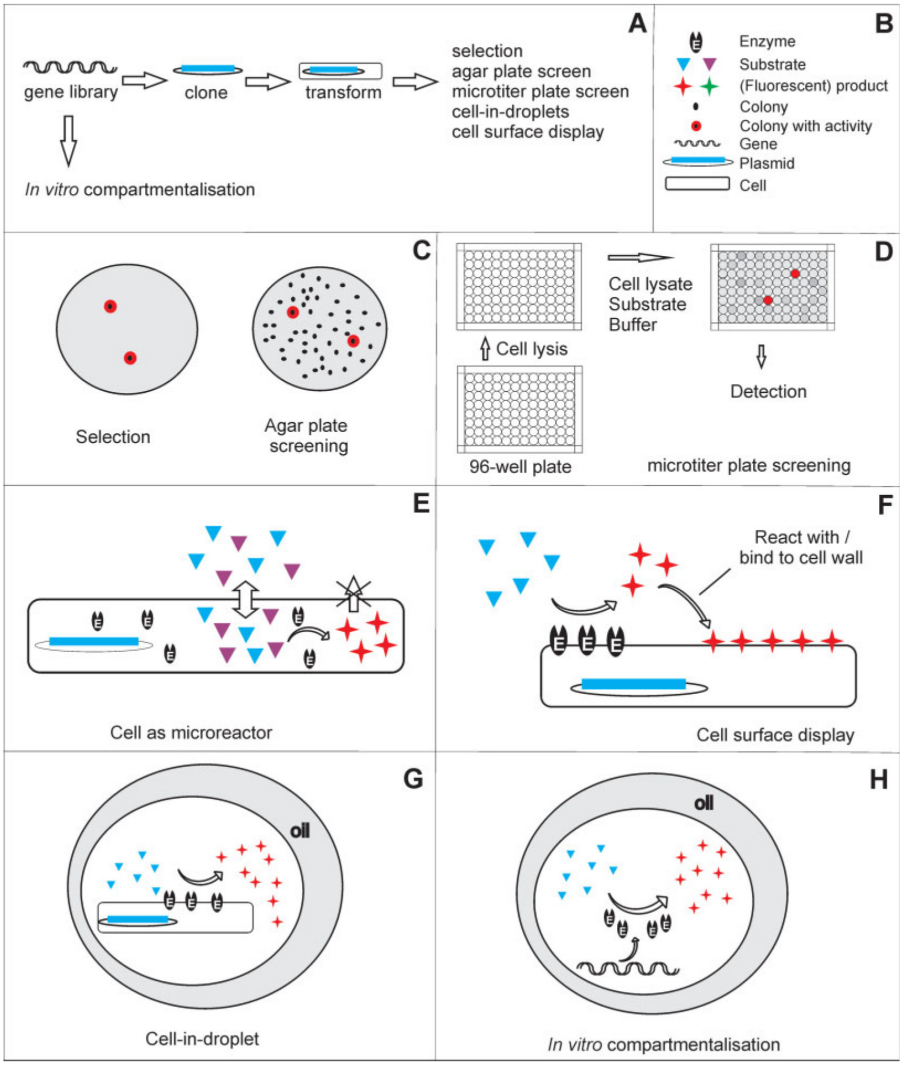

Comparison of screening and selection technologies

Strategy	Library size	Advantage	Disadvantage
Selection	$\sim 10^9$	Yields desirable variants only	Only possible if activity gives growth advantage
Agar plate screen	$\sim 10^5$	Simple to operate	Limited dynamic range
Microtiter plate screen	$\sim 10^4$	All analytical methods possible Excellent dynamic range	Relatively low screening capacity
Cell-in-droplet screen	$\sim 10^9$	Large libraries	Fluorescence detection and DNA modifying enzymes only
Cell as microreactor	$\sim 10^9$	Large libraries	Fluorescence detection only
Cell surface display	$\sim 10^9$	Large libraries	Fluorescence detection only
In vitro compartmentalization	$\sim 10^{10}$	No cloning steps Large libraries	Fluorescence detection and DNA modifying enzymes only

Figure 2. Overview of screening technologies. (A) Experimental steps from obtaining the gene library as PCR product to the actual screen. Note that cloning and transformation efficiency are often limiting library size; (B) Explanation of symbols; (C) Cell growth/survival selection and agar plate screening; (D) Microtiter plate screening; (E) Cell as micro-reactor; (F) Cell surface display; (G) Cell-in-droplet; and (H) *In vitro* compartmentalization (73).

2.2 Directed enzyme evolution for pH tolerance of enzymes

Application of enzymes in processes at a specified pH necessitates protein engineering to change their pH performance. Directed evolution and rational design method were applied to improve enzyme specific activity at certain pH or shift their pH profiles. Some representative success stories of directed protein evolution improving pH performance are summarized in Table 1.

Table 1. Improvement obtained from directed evolution or rational design for pH performance.

Enzymes	Mutagenesis methods	Screening methods	Improvements	References
Human β-glucuronidase	EpPCR and saturation mutagenesis	Flow cytometry	60-fold more active (k_{cat}/K_m) at pH 7.0 and were up to an order of magnitude more effective at catalyzing the conversion of two structurally disparate glucuronide prodrugs to anticancer agents	2008 (74)
Bacterial xylanase	DNA shuffling	Agar plate assay	About 5-fold improvement of specific activity at pH 9.0	2008 (75)
Human pancreatic lipase	EpPCR	Agar plate and microtiter plate assay	1.5-fold of activity improvement at acidic pH	2010 (76)
Bacterial arginine deiminase	EpPCR and site directed mutagenesis	Microtiter plate assay	pH optimum shifted from pH 6.5 to pH 7; 4-fold of activity improvement at pH 7.4	2010 (3)
Bacterial α-amylase	EpPCR	Microtiter plate assay	5-fold higher activity at pH 10 than wild type	2003 (77)
Eukaryote D-pantonohydrolase	EpPCR and DNA shuffling	Agar plate assay	10.5-fold higher specific activity and retain 85% of its original activity after incubation under low pH	2006 (78)
Vanadium chloroperoxidase	EpPCR, site saturation mutagenesis and site directed mutagenesis	Microtiter plate assay	About 100-fold improvement of specific activity at pH 8	2006 (79)
Bacterial class-A non-specific acid phosphatase (PhoN)	Site directed mutagenesis		1.6-fold of activity improvement over broder pH range	2006 (80)
Aspergillus niger PhyA phytase	Site directed mutagenesis		pH shifted from 5.5 to 3.8 (1.7 unit); 2.66 -fold improvement of activity at pH 3.5 than wild type.	2006 (81)
Bacillus cereus β-amylase	Site directed mutagenesis		pH optimum shifted to pH 4.2-4.8 by 2 pH units.	2004 (82)
Phytase	Site directed mutagenesis		pH optimum shifted by 0.5-1 pH unit; a slight increase in maximum specific activity	2002 (83)
Alcohol dehydrogenase	Site directed mutagenesis		pH optimum shifted from 7.8 to 9.0; about 2-fold improvement of maximum activity at pH 9.0 than that of wild type	1991 (84)

Many examples of rational reengineering of an enzyme pH optimum exist (Table 1). For shifting the pH optimum, a deep understanding of molecular dynamics is essential part of understanding enzyme flexibility. Rational design method successfully shifted enzyme pH profile. pH dependence of an enzyme is determined by the ionization of the catalytic groups, which is affected by various interactions involved in their microenvironments. In order to catalyze certain reactions, ionizable residues in active site should act as nucleophile or acid/base catalyst and they need to maintain proper ionization state for proper activities of proteins. The p*K*a value of the proton donor and the catalytic nucleophilic residue are therefore limiting the pH range at which the enzyme can function, and therefore pH-dependent activity can be differed by the p*K*a of the key residues. The p*K*a value of the residue is governed by intrinsic acidity of the functional group and other factors (electrostatic interaction from neighboring and the heterogeneous dielectric environment in the protein solution system). The electrostatic potential generated by the charged titratable residues affects the ground state of the protein, such as stability, binding to ligands and p*K*a values of ionizable groups. The electrostatic potential of proteins can be calculated by using computational procedures (Delphi, UHBD, CHARMM) and can be increased or decreased through mutations. For shifting the pH optimum of enzymes, many researchers have tried to substitute catalytic residue by site-directed mutagenesis (Table 1).

Yoo and coworkers (85) analyzed the relation between the shift of pH optimum and change in electrostatic potential due to mutation using Delphi. They identified key residues of xylanase responsible for electrostatic potential of catalytic residues but not affecting the catalysis directly. The latter hypothesis was proven by site directed mutagenesis in a later report. Wyss and coworkers (83) summarized strategies for enzyme pH profile modification, 1) replacement of ionizable groups that are directly involved in substrate or product binding and/or catalysis by nonionizable ones or by amino acids with different charge or p*K*a values; 2) replacement of residues that are in direct contact with residues

mentioned in 1) by forming hydrogen bonds and/or salt bridges; 3) alteration of longer-range (indirect) charge-charge interactions by modification of the surface charge of the enzyme.

When there is no structure-function relationship information available for an enzyme, directed evolution is the best option to tailor the pH performance of enzyme for application demands (Table 1). Directed evolution allows improving all properties that can be reflected in a screening system through iterative rounds of diversity generation and screening. Small libraries of a few thousand variants are often sufficient to find improved muteins even without rational understanding of the targeted property (76, 86). Using MTP assay, epPCR mutant libraries with a ratio of 50 % active and 50 % inactive clones have often been used successfully in directed evolution, improving enzyme properties by gradual changes (one or two amino acids changes per round of mutagenesis and screening).

2.3 Directed enzyme evolution for medical application

Directed evolution has been very useful for improving enzymes for industrial needs. In recent years, there is also growing number of enzymes applied for therapeutic purpose. For the development of protein therapeutics, directed evolution started to be used to tailor enzyme properties in medical field, for example drug delivery (87, 88) and has proven to be a useful tool for generating protein variants with enhanced therapeutic potential (88), for example, improving the effectiveness of therapeutic enzymes, antibodies, vaccines and viruses. Here, the improvements of therapeutic protein for anti-tumor application by directed evolution are discussed in more details.

2.3.1 Prodrug enzymes for tumor chemotherapy

Prodrug cancer chemotherapy has attracted considerable interest due to the possibilities it provids to overcome various barriers to drug formulation and delivery (such as poor aqueous solubility, chemical instability, insufficient oral

adsorption, rapid pre-systemic metabolism, inadequate brain penetration, toxicity and local irritation) (89). Examples of such drugs currently in use in cancer treatment include 5-fluorocytosine, cyclophosphamide, capecitabine, mitomycin C, and AQ4N (90). However, the side effects of prodrug therapy remain a serious concern which arises from the fact that noncancerous cells also possess the capacity to degrade them. This has triggered the interest to generate more effective prodrug-activating enzymes so that prodrugs can kill tumor cells at concentrations that generate little or no side effects. Further goals are to design more powerful and tumor-specific drugs, and to devise more effective methods for delivering them specifically to tumors.

By applying directed evolution through the technique of error-prone PCR, Martin and coworkers (90) indentified YieF variant exhibiting >5-fold increased capacity to kill HeLa cells. Furthermore, YieF variant was proved to be effectively delivered to tumor cells using a strain of *Salmonella typhimurium* (SL 7838).

Human β-glucuronidase, due to low intrinsic immunogenicity in humans, is an attractive enzyme for tumor-specific prodrug activation. However its utility is limited by low activity at physiological pH. Roffler and coworkers (74) developed a high-throughput screening procedure for enzymatic activity based on the stable retention of fluorescent reaction product in mammalian cells expressing properly folded glycoproteins on their surface. This procedure was utilized to screen error-prone PCR and saturation mutagenesis libraries to isolate β-glucuronidase tetramers that were up to 60-fold more active (k_{cat}/K_m) at pH 7.0 and were up to one order of magnitude more effective at catalyzing the conversion of two structurally disparate glucuronide prodrugs to anticancer agents.

2.3.2 Oncolytic viruses for tumor chemotherapy

Viral-mediated oncolysis is a novel cancer therapeutic approach with the potential to be more effective and less toxic than current therapies due to the agents' selective growth and amplification in tumor cells. To date, these agents

have been regarded as highly safe in patients but have generally fallen short of their expected therapeutic value as monotherapies.

Consequently, new approaches to generate highly potent oncolytic viruses are required. For the latter purpose, Hermiston and coworkers (91) developed a new method and termed it also ‘‘Directed Evolution’’ for creating highly potent oncolytic viruses. Viral serotypes representing Ad subgroups B-F were pooled and passaged twice on sub-confluent cultures of the target tumor cell lines at a particle-per-cell ratio of approximately 200 to invite recombination between serotypes (Figure 3). Supernatants from the second round of the high viral particle-per-cell infection of sub-confluent cultures were then used in a 10-fold dilution series to infect confluent T-75 tissue culture flasks of target tumor cell lines PC-3, HT-29, Panc-1 and MDA-231. Using this ‘‘Directed Evolution’’ methodology, the novel generated chimeric oncolytic virus ColoAd1 demonstrated ~ 2 log increase in both potency and selectivity when compared to ONYX-015 on colon cancer cells. *In vivo* and *ex vivo* studies therefore validated the innovative general approach for deriving clinically-relevant and potent anti-cancer virotherapies.

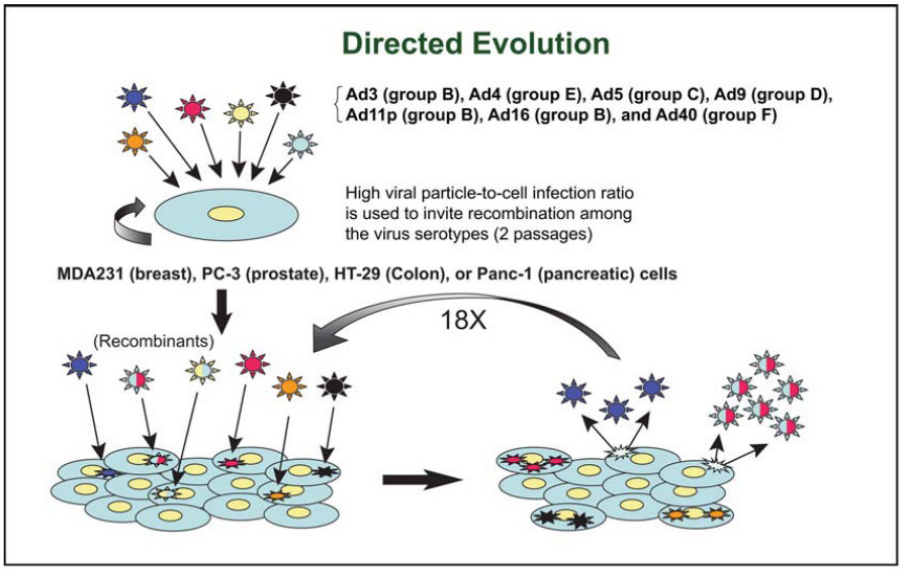

Figure 3. Hermiston’s “Directed Evolution” process of viruses and derivative viral pools (91).

2.3.3 Amino acid depriving enzyme for anti-tumor applications

Naturally available enzymes are usually not optimally suited for therapeutic purposes. This incompatibility often relates to the stability or activity of the enzymes under body conditions.

Despite many successful efforts to broaden the understanding of the structural basis of protein stability, there is still no universal strategy to stabilize protein by a limited number of rationally designed mutations. Well-known and reasonably successful types of rational engineering work include substitutions that increase rigidity (e.g. substitute amino acid Xxx with Pro or substitute Gly with other amino acid Xxx or the introduction of disulfides). These substitutions have effects on the entropy of the unfolded state, improvement of molecular packing (e.g. shortening of loops, improvement of interactions in the hydrophobic core, for example, by the removal of internal cavities), modification of surface charge networks or reinforcement of a higher oligomerization state.

Directed evolution provides a powerful approach for improving thermostability and does not need understanding of structure-function relationship. Most strategies for screening for enzyme stability rely on measuring residual enzyme activity before and after exposure to a denaturing challenge (e.g. high temperature, organic solvents, extreme pH) (92).

Bacterial L-asparaginases have been used as therapeutic agents in the treatment of lymphoblastic leukaemia. The main restrictions to the therapeutic use of L-asparaginase include its premature inactivation. As a result frequent injections are required to maintain therapeutic levels. Repeated injections and high dose can cause several types of side reactions from mild allergies and the development of immune responses to dangerous anaphylactic shocks (93). Enhancing the stability of L-asparaginase by protein engineering improves its body-residence time, and thereby minimizes immunosuppressive effects by lowering the therapeutic dose. Labrou and coworkers (94) obtained a

reengineered L-asparaginase with enhanced thermal stability. Single mutation on the surface of the protein resulted in ~10 degree increased T_m value (half-inactivation temperature). The thermostable variant has to be tested further on animals and/or humans in order to be advanced to a potent therapeutic drug.

Another example of a reengineered amino acid-deprivating enzyme is PpADI. PpADI is a promising anti-tumor enzyme however with a non-physiological optimal pH and relative high K_m value which hindering its medical application. By directed evolution and site saturation mutagenesis, PpADI variants with higher activity at physiological pH and at low arginine concentration of were obtained with improved properties to become a potent anti-tumor drug (see chapter 3 and chapter 4). *In vitro* and *in vivo* test of the improved variants are required to evaluate the anti-tumor effectiveness.

2.3.4 Affibody molecules for cancer prognosis

Affibody molecules represent a new class of affinity proteins that are based on the Z-domain scaffold derived from staphylococcal protein A (95). Among the scaffold proteins, Affibody molecules constitute the smallest non-cysteine-containing protein scaffold. The small size (~ 7 kDa), robust structure, and straightforward production procedures (either by recombinant production in bacteria or by chemical synthesis) make Affibody molecules attractive targeting agents for *in vivo* radionuclide imaging (96) as well as for various biotechnological applications (97, 98). The small size offers a convenient affinity maturation principle. Gene synthesis allows randomizing the whole gene to generate diverse mutant library. The potential use of radiolabeled Affibody molecules for high-contrast radionuclide imaging of biomarkers has been demonstrated in preclinical studies and in pilot clinical studies. Affibody molecules are non-immunoglobulin-derived affinity proteins based on a three-helical bundle protein domain.

Several of affinity proteins have been investigated for both *in vivo* diagnostics and therapy of tumor in radionuclide molecular imaging. Affinity proteins in tumor-targeted therapy can affect tumor progression by altering signal transduction or by delivering a payload of toxin, drug or radionuclide. EGFR (epidermal growth factor receptor), one of the receptor in ErbB family, has been extensively studied as biomarkers in tumor targeting and over expressed in various malignancies, associated with poor patient prognosis and are therefore interesting targets for solid tumors. High affinity and especially slow dissociation rate are important for obtaining high contrast images. Affinity in the low nanomolar range is considered as a prerequisite for successful use of peptide-based tracers.

Ståhl and coworkers (99) described the affinity maturation procedure for the generation of Affibody molecules binding with high affinity and specificity to EGFR. The library for affinity maturation was constructed using a single oligonucleotide for the rerandomization of desired positions. The new binders were selected with phage display technology and the best second-generation binders were characterized *in vitro* using real-time biospecific interaction analysis (BIA) for their binding to recombinant EGFR and with flow cytometry for their binding to native EGFR. Second-generation binders achieved an approximately 30-fold improvement in affinity (K_d = 5-10 nM) for the soluble extracellular domain of EGFR in biospecific interaction analysis using Biacore.

2.3.5 Interferon for anti-tumor applicaiton

Alpha interferons (IFN-as) are members of the diverse helical-bundle superfamily of cytokine genes, which have potent antiviral and antiproliferative activities and therefore can be used as anticancer and antiviral agents. However, doselimiting toxicity, receptor cross-reactivity, and short serum half-lives significantly reduce the clinical use of many of these cytokines.

Patten and coworkers (100) performed a family shuffling experiment with over 20 human interferon-α (Hu-IFN-α) genes. Antiviral assay and proliferation assay

were used to indentify clones with improved activity on Hu-IFN-α receptor. One clone showed 285,000-fold improved activity relative to Hu-IFN-α2a and 185-fold relative to Hu-IFN-α1 (most active native human interferon).

Selective breeding using DNA shuffling has proved to be very effective method to rapidly improve pharmaceutical proteins by which initially have low levels of the desired “activity” (101, 102). Backcrossing of evolved recommbinants with the wild type genes removes functionally neutral changes, which might reduce the immunogenicity of evolved proteins (103).

2.4 Conclusion

Proteins, especially enzymes, have gained a central role in modern chemical, biotechnological, and biopharmaceutical industries. Directed evolution has over the past proved to be a versatile and successful approach for tailoring protein properties to industrial, agricultural and medical demands and for advancing our understanding of structure-function relationships in biocatalysts. Appropriate library generation and screening methods should be employed concerning the target protein and desired property. To set up a sophisticated screening method, complex conditions in human body (pH, ion concentration, proteases, hormones etc.) should be considered. Subsequent *in vivo* or *in vitro* test of improved variants should be carried out to further validate the screening assay. Development of diversity generation and high-throughput screening method will enable evolution to solve problems efficiently. Especially, directed evolution provides a powerful strategy to rapidly advance the development of improved protein-based drugs (enzymes and antibodies, peptide and ligands). Directed evolution promises to play an increasingly important role to generate “desirable” drugs.

Chapter 3. Directed evolution of Arginine deiminase for increased activity at physiological pH

3. 1 Abstract

Arginine deiminase (ADI; EC 3.5.3.6) has been studied as a potential anti-tumor drug for the treatment of arginine-auxotrophic tumors, such as hepatocellular carcinomas (HCCs) and melanomas. Studies with human lymphatic leukemia cell lines confirmed that ADI is a potential anti-angiogenic agent effective in the treatment of leukemia. ADI from *Pseudomonas plecoglossicida* (PpADI) was cloned and expressed in *E.coli*. A main limitation of PpADI lies in its pH-dependent activity profile with a pH optimum at 6.5. A pH shift from 6.5 to 7.5 results in ~80 % activity drop (pH of human plasma is 7.35 to 7.45). For shifting PpADI pH optimum to netrual pH, a directed evolution protocol based on an adapted citrulline screening protocol in microtiter plate (MTP) format was developed and validated. Proof of concept for ADI engineering resulted in a pH optimum of pH 7.0 and increased activity under physiological conditions: at pH 7.4, variant M2 (K5T, D44E and H404R) is 4-fold more active than the wild type PpADI and retains ~30 % of its activity relative to its pH optimum, compared to ~10 % in the case of the wild type PpADI.

3.2 Introduction

Arginine deiminase (ADI) is a potential cancer therapy agent for the treatment of arginine-auxotrophic tumors (e.g. hepatocellular carcinomas and melanomas). The hepatocellular carcinoma (HCC) accounts annually for approximately 1 million new cases worldwide. In the US the incidence rate (per 100,000 persons; 1992-2002) of HCC is 8.6 with a mortality rate of 6.5 due to low responses of hepatoma to chemotherapeutic treatments (27). Current research efforts are

focused on ADI's *in vivo* inhibitory effect towards HCCs, leukemia, melanomas and human umbilical vein endothelial cells (HUVEC) (104-106), clinical trials for HCC (phase III) and melanoma (phase I/II) (105, 107), and PEG formulation of ADI to improve its efficacy as a clinical drug, including serum half-life and antigenicity (16, 108). ADI inhibited the growth of cultured leukemia cells at concentrations of 5-10 ng/ml, which were about 20-100 times lower than those of the L-asparaginase standard resulting in fewer side effects (106, 109). Arginine deprivation is speculated to be the molecular reason for ADI's inhibitory effect on human lymphatic leukemia (106). ADIs catalyze the first step of the arginine deiminase (ADI) pathway by hydrolyzing arginine to citrulline and ammonium. Several ADI genes have been identified, purified, and characterized from bacteria, archaea and some eukaryotes excluding mammalian cells and summarized in a recent review (27). None of these ADIs is from a kinetic point of view ideally suited for *in vivo* applications in humans under physiological conditions.

Protein engineering by rational design and directed evolution offers opportunities to tailor ADI properties to physiological conditions. For the proof of concept, an ADI isolated from *Pseudomonas plecoglossicida* CGMCC2039 (accession number: ABS70718) which can be functionally expressed in *E. coli* has been employed. Directed evolution approaches employ mainly *E. coli* as host due to its fast growth and high transformation efficiency which is a prerequisite for generating complex mutant libraries. Over the last decades, directed protein evolution has become a versatile and successful approach for tailoring protein properties for industrial demands (mainly in chemical synthesis) and for advancing our understanding of structure-function relationships in enzymes. A directed evolution experiment comprises iterative cycles of diversity generation and functional selection for improved variants. Only a few manuscripts for phytases (83), xylanases (110), amylases (77, 82, 111), and an alcohol deyhdrogenase (112) reported a shift of pH optima using directed evolution algorithms. None of these directed evolution campaigns targeted a medical

application and arginine deiminase has to our best knowledge not been altered in its pH activity/resistance by directed evolution.

Comparison of PaADI (*Pseudomonas aeruginosa*, pH optimum 5.6; His405) and MaADI (*Mycoplasma arginini* ADI, pH optimum 6.5, Arg397) led to the speculation that substitution of His by Arg might contribute to MaADI's increased pH optimum (17). A sequence alignment of four ADIs (MaADI, MyADI (*Mycoplasma arthritidis* ADI), PaADI and PpADI) shows that for both Pseudomonas ADIs the synonymous amino acid positions (404 & 405), contain a His whereas both Mycoplasma ADIs contain at corresponding positions an Arg. Interestingly, both Mycoplasma ADIs have an pH optimum approximately one pH unit higher than both Pseudomonas ADIs.

In this study we report the first directed ADI evolution protocol in which the pH profile of PpADI was shifted to higher pH values representing a conceptional proof that ADI properties can be tailored for demands *in vivo* treatment of arginine-auxotrophic tumors. An emphasis is given on detailed description of directed evolution conditions (mutagenic and screening).

3.3 Materials and methods

3.3.1 Materials

All chemicals were of analytical-reagent grade or higher quality and were purchased from Fluka (Neu-Ulm, Germany), Sigma-Aldrich (Steinheim, Germany) and Applichem (Darmstadt, Germany), except the resins for purification (TOSOH, Stuttgart, Germany). All enzymes were purchased from New England Biolabs (Frankfurt, Germany), Fermentas (St. Leon-Rt, Germany), and Sigma-Aldrich Chemie (Taufkirchen, Germany), unless stated otherwise.

Thermal cycler (Mastercyler gradient; Eppendorf, Hamburg, Germany) and thin-wall PCR tubes (Multi-ultra tubes; 0.2 µl; Carl Roth, Germany) were used in all PCRs. The PCR volume was always 50 µl except for Megaprimer PCR of whole

plasmid (MEGAWHOP, 20 µl); larger volumes were prepared in multiple 50-µl PCRs. The amount of DNA in cloning experiments was quantified by using a NanoDrop photometer (NanoDrop Technologies, Germany).

Pseudomonas plecoglossicida CGMCC2039 was provided by Professor Zhihao Sun (Jiangnan University, Wuxi, China).

3.3.2 Methods

3.3.2.1 Reagents used in assays

Acid-ferric solution

To dH_2O (600 ml), concentrated H_3PO_4 (70 ml, 85 %) and concentrated H_2SO_4 (160 ml, 90-91 %) were added slowly. After cooling to room temperature, $FeCl_3 \cdot 6H_2O$ (10 ml, 10 g/L) was added in the above solution, finally the total volume was adjusted to 1 liter with dH_2O.

Diacetyl monoxime -thiosemicarbazide (DAM-TSC) solution

DAM solution (10 g/L) and TSC solution (0.3 g/L) were prepared separately. The two solutions were mixed (volume ratio = 1:1) just prior to use.

3.3.2.2 Cloning of ADI into pET42b(+)

The arginine deiminase (ADI) gene was amplified from *Pseudomonas plecoglossicida* CGMCC2039 by colony PCR (94℃ for 10 min, 1 cycle; 94℃, 30 s/ 54℃, 30 s/ 72℃, 165 s, 29 cycles; 72℃ for 5 min, 1 cycle) using primer (5'-CCGCATTCCGCTGAAAAACAGAAGTACGG-3' and 5'-CTTCTCGAGTTAGTAGTTGATCGGGTCGCGCACG-3'), 1.5 U of Pfu DNA polymerase, 0.20 mM of dNTP mix and a colony of *Pseudomonas plecoglossicida* CGMCC2039. Amplification product was purified by gel extraction, digested using NdeI (20 U) and XhoI (20 U) and purified using QIAquick PCR purification kit (QIAGEN, Hilden, Germany). Cloning vector pET42b(+) was digested with NdeI (20 U) and XhoI (20 U), and purified by gel extraction kit (QIAGEN, Hilden, Germany). Digested ADI gene and pET42b(+)

were ligated using T4 DNA ligase (1 U) to give pET42b(+)-ADI and transformed into *E. coli* BL21-Gold (DE3).

3.3.2.3 Site directed mutagenesis of PpADI gene at position H404

Site directed mutagenesis of ADI gene was performed according to the published method (113) on plasmid pET42b(+)-ADI. The following oligonucleotides were used for mutagenesis of H404R: 5'-GGCCGTGGCGGCGGCCGTTGCATGACCTGCCCG-3' and 5'-CGGGCAGGTCATGCAACGGCCGCCGCCACGGCC-3' (underlining indicated the substituted nucleotide). For the mutagenic PCR (First stage: 95℃ for 30 s, 1 cycle; 95℃, 30 s/ 55℃, 1 min/ 72℃, 130 s, 3 cycles. Second stage: 95℃ for 30 s, 1 cycle; 95℃, 30 s/ 55℃, 1 min/ 72℃, 130 s, 15 cycles; 68℃ for 30 min, 1 cycle), 2 U of Phusion™ Hot Start DNA polymerase (Finnzymes, Keilaranta, Finland), 0.20 mM of dNTP mix, 25 pmol of each primer together with 100 ng of template (pET42b(+) harboring ADI gene) were used. Following the PCR, DpnI (40 U; New England Biolabs) was added, and incubated overnight at 37℃. The PCR products were purified by using a QIAquick PCR Purification Kit (Qiagen) and transformed into *E. coli* BL21-Gold (DE3) for expression.

3.3.2.4 Site sturation mutagenesis of PpADI gene at nine amino acid position

Site saturation mutagenesis of ADI gene was performed according to the published method (113) on plasmid pET42b(+)-ADI. The oligonucleotides were used for mutagenesis were listed in table 1 (underlining indicated the substituted nucleotide). For the mutagenic PCR (First stage: 95℃ for 30 s, 1 cycle; 95℃, 30 s/ 55℃, 1 min/ 72℃, 130 s, 3 cycles. Second stage: 95℃ for 30 s, 1 cycle; 95℃, 30 s/ 55℃, 1 min/ 72℃, 130 s, 15 cycles; 68℃ for 30 min, 1 cycle), 2 U of Phusion™ Hot Start DNA polymerase (Finnzymes, Keilaranta, Finland), 0.20 mM of dNTP mix, 25 pmol of each primer together with 100 ng of template (pET42b(+) harboring ADI gene) were used. Following the PCR, DpnI (40 U; New England Biolabs) was added, and incubated overnight at 37℃. The PCR products were

purified by using a QIAquick PCR Purification Kit (Qiagen) and transformed into *E. coli* BL21-Gold (DE3) for expression.

Table 1. Primer sequences for site saturation mutagenesis.

Primer name	Sequences
Leu 41 FP	AACTGCGACGAGCTGNNNTTCGACGATGTGATC
Leu 41 RP	GATCACATCG TCGAANNNCA GCTCGTCGCAGTT
Asn 360 FP	TGGGATGACGGCAACAACNNNGTGGCGCTGGAG
Asn 360 RP	CTCCAGCGCC ACCACNNNGT TGCCGTCATCCCA
Arg401 FP	GAACTGGGCCGGGGCNNNGGCGGCGGCCACTGC
Arg401 RP	GCAGTGGCCGCCGCCNNNGCCCCGGCCCAGTTC
Phe163 FP	CTGCCCAACACCCAGNNNACCCGCGACACCACC
Phe163 RP	GGTGGTGTCGCGGGTNNNCTGGGTGTTGGGCAG
Asn160 FP	CTGCCGCCGCTGCCCNNNACCCAGTTCACCCGC
Asn160 RP	GCGGGTGAACTGGGTNNNGGGCAGCGGCGGCAG
Arg185 FP	ATGTACTGGCCGGCNNNCGCCAGGAAACCCTG
Arg185 RP	CAGGGTTTCCTGGCGNNNGCCGGCCAGTACAT
Arg243 FP	ATCGGCATGGGTGAGNNNACCTCGCGCCAGGCC
Arg243 RP	GGCCTGGCGCGAGGTNNNCTCACCCATGCCGAT
His405 FP	GGCCGTGGCGGCGGCNNNTGCATGACCTGCCCG
His405 RP	CGGGCAGGTCATGCANNNGCCGCCGCCACGGCC
Gly403 FP	GCCGGGGCCGTGGCNNNGGCCACTGCATGACC
Gly403 RP	GGTCATGCAGTGGCCNNNGCCACGGCCCCGGCC

3.3.2.5 Construction of PpADI error-prone library

The library was generated by the standard error-prone PCR (epPCR) using improved variant H404R as template. For the mutagenic PCR (95℃ for 2 min, 1 cycle; 95℃, 30 s/ 55℃, 30 s/ 72℃, 30 s, 29 cycles; 72℃ for 3 min, 1 cycle), 2.5 U of Taq DNA polymerase, 0.20 mM of dNTP mix, 50 ng of template (pET42b(+) harboring ADI gene H404R), 0.01-0.1 mM of $MnCl_2$ and 10 pmol of each primer (5'-TACATATGTCCGCTGAAAAACAGAAG-3' and 5'- GTGCTCGAGTTAGTAGT TGATCGG-3') were used. The PCR products were purified by using a QIAquick PCR Purification Kit. The purified epPCR products were cloned into expression

plasmid pET42b(+) by MEGAWHOP(114). For MEGAWHOP (68℃ for 5 min, 1 cycle; 95℃ for 5 min, 1 cycle; 95℃, 1 min/ 55℃, 1 min/ 68℃, 13 min 30 s, 24 cycles; 68℃ for 30 min, 1 cycle), 1 U of Taq DNA polymerase, 0.1 U of Pfu DNA polymerase, 0.20 mM of dNTP mix together with 200 ng of template (pET42b(+) harboring ADI gene H404R) were used. Following the PCR, DpnI (40 U; New England Biolabs) was added, and incubated (4 h; 37℃). The MEGAWHOP products were transformed into *E. coli* BL21-Gold (DE3) for expression and screening.

3.3.2.6 Expression of PpADI in LB media with IPTG induction

The strain *E. coli* BL21-Gold (DE3)/ pET42b-PpADI was cultured at 37℃ in 20 ml of LB media that contained 50 μg/ml kanamycine to an absorbance of 0.6 at 578nm. Then, isopropyl β-D-thio-galactopyranoside (IPTG) was added to a final concentration 0.2 mM. The cells were harvested after 9 h induction with IPTG at 37℃. The expressed rADI was analyzed by SDS-PAGE.

3.3.2.7 Expression of PpADI in auto-induction media

A chemically defined auto-induction medium (115) containing salts and trace metals, vitamins including vitamin B12, and glucose, glycerol, and lactose were test for PpADI expression. Five kinds of auto-induction media LS-5052, P-5052, MD-5052, TYM-5052 and TYP-5052 were tested for the ADI expression, under the following conditions: 20 ml LB media in 100 ml flask, 37℃, 250 rpm, 20 h. The expressed rADI was analyzed by SDS-PAGE.

3.3.2.8 Cultivation and expression of PpADI in 96-well plates

Colonies grown on LB_{kan} agar plates were transferred, by using toothpicks, into 96-well microtiter plates (flat bottom, polystyrene plates; Greiner Bio-One GmbH, Frickenhausen, Germany), containing non-inducing medium LSG (150 μL) (115) supplemented with kanamycin (50 μg/ml). After 16 h of cultivation in a microtiter plate shaker (Multitron II, Infors GmbH, Einsbach, Germany; 37℃, 900 rpm, 70 % humidity), each well was replicated using a replicator (EnzyScreen BV, Leiden,

Netherlands) into a second series of 96-well microtiter plates containing 150 µL of auto-induction media LS-5052 (115) supplemented with kanamycin (50 µg/ml). The first set of plates was stored at -80°C after addition of glycerol. The clones in the second set of plates were cultivated for 12 h (Multitron II, Infors GmbH, 37°C, 900 rpm) and used for screening.

3.3.2.9 Screening Procedure

96-well plate format citrulline colorimetric screening assay

A modified protocol of citrulline detection based on carbamido-diacetyl reaction (116) (see Figure 1A for assay mechanism) was used for ADI activity measurement. Screening for increased activity was carried out by measuring the activity at pH 7.4 and 6.4. 20 µl of cell culture was transferred to 96-well microtiter plate. Enzyme reaction was initiated by addition of arginine solution (100 µl, 100 mM) supplemented with cetyltrimethylammoniumbromide (CTAB, 4 mM), and incubated (20 min, 37°C). Subsequently, acid-ferric solution (60 µl) and diacetyl monoxime (DAM, 20 µl, 0.5 M) were added. The reaction mixture was further incubated (15 min, 55°C). Absorbance was measured at 492 nm using a microtiter plate reader (Tecan Sunrise, Tecan Group AG, Zurich, Switzerland).

Standard deviation measurements were performed in 96-well plate format using culture from BL21-Gold (DE3) lacking ADI and in a separate experiment containing ADI. Apparent standard deviation was based on the absolute absorbance values obtained from the ADI wild type plate. The true standard deviation was calculated by subtracting the background absorbance value of the microtiter plate lacking ADI from the apparent values.

Cuvette format citrulline colorimetric assay

ADI activity was routinely measured using a modified protocol of the citrulline detection with DAM and TSC (117) (see Figure 1A for assay mechanism) in Eppendorf tubes. Enzyme reaction was initiated by addition of arginine solution (200 µl, 100 mM) to a 2-ml eppendorf tube containing crude cell lysate (50 µl), and incubated (20 min, 37°C). Subsequently, acid-ferric solution (250 µl) was

added to stop the enzyme reaction. After appropriate dilution with deionized water to ensure the concentration of produced citrulline is within linear detection range, the reaction mixture (400 µl) was mixed with acid-ferric solution (600 µl) and DAM-TSC solution (100 µl). The reaction mixture was further incubated (30 min, 70°C), followed by incubation in ice water to stop color development. Absorbance was measured at 530 nm using a Specord 200 (Analytik Jena AG, Jena, Germany).

Normalization of protein expression for wild type ADI and variants

Agilent Protein 230 Kit (Agilent Protein 230 Kit, Agilent Technologies Deutschland GmbH, Böblingen, Germany) and Agilent 2100 Bioanalyzer (Agilent 2100 Bioanalyzer, Agilent Technologies Deutschland GmbH, Böblingen, Germany) were used for normalization of protein expression in crude cell extract. The protocol used was according to Agilent protein 230 Kit Guide except BSA was used as an internal standard.

3.3.2.10 Expression of ADI in shaking flask and purification

Shaking flasks (1 liter) containing auto induction media LS-5052 (200 ml) supplemented with kanamycin (50 µg/ml) were inoculated with a 1:200 dilution of overnight culture (*E. coli* BL21-Gold(DE3) harboring pET42b-ADI) grown in non-inducing media LSG. After 12 h of expression, *E. coli* cells were harvested by centrifugation (Eppendorf 5810R 4°C, 3220 g, 30 min) and resuspended in phosphate buffer (20 ml, Na_xPO_4, 20 mM, pH 7.0). *E. coli* cells were subsequently lysed by using a high-pressure homogenizer (1500 bar, 2 cycles; Avestin Emulsiflex, Mannheim, Germany). The disrupted cells were centrifuged (Eppendorf 5417R, 4°C, 13000 g, 20 min) and the supernatant was further cleared by filtration through a low protein-binding filter (0.45 µm; Minisart RC 25 single use syringe filter; Sartorius, Hamburg, Germany). ADI wild type and mutants (H404R and K5T D44E H404R) were subsequently purified by a column chromatography procedure: (i) The filtered cell lysates were subjected to a Super-Q anion exchange column, which had been pre-equilibrated with 50 mM

phosphate buffer (Na_xPO_4, pH 7.0). 20 ml of cell lysate was loaded. ADI were eluted by a NaCl step elution in phosphate buffer (Na_xPO_4, 50 mM, pH 7.0) at a rate of 3 ml/min. (ii) The obtained ADI protein from ion exchange chromatography was subjected to a gel filtration column (Matrix: Toyoperl HW-55S, Bed volume: 33 ml, Bed height: 40 cm, Column: Omnifit).

Purified ADI was subsequently concentrated using a Amicon ultra-4 centrifugal filter device (Millipore Corporation, Billerica, U.S.A.) with a 30-kDa cut-off membrane. Total protein concentration was determined by BCA^{TM} assay kit (Pierce, Born, Germany) and homogeneity of the purified sample was controlled by SDS-page electrophoresis using standard molecular biology techniques.

3.3.2.11 Characterization of ADI wild type and mutants

Determination of k_{cat} and K_m of ADI wild type and the mutants

The k_{cat} and K_m values were determined from initial velocity data measured as a function of substrate concentration. Enzyme reaction was carried out at 37°C in a water bath. After 10 min preincubation at 37°C, the enzyme reaction was initiated by addition of purified enzyme (50 µl, 0.2-0.5 µM) to the substrate solution (200 µl, 0.2 mM to 10 mM of arginine, 0.5 M phosphate buffer, pH 7.4) in deep well plates. The reaction mixture was incubated (37°C) and every two minutes reaction mixture (30 µl) of each well was transferred to acid-ferric solution (30 µl) to stop the enzyme reaction. The color development was subsequently performed in 96-well PCR plate. Ferric-acid solution (90 µl) and DAM-TSC solution (15 µl) were added to each well. The 96-well PCR plate was then incubated (70°C, 30 min) in thermal cycler (Eppendorf Mastercyler gradient) for color development, followed by incubation in ice water to stop color development. Absorbance was measured at 530 nm using a microtiter plate reader (SPECTROstar Omega, BMG LABTECH, Offenburg, Germany). The initial velocity data obtained were fitted to the equation $v = V_{max}[S]/([S] + K_m)$ (where v is the initial velocity, V_{max} the maximum velocity, [S] the substrate concentration, and K_m the Michaelis constant) using GraphPad Prism software (GraphPad

software, San Diego, CA, USA). The k_{cat} was calculated from the ratio of V_{max} and enzyme concentration.

Determination of pH profile

Enzyme reaction was carried out at 37°C in a water bath using the following substrate solution: arginine 0.1 M, pH 5-8 phosphate/acetate buffer (0.5 M phosphate, 50 mM acetate). After 10 min preincubation at 37°C, the enzyme reaction was initiated by addition of purified enzyme (50 µl, 0.2-0.5 µM) to the substrate solution (200 µl) in deep well plates. The reaction mixture was incubated (37°C, 10 min) and acid-ferric solution (250 µl) was transferred to each well to stop the enzyme reaction. The color development was subsequently performed in 96-well PCR plate. The reaction mixture (60 µl), ferric-acid solution (90 µl) and DAM-TSC solution (15 µl) were transferred to a 96-well PCR plate. The 96-well PCR plate was then incubated (70°C, 30 min) in thermal cycler (Eppendorf Mastercyler gradient) for color development, followed by incubation in ice water to stop color development. Absorbance was measured at 530 nm using a microtiter plate reader (SPECTROstar Omega, Germany).

3.3.2.12 Molecular Modeling

Two crystal structures of PaADI (PDB codes: 1RXX, 2A9G) were used to model the mutations H405R and D44E. Only one monomeric unit of the tetrameric PaADI was used for the modeling study employing Swiss-PDB viewer (118) (www.expasy.org/spdbv). PaADI variants (H405R; D44E) were generated using the mutate command of Swiss-PDB viewer. The side chain rotamer with the best score was used for subsequent energy optimized with parameter of GROMOS96 force field for in vacuum minimization (119).

3.3.2.13 Stability of PpADI in presence of serum

Purified PpADI (wild type, M1, M2; 20 µl) was incubated (37°C, 60 min) with AB--human serum (80 ul, Invitrogen, Karlsruhe, Germany) and PBS buffer (pH7.4, 80 ul), respectively. Subsequently, the incubated ADI-serum/PBS mix (20 µl) was

added to microtiter plate containing arginine solution (100 µl, 10 mM arginine in PBS buffer, pH 7.4) and incubated (37℃, 30 min). Acid-ferric solution (120 µl) was added to stop the enzyme reaction. The produced citrulline was detected using the assay procedure employed in "Determination of kcat and Km of ADI wild type and the mutants". Before measuring absorbance at 530 nm, centrifugation (Eppendorf, 5810R 4℃, 3000 g, 10 min) was performed to remove the precipitation in the assay solution (likely proteins in serum were precipitated in acidic condition during assay procedure). Meanwhile, a serum control was test for the original citrulline concentration of serum using the same procedure mentioned above except that instead of PpADI, elution buffer of gel filtration (NaxPO4, 50 mM, pH 7.4) was used. All the absorbance values at 530 nm of ADI-serum sample were subtracted the value of serum control to get the citrulline concentration produced by PpADI. The residual activities of PpADI after incubation in serum compared to that in PBS buffer were calculated to show the stability of PpADI after incubated in human serum.

3.3.2.14 Activity of PpADI (wild type, M1, M2) towards arginine derivative dimethylarginine

Purified PpADI (wild type, M1, M2; 15 µl, ~0.2 mg/ml final concentration; >20-fold concentration used for kinetic constant determination) was incubated (37℃, 4 h) with (N^G, N^G)-dimethylarginine solution (20 mM, 100 µl). Acid-ferric solution (120 µl) was added to stop the enzyme reaction. Activity was recorded by citrulline detection using citrulline colorimetric assay (see 3.3.2.11 Characterization of ADI wild type and mutants).

3.4 Results

3.4.1 PpADI cloning

PpADI was cloned into pET42b(+) and expressed in *E.coli* BL21-Gold(DE3) using auto-induction media LS-5052 (see figure 2). The nucleotide sequence of PpADI comprises 1,254 bp nucleotide (figure 1) encoding 417 amino acids which have 85% identity to ADI from *P. aeruginosa* (PaADI). The PpADI cloned into

pET42b(+) was confirmed by nucleotide sequencing. As indicated in Figure 1, sequence analysis of ADI gene showed that there was one synonymous mutation at amino acid position D78 (GAT to GAC) compared to ADI-sequence of *P. plecoglossicida* CGMCC2039 deposited in NCBI (accession number: EU030267). The deduced ADI protein sequence has a calculated molecular weight of 46.5 kDa and shows 85% identity to ADI from *P. aeruginosa*. This clone was used for subsequent directed evolution experiments.

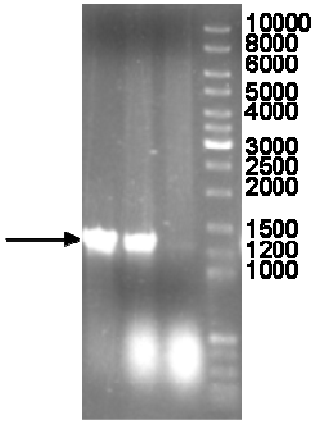

Figure 1. DNA electrophoresis of *PpADI*.

```
1       ATGTCCGCTG AAAAACAGAA GTACGGTGTC CACTCCGAAG CAGGCAAGCT GCGCAAGGTA
61      ATGGTCTGCG CTCCGGGACT GGCGCACAAG CGCCTGACCC CGAGCAACTG CGACGAGCTG
121     CTGTTCGACG ATGTGATCTG GGTCGACCAG GCCAAGCGCG ACCACTTCGA CTTCGTCACC
181     AAGATGCGCG AGCGCGGCGT GGATGTGCTG GAAATGCATA ACCTGCTCAC CGACATCGTG
241     CAGAACCCCG AGGCCCTGAA GTGGATCCTC GACCGCAAGA TCACCCCTGA CACCGTCGGG
301     GTGGGCCTGA CCAACGAAGT GCGCAGCTGG CTGGAGGGCC AGGAGCCACG CCACCTCGCC
361     GAGTTCCTGA TCGGCGGCGT GGCCGGCCAG GACCTGCCGG AGAGCGAAGG TGCCAGCGTG
421     GTCAAGATGT ACAACGACTA CCTGGGCCAC TCCAGCTTCA TCCTGCCGCC GCTGCCCAAC
481     ACCCAGTTCA CCCGCGACAC CACCTGCTGG ATCTACGGCG GCGTGACCCT CAACCCGATG
541     TACTGGCCGG CGCGACGCCA GGAAACCCTG CTGACCACCG CCATCTACAA GTTCCACCCC
601     GAGTTCACCA AGGCCGACTT CCAGGTCTGG TACGGCGACC CGGACCAAGA GCACGGCCAG
661     GCCACCCTCG AAGGCGGCGA CGTCATGCCG ATCGGCAAGG GCATCGTGCT GATCGGCATG
721     GGTGAGCGCA CCTCGCGCCA GGCCATCGGC CAACTGGCAC AGAACCTCTT CGCCAAGGGC
781     GCAGTGGAGC AAGTGATCGT CGCCGGGCTG CCGAAGTCCC GTGCGGCCAT GCACCTGGAC
841     ACCGTGTTCA GCTTCTGCGA CCGCGACCTG GTCACGGTTT TCCCGGAAGT GGTGCGCGAG
901     ATCGTGCCGT TCATCATCCG CCCGGACGAA AGCAAGCCCT ACGGCATGGA CGTACGCCGC
961     GAGAACAAGT CGTTCATCGA GGTGGTCGGC GAGCAGCTGG GCGTCAAGCT GCGTGTGGTC
1021    GAGACCGGCG GCAACAGCTT CGCCGCCGAG CGCGAGCAGT GGGATGACGG CAACAACGTG
1081    GTGGCGCTGG AGCCAGGTGT GGTCATCGGC TACGACCGCA ACACCTACAC CAATACCTTG
1141    CTGCGCAAGG CCGGGATAGA GGTCATCACC ATCAGTGCCG GCGAACTGGG CCGGGGCCGT
1201    GGCGGCGGCC ACTGCATGAC CTGCCCGATC GTGCGCGACC CGATCAACTA CTAA
```

Figure 2. PpADI sequencing results.

3.4.2 PpADI expression in LB media with IPTG as inducer

PpADI was successfully expressed in LB media with IPTG as inducer. Figure 3 (lane 4) shows the expression band of PpADI observed at ~45 kDa, which is similar to the calculated molecular weight of 46 kDa (based on http://expasy.org/tools/pi_tool.html).

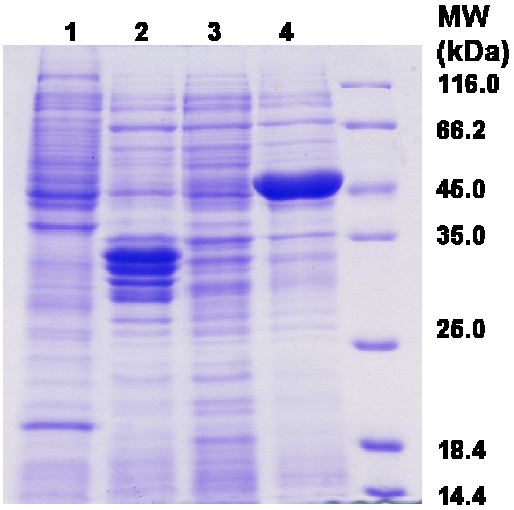

Figure 3. SDS-PAGE of PpADI expression. Lane 1: *P. plecoglossicida*; Lane 2: E. coli BL21-Gold (DE3)/ pET42b; Lane 3: E. coli BL21-Gold (DE3)/ pET42b-PpADI WT, without IPTG; Lane 4: E. coli BL21-Gold (DE3)/ pET42b- PpADI WT.

3.4.3 PpADI expression in auto-induction media

Expressing recombinant protein in auto-induction media is based upon the preferences of bacteria to selectively use different carbon sources during diauxic growth and upon the often-observed negative regulation of gene expression by catabolite repression. Auto-induction is more convenient than IPTG induction because the expression strain is simply inoculated into auto-inducing medium and grown to saturation without the need to follow culture growth and add inducer at the proper time. For high-throughput applications, the auto-induction approach has many advantages over traditional induction methods including avoidance of the strong induction and apparent toxicity associated with chemical inducers such as IPTG.

Five kinds of auto-induction media LS-5052, P-5052, MD-5052, TYM-5052 and TYP-5052 were tested for the ADI expression. Figure 4(A) and 4(B) show ADI

activity and corresponding SDS-PAGE band of the PpADI expression in different auto-induction media. The expression in auto-induction media LS-5052 is shows the highest activity and therefore LS-5052 was used for the following directed evolution experiments.

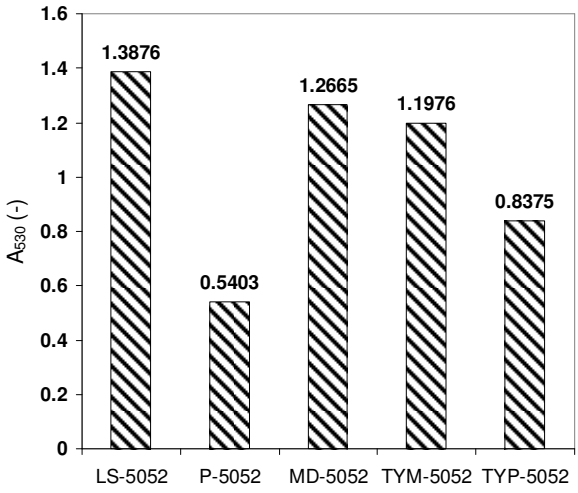

Figure 4(A). Activity of PpADI expressed in auto-induction media.

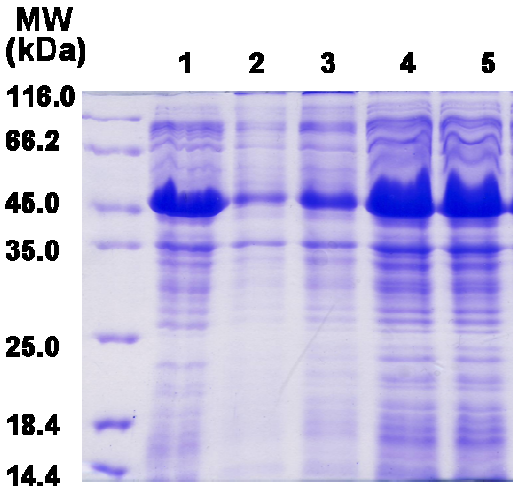

Figure 4(B). SDS-PAGE of ADI expressed in auto-induction media 1, LS-5052; 2, P-5052; 3, MD-5052; 4 TYM-5052; 5, TYP-5052.

3.4.4 PpADI assay based on citrulline detection

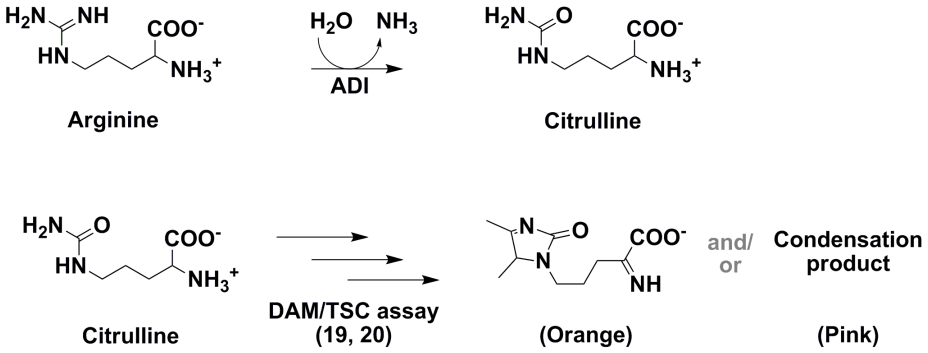

Figure 5. Arginine conversion by ADI and detection of citrulline using DAM/TSC assay.

ADI activity was measured by detecting the production of citrulline from arginine, according to carbamido diacetyl reaction (colorimetric reaction). The conditions of the carbamido diacetyl reaction is as follows： strong acid solution (H_3PO_4, H_2SO_4), oxidizing agent (Fe^{3+}), diacetyl monoxime (DAM), thiosemicarbazide (TSC), and boiling water bath. Figure 5 shows one postulated reaction mechanism for the assay which depicts the reaction between citrulline and DAM. By the addition of TSC to the reaction system, Coulombe and Favreau(120) obtained linearity of response with a more stable pink color which A_{max} was shifted from 490nm to 530nm.

Figure 6 describes the assay procedure for measuring ADI activity in 2 ml eppendorf tube. A calibration curve was prepared using citrulline standard solution (Figure 7) for determining the citrulline production during the assay.

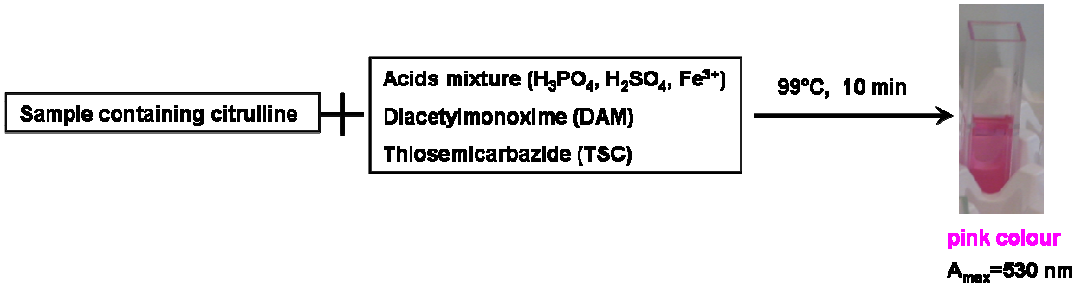

Figure 6. Citrulline colorimetric assay in cuvette format using DAM/TSC assay.

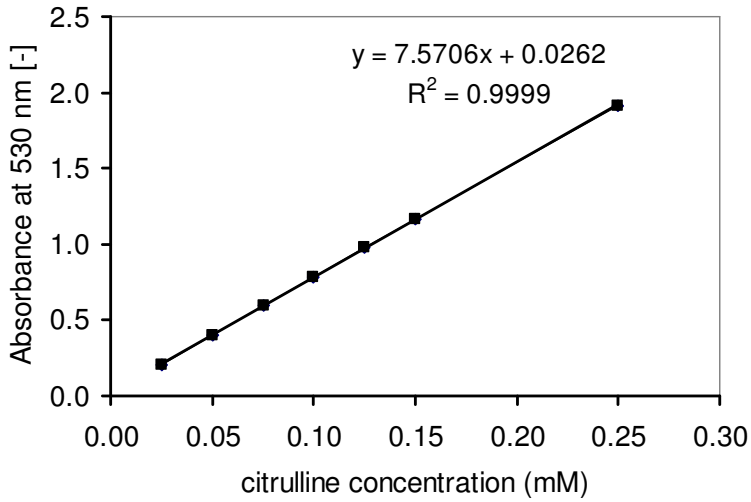

Figure 7. Calibration curve of cuvette format citrulline colorimetric assay.

3.4.5 PpADI screening system for citrulline production in microtiter plates

Two key performance parameters for identifying improved variants in microtiter plate based screening systems are the true standard variation and the linear detection range of the employed assay. Standard deviations have been reduced by optimizing expression and screening conditions (various auto-induction media and assay conditions such as amount of cell, conversion time and color development procedure). A modified version of the DAM-TSC assay for citrulline detection (Scheme 1) was selected for directed evolution of PpADI. The microtiter plate screening format was optimized for simplified handling by lowering the color development temperature (55℃ instead of 100℃), increasing the diacetylmonoxime concentration (~22-fold) and avoiding the use of the sensitizer thiosemicarbazide. Figure 8 shows the procedure of screening assay of citrulline detection.

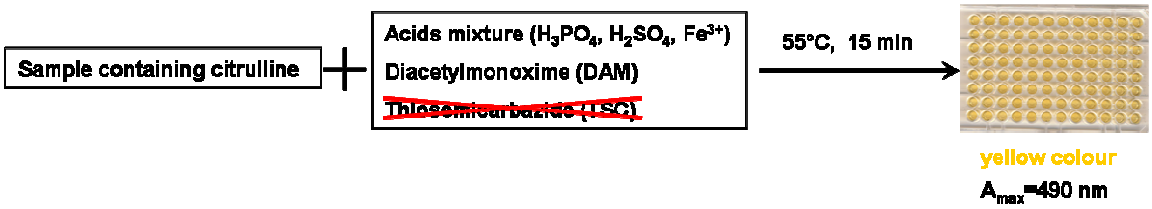

Figure 8. Citrulline colorimetric assay in MTP format using DAM assay.

Standard deviations of the modified citrulline detection assay have been reduced by optimizing expression and screening conditions (various auto-induction media and assay conditions such as amount of cell, conversion time and color development procedure). The preferred combination (150 µl LS5052 auto-induction media and 20 µl cell culture, 20 min conversion time and 15 min color develop time) resulted in a true standard deviation of 12.8 % after subtracting the background (Figure 10). Screening systems with standard deviations around 10 % have successfully been used in directed evolution experiments (121, 122). A wide linear detection window is important for identifying beneficial mutants in directed evolution experiments and screening systems for evolved mutants have to be constantly adapted for hitting the linear detection window. A linear detection range up to 6 mM citrulline could be detected (Figure 9).

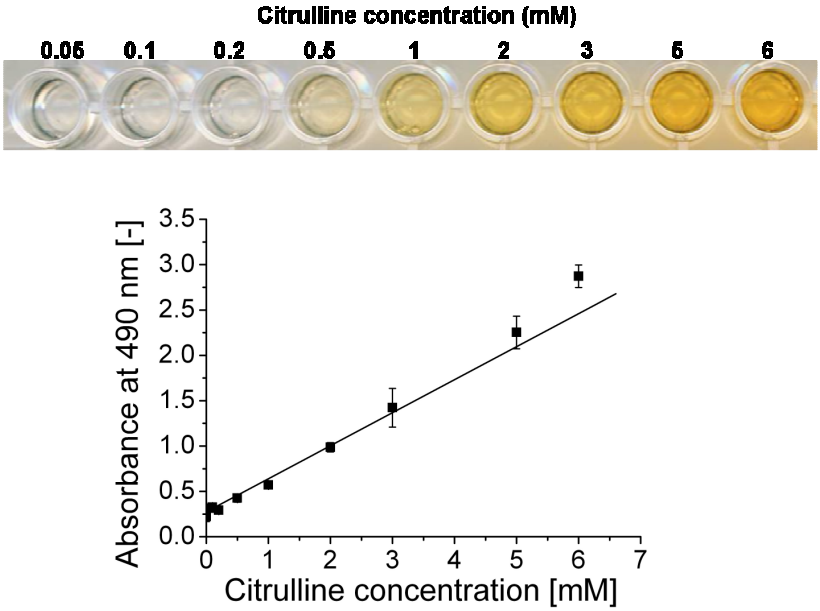

Figure 9. Calibration curve of 96-well microtiter plate format citrulline colorimetric screening assay.

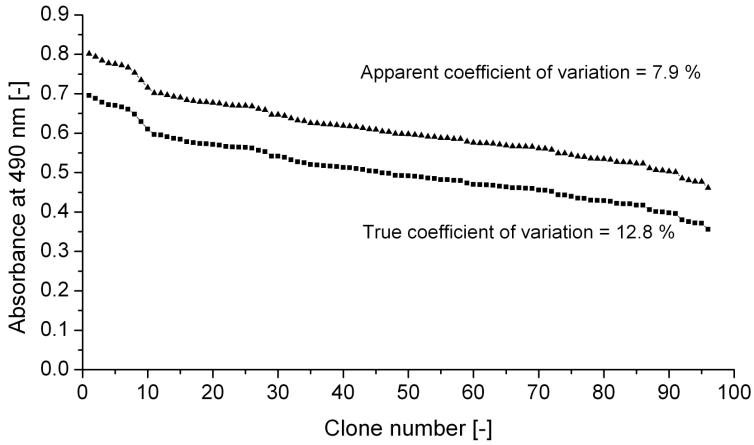

Figure 10. Activity values in descending order of the ADI wild-type conversion of arginine to citrulline in a 96-well microtiter plate using the optimized assay protocol. The apparent coefficients of variation were calculated without subtracting the background and the true coefficients of variation after background subtraction.

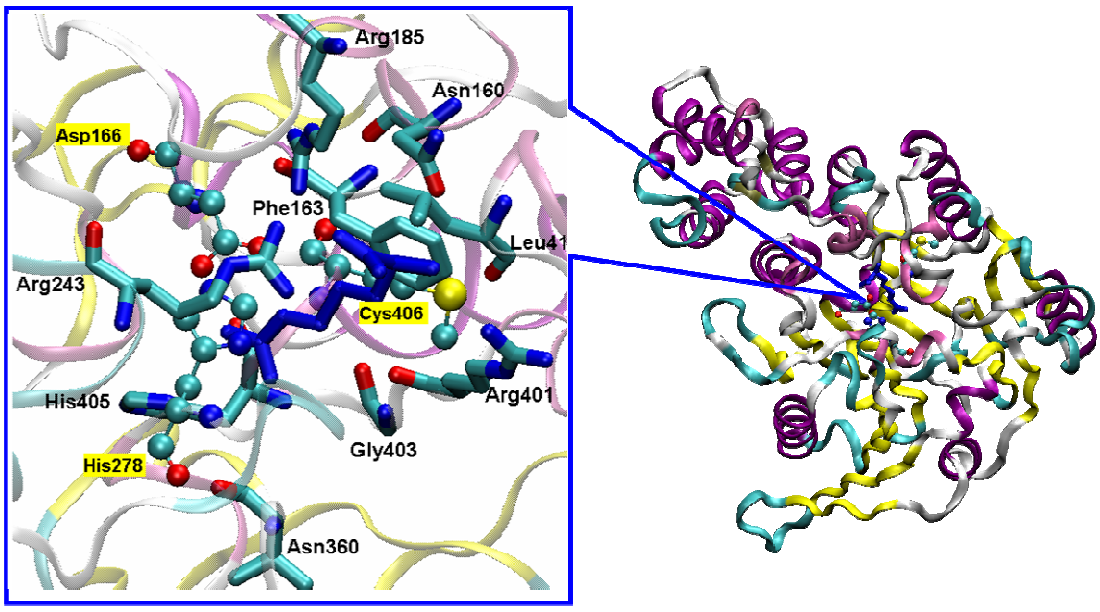

Figure 11. PpADI model derived from PaADI crystal structure (PDB code 2a9gD) by SWISS MODEL WORKSPACE.

3.4.6 Focused libraries generated by saturation mutagenesis

PpADI gene shares 83 % sequence identity with PaADI of which the crystal structure was solved (123). After submitting the ADI sequence to SWISS MODEL WORKSPACE, a proposed ADI model based on the PaADI crystal structure (PDB code 2a9gD) was obtained (Figure 11). According to this model and published literatures, 9 amino acid residues: Leu41, Asn160, Phe163, Arg185, Arg243, Asn360, Arg401, His404, Gly 403 (Figure 11) close to the active center (catalytic triad: Cys406-His278-Glu224) or known to interact with substrate arginine were selected for saturation mutagenesis.

Site saturation mutagenesis at position Leu41, Asn160, Phe163, Arg185, Arg243, Asn360, Arg401, His404 and Gly 403 were performed. 300 clones were screened for each position. However, no improved variant was identified.

3.4.7 Validation of variant M1 (H404R) citrulline colorimetric assay in cuvette format

Position H404 which was suspected to influence ADI pH profile by substitution to R404 (15). Compared to wild type PpADI, variant M1 (H404R) shows higher activity (1.8-fold) and improved activity ratio of pH 7.4 to 6.4 (4.7-fold). Therefore, M1 (H404R) was selected for directed evolution.

3.4.8 epPCR library generation and screening with citrulline detection assay by screening error-prone mutant libraries

Various concentrations of $MnCl_2$ (0.01-0.10 mM) were used in epPCR library generation to adjust the ratio of active to inactive clones. Figure 12 (A) and 12 (B) show the epPCR products and the corresponding MEGAWHOP products. Concentration of 0.01 mM $MnCl_2$ which generated 53 % inactive mutant was selected for library generation. EpPCR mutant libraries with a ratio of 50 % active and 50 % inactive clones have often been used successfully in directed evolution, improving enzyme properties by gradual changes (one or two amino acids changes per round of mutagenesis and screening). A total of 7 variants (listed in

Table 2) were identified from an epPCR library of 2400 mutants and used for further characterization. The most active variant was sequenced and two additional amino acid substitutions (K5T D44E) were identified.

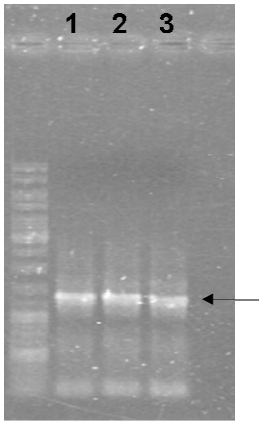

Figure 12 (A). Electrophoresis of epPCR products. Lane 1, 0.01 mM of $MnCl_2$; Lane 2, 0.02 mM of $MnCl_2$; Lane 3, 0.05 mM of $MnCl_2$.

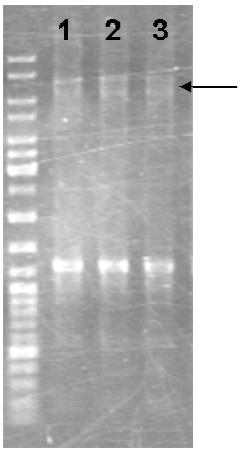

Figure 12 (B). Electrophoresis of MEGAWHOP product with epPCR products as megaprimer. Lane 1, 0.01 mM of $MnCl_2$; Lane 2, 0.02 mM of $MnCl_2$; Lane 3, 0.05 mM of $MnCl_2$.

Table 2. Activity of ADI variants towards arginine determined using citrulline colorimetric assay in cuvette format. Samples were diluted to ensure that detected citrulline concentrations are within the linear detection range of the citrulline colorimetric assay. Wild type, mutant M1 and the "best variant" M2 are in bold and prominent expression mutants (9-B3-1; 21-D5-1) are italized.

	Normalized [ADI][a]				
	Citrulline production (mM/mg)		Relative to activity at pH 7.4 of WT		Activity at pH 7.4/ activity at pH 6.4
ADI variants	pH 7.4	pH 6.4	pH 7.4	pH 6.4	
WT	9.83 (0.74)[b]	124.92 (1.98)	1.00 (0.15)	12.69 (0.01)	0.08 (0.01)
M1 (H404R)	17.80 (0.49)	45.95 (0.87)	1.81 (0.06)	4.67 (0.02)	0.39 (0.02)
M2 (K5T D44E H404R)	38.99 (0.79)	39.20 (0.31)	3.96 (0.02)	3.98 (0.02)	0.99 (0.03)
9-B3-1	24.89 (0.45)	54.50 (1.80)	2.53 (0.03)	5.54 (0.03)	0.46 (0.02)
21-D5-1	25.68 (2.68)	50.95 (2.36)	2.61 (0.07)	5.18 (0.02)	0.50 (0.01)
15-G10-2	13.11 (0.53)	47.02 (0.47)	1.33 (0.09)	4.78 (0.02)	0.28 (0.01)
2-H4-2	12.50 (0.07)	21.58 (0.09)	1.27 (0.06)	2.19 (0.04)	0.58 (0.01)
1-G11-1	24.91 (0.20)	29.12 (0.33)	2.53 (0.03)	2.96 (0.03)	0.85 (0.02)
24-E10-1	14.62 (0.62)	32.82 (0.52)	1.49 (0.08)	3.34 (0.03)	0.45 (0.02)

[a] (Based on quantification employing Agilent 2100 Bioanalyzer (Agilent Protein 230 Kit))
[b] (Standard error of triplicate measurements are given in brackets below each absolute and normalized value.)

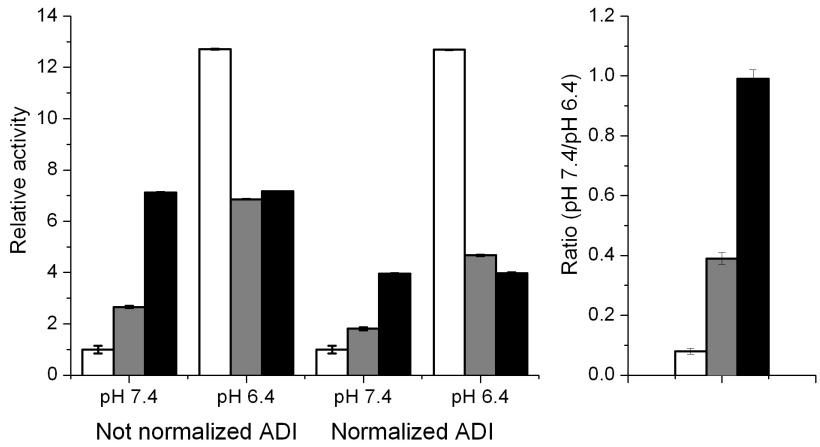

Figure 13. Relative activity of ADI variants towards arginine. The relative activity is the ratio of the activity at the pH of each variant relative to the activity at pH 7.4 of wild type ADI. White: ADI wild type, grey: M1 (H404R), black: M2 (K5T D44E H404R).

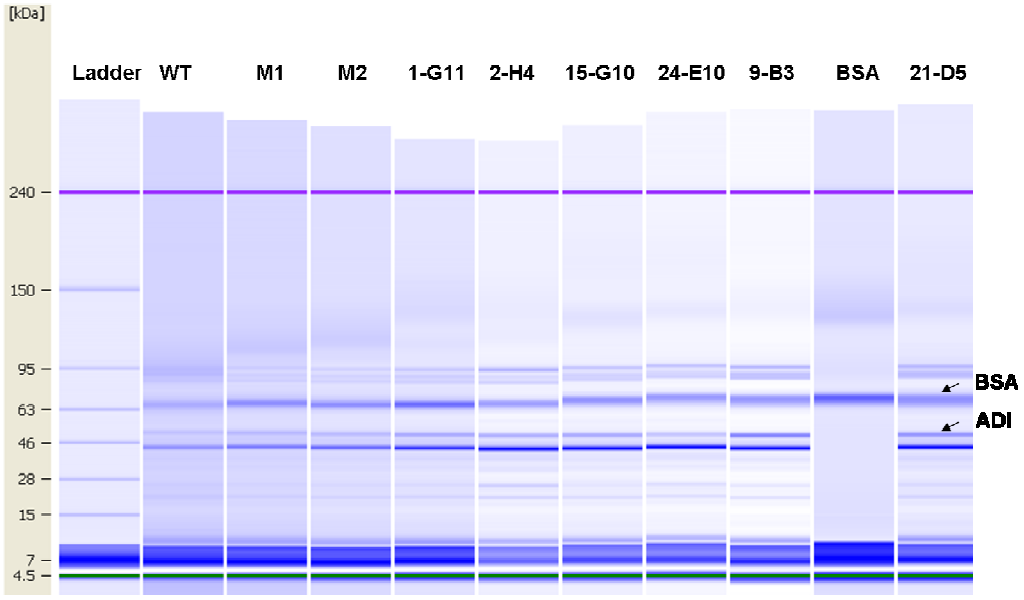

Figure 14. Elution profile of wild type PpADI and improved variants from epPCR library, generated with Protein 230 Kit using a mircofluidic device (Agilent Bioanalyzer). BSA was added as an internal standard.

3.4.9 Characterization of PpADI variants

3.4.9.1 Determination of k_{cat} and K_m of ADI wild type and the mutants

Variants selected from epPCR were first characterized using the crude cell extract to identify the most promising variants (Table 2). Using an activity ratio of pH 7.4 to 6.4 proved to be an effective method to eliminate expression mutants. Additionally ADI concentration in crude cell extract was determined using the Agilent Protein 230 Kit. Microfluidic elution profiles (Figure 14) semi-quantify differences in expression between the wild type PpADI and variants. Normalization of activities against the corresponding ADI concentrations reveals improvements in specific activities of ADI mutants (Table 2). M1, the starting variant for the directed evolution campaign, and M2 were selected for detailed characterization studies. M2 has as “best identified variants” (Figure 13) a more than 2.5-fold higher activity ratio at pH 7.4 to pH 6.4 than M1 and a 12-fold higher activity ratio than wild type in crude cell lysates.

For kinetic characterization of ADI variants the citrulline production was maintained between 0.2-0.8 mM. Calibration curve in Figure 4 shows the linear detection range in the employed 96-well PCR plate format citrulline colorimetric assay system. Figure 15 summarizes the k_{cat} and K_m values of wild type PpADI, identified variants M1 (H404) and M2 (K5T D44E H404R) which were expressed in shaking flasks cultures and purified using a two step procedure (anion exchange followed by gel filtration). Both variants M1 and M2 show an increase in k_{cat} and K_m for citrulline production at pH 7.4. Variant M2 shows a 4-fold higher k_{cat} as also obtained for specific activity in Table 2 using the crude cell extract, validating the characterization procedure with crude cell lysate. Furthermore, an increased K_m from 0.7 mM (wild type PpADI) to 1.2 mM (M1) and 2.5 mM (M2) was found.

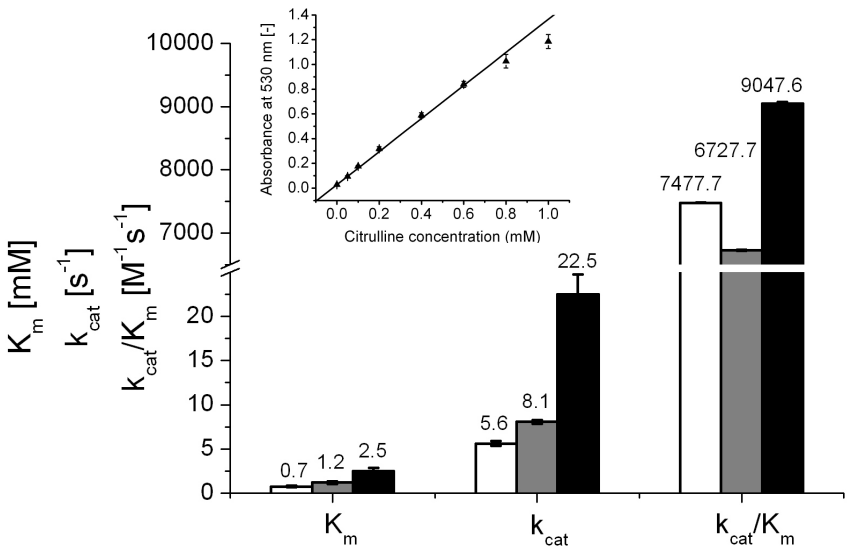

Figure 15. Kinetic parameters of ADI and mutants for conversion of arginine to citrulline. White: ADI wild type, grey: M1 (H404R), black: M2 (K5T D44E H404R). Values reported are the average of three measurements, and average deviations from the mean values are shown. Embedded calibration curve shows linearity of citrulline colorimetric assay in 96-well PCR plate format which was used to determine arginine conversions and kinetic constants.

3.4.9.2 Relative pH profile of wild type and mutant

The relative pH profile (Figure 16) of wild type PpADI and M1 (H404R) shows an identical pH optimum at pH 6.5. Compared to wild type PpADI, variant M2 (K5T

D44E H404R) shows a pH optimum at pH 7.0 which is shifted remarkably (0.5 pH units). Both M1 and M2 show decreased specific activities at pH 6.5, and increased specific activity at pH 7.5. At pH 7.0, the specific activity of M2 exceeds that of wild type PaADI (data not shown).

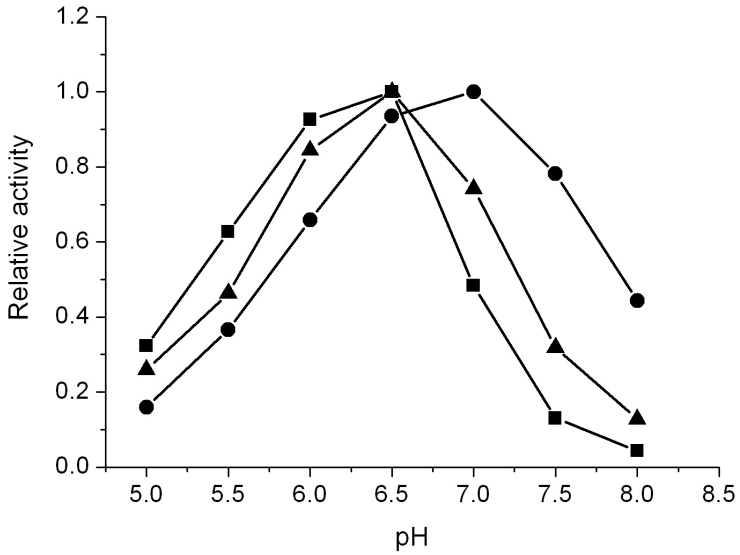

Figure 16. pH profile of wild type ADI, M1(H404R), M2(K5T/D44E/H404R). The relative activity is the ratio of the catalytic activity at the pH relative to the maximum activity of each enzyme. (■) WT, (▲) M1 (H404R), (●) M2 (K5T/D44E/H404R).

3.4.10 Stability of PpADI in the presence of human serum

Table 3 summarizes the stability of PpADI variants in serum (37℃, 60 min; standard deviation of three measurements in brackets). The mutants M1 and M2 have a similar stability in serum when compared to the wild-type PpADI wild type. The substitution D44E and H404R do not destabilize further the PpADI in serum.

Table 3. Stability of PpADI variants in the presence of human serum.

	PpADI WT	M1	M2
No incubation (A_{530})	0.08	0.27	0.98
Incubation with serum (37℃, 60 min) (A_{530})	0.05	0.15	0.69
Residual activity	60 %	55 %	70 %

3.4.11 Activity of PpADI (wild type, M1, M2) towards arginine derivative (N^G, N^G)-dimethylarginine

No detectable conversion of (N^G, N^G)-dimethylarginine could be detected with PpADI variants.

3.5 Discussion

ADI properties have to date not been engineered through directed evolution algorithms despite their often poor performances under physiological conditions and their medical importance as potential anti-tumor drug. Chemically modified of ADI (e.g. through PEGylation) (27) and fusion protein (e. g. Human serum albumin fusion, HSA) (124) have been used for addressing activity and stability demands *in vivo*. Directed evolution offers opportunities to directly improve ADI properties for *in vivo* applications and small libraries of a few thousand variants have often been sufficient to find improved muteins in directed evolution experiments (55, 125).

Our main intention in this report is to provide a validated protocol for directed ADI evolution and improving the activity at the physiological pH 7.4. *Pseudomonas plecoglossicida* CGMCC2039 (PpADI, 7.8 U/mg; pH optimum 6.5) was selected for the directed evolution studies due to its functional expression in *E. coli,* coverage of sequence space in patents and "potential" for activity improvement. PpADI is a relatively slow ADI when compared to Mycoplasma ADIs like MhADI (*Mycoplasma hominus* ADI, 35 U/mg) which would have been good alternatives for directed evolution studies (105). Reported ADI activities range from 0.115 to 140.3 IU/mg. One unit is commonly defined as the ADI amount that converts 1 µmol of L-arginine into 1 µmol of L-citrulline per minute (27).

Screening of PpADI variants yielded three amino acid positions 5, 44 and 404. Positions 44 and 404 resulted in a 4-fold higher k_{cat} at pH 7.4 and a significant shift in the pH optimum (0.5 units) when compared to wild type PpADI (Figure 17 & 8). Position 5 did not show any effect on PpADI activity.

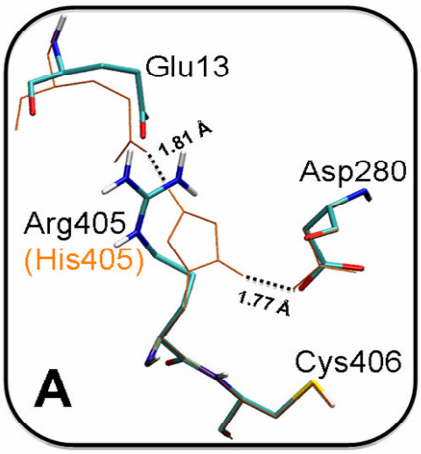

Figure 17. Structural alignment of mutant M1 model with corresponding residues of the crystal structures of the PaADI (in orange). The crystal structure of PaADI which was diffracted in absence of the substrate arginine (1RXX) was used to investigate the substitution of His405 to Arg405. The Arg405 variant shows with respect the Asp280 a different orientation of the guanidinium group when compared to side chain of His405 (in orange).

Galkin and coworkers postulated that the histidine in position 404 (corresponding position in “their” PaADI is 405) is a key residue in controlling activity at acidic and neutral pH. In protonated state of the imidazolium ring a hydrogen bonding interaction can be formed with the oxygen of Asp280 (carboxyl group). This hydrogen bond favors stabilizing interactions between Asp280 and the substrate arginine. His405 in PaADI was reported (17) to share protons with Asp280 and Glu13 and to be important for modulating electrostatic environments of closely located catalytic groups. The same report postulated that H405 is likely to be protonated when the substrate arginine binds to catalytic triad (His278, Glu224, Cys406) [(2)]. Based on these reports the His404 in PpADI was subjected to a site directed mutagenesis to Arg404 and named M1. The M1 variant (H404R) shows 40 % residual activity compared to wild type PpADI at pH 6.4 and a 1.8-fold increase in activity at pH 7.4 (see Table 1). In the M1 (H404R) mutant (see the model in Figure 17; based PaADI 1RXX; residue His404 in PpADI corresponds to His405 in PaADI), the conformational effect due to the extended side chain of Arg likely weakens the hydrogen bond to Asp280 and thus reduces the stabilizing effect on arginine binding. As a result the activity of M1 is reduced, especially at

lower pH values at which His405 is protonated. However at elevated pHs, His405 becomes increasingly deprotonated whereas Arg405 remains protonated and can therefore still stabilize Asp280 for arginine binding. The electrostatic effect suggested by theoretical and experimental studies have evidenced the importance of positively charged residues to modulate the reaction rate of PaADI (126). At pH 6.4, histidine in wild type PpADI and arginine in M1 are both positively charged. At pH 7.4, histidine is only partially positive charged and PpADI's activity is reduced (>90 %) while arginine in M1 remains positively charged preserving M1's activity (Figure 17).

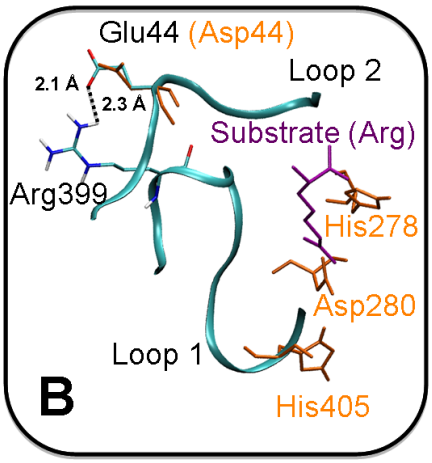

Figure 18. Structural alignment of mutant M2 model with corresponding residues of the crystal structures of the PaADI (in orange). The PaADI crystal structure in presence of substrate arginine was used (2A9G) to investigate the role of the substitution Asp44 to Glu44. The latter was solved for an inactive variant in which Cys406 was replaced by Ala406. The extended side chain of Glu44 might improve the hydrogen bond interaction with the Arg399 inducing a conformational shift of loop 1.

The PpADI H404R was used as starting variant for directed evolution. The amino acid position 44 was identified from a epPCR library (2400 variants screened) resulting in a triple mutant M2 (K5T D44E H404R). For investigating the role of each position the double mutants (K5T H404R) and (D44E H404R) were generated. Only the double mutant (D44E H404R) revealed improvements in k_{cat} (4-fold, pH 7.4; Figure 18). The rationale behind the effects of the mutation D44E on the PpADI activity is more complex to extrapolate from the available ADI crystal structures. Comparative crystallographic studies have shown that the

entrance of the active site is decorated by 4 loops that undergo conformational transitions upon arginine binding (17). The loops exhibit significant shifts that limit the access of water molecules to the active site. The Asp44 is located in loop 1 (residues 30-46) and upon binding of the substrate, Asp44 comes closer to the positively charged Arg399 located on loop 4 (residues 392 to 403). In the D44E mutant, the longer side chain reduces the distance with Arg399 favoring the formation of hydrogen bond (see model in Figure 18). The reinforced interaction between Glu44 and Arg399 might expedite conformational changes in loops, probably confining the arginine substrate in the active site and hence promote arginine conversion. In the future, we plan to further investigate the influence of H404R and D44E using molecular dynamics simulations, further boost the k_{cat} at pH 7.4 and reduce the K_m value of PpADI.

Overall site directed mutagenesis of position H404R and one round of directed evolution (2400 variants screened) resulted in a triple mutant M2 (K5T D44E H404R) with 4-fold higher k_{cat} at pH 7.4 (compared to wild type; Figure 4). The best mutant isolated, M2, has specific activity of 31.3 U/mg at pH 7.4 which is already after one round of evolution close to the specific activity of MhADI (35 U/mg) (127) at its pH optimum. The stability and specificity of improved PpADI variants are furthermore important for cancer treatment *in vivo*. First experiments in AB-human serum (Invitrogen) showed an unaltered stability of M2 compared to the wild type PpADI and (N^G, N^G)-dimethylarginine conversion could not detect with the citrulline colorimetic assay.

3.6 Conclusion

In summary, a directed evolution protocol has been developed for PpADI and validated by increasing the k_{cat} of PpADI at physiological pH (7.4). The reported screening system is the first one employed in directed ADI evolution and can likely be used for other ADIs and other properties such as temperature stability, salt/detergent stability or protease resistance.

Chapter 4. PpADI reengineered for efficient operation under physiological conditions

4.1 Abstract

The proof of concept for ADI engineering by directed evolution resulted in variant M2 (K5T/D44E/H404R). M2 has a pH optimum of pH 7.0 and 4-fold higher k_{cat} value than the wild type PpADI (pH 7.4, 0.5 M phosphate buffer) and an increased K_m value for substrate arginine. In this chapter, in order to improve the catalytic efficiency of PpADI at low concentration of arginine, variant M5 (K5T/D38H/D44E/A128T/H404R) and M6 (K5T/D38H/D44E/A128T/E296K/H404R) were generated from an epPCR library: at pH 7.4 (PBS buffer), the $S_{0.5}$ value decreased from 2.01 mM (parent M3, K5T/D44E/A128T/H404R) to 1.48 mM (M5) and 0.81 mM (M6). The $S_{0.5}$ value of M6 (0.81 mM) is lower than that of PpADI wild type (1.30 mM); the k_{cat} value improved from 0.18 s^{-1} (PpADI wild type) to 17.56 s^{-1} (M5, 97.6-folds) and 11.64 s^{-1} (M6, 64.7-fold).

4.2 Introduction

ADI-based arginine depletion is a target specific therapy for arginine-auxotrophic tumors (e.g. hepatocellular carcinomas and melanomas) and pegylated ADI is currently under clinical trials for HCC with promising results (45). HCC is the third leading cause of cancer mortality world wide with a less than 10 % 5-year survival rate (EU and USA) (128) due to low responses of hepatoma to chemotherapeutic treatments. In 1999, US Food and Drug Administration (FDA) designated ADI-PEG-20 orphan drug status for the treatment of HCC and invasive malignant melanomas, and in 2005 European Agency for the Evaluation of Medicinal Products (EMEA) also granted ADI-PEG-20 orphan drug status for the treatment of HCC. Phase II trials of ADI-PEG-20 in patients with metastatic

hepatocellular carcinomas have shown that the drug is safe, well tolerated, and may benefit patients with unresectable HCC. Izzo and coworker suspected that combination therapies of arginine deprivation and growth inhibition via kinase inhibitors might improve the survival rate further more. Additionally, ADI can enhance radio sensitivity of human mammary adenocarcinoma (MCF-7 cells) (48), exerts anti-proliferative and anti-angiogenic activities and inhibits the growth of viruses such as HIV-1 and hepatitis (49, 50). Current research efforts are focused on ADI's *in vivo* inhibitory effect towards leukemia, melanoma, prostate cancer, renal cell carcinoma, and human umbilical vein endothelial cells (HUVEC) (19, 44, 51-53), clinical trials for HCC (phase II) (45) and melanoma (phase I/II) (46), and inhibitory mechanisms of ADI to tumors (54).

Arginine deprivation is believed to be a main molecular reason for ADI's inhibitory effects on arginine auxotrophic tumors which do not express argininosuccinate synthetase (ASS). ADIs catalyze the first step of the arginine dehydrolase pathway by hydrolyzing arginine to citrulline and ammonium. ADI genes have been identified, purified, and characterized from bacteria, archaea and some eukaryotes excluding mammalian cells (see review (27)). Enzymatic properties of several recombinant ADIs have been examined, such as specific activity, functional expression level, temperature optimum, pH optimum, substrate affinity for arginine, and half-life in human plasma. Only the ADI from *Mycoplasma hominis* has so far been developed as orphan drug by Pheonix Pharmacologics Inc. for HCC and melanoma (129). From enzyme kinetic point of view, none of the ADIs is ideally suited for *in vivo* applications under physiological conditions. Protein engineering by rational design and directed evolution offers opportunities to tailor ADI properties to physiological conditions. PpADI (ADI from *Pseudomonas plecoglossicida*) was functionally expressed in *E. coli* with a simple protocol and has been engineered for the first time by directed evolution for improved activity at physiological pH (3). The variant M2 (K5T/D44E/H404R), by our group reported, showed a 4-fold higher specific activity than the wild type PpADI (0.5 M phosphate buffer, pH 7.4), but a increased K_m value (3.5-fold).

High activity at low arginine concentration is an important prerequisite for ADI's medical application, allowing low ADI dose required per treatment.
In the present work, we improved the directed evolution protocol and identified a PpADI variant with further improved activity and slightly decreased "K_m value" and PpADI variant with lowered K_m value maintaining its high catalytic activity. Those variants were characterized in respect to their kinetic constants.

4.3 Materials and methods

4.3.1 Materials

All chemicals were of analytical-reagent grade or higher quality and were purchased from Fluka (Neu-Ulm, Germany), Sigma-Aldrich (Steinheim, Germany) and Applichem (Darmstadt, Germany), except the resins for purification (TOSOH, Stuttgart, Germany). All enzymes were purchased from New England Biolabs (Frankfurt, Germany), Fermentas (St. Leon-Rt, Germany), and Sigma-Aldrich Chemie (Taufkirchen, Germany), unless stated otherwise.
Thermal cycler (Mastercyler gradient; Eppendorf, Hamburg, Germany) and thin-wall PCR tubes (Multi-ultra tubes; 0.2 µl; Carl Roth, Germany) were used in all PCRs. The PCR volume was always 50 µl except for Megaprimer PCR of whole plasmid (MEGAWHOP, 25 µl); larger volumes were prepared in multiple 50-µl PCRs. The amount of DNA in cloning experiments was quantified by using a NanoDrop photometer (NanoDrop Technologies, Germany).

4.3.2 Methods

4.3.2.1 Site saturation mutagenesis of *PpADI* M2 at position A128

Site directed mutagenesis of *PpADI* M2 (K5T/D44E/H404R) at position A128 was performed according to the published method (130). The following oligonucleotides were used for mutagenesis of A128: 5'-CTGATCGGCGGCGTGNNNGGCCAGGACCTGCCG-3' and 5'-CGGCAGGTCCTGGCCNNNCACGCCGCCGATCAG-3' (underlining indicated the substituted nucleotide). For the mutagenic PCR (First stage: 98°C for 30 s, 1 cycle; 98°C, 30 s/ 55°C, 1 min/ 72°C, 3 min, 3 cycles. Second stage: 98°C for 30

s, 1 cycle; 98℃, 30 s/ 55℃, 1 min/ 72℃, 3 min, 15 cycles; 72℃ for 3 min, 1 cycle), 2 U of PhuS DNA polymerase, 0.20 mM of dNTP mix, 25 pmol of each primer together with 100 ng of template (pET42b(+) harboring PpADI M2 gene) were used. Following the PCR, DpnI (40 U; New England Biolabs) was added, and incubated overnight at 37℃. The PCR products were purified by using a QIAquick PCR Purification Kit (Qiagen) and transformed into *E. coli* BL21-Gold (DE3) for expression.

4.3.2.2 Construction of PpADI error-prone library

EpPCR library was generated by the standard error-prone PCR (epPCR) using improved variant M3 (K5T/D44E/A128T/H404R) as template. For the mutagenic PCR (95℃ for 2 min, 1 cycle; 95℃, 30 s/ 55℃, 30 s/ 72℃, 30 s, 29 cycles; 72℃ for 3 min, 1 cycle), 2.5 U of Taq DNA polymerase, 0.20 mM of dNTP mix, 50 ng of template (pET42b(+) harboring PpADI M3 gene), 0.01-0.1 mM of $MnCl_2$ and 10 pmol of each primer (5'-TACATATGTCCGCTGAAACACAGAAG-3' and 5'-GTGCTCGAGTTAGTAGTTGATCGG-3') were used. The PCR products were purified by using a QIAquick PCR Purification Kit. The purified epPCR products were cloned into expression plasmid pET42b(+) by MEGAWHOP (114). For MEGAWHOP (72℃ for 5 min, 1 cycle; 98℃ for 1 min 30 s, 1 cycle; 98℃, 45 s/ 55℃, 45 s/72℃, 4 min, 24 cycles; 72℃ for 10 min, 1 cycle), 1.2 U of PfuS DNA polymerase, 0.20 mM of dNTP mix, 500 ng of epPCR products together with 50 ng of template (pET42b(+) harboring PpADI gene of variant M3) were used. Following the PCR, DpnI (40 U; New England Biolabs) was added, and incubated (overnight; 37℃). The MEGAWHOP products were transformed into *E. coli* BL21-Gold (DE3) for expression and screening.

4.3.2.3 Site directed mutagenesis at position D38 of *PpADI* M4

Site directed mutagenesis of *PpADI* variant M4 at position D38 was performed according to the published method on plasmid pET42b(+)-ADI-M4 (K5T/D44E/A128T/E296K/H404R). The following oligonucleotides were used for mutagenesis of D38H: 5'-ACCCCGAGCAACTGCCACGAGCTGCTGTTCGAC-3'

and 5'-GTCGAACAGCAGCTCGTGGCAGTTGCTCGGGGT-3' (underlining indicated the substituted nucleotide). Conditions for mutagenic PCR are as described in "Site saturation mutagenesis of *PpADI* M2 at position A128".The PCR products were purified by using a QIAquick PCR Purification Kit (Qiagen) and transformed into *E. coli* BL21-Gold (DE3) for expression.

4.3.2.4 Site saturation mutagenesis at position D38 and E296 of *PpADI* M3

Site saturation mutagenesis library at position D38 and E296 of *PpADI* variant M3 (K5T/D44E/A128T/H404R) were generated according to the published method on plasmid pET42b(+)-ADI-M3 using the following oligonucleotides: D38FP (5'-ACCCCGAGCAACTGCNNNGAGCTGCTGTTCGAC-3'), D38RP (5'-GTCGAACAGCAGCTCNNNGCAGTTGCTCGGGGT-3') and E296FP (5'-GTCACGGTTTTCCCGNNNGTGGTGCGCGAGATC-3'), E296RP (5'-GATCTCGCGCACCACNNNCGGGAAAACCGTGAC-3') (underlining indicated the substituted nucleotide). Conditions for mutagenic PCR are as described in "Site saturation mutagenesis of PpADI M3 gene at position A128".The PCR products were purified by using a QIAquick PCR Purification Kit (Qiagen) and transformed into *E. coli* BL21-Gold (DE3) for expression.

4.3.2.5 Cultivation and expression of PpADI in 96-well plates

Cultivation and expression in 96-well plates (flat bottom, polystyrene plates; Greiner Bio-One GmbH, Frickenhausen, Germany) were performed as previously described in 3.3.2.8.

4.3.2.6 Improved screening system in 96-well plate to identify PpADI variants with high activities at low arginine concentration

As describe previously, the modified protocol of citrulline detection based on carbamido-diacetyl reaction was used for screening for improved ADI affinity to arginine at pH 7.4. 15 µl of cell culture was transferred to 96-well microtiter plate. Enzyme reaction was initiated by addition of arginine solution (105 µl, 1mM arginine in PBS buffer, pH 7.4) supplemented with

cetyltrimethylammoniumbromide (CTAB, 4 mM), and incubated (10 min, 37°C). The following color development procedure was carried out as described previously (3).

Standard deviation measurements were performed in 96-well plate format using culture from BL21-Gold (DE3) lacking PpADI and in a separate experiment containing PpADI variant M3. Apparent standard deviation was based on the absolute absorbance values obtained from the PpADI variant M3 plate. The true standard deviation was calculated by subtracting the background absorbance value of the microtiter plate lacking ADI from the apparent values.

4.3.2.7 Expression of PpADI in shaking flask and purification

Expression of PpADI in shaking flasks and purification (by anion exchange chromatography and gel filtration) was performed as previously described in 3.3.2.10.

4.3.2.8 Characterization of PpADI variants

Preliminary determination of kinetic constants for site saturation mutagenesis variants of position 38 and 296

The k_{cat} and K_m values were determined from initial velocity data measured as a function of substrate concentration. Enzyme reaction was carried out at 37°C in incubator (Heraeus Holding GmbH, Hanau, Germany) using cell crude extract. 2 ml of expression culture was harvested by centrifugation (Eppendorf 5415R 4°C, 13,000 g, 10 min) and then freezed (-20°C, overnight). Cell lysate was prepared by resuspending the cell pellet in lysozyme (91000 U, 50 mM phosphate buffer, pH 7.4, 1.3 ml) followed by incubation (37°C, 40 min) and centrifugation (4°C, 13,000 g, 10 min). 15 µl of diluted (4 times diluted with 50 mM phosphate buffer, pH 7.4) cell lysate was transferred to 96-well microtiter plates. Enzyme reaction was initiated by addition of arginine solution (105 µl, 0.25-10 mM arginine in PBS buffer, pH 7.4) and incubated (7 min, 37°C). Subsequently, ferric-acid solution (120 µl) was added to each well to stop enzyme reaction. 60 µl of terminated

enzyme reaction mixture was transferred to 96-well PCR plate for color development. Ferric-acid solution (90 µl) and DAM-TSC solution (15 µl) were added to each well. The 96-well PCR plate was then incubated (70°C, 30 min) in thermal cycler (Eppendorf Mastercyler gradient) for color development, followed by incubation in ice water to stop color development. Absorbance was measured at 530 nm using a microtiter plate reader (Tecan Sunrise TC reader, Tecan Group AG, Zurich, Switzerland). The initial velocity data obtained were fitted to the equation $v = V_{max}[S]/([S] + K_m)$ (where v is the initial velocity, Vmax the maximum velocity, [S] the substrate concentration, and Km the Michaelis constant) using GraphPad Prism software (GraphPad software, San Diego, CA, USA). The kcat was calculated from the ratio of V_{max} and enzyme concentration.

Determination of kinetic constants of PpADI wild type and variants M3, M4, M5, M6

The k_{cat} and $S_{0.5}$ values were determined from initial velocity data measured as a function of substrate concentration. Enzyme reaction was carried out at 37°C in a water bath as described previously using purified enzyme (50 µl, 0.1-1.8 µM) to and substrate solution (200 µl, 0.5 mM to 10 mM of arginine, PBS buffer, pH 7.4) in deep well plates.

The initial velocity data obtained were fitted to the sigmoidal model of kinetics equation $v = V_{max}^{n}/(S_{0.5}^{n} + K^{n})$ (where v is the initial velocity, V_{max} is the maximum velocity, K is the substrate concentration, and $S_{0.5}$ is the ligand concentration producing half occupation (131)) using GraphPad Prism software (GraphPad software, San Diego, CA, USA). The k_{cat} was calculated from the ratio of V_{max} and enzyme concentration.

4.3.2.9 Native polyacrylamide gel electrophoresis of PpADI variants

10% of polyacrylamide native gels were used for protein electrophoresis to analyze the native form of PpADI variants. Purified protein of PpADI variants (7 µl of protein and 3 µl of loading dye) were loaded into each lane of native gel. The

molecular marker used in the gel is NativeMark™ Unstained Protein Standard (Invitrogen, Darmstadt, Germany). The electrophoresis was performed with tris/glycine buffer (pH 8.3) and electrophoresis chamber was incubated in ice-water bath. Protein bands were stained with Coomassie brilliant blue solution.

4.3.2.10 Homology modeling

Homology modeling approach was used for the structure prediction of PpADI. The model was built by using the automated structure prediction tool, Protein homology/analogy recognition engine (Phyre: http://www.sbg.bio.ic.ac.uk/~phyre/) (132). The crystal structure of PaADI (PDB ID: 2A9G) was used as template by the server and It has 84.9% sequence identity (http://blast.ncbi.nlm.nih.gov/Blast) with PpADI. Procheck program suit (http://www.ebi.ac.uk/thornton-srv/software/PROCHECK/) (133) was used to assess the stereochemical quality of the model. Ramachandran plot which represented that 84.7% residues were present in the most favoured region and 14.7% in additional allowed region (Figure 3). Dfire was used to access non bonded atomic interaction in the model (http://sparks.informatics.iupui.edu/hzhou/dfire.html/) (134), and Qmean (http://swissmodel.expasy.org/qmean/cgi/index.cgi) (135) for the estimation of global protein quality. Swiss-PdbViewer (118) was used to create the tetramer structure by fitting the monomer model on the 4 units of the 2A9G template. The variant M6 (D38H, D44E, A128T, E296K, H404R) were created by using the “mutate” tool of the Swiss-PdbViewer and by selecting rotamers with the best fitness score. All tetramers were energy minimized in vacuum using GROMOS 43B1 force field (119).

4.4 Results

4.4.1 Improved screening system in microtiter plates to identify PpADI variants with high activities at low arginine concentration

Screening assay was based on the validated citrulline colorimetric screening protocol in microtiter plate, as reported previously (3). In order to screen for variants with high activity at low arginine concentration under physiological

condition concerning pH and ion concentrations, 1 mM arginine in PBS buffer (pH 7.4) as substrate solution was employed in screening assay and enzyme reaction time was controlled accordingly (10 min). The coefficient of variation is an important performance criterion of a screening system to determine its accuracy. Optimized assay condition with 1 mM arginine (PBS buffer, pH 7.4) as substrate resulted in true coefficient of variation of 14.9 % (Figure 1). The resulting low absolute absorbance value is a main reason for the high true coefficient of variation (14.9 %). In the previous screening system, 100 mM arginine in 0.5 M sodium phosphate buffer was used and yielded higher activity variants but with higher K_m value.

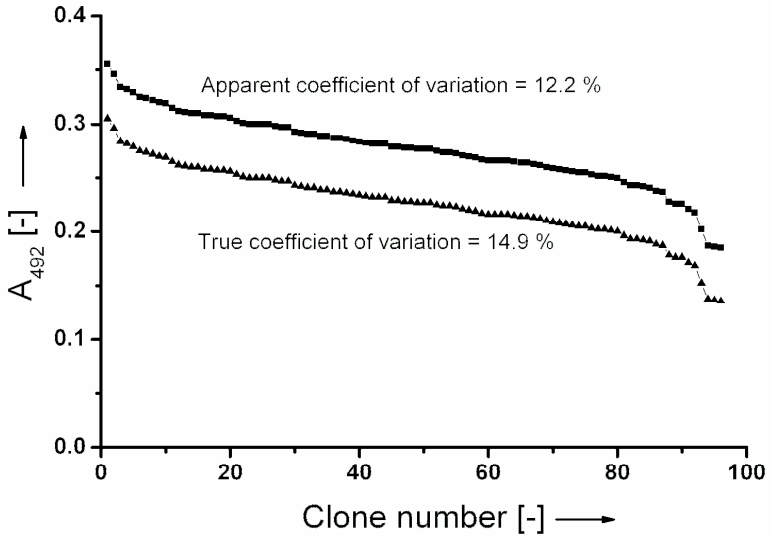

Figure 1. Activity values in descending order of the PpADI variant M3 conversion of arginine to citrulline in a 96-well microtiter plate using the optimized assay protocol. The apparent coefficients of variation were calculated without subtracting the background and the true coefficients of variation after background subtraction.

4.4.2 Genealogic tree of directed PpADI evolution

Figure 2 shows the two rounds of PpADI evolution, generation of saturation mutagenesis libraries and recombination of beneficial positions to finally obtain the PpADI variant M6 with 64.7-fold higher k_{cat} and reduced $S_{0.5}$ (1.3 mM (WT) to 0.81 mM (M6). Based on structure-function analysis of PaADI[16], M1 was generated by substitute His at position 404 with Arg. Position 404 is through

interactions with position Asp280 involved in substrate stabilization during catalysis. M1 was subject to the first round of epPCR library, from which M2 was identified showing a 4-fold improved k_{cat} value and increased K_m value (2.5 mM in 0.5 mM sodium phosphate buffer, pH 7.4)[15]. M3 was generated by a site saturation mutagenesis library at position 128 which increased in another clone the expression level (data not shown). In order to improve PpADI towards medical application demands (high activity at low arginine concentration), a second epPCR mutant library was constructed using M3 as parent. M4 with decreased $S_{0.5}$ value (0.81 mM) and M5 with increased K_{cat} value (17.56 s^{-1}) were identified after screening of ~1400 clones. In M4 the position E296 was identified to be important for lowering $S_{0.5}$ and in M5 position D38 was identified to be important for activity increase. M6 was finally constructed by combining the substations at position D38 and E296. Saturation mutagenesis of these two positions did not yield any further improved $S_{0.5}$ or activity variant.

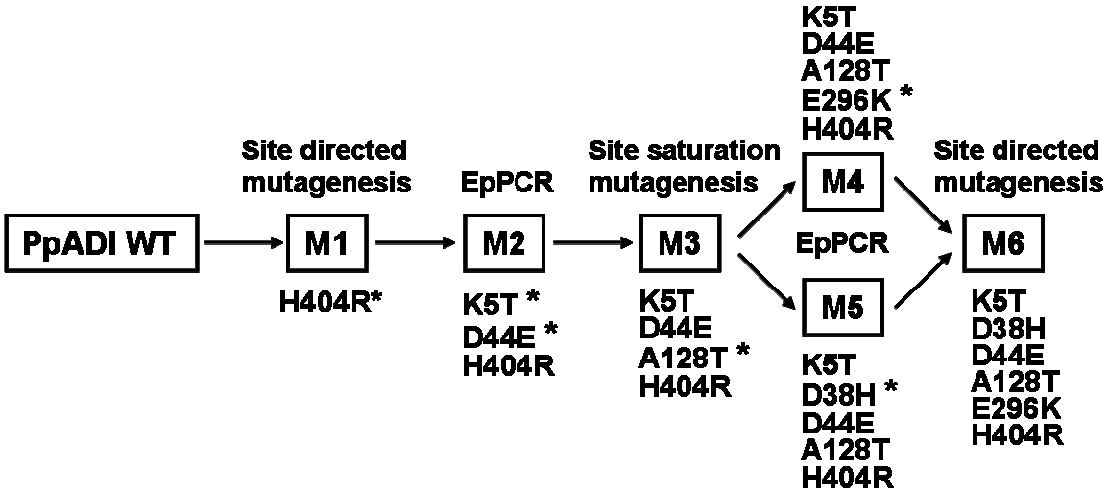

Figure 2. Genealogic tree of PpADI variants (M1 to M6) with generated amino acid substitutions. Novel substitutions are indicated by an asterisk.

4.4.3 EpPCR library construction and screening for variants with high activities at low arginine concentration

Variant M2 was used as a starting template. As described previously, M2 shifts the pH optimum from pH 6.5 to pH 7.0 and has a 4-fold faster k_{cat} than PpADI wild type. In one sequenced mutant, position A128 was identified to be

responsible for higher expression (data not shown). Site saturation mutagenesis on M2 therefore was carried out at position A128. The resulting variant M3 (K5T/D44E/A128T/H404R) showed a ~2-fold improved expression and was subsequently used as parent template for epPCR library.

Three concentrations of $MnCl_2$ (0.01-0.10 mM) were used in epPCR library generation to adjust the ratio of active to inactive clones. Instead of 0.02 mM $MnCl_2$, 0.05 mM $MnCl_2$ which generated 46 % of inactive mutant was selected for library generation. EpPCR mutant libraries with a ratio of ~50 % active and ~50 % inactive clones have often been used successfully in directed evolution, improving enzyme properties by gradual changes (one or two amino acids changes per round of mutagenesis and screening). Two variants M4 and M5 were identified from this epPCR library (~1400 clones) and further characterized. Variant M4 and M5 were sequenced and one additional amino acid substitution was identified for each variant, E296K and D38H, respectively.

4.4.4 Site saturation mutagenesis of *PpADI* at position D38 and E296

To investigate their role in improving of catalytic performance for arginine, site saturation mutagenesis library at position D38 and E296 were generated using PpADI M3 as template. For each position, ~300 clones were screened at low concentration of arginine (1 mM, PBS buffer, pH 7.4), using 96-well plate format citrulline colorimetric screening assay.

After the screening of site saturation mutagenesis libraries of position 38 and 296, variants with higher activity were chosen for preliminary kinetic investigation using crude cell extract. Beneficial mutants were identified and sequenced from both sites (Table 1). At position 38, the following beneficial substitutions were found: D38R (three times, AGA, CGG, CGT) and D38K (twice, AAG, AAA). In all cases, the negatively charged acidic amino Asp had been replaced by positively charged amino acids, Arg or His. Substitution by negatively charged Glu resulted in a clone showing a parent M3-like kinetic behavior. Hydrophobic amino acid

substitution by Pro resulted inactive clone under assay conditions. At position 296, the following substitutions were found to be beneficial: E296K (twice, AAA, AAG), E296N (once, AAC), E296T (once, ACC), E296G (once, GGA). Among these substitutions, variants with substitution to positively charged residue Lys show lowest $S_{0.5}$ value for arginine while substitution by uncharged amino acids (Asn, Thr, Gly) shows relatively marginal improvement compared to E296K. Hydrophobic amino acid substitution by Pro and Trp resulted in very low activity clones.

Table 1. Nucleotide and amino acid substitutions at position 38 in PpADI M3.

PpADI variants	Substitution at position 38	k_m (mM)
M3 (parent)	Asp (GAC)	3.74 ± 0.35
SSM-D38R	Arg (AGA, CGG, CGT)	1.16 ± 0.21
SSM-D38K	Lys (AAG, AAA)	1.01 ± 0.28
SSM-D38E	Glu (GAG)	2.95 ± 0.77
SSM-D38P	Pro (CCA)	n. d.
SSM-D38T	Thr (ACC)	n. d.
M5	His (CAC)	1.26 ± 0.12

Kinetic experiments were performed with crude cell extracts.

Table 2. Nucleotide and amino acid substitutions at position 296 in PpADI M3.

PpADI variants	Substitution at position 296	k_m (mM)
M3 (parent)	Glu (GAA)	3.74 ± 0.35
SSM-E296K	Lys (AAA, AAG)	0.20 ± 0.01
SSM-E296N	Asn (AAC)	0.53 ± 0.04
SSM-E296T	Thr (ACC)	0.61 ± 0.04
SSM-E296Q	Gln (CAA)	0.79 ± 0.06
SSM-E296G	Gly (GGA)	1.29 ± 0.12
SSM-E296W	Trp (TGG)	n. d.
SSM-E296P	Pro (CCT)	n. d.
M4	Lys (AAA)	0.27 ± 0.02

Kinetic experiments were performed with crude cell extracts.
* n. d. activity not detectable under assay conditions.

4.4.5 Determination of kinetic constants (k_{cat} and $S_{0.5}$) of PpADI wild type and variants M3, M4, M5 and M6

Table 3. Kinetic constants of wild type PpADI and variants.

	Wild type	M3 (parent)	M4	M5	M6
k_{cat} (s^{-1})	0.18 ± 0.05	10.13 ± 0.36	5.88 ± 0.09	17.56 ± 1.15	11.64 ± 0.50
$S_{0.5}$ (mM)	1.30 ± 0.25	2.01 ± 0.19	0.81 ± 0.03	1.48 ± 0.17	0.81 ± 0.09

* Kinetic contants of PpADI wild type is different from our previous report because in stead of 0.5 M phosphate buffer, PBS buffer was used for kinetic measurements. K_{cat} value of PpADI wild type dropped from 5.6 s^{-1} to 0.18 s^{-1} and k_{cat} value of M2 is reduced ~2-fold.

M3, the parent of the second round of PpADI epPCR library, M4 with decreased $S_{0.5}$, M5 with increased k_{cat} and best variant M6 with best combination of k_{cat} value and $S_{0.5}$ were selected for detailed characterization studies.

Kinetic characterization of PpADI variants was performed using PBS buffer (pH 7.4), which is commonly used in biological research. PBS buffer helps to maintain a constant pH and its osmolarity and ion concentrations usually match those of the human body. Citrulline production of PpADI variants was maintained between 0.2-0.8 mM. Table 3 summarizes the k_{cat} and $S_{0.5}$ values of parent M3 (K5T/D44E/A128T/H404R), variants M4 (K5T/D44E/A128T/E296K/H404R), M5 (K5T/D44E/A128T/D38H/H404R) and M6 (K5T/D38H/D44E/A128T/E296K/H404R), which were expressed in shaking flasks cultures and purified using a two step procedure (anion exchange follows by gel filtration). Compared to parent M3 ($S_{0.5}$ = 2.01 mM), both variants M4 and M5 have a lower $S_{0.5}$ for arginine conversion at pH 7.4, 0.81 mM and 1.48 mM, respectively. Variant M4 shows a decreased k_{cat} value, 58% of parent M3 while M5 shows a 1.7-fold higher k_{cat} compared to parent M3. Variant M6 with combined mutations (K5T/D38H/D44E/A128T/E296K/H404R) shows decreased $S_{0.5}$ value, 40 % of parent M3 (K5T/D44E/A128T/H404R), 62 % of PpADI wild type, and a 64.7-fold faster k_{cat} value than PpADI wild type. M6 is 42.3-fold faster than PpADI wild type with 0.4 mM arginine (PBS buffer, pH 7.4) as substrate.

After two rounds of epPCR libraries coupled with site directed mutagenesis, a variant M6 with 64.7-fold higher k_{cat} and lower $S_{0.5}$ value (0.81 mM) than PpADI wild type (0.31 mM). At low concentration of arginine, activity of M6 enhanced dramatically than M3 and wild type. For example, M6 is 42.3-fold faster than PpADI wild type in 0.4 mM arginine (PBS buffer, pH 7.4).

4.4.6 Native polyacrylamide gel electrophoresis of PpADI variants

Multimeric form of PpADI variants were investigated by native polyacrylamide gel electrophoresis. As shown in Figure 3, two distinct protein bands representing two multimeric forms tetramer and dimer (molecular weight of a subunit is ~ 46 kDa) were observed, but with different concentration percentage. The major multimeric form of M3 is dimer. Compared to M3, M4 with an additional mutation E296K shows a very different pattern: tetramer is the main form; while M5 with an additional mutation D38H contains more or less equal amount of dimer and tetramer. M6, with both mutations E296K and D38H, contains more tetramer than dimer.

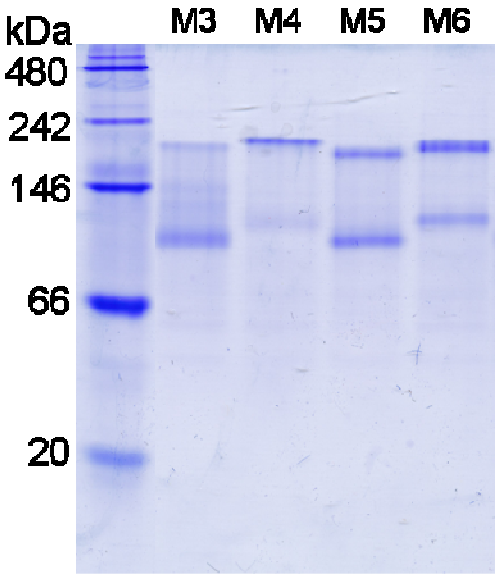

Figure 3. Native polyacrylamide gel electrophoresis of PpADI variants (M3 to M6) with different dimer/tetramer distribution. Single subunit has a molecular weight of ~46 kDa.

4.5 Discussion

Directed evolution allows improving all properties that can be reflected in a screening system through iterative rounds of diversity generation and screening. Small libraries of a few thousand variants are often sufficient to find improved variants [18] even without rational understanding of the targeted property. After establishing a first directed ADI evolution protocol yielding mutant M2, we adjusted the screening system to better reflect ADI's application conditions. Prerequisite for ADI to become an effective anti-tumor agent is that low concentrations of arginine in human plasma can effectively be converted.

Figure 2 shows the genealogic tree of PpADI evolution and before discussing the influence of each substitution individually the effect on kinetics are briefly summarized. Amino acid substitution D44E (M2) increases k_{cat} and $S_{0.5}$, substitution A128T (M3) increases the expression level, and substitution E296K (M4) decreases k_{cat} and $S_{0.5}$ and is responsible for tetramer formation. Substitution D38H (M5) increase largely k_{cat} and reduces slightly $S_{0.5}$. The combination of all mentioned residues in M6 result in a finally 64.7-fold improved PpADI activity and reduced $S_{0.5}$ (1.30 to 0.81 mM).

PpADI M3 was obtained from site saturation mutagenesis library at position A128 using M2 as template (Figure 2). M3 shows improved functional expression level of ADI (data not shown) and was used as parent for generating an epPCR library. Screening of epPCR library yielded two improved variants M4 and M5, carrying an additional mutation, E296K (M4) and D38H (M5). M4 has a decreased $S_{0.5}$ (0.81 mM) and a decreased k_{cat} value (5.88 s^{-1}; see Table 3). M5 has a decreased $S_{0.5}$ (1.48 mM) and an increased k_{cat} value (17.56 s^{-1}) when compared to parent M3 ($S_{0.5}$, 2.01 mM; k_{cat}, 10.03 s^{-1}; see Table 3). M6 which harbors both substitutions (E296K and D38H) has a decreased $S_{0.5}$ value (0.81 mM) compared to the parent M3 (1.30 mM) and the wild type (2.01 mM), and a 64.7-fold higher k_{cat} value than the PpADI wild type.

Despite further enhancing the activity of PpADI, it is crucial for an efficient conversion of the substrate arginine in human plasma (100-120 µM arginine) to reduce PpADI's "K_m" ($S_{0.5}$) value. Figure 4 shows the kinetics of PpADI WT, parent M3, and the variants M4, M5 and M6. M3 has a significantly higher k_{cat} value compared to WT, but its activity at low concentration of arginine (<1.0 mM) is very low ($S_{0.5}$ value 2.01 mM). In contrast, the most efficient variant M6 with a decreased $S_{0.5}$ value (0.81 mM) shows a remarkable activity improvement at low concentrations of arginine (<0.5 mM; see Figure 4). M6 has additional two amino acid substitutions (D38H and E296K) compared to M3 which increases k_{cat} and reduces the $S_{0.5}$ value. The combination of D38H and E296K improves especially the activity of M6 at low arginine concentrations (< 0.5 mM; see Figure 4).

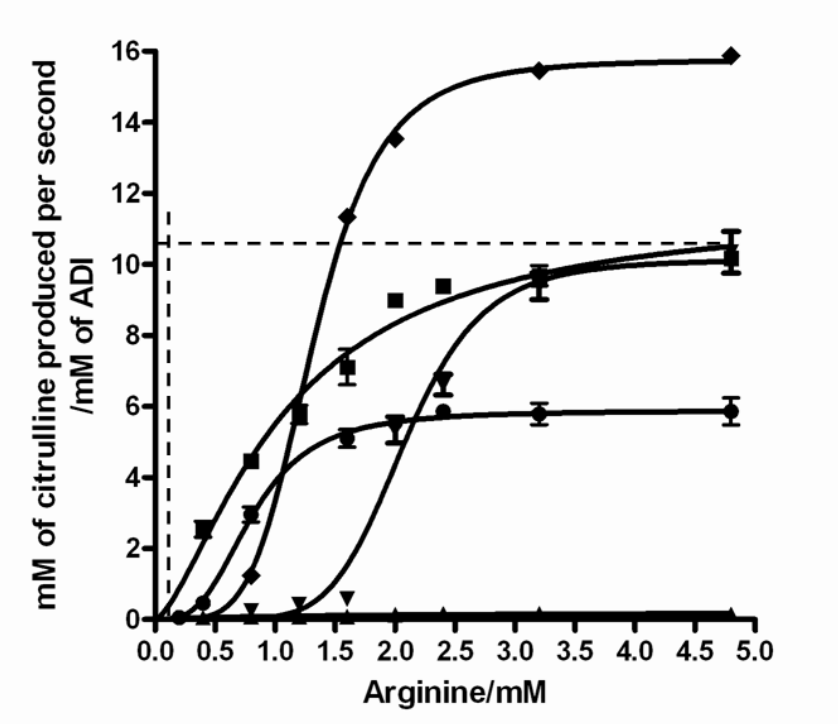

Figure 4. Kinetic curve of PpADI wild type, M3, M5 and M6. (▲) PpADI wild type, (▼) M3, (●) M4, (♦) M5 and (■) M6.

Figure 5 shows the tetrameric model (based on PaADI, PDB code 2A9G) of PpADI WT (Figure 5A) and variant M6 (Figure 5B). Monomeric units are

indicated with the letters a, b, c and d. The access channel to the active sites of each monomer is highlighted in square and faces an internal cavity generated by the assembly of four PpADI monomers. The substitutions D38H (in blue) and D44E (in green) are localized at the interface of monomer pair a-b and c-d. The substitution of Glu by Asp at position 44 provides a longer side chain in close proximity of the also negatively charged residue Asp43 (Figure 6A). The substitution E296K is localized at the border of the entrance to the internal cavity of the PpADI tetramer. E296K promotes the tetramer formation likely by introducing stabilizing interactions with other residues, for example with Thr33 (hydrogen bond). E296K inverts the charge at this position and its increased length of the side chain might promote further interactions to a neighboring monomer (Figure 6A). The combination of D44E and E296K results in a population consisting of mainly tetramers (see Figure 3; mutein M4). Interestingly with the formation of a tetramer (M4) the $S_{0.5}$ value is reduced which indicates that the tetramer complex formation promotes interactions with the substrate arginine at low concentrations. The substitution D38H together with the E296K in the mutein M6 reestablishes an almost equal population of PpADI dimers and tetramers. A hypothesis is that Lys of the E296K has an electrostatic stabilizing interaction with the Glu38 in the M4 but not to the neutral His38.

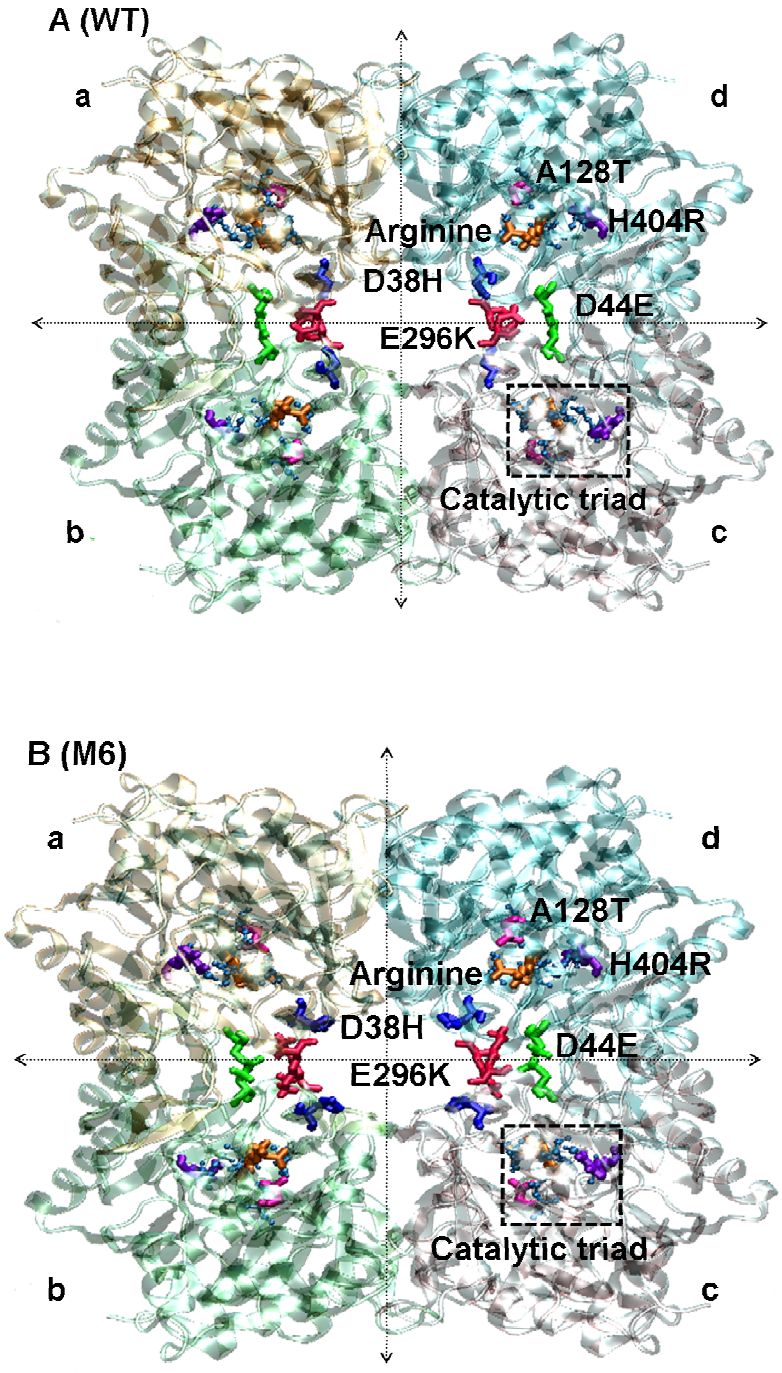

Figure 5. A). The model of WT tetramer after energy minimization in vacuum (GROMOS 43B1). B). The model of M6 tetramer after energy minimization in vacuum (GROMOS 43B1). Active site residues are represented in CRK format in a square (Blue). Mutated residues are shown in licorice format in different colors like D38H (blue), D44E (green), A128T (magenta), E296K (red) and H404R (violet). Substrate arginine is represented in orange color by licorice format.

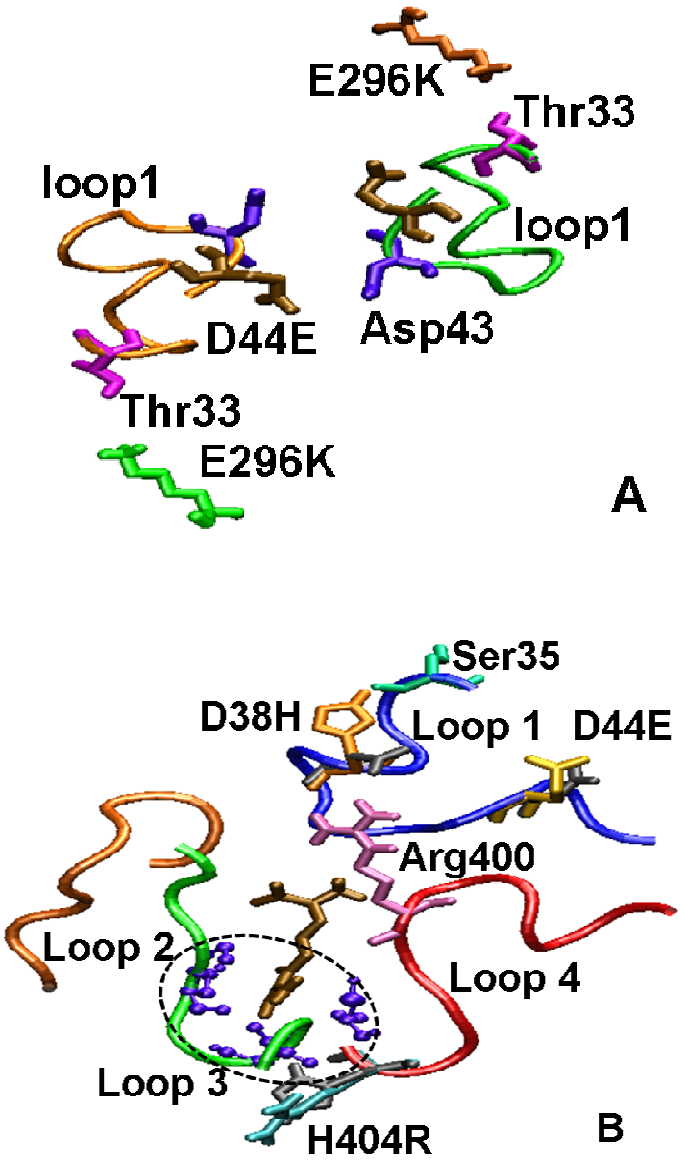

Figure 6. A). Structure model of variant M6. E296K is involved in intermonomer interaction (between chain a (orange) and b (green)) with Thr33. D44E is involved in intermonomer interaction, between chain A (orange) and B (green), with Asp43 (violet). B). Structure alignment of PpADI WT model and M6 model with four loops (loop 1:30-46, loop 2:178-175, loop 3:271-281 and loop 4: 393-404) surrounding the entrance of the active site. The substitutions in these loops and the residues involved in the interaction with those substitutions are representing: D38H (orange), D44E (yellow) and H404R (cyan, in M6; gray, in WT), Ser35 (green), Arg 400 (pink), substrate arginine (ochre), catalytic triad His278, Asp280 and Cys406 (violet, highlighted in an oval)

Figure 6B shows that the active site of the PaADI is surrounded by four loops (loop 1: 30-46, loop 2: 178-185, loop 3: 271-281, and loop 4: 393-404). These four loops undergo a conformational transition upon arginine binding and tighten

the surrounding of the arginine substrate[16]. D38 is located in loop 1 and faces towards the substrate access channel. In PpADI model (Figure 6B), the D38H mutation promotes the formation of a hydrogen bond interaction with the neighboring residues Ser35, contributing to the stability of the entropically unfavorable folded conformation of loop1. The rigidified loop 1 might be beneficial for arginine conversion. According to PaADI structure analysis, the side chain of gating residue Arg401 (Arg400 in PpADI) is located at the active site entrance and fills the substrate-binding site. The structure analysis of the C406A PaADI-L-arginine complex[16] shows that the Arg401 side chain (Arg400 in PpADI) is displaced by the substrate arginine to a position near the active site entrance that allows its hydrocarbon chain to assist shielding the catalytic site from solvent. D38 is involved in an ionic interaction and hydrogen bonding with Arg400. The substitution of Asp to His at position 38 results in a loss of ionic interactions to Arg400 due to the different lengths of the side chains. His38 can form only a hydrogen bond with active site gating residue Arg400. A weakened interaction between position 38 and Arg400 might increase the flexibility of the side chain of Arg400 which then might block less efficiently the access of arginine to the active site. As a result the variant M5 shows an improved k_{cat} value (1.7-fold compared to parent M3) due to the substitution D38H.

For elucidating further the individual role of the five identified amino acid substitutions and their influence on the active site geometry and tetramer formation crystal structures of variant M4 and M6 have to be solved.

4.6 Conclusion

In summary, with the modified screening protocol, PpADI variants with improved k_{cat} and $S_{0.5}$ were identified. The increased k_{cat} value and decreased $S_{0.5}$ value result in significant activity improvement of PpADI at low arginine concentrations. Especially the kinetic constants of PpADI variant M6 demonstrate that PpADI properties can be tailored by directed evolution. The generated PpADI variants match from their kinetic behavior therapeutic application demands much better

than the wild type PpADI. We therefore hope that by directed evolution improved PpADIs will further be investigated *in vivo* for tumor therapy.

References

1. Li L, Li ZM, Chen DQ*, et al.* Inactivation of microbial arginine deiminases by L-canavanine. Journal of the American Chemical Society, 2008; 130(6): 1918-31.

2. Lu XF, Li L, Wu R*, et al.* Kinetic analysis of *Pseudomonas aeruginosa* arginine deiminase mutants and alternate substrates provides insight into structural determinants of function. Biochemistry, 2006; 45(4): 1162-72.

3. Zhu LL, Tee KL, Roccatano D*, et al.* Directed evolution of an antitumor drug (arginine deiminase PpADI) for increased activity at physiological pH. Chembiochem, 2010; 11(5): 691-7.

4. Das K, Butler GH, Kwiatkowski V, Clark AD, Yadav P, Arnold E. Crystal structures of arginine deiminase with covalent reaction intermediates: Implications for catalytic mechanism. Structure, 2004; 12(4): 657-67.

5. Schofield PJ, Edwards MR, Matthews J, Wilson JR. The pathway of arginine catabolism in *Giardia intestinalis*. Molecular and Biochemical Parasitology, 1992; 51(1): 29-36.

6. Linstead D, Cranshaw MA. The pathway of arginine catabolism in the parasitic flagellate *Trichomonas vaginalis*. Molecular and Biochemical Parasitology, 1983; 8(3): 241-52.

7. Yarlett N, Lindmark DG, Goldberg B, Moharrami MA, Bacchi CJ. Subcellular localization of the enzymes of the arginine dihydrolase pathway in Trichomonas vaginalis and Tritrichomonas foetus. J Eukaryot Microbiol, 1994; 41(6): 554-9.

8. Biagini GA, Yarlett N, Ball GE*, et al.* Bacterial-like energy metabolism in the amitochondriate protozoon Hexamita inflata. Mol Biochem Parasitol, 2003; 128(1): 11-9.

9. Makhlin J, Kofman T, Borovok I*, et al.* Staphylococcus aureus ArcR controls expression of the arginine deiminase operon. Journal of Bacteriology, 2007; 189(16): 5976-86.

10. Seggewiss J, Becker K, Kotte O*, et al.* Reporter metabolite analysis of transcriptional profiles of a Staphylococcus aureus strain with normal phenotype

and its isogenic hemB mutant displaying the small-colony-variant phenotype. Journal of Bacteriology, 2006; 188(22): 7765-77.

11. Altucci P, Sapio V, Vitale P, de Vargas F. Mycoplasma in human pathology. Current status of the problem, with special reference to respiratory pathology. Recenti Prog Med, 1966; 41(5): 409-55.

12. Harasawa R, Koshimizu K, Kitagawa M, Asada K, Kato I. Nucleotide sequence of the arginine deiminase gene of *Mycoplasma hominis*. Microbiology and Immunology, 1992; 36(6): 661-5.

13. Takaku H, Matsumoto M, Misawa S, Miyazaki K. Antitumor activity of arginine deiminase from *Mycoplasma arginini* and its growth inhibitory mechanism. Japanese Journal of Cancer Research, 1995; 86(9): 840-6.

14. Fenske JD, Kenny GE. Role of arginine deiminase in growth of *Mycoplasma hominis*. Journal of Bacteriology, 1976; 126(1): 501-10.

15. Wei YZ, Zhou H, Sun Y, He YB, Luo YZ. Insight into the catalytic mechanism of arginine deiminase: Functional studies on the crucial sites. Proteins-Structure Function and Bioinformatics, 2007; 66(3): 740-50.

16. Ensor CM, Holtsberg FW, Bomalaski JS, Clark MA. Pegylated arginine deiminase (ADI-SS PEG(20,000) (mw)) inhibits human melanomas and hepatocellular carcinomas in vitro and in vivo. Cancer Research, 2002; 62(19): 5443-50.

17. Galkin A, Lu XF, Dunaway-Mariano D, Herzberg O. Crystal structures representing the Michaelis complex and the thiouronium reaction intermediate of Pseudomonas aeruginosa arginine deiminase. Journal of Biological Chemistry, 2005; 280(40): 34080-7.

18. Kundu M, Thomas J, Fialho AM*, et al.* The anticancer activity of the N-terminal CARD-Like domain of arginine deiminase (ADI) from *Pseudomonas aeruginosa*. Letters in Drug Design & Discovery, 2009; 6(6): 403-12.

19. Beloussow K, Wang L, Wu J, Ann D, Shen WC. Recombinant arginine deiminase as a potential anti-angiogenic agent. Cancer Letters, 2002; 183(2): 155-62.

20. Misawa S, Aoshima M, Takaku H, Matsumoto M, Hayashi H. High-Level expression of Mycoplasma arginine deiminase in *Escherichia coli* and Its efficient renaturation as an antitumor enzyme. Journal of Biotechnology, 1994; 36(2): 145-55.
21. Gong H, Zolzer F, von Recklinghausen G*, et al.* Arginine deiminase inhibits cell proliferation by arresting cell cycle and inducing apoptosis. Biochemical and Biophysical Research Communications, 1999; 261(1): 10-4.
22. Takaku H, Takase M, Abe S, Hayashi H, Miyazaki K. *In vivo* antitumor activity of arginine deiminase purified from *Mycoplasma arginini*. International Journal of Cancer, 1992; 51(2): 244-9.
23. Kim JE, Jeong DW, Lee HJ. Expression, purification, and characterization of arginine deiminase from Lactococcus lactis ssp lactis ATCC 7962 in Escherichia coli BL21. Protein Expression and Purification, 2007; 53(1): 9-15.
24. Kakimoto T, Shibatan.T, Chibata I. Crystallization of L-arginine deiminase from *Pseudomonas putida*. Febs Letters, 1971; 19(2): 166-8.
25. Shibatani T, Kakimoto T, Chibata I. Crystallization and properties of L-arginine deiminase of *Pseudomonas Putida* 2. Journal of Biological Chemistry, 1975; 250(12): 4580-3.
26. Galkin A, Kulakova L, Sarikaya E, Lim K, Howard A, Herzberg O. Structural insight into arginine degradation by arginine deiminase, an antibacterial and parasite drug target. Journal of Biological Chemistry, 2004; 279(14): 14001-8.
27. Ni Y, Schwaneberg U, Sun ZH. Arginine deiminase, a potential anti-tumor drug. Cancer Lett, 2008; 261(1): 1-11.
28. Galkin A, Kulakova L, Sarikaya E, Lim K, Howard A, Herzberg O. J Biol Chem, 2004; 279: 14001.
29. Galkin A, Lu XF, Dunaway-Mariano D, Herzberg O. J Biol Chem, 2005; 280: 34080.
30. Holle LM. Pegaspargase: an alternative? Annals of Pharmacotherapy, 1997; 31(5): 616-24.

31. Yoshioka T, Wada T, Uchida N*, et al.* Anticancer efficacy in vivo and in vitro, synergy with 5-fluorouracil, and safety of recombinant methioninase. Cancer Research, 1998; 58(12): 2583-7.
32. Lam TL, Wong GKY, Chong HC*, et al.* Recombinant human arginase inhibits proliferation of human hepatocellular carcinoma by inducing cell cycle arrest. Cancer Letters, 2009; 277(1): 91-100.
33. Shen RS, Fritz RR, Abell CW. Biochemical-Properties and Immunogenicity of L-Phenylalanine Ammonia-Lyase - Effects on Tumor-Bearing Mice. Cancer Treatment Reports, 1979; 63(6): 1063-8.
34. Yoshimoto T, Chao SG, Saito Y, Imamura I, Wada H, Inada Y. Chemical modification of tryptophanase from E. coli with polyethylene glycol to reduce its immunoreactivity towards anti-tryptophanase antibodies. Enzyme, 1986; 36(4): 261-5.
35. Feun LG, Savaraj N, Marini A*, et al.* Phase II study of pegylated arginine deiminase (ADI-PEG20), a novel targeted therapy for melanoma. Journal of Clinical Oncology, 2006; 24(18): 464s-s.
36. Gong H, Zolzer F, von Recklinghausen G, Havers W, Schweigerer L. Arginine deiminase inhibits proliferation of human leukemia cells more potently than asparaginase by inducing cell cycle arrest and apoptosis. Leukemia, 2000; 14(5): 826-9.
37. Morris SM, Jr. Regulation of enzymes of the urea cycle and arginine metabolism. Annu Rev Nutr, 2002; 22: 87-105.
38. Scott L, Lamb J, Smith S, Wheatley DN. Single amino acid (arginine) deprivation: rapid and selective death of cultured transformed and malignant cells. British Journal of Cancer, 2000; 83(6): 800-10.
39. Wheatley DN, Campbell E. Arginine catabolism, liver extracts and cancer. Pathol Oncol Res, 2002; 8(1): 18-25.
40. Thomas JB, Holtsberg FW, Ensor CM, Bomalaski JS, Clark MA. Enzymatic degradation of plasma arginine using arginine deiminase inhibits nitric oxide production and protects mice from the lethal effects of tumor necrosis factor and endotoxin. Molecular Biology of the Cell, 2001; 12: 404a-a.

41. Cheng PNM, Leung YC, Lo WH, Tsui SM, Lam KC. Remission of hepatocellular carcinoma with arginine depletion induced by systemic release of endogenous hepatic arginase due to transhepatic arterial embolisation, augmented by high-dose insulin: arginase as a potential drug candidate for hepatocellular carcinoma. Cancer Letters, 2005; 224(1): 67-80.
42. Cheng PNM, Lam TL, Lam WM*, et al.* Pegylated recombinant human arginase (rhArg-peg(5,000mw)) inhibits the in vitro and in vivo proliferation of human hepatocellular carcinoma through arginine depletion. Cancer Research, 2007; 67(1): 309-17.
43. Kim JH, Yu YS, Kim DH, Min BH, Kim KW. Anti-tumor activity of arginine deiminase via arginine deprivation in retinoblastoma. Oncol Rep, 2007; 18(6): 1373-7.
44. Kim RH, Coates JM, Bowles TL*, et al.* Arginine deiminase as a novel therapy for prostate cancer induces autophagy and caspase-independent apoptosis. Cancer Research, 2009; 69(2): 700-8.
45. Glazer ES, Piccirillo M, Albino V*, et al.* Phase II study of pegylated arginine deiminase for nonresectable and metastatic hepatocellular carcinoma. Journal of Clinical Oncology, 2010; 28(13): 2220-6.
46. Ascierto PA, Scala S, Castello G*, et al.* Pegylated arginine deiminase treatment of patients with metastatic melanoma: Results from phase I and II studies. Journal of Clinical Oncology, 2005; 23(30): 7660-8.
47. Shen LJ, Beloussow K, Shen WC. Accessibility of endothelial and inducible nitric oxide synthase to the intracellular citrulline-arginine regeneration pathway. Biochemical Pharmacology, 2005; 69(1): 97-104.
48. Park H, Lee JB, Shim YJ*, et al.* Arginine deiminase enhances MCF-7 cell radiosensitivity by inducing changes in the expression of cell cycle-related proteins. Molecules and Cells, 2008; 25(2): 305-11.
49. Kubo M, Nishitsuji H, Kurihara K, Hayashi T, Masuda T, Kannagi M. Suppression of human immunodeficiency virus type 1 replication by arginine deiminase of *Mycoplasma arginini*. Journal of General Virology, 2006; 87: 1589-93.

50. Izzo F, Montella M, Orlando AP*, et al.* Pegylated arginine deiminase lowers hepatitis C viral titers and inhibits nitric oxide synthesis. Journal of Gastroenterology and Hepatology, 2007; 22(1): 86-91.
51. Kwan JM, Fialho AM, Kundu M*, et al.* Bacterial proteins as potential drugs in the treatment of leukemia. Leukemia Research, 2009; 33(10): 1392-9.
52. Tsai WB, Aiba I, Lee SY, Feun L, Savaraj N, Kuo MT. Resistance to arginine deiminase treatment in melanoma cells is associated with induced argininosuccinate synthetase expression involving c-Myc/HIF-1 alpha/Sp4. Molecular Cancer Therapeutics, 2009; 8(12): 3223-33.
53. Yoon CY, Shim YJ, Kim EH*, et al.* Renal cell carcinoma does not express argininosuccinate synthetase and is highly sensitive to arginine deprivation via arginine deiminase. International Journal of Cancer, 2007; 120(4): 897-905.
54. Feun L, You M, Wu CJ*, et al.* Arginine deprivation as a targeted therapy for cancer. Current Pharmaceutical Design, 2008; 14(11): 1049-57.
55. Zhu ZW, Momeu C, Zakhartsev M, Schwaneberg U. Making glucose oxidase fit for biofuel cell applications by directed protein evolution. Biosens Bioelectron, 2006; 21(11): 2046-51.
56. Panke S, Held M, Wubbolts M. Trends and innovations in industrial biocatalysis for the production of fine chemicals. Current Opinion in Biotechnology, 2004; 15(4): 272-9.
57. Patel RN. Chemo-enzymatic synthesis of pharmaceutical intermediates. Expert Opinion on Drug Discovery, 2008; 3(2): 187-245.
58. Yokobayashi Y, Weiss R, Arnold FH. Directed evolution of a genetic circuit. Proc Natl Acad Sci U S A, 2002; 99(26): 16587-91.
59. Ellington AD, Chen X, Robertson M, Syrett A. Evolutionary origins and directed evolution of RNA. International Journal of Biochemistry & Cell Biology, 2009; 41(2): 254-65.
60. Alper H, Fischer C, Nevoigt E, Stephanopoulos G. Tuning genetic control through promoter engineering. Proceedings of the National Academy of Sciences of the United States of America, 2005; 102(36): 12678-83.

61. Drummond DA, Iverson BL, Georgiou G, Arnold FH. Why high-error-rate random mutagenesis libraries are enriched in functional and improved proteins. J Mol Biol, 2005; 350(4): 806-16.
62. Wong TS, Roccatano D, Schwaneberg U. Steering directed protein evolution: strategies to manage combinatorial complexity of mutant libraries. Environmental Microbiology, 2007; 9(11): 2645-59.
63. Wong TS, Zhurina D, Schwaneberg U. The diversity challenge in directed protein evolution. Combinatorial Chemistry & High Throughput Screening, 2006; 9(4): 271-88.
64. Fasan R, Chen MM, Crook NC, Arnold FH. Engineered alkane-hydroxylating cytochrome P450(BM3) exhibiting nativelike catalytic properties. Angewandte Chemie-International Edition, 2007; 46(44): 8414-8.
65. Titus SA, Xiao L, Southall N*, et al.* Cell-based PDE4 assay in 1536-well plate format for high-throughput screening. Journal of Biomolecular Screening, 2008; 13(7): 609-18.
66. Lafferty M, Dycaico MJ. GigaMatrix^{TM}: an ultra highthroughput tool for accessing biodiversity. JALA, 2009; 9: 200-8.
67. Yang GY, Withers SG. Ultrahigh-throughput FACS-based screening for directed enzyme evolution. Chembiochem, 2009; 10(17): 2704-15.
68. Miller OJ, Hibbert EG, Ingram CU, Lye GJ, Dalby PA. Optimisation and evaluation of a generic microplate-based HPLC screen for transketolase activity. Biotechnology Letters, 2007; 29(11): 1759-70.
69. Yoshikuni Y, Ferrin TE, Keasling JD. Designed divergent evolution of enzyme function. Nature, 2006; 440(7087): 1078-82.
70. Becker S, Schmoldt HU, Adams TM, Wilhelm S, Kolmar H. Ultra-high-throughput screening based on cell-surface display and fluorescence-activated cell sorting for the identification of novel biocatalysts. Current Opinion in Biotechnology, 2004; 15(4): 323-9.
71. Farinas ET. Fluorescence activated cell sorting for enzymatic activity. Combinatorial Chemistry & High Throughput Screening, 2006; 9(4): 321-8.

72. Agresti JJ, Antipov E, Abate AR*, et al.* Ultrahigh-throughput screening in drop-based microfluidics for directed evolution. Proceedings of the National Academy of Sciences of the United States of America, 2010; 107(9): 4004-9.
73. Leemhuis H, Kelly RM, Dijkhuizen L. Directed evolution of enzymes: library screening strategies. Iubmb Life, 2009; 61(3): 222-8.
74. Chen KC, Wu CH, Chang CY*, et al.* Directed evolution of a lysosomal enzyme with enhanced activity at neutral pH by mammalian cell-surface display. Chem Biol, 2008; 15(12): 1277-86.
75. Wang Q, Xia T. Enhancement of the activity and alkaline pH stability of Thermobifida fusca xylanase A by directed evolution. Biotechnology Letters, 2008; 30(5): 937-44.
76. Colin DY, Deprez-Beauclair P, Silva N, Infantes L, Kerfelec B. Modification of pancreatic lipase properties by directed molecular evolution. Protein Engineering Design & Selection, 2010; 23(5): 365-73.
77. Bessler C, Schmitt J, Maurer KH, Schmid RD. Directed evolution of a bacterial alpha-araylase: Toward enhanced pH-performance and higher specific activity. Protein Sci, 2003; 12(10): 2141-9.
78. Liu ZQ, Sun ZH, Leng Y. Directed evolution and characterization of a novel D-pantonohydrolase from Fusarium moniliforme. Journal of Agricultural and Food Chemistry, 2006; 54(16): 5823-30.
79. Hasan Z, Renirie R, Kerkman R, Ruijssenaars HJ, Hartog AF, Wever R. Laboratory-evolved vanadium chloroperoxidase exhibits 100-fold higher halogenating activity at alkaline pH - Catalytic effects from first and second coordination sphere mutations. Journal of Biological Chemistry, 2006; 281(14): 9738-44.
80. Makde RD, Dikshit K, Kumar V. Protein engineering of class-A non-specific acid phosphatase (PhoN) of Salmonella typhimurium: Modulation of the pH-activity profile. Biomolecular Engineering, 2006; 23(5): 247-51.
81. Kim T, Mullaney EJ, Porres JM*, et al.* Shifting the pH profile of *Aspergillus niger* PhyA phytase to match the stomach pH enhances its effectiveness as an

animal feed additive. Applied and Environmental Microbiology, 2006; 72(6): 4397-403.
82. Hirata A, Adachi M, Utsumi S, Mikami B. Engineering of the pH optimum of Bacillus cereus beta-amylase: Conversion of the pH optimum from a bacterial type to a higher-plant type. Biochemistry, 2004; 43(39): 12523-31.
83. Tomschy A, Brugger R, Lehmann M*, et al.* Engineering of phytase for improved activity at low pH. Appl Environ Microbiol, 2002; 68(4): 1907-13.
84. Sakoda H, Imanaka T. Cloning and sequencing of the gene coding for alcohol dehydrogenase of Bacillus stearothermophilus and rational shift of the optimum pH. J Bacteriol, 1992; 174(4): 1397-402.
85. Yang JH, Park JY, Kim SH, Yoo YJ. Shifting pH optimum of Bacillus circulans xylanase based on molecular modeling. Journal of Biotechnology, 2008; 133(3): 294-300.
86. MacPherson IS, Rosell FI, Scofield M, Mauk AG, Murphy MEP. Directed evolution of copper nitrite reductase to a chromogenic reductant. Protein Engineering Design & Selection, 2010; 23(3): 137-45.
87. Hida K, Hanes J, Ostermeier M. Directed evolution for drug and nucleic acid delivery. Adv Drug Deliv Rev, 2007; 59(15): 1562-78.
88. Yuan L, Kurek I, English J, Keenan R. Laboratory-directed protein evolution. Microbiology and Molecular Biology Reviews, 2005; 69(3): 373-92.
89. Rautio J, Kumpulainen H, Heimbach T*, et al.* Prodrugs: design and clinical applications. Nat Rev Drug Discov, 2008; 7(3): 255-70.
90. Barak Y, Thorne SH, Ackerley DF, Lynch SV, Contag CH, Matin A. New enzyme for reductive cancer chemotherapy, YieF, and its improvement by directed evolution. Molecular Cancer Therapeutics, 2006; 5(1): 97-103.
91. Kuhn I, Harden P, Bauzon M*, et al.* Directed evolution generates a novel oncolytic virus for the treatment of colon cancer. PLoS One, 2008; 3(6): e2409.
92. Robertson DE, Steer BA. Recent progress in biocatalyst discovery and optimization. Current Opinion in Chemical Biology, 2004; 8(2): 141-9.
93. Soares AL, Guirmaraes GM, Polakiewicz B, Pitombo RND, Abrahao-Neto J. Effects of polyethylene glycol attachment on physicochemical and biological

stability of E-coli L-asparaginase. International Journal of Pharmaceutics, 2002; 237(1-2): 163-70.
94. Kotzia GA, Labrou NE. Engineering thermal stability of L-asparaginase by in vitro directed evolution. Febs Journal, 2009; 276(6): 1750-61.
95. Orlova A, Feldwisch J, Abrahmsen L, Tolmachev V. Affibody molecules for molecular imaging and therapy for cancer. Cancer Biotherapy and Radiopharmaceuticals, 2007; 22(5): 573-84.
96. Nilsson FY, Tolmachev V. Affibody (R) molecules: New protein domains for molecular imaging and targeted tumor therapy. Current Opinion in Drug Discovery & Development, 2007; 10(2): 167-75.
97. Gronwall C, Sjoberg A, Ramstrom M*, et al.* Affibody-mediated transferrin depletion for proteomics applications. Biotechnol J, 2007; 2(11): 1389-98.
98. Renberg B, Shiroyama I, Engfeldt T, Nygren PA, Karlstrom AE. Affibody protein capture microarrays: Synthesis and evaluation of random and directed immobilization of affibody molecules. Analytical Biochemistry, 2005; 341(2): 334-43.
99. Friedman M, Orlova A, Johansson E*, et al.* Directed evolution to low nanomolar affinity of a tumor-targeting epidermal growth factor receptor-binding affibody molecule. Journal of Molecular Biology, 2008; 376(5): 1388-402.
100. Chang CCJ, Chen TT, Cox BW*, et al.* Evolution of a cytokine using DNA family shuffling. Nature Biotechnology, 1999; 17(8): 793-7.
101. Zhang JH, Dawes G, Stemmer WPC. Directed evolution of a fucosidase from a galactosidase by DNA shuffling and screening. Proceedings of the National Academy of Sciences of the United States of America, 1997; 94(9): 4504-9.
102. Crameri A, Cwirla S, Stemmer WPC. Construction and evolution of antibody-phage libraries by DNA shuffling. Nature Medicine, 1996; 2(1): 100-2.
103. Patten PA, Howard RJ, Stemmer WP. Applications of DNA shuffling to pharmaceuticals and vaccines. Curr Opin Biotechnol, 1997; 8(6): 724-33.
104. Park IS, Kang SW, Shin YJ*, et al.* Arginine deiminase: a potential inhibitor of angiogenesis and tumour growth. Br J Cancer, 2003; 89(5): 907-14.

105. Izzo F, Marra P, Beneduce G*, et al.* Pegylated arginine deiminase treatment of patients with unresectable hepatocellular carcinoma: Results from phase I/II studies. J Clin Oncol, 2004; 22(10): 1815-22.
106. Gong H, Zölzer F, von Recklinghausen G, Havers W, Schweigerer L. Arginine deiminase inhibits proliferation of human leukemia cells more potently than asparaginase by inducing cell cycle arrest and apoptosis. Leukemia, 2000; 14(5): 826-9.
107. Shen LJ, Shen WC. Drug evaluation: ADI-PEG-20 - a PEGylated arginine deiminase for arginine-auxotrophic cancers. Curr Opin in Mol Ther, 2006; 8(3): 240-8.
108. Holtsberg FW, Ensor CM, Steiner MR, Bomalaski JS, Clark MA. Poly(ethylene glycol) (PEG) conjugated arginine deiminase: effects of PEG formulations on its pharmacological properties. J Controlled Release, 2002; 80(1-3): 259-71.
109. Mûller HJ, Boos J. Use of L-asparaginase in childhood all. Crit Rev Oncol Hematol, 1998; 28(2): 97-113.
110. Turunen O, Janis J, Fenel F, Leisola M. Engineering the thermotolerance and pH optimum of family 11 xylanases by site-directed mutagenesis. Methods Enzymol, 2004; 388: 156-67.
111. Fang TY, Ford C. Protein engineering of *Aspergillus awamori* glucoamylase to increase its pH optimum. Protein Eng, 1998; 11(5): 383-8.
112. Sakoda H, Imanaka T. Cloning and sequencing of the gene coding for alcohol-dehydrogenase of *Bacillus stearothermophilus* and rational shift of the optimum pH. J Bacteriol, 1992; 174(4): 1397-402.
113. Wang WY, Malcolm BA. Two-stage PCR protocol allowing introduction of multiple mutations, deletions and insertions using QuikChange™ site-directed mutagenesis. BioTechniques, 1999; 26(4): 680-2.
114. Miyazaki K, Takenouchi M. Creating random mutagenesis libraries using megaprimer PCR of whole plasmid. Biotechniques, 2002; 33(5): 1033-8.
115. Studier FW. Protein production by auto-induction in high-density shaking cultures. Protein Expression and Purification, 2005; 41(1): 207-34.

116. Archibald RM. Deternination of citrulline and allantoin and demonstration of citrulline in blood plasma. J Biol Chem, 1944; 156(1): 121-42.
117. Boyde TRC, Rahmatullah M. Optimization of conditions for the colorimetric determination of citrulline, using diacetyl monoxime. Anal Biochem, 1980; 107(2): 424-31.
118. Guex N, Peitsch MC. SWISS-MODEL and the Swiss-PdbViewer: an environment for comparative protein modeling. Electrophoresis, 1997; 18(15): 2714-23.
119. van Gunsteren WF, Billeter SR, Eising AA*, et al.* Biomolecular simulation: the gromos 96 manual and user guide ETH Zürich; 1996.
120. Mather A, Roland D. Automated thiosemicarbazide-diacetyl monoxime method for plasma urea. Clinical Chemistry, 1969; 15(5): 393-6.
121. Wong TS, Arnold FH, Schwaneberg U. Laboratory evolution of cytochrome P450BM-3 monooxygenase for organic cosolvents. Biotechnol Bioeng, 2004; 85(3): 351-8.
122. Glieder A, Farinas ET, Arnold FH. Laboratory evolution of a soluble, self-sufficient, highly active alkane hydroxylase. Nat Biotechnol, 2002; 20(11): 1135-9.
123. Galkin A, Lu X, Dunaway-Mariano D, Herzberg O. Crystal structures representing the Michaelis complex and the thiouronium reaction intermediate of Pseudomonas aeruginosa arginine deiminase. Journal of biological chemistry, 2005; 280(40): 34080-7.
124. Chuang VTG, Kragh-Hansen U, Otagiri M. Pharmaceutical strategies utilizing recombinant human serum albumin. Pharm Res, 2002; 19(5): 569-77.
125. Tee KL, Dmytrenko O, Otto K, Schmid A, Schwaneberg U. A p-nitrothiophenolate screening system for the directed evolution of a two-component epoxygenase (StyAB). J Mol Catal B: Enzym, 2008; 50(2-4): 121-7.
126. Li L, Li ZM, Wang CH*, et al.* The electrostatic driving force for nucleophilic catalysis in L-arginine deiminase: a combined experimental and theoretical study. Biochemistry (Mosc), 2008; 47(16): 4721-32.

127. Takaku H, Matsumoto M, Misawa S, Miyazaki K. Antitumor-activity of arginine deiminase from *Mycoplasma arginini* and its growth-Inhibitory mechanism. Jap J Cancer Res, 1995; 86(9): 840-6.
128. Capocaccia R, Sant M, Berrino F, Simonetti A, Santi V, Trevisani F. Hepatocellular carcinoma: trends of incidence and survival in Europe and the United States at the end of the 20th century. American Journal of Gastroenterol, 2007; 102(8): 1661-70.
129. Shen LJ, Shen WC. Drug evaluation: ADI-PEG-20 - a PEGylated arginine deiminase for arginine-auxotrophic cancers. Current Opinion in Molecular Therapeutics, 2006; 8(3): 240-8.
130. Wang WY, Malcolm BA. Two-stage PCR protocol allowing introduction of multiple mutations, deletions and insertions using QuikChange (TM) site-directed mutagenesis. Biotechniques, 1999; 26(4): 680-2.
131. Vaughn WK, Neal RA, Anderson AJ. Computer estimation of the parameters of the sigmoidal kinetic model. Computers in Biology and Medicine, 1976; 6(1): 1-7.
132. Kelley LA, Sternberg MJE. Protein structure prediction on the web: a case study using the Phyre server. Nature Protocols, 2009; 4(3): 363-71.
133. Laskowski RA, Macarthur MW, Moss DS, Thornton JM. Procheck - a program to check the stereochemical quality of protein structures. Journal of Applied Crystallography, 1993; 26: 283-91.
134. Zhou HY, Zhou YQ. Distance-scaled, finite ideal-gas reference state improves structure-derived potentials of mean force for structure selection and stability prediction. Protein Science, 2002; 11(11): 2714-26.
135. Benkert P, Tosatto SCE, Schomburg D. QMEAN: A comprehensive scoring function for model quality assessment. Proteins-Structure Function and Bioinformatics, 2008; 71(1): 261-77.
136. Berendsen HJC, Postman JPM, van Gunsteren WF, Hermans J. Interaction models for water in relation to protein hydration. Intermolecular Forces, 1981: 331-42.

137. Hess B, Bekker H, Berendsen HJC, Fraaije JGEM. LINCS: A linear constraint solver for molecular simulations. Journal of Computational Chemistry, 1997; 18(12): 1463-72.
138. Miyamoto S, Kollman PA. Settle - an analytical version of the shake and rattle algorithm for rigid water models. Journal of Computational Chemistry, 1992; 13(8): 952-62.
139. Darden T, York D, Pedersen L. Particle mesh ewald - an N.Log(N) method for ewald sums in large systems. Journal of Chemical Physics, 1993; 98(12): 10089-92.
140. Berendsen HJC, Postma JPM, Vangunsteren WF, Dinola A, Haak JR. Molecular dynamics with coupling to an external bath. Journal of Chemical Physics, 1984; 81(8): 3684-90.
141. Hess B, Kutzner C, van der Spoel D, Lindahl E. GROMACS 4: algorithms for highly efficient, load-balanced, and scalable molecular simulation. Journal of Chemical Theory and Computation, 2008; 4(3): 435-47.

Summary and outlook

Arginine depletion based on ADI is an emerging strategy for anti-tumor treatment. ADIs have been studied for the therapy of HCCs and melanomas and were approved as an orphan drug for both kinds of tumors. ADI is proved to be effective in the treatment of leukemia. The effectiveness of ADIs as anti-tumor agent depends on their enzymatic properties (such as K_m, k_{cat}, optimum pH, stability at neutral pH). Directed evolution, without rational understanding of the targeted property, allows improving all properties that can be reflected in a screening system through iterative rounds of diversity generation and screening.

In order to improve PpADI activity at physiological pH by directed evolution, a colorimetric screening assay based on citrulline detection has been developed in 96-well microtiter plate format. Single mutation H404R was identified according to PpADI homology model (based on PaADI crystal structure), introduced to PpADI wild type and eventually resulted in 1.4-fold of increase in k_{cat}. M1 (H404R) was used as template for the first round of epPCR library generation. M2 (K5T/D44E/H404R) obtained from the first round of epPCR library showed 4-fold improved k_{cat} value when compared to the PpADI wild type. Furthermore, a shift of pH optimum from pH 6.5 to pH 7.0 was observed, combined with an increased K_m value (2.5 mM) under assay conditions (0.5 M sodium phosphate buffer, pH 7.4), compared to PpADI wild type (0.7 mM).

Arginine concentration in human plasma is however relatively low (100-120 µM). Therefore the second round of epPCR library was performed to decrease K_m value and further improve k_{cat} value. The validated screening assay was modified to reflect more close physiological condition (1 mM arginine in PBS buffer, pH 7.4). Two important variants with one additional mutation, M4 (K5T/D44E/A128T/E296K/H404R) with decreased $S_{0.5}$ vaule, and M5 (K5T/D38H/D44E/A128T/H404R) with improved k_{cat} were obtained. Their two mutations were combined and resulted in variants M6

(K5T/D38H/D44E/A128T/E296K/H404R). Under physiological pH in PBS buffer, the $S_{0.5}$ value of M6 (0.81 mM) is lower than that of PpADI wild type (1.30 mM); the k_{cat} value improved from 0.18 s^{-1} (PpADI wild type) to 17.56 s^{-1} (M5, 97.6-folds) and 11.64 s^{-1} (M6, 64.7-fold).

A reamaining challenge facing PpADI's anti-tumor application is to decrease the K_m ($S_{0.5}$) value further close to arginine concentration level in human plasma. A more sensitive assay for screening has to be developed with the addition of sensitizer like thiosemicarbazide (TSC), optimized temperature and incubation time. Improved variants should be tested tested in human plasma or with human plasma composition. *In vitro* testing of ADI variants with arginine auxotrophic tumor cell lines is the first step towards *in vivo* in human.

In summary, directed evolution has been very useful algorithim for improving ADI's k_{cat} and K_m at physiological pH (pH 7.4) for its medical application. Hope that directed evolution will be become a standard method for therapeutic protein like its use in industry.

Publications

1. **Leilei Zhu**, Kang Lan Tee, Danilo Roccatano, Burcu Sonmez, Ye Ni, Zhi-Hao Sun, and Ulrich Schwaneberg. Directed evolution of an antitumor drug (Arginine Deiminase PpADI) for increased activity at physiological pH. ChemBioChem. 2010, 11, 691-697.

2. **Leilei Zhu**, Rajni Verma, Danilo Roccatano, Ye Ni, Zhi-Hao Sun, and Ulrich Schwaneberg. A potential anti-tumor drug (arginine deiminase) reengineered for efficient operation under physiological conditions. ChemBioChem. *In press*.

3. Ye Ni, Zhenwei Li, Zhihao Sun, Pu Zheng, Yongmei Liu and **Leilei Zhu**, Ulrich Schwaneberg. Expression of arginine deiminase from *Pseudomonas plecoglossicida* CGMCC2039 in *Escherichia coli* and its anti-tumor activity. Current Microbiology. 2009, 58(6):593-598.

Patent

1. Directed evolution of arginine deiminase for increased activity at physiological pH. Application number: PCT/EP2010/061884.

Curriculum vitae

Personal data

Name:	Leilei Zhu
Gender:	Female
Date of Birth:	27th April, 1982
Place of Birth:	Weifang, China
Marital Status:	Married
Nationality:	Chinese

Education

2009-	PhD fellow of biotechnology, RWTH Aachen University, Aachen, Germany
2007-2009	PhD fellow of engineering and science, Jacobs University Bremen, Bremen, Germany
2005-2007	Master of biochemical engineering, Jiangnan University (Southern Yantze University), Wuxi, China
2001-2005	Bachelor of biotechnology, Jiangnan University (Southern Yantze University), Wuxi, China

2001-1998	The first high school of Hanting, Weifang, China
1998-1994	The sixth middle school of Hanting, Weifang, China
1989-1994	Primary school of Liuhe, Weifang, China

Directed Evolution of Arginine Deiminase (ADI) for Anti-tumor Application

Von der Fakultät für Mathematik, Informatik und Naturwissenschaften der RWTH Aachen University zur Erlangung des akademischen Grades eines(r) Doktors(in) der Naturwissenschaften oder eines(r) Doktors(in) der Ingenieurwissenschaften genehmigte Dissertation

vorgelegt von

Master of Biochemistry

Leilei Zhu

Aus Weifang China

Berichter: **Universitätsprofessor Dr. Ulrich Schwaneberg**
Universitätsprofessor Dr. Lothar Elling

Tag der mündlichen Prüfung: 14.09.2010

Diese Dissertation ist auf den Internetseiten der Hochschulbibliothek online verfügbar.

Table of contents

Acknowledgement.....I
Abstract.....III
Abbreviations V
List of figures..... VI
List of tables..... IX
Chapter 1 Arginine deiminase (ADI) 1
1.1 Arginine deiminase (ADI).....1
1.2 ADI structure 5
1.3 Catalytic reaction mechanism of ADI.....10
1.4 Anti-tumor application of ADI.....11
1.5 Conclusion.....16
Chapter 2 Directed evolution 17
2.1 Introduction to directed evolution.....17
2.2 Directed enzyme evolution for pH tolerance of enzymes 22
2.3 Directed enzyme evolution for medical application.....24
2.3.1 Prodrug enzymes for tumor chemotherapy.....24
2.3.2 Oncolytic viruses for tumor chemotherapy.....25
2.3.3 Amino acid depriving enzyme for anti-tumor applications.....27
2.3.4 Affibody molecules for cancer prognosis 28
2.3.5 Interferon for anti-tumor applicaiton 29
2.4 Conclusion.....30
Chapter 3. Directed evolution of Arginine deiminase for increased activity at physiological pH.....31
3. 1 Abstract 31
3.2 Introduction.....31
3.3 Materials and methods 33
3.3.1 Materials 33
3.3.2 Methods 34

3.3.2.1 Reagents used in assays 34
3.3.2.2 Cloning of ADI into pET42b(+) 34
3.3.2.3 Site directed mutagenesis of PpADI gene at position H404 35
3.3.2.4 Site sturation mutagenesis of PpADI gene at nine amino acid position 35
3.3.2.5 Construction of PpADI error-prone library 36
3.3.2.6 Expression of PpADI in LB media with IPTG induction 37
3.3.2.7 Expression of PpADI in auto-induction media 37
3.3.2.8 Cultivation and expression of PpADI in 96-well plates 37
3.3.2.9 Screening Procedure 38
3.3.2.10 Expression of ADI in shaking flask and purification 39
3.3.2.11 Characterization of ADI wild type and mutants 40
3.3.2.12 Molecular Modeling 41
3.3.2.13 Stability of PpADI in presence of serum 41
3.3.2.14 Activity of PpADI (wild type, M1, M2) towards arginine derivative dimethylarginine 42
3.4 Results 42
3.4.1 PpADI cloning 42
3.4.2 PpADI expression in LB media with IPTG as inducer 44
3.4.3 PpADI expression in auto-induction media 44
3.4.4 PpADI assay based on citrulline detection 46
3.4.5 PpADI screening system for citrulline production in microtiter plates 47
3.4.6 Focused libraries generated by saturation mutagenesis 50
3.4.7 Validation of variant M1 (H404R) citrulline colorimetric assay in cuvette format 50
3.4.8 epPCR library generation and screening with citrulline detection assay by screening error-prone mutant libraries 50
3.4.9 Characterization of PpADI variants 53
3.4.9.1 Determination of k_{cat} and K_m of ADI wild type and the mutants 53
3.4.9.2 Relative pH profile of wild type and mutant 54
3.4.10 Stability of PpADI in the presence of human serum 55

3.4.11 Activity of PpADI (wild type, M1, M2) towards arginine derivative (N^G, N^G)-dimethylarginine 56
3.5 Discussion 56
3.6 Conclusion 59
Chapter 4. PpADI reengineered for efficient operation under physiological conditions 60
4.1 Abstract 60
4.2 Introduction 60
4.3 Materials and methods 62
4.3.1 Materials 62
4.3.2 Methods 62
4.3.2.1 Site saturation mutagenesis of *PpADI* M2 at position A128 62
4.3.2.2 Construction of PpADI error-prone library 63
4.3.2.3 Site directed mutagenesis at position D38 of *PpADI* M4 63
4.3.2.4 Site saturation mutagenesis at position D38 and E296 of *PpADI* M3 64
4.3.2.5 Cultivation and expression of PpADI in 96-well plates 64
4.3.2.6 Improved screening system in 96-well plate to identify PpADI variants with high activities at low arginine concentration 64
4.3.2.7 Expression of PpADI in shaking flask and purification 65
4.3.2.8 Characterization of PpADI variants 65
4.3.2.9 Native polyacrylamide gel electrophoresis of PpADI variants 66
4.3.2.10 Homology modeling 67
4.4 Results 67
4.4.1 Improved screening system in microtiter plates to identify PpADI variants with high activities at low arginine concentration 67
4.4.2 Genealogic tree of directed PpADI evolution 68
4.4.3 EpPCR library construction and screening for variants with high activities at low arginine concentration 69
4.4.4 Site saturation mutagenesis of *PpADI* at position D38 and E296 70

4.4.5 Determination of kinetic constants (k_{cat} and $S_{0.5}$) of PpADI wild type and variants M3, M4, M5 and M6 72
4.4.6 Native polyacrylamide gel electrophoresis of PpADI variants 73
4.5 Discussion 74
Summary and outlook 95
Publication list 97
Curriculum vitae 98

Acknowledgement

First and foremost I want to thank my supervisor Prof. Dr. Ulrich Schwaneberg for offering me the opportunity to study in Germany, his continuous support of my PhD study and research, for his patience, motivation, enthusiasm, and immense knowledge, which influence my view of science and life. His guidance helped me all the time in research and writing of paper and thesis. I could not have imagined having a better advisor and mentor for my PhD study.

Besides my supervisor, I would like to thank other two committee member Prof. Dr. Lothar Elling and Prof. Dr. Anett Kirschner. I appreciate their taking time to read this thesis and give valuable comments.

My sincere thanks also go to Kang Lan, who became a great friend of mine after I came to Bremen of Germany three years ago. She helped me a lot with my PhD project and she was a great company in my daily life. I will never forget the two months I spent on the first cloning working in my life and how Kang Lan taught me and encouraged me.

I am grateful to Prof. Dr. Danilo Roccatano for spending a lot of time discussing my results. After the first meeting with Prof. Roccatano, I started to know and learn computational tools which are really useful for my PhD study. I also thank Rajni for her contribution of homology modeling to my project.

The members of the Schwaneberg group have contributed immensely to my personal and professional time in Jacobs University Bremen and RWTH Aachen University. The group has been a source of friendships as well as good advice and collaboration. I appreciate the help from Marina, Daniela, Gisela, Wolfgang and Brigitta in lab and Marina, Monika and Anita's patient explanation of the registration regulation RWTH Aachen University. I would like to acknowledge honorary group members. I thank Liqing for her sharing apartment with me and helped me start my life in Germany and also thank Haiyan for her offering me a room later and often cooked nice food for us. Ran shared a lot of lab techniques which are very useful for my experiments. I always admire her professional and

accurate attitude towards work. I thank other labmates who I got to know in Jacobs university: Ronny, Hemu, Chaoning, Amol, Dominik and Amir for the stimulating discussions, little help in lab and all the fun we have had in the last three years; Dragana, Ljubica, Noor, Pravine and Raluca helped me move to Aachen and we finally got through the tough transition period from Bremen to Aachen. I thank our group leaders Marco, Jan and Radivoje, who are not my direct supervisor, but are always helpful when I have questions. I thank my fellow labmates who I got to know in RWTH Aachen University: Tamara, Felix, Alex, Christian, Joelle, André, Joana……, who are always helpful with all the problems (PhD registration, Germany letters from university…….) because of my poor German.

I also want to acknowledge my students, Burcu and Alice, both of whom were hard-working and smart. They were all a great help in the lab and I really enjoyed working with them.

I would like to thank my family because of their love, support and trust. They love me the most in the world. I thank for their efforts that they made over the years to make sure I have a good growth and education environment. I wish them healthy and happy life. I thank my elder sister for her love and understanding and always taking good care of my parents these years when I am not around. I thank my husband, Haifeng, who supports me all the time and always is there for me. I am lucky to have him with me.

The financial support of the Jacobs University Bremen and RWTH Aachen University is gratefully acknowledged.

Abstract

Arginine deiminase (ADI), an arginine-degrading enzyme, is involved in the first step of arginine dihydrolase pathway. It catalyzes the hydrolysis of L-arginine to form citrulline and ammonia. ADI has been studied as a potential cancer therapeutic agent for the arginine-auxotrophic tumors, such as hepatocellular carcinomas (HCC) and melanomas. Furthermore, studies also indicate that ADI is a potential anti-angiogenic agent; therefore it could become a novel anti-cancer drug targeting the neovascularization-related tumors. Studies show ADI is more potent for the treatment of leukemia than L-asparaginase. However, the anti-tumor application of ADI for therapeutic purpose faces considerable challenges, such as, microbial ADI has low activity at physiological pH (7.35~7.45), short circulating half-life (~5 h) and high antigenicity. Pegylation of ADI improved its efficacy as a clinical drug, including its half-life in serum and antigenicity. The aim of the project is to improve ADI catalytic performance at physiological pH by directed evolution.

Protein engineering by rational design and directed evolution offers opportunities to tailor ADI properties to physiological conditions. Directed protein evolution has over the last decades become a versatile and successful approach for tailoring protein properties to industrial demands and for advancing our understanding of structure-function relationships in biocatalysts. Unlike rational design relying on the gathering of extensive structure-function relationships of enzymes, directed evolution is used to reengineer enzyme properties through iterative rounds of diversity generation and function selection for improved variants.

In order to improve the ADI activity at physiological pH, we established a directed evolution protocol for this purpose. A microtiter plate (MTP) format colorimetric screening assay based on citrulline detection with diacetyl monoxime (DAM) was developed. Reaction temperature for color development and DAM concentration

were optimized to ensure sufficient sensitivity, appropriate linear range and throughput. With the optimized assay and PpADI wild type expressed in *E. coli* as a model protein, true standard deviation 12.8 % was obtained, which is appropriate for the library screening.

With the established microtiter plate assay system, for the first time, we reengineered ADI for improved activity at physiological pH (pH 7.4) with higher potency in medical application. After one site directed mutagenesis and one round of epPCR library screening, variant M2 (K5T/D44E/H404R) was obtained. M2 shows 4-fold improved k_{cat} value than the PpADI wild type, a shifted pH optimum at pH 7.0 (by 0.5 pH unit), and however an increased K_m value, 3.6-fold under assay conditions (0.5 M sodium phosphate buffer).

Low K_m ($S_{0.5}$) value for ADI is an important factor for efficient consume of arginine in plasma because of the low arginine concentration in human plasma (100-120 µM). Therefore after our proof of concept of reengineering PpADI by directed evolution, we aim to decrease the K_m value of PpADI towards arginine and improve the k_{cat} furthermore thereby improve the efficiency of arginine depletion by ADI. The established citrulline colorimetric assay in 96-well microtiter plate is improved to reflect application conditions: PBS buffer and 1 mM arginine were used in screening system. After the second round of epPCR library and site directed mutagenesis, variant M5 (K5T/D38H/D44E/A128T/H404R) and M6 (K5T/D38H/D44E/A128T/E296K/H404R) were generated: at pH 7.4 (PBS buffer), the $S_{0.5}$ value decrease from 2.01 mM (parent M3, K5T/D44E/A128T/H404R) to 1.48 mM (M5) and 0.81 mM (M6). Under physiological pH in PBS buffer, the $S_{0.5}$ value of M6 (0.81 mM) is lower than that of PpADI wild type (1.30 mM); the k_{cat} value improved from 0.18 s^{-1} (PpADI wild type) to 17.56 s^{-1} (M5, 97.6-folds) and 11.64 s^{-1} (M6, 64.7-fold).

Abbreviations

ADI	arginine deiminase
ADH	arginine degradation pathway
ASS	argininosuccinate synthetase
ASL	argininosuccinate lyase
CARD	caspase recruitment domain
PCR	polymerase chain reaction
epPCR	error prone PCR
DAM	diacetyl monoxime
Da	dalton
DNA	deoxyribonucleic acid
E. coli	*Escherichia coli*
GMSF	guanidino-group modifying enzyme superfamily
HCC	hepatocellular carcinomas
HUVEC	human umbilical vein endothelial cells
IPTG	isopropyl β-D-1-thiogalactopyranoside
iNOs	inducible nitric oxide synthase
LB	Luria-Bertani-medium
MTP	microtiter plate
OD_{600}	optical density at 600 nm
OTC	ornithine carbamoyl transferase
PEG	polyethylene glycol
PDB	protein data bank
TSC	thiosemicarbazide
WT	wild type

List of tables

Figures	Pages
Chapter 1	
Scheme 1. Arginine dihydrolase pathway. OTC, ornithine transcarbamylase; CK, carbamate kinase.	1
Figure 1. Structural of ADIs from *P. aeruginosa* and *M. arginini*.	5
Figure 2 (A). stereoscopic view of PaADI key active site residues. 2 (B). stereoscopic view of a modeled arginine substrate (green) docked in the active site of ADI. Atomic colors are red, oxygen; blue, nitrogen; yellow, sulfur; and gray, carbon. Ion pair interactions are shown as dashed lines.	7
Figure 3. Structural characteristics of the PaADI.	9
Figure 4 (A). Stereoscopic view of ADI in the unbound and bound states. 4 (B). Structural relationship between ADI (yellow) and PAD4 (cyan).	10
Figure 5. Mechanism of PaADI catalysis of arginine to citrulline and ammonia.	11
Firgure 6. Urea cycle.	13
Firgure 7. Summary of ADI effects on arginine-related cellular functions.	15
Chapter 2	
Figure 1. Procedure of a directed evolution experiment.	18
Figure 2. Overview of screening technologies.	21
Figure 3. Hermiston's "Directed Evolution" process of viruses and derivative viral pools.	26
Chapter 3	
Figure 1. DNA electrophoresis of PpADI.	43
Figure 2. PpADI sequencing results.	43
Figure 3. SDS-PAGE of PpADI expression.	44

Figures Pages

Figure 4(A). Activity of PpADI expressed in auto-induction media. 45

Figure 4(B). SDS-PAGE of ADI expressed in auto-induction media 1, LS-5052; 2, P-5052; 3, MD-5052; 4 TYM-5052; 5, TYP-5052. 45

Figure 5. Arginine conversion by ADI and detection of citrulline using DAM/TSC assay. 46

Figure 6. Citrulline colorimetric assay in cuvette format using DAM/TSC assay. 46

Figure 7. Calibration curve of cuvette format citrulline colorimetric assay. 47

Figure 8. Citrulline colorimetric assay in MTP format using DAM assay. 47

Figure 9. Calibration curve of 96-well microtiter plate format citrulline colorimetric screening assay. 48

Figure 10. Activity values in descending order of the ADI wild-type conversion of arginine to citrulline in a 96-well microtiter plate using the optimized assay protocol. 49

Figure 11. PpADI model derived from PaADI crystal structure (PDB code 2a9gD) by SWISS MODEL WORKSPACE. 49

Figure 12 (A). Electrophoresis of epPCR products. Lane 1, 0.01 mM of $MnCl_2$; Lane 2, 0.02 mM of $MnCl_2$; Lane 3, 0.05 mM of $MnCl_2$. 51

Figure 12 (B). Electrophoresis of MEGAWHOP product with epPCR products as megaprimer. 51

Figure 13. Relative activity of ADI variants towards arginine. The relative activity is the ratio of the activity at the pH of each variant relative to the activity at pH 7.4 of wild type ADI. 52

Figure 14. Elution profile of wild type PpADI and improved variants from epPCR library, generated with Protein 230 Kit using a mircofluidic device (Agilent Bioanalyzer). BSA was added as an internal standard. 53

Figure 15. Kinetic parameters of ADI and mutants for conversion of arginine to citrulline. White: ADI wild type, grey: M1 (H404R), black: M2 (K5T D44E H404R). 54

Figure 16. pH profile of wild type ADI, M1(H404R), M2(K5T/D44E /H404R. 55

Figures Pages

Figure 17. Structural alignment of mutant M1 model with corresponding residues of the crystal structures of the PaADI (in orange). 57

Figure 18. Structural alignment of mutant M2 model with corresponding residues of the crystal structures of the PaADI (in orange). 58

Chaper 4

Figure 1. Figure 1. Activity values in descending order of the PpADI variant M3 conversion of arginine to citrulline in a 96-well microtiter plate using the optimized assay protocol. 68

Figure 2. Genealogic tree of PpADI variants (M1 to M6) with generated amino acid substitutions. Novel substitutions are indicated by an asterisk. 69

Figure 3. Native polyacrylamide gel electrophoresis of PpADI variants (M3 to M6) with different dimer/tetramer distribution 73

Figure 4. Kinetic curve of PpADI wild type, M3, M5 and M6. 75

Figure 5. A). The model of WT tetramer after energy minimization in vacuum (GROMOS 43B1). B). The model of M6 tetramer after energy minimization in vacuum (GROMOS 43B1). 77

Figure 6. A). Structure model of variant M6. B). Structure alignment of PpADI WT model and M6 model with four loops 78

List of tables

Tables Page

Chapter 1

Table 1. ADI expression, enzymatic properties and medical applications. 3

Table 2. Crystal structures of ADI in protein data bank (PDB). 6

Table 3. Residues important for catalytic function of PaADI. 8

Chapter 2

Table 1. Improvement obtained from directed evolution or rational design for pH performance. 22

Chapter 3

Table 1. Primer sequences for site saturation mutagenesis. 36

Table 2. Activity of ADI variants towards arginine determined using citrulline colorimetric assay in cuvette format. 52

Table 3. Stability of PpADI variants in the presence of human serum. 55

Chapter 4

Table 1. Nucleotide and amino acid substitutions at position 38 71

Table 2. Nucleotide and amino acid substitutions at position 296 71

Table 3. Kinetic constants of wild type PpADI and variants. 72

Arginine deiminase (ADI)

1.1 Arginine deiminase (ADI)

Arginine deiminase (ADI, EC 3.5.3.6), an arginine-metabolizing hydrolase, catalyzes the hydrolysis of L-arginine to form citrulline and ammonia. This reaction is the first step in the L-arginine degradation pathway (ADH, scheme 1, (1). First, arginine is deiminated by arginine deiminase. The resulting citrulline is converted to carbamoyl phosphate and ornithine by ornithine transcarbamylase (EC 2.1.3.3), and finally the carbamoyl phosphate is used to phosphorylate ADP by carbamate kinase (EC 2.7.2.2), producing one ATP molecule. ADI is absent in humans but present in a wide range of bacterial species such as *Pseudomonas aeruginosa* (2), *Pseudomonas plecoglossicida* (3) and *Mycoplasma arginini* (4) and in parasitic protists such as *Giardia intestinalis* (5), *Trichomonas Vaginalis* (6), *Trichomonas fetus* (7), and *Hexamita inflate* (8). For pathogenic bacteria, ADI is required in arginine dehydrolase pathway for virulence and for energy production under anaerobic conditions (9, 10).

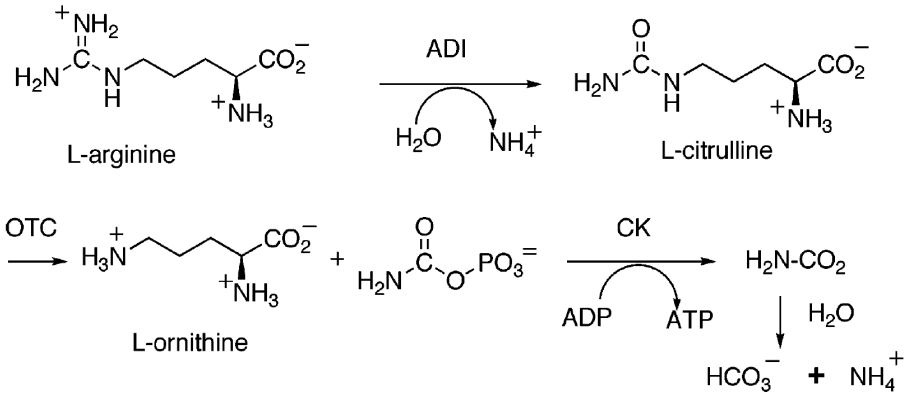

Scheme 1. Arginine dihydrolase pathway. OTC, ornithine transcarbamylase; CK, carbamate kinase.

The establishment of a high-level production system for ADI is an essential step for further research and development of this enzyme. After ADI was discovered from Mycoplasma in 1960s (11), various ADI genes have been cloned, expressed in *E. coli* strains, and the enzyme properties were also studied (Table 1).

Table 1. ADI expression, enzymatic properties and medical applications.

ADIs	Origin	Expression host/vector	Multimeric form	K_m; k_{cat}	Optimum pH	Specific activity	Medical application	References
MhADI (SYN1903)	*Mycoplasma hominis* PG21*	*E.coli* BL21 (DE3)/pET-47b	Dimer			0.618 U/mg (pH 6.5)	Human melanoma (G361), 0.036 U/ml for 50 % IC_{50}	Japan, Harasawa, 2009 (12)
MhADI	*Mycoplasma hominis* (ATCC 23114)	-	Dimer		6.0	35.5 U/mg (pH 6.0) ; 3.9 U/mg (pH 7.4)	Mouse melanoma (MH134) *in vitro*, 100 ng/ml for 50 % IC_{50}	Japan, Takaku, 1995 (13)
MhADI	*Mycoplasma hominis* (ATCC 14027)	-	Dimer	0.17 mM (pH6.6)				USA, Fenske, 1976(14)
MhADI	*Mycoplasma hominis*	*E.coli* BL21 (DE3)/pET25b		0.24 mM; 0.151 s^{-1}				China, Luo, 2007 (15)
MhADI	*Mycoplasma hominis*	*E.coli*				20 U/mg ADI (37℃). [a]	ADI-SS PEG_{20000}, human melanoma, human HCC	USA, Pheonix Pharmacologics, Inc., Clark, 2002 (16)
PaADI (PA5171)	*Pseudomonas aeruginosa* (ATCC 47085D)	*E. coli* BL21(DE3)/pET100	Tetramer	0.14±0.01 mM (pH 5.6)	5.6			USA, Dunaway-Mariano, 2005 (17)
PaADI	*Pseudomonas aeruginosa*	*E. coli* BL21 (DE3)/ pET SUMO				CARD-like domain, no catalytic activity	Human cancer cell line SKOV-3	USA, Chakrabarty, 2006 (18)
PpADI	*Pseudomonas plecoglossicida*	*E. coli* BL21 Gold-(DE3)/ pET42b		0.7 mM; 5.6 s^{-1} (pH 7.4, 0.5 M sodium phosphate buffer)	6.5	31.3 U/mg (pH 7.4, 0.5 M sodium phosphate buffer)		Germany, Schwaneberg, 2010 (3)

MaADI	*Mycoplasma arginini* (ATCC 23838D)	*E. coli* DH5α/PTTQ118				32.7 U/mg. [a]	Human umbilical vein endothelial (HUVE)	USA, Shen, 2002 (19)
MaADI	*Mycoplasma arginini* (ATCC 23838)	*E. coli* JM101/pADTc1	Dimer			33.6 U/mg (37℃, pH 6.5). [a]	Mouse hepatoma, 17 ng/ml for 50 % IC_{50}; mouse fibrosarcoma, 15 ng/ml for 50 % IC_{50}	Japan, Hayashi, 1994 (20)
MaADI	*Mycoplasma arginini* (ATCC 23838)					42 U/mg (37℃, pH 6.5); 29.9 U/mg (37℃, pH 7.4)	Mouse melanoma (MH134) *in vitro*, 10 ng/ml for 50 % IC_{50}	Japan, Takaku, 1995 (13)
MaADI	*Mycoplasma arginini* (ATCC 23838)	-					HUVE, neuroblastoma, retinoblastoma, osteosarcoma, 5~10 ng/ml for 50 % IC_{50}	Germany, Schweigerer, 1999 (21)
MaADI	*Mycoplasma arginini* (ATCC 23838)	-	Dimer	0.2 mM	6.0-7.5	50 U/mg	Mouse tumor carcinoma, fibrosarcoma and melanoma, 5~20 ng/ml for 50 % IC_{50}	Japan, Takaku, 1992 (22)
LlADI	*L. lactis* (ATCC 7962)	*E. coli* BL21Gold(DE3)/pGEM-T Easy	Trimer	8.67 mM	7.2	140.27 U/mg		Korea, Lee, 2007 (23)

[a] ADI was expressed in inclusion body and denaturation-renaturation had to be employed to get soluble protein.

1.2 ADI structure

In 1970s, Kakimoto et al. (24, 25) diffracted the first ADI crystals from *P. putida* through multiple-step chromatography followed by crystallization. Almost three decades later, the X-ray crystal structure of ADI from *P. aeruginosa* (PaADI, Figure 1A) (26) and *M. arginini* (MaADI, Figure 1B) (4) were solved to assist in understanding structure-function relationships. PaADI and MaADI share 27 % sequence identity and belong to guanidino group-modifying enzyme superfamily (GMSF). The catalytic triad (Cys-His-Glu/Asp) is conserved in members of the GMSF. Both crystal structures of PaADI and MaADI show a characteristic 5-fold pseudosymmetrical barrel with ββαβ subunits. Table 2 summarizes the crystal structures of PaADI and MaADI.

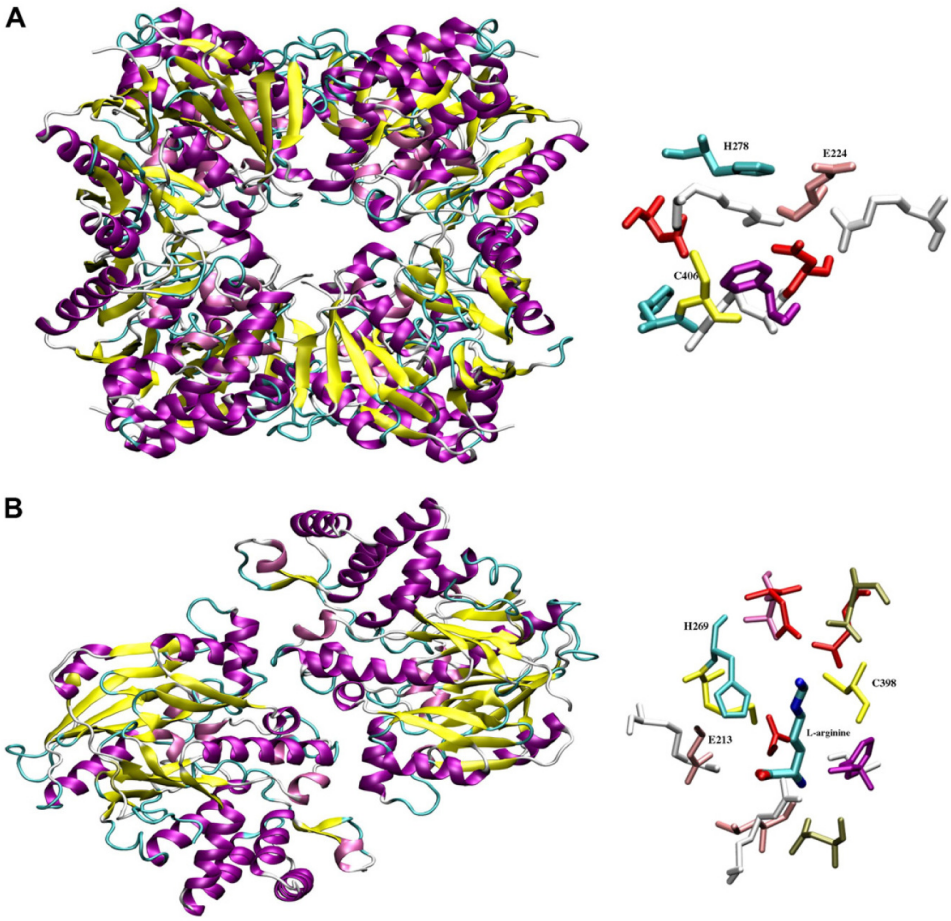

Figure 1. Structural of ADIs from *P. aeruginosa* and *M. arginini*. (A) PaADI (PDB ID: 1RXX) and stereo view of its catalytic triad (C406-H278-E224). (B) MaADI (PDB ID: 1S9R) and stereo view of its catalytic triad (C398-H269-E213) with substrate L-arginine (27).

Table 2. Crystal structures of ADI in protein data bank (PDB).

PDB code	Ligand in crystal structure	Description	Resolution (year)
2A9G	Arginine	Crystal structure of PaADI variant C406A in complex with L-arginine	2.30 Å (2005)
2AAF		Crystal structure of PaADI variant H278A forming a S-alkylthiouronium reaction intermediate	2.30 Å (2005)
2ABR		Crystal structure of PaADI variant D280A with L-arginine forming a S-alkylthiouronium reaction intermediate	2.9 Å (2005)
2ACI		Crystal structure of D166A arginine deiminase	2.50 Å (2005)
1S9R	Arginine	Crystal structure of MaADI covalently linker with a reaction in intermediate	1.60 Å (2004)
1LXY	Citrulline	Crystal Structure of MaADI covalently linked with L-citrulline	2.00 Å (2004)
1RXX		Crystal structure of MaADI	2.45 Å (2004)

MaADI was crystallized as a homodimer and its catalytic triad is formed by Cys398-His269-Glu213. MaADI has a catalytic domain and a five-helix bundle domain (Figure 3). The buried and compact substrate binding pocket is located approximately at the center of the molecule, from which a small solvent channel leads to the surface of the enzyme. The opening to the channel is located adjacent to the dimer interface region, which is at the opposite side of the 5-fold pseudosymmetric moiety of ADI. The shape and size of the channel does not permit transport of the substrate (L-arginine and end product (L-citrulline) in and out of the pocket. Substantial conformational changes in ADI are required to permit entry of the substrate and expulsion of the end product. The occurrence of "closed" and "open" form was suspected to be dependent on binding of substrate.

PaADI has a tetrametric structure with 1630 amino acid residues in total, which makes it the largest enzyme of its structural superfamily. The catalytic triad of PaADI is Cys406-His278-Glu224. Similar to MaADI, the active site of PaADI is

located in a narrow crevice formed by a network of charged residues. Ligand binding energy is derived from ion pair and hydrogen bonding interactions between active site residues and the guanidinium, carboxylate and ammonium groups of the substrate. The proposed substrate-binding model shows that the catalytic center contains abundant charged residues (e.g. Asp280, His405, Glu13 and Arg165). The ion pairing interactions between these residues contribute to the integrity and activity of ADI. In addition, Asp116, Asp227, Arg185, Arg401, His278, Glu118, and Glu224 are part of an extended charged network. The proposed catalytic mechanism suggests that the active site of PaADI is blocked by Arg401, and therefore a conformational transition is taking place upon the substrate binding. Based on the proposed reaction mechanism, Cys406 is as a key residue responsible for the nucleophilic attack on the guanidinium carbon atom of arginine. PaADI contains only one hydrophobic residue, Phe-163 and a Cys-406 with an unknown protonation state. The known functions of important residues are shown in Table 3, and the interactions between important residues and substrate arginine are shown in Figure 2.

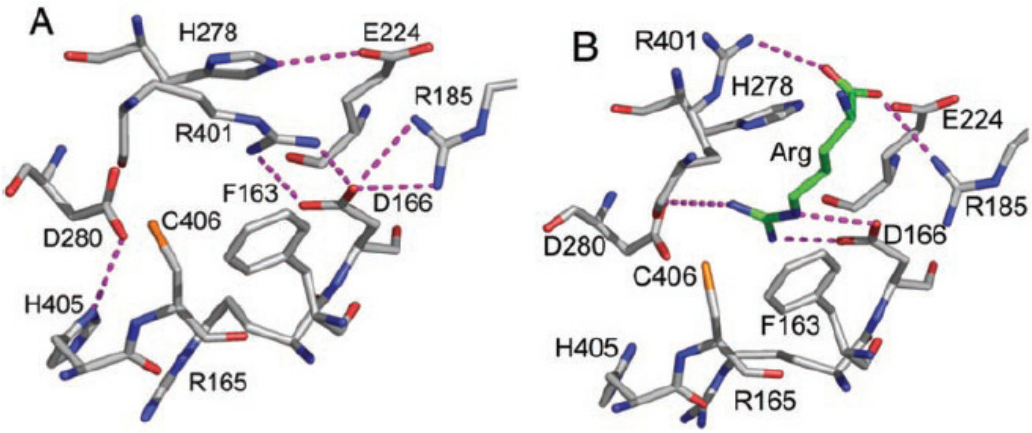

Figure 2. A. stereoscopic view of PaADI key active site residues. B. stereoscopic view of a modeled arginine substrate (green) docked in the active site of ADI. Atomic colors are red, oxygen; blue, nitrogen; yellow, sulfur; and gray, carbon. Ion pair interactions are shown as dashed lines (26).

Table 3. Residues important for catalytic function of PaADI (28, 29).	
Residues	Known/postulated function or comment
Cys406	Mounts the nucleophilic attack on the carbon atom of the guanidinium group of arginine
His278	Serves as a general base and activate the water molecule
Glu224	Modulate the ionization state of His278
Asp280	Interacts with the imidazole group of His405 F via the carboxylate group, which in turn interacts with Glu13. Invariant residue in all known ADIs
Asp280, Asp166	Fix the guanidinium group of the arginine substrate tightly by interactions with the carboxyl groups
Arg401, Arg185	Form ionic interaction with The carboxyl group of the arginine substrate
Phe163	Interacts with the hydrophobic part of arginine substrate
Glu13	Interacts His405 and is invariant in all known ADIs
His405	Sometimes is replaced by an arginine, as in the case of McADI. This may explain the low pH optimum of PaADI (5.6) in contrast to the neutral pH optimum of McADI, the enzyme that contains an arginine residue instead of His405
Arg165	Is fixed by electrostatic interactions with the main chain oxygen atoms of Thr408 and His405 and with the hydroxyl group of Thr-408
Arg401	Blocks the ADI active site via the side chain by forming an ion pair with the carboxyl group of Asp166 and occupies approximately the same position as the guanidinium group of an arginine substrate

The overall fold of MaADI and PaADI consist of five ββαβ modules in cyclical arrangement, generating a pseudo 5-fold symmetrical barrel and an additional 85-residue α-helical domain inserted between the first and the second ββαβ modules giving the typical “Clip-on-fan” moiety. The α-helical domain of PaADI mediates tetramer formation and the α-helical domain of MaADI was speculated to play a role in activating the series of reaction in arginine dehydrolysis pathway (4). Structural alignments by Chakrabarty et al. (18) demonstrated the unique 85 residue 5-α-helical bundle domain exhibiting structural similarity to the mammalian CARD (caspase recruitment domains)-containing proteins and this CARD-like domain is present only in the PaADI and MaADI but not in the other

GMSF members (Figure 3B). Furthermore, PaADI putative CARD-like domain induced apoptosis to cancer cells.

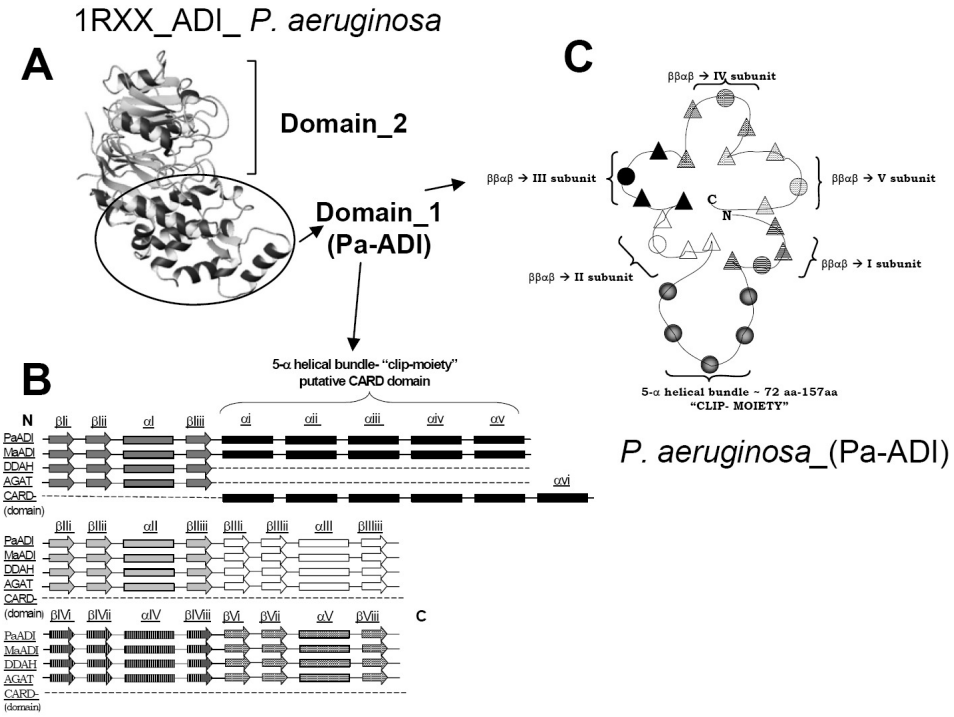

Figure 3. Structural characteristics of the PaADI. A. Ribbon drawing of PaADI (1RXX_A) highlighting the two domains. B. The presence of the CARD domain in PaADI and MaADI but its absence in other members of the GMSF (guanidino-group modifying superfamily) enzymes such as DDAH and AGAT, as shown from the structure-based sequence alignments. The CARD domain represents that of caspase-9. DDAH, dimethylarginine dimethylaminohydrolase; AGAT, arginine: glycine amidinotransferase. The β-strand and α-helices are shown as arrows and strips respectively. Roman numericals I to V are the five ββαβ subunits. The clip moiety (α-helical module) in Figure 3 is seen only in PaADI and MaADI which bears structural homology to the six-α-helical modules that form the CARD domain of the caspase-9 protein molecule. N, N-terminal; C, C-terminal. C. A schematic diagram showing the overall fold and topology of PaADI, as reported (18).

Comparison of substrate free and substrate bound structure of PaADI gives interesting insight into structure changes upon substrate binding (17). Pairwise superposition of the free wild-type PaADI (PDB code: 1rxx) and the mutant enzyme substrate complexes (PDB code: 2a9g) show that the overall fold of the structures remains similar, yet with some local changes. In particular, four loops (Figure 4) associated with the active site undergo conformational transitions not

related to crystal packing: loop 1 (residues 30-46), loop 2 (residues 178-185), loop 3 (residues 271-281, part of this loop is disordered in the apoADI structure), and loop 4 (residues 393-404). Residues adjacent to the substrate exhibit the most significant shifts. For example, the α-carbon atom of Leu41 (loop 1) shifts by 2.7Å and that of Arg185 (loop 2) by 1.8 Å; the α-carbon atom of His278 (loop 3) shifts by 0.9 Å and that of Gly400 (loop 4) by 4.4 Å. These are localized but mechanistically important conformational transitions that tighten the surrounding of the substrate. Simultaneously, substrate binding is accompanied by displacement of the side chain of Arg401 (loop 4) by more than 8 Å to enable access to the active site. The superposition of ADI and PAD4 ADI active site is shielded from the solvent by a long loop (residues 25-48 in PaADI) and the following two turns of α-helix (residues 49-56).

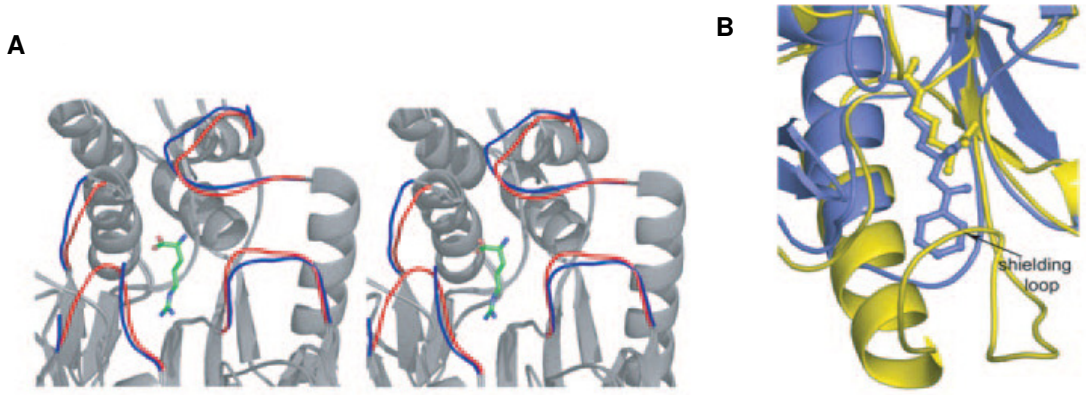

Figure 4 (A). Stereoscopic view of ADI in the unbound and bound states. Superposed molecules are colored gray where the trace of the polypeptide chain is similar in both structures. For regions exhibiting differences, loops of the apoADI structure are highlighted in blue, and loops of the ADI structure complexed with arginine are highlighted in red. 4(B). Structural relationship between ADI (yellow) and PAD4 (cyan) (17).

1.3 Catalytic reaction mechanism of ADI

The overall reaction catalyzed by ADI is the hydrolytic substitution of the ηNH_2 group from the guanidinium group Cζ of L-arginine, leading to citrulline and ammonia (Figure 5). Herzberg (17) and Arnold (4) proposed ADI catalysis mechanism for PaADI (Figure 5) and MaADI, respectively. Basically, both of the proposed mechanisms are composed of three main steps: 1) thiol group of

Cys406 mount a nucleophilic attack on the guanidinium group of arginine and a proton is transferred first to ηNH$_2$ group; 2) water molecule is activated by His278 and followed by attacking the covalent intermediate to replace and release NH$_3$; 3) the C-S covalent bond between enzyme and the resulting citrulline is cleaved and thus end product citrulline is released and free enzyme is generated for next catalytic cycle.

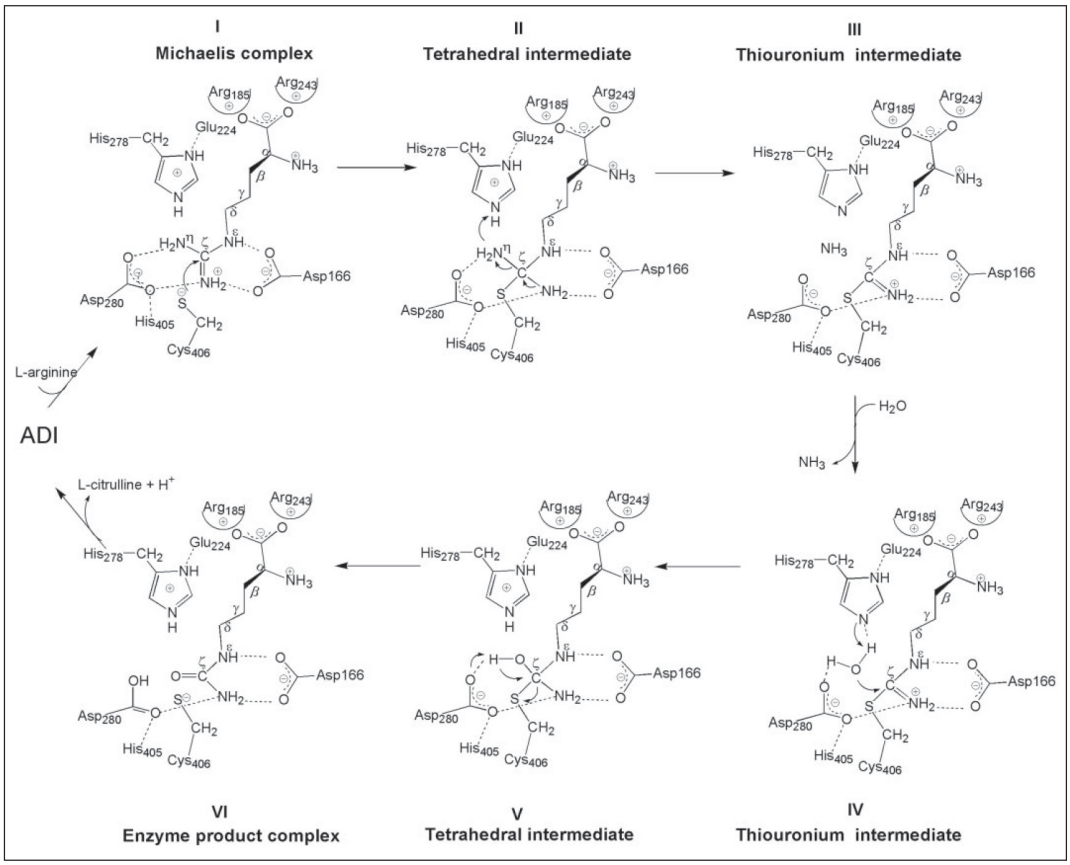

Figure 5. Mechanism of PaADI catalysis of arginine to citrulline and ammonia (17).

1.4 Anti-tumor application of ADI

Amino acids depletion is one type of targeted therapy for human cancers which are auxotrophic for a particular amino acid. Amino acids degrading enzymes, such as asparaginase (30), methioninase (31), arginase (32), arginine deiminase (27), phenylalanine ammonialyase (33) and tryptophanase (34) have been

studied for inhibition of tumor cells *in vitro*. The most representative anticancer enzyme is asparaginase, which is particularly effective in acute lymphoblastic leukaemia. PEG asparaginase is commercialized for acute lymphoblastic leukaemia treatment (Oncaspar®, pegaspargase) (35). However, asparaginase treatment is sometimes accompanied by serous side-effects including anaphylactic shock, coagulapathies as well as liver and pancreatic toxicity (36).

Arginine is an important amino acid involved in the synthesis of a wide range of peptides and proteins, production of creatine and nitric oxide, and a myriad of metabolic pathways and cellular events. It is a precursor of proline, polyamines, glutamine, glutamate, and other neurotransmitters, such as g-aminobutyric acid and also serves as a substrate for two important enzymes, arginase and nitric oxide synthetase (37). Arginine is an indispensable amino acid to children but a semi-essential amino acid in adult humans since many adult somatic cells can synthesize it from citrulline in two steps via urea cycles (Figure 6). The enzyme argininosuccinate synthetase (ASS) catalyzes the conversion of citrulline and aspartic acid to argininosuccinate which is then further converted to arginine and fumaric acid by argininosuccinate lyase (ASL). Arginine can be degraded to ornithine by the urea cycle enzyme arginase. Ornithine is then converted back to citrulline by ornithine carbamoyl transferase (OTC) and then recycles back to arginine from citrulline by ASS/ASL. Thus, the ability to regenerate arginine from citrulline depends on the amount/activity of ASS and ASL, which are tightly coupled. The sensitivity of cells to arginine deprivation depends on the ability of ASS and ASL to regenerate arginine from the alternative intermediate (ornithine, citrulline and argininosuccinate) in the urea cycle.

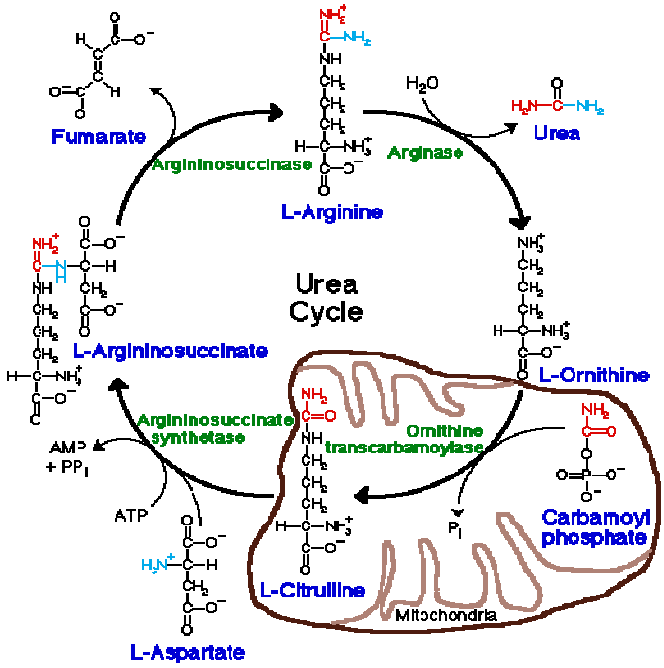

Firgure 6. Urea cycle. Argininosuccinate synthetase (ASS) catalyzes the conversion of citrulline and aspartic acid to argininosuccinate which is then further converted to arginine and fumaric acid by argininosuccinate lyase (ASL). Arginine can be degraded to ornithine by the urea cycle enzyme arginase. Ornithine is then converted back to citrulline by ornithine carbamoyl transferase (OTC) and then recycles back to arginine from citrulline by ASS/ASL.

Arginine begins to become limiting at ~10^{-4} M, whereas other amino acids can sustain growth at 10^{-5}-10^{-6} M. Wheatley et al. showed that most tumour cell lines die considerably more quickly during arginine deprivation than in the absence of any other single (or group of) essential amino acids (38). Since 1930 for the first time arginine known is essential for the growth of some forms of cancer, the potential of arginine degrading enzymes as therapeutic agents was recognized, investigated and employed for arginine auxotrophic tumor treatments. Enzymes capable of depleting arginine *in vitro* include arginase existing in human liver, arginine decarboxylase from bacterial, plant and human, and ADI from microorganism.

Arginine decarboxylase converts arginine to agmatine, which is toxic at high plasma concentration. Furthermore, arginine decarboxylase has a short half-life and it loses virtually all enzymatic activities upon pegylation though pegylation of

arginine decarboxylase is inefficient because not enough lysine residues for polyethylene glycol to attach (39).

Arginase is limited for anti-tumor application because of its low substrate affinity (K_m value 2-4 mM; plasma arginine 100-120 μM), short circulatory half-life (10-15 min) and sub-optimal enzymatic activity at physiological pH (alkaline pH optimum, pH 9.3)(40). Despite these disadvantages of arginase, Lam et al. reported remission of hepatocellular carcinoma induced by systemic release of endogenous hepatic arginase (41) and Leung et al. proved pegylated recombinant human arginase (rhArg-peg 5,000mw) can inhibit ASS-positive HCCs while ADI can not (42).

In addition, ADI, another arginine-degrading microbial enzyme, has various biological activities including anti-proliferation, anti-angiogenesis and inhibition of inducible nitric oxide synthase (iNOs). Figure 7 summarizes how ADI affect many arginine-related cellular functions. ADIs (Table 1) have been shown to have strong *in vitro* and *in vivo* inhibition for arginine auxotrophic tumors (e.g. hepatocellular carcinomas (HCCs), melanomas, retinoblastoma (43), prostate cancer(44)) and ADI from *M. hominis* (MhADI) is currently under clinical trial for HCC (phase II) (45) and melanomas (phase I/II) (46). Studies on human lymphatic leukemia cell lines confirmed ADI's anti-angiogenic activity. Among all the ADIs, MhADI and MaADI were studied most intensively (Table 1).

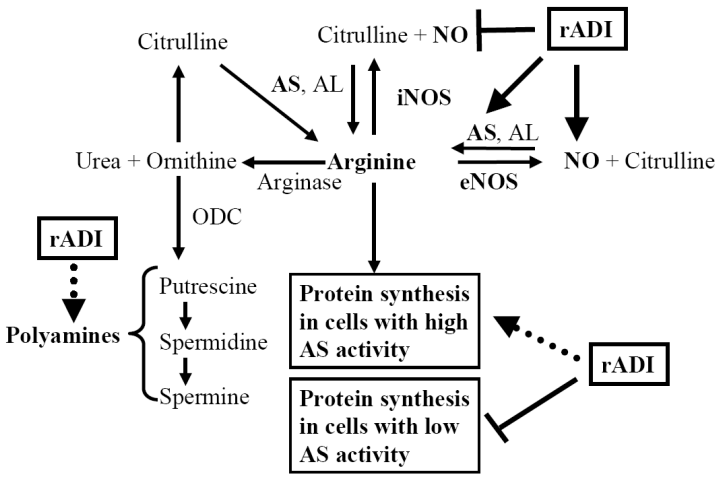

Firgure 7. Summary of ADI effects on arginine-related cellular functions. rADI inhibits NO production via iNOS, but potentiates NO production via eNOS in the cultured endothelial cell model. rADI enhances or inhibits AS activity in different cells. rADI inhibits de novo protein synthesis in cells with low AS activity, but not in cells with high AS activity. Polyamine synthesis was not significantly affected by rADI, even in cells with low AS activity. Arrow representation: solid, potentiates; blocked, inhibits; dotted, no effect (47).

In 1999, US Food and Drug Administration (FDA) designated ADI-PEG-20 orphan drug status for treating HCC and invasive malignant melanomas. In 2005, also the European Agency for the Evaluation of Medicinal Products (EMEA) also granted ADI-PEG-20 orphan drug status for HCC. Phase II trials of ADI-PEG-20 in patients with metastatic hepatocellular carcinomas have shown that the drug is safe, well tolerated, and may benefit patients with unresectable HCC. Izzo and coworker suspected that combination therapies of arginine deprivation and growth inhibition via kinase inhibitors might improve the survival rate further. Additionally, ADI enhances radio sensitivity of human mammary adenocarcinoma (MCF-7 cells) (48), exerts anti-proliferative as well as anti-angiogenic activities and inhibits the growth of viruses such as HIV-1 and hepatitis (49, 50). Current research efforts are focused on ADI's *in vivo* inhibitory effect towards leukemia, melanoma, prostate cancer, renal cell carcinoma, and human umbilical vein endothelial cells (HUVEC) (19, 44, 51-53), clinical trials for HCC (phase II) (45) and melanoma (phase I/II) (46), and tumor inhibitory mechanisms of ADI (54).

The effectiveness of ADIs as anti-tumor agent depends on their enzymatic properties (such as K_m, k_{cat}, optimum pH, stability at neutral pH), selectivity on tumor cells, stability in blood circulation and immunogenicity. Pegylation (35) has been effective in reducing their immunogenicity in animal and increase their stability to various hydrolytic enzymes in plasma. Directed evolution as powerful algorithm to design proteins allows improving all properties that can be reflected in a screening system through iterative rounds of diversity generation and screening. Small libraries of a few thousand variants are often sufficient to find improved variants (55) even without rational understanding of the targeted property. The first example of directed ADI evolution by our group (3) provides a simple and effective screening system to improve activity of PpADI at physiological pH.

1.5 Conclusion

ADI-based arginine deprivation is a novel and promising targeted approach to the treatment arginine auxotrophic tumors, in particular, melanoma, hepatocellular carcinoma and leukemia. Certain mesotheliomas and renal cell cancers were also proved to be sensitive to ADI therapy. Due to its low incidence of major side effects (myelosuppression and gastrointestinal toxicity or other major organ toxicity) arginine deprivation treatment should be combined with other anticancer treatments to increase the response rate. Reengineering of ADI by protein engineering is a promising strayegy to tailor ADI properties for demands in medical applications. Solved ADI crystal structure enables to understand structure function relationships and to guide protein engineering.

Directed evolution

2.1 Introduction to directed evolution

Enzymes are increasingly being used in the generation of products that are traditionally made using chemical synthesis and the field continues to expand its horizons, particularly as applied to the synthesis of the fine chemicals and pharmaceuticals (56, 57). Naturally occurring enzymes are often not designed for the applications of interest, since after all they are evolved in nature for a purpose other than being the catalysts of industrial processes. Directed evolution, rational design and biodiversity screening and combined approches are the main strategies to reengineer enzymes for addressing application demands. Directed evolution has emerged as a powerful enabling method for improving enzyme properties in iterative cycles of diversity generation and screening (Figure 1).

A main advantage of directed evolution compared to rational design is that it does not require structural or mechanistic information for protein optimization. Directed protein evolution has been successfully used for altering and improving protein properties (solubility, expression, enantioselectivity, stability and activity in unusual environment, allosteric interactions, tolerance to pH), as well as for regulating other molecules and systems, including RNA, DNA regulatory elements, biosynthetic pathways and genetic regulatory circuits (58-60).

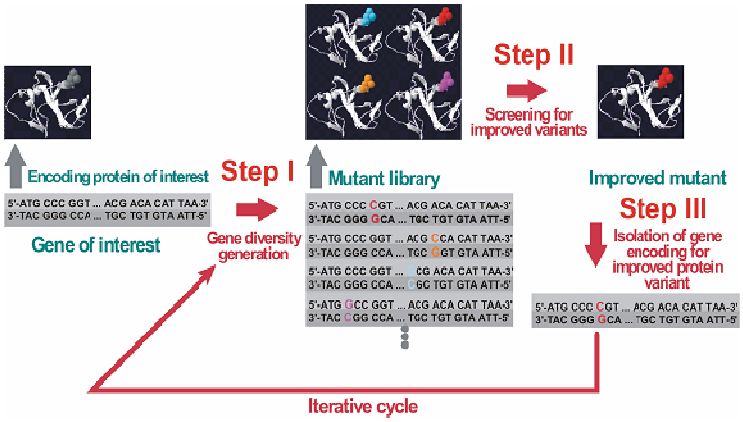

Figure 1. Procedure of a directed evolution experiment. It involves three key steps: 1) selection a good starting sequence and mutating the parent to create a library of variants; 2) identification variants with improved function and 3) isolation of gene encoding for improved variant and repeating the process until the desired function is achieved.

A parent sequence (or sequences) is chosen based on its perceived proximity to the desired function and its evolvability (the ability of a protein to adapt in response to mutation and selective pressure). A parent protein for directed evolution should exhibit enough of the desired function that small improvements can be reliably discerned in a high-throughput screen.

Variants library should be generated with high probability of finding improved variants given the screening capacity. With a high-throughput screening method, a library can be constructed to generate the large potential improvement. Arnold and coworkers(61) showed that very low mutation rates result in many functional sequences but only a small number are unique sequences, however very high mutation rates produce diverse sequences but few retain function. Schwaneberg and coworkers(62) reviewed random mutagenesis methods, focused library generation methods and computational tools for high-quality mutant libraries generation. Schwaneberg and coworkers (63) also summarized criteria for an ideal mutagenesis methods: unbiased mutational spectrum, controllable mutation frequency, consecutive nucleotide substitutions or codon-based substitutions, enable subset mutagenesis (e.g. introduction mainly positively or negatively charged amino acid), independent of gene length, technically simple and reproducible, and economical.

Screening is used to identify library members improved in the targeted property. Identification of improved variants though selection or screening is “analogous” to evolutionary pressure in natural evolution (i.e. only the fittest survive). As the word “directed” in directed evolution implies, laboratory evolutionary pressure is defined and applied by the researcher in screening system. Gradually increasing the selection pressure or evolving against a series of intermediate challenges often accumulates useful single mutations and yields desired variants (64).

Traditional methods for screening employ microtiter plate formats (96-well, 384-well, 1,536-well (65) and even 1,000,000-well (66)) or solid phase assay (agar plate, filter paper and nitrocellulose membrane), which typically enable the screening of no more than 10^6 variants by using robotic automation (67). Sometimes, fast and universal analytic methods like HPLC (68) or GC-MS (69) are utilized for performing an efficient screen of a non-natural substrate. However, the number of screened mutants is limited to 10^4-10^6. In recent years flow cytometry systems (67, 70, 71) have become increasingly attractive, especially after the development of emulsion technology offering compartmentalization and high throughput up to 10^7/h. In addition, Weitz and coworkers (72) recently reported a promising ultrahigh-throughput screening in drop-based microfluidics, by which one can screen a library of 10^8 in about 10 h. Dijkhuizen et al. compared in a review (73) six kinds of library screening strategies (Figure 2). Selection techniques rely on a direct link between cell growth and improved or acquired enzyme function and therefore it is limited to engineering detoxifying enzymes (e.g. b-lactamase) or enzymes that synthesize essential nutrients for cell growth and survival. The traditional microtiter plate screenings are medium-throughput and the most simplistic format of screening. It involves the incubation of colonies with the substrate of targeted enzyme. The crucial factor with this screening technique is that substrate conversion creates a visual signal, such as fluorescence or color, to identify colonies expressing an enzyme with desirable properties. Microtiter plate based screenings are the most commonly applied method in identifying desirable enzyme variants. Microtiter plate based

screenings enable the use of various analytical tools and in the mean while they offer a great dynamic range. Their screening capacity is usually limited to less than 10^4 variants per day. Screening based on microfluidic device and sorting device is a new screening platform for directed evolution, which offers ultra-high-throughput. It allows the discriminate between wild-type and a less active mutant and allows for the addition of substrates and quenchers at desired time thus extending the scope of directed evolution screening strategies. Cell as micro-rector, cell surface display and *in vitro* compartmentalization technology are also FACS (fluorescence-activated cell sorting system) dependent methods for high-throughput screening and allow 10^9-10^{10} screening capacity.

Once improved enzymes are identified, encoding genes are isolated and subjected to further iterative cycles of mutation and screening in order to accumulate beneficial mutations until the targeted improvement is hopefully achieved. The number of iterations required depends on the starting point, the protein fold and the selected properties which determine the possible mutational load and achievable improvement.

Four accepted requirements for successful directed evolution (http://www.che.caltech.edu/groups/fha/) are, 1) the desired function must be physically possible; 2) the function must also be biologically, or evolutionarily, feasible. In practice, this means that there exists a mutational pathway to get from here to there through ever-improving variants (see above). A good experiment will maximize the likelihood; 3) Suitable host (*E. coli* or *S. cerevisiae*) which allows functional expression of more than 10^6 variants per µg of DNA. 4) A rapid screen or selection that reflects the desired function. How rapid the screen must be depends on how rare mutations leading to the desired property are and how many must be accumulated to achieve the desired result.

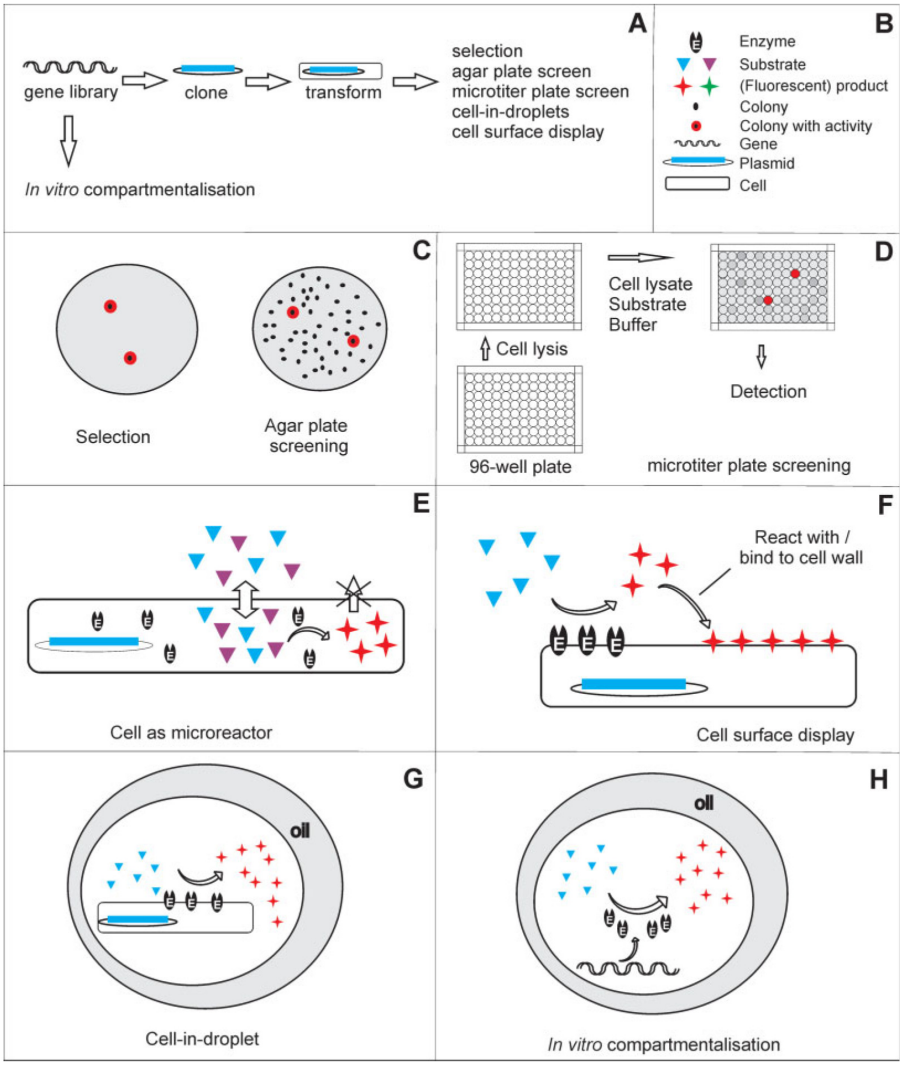

Comparison of screening and selection technologies

Strategy	Library size	Advantage	Disadvantage
Selection	$\sim 10^9$	Yields desirable variants only	Only possible if activity gives growth advantage
Agar plate screen	$\sim 10^5$	Simple to operate	Limited dynamic range
Microtiter plate screen	$\sim 10^4$	All analytical methods possible Excellent dynamic range	Relatively low screening capacity
Cell-in-droplet screen	$\sim 10^9$	Large libraries	Fluorescence detection and DNA modifying enzymes only
Cell as microreactor	$\sim 10^9$	Large libraries	Fluorescence detection only
Cell surface display	$\sim 10^9$	Large libraries	Fluorescence detection only
In vitro compartmentalization	$\sim 10^{10}$	No cloning steps Large libraries	Fluorescence detection and DNA modifying enzymes only

Figure 2. Overview of screening technologies. (A) Experimental steps from obtaining the gene library as PCR product to the actual screen. Note that cloning and transformation efficiency are often limiting library size; (B) Explanation of symbols; (C) Cell growth/survival selection and agar plate screening; (D) Microtiter plate screening; (E) Cell as micro-reactor; (F) Cell surface display; (G) Cell-in-droplet; and (H) *In vitro* compartmentalization (73).

2.2 Directed enzyme evolution for pH tolerance of enzymes

Application of enzymes in processes at a specified pH necessitates protein engineering to change their pH performance. Directed evolution and rational design method were applied to improve enzyme specific activity at certain pH or shift their pH profiles. Some representative success stories of directed protein evolution improving pH performance are summarized in Table 1.

Table 1. Improvement obtained from directed evolution or rational design for pH performance.

Enzymes	Mutagenesis methods	Screening methods	Improvements	References
Human β-glucuronidase	EpPCR and saturation mutagenesis	Flow cytometry	60-fold more active (k_{cat}/K_m) at pH 7.0 and were up to an order of magnitude more effective at catalyzing the conversion of two structurally disparate glucuronide prodrugs to anticancer agents	2008 (74)
Bacterial xylanase	DNA shuffling	Agar plate assay	About 5-fold improvement of specific activity at pH 9.0	2008 (75)
Human pancreatic lipase	EpPCR	Agar plate and microtiter plate assay	1.5-fold of activity improvement at acidic pH	2010 (76)
Bacterial arginine deiminase	EpPCR and site directed mutagenesis	Microtiter plate assay	pH optimum shifted from pH 6.5 to pH 7; 4-fold of activity improvement at pH 7.4	2010 (3)
Bacterial α-amylase	EpPCR	Microtiter plate assay	5-fold higher activity at pH 10 than wild type	2003 (77)
Eukaryote D-pantonohydrolase	EpPCR and DNA shuffling	Agar plate assay	10.5-fold higher specific activity and retain 85% of its original activity after incubation under low pH	2006 (78)
Vanadium chloroperoxidase	EpPCR, site saturation mutagenesis and site directed mutagenesis	Microtiter plate assay	About 100-fold improvement of specific activity at pH 8	2006 (79)
Bacterial class-A non-specific acid phosphatase (PhoN)	Site directed mutagenesis		1.6-fold of activity improvement over broder pH range	2006 (80)
Aspergillus niger PhyA phytase	Site directed mutagenesis		pH shifted from 5.5 to 3.8 (1.7 unit); 2.66 -fold improvement of activity at pH 3.5 than wild type.	2006 (81)
Bacillus cereus β-amylase	Site directed mutagenesis		pH optimum shifted to pH 4.2-4.8 by 2 pH units.	2004 (82)
Phytase	Site directed mutagenesis		pH optimum shifted by 0.5-1 pH unit; a slight increase in maximum specific activity	2002 (83)
Alcohol dehydrogenase	Site directed mutagenesis		pH optimum shifted from 7.8 to 9.0; about 2-fold improvement of maximum activity at pH 9.0 than that of wild type	1991 (84)

Many examples of rational reengineering of an enzyme pH optimum exist (Table 1). For shifting the pH optimum, a deep understanding of molecular dynamics is essential part of understanding enzyme flexibility. Rational design method successfully shifted enzyme pH profile. pH dependence of an enzyme is determined by the ionization of the catalytic groups, which is affected by various interactions involved in their microenvironments. In order to catalyze certain reactions, ionizable residues in active site should act as nucleophile or acid/base catalyst and they need to maintain proper ionization state for proper activities of proteins. The p*K*a value of the proton donor and the catalytic nucleophilic residue are therefore limiting the pH range at which the enzyme can function, and therefore pH-dependent activity can be differed by the p*K*a of the key residues. The p*K*a value of the residue is governed by intrinsic acidity of the functional group and other factors (electrostatic interaction from neighboring and the heterogeneous dielectric environment in the protein solution system). The electrostatic potential generated by the charged titratable residues affects the ground state of the protein, such as stability, binding to ligands and p*K*a values of ionizable groups. The electrostatic potential of proteins can be calculated by using computational procedures (Delphi, UHBD, CHARMM) and can be increased or decreased through mutations. For shifting the pH optimum of enzymes, many researchers have tried to substitute catalytic residue by site-directed mutagenesis (Table 1).

Yoo and coworkers (85) analyzed the relation between the shift of pH optimum and change in electrostatic potential due to mutation using Delphi. They identified key residues of xylanase responsible for electrostatic potential of catalytic residues but not affecting the catalysis directly. The latter hypothesis was proven by site directed mutagenesis in a later report. Wyss and coworkers (83) summarized strategies for enzyme pH profile modification, 1) replacement of ionizable groups that are directly involved in substrate or product binding and/or catalysis by nonionizable ones or by amino acids with different charge or p*K*a values; 2) replacement of residues that are in direct contact with residues

mentioned in 1) by forming hydrogen bonds and/or salt bridges; 3) alteration of longer-range (indirect) charge-charge interactions by modification of the surface charge of the enzyme.

When there is no structure-function relationship information available for an enzyme, directed evolution is the best option to tailor the pH performance of enzyme for application demands (Table 1). Directed evolution allows improving all properties that can be reflected in a screening system through iterative rounds of diversity generation and screening. Small libraries of a few thousand variants are often sufficient to find improved muteins even without rational understanding of the targeted property (76, 86). Using MTP assay, epPCR mutant libraries with a ratio of 50 % active and 50 % inactive clones have often been used successfully in directed evolution, improving enzyme properties by gradual changes (one or two amino acids changes per round of mutagenesis and screening).

2.3 Directed enzyme evolution for medical application

Directed evolution has been very useful for improving enzymes for industrial needs. In recent years, there is also growing number of enzymes applied for therapeutic purpose. For the development of protein therapeutics, directed evolution started to be used to tailor enzyme properties in medical field, for example drug delivery (87, 88) and has proven to be a useful tool for generating protein variants with enhanced therapeutic potential (88), for example, improving the effectiveness of therapeutic enzymes, antibodies, vaccines and viruses. Here, the improvements of therapeutic protein for anti-tumor application by directed evolution are discussed in more details.

2.3.1 Prodrug enzymes for tumor chemotherapy

Prodrug cancer chemotherapy has attracted considerable interest due to the possibilities it provids to overcome various barriers to drug formulation and delivery (such as poor aqueous solubility, chemical instability, insufficient oral

adsorption, rapid pre-systemic metabolism, inadequate brain penetration, toxicity and local irritation) (89). Examples of such drugs currently in use in cancer treatment include 5-fluorocytosine, cyclophosphamide, capecitabine, mitomycin C, and AQ4N (90). However, the side effects of prodrug therapy remain a serious concern which arises from the fact that noncancerous cells also possess the capacity to degrade them. This has triggered the interest to generate more effective prodrug-activating enzymes so that prodrugs can kill tumor cells at concentrations that generate little or no side effects. Further goals are to design more powerful and tumor-specific drugs, and to devise more effective methods for delivering them specifically to tumors.

By applying directed evolution through the technique of error-prone PCR, Martin and coworkers (90) indentified YieF variant exhibiting >5-fold increased capacity to kill HeLa cells. Furthermore, YieF variant was proved to be effectively delivered to tumor cells using a strain of *Salmonella typhimurium* (SL 7838).

Human β-glucuronidase, due to low intrinsic immunogenicity in humans, is an attractive enzyme for tumor-specific prodrug activation. However its utility is limited by low activity at physiological pH. Roffler and coworkers (74) developed a high-throughput screening procedure for enzymatic activity based on the stable retention of fluorescent reaction product in mammalian cells expressing properly folded glycoproteins on their surface. This procedure was utilized to screen error-prone PCR and saturation mutagenesis libraries to isolate β-glucuronidase tetramers that were up to 60-fold more active (k_{cat}/K_m) at pH 7.0 and were up to one order of magnitude more effective at catalyzing the conversion of two structurally disparate glucuronide prodrugs to anticancer agents.

2.3.2 Oncolytic viruses for tumor chemotherapy

Viral-mediated oncolysis is a novel cancer therapeutic approach with the potential to be more effective and less toxic than current therapies due to the agents' selective growth and amplification in tumor cells. To date, these agents

have been regarded as highly safe in patients but have generally fallen short of their expected therapeutic value as monotherapies.

Consequently, new approaches to generate highly potent oncolytic viruses are required. For the latter purpose, Hermiston and coworkers (91) developed a new method and termed it also ‘‘Directed Evolution’’ for creating highly potent oncolytic viruses. Viral serotypes representing Ad subgroups B-F were pooled and passaged twice on sub-confluent cultures of the target tumor cell lines at a particle-per-cell ratio of approximately 200 to invite recombination between serotypes (Figure 3). Supernatants from the second round of the high viral particle-per-cell infection of sub-confluent cultures were then used in a 10-fold dilution series to infect confluent T-75 tissue culture flasks of target tumor cell lines PC-3, HT-29, Panc-1 and MDA-231. Using this ‘‘Directed Evolution’’ methodology, the novel generated chimeric oncolytic virus ColoAd1 demonstrated ~ 2 log increase in both potency and selectivity when compared to ONYX-015 on colon cancer cells. *In vivo* and *ex vivo* studies therefore validated the innovative general approach for deriving clinically-relevant and potent anti-cancer virotherapies.

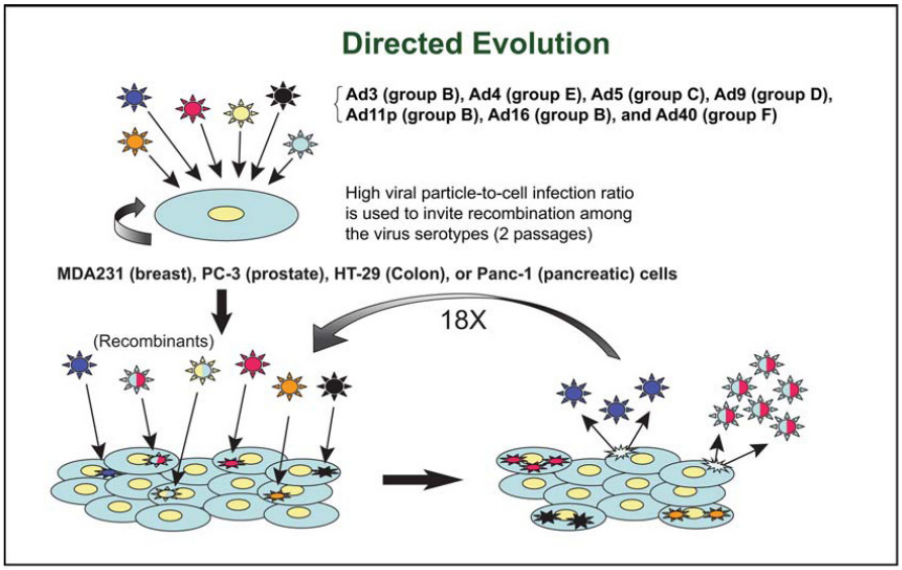

Figure 3. Hermiston’s “Directed Evolution” process of viruses and derivative viral pools (91).

2.3.3 Amino acid depriving enzyme for anti-tumor applications

Naturally available enzymes are usually not optimally suited for therapeutic purposes. This incompatibility often relates to the stability or activity of the enzymes under body conditions.

Despite many successful efforts to broaden the understanding of the structural basis of protein stability, there is still no universal strategy to stabilize protein by a limited number of rationally designed mutations. Well-known and reasonably successful types of rational engineering work include substitutions that increase rigidity (e.g. substitute amino acid Xxx with Pro or substitute Gly with other amino acid Xxx or the introduction of disulfides). These substitutions have effects on the entropy of the unfolded state, improvement of molecular packing (e.g. shortening of loops, improvement of interactions in the hydrophobic core, for example, by the removal of internal cavities), modification of surface charge networks or reinforcement of a higher oligomerization state.

Directed evolution provides a powerful approach for improving thermostability and does not need understanding of structure-function relationship. Most strategies for screening for enzyme stability rely on measuring residual enzyme activity before and after exposure to a denaturing challenge (e.g. high temperature, organic solvents, extreme pH) (92).

Bacterial L-asparaginases have been used as therapeutic agents in the treatment of lymphoblastic leukaemia. The main restrictions to the therapeutic use of L-asparaginase include its premature inactivation. As a result frequent injections are required to maintain therapeutic levels. Repeated injections and high dose can cause several types of side reactions from mild allergies and the development of immune responses to dangerous anaphylactic shocks (93). Enhancing the stability of L-asparaginase by protein engineering improves its body-residence time, and thereby minimizes immunosuppressive effects by lowering the therapeutic dose. Labrou and coworkers (94) obtained a

reengineered L-asparaginase with enhanced thermal stability. Single mutation on the surface of the protein resulted in ~10 degree increased T_m value (half-inactivation temperature). The thermostable variant has to be tested further on animals and/or humans in order to be advanced to a potent therapeutic drug.

Another example of a reengineered amino acid-deprivating enzyme is PpADI. PpADI is a promising anti-tumor enzyme however with a non-physiological optimal pH and relative high K_m value which hindering its medical application. By directed evolution and site saturation mutagenesis, PpADI variants with higher activity at physiological pH and at low arginine concentration of were obtained with improved properties to become a potent anti-tumor drug (see chapter 3 and chapter 4). *In vitro* and *in vivo* test of the improved variants are required to evaluate the anti-tumor effectiveness.

2.3.4 Affibody molecules for cancer prognosis

Affibody molecules represent a new class of affinity proteins that are based on the Z-domain scaffold derived from staphylococcal protein A (95). Among the scaffold proteins, Affibody molecules constitute the smallest non-cysteine-containing protein scaffold. The small size (~ 7 kDa), robust structure, and straightforward production procedures (either by recombinant production in bacteria or by chemical synthesis) make Affibody molecules attractive targeting agents for *in vivo* radionuclide imaging (96) as well as for various biotechnological applications (97, 98). The small size offers a convenient affinity maturation principle. Gene synthesis allows randomizing the whole gene to generate diverse mutant library. The potential use of radiolabeled Affibody molecules for high-contrast radionuclide imaging of biomarkers has been demonstrated in preclinical studies and in pilot clinical studies. Affibody molecules are non-immunoglobulin-derived affinity proteins based on a three-helical bundle protein domain.

Several of affinity proteins have been investigated for both *in vivo* diagnostics and therapy of tumor in radionuclide molecular imaging. Affinity proteins in tumor-targeted therapy can affect tumor progression by altering signal transduction or by delivering a payload of toxin, drug or radionuclide. EGFR (epidermal growth factor receptor), one of the receptor in ErbB family, has been extensively studied as biomarkers in tumor targeting and over expressed in various malignancies, associated with poor patient prognosis and are therefore interesting targets for solid tumors. High affinity and especially slow dissociation rate are important for obtaining high contrast images. Affinity in the low nanomolar range is considered as a prerequisite for successful use of peptide-based tracers.

Ståhl and coworkers (99) described the affinity maturation procedure for the generation of Affibody molecules binding with high affinity and specificity to EGFR. The library for affinity maturation was constructed using a single oligonucleotide for the rerandomization of desired positions. The new binders were selected with phage display technology and the best second-generation binders were characterized *in vitro* using real-time biospecific interaction analysis (BIA) for their binding to recombinant EGFR and with flow cytometry for their binding to native EGFR. Second-generation binders achieved an approximately 30-fold improvement in affinity (K_d = 5-10 nM) for the soluble extracellular domain of EGFR in biospecific interaction analysis using Biacore.

2.3.5 Interferon for anti-tumor applicaiton

Alpha interferons (IFN-as) are members of the diverse helical-bundle superfamily of cytokine genes, which have potent antiviral and antiproliferative activities and therefore can be used as anticancer and antiviral agents. However, doselimiting toxicity, receptor cross-reactivity, and short serum half-lives significantly reduce the clinical use of many of these cytokines.

Patten and coworkers (100) performed a family shuffling experiment with over 20 human interferon-α (Hu-IFN-α) genes. Antiviral assay and proliferation assay

were used to indentify clones with improved activity on Hu-IFN-α receptor. One clone showed 285,000-fold improved activity relative to Hu-IFN-α2a and 185-fold relative to Hu-IFN-α1 (most active native human interferon).

Selective breeding using DNA shuffling has proved to be very effective method to rapidly improve pharmaceutical proteins by which initially have low levels of the desired “activity” (101, 102). Backcrossing of evolved recommbinants with the wild type genes removes functionally neutral changes, which might reduce the immunogenicity of evolved proteins (103).

2.4 Conclusion

Proteins, especially enzymes, have gained a central role in modern chemical, biotechnological, and biopharmaceutical industries. Directed evolution has over the past proved to be a versatile and successful approach for tailoring protein properties to industrial, agricultural and medical demands and for advancing our understanding of structure-function relationships in biocatalysts. Appropriate library generation and screening methods should be employed concerning the target protein and desired property. To set up a sophisticated screening method, complex conditions in human body (pH, ion concentration, proteases, hormones etc.) should be considered. Subsequent *in vivo* or *in vitro* test of improved variants should be carried out to further validate the screening assay. Development of diversity generation and high-throughput screening method will enable evolution to solve problems efficiently. Especially, directed evolution provides a powerful strategy to rapidly advance the development of improved protein-based drugs (enzymes and antibodies, peptide and ligands). Directed evolution promises to play an increasingly important role to generate “desirable” drugs.

Chapter 3. Directed evolution of Arginine deiminase for increased activity at physiological pH

3. 1 Abstract

Arginine deiminase (ADI; EC 3.5.3.6) has been studied as a potential anti-tumor drug for the treatment of arginine-auxotrophic tumors, such as hepatocellular carcinomas (HCCs) and melanomas. Studies with human lymphatic leukemia cell lines confirmed that ADI is a potential anti-angiogenic agent effective in the treatment of leukemia. ADI from *Pseudomonas plecoglossicida* (PpADI) was cloned and expressed in *E.coli*. A main limitation of PpADI lies in its pH-dependent activity profile with a pH optimum at 6.5. A pH shift from 6.5 to 7.5 results in ~80 % activity drop (pH of human plasma is 7.35 to 7.45). For shifting PpADI pH optimum to netrual pH, a directed evolution protocol based on an adapted citrulline screening protocol in microtiter plate (MTP) format was developed and validated. Proof of concept for ADI engineering resulted in a pH optimum of pH 7.0 and increased activity under physiological conditions: at pH 7.4, variant M2 (K5T, D44E and H404R) is 4-fold more active than the wild type PpADI and retains ~30 % of its activity relative to its pH optimum, compared to ~10 % in the case of the wild type PpADI.

3.2 Introduction

Arginine deiminase (ADI) is a potential cancer therapy agent for the treatment of arginine-auxotrophic tumors (e.g. hepatocellular carcinomas and melanomas). The hepatocellular carcinoma (HCC) accounts annually for approximately 1 million new cases worldwide. In the US the incidence rate (per 100,000 persons; 1992-2002) of HCC is 8.6 with a mortality rate of 6.5 due to low responses of hepatoma to chemotherapeutic treatments (27). Current research efforts are

focused on ADI's *in vivo* inhibitory effect towards HCCs, leukemia, melanomas and human umbilical vein endothelial cells (HUVEC) (104-106), clinical trials for HCC (phase III) and melanoma (phase I/II) (105, 107), and PEG formulation of ADI to improve its efficacy as a clinical drug, including serum half-life and antigenicity (16, 108). ADI inhibited the growth of cultured leukemia cells at concentrations of 5-10 ng/ml, which were about 20-100 times lower than those of the L-asparaginase standard resulting in fewer side effects (106, 109). Arginine deprivation is speculated to be the molecular reason for ADI's inhibitory effect on human lymphatic leukemia (106). ADIs catalyze the first step of the arginine deiminase (ADI) pathway by hydrolyzing arginine to citrulline and ammonium. Several ADI genes have been identified, purified, and characterized from bacteria, archaea and some eukaryotes excluding mammalian cells and summarized in a recent review (27). None of these ADIs is from a kinetic point of view ideally suited for *in vivo* applications in humans under physiological conditions.

Protein engineering by rational design and directed evolution offers opportunities to tailor ADI properties to physiological conditions. For the proof of concept, an ADI isolated from *Pseudomonas plecoglossicida* CGMCC2039 (accession number: ABS70718) which can be functionally expressed in *E. coli* has been employed. Directed evolution approaches employ mainly *E. coli* as host due to its fast growth and high transformation efficiency which is a prerequisite for generating complex mutant libraries. Over the last decades, directed protein evolution has become a versatile and successful approach for tailoring protein properties for industrial demands (mainly in chemical synthesis) and for advancing our understanding of structure-function relationships in enzymes. A directed evolution experiment comprises iterative cycles of diversity generation and functional selection for improved variants. Only a few manuscripts for phytases (83), xylanases (110), amylases (77, 82, 111), and an alcohol deyhdrogenase (112) reported a shift of pH optima using directed evolution algorithms. None of these directed evolution campaigns targeted a medical

application and arginine deiminase has to our best knowledge not been altered in its pH activity/resistance by directed evolution.

Comparison of PaADI (*Pseudomonas aeruginosa*, pH optimum 5.6; His405) and MaADI (*Mycoplasma arginini* ADI, pH optimum 6.5, Arg397) led to the speculation that substitution of His by Arg might contribute to MaADI's increased pH optimum (17). A sequence alignment of four ADIs (MaADI, MyADI (*Mycoplasma arthritidis* ADI), PaADI and PpADI) shows that for both Pseudomonas ADIs the synonymous amino acid positions (404 & 405), contain a His whereas both Mycoplasma ADIs contain at corresponding positions an Arg. Interestingly, both Mycoplasma ADIs have an pH optimum approximately one pH unit higher than both Pseudomonas ADIs.

In this study we report the first directed ADI evolution protocol in which the pH profile of PpADI was shifted to higher pH values representing a conceptional proof that ADI properties can be tailored for demands *in vivo* treatment of arginine-auxotrophic tumors. An emphasis is given on detailed description of directed evolution conditions (mutagenic and screening).

3.3 Materials and methods

3.3.1 Materials

All chemicals were of analytical-reagent grade or higher quality and were purchased from Fluka (Neu-Ulm, Germany), Sigma-Aldrich (Steinheim, Germany) and Applichem (Darmstadt, Germany), except the resins for purification (TOSOH, Stuttgart, Germany). All enzymes were purchased from New England Biolabs (Frankfurt, Germany), Fermentas (St. Leon-Rt, Germany), and Sigma-Aldrich Chemie (Taufkirchen, Germany), unless stated otherwise.

Thermal cycler (Mastercyler gradient; Eppendorf, Hamburg, Germany) and thin-wall PCR tubes (Multi-ultra tubes; 0.2 µl; Carl Roth, Germany) were used in all PCRs. The PCR volume was always 50 µl except for Megaprimer PCR of whole

plasmid (MEGAWHOP, 20 µl); larger volumes were prepared in multiple 50-µl PCRs. The amount of DNA in cloning experiments was quantified by using a NanoDrop photometer (NanoDrop Technologies, Germany).

Pseudomonas plecoglossicida CGMCC2039 was provided by Professor Zhihao Sun (Jiangnan University, Wuxi, China).

3.3.2 Methods

3.3.2.1 Reagents used in assays

Acid-ferric solution

To dH_2O (600 ml), concentrated H_3PO_4 (70 ml, 85 %) and concentrated H_2SO_4 (160 ml, 90-91 %) were added slowly. After cooling to room temperature, $FeCl_3 \cdot 6H_2O$ (10 ml, 10 g/L) was added in the above solution, finally the total volume was adjusted to 1 liter with dH_2O.

Diacetyl monoxime -thiosemicarbazide (DAM-TSC) solution

DAM solution (10 g/L) and TSC solution (0.3 g/L) were prepared separately. The two solutions were mixed (volume ratio = 1:1) just prior to use.

3.3.2.2 Cloning of ADI into pET42b(+)

The arginine deiminase (ADI) gene was amplified from *Pseudomonas plecoglossicida* CGMCC2039 by colony PCR (94℃ for 10 min, 1 cycle; 94℃, 30 s/ 54℃, 30 s/ 72℃, 165 s, 29 cycles; 72℃ for 5 min, 1 cycle) using primer (5'-CCGCATTCCGCTGAAAAACAGAAGTACGG-3' and 5'-CTTCTCGAGTTAGTAGTTGATCGGGTCGCGCACG-3'), 1.5 U of Pfu DNA polymerase, 0.20 mM of dNTP mix and a colony of *Pseudomonas plecoglossicida* CGMCC2039. Amplification product was purified by gel extraction, digested using NdeI (20 U) and XhoI (20 U) and purified using QIAquick PCR purification kit (QIAGEN, Hilden, Germany). Cloning vector pET42b(+) was digested with NdeI (20 U) and XhoI (20 U), and purified by gel extraction kit (QIAGEN, Hilden, Germany). Digested ADI gene and pET42b(+)

were ligated using T4 DNA ligase (1 U) to give pET42b(+)-ADI and transformed into *E. coli* BL21-Gold (DE3).

3.3.2.3 Site directed mutagenesis of PpADI gene at position H404

Site directed mutagenesis of ADI gene was performed according to the published method (113) on plasmid pET42b(+)-ADI. The following oligonucleotides were used for mutagenesis of H404R: 5'-GGCCGTGGCGGCGGCCGTTGCATGACCTGCCCG-3' and 5'-CGGGCAGGTCATGCAACGGCCGCCGCCACGGCC-3' (underlining indicated the substituted nucleotide). For the mutagenic PCR (First stage: 95℃ for 30 s, 1 cycle; 95℃, 30 s/ 55℃, 1 min/ 72℃, 130 s, 3 cycles. Second stage: 95℃ for 30 s, 1 cycle; 95℃, 30 s/ 55℃, 1 min/ 72℃, 130 s, 15 cycles; 68℃ for 30 min, 1 cycle), 2 U of Phusion™ Hot Start DNA polymerase (Finnzymes, Keilaranta, Finland), 0.20 mM of dNTP mix, 25 pmol of each primer together with 100 ng of template (pET42b(+) harboring ADI gene) were used. Following the PCR, DpnI (40 U; New England Biolabs) was added, and incubated overnight at 37℃. The PCR products were purified by using a QIAquick PCR Purification Kit (Qiagen) and transformed into *E. coli* BL21-Gold (DE3) for expression.

3.3.2.4 Site sturation mutagenesis of PpADI gene at nine amino acid position

Site saturation mutagenesis of ADI gene was performed according to the published method (113) on plasmid pET42b(+)-ADI. The oligonucleotides were used for mutagenesis were listed in table 1 (underlining indicated the substituted nucleotide). For the mutagenic PCR (First stage: 95℃ for 30 s, 1 cycle; 95℃, 30 s/ 55℃, 1 min/ 72℃, 130 s, 3 cycles. Second stage: 95℃ for 30 s, 1 cycle; 95℃, 30 s/ 55℃, 1 min/ 72℃, 130 s, 15 cycles; 68℃ for 30 min, 1 cycle), 2 U of Phusion™ Hot Start DNA polymerase (Finnzymes, Keilaranta, Finland), 0.20 mM of dNTP mix, 25 pmol of each primer together with 100 ng of template (pET42b(+) harboring ADI gene) were used. Following the PCR, DpnI (40 U; New England Biolabs) was added, and incubated overnight at 37℃. The PCR products were

purified by using a QIAquick PCR Purification Kit (Qiagen) and transformed into *E. coli* BL21-Gold (DE3) for expression.

Table 1. Primer sequences for site saturation mutagenesis.

Primer name	Sequences
Leu 41 FP	AACTGCGACGAGCTGNNNTTCGACGATGTGATC
Leu 41 RP	GATCACATCG TCGAANNNCA GCTCGTCGCAGTT
Asn 360 FP	TGGGATGACGGCAACAACNNNGTGGCGCTGGAG
Asn 360 RP	CTCCAGCGCC ACCACNNNGT TGCCGTCATCCCA
Arg401 FP	GAACTGGGCCGGGGCNNNGGCGGCGGCCACTGC
Arg401 RP	GCAGTGGCCGCCGCCNNNGCCCCGGCCCAGTTC
Phe163 FP	CTGCCCAACACCCAGNNNACCCGCGACACCACC
Phe163 RP	GGTGGTGTCGCGGGTNNNCTGGGTGTTGGGCAG
Asn160 FP	CTGCCGCCGCTGCCCNNNACCCAGTTCACCCGC
Asn160 RP	GCGGGTGAACTGGGTNNNGGGCAGCGGCGGCAG
Arg185 FP	ATGTACTGGCCGGCNNNCGCCAGGAAACCCTG
Arg185 RP	CAGGGTTTCCTGGCGNNNGCCGGCCAGTACAT
Arg243 FP	ATCGGCATGGGTGAGNNNACCTCGCGCCAGGCC
Arg243 RP	GGCCTGGCGCGAGGTNNNCTCACCCATGCCGAT
His405 FP	GGCCGTGGCGGCGGCNNNTGCATGACCTGCCCG
His405 RP	CGGGCAGGTCATGCANNNGCCGCCGCCACGGCC
Gly403 FP	GCCGGGGCCGTGGCNNNGGCCACTGCATGACC
Gly403 RP	GGTCATGCAGTGGCCNNNGCCACGGCCCCGGCC

3.3.2.5 Construction of PpADI error-prone library

The library was generated by the standard error-prone PCR (epPCR) using improved variant H404R as template. For the mutagenic PCR (95℃ for 2 min, 1 cycle; 95℃, 30 s/ 55℃, 30 s/ 72℃, 30 s, 29 cycles; 72℃ for 3 min, 1 cycle), 2.5 U of Taq DNA polymerase, 0.20 mM of dNTP mix, 50 ng of template (pET42b(+) harboring ADI gene H404R), 0.01-0.1 mM of $MnCl_2$ and 10 pmol of each primer (5'-TACATATGTCCGCTGAAAAACAGAAG-3' and 5'- GTGCTCGAGTTAGTAGT TGATCGG-3') were used. The PCR products were purified by using a QIAquick PCR Purification Kit. The purified epPCR products were cloned into expression

plasmid pET42b(+) by MEGAWHOP(114). For MEGAWHOP (68℃ for 5 min, 1 cycle; 95℃ for 5 min, 1 cycle; 95℃, 1 min/ 55℃, 1 min/ 68℃, 13 min 30 s, 24 cycles; 68℃ for 30 min, 1 cycle), 1 U of Taq DNA polymerase, 0.1 U of Pfu DNA polymerase, 0.20 mM of dNTP mix together with 200 ng of template (pET42b(+) harboring ADI gene H404R) were used. Following the PCR, DpnI (40 U; New England Biolabs) was added, and incubated (4 h; 37℃). The MEGAWHOP products were transformed into *E. coli* BL21-Gold (DE3) for expression and screening.

3.3.2.6 Expression of PpADI in LB media with IPTG induction

The strain *E. coli* BL21-Gold (DE3)/ pET42b-PpADI was cultured at 37℃ in 20 ml of LB media that contained 50 μg/ml kanamycine to an absorbance of 0.6 at 578nm. Then, isopropyl β-D-thio-galactopyranoside (IPTG) was added to a final concentration 0.2 mM. The cells were harvested after 9 h induction with IPTG at 37℃. The expressed rADI was analyzed by SDS-PAGE.

3.3.2.7 Expression of PpADI in auto-induction media

A chemically defined auto-induction medium (115) containing salts and trace metals, vitamins including vitamin B12, and glucose, glycerol, and lactose were test for PpADI expression. Five kinds of auto-induction media LS-5052, P-5052, MD-5052, TYM-5052 and TYP-5052 were tested for the ADI expression, under the following conditions: 20 ml LB media in 100 ml flask, 37℃, 250 rpm, 20 h. The expressed rADI was analyzed by SDS-PAGE.

3.3.2.8 Cultivation and expression of PpADI in 96-well plates

Colonies grown on LB_{kan} agar plates were transferred, by using toothpicks, into 96-well microtiter plates (flat bottom, polystyrene plates; Greiner Bio-One GmbH, Frickenhausen, Germany), containing non-inducing medium LSG (150 μL) (115) supplemented with kanamycin (50 μg/ml). After 16 h of cultivation in a microtiter plate shaker (Multitron II, Infors GmbH, Einsbach, Germany; 37℃, 900 rpm, 70 % humidity), each well was replicated using a replicator (EnzyScreen BV, Leiden,

Netherlands) into a second series of 96-well microtiter plates containing 150 µL of auto-induction media LS-5052 (115) supplemented with kanamycin (50 µg/ml). The first set of plates was stored at -80°C after addition of glycerol. The clones in the second set of plates were cultivated for 12 h (Multitron II, Infors GmbH, 37°C, 900 rpm) and used for screening.

3.3.2.9 Screening Procedure

96-well plate format citrulline colorimetric screening assay

A modified protocol of citrulline detection based on carbamido-diacetyl reaction (116) (see Figure 1A for assay mechanism) was used for ADI activity measurement. Screening for increased activity was carried out by measuring the activity at pH 7.4 and 6.4. 20 µl of cell culture was transferred to 96-well microtiter plate. Enzyme reaction was initiated by addition of arginine solution (100 µl, 100 mM) supplemented with cetyltrimethylammoniumbromide (CTAB, 4 mM), and incubated (20 min, 37°C). Subsequently, acid-ferric solution (60 µl) and diacetyl monoxime (DAM, 20 µl, 0.5 M) were added. The reaction mixture was further incubated (15 min, 55°C). Absorbance was measured at 492 nm using a microtiter plate reader (Tecan Sunrise, Tecan Group AG, Zurich, Switzerland).

Standard deviation measurements were performed in 96-well plate format using culture from BL21-Gold (DE3) lacking ADI and in a separate experiment containing ADI. Apparent standard deviation was based on the absolute absorbance values obtained from the ADI wild type plate. The true standard deviation was calculated by subtracting the background absorbance value of the microtiter plate lacking ADI from the apparent values.

Cuvette format citrulline colorimetric assay

ADI activity was routinely measured using a modified protocol of the citrulline detection with DAM and TSC (117) (see Figure 1A for assay mechanism) in Eppendorf tubes. Enzyme reaction was initiated by addition of arginine solution (200 µl, 100 mM) to a 2-ml eppendorf tube containing crude cell lysate (50 µl), and incubated (20 min, 37°C). Subsequently, acid-ferric solution (250 µl) was

added to stop the enzyme reaction. After appropriate dilution with deionized water to ensure the concentration of produced citrulline is within linear detection range, the reaction mixture (400 µl) was mixed with acid-ferric solution (600 µl) and DAM-TSC solution (100 µl). The reaction mixture was further incubated (30 min, 70°C), followed by incubation in ice water to stop color development. Absorbance was measured at 530 nm using a Specord 200 (Analytik Jena AG, Jena, Germany).

Normalization of protein expression for wild type ADI and variants

Agilent Protein 230 Kit (Agilent Protein 230 Kit, Agilent Technologies Deutschland GmbH, Böblingen, Germany) and Agilent 2100 Bioanalyzer (Agilent 2100 Bioanalyzer, Agilent Technologies Deutschland GmbH, Böblingen, Germany) were used for normalization of protein expression in crude cell extract. The protocol used was according to Agilent protein 230 Kit Guide except BSA was used as an internal standard.

3.3.2.10 Expression of ADI in shaking flask and purification

Shaking flasks (1 liter) containing auto induction media LS-5052 (200 ml) supplemented with kanamycin (50 µg/ml) were inoculated with a 1:200 dilution of overnight culture (*E. coli* BL21-Gold(DE3) harboring pET42b-ADI) grown in non-inducing media LSG. After 12 h of expression, *E. coli* cells were harvested by centrifugation (Eppendorf 5810R 4°C, 3220 g, 30 min) and resuspended in phosphate buffer (20 ml, Na_xPO_4, 20 mM, pH 7.0). *E. coli* cells were subsequently lysed by using a high-pressure homogenizer (1500 bar, 2 cycles; Avestin Emulsiflex, Mannheim, Germany). The disrupted cells were centrifuged (Eppendorf 5417R, 4°C, 13000 g, 20 min) and the supernatant was further cleared by filtration through a low protein-binding filter (0.45 µm; Minisart RC 25 single use syringe filter; Sartorius, Hamburg, Germany). ADI wild type and mutants (H404R and K5T D44E H404R) were subsequently purified by a column chromatography procedure: (i) The filtered cell lysates were subjected to a Super-Q anion exchange column, which had been pre-equilibrated with 50 mM

phosphate buffer (Na_xPO_4, pH 7.0). 20 ml of cell lysate was loaded. ADI were eluted by a NaCl step elution in phosphate buffer (Na_xPO_4, 50 mM, pH 7.0) at a rate of 3 ml/min. (ii) The obtained ADI protein from ion exchange chromatography was subjected to a gel filtration column (Matrix: Toyoperl HW-55S, Bed volume: 33 ml, Bed height: 40 cm, Column: Omnifit).

Purified ADI was subsequently concentrated using a Amicon ultra-4 centrifugal filter device (Millipore Corporation, Billerica, U.S.A.) with a 30-kDa cut-off membrane. Total protein concentration was determined by BCA^{TM} assay kit (Pierce, Born, Germany) and homogeneity of the purified sample was controlled by SDS-page electrophoresis using standard molecular biology techniques.

3.3.2.11 Characterization of ADI wild type and mutants

Determination of k_{cat} and K_m of ADI wild type and the mutants

The k_{cat} and K_m values were determined from initial velocity data measured as a function of substrate concentration. Enzyme reaction was carried out at 37°C in a water bath. After 10 min preincubation at 37°C, the enzyme reaction was initiated by addition of purified enzyme (50 µl, 0.2-0.5 µM) to the substrate solution (200 µl, 0.2 mM to 10 mM of arginine, 0.5 M phosphate buffer, pH 7.4) in deep well plates. The reaction mixture was incubated (37°C) and every two minutes reaction mixture (30 µl) of each well was transferred to acid-ferric solution (30 µl) to stop the enzyme reaction. The color development was subsequently performed in 96-well PCR plate. Ferric-acid solution (90 µl) and DAM-TSC solution (15 µl) were added to each well. The 96-well PCR plate was then incubated (70°C, 30 min) in thermal cycler (Eppendorf Mastercyler gradient) for color development, followed by incubation in ice water to stop color development. Absorbance was measured at 530 nm using a microtiter plate reader (SPECTROstar Omega, BMG LABTECH, Offenburg, Germany). The initial velocity data obtained were fitted to the equation $v = V_{max}[S]/([S] + K_m)$ (where v is the initial velocity, V_{max} the maximum velocity, [S] the substrate concentration, and K_m the Michaelis constant) using GraphPad Prism software (GraphPad

software, San Diego, CA, USA). The k_{cat} was calculated from the ratio of V_{max} and enzyme concentration.

Determination of pH profile

Enzyme reaction was carried out at 37°C in a water bath using the following substrate solution: arginine 0.1 M, pH 5-8 phosphate/acetate buffer (0.5 M phosphate, 50 mM acetate). After 10 min preincubation at 37°C, the enzyme reaction was initiated by addition of purified enzyme (50 µl, 0.2-0.5 µM) to the substrate solution (200 µl) in deep well plates. The reaction mixture was incubated (37°C, 10 min) and acid-ferric solution (250 µl) was transferred to each well to stop the enzyme reaction. The color development was subsequently performed in 96-well PCR plate. The reaction mixture (60 µl), ferric-acid solution (90 µl) and DAM-TSC solution (15 µl) were transferred to a 96-well PCR plate. The 96-well PCR plate was then incubated (70°C, 30 min) in thermal cycler (Eppendorf Mastercyler gradient) for color development, followed by incubation in ice water to stop color development. Absorbance was measured at 530 nm using a microtiter plate reader (SPECTROstar Omega, Germany).

3.3.2.12 Molecular Modeling

Two crystal structures of PaADI (PDB codes: 1RXX, 2A9G) were used to model the mutations H405R and D44E. Only one monomeric unit of the tetrameric PaADI was used for the modeling study employing Swiss-PDB viewer (118) (www.expasy.org/spdbv). PaADI variants (H405R; D44E) were generated using the mutate command of Swiss-PDB viewer. The side chain rotamer with the best score was used for subsequent energy optimized with parameter of GROMOS96 force field for in vacuum minimization (119).

3.3.2.13 Stability of PpADI in presence of serum

Purified PpADI (wild type, M1, M2; 20 µl) was incubated (37°C, 60 min) with AB--human serum (80 ul, Invitrogen, Karlsruhe, Germany) and PBS buffer (pH7.4, 80 ul), respectively. Subsequently, the incubated ADI-serum/PBS mix (20 µl) was

added to microtiter plate containing arginine solution (100 µl, 10 mM arginine in PBS buffer, pH 7.4) and incubated (37℃, 30 min). Acid-ferric solution (120 µl) was added to stop the enzyme reaction. The produced citrulline was detected using the assay procedure employed in "Determination of kcat and Km of ADI wild type and the mutants". Before measuring absorbance at 530 nm, centrifugation (Eppendorf, 5810R 4℃, 3000 g, 10 min) was performed to remove the precipitation in the assay solution (likely proteins in serum were precipitated in acidic condition during assay procedure). Meanwhile, a serum control was test for the original citrulline concentration of serum using the same procedure mentioned above except that instead of PpADI, elution buffer of gel filtration (NaxPO4, 50 mM, pH 7.4) was used. All the absorbance values at 530 nm of ADI-serum sample were subtracted the value of serum control to get the citrulline concentration produced by PpADI. The residual activities of PpADI after incubation in serum compared to that in PBS buffer were calculated to show the stability of PpADI after incubated in human serum.

3.3.2.14 Activity of PpADI (wild type, M1, M2) towards arginine derivative dimethylarginine

Purified PpADI (wild type, M1, M2; 15 µl, ~0.2 mg/ml final concentration; >20-fold concentration used for kinetic constant determination) was incubated (37℃, 4 h) with (N^G, N^G)-dimethylarginine solution (20 mM, 100 µl). Acid-ferric solution (120 µl) was added to stop the enzyme reaction. Activity was recorded by citrulline detection using citrulline colorimetric assay (see 3.3.2.11 Characterization of ADI wild type and mutants).

3.4 Results

3.4.1 PpADI cloning

PpADI was cloned into pET42b(+) and expressed in *E.coli* BL21-Gold(DE3) using auto-induction media LS-5052 (see figure 2). The nucleotide sequence of PpADI comprises 1,254 bp nucleotide (figure 1) encoding 417 amino acids which have 85% identity to ADI from *P. aeruginosa* (PaADI). The PpADI cloned into

pET42b(+) was confirmed by nucleotide sequencing. As indicated in Figure 1, sequence analysis of ADI gene showed that there was one synonymous mutation at amino acid position D78 (GAT to GAC) compared to ADI-sequence of *P. plecoglossicida* CGMCC2039 deposited in NCBI (accession number: EU030267). The deduced ADI protein sequence has a calculated molecular weight of 46.5 kDa and shows 85% identity to ADI from *P. aeruginosa*. This clone was used for subsequent directed evolution experiments.

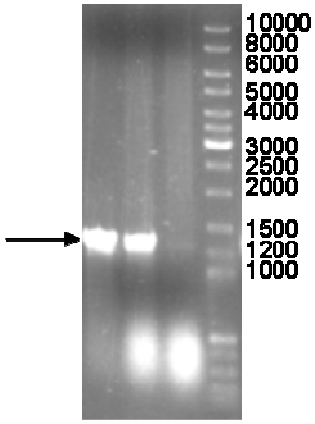

Figure 1. DNA electrophoresis of *PpADI*.

```
1       ATGTCCGCTG AAAAACAGAA GTACGGTGTC CACTCCGAAG CAGGCAAGCT GCGCAAGGTA
61      ATGGTCTGCG CTCCGGGACT GGCGCACAAG CGCCTGACCC CGAGCAACTG CGACGAGCTG
121     CTGTTCGACG ATGTGATCTG GGTCGACCAG GCCAAGCGCG ACCACTTCGA CTTCGTCACC
181     AAGATGCGCG AGCGCGGCGT GGATGTGCTG GAAATGCATA ACCTGCTCAC CGACATCGTG
241     CAGAACCCCG AGGCCCTGAA GTGGATCCTC GACCGCAAGA TCACCCCTGA CACCGTCGGG
301     GTGGGCCTGA CCAACGAAGT GCGCAGCTGG CTGGAGGGCC AGGAGCCACG CCACCTCGCC
361     GAGTTCCTGA TCGGCGGCGT GGCCGGCCAG GACCTGCCGG AGAGCGAAGG TGCCAGCGTG
421     GTCAAGATGT ACAACGACTA CCTGGGCCAC TCCAGCTTCA TCCTGCCGCC GCTGCCCAAC
481     ACCCAGTTCA CCCGCGACAC CACCTGCTGG ATCTACGGCG GCGTGACCCT CAACCCGATG
541     TACTGGCCGG CGCGACGCCA GGAAACCCTG CTGACCACCG CCATCTACAA GTTCCACCCC
601     GAGTTCACCA AGGCCGACTT CCAGGTCTGG TACGGCGACC CGGACCAAGA GCACGGCCAG
661     GCCACCCTCG AAGGCGGCGA CGTCATGCCG ATCGGCAAGG GCATCGTGCT GATCGGCATG
721     GGTGAGCGCA CCTCGCGCCA GGCCATCGGC CAACTGGCAC AGAACCTCTT CGCCAAGGGC
781     GCAGTGGAGC AAGTGATCGT CGCCGGGCTG CCGAAGTCCC GTGCGGCCAT GCACCTGGAC
841     ACCGTGTTCA GCTTCTGCGA CCGCGACCTG GTCACGGTTT TCCCGGAAGT GGTGCGCGAG
901     ATCGTGCCGT TCATCATCCG CCCGGACGAA AGCAAGCCCT ACGGCATGGA CGTACGCCGC
961     GAGAACAAGT CGTTCATCGA GGTGGTCGGC GAGCAGCTGG GCGTCAAGCT GCGTGTGGTC
1021    GAGACCGGCG GCAACAGCTT CGCCGCCGAG CGCGAGCAGT GGGATGACGG CAACAACGTG
1081    GTGGCGCTGG AGCCAGGTGT GGTCATCGGC TACGACCGCA ACACCTACAC CAATACCTTG
1141    CTGCGCAAGG CCGGGATAGA GGTCATCACC ATCAGTGCCG GCGAACTGGG CCGGGGCCGT
1201    GGCGGCGGCC ACTGCATGAC CTGCCCGATC GTGCGCGACC CGATCAACTA CTAA
```

Figure 2. PpADI sequencing results.

3.4.2 PpADI expression in LB media with IPTG as inducer

PpADI was successfully expressed in LB media with IPTG as inducer. Figure 3 (lane 4) shows the expression band of PpADI observed at ~45 kDa, which is similar to the calculated molecular weight of 46 kDa (based on http://expasy.org/tools/pi_tool.html).

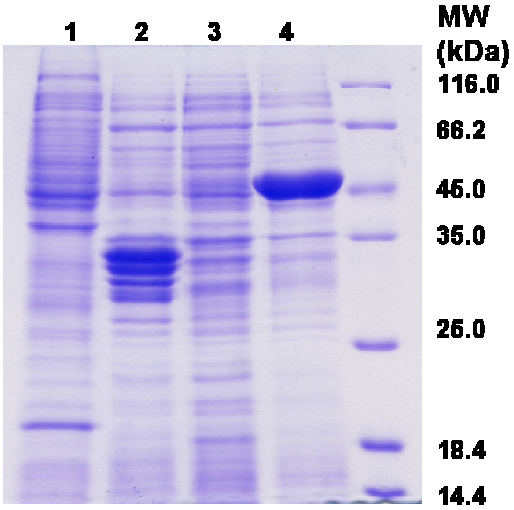

Figure 3. SDS-PAGE of PpADI expression. Lane 1: *P. plecoglossicida*; Lane 2: E. coli BL21-Gold (DE3)/ pET42b; Lane 3: E. coli BL21-Gold (DE3)/ pET42b-PpADI WT, without IPTG; Lane 4: E. coli BL21-Gold (DE3)/ pET42b- PpADI WT.

3.4.3 PpADI expression in auto-induction media

Expressing recombinant protein in auto-induction media is based upon the preferences of bacteria to selectively use different carbon sources during diauxic growth and upon the often-observed negative regulation of gene expression by catabolite repression. Auto-induction is more convenient than IPTG induction because the expression strain is simply inoculated into auto-inducing medium and grown to saturation without the need to follow culture growth and add inducer at the proper time. For high-throughput applications, the auto-induction approach has many advantages over traditional induction methods including avoidance of the strong induction and apparent toxicity associated with chemical inducers such as IPTG.

Five kinds of auto-induction media LS-5052, P-5052, MD-5052, TYM-5052 and TYP-5052 were tested for the ADI expression. Figure 4(A) and 4(B) show ADI

activity and corresponding SDS-PAGE band of the PpADI expression in different auto-induction media. The expression in auto-induction media LS-5052 is shows the highest activity and therefore LS-5052 was used for the following directed evolution experiments.

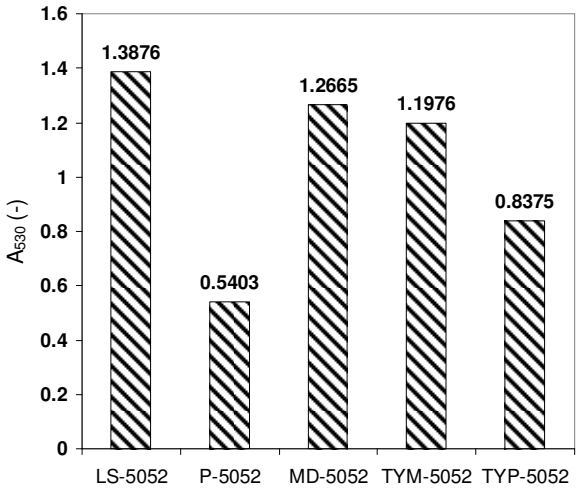

Figure 4(A). Activity of PpADI expressed in auto-induction media.

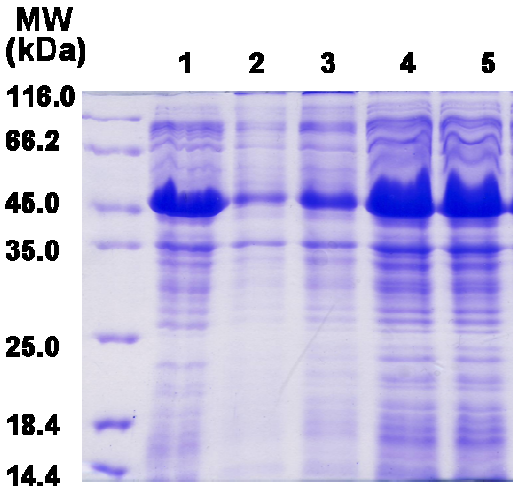

Figure 4(B). SDS-PAGE of ADI expressed in auto-induction media 1, LS-5052; 2, P-5052; 3, MD-5052; 4 TYM-5052; 5, TYP-5052.

3.4.4 PpADI assay based on citrulline detection

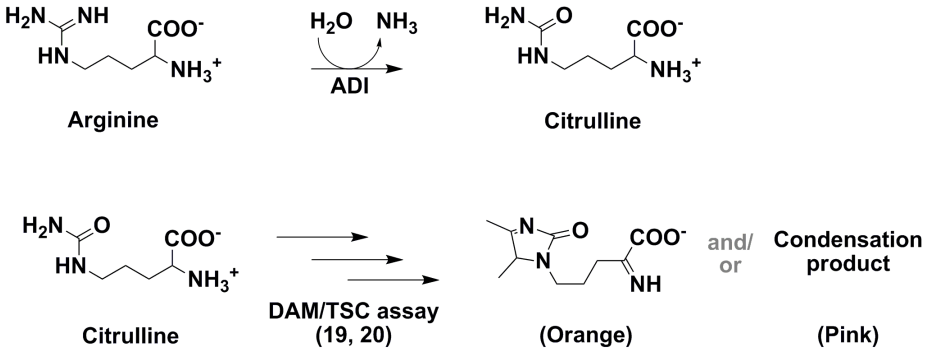

Figure 5. Arginine conversion by ADI and detection of citrulline using DAM/TSC assay.

ADI activity was measured by detecting the production of citrulline from arginine, according to carbamido diacetyl reaction (colorimetric reaction). The conditions of the carbamido diacetyl reaction is as follows： strong acid solution (H_3PO_4, H_2SO_4), oxidizing agent (Fe^{3+}), diacetyl monoxime (DAM), thiosemicarbazide (TSC), and boiling water bath. Figure 5 shows one postulated reaction mechanism for the assay which depicts the reaction between citrulline and DAM. By the addition of TSC to the reaction system, Coulombe and Favreau(120) obtained linearity of response with a more stable pink color which A_{max} was shifted from 490nm to 530nm.

Figure 6 describes the assay procedure for measuring ADI activity in 2 ml eppendorf tube. A calibration curve was prepared using citrulline standard solution (Figure 7) for determining the citrulline production during the assay.

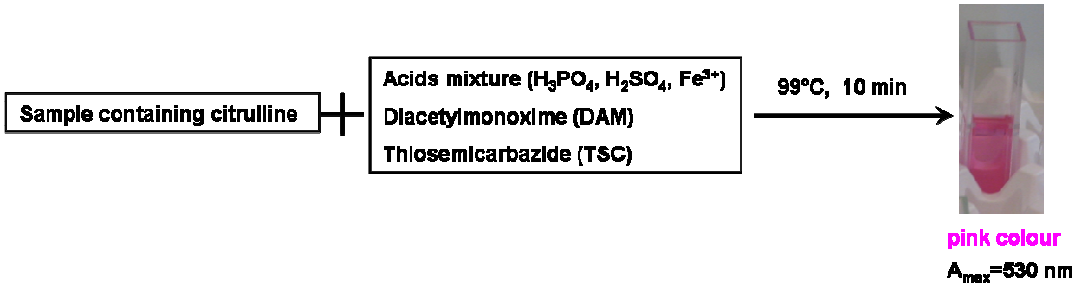

Figure 6. Citrulline colorimetric assay in cuvette format using DAM/TSC assay.

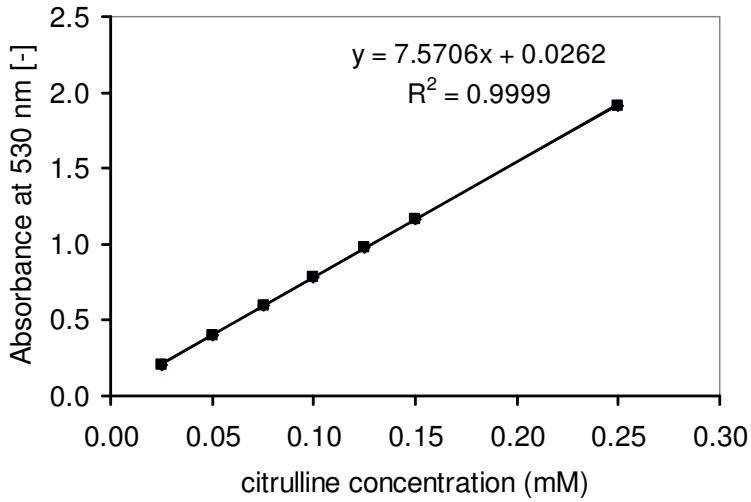

Figure 7. Calibration curve of cuvette format citrulline colorimetric assay.

3.4.5 PpADI screening system for citrulline production in microtiter plates

Two key performance parameters for identifying improved variants in microtiter plate based screening systems are the true standard variation and the linear detection range of the employed assay. Standard deviations have been reduced by optimizing expression and screening conditions (various auto-induction media and assay conditions such as amount of cell, conversion time and color development procedure). A modified version of the DAM-TSC assay for citrulline detection (Scheme 1) was selected for directed evolution of PpADI. The microtiter plate screening format was optimized for simplified handling by lowering the color development temperature (55℃ instead of 100℃), increasing the diacetylmonoxime concentration (~22-fold) and avoiding the use of the sensitizer thiosemicarbazide. Figure 8 shows the procedure of screening assay of citrulline detection.

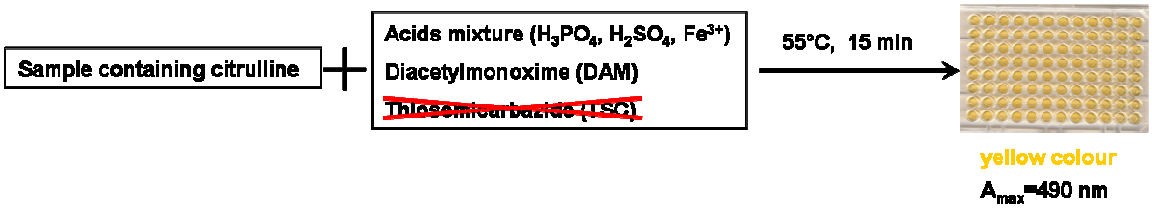

Figure 8. Citrulline colorimetric assay in MTP format using DAM assay.

Standard deviations of the modified citrulline detection assay have been reduced by optimizing expression and screening conditions (various auto-induction media and assay conditions such as amount of cell, conversion time and color development procedure). The preferred combination (150 µl LS5052 auto-induction media and 20 µl cell culture, 20 min conversion time and 15 min color develop time) resulted in a true standard deviation of 12.8 % after subtracting the background (Figure 10). Screening systems with standard deviations around 10 % have successfully been used in directed evolution experiments (121, 122). A wide linear detection window is important for identifying beneficial mutants in directed evolution experiments and screening systems for evolved mutants have to be constantly adapted for hitting the linear detection window. A linear detection range up to 6 mM citrulline could be detected (Figure 9).

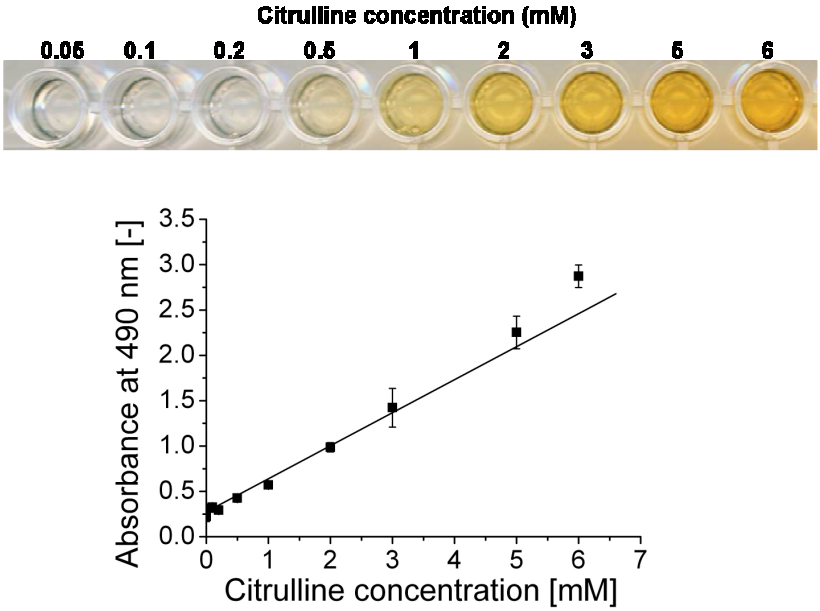

Figure 9. Calibration curve of 96-well microtiter plate format citrulline colorimetric screening assay.

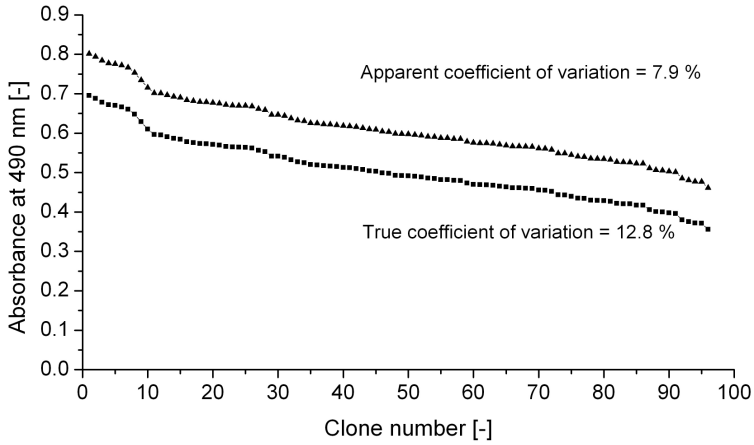

Figure 10. Activity values in descending order of the ADI wild-type conversion of arginine to citrulline in a 96-well microtiter plate using the optimized assay protocol. The apparent coefficients of variation were calculated without subtracting the background and the true coefficients of variation after background subtraction.

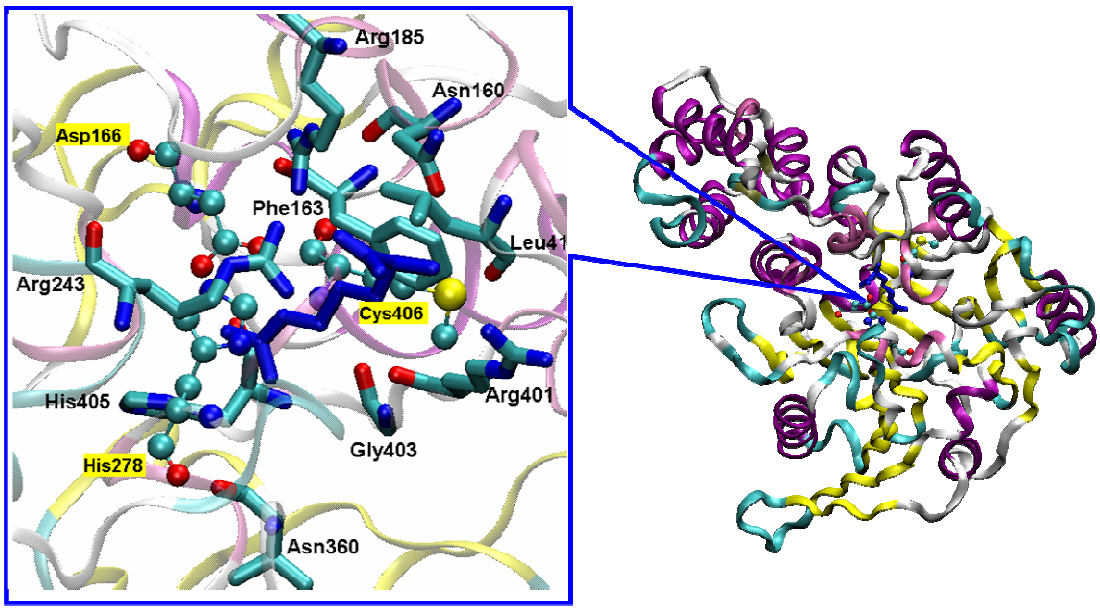

Figure 11. PpADI model derived from PaADI crystal structure (PDB code 2a9gD) by SWISS MODEL WORKSPACE.

3.4.6 Focused libraries generated by saturation mutagenesis

PpADI gene shares 83 % sequence identity with PaADI of which the crystal structure was solved (123). After submitting the ADI sequence to SWISS MODEL WORKSPACE, a proposed ADI model based on the PaADI crystal structure (PDB code 2a9gD) was obtained (Figure 11). According to this model and published literatures, 9 amino acid residues: Leu41, Asn160, Phe163, Arg185, Arg243, Asn360, Arg401, His404, Gly 403 (Figure 11) close to the active center (catalytic triad: Cys406-His278-Glu224) or known to interact with substrate arginine were selected for saturation mutagenesis.

Site saturation mutagenesis at position Leu41, Asn160, Phe163, Arg185, Arg243, Asn360, Arg401, His404 and Gly 403 were performed. 300 clones were screened for each position. However, no improved variant was identified.

3.4.7 Validation of variant M1 (H404R) citrulline colorimetric assay in cuvette format

Position H404 which was suspected to influence ADI pH profile by substitution to R404 (15). Compared to wild type PpADI, variant M1 (H404R) shows higher activity (1.8-fold) and improved activity ratio of pH 7.4 to 6.4 (4.7-fold). Therefore, M1 (H404R) was selected for directed evolution.

3.4.8 epPCR library generation and screening with citrulline detection assay by screening error-prone mutant libraries

Various concentrations of $MnCl_2$ (0.01-0.10 mM) were used in epPCR library generation to adjust the ratio of active to inactive clones. Figure 12 (A) and 12 (B) show the epPCR products and the corresponding MEGAWHOP products. Concentration of 0.01 mM $MnCl_2$ which generated 53 % inactive mutant was selected for library generation. EpPCR mutant libraries with a ratio of 50 % active and 50 % inactive clones have often been used successfully in directed evolution, improving enzyme properties by gradual changes (one or two amino acids changes per round of mutagenesis and screening). A total of 7 variants (listed in

Table 2) were identified from an epPCR library of 2400 mutants and used for further characterization. The most active variant was sequenced and two additional amino acid substitutions (K5T D44E) were identified.

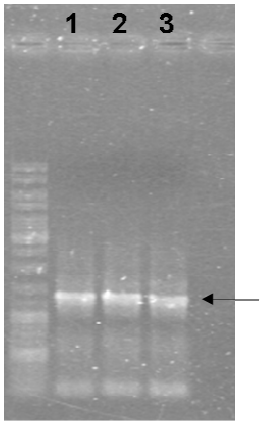

Figure 12 (A). Electrophoresis of epPCR products. Lane 1, 0.01 mM of $MnCl_2$; Lane 2, 0.02 mM of $MnCl_2$; Lane 3, 0.05 mM of $MnCl_2$.

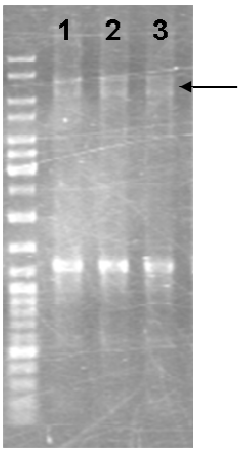

Figure 12 (B). Electrophoresis of MEGAWHOP product with epPCR products as megaprimer. Lane 1, 0.01 mM of $MnCl_2$; Lane 2, 0.02 mM of $MnCl_2$; Lane 3, 0.05 mM of $MnCl_2$.

Table 2. Activity of ADI variants towards arginine determined using citrulline colorimetric assay in cuvette format. Samples were diluted to ensure that detected citrulline concentrations are within the linear detection range of the citrulline colorimetric assay. Wild type, mutant M1 and the "best variant" M2 are in bold and prominent expression mutants (9-B3-1; 21-D5-1) are italized.

	Normalized [ADI][a]				
	Citrulline production (mM/mg)		Relative to activity at pH 7.4 of WT		Activity at pH 7.4/ activity at pH 6.4
ADI variants	pH 7.4	pH 6.4	pH 7.4	pH 6.4	
WT	9.83 (0.74)[b]	124.92 (1.98)	1.00 (0.15)	12.69 (0.01)	0.08 (0.01)
M1 (H404R)	17.80 (0.49)	45.95 (0.87)	1.81 (0.06)	4.67 (0.02)	0.39 (0.02)
M2 (K5T D44E H404R)	38.99 (0.79)	39.20 (0.31)	3.96 (0.02)	3.98 (0.02)	0.99 (0.03)
9-B3-1	24.89 (0.45)	54.50 (1.80)	2.53 (0.03)	5.54 (0.03)	0.46 (0.02)
21-D5-1	25.68 (2.68)	50.95 (2.36)	2.61 (0.07)	5.18 (0.02)	0.50 (0.01)
15-G10-2	13.11 (0.53)	47.02 (0.47)	1.33 (0.09)	4.78 (0.02)	0.28 (0.01)
2-H4-2	12.50 (0.07)	21.58 (0.09)	1.27 (0.06)	2.19 (0.04)	0.58 (0.01)
1-G11-1	24.91 (0.20)	29.12 (0.33)	2.53 (0.03)	2.96 (0.03)	0.85 (0.02)
24-E10-1	14.62 (0.62)	32.82 (0.52)	1.49 (0.08)	3.34 (0.03)	0.45 (0.02)

[a] (Based on quantification employing Agilent 2100 Bioanalyzer (Agilent Protein 230 Kit))
[b] (Standard error of triplicate measurements are given in brackets below each absolute and normalized value.)

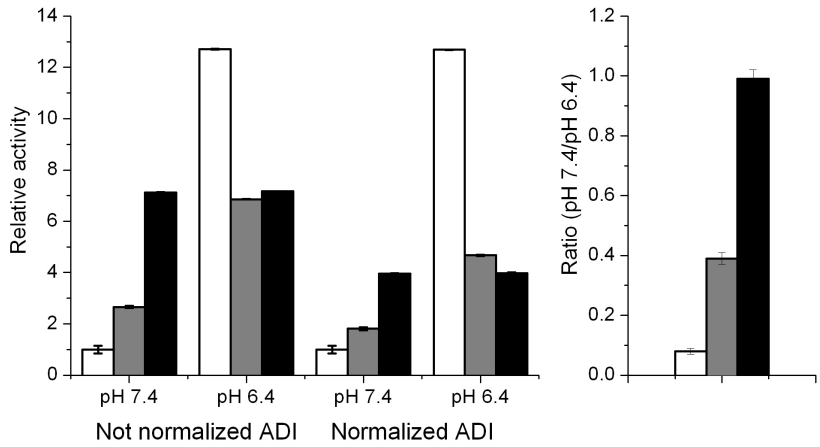

Figure 13. Relative activity of ADI variants towards arginine. The relative activity is the ratio of the activity at the pH of each variant relative to the activity at pH 7.4 of wild type ADI. White: ADI wild type, grey: M1 (H404R), black: M2 (K5T D44E H404R).

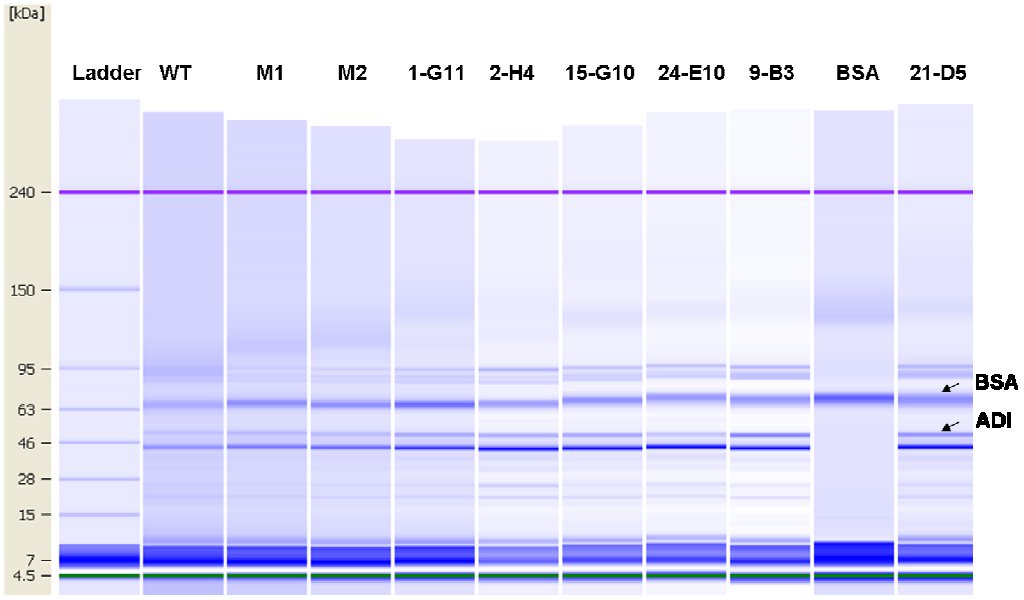

Figure 14. Elution profile of wild type PpADI and improved variants from epPCR library, generated with Protein 230 Kit using a mircofluidic device (Agilent Bioanalyzer). BSA was added as an internal standard.

3.4.9 Characterization of PpADI variants

3.4.9.1 Determination of k_{cat} and K_m of ADI wild type and the mutants

Variants selected from epPCR were first characterized using the crude cell extract to identify the most promising variants (Table 2). Using an activity ratio of pH 7.4 to 6.4 proved to be an effective method to eliminate expression mutants. Additionally ADI concentration in crude cell extract was determined using the Agilent Protein 230 Kit. Microfluidic elution profiles (Figure 14) semi-quantify differences in expression between the wild type PpADI and variants. Normalization of activities against the corresponding ADI concentrations reveals improvements in specific activities of ADI mutants (Table 2). M1, the starting variant for the directed evolution campaign, and M2 were selected for detailed characterization studies. M2 has as “best identified variants” (Figure 13) a more than 2.5-fold higher activity ratio at pH 7.4 to pH 6.4 than M1 and a 12-fold higher activity ratio than wild type in crude cell lysates.

For kinetic characterization of ADI variants the citrulline production was maintained between 0.2-0.8 mM. Calibration curve in Figure 4 shows the linear detection range in the employed 96-well PCR plate format citrulline colorimetric assay system. Figure 15 summarizes the k_{cat} and K_m values of wild type PpADI, identified variants M1 (H404) and M2 (K5T D44E H404R) which were expressed in shaking flasks cultures and purified using a two step procedure (anion exchange followed by gel filtration). Both variants M1 and M2 show an increase in k_{cat} and K_m for citrulline production at pH 7.4. Variant M2 shows a 4-fold higher k_{cat} as also obtained for specific activity in Table 2 using the crude cell extract, validating the characterization procedure with crude cell lysate. Furthermore, an increased K_m from 0.7 mM (wild type PpADI) to 1.2 mM (M1) and 2.5 mM (M2) was found.

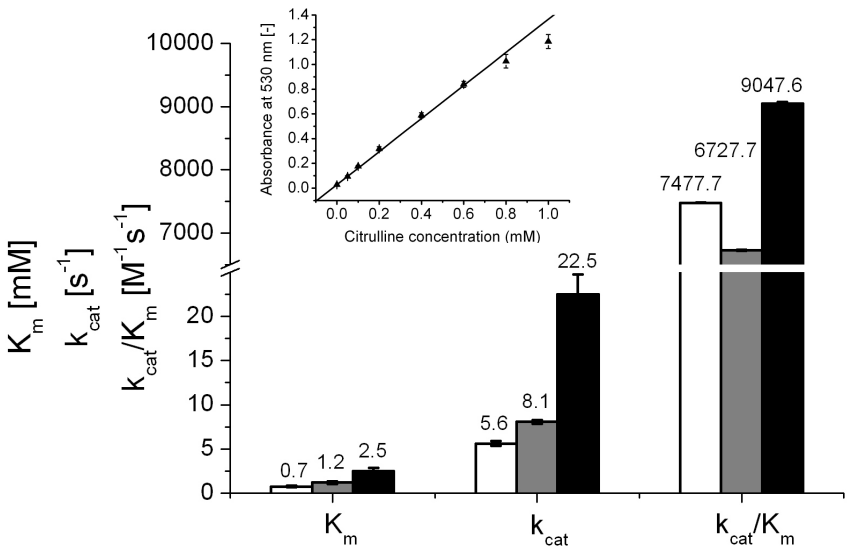

Figure 15. Kinetic parameters of ADI and mutants for conversion of arginine to citrulline. White: ADI wild type, grey: M1 (H404R), black: M2 (K5T D44E H404R). Values reported are the average of three measurements, and average deviations from the mean values are shown. Embedded calibration curve shows linearity of citrulline colorimetric assay in 96-well PCR plate format which was used to determine arginine conversions and kinetic constants.

3.4.9.2 Relative pH profile of wild type and mutant

The relative pH profile (Figure 16) of wild type PpADI and M1 (H404R) shows an identical pH optimum at pH 6.5. Compared to wild type PpADI, variant M2 (K5T

D44E H404R) shows a pH optimum at pH 7.0 which is shifted remarkably (0.5 pH units). Both M1 and M2 show decreased specific activities at pH 6.5, and increased specific activity at pH 7.5. At pH 7.0, the specific activity of M2 exceeds that of wild type PaADI (data not shown).

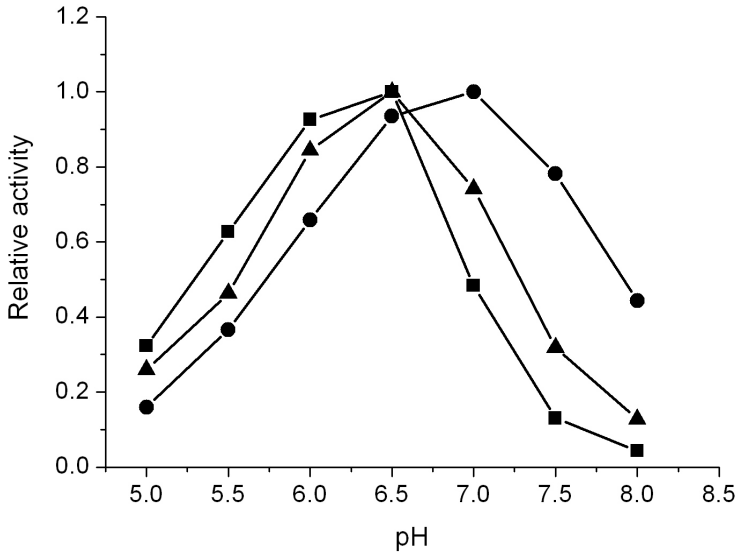

Figure 16. pH profile of wild type ADI, M1(H404R), M2(K5T/D44E/H404R). The relative activity is the ratio of the catalytic activity at the pH relative to the maximum activity of each enzyme. (■) WT, (▲) M1 (H404R), (●) M2 (K5T/D44E/H404R).

3.4.10 Stability of PpADI in the presence of human serum

Table 3 summarizes the stability of PpADI variants in serum (37℃, 60 min; standard deviation of three measurements in brackets). The mutants M1 and M2 have a similar stability in serum when compared to the wild-type PpADI wild type. The substitution D44E and H404R do not destabilize further the PpADI in serum.

Table 3. Stability of PpADI variants in the presence of human serum.

	PpADI WT	M1	M2
No incubation (A_{530})	0.08	0.27	0.98
Incubation with serum (37℃, 60 min) (A_{530})	0.05	0.15	0.69
Residual activity	60 %	55 %	70 %

3.4.11 Activity of PpADI (wild type, M1, M2) towards arginine derivative (N^G, N^G)-dimethylarginine

No detectable conversion of (N^G, N^G)-dimethylarginine could be detected with PpADI variants.

3.5 Discussion

ADI properties have to date not been engineered through directed evolution algorithms despite their often poor performances under physiological conditions and their medical importance as potential anti-tumor drug. Chemically modified of ADI (e.g. through PEGylation) (27) and fusion protein (e. g. Human serum albumin fusion, HSA) (124) have been used for addressing activity and stability demands *in vivo*. Directed evolution offers opportunities to directly improve ADI properties for *in vivo* applications and small libraries of a few thousand variants have often been sufficient to find improved muteins in directed evolution experiments (55, 125).

Our main intention in this report is to provide a validated protocol for directed ADI evolution and improving the activity at the physiological pH 7.4. *Pseudomonas plecoglossicida* CGMCC2039 (PpADI, 7.8 U/mg; pH optimum 6.5) was selected for the directed evolution studies due to its functional expression in *E. coli,* coverage of sequence space in patents and "potential" for activity improvement. PpADI is a relatively slow ADI when compared to Mycoplasma ADIs like MhADI (*Mycoplasma hominus* ADI, 35 U/mg) which would have been good alternatives for directed evolution studies (105). Reported ADI activities range from 0.115 to 140.3 IU/mg. One unit is commonly defined as the ADI amount that converts 1 µmol of L-arginine into 1 µmol of L-citrulline per minute (27).

Screening of PpADI variants yielded three amino acid positions 5, 44 and 404. Positions 44 and 404 resulted in a 4-fold higher k_{cat} at pH 7.4 and a significant shift in the pH optimum (0.5 units) when compared to wild type PpADI (Figure 17 & 8). Position 5 did not show any effect on PpADI activity.

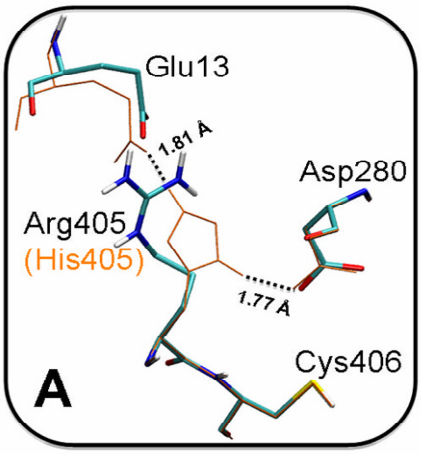

Figure 17. Structural alignment of mutant M1 model with corresponding residues of the crystal structures of the PaADI (in orange). The crystal structure of PaADI which was diffracted in absence of the substrate arginine (1RXX) was used to investigate the substitution of His405 to Arg405. The Arg405 variant shows with respect the Asp280 a different orientation of the guanidinium group when compared to side chain of His405 (in orange).

Galkin and coworkers postulated that the histidine in position 404 (corresponding position in “their” PaADI is 405) is a key residue in controlling activity at acidic and neutral pH. In protonated state of the imidazolium ring a hydrogen bonding interaction can be formed with the oxygen of Asp280 (carboxyl group). This hydrogen bond favors stabilizing interactions between Asp280 and the substrate arginine. His405 in PaADI was reported (17) to share protons with Asp280 and Glu13 and to be important for modulating electrostatic environments of closely located catalytic groups. The same report postulated that H405 is likely to be protonated when the substrate arginine binds to catalytic triad (His278, Glu224, Cys406) [(2)]. Based on these reports the His404 in PpADI was subjected to a site directed mutagenesis to Arg404 and named M1. The M1 variant (H404R) shows 40 % residual activity compared to wild type PpADI at pH 6.4 and a 1.8-fold increase in activity at pH 7.4 (see Table 1). In the M1 (H404R) mutant (see the model in Figure 17; based PaADI 1RXX; residue His404 in PpADI corresponds to His405 in PaADI), the conformational effect due to the extended side chain of Arg likely weakens the hydrogen bond to Asp280 and thus reduces the stabilizing effect on arginine binding. As a result the activity of M1 is reduced, especially at

lower pH values at which His405 is protonated. However at elevated pHs, His405 becomes increasingly deprotonated whereas Arg405 remains protonated and can therefore still stabilize Asp280 for arginine binding. The electrostatic effect suggested by theoretical and experimental studies have evidenced the importance of positively charged residues to modulate the reaction rate of PaADI (126). At pH 6.4, histidine in wild type PpADI and arginine in M1 are both positively charged. At pH 7.4, histidine is only partially positive charged and PpADI's activity is reduced (>90 %) while arginine in M1 remains positively charged preserving M1's activity (Figure 17).

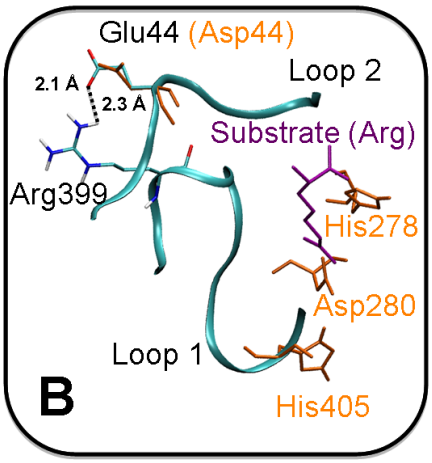

Figure 18. Structural alignment of mutant M2 model with corresponding residues of the crystal structures of the PaADI (in orange). The PaADI crystal structure in presence of substrate arginine was used (2A9G) to investigate the role of the substitution Asp44 to Glu44. The latter was solved for an inactive variant in which Cys406 was replaced by Ala406. The extended side chain of Glu44 might improve the hydrogen bond interaction with the Arg399 inducing a conformational shift of loop 1.

The PpADI H404R was used as starting variant for directed evolution. The amino acid position 44 was identified from a epPCR library (2400 variants screened) resulting in a triple mutant M2 (K5T D44E H404R). For investigating the role of each position the double mutants (K5T H404R) and (D44E H404R) were generated. Only the double mutant (D44E H404R) revealed improvements in k_{cat} (4-fold, pH 7.4; Figure 18). The rationale behind the effects of the mutation D44E on the PpADI activity is more complex to extrapolate from the available ADI crystal structures. Comparative crystallographic studies have shown that the

entrance of the active site is decorated by 4 loops that undergo conformational transitions upon arginine binding (17). The loops exhibit significant shifts that limit the access of water molecules to the active site. The Asp44 is located in loop 1 (residues 30-46) and upon binding of the substrate, Asp44 comes closer to the positively charged Arg399 located on loop 4 (residues 392 to 403). In the D44E mutant, the longer side chain reduces the distance with Arg399 favoring the formation of hydrogen bond (see model in Figure 18). The reinforced interaction between Glu44 and Arg399 might expedite conformational changes in loops, probably confining the arginine substrate in the active site and hence promote arginine conversion. In the future, we plan to further investigate the influence of H404R and D44E using molecular dynamics simulations, further boost the k_{cat} at pH 7.4 and reduce the K_m value of PpADI.

Overall site directed mutagenesis of position H404R and one round of directed evolution (2400 variants screened) resulted in a triple mutant M2 (K5T D44E H404R) with 4-fold higher k_{cat} at pH 7.4 (compared to wild type; Figure 4). The best mutant isolated, M2, has specific activity of 31.3 U/mg at pH 7.4 which is already after one round of evolution close to the specific activity of MhADI (35 U/mg) (127) at its pH optimum. The stability and specificity of improved PpADI variants are furthermore important for cancer treatment *in vivo*. First experiments in AB-human serum (Invitrogen) showed an unaltered stability of M2 compared to the wild type PpADI and (N^G, N^G)-dimethylarginine conversion could not detect with the citrulline colorimetic assay.

3.6 Conclusion

In summary, a directed evolution protocol has been developed for PpADI and validated by increasing the k_{cat} of PpADI at physiological pH (7.4). The reported screening system is the first one employed in directed ADI evolution and can likely be used for other ADIs and other properties such as temperature stability, salt/detergent stability or protease resistance.

Chapter 4. PpADI reengineered for efficient operation under physiological conditions

4.1 Abstract

The proof of concept for ADI engineering by directed evolution resulted in variant M2 (K5T/D44E/H404R). M2 has a pH optimum of pH 7.0 and 4-fold higher k_{cat} value than the wild type PpADI (pH 7.4, 0.5 M phosphate buffer) and an increased K_m value for substrate arginine. In this chapter, in order to improve the catalytic efficiency of PpADI at low concentration of arginine, variant M5 (K5T/D38H/D44E/A128T/H404R) and M6 (K5T/D38H/D44E/A128T/E296K/H404R) were generated from an epPCR library: at pH 7.4 (PBS buffer), the $S_{0.5}$ value decreased from 2.01 mM (parent M3, K5T/D44E/A128T/H404R) to 1.48 mM (M5) and 0.81 mM (M6). The $S_{0.5}$ value of M6 (0.81 mM) is lower than that of PpADI wild type (1.30 mM); the k_{cat} value improved from 0.18 s^{-1} (PpADI wild type) to 17.56 s^{-1} (M5, 97.6-folds) and 11.64 s^{-1} (M6, 64.7-fold).

4.2 Introduction

ADI-based arginine depletion is a target specific therapy for arginine-auxotrophic tumors (e.g. hepatocellular carcinomas and melanomas) and pegylated ADI is currently under clinical trials for HCC with promising results (45). HCC is the third leading cause of cancer mortality world wide with a less than 10 % 5-year survival rate (EU and USA) (128) due to low responses of hepatoma to chemotherapeutic treatments. In 1999, US Food and Drug Administration (FDA) designated ADI-PEG-20 orphan drug status for the treatment of HCC and invasive malignant melanomas, and in 2005 European Agency for the Evaluation of Medicinal Products (EMEA) also granted ADI-PEG-20 orphan drug status for the treatment of HCC. Phase II trials of ADI-PEG-20 in patients with metastatic

hepatocellular carcinomas have shown that the drug is safe, well tolerated, and may benefit patients with unresectable HCC. Izzo and coworker suspected that combination therapies of arginine deprivation and growth inhibition via kinase inhibitors might improve the survival rate further more. Additionally, ADI can enhance radio sensitivity of human mammary adenocarcinoma (MCF-7 cells) (48), exerts anti-proliferative and anti-angiogenic activities and inhibits the growth of viruses such as HIV-1 and hepatitis (49, 50). Current research efforts are focused on ADI's *in vivo* inhibitory effect towards leukemia, melanoma, prostate cancer, renal cell carcinoma, and human umbilical vein endothelial cells (HUVEC) (19, 44, 51-53), clinical trials for HCC (phase II) (45) and melanoma (phase I/II) (46), and inhibitory mechanisms of ADI to tumors (54).

Arginine deprivation is believed to be a main molecular reason for ADI's inhibitory effects on arginine auxotrophic tumors which do not express argininosuccinate synthetase (ASS). ADIs catalyze the first step of the arginine dehydrolase pathway by hydrolyzing arginine to citrulline and ammonium. ADI genes have been identified, purified, and characterized from bacteria, archaea and some eukaryotes excluding mammalian cells (see review (27)). Enzymatic properties of several recombinant ADIs have been examined, such as specific activity, functional expression level, temperature optimum, pH optimum, substrate affinity for arginine, and half-life in human plasma. Only the ADI from *Mycoplasma hominis* has so far been developed as orphan drug by Pheonix Pharmacologics Inc. for HCC and melanoma (129). From enzyme kinetic point of view, none of the ADIs is ideally suited for *in vivo* applications under physiological conditions. Protein engineering by rational design and directed evolution offers opportunities to tailor ADI properties to physiological conditions. PpADI (ADI from *Pseudomonas plecoglossicida*) was functionally expressed in *E. coli* with a simple protocol and has been engineered for the first time by directed evolution for improved activity at physiological pH (3). The variant M2 (K5T/D44E/H404R), by our group reported, showed a 4-fold higher specific activity than the wild type PpADI (0.5 M phosphate buffer, pH 7.4), but a increased K_m value (3.5-fold).

High activity at low arginine concentration is an important prerequisite for ADI's medical application, allowing low ADI dose required per treatment.
In the present work, we improved the directed evolution protocol and identified a PpADI variant with further improved activity and slightly decreased "K_m value" and PpADI variant with lowered K_m value maintaining its high catalytic activity. Those variants were characterized in respect to their kinetic constants.

4.3 Materials and methods

4.3.1 Materials

All chemicals were of analytical-reagent grade or higher quality and were purchased from Fluka (Neu-Ulm, Germany), Sigma-Aldrich (Steinheim, Germany) and Applichem (Darmstadt, Germany), except the resins for purification (TOSOH, Stuttgart, Germany). All enzymes were purchased from New England Biolabs (Frankfurt, Germany), Fermentas (St. Leon-Rt, Germany), and Sigma-Aldrich Chemie (Taufkirchen, Germany), unless stated otherwise.
Thermal cycler (Mastercyler gradient; Eppendorf, Hamburg, Germany) and thin-wall PCR tubes (Multi-ultra tubes; 0.2 µl; Carl Roth, Germany) were used in all PCRs. The PCR volume was always 50 µl except for Megaprimer PCR of whole plasmid (MEGAWHOP, 25 µl); larger volumes were prepared in multiple 50-µl PCRs. The amount of DNA in cloning experiments was quantified by using a NanoDrop photometer (NanoDrop Technologies, Germany).

4.3.2 Methods

4.3.2.1 Site saturation mutagenesis of *PpADI* M2 at position A128

Site directed mutagenesis of *PpADI* M2 (K5T/D44E/H404R) at position A128 was performed according to the published method (130). The following oligonucleotides were used for mutagenesis of A128: 5'-CTGATCGGCGGCGTGNNNGGCCAGGACCTGCCG-3' and 5'-CGGCAGGTCCTGGCCNNNCACGCCGCCGATCAG-3' (underlining indicated the substituted nucleotide). For the mutagenic PCR (First stage: 98°C for 30 s, 1 cycle; 98°C, 30 s/ 55°C, 1 min/ 72°C, 3 min, 3 cycles. Second stage: 98°C for 30

s, 1 cycle; 98℃, 30 s/ 55℃, 1 min/ 72℃, 3 min, 15 cycles; 72℃ for 3 min, 1 cycle), 2 U of PhuS DNA polymerase, 0.20 mM of dNTP mix, 25 pmol of each primer together with 100 ng of template (pET42b(+) harboring PpADI M2 gene) were used. Following the PCR, DpnI (40 U; New England Biolabs) was added, and incubated overnight at 37℃. The PCR products were purified by using a QIAquick PCR Purification Kit (Qiagen) and transformed into *E. coli* BL21-Gold (DE3) for expression.

4.3.2.2 Construction of PpADI error-prone library

EpPCR library was generated by the standard error-prone PCR (epPCR) using improved variant M3 (K5T/D44E/A128T/H404R) as template. For the mutagenic PCR (95℃ for 2 min, 1 cycle; 95℃, 30 s/ 55℃, 30 s/ 72℃, 30 s, 29 cycles; 72℃ for 3 min, 1 cycle), 2.5 U of Taq DNA polymerase, 0.20 mM of dNTP mix, 50 ng of template (pET42b(+) harboring PpADI M3 gene), 0.01-0.1 mM of $MnCl_2$ and 10 pmol of each primer (5'-TACATATGTCCGCTGAAACACAGAAG-3' and 5'-GTGCTCGAGTTAGTAGTTGATCGG-3') were used. The PCR products were purified by using a QIAquick PCR Purification Kit. The purified epPCR products were cloned into expression plasmid pET42b(+) by MEGAWHOP (114). For MEGAWHOP (72℃ for 5 min, 1 cycle; 98℃ for 1 min 30 s, 1 cycle; 98℃, 45 s/ 55℃, 45 s/72℃, 4 min, 24 cycles; 72℃ for 10 min, 1 cycle), 1.2 U of PfuS DNA polymerase, 0.20 mM of dNTP mix, 500 ng of epPCR products together with 50 ng of template (pET42b(+) harboring PpADI gene of variant M3) were used. Following the PCR, DpnI (40 U; New England Biolabs) was added, and incubated (overnight; 37℃). The MEGAWHOP products were transformed into *E. coli* BL21-Gold (DE3) for expression and screening.

4.3.2.3 Site directed mutagenesis at position D38 of *PpADI* M4

Site directed mutagenesis of *PpADI* variant M4 at position D38 was performed according to the published method on plasmid pET42b(+)-ADI-M4 (K5T/D44E/A128T/E296K/H404R). The following oligonucleotides were used for mutagenesis of D38H: 5'-ACCCCGAGCAACTGCCACGAGCTGCTGTTCGAC-3'

and 5'-GTCGAACAGCAGCTCGTGGCAGTTGCTCGGGGT-3' (underlining indicated the substituted nucleotide). Conditions for mutagenic PCR are as described in "Site saturation mutagenesis of *PpADI* M2 at position A128".The PCR products were purified by using a QIAquick PCR Purification Kit (Qiagen) and transformed into *E. coli* BL21-Gold (DE3) for expression.

4.3.2.4 Site saturation mutagenesis at position D38 and E296 of *PpADI* M3

Site saturation mutagenesis library at position D38 and E296 of *PpADI* variant M3 (K5T/D44E/A128T/H404R) were generated according to the published method on plasmid pET42b(+)-ADI-M3 using the following oligonucleotides: D38FP (5'-ACCCCGAGCAACTGCNNNGAGCTGCTGTTCGAC-3'), D38RP (5'-GTCGAACAGCAGCTCNNNGCAGTTGCTCGGGGT-3') and E296FP (5'-GTCACGGTTTTCCCGNNNGTGGTGCGCGAGATC-3'), E296RP (5'-GATCTCGCGCACCACNNNCGGGAAAACCGTGAC-3') (underlining indicated the substituted nucleotide). Conditions for mutagenic PCR are as described in "Site saturation mutagenesis of PpADI M3 gene at position A128".The PCR products were purified by using a QIAquick PCR Purification Kit (Qiagen) and transformed into *E. coli* BL21-Gold (DE3) for expression.

4.3.2.5 Cultivation and expression of PpADI in 96-well plates

Cultivation and expression in 96-well plates (flat bottom, polystyrene plates; Greiner Bio-One GmbH, Frickenhausen, Germany) were performed as previously described in 3.3.2.8.

4.3.2.6 Improved screening system in 96-well plate to identify PpADI variants with high activities at low arginine concentration

As describe previously, the modified protocol of citrulline detection based on carbamido-diacetyl reaction was used for screening for improved ADI affinity to arginine at pH 7.4. 15 µl of cell culture was transferred to 96-well microtiter plate. Enzyme reaction was initiated by addition of arginine solution (105 µl, 1mM arginine in PBS buffer, pH 7.4) supplemented with

cetyltrimethylammoniumbromide (CTAB, 4 mM), and incubated (10 min, 37°C). The following color development procedure was carried out as described previously (3).

Standard deviation measurements were performed in 96-well plate format using culture from BL21-Gold (DE3) lacking PpADI and in a separate experiment containing PpADI variant M3. Apparent standard deviation was based on the absolute absorbance values obtained from the PpADI variant M3 plate. The true standard deviation was calculated by subtracting the background absorbance value of the microtiter plate lacking ADI from the apparent values.

4.3.2.7 Expression of PpADI in shaking flask and purification

Expression of PpADI in shaking flasks and purification (by anion exchange chromatography and gel filtration) was performed as previously described in 3.3.2.10.

4.3.2.8 Characterization of PpADI variants

Preliminary determination of kinetic constants for site saturation mutagenesis variants of position 38 and 296

The k_{cat} and K_m values were determined from initial velocity data measured as a function of substrate concentration. Enzyme reaction was carried out at 37°C in incubator (Heraeus Holding GmbH, Hanau, Germany) using cell crude extract. 2 ml of expression culture was harvested by centrifugation (Eppendorf 5415R 4°C, 13,000 g, 10 min) and then freezed (-20°C, overnight). Cell lysate was prepared by resuspending the cell pellet in lysozyme (91000 U, 50 mM phosphate buffer, pH 7.4, 1.3 ml) followed by incubation (37°C, 40 min) and centrifugation (4°C, 13,000 g, 10 min). 15 µl of diluted (4 times diluted with 50 mM phosphate buffer, pH 7.4) cell lysate was transferred to 96-well microtiter plates. Enzyme reaction was initiated by addition of arginine solution (105 µl, 0.25-10 mM arginine in PBS buffer, pH 7.4) and incubated (7 min, 37°C). Subsequently, ferric-acid solution (120 µl) was added to each well to stop enzyme reaction. 60 µl of terminated

enzyme reaction mixture was transferred to 96-well PCR plate for color development. Ferric-acid solution (90 µl) and DAM-TSC solution (15 µl) were added to each well. The 96-well PCR plate was then incubated (70°C, 30 min) in thermal cycler (Eppendorf Mastercyler gradient) for color development, followed by incubation in ice water to stop color development. Absorbance was measured at 530 nm using a microtiter plate reader (Tecan Sunrise TC reader, Tecan Group AG, Zurich, Switzerland). The initial velocity data obtained were fitted to the equation $v = V_{max}[S]/([S] + K_m)$ (where v is the initial velocity, Vmax the maximum velocity, [S] the substrate concentration, and Km the Michaelis constant) using GraphPad Prism software (GraphPad software, San Diego, CA, USA). The kcat was calculated from the ratio of V_{max} and enzyme concentration.

Determination of kinetic constants of PpADI wild type and variants M3, M4, M5, M6

The k_{cat} and $S_{0.5}$ values were determined from initial velocity data measured as a function of substrate concentration. Enzyme reaction was carried out at 37°C in a water bath as described previously using purified enzyme (50 µl, 0.1-1.8 µM) to and substrate solution (200 µl, 0.5 mM to 10 mM of arginine, PBS buffer, pH 7.4) in deep well plates.

The initial velocity data obtained were fitted to the sigmoidal model of kinetics equation $v = V_{max}^{n}/(S_{0.5}^{n} + K^{n})$ (where v is the initial velocity, V_{max} is the maximum velocity, K is the substrate concentration, and $S_{0.5}$ is the ligand concentration producing half occupation (131)) using GraphPad Prism software (GraphPad software, San Diego, CA, USA). The k_{cat} was calculated from the ratio of V_{max} and enzyme concentration.

4.3.2.9 Native polyacrylamide gel electrophoresis of PpADI variants

10% of polyacrylamide native gels were used for protein electrophoresis to analyze the native form of PpADI variants. Purified protein of PpADI variants (7 µl of protein and 3 µl of loading dye) were loaded into each lane of native gel. The

molecular marker used in the gel is NativeMark™ Unstained Protein Standard (Invitrogen, Darmstadt, Germany). The electrophoresis was performed with tris/glycine buffer (pH 8.3) and electrophoresis chamber was incubated in ice-water bath. Protein bands were stained with Coomassie brilliant blue solution.

4.3.2.10 Homology modeling

Homology modeling approach was used for the structure prediction of PpADI. The model was built by using the automated structure prediction tool, Protein homology/analogy recognition engine (Phyre: http://www.sbg.bio.ic.ac.uk/~phyre/) (132). The crystal structure of PaADI (PDB ID: 2A9G) was used as template by the server and It has 84.9% sequence identity (http://blast.ncbi.nlm.nih.gov/Blast) with PpADI. Procheck program suit (http://www.ebi.ac.uk/thornton-srv/software/PROCHECK/) (133) was used to assess the stereochemical quality of the model. Ramachandran plot which represented that 84.7% residues were present in the most favoured region and 14.7% in additional allowed region (Figure 3). Dfire was used to access non bonded atomic interaction in the model (http://sparks.informatics.iupui.edu/hzhou/dfire.html/) (134), and Qmean (http://swissmodel.expasy.org/qmean/cgi/index.cgi) (135) for the estimation of global protein quality. Swiss-PdbViewer (118) was used to create the tetramer structure by fitting the monomer model on the 4 units of the 2A9G template. The variant M6 (D38H, D44E, A128T, E296K, H404R) were created by using the “mutate” tool of the Swiss-PdbViewer and by selecting rotamers with the best fitness score. All tetramers were energy minimized in vacuum using GROMOS 43B1 force field (119).

4.4 Results

4.4.1 Improved screening system in microtiter plates to identify PpADI variants with high activities at low arginine concentration

Screening assay was based on the validated citrulline colorimetric screening protocol in microtiter plate, as reported previously (3). In order to screen for variants with high activity at low arginine concentration under physiological

condition concerning pH and ion concentrations, 1 mM arginine in PBS buffer (pH 7.4) as substrate solution was employed in screening assay and enzyme reaction time was controlled accordingly (10 min). The coefficient of variation is an important performance criterion of a screening system to determine its accuracy. Optimized assay condition with 1 mM arginine (PBS buffer, pH 7.4) as substrate resulted in true coefficient of variation of 14.9 % (Figure 1). The resulting low absolute absorbance value is a main reason for the high true coefficient of variation (14.9 %). In the previous screening system, 100 mM arginine in 0.5 M sodium phosphate buffer was used and yielded higher activity variants but with higher K_m value.

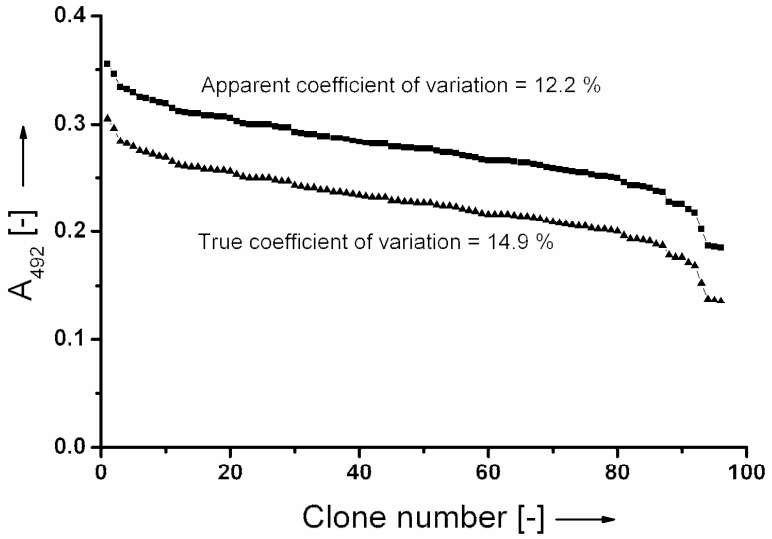

Figure 1. Activity values in descending order of the PpADI variant M3 conversion of arginine to citrulline in a 96-well microtiter plate using the optimized assay protocol. The apparent coefficients of variation were calculated without subtracting the background and the true coefficients of variation after background subtraction.

4.4.2 Genealogic tree of directed PpADI evolution

Figure 2 shows the two rounds of PpADI evolution, generation of saturation mutagenesis libraries and recombination of beneficial positions to finally obtain the PpADI variant M6 with 64.7-fold higher k_{cat} and reduced $S_{0.5}$ (1.3 mM (WT) to 0.81 mM (M6). Based on structure-function analysis of PaADI[16], M1 was generated by substitute His at position 404 with Arg. Position 404 is through

interactions with position Asp280 involved in substrate stabilization during catalysis. M1 was subject to the first round of epPCR library, from which M2 was identified showing a 4-fold improved k_{cat} value and increased K_m value (2.5 mM in 0.5 mM sodium phosphate buffer, pH 7.4)[15]. M3 was generated by a site saturation mutagenesis library at position 128 which increased in another clone the expression level (data not shown). In order to improve PpADI towards medical application demands (high activity at low arginine concentration), a second epPCR mutant library was constructed using M3 as parent. M4 with decreased $S_{0.5}$ value (0.81 mM) and M5 with increased K_{cat} value (17.56 s^{-1}) were identified after screening of ~1400 clones. In M4 the position E296 was identified to be important for lowering $S_{0.5}$ and in M5 position D38 was identified to be important for activity increase. M6 was finally constructed by combining the substations at position D38 and E296. Saturation mutagenesis of these two positions did not yield any further improved $S_{0.5}$ or activity variant.

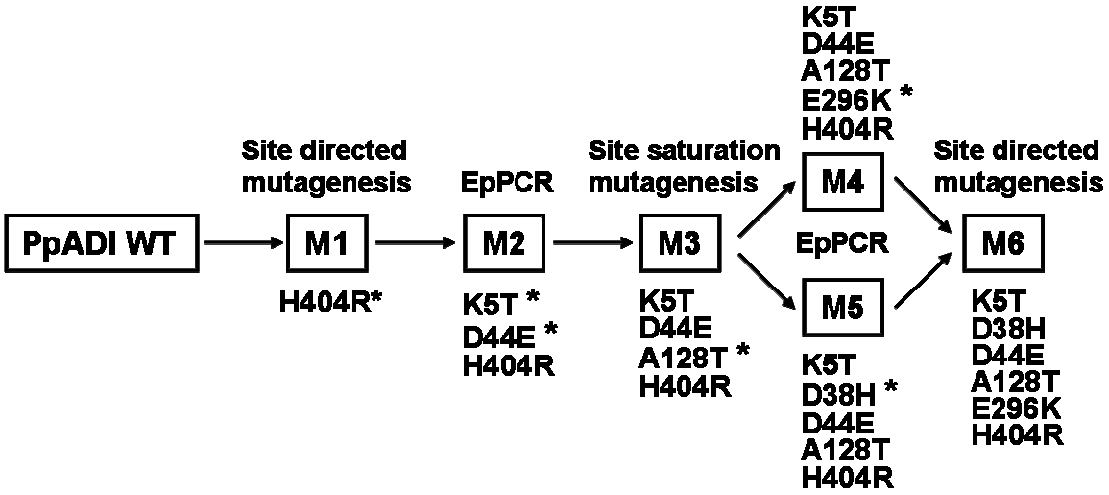

Figure 2. Genealogic tree of PpADI variants (M1 to M6) with generated amino acid substitutions. Novel substitutions are indicated by an asterisk.

4.4.3 EpPCR library construction and screening for variants with high activities at low arginine concentration

Variant M2 was used as a starting template. As described previously, M2 shifts the pH optimum from pH 6.5 to pH 7.0 and has a 4-fold faster k_{cat} than PpADI wild type. In one sequenced mutant, position A128 was identified to be

responsible for higher expression (data not shown). Site saturation mutagenesis on M2 therefore was carried out at position A128. The resulting variant M3 (K5T/D44E/A128T/H404R) showed a ~2-fold improved expression and was subsequently used as parent template for epPCR library.

Three concentrations of $MnCl_2$ (0.01-0.10 mM) were used in epPCR library generation to adjust the ratio of active to inactive clones. Instead of 0.02 mM $MnCl_2$, 0.05 mM $MnCl_2$ which generated 46 % of inactive mutant was selected for library generation. EpPCR mutant libraries with a ratio of ~50 % active and ~50 % inactive clones have often been used successfully in directed evolution, improving enzyme properties by gradual changes (one or two amino acids changes per round of mutagenesis and screening). Two variants M4 and M5 were identified from this epPCR library (~1400 clones) and further characterized. Variant M4 and M5 were sequenced and one additional amino acid substitution was identified for each variant, E296K and D38H, respectively.

4.4.4 Site saturation mutagenesis of *PpADI* at position D38 and E296

To investigate their role in improving of catalytic performance for arginine, site saturation mutagenesis library at position D38 and E296 were generated using PpADI M3 as template. For each position, ~300 clones were screened at low concentration of arginine (1 mM, PBS buffer, pH 7.4), using 96-well plate format citrulline colorimetric screening assay.

After the screening of site saturation mutagenesis libraries of position 38 and 296, variants with higher activity were chosen for preliminary kinetic investigation using crude cell extract. Beneficial mutants were identified and sequenced from both sites (Table 1). At position 38, the following beneficial substitutions were found: D38R (three times, AGA, CGG, CGT) and D38K (twice, AAG, AAA). In all cases, the negatively charged acidic amino Asp had been replaced by positively charged amino acids, Arg or His. Substitution by negatively charged Glu resulted in a clone showing a parent M3-like kinetic behavior. Hydrophobic amino acid

substitution by Pro resulted inactive clone under assay conditions. At position 296, the following substitutions were found to be beneficial: E296K (twice, AAA, AAG), E296N (once, AAC), E296T (once, ACC), E296G (once, GGA). Among these substitutions, variants with substitution to positively charged residue Lys show lowest $S_{0.5}$ value for arginine while substitution by uncharged amino acids (Asn, Thr, Gly) shows relatively marginal improvement compared to E296K. Hydrophobic amino acid substitution by Pro and Trp resulted in very low activity clones.

Table 1. Nucleotide and amino acid substitutions at position 38 in PpADI M3.

PpADI variants	Substitution at position 38	k_m (mM)
M3 (parent)	Asp (GAC)	3.74 ± 0.35
SSM-D38R	Arg (AGA, CGG, CGT)	1.16 ± 0.21
SSM-D38K	Lys (AAG, AAA)	1.01 ± 0.28
SSM-D38E	Glu (GAG)	2.95 ± 0.77
SSM-D38P	Pro (CCA)	n. d.
SSM-D38T	Thr (ACC)	n. d.
M5	His (CAC)	1.26 ± 0.12

Kinetic experiments were performed with crude cell extracts.

Table 2. Nucleotide and amino acid substitutions at position 296 in PpADI M3.

PpADI variants	Substitution at position 296	k_m (mM)
M3 (parent)	Glu (GAA)	3.74 ± 0.35
SSM-E296K	Lys (AAA, AAG)	0.20 ± 0.01
SSM-E296N	Asn (AAC)	0.53 ± 0.04
SSM-E296T	Thr (ACC)	0.61 ± 0.04
SSM-E296Q	Gln (CAA)	0.79 ± 0.06
SSM-E296G	Gly (GGA)	1.29 ± 0.12
SSM-E296W	Trp (TGG)	n. d.
SSM-E296P	Pro (CCT)	n. d.
M4	Lys (AAA)	0.27 ± 0.02

Kinetic experiments were performed with crude cell extracts.
* n. d. activity not detectable under assay conditions.

4.4.5 Determination of kinetic constants (k_{cat} and $S_{0.5}$) of PpADI wild type and variants M3, M4, M5 and M6

Table 3. Kinetic constants of wild type PpADI and variants.

	Wild type	M3 (parent)	M4	M5	M6
k_{cat} (s^{-1})	0.18 ± 0.05	10.13 ± 0.36	5.88 ± 0.09	17.56 ± 1.15	11.64 ± 0.50
$S_{0.5}$ (mM)	1.30 ± 0.25	2.01 ± 0.19	0.81 ± 0.03	1.48 ± 0.17	0.81 ± 0.09

* Kinetic contants of PpADI wild type is different from our previous report because in stead of 0.5 M phosphate buffer, PBS buffer was used for kinetic measurements. K_{cat} value of PpADI wild type dropped from 5.6 s^{-1} to 0.18 s^{-1} and k_{cat} value of M2 is reduced ~2-fold.

M3, the parent of the second round of PpADI epPCR library, M4 with decreased $S_{0.5}$, M5 with increased k_{cat} and best variant M6 with best combination of k_{cat} value and $S_{0.5}$ were selected for detailed characterization studies.

Kinetic characterization of PpADI variants was performed using PBS buffer (pH 7.4), which is commonly used in biological research. PBS buffer helps to maintain a constant pH and its osmolarity and ion concentrations usually match those of the human body. Citrulline production of PpADI variants was maintained between 0.2-0.8 mM. Table 3 summarizes the k_{cat} and $S_{0.5}$ values of parent M3 (K5T/D44E/A128T/H404R), variants M4 (K5T/D44E/A128T/E296K/H404R), M5 (K5T/D44E/A128T/D38H/H404R) and M6 (K5T/D38H/D44E/A128T/E296K/H404R), which were expressed in shaking flasks cultures and purified using a two step procedure (anion exchange follows by gel filtration). Compared to parent M3 ($S_{0.5}$ = 2.01 mM), both variants M4 and M5 have a lower $S_{0.5}$ for arginine conversion at pH 7.4, 0.81 mM and 1.48 mM, respectively. Variant M4 shows a decreased k_{cat} value, 58% of parent M3 while M5 shows a 1.7-fold higher k_{cat} compared to parent M3. Variant M6 with combined mutations (K5T/D38H/D44E/A128T/E296K/H404R) shows decreased $S_{0.5}$ value, 40 % of parent M3 (K5T/D44E/A128T/H404R), 62 % of PpADI wild type, and a 64.7-fold faster k_{cat} value than PpADI wild type. M6 is 42.3-fold faster than PpADI wild type with 0.4 mM arginine (PBS buffer, pH 7.4) as substrate.

After two rounds of epPCR libraries coupled with site directed mutagenesis, a variant M6 with 64.7-fold higher k_{cat} and lower $S_{0.5}$ value (0.81 mM) than PpADI wild type (0.31 mM). At low concentration of arginine, activity of M6 enhanced dramatically than M3 and wild type. For example, M6 is 42.3-fold faster than PpADI wild type in 0.4 mM arginine (PBS buffer, pH 7.4).

4.4.6 Native polyacrylamide gel electrophoresis of PpADI variants

Multimeric form of PpADI variants were investigated by native polyacrylamide gel electrophoresis. As shown in Figure 3, two distinct protein bands representing two multimeric forms tetramer and dimer (molecular weight of a subunit is ~ 46 kDa) were observed, but with different concentration percentage. The major multimeric form of M3 is dimer. Compared to M3, M4 with an additional mutation E296K shows a very different pattern: tetramer is the main form; while M5 with an additional mutation D38H contains more or less equal amount of dimer and tetramer. M6, with both mutations E296K and D38H, contains more tetramer than dimer.

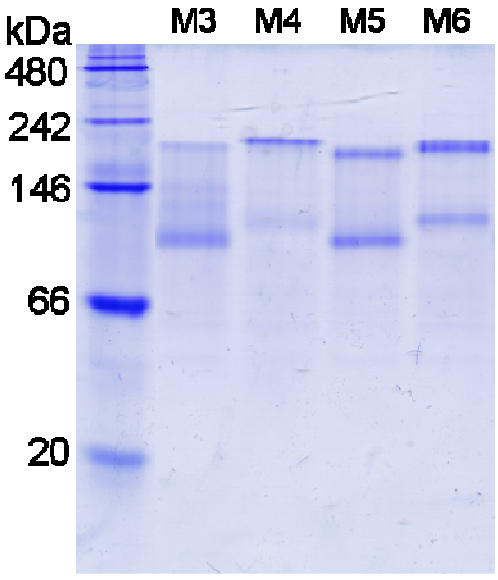

Figure 3. Native polyacrylamide gel electrophoresis of PpADI variants (M3 to M6) with different dimer/tetramer distribution. Single subunit has a molecular weight of ~46 kDa.

4.5 Discussion

Directed evolution allows improving all properties that can be reflected in a screening system through iterative rounds of diversity generation and screening. Small libraries of a few thousand variants are often sufficient to find improved variants [18] even without rational understanding of the targeted property. After establishing a first directed ADI evolution protocol yielding mutant M2, we adjusted the screening system to better reflect ADI's application conditions. Prerequisite for ADI to become an effective anti-tumor agent is that low concentrations of arginine in human plasma can effectively be converted.

Figure 2 shows the genealogic tree of PpADI evolution and before discussing the influence of each substitution individually the effect on kinetics are briefly summarized. Amino acid substitution D44E (M2) increases k_{cat} and $S_{0.5}$, substitution A128T (M3) increases the expression level, and substitution E296K (M4) decreases k_{cat} and $S_{0.5}$ and is responsible for tetramer formation. Substitution D38H (M5) increase largely k_{cat} and reduces slightly $S_{0.5}$. The combination of all mentioned residues in M6 result in a finally 64.7-fold improved PpADI activity and reduced $S_{0.5}$ (1.30 to 0.81 mM).

PpADI M3 was obtained from site saturation mutagenesis library at position A128 using M2 as template (Figure 2). M3 shows improved functional expression level of ADI (data not shown) and was used as parent for generating an epPCR library. Screening of epPCR library yielded two improved variants M4 and M5, carrying an additional mutation, E296K (M4) and D38H (M5). M4 has a decreased $S_{0.5}$ (0.81 mM) and a decreased k_{cat} value (5.88 s^{-1}; see Table 3). M5 has a decreased $S_{0.5}$ (1.48 mM) and an increased k_{cat} value (17.56 s^{-1}) when compared to parent M3 ($S_{0.5}$, 2.01 mM; k_{cat}, 10.03 s^{-1}; see Table 3). M6 which harbors both substitutions (E296K and D38H) has a decreased $S_{0.5}$ value (0.81 mM) compared to the parent M3 (1.30 mM) and the wild type (2.01 mM), and a 64.7-fold higher k_{cat} value than the PpADI wild type.

Despite further enhancing the activity of PpADI, it is crucial for an efficient conversion of the substrate arginine in human plasma (100-120 µM arginine) to reduce PpADI's "K_m" ($S_{0.5}$) value. Figure 4 shows the kinetics of PpADI WT, parent M3, and the variants M4, M5 and M6. M3 has a significantly higher k_{cat} value compared to WT, but its activity at low concentration of arginine (<1.0 mM) is very low ($S_{0.5}$ value 2.01 mM). In contrast, the most efficient variant M6 with a decreased $S_{0.5}$ value (0.81 mM) shows a remarkable activity improvement at low concentrations of arginine (<0.5 mM; see Figure 4). M6 has additional two amino acid substitutions (D38H and E296K) compared to M3 which increases k_{cat} and reduces the $S_{0.5}$ value. The combination of D38H and E296K improves especially the activity of M6 at low arginine concentrations (< 0.5 mM; see Figure 4).

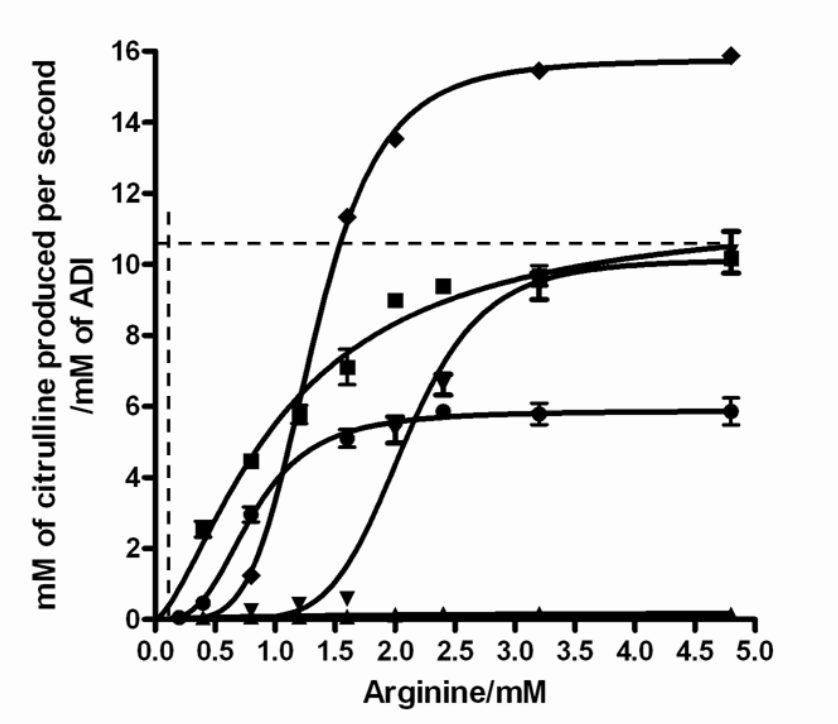

Figure 4. Kinetic curve of PpADI wild type, M3, M5 and M6. (▲) PpADI wild type, (▼) M3, (●) M4, (♦) M5 and (■) M6.

Figure 5 shows the tetrameric model (based on PaADI, PDB code 2A9G) of PpADI WT (Figure 5A) and variant M6 (Figure 5B). Monomeric units are

indicated with the letters a, b, c and d. The access channel to the active sites of each monomer is highlighted in square and faces an internal cavity generated by the assembly of four PpADI monomers. The substitutions D38H (in blue) and D44E (in green) are localized at the interface of monomer pair a-b and c-d. The substitution of Glu by Asp at position 44 provides a longer side chain in close proximity of the also negatively charged residue Asp43 (Figure 6A). The substitution E296K is localized at the border of the entrance to the internal cavity of the PpADI tetramer. E296K promotes the tetramer formation likely by introducing stabilizing interactions with other residues, for example with Thr33 (hydrogen bond). E296K inverts the charge at this position and its increased length of the side chain might promote further interactions to a neighboring monomer (Figure 6A). The combination of D44E and E296K results in a population consisting of mainly tetramers (see Figure 3; mutein M4). Interestingly with the formation of a tetramer (M4) the $S_{0.5}$ value is reduced which indicates that the tetramer complex formation promotes interactions with the substrate arginine at low concentrations. The substitution D38H together with the E296K in the mutein M6 reestablishes an almost equal population of PpADI dimers and tetramers. A hypothesis is that Lys of the E296K has an electrostatic stabilizing interaction with the Glu38 in the M4 but not to the neutral His38.

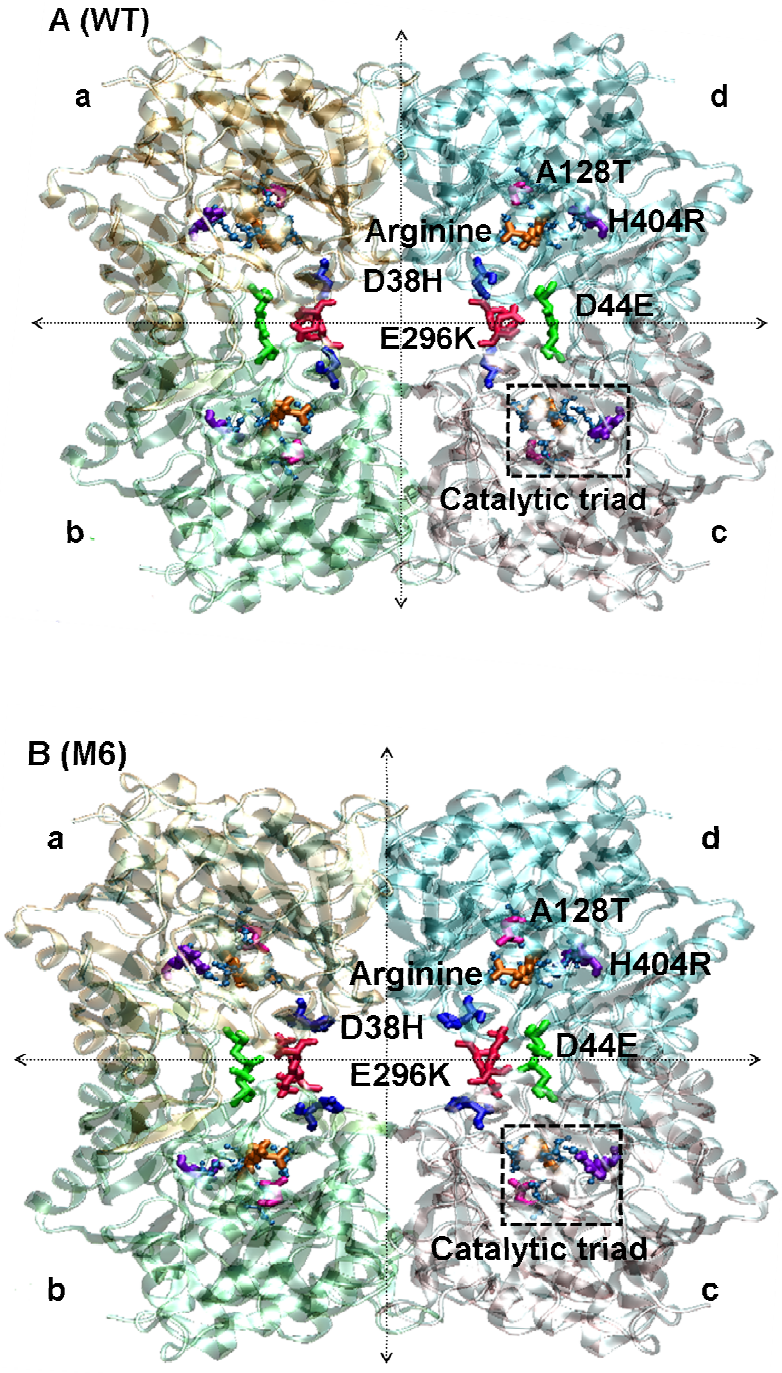

Figure 5. A). The model of WT tetramer after energy minimization in vacuum (GROMOS 43B1). B). The model of M6 tetramer after energy minimization in vacuum (GROMOS 43B1). Active site residues are represented in CRK format in a square (Blue). Mutated residues are shown in licorice format in different colors like D38H (blue), D44E (green), A128T (magenta), E296K (red) and H404R (violet). Substrate arginine is represented in orange color by licorice format.

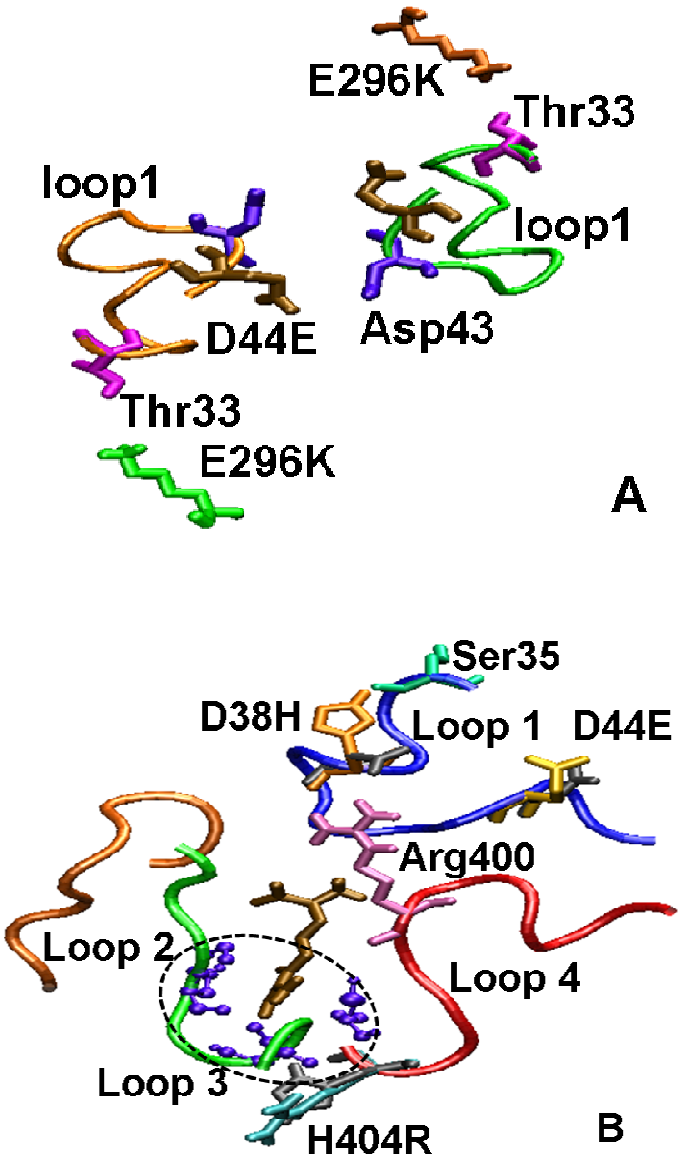

Figure 6. A). Structure model of variant M6. E296K is involved in intermonomer interaction (between chain a (orange) and b (green)) with Thr33. D44E is involved in intermonomer interaction, between chain A (orange) and B (green), with Asp43 (violet). B). Structure alignment of PpADI WT model and M6 model with four loops (loop 1:30-46, loop 2:178-175, loop 3:271-281 and loop 4: 393-404) surrounding the entrance of the active site. The substitutions in these loops and the residues involved in the interaction with those substitutions are representing: D38H (orange), D44E (yellow) and H404R (cyan, in M6; gray, in WT), Ser35 (green), Arg 400 (pink), substrate arginine (ochre), catalytic triad His278, Asp280 and Cys406 (violet, highlighted in an oval)

Figure 6B shows that the active site of the PaADI is surrounded by four loops (loop 1: 30-46, loop 2: 178-185, loop 3: 271-281, and loop 4: 393-404). These four loops undergo a conformational transition upon arginine binding and tighten

the surrounding of the arginine substrate[16]. D38 is located in loop 1 and faces towards the substrate access channel. In PpADI model (Figure 6B), the D38H mutation promotes the formation of a hydrogen bond interaction with the neighboring residues Ser35, contributing to the stability of the entropically unfavorable folded conformation of loop1. The rigidified loop 1 might be beneficial for arginine conversion. According to PaADI structure analysis, the side chain of gating residue Arg401 (Arg400 in PpADI) is located at the active site entrance and fills the substrate-binding site. The structure analysis of the C406A PaADI-L-arginine complex[16] shows that the Arg401 side chain (Arg400 in PpADI) is displaced by the substrate arginine to a position near the active site entrance that allows its hydrocarbon chain to assist shielding the catalytic site from solvent. D38 is involved in an ionic interaction and hydrogen bonding with Arg400. The substitution of Asp to His at position 38 results in a loss of ionic interactions to Arg400 due to the different lengths of the side chains. His38 can form only a hydrogen bond with active site gating residue Arg400. A weakened interaction between position 38 and Arg400 might increase the flexibility of the side chain of Arg400 which then might block less efficiently the access of arginine to the active site. As a result the variant M5 shows an improved k_{cat} value (1.7-fold compared to parent M3) due to the substitution D38H.

For elucidating further the individual role of the five identified amino acid substitutions and their influence on the active site geometry and tetramer formation crystal structures of variant M4 and M6 have to be solved.

4.6 Conclusion

In summary, with the modified screening protocol, PpADI variants with improved k_{cat} and $S_{0.5}$ were identified. The increased k_{cat} value and decreased $S_{0.5}$ value result in significant activity improvement of PpADI at low arginine concentrations. Especially the kinetic constants of PpADI variant M6 demonstrate that PpADI properties can be tailored by directed evolution. The generated PpADI variants match from their kinetic behavior therapeutic application demands much better

than the wild type PpADI. We therefore hope that by directed evolution improved PpADIs will further be investigated *in vivo* for tumor therapy.

References

1. Li L, Li ZM, Chen DQ*, et al.* Inactivation of microbial arginine deiminases by L-canavanine. Journal of the American Chemical Society, 2008; 130(6): 1918-31.

2. Lu XF, Li L, Wu R*, et al.* Kinetic analysis of *Pseudomonas aeruginosa* arginine deiminase mutants and alternate substrates provides insight into structural determinants of function. Biochemistry, 2006; 45(4): 1162-72.

3. Zhu LL, Tee KL, Roccatano D*, et al.* Directed evolution of an antitumor drug (arginine deiminase PpADI) for increased activity at physiological pH. Chembiochem, 2010; 11(5): 691-7.

4. Das K, Butler GH, Kwiatkowski V, Clark AD, Yadav P, Arnold E. Crystal structures of arginine deiminase with covalent reaction intermediates: Implications for catalytic mechanism. Structure, 2004; 12(4): 657-67.

5. Schofield PJ, Edwards MR, Matthews J, Wilson JR. The pathway of arginine catabolism in *Giardia intestinalis*. Molecular and Biochemical Parasitology, 1992; 51(1): 29-36.

6. Linstead D, Cranshaw MA. The pathway of arginine catabolism in the parasitic flagellate *Trichomonas vaginalis*. Molecular and Biochemical Parasitology, 1983; 8(3): 241-52.

7. Yarlett N, Lindmark DG, Goldberg B, Moharrami MA, Bacchi CJ. Subcellular localization of the enzymes of the arginine dihydrolase pathway in Trichomonas vaginalis and Tritrichomonas foetus. J Eukaryot Microbiol, 1994; 41(6): 554-9.

8. Biagini GA, Yarlett N, Ball GE*, et al.* Bacterial-like energy metabolism in the amitochondriate protozoon Hexamita inflata. Mol Biochem Parasitol, 2003; 128(1): 11-9.

9. Makhlin J, Kofman T, Borovok I*, et al.* Staphylococcus aureus ArcR controls expression of the arginine deiminase operon. Journal of Bacteriology, 2007; 189(16): 5976-86.

10. Seggewiss J, Becker K, Kotte O*, et al.* Reporter metabolite analysis of transcriptional profiles of a Staphylococcus aureus strain with normal phenotype

and its isogenic hemB mutant displaying the small-colony-variant phenotype. Journal of Bacteriology, 2006; 188(22): 7765-77.

11. Altucci P, Sapio V, Vitale P, de Vargas F. Mycoplasma in human pathology. Current status of the problem, with special reference to respiratory pathology. Recenti Prog Med, 1966; 41(5): 409-55.

12. Harasawa R, Koshimizu K, Kitagawa M, Asada K, Kato I. Nucleotide sequence of the arginine deiminase gene of *Mycoplasma hominis*. Microbiology and Immunology, 1992; 36(6): 661-5.

13. Takaku H, Matsumoto M, Misawa S, Miyazaki K. Antitumor activity of arginine deiminase from *Mycoplasma arginini* and its growth inhibitory mechanism. Japanese Journal of Cancer Research, 1995; 86(9): 840-6.

14. Fenske JD, Kenny GE. Role of arginine deiminase in growth of *Mycoplasma hominis*. Journal of Bacteriology, 1976; 126(1): 501-10.

15. Wei YZ, Zhou H, Sun Y, He YB, Luo YZ. Insight into the catalytic mechanism of arginine deiminase: Functional studies on the crucial sites. Proteins-Structure Function and Bioinformatics, 2007; 66(3): 740-50.

16. Ensor CM, Holtsberg FW, Bomalaski JS, Clark MA. Pegylated arginine deiminase (ADI-SS PEG(20,000) (mw)) inhibits human melanomas and hepatocellular carcinomas in vitro and in vivo. Cancer Research, 2002; 62(19): 5443-50.

17. Galkin A, Lu XF, Dunaway-Mariano D, Herzberg O. Crystal structures representing the Michaelis complex and the thiouronium reaction intermediate of Pseudomonas aeruginosa arginine deiminase. Journal of Biological Chemistry, 2005; 280(40): 34080-7.

18. Kundu M, Thomas J, Fialho AM*, et al.* The anticancer activity of the N-terminal CARD-Like domain of arginine deiminase (ADI) from *Pseudomonas aeruginosa*. Letters in Drug Design & Discovery, 2009; 6(6): 403-12.

19. Beloussow K, Wang L, Wu J, Ann D, Shen WC. Recombinant arginine deiminase as a potential anti-angiogenic agent. Cancer Letters, 2002; 183(2): 155-62.

20. Misawa S, Aoshima M, Takaku H, Matsumoto M, Hayashi H. High-Level expression of Mycoplasma arginine deiminase in *Escherichia coli* and Its efficient renaturation as an antitumor enzyme. Journal of Biotechnology, 1994; 36(2): 145-55.
21. Gong H, Zolzer F, von Recklinghausen G*, et al.* Arginine deiminase inhibits cell proliferation by arresting cell cycle and inducing apoptosis. Biochemical and Biophysical Research Communications, 1999; 261(1): 10-4.
22. Takaku H, Takase M, Abe S, Hayashi H, Miyazaki K. *In vivo* antitumor activity of arginine deiminase purified from *Mycoplasma arginini*. International Journal of Cancer, 1992; 51(2): 244-9.
23. Kim JE, Jeong DW, Lee HJ. Expression, purification, and characterization of arginine deiminase from Lactococcus lactis ssp lactis ATCC 7962 in Escherichia coli BL21. Protein Expression and Purification, 2007; 53(1): 9-15.
24. Kakimoto T, Shibatan.T, Chibata I. Crystallization of L-arginine deiminase from *Pseudomonas putida*. Febs Letters, 1971; 19(2): 166-8.
25. Shibatani T, Kakimoto T, Chibata I. Crystallization and properties of L-arginine deiminase of *Pseudomonas Putida* 2. Journal of Biological Chemistry, 1975; 250(12): 4580-3.
26. Galkin A, Kulakova L, Sarikaya E, Lim K, Howard A, Herzberg O. Structural insight into arginine degradation by arginine deiminase, an antibacterial and parasite drug target. Journal of Biological Chemistry, 2004; 279(14): 14001-8.
27. Ni Y, Schwaneberg U, Sun ZH. Arginine deiminase, a potential anti-tumor drug. Cancer Lett, 2008; 261(1): 1-11.
28. Galkin A, Kulakova L, Sarikaya E, Lim K, Howard A, Herzberg O. J Biol Chem, 2004; 279: 14001.
29. Galkin A, Lu XF, Dunaway-Mariano D, Herzberg O. J Biol Chem, 2005; 280: 34080.
30. Holle LM. Pegaspargase: an alternative? Annals of Pharmacotherapy, 1997; 31(5): 616-24.

31. Yoshioka T, Wada T, Uchida N*, et al.* Anticancer efficacy in vivo and in vitro, synergy with 5-fluorouracil, and safety of recombinant methioninase. Cancer Research, 1998; 58(12): 2583-7.
32. Lam TL, Wong GKY, Chong HC*, et al.* Recombinant human arginase inhibits proliferation of human hepatocellular carcinoma by inducing cell cycle arrest. Cancer Letters, 2009; 277(1): 91-100.
33. Shen RS, Fritz RR, Abell CW. Biochemical-Properties and Immunogenicity of L-Phenylalanine Ammonia-Lyase - Effects on Tumor-Bearing Mice. Cancer Treatment Reports, 1979; 63(6): 1063-8.
34. Yoshimoto T, Chao SG, Saito Y, Imamura I, Wada H, Inada Y. Chemical modification of tryptophanase from E. coli with polyethylene glycol to reduce its immunoreactivity towards anti-tryptophanase antibodies. Enzyme, 1986; 36(4): 261-5.
35. Feun LG, Savaraj N, Marini A*, et al.* Phase II study of pegylated arginine deiminase (ADI-PEG20), a novel targeted therapy for melanoma. Journal of Clinical Oncology, 2006; 24(18): 464s-s.
36. Gong H, Zolzer F, von Recklinghausen G, Havers W, Schweigerer L. Arginine deiminase inhibits proliferation of human leukemia cells more potently than asparaginase by inducing cell cycle arrest and apoptosis. Leukemia, 2000; 14(5): 826-9.
37. Morris SM, Jr. Regulation of enzymes of the urea cycle and arginine metabolism. Annu Rev Nutr, 2002; 22: 87-105.
38. Scott L, Lamb J, Smith S, Wheatley DN. Single amino acid (arginine) deprivation: rapid and selective death of cultured transformed and malignant cells. British Journal of Cancer, 2000; 83(6): 800-10.
39. Wheatley DN, Campbell E. Arginine catabolism, liver extracts and cancer. Pathol Oncol Res, 2002; 8(1): 18-25.
40. Thomas JB, Holtsberg FW, Ensor CM, Bomalaski JS, Clark MA. Enzymatic degradation of plasma arginine using arginine deiminase inhibits nitric oxide production and protects mice from the lethal effects of tumor necrosis factor and endotoxin. Molecular Biology of the Cell, 2001; 12: 404a-a.

41. Cheng PNM, Leung YC, Lo WH, Tsui SM, Lam KC. Remission of hepatocellular carcinoma with arginine depletion induced by systemic release of endogenous hepatic arginase due to transhepatic arterial embolisation, augmented by high-dose insulin: arginase as a potential drug candidate for hepatocellular carcinoma. Cancer Letters, 2005; 224(1): 67-80.
42. Cheng PNM, Lam TL, Lam WM*, et al.* Pegylated recombinant human arginase (rhArg-peg(5,000mw)) inhibits the in vitro and in vivo proliferation of human hepatocellular carcinoma through arginine depletion. Cancer Research, 2007; 67(1): 309-17.
43. Kim JH, Yu YS, Kim DH, Min BH, Kim KW. Anti-tumor activity of arginine deiminase via arginine deprivation in retinoblastoma. Oncol Rep, 2007; 18(6): 1373-7.
44. Kim RH, Coates JM, Bowles TL*, et al.* Arginine deiminase as a novel therapy for prostate cancer induces autophagy and caspase-independent apoptosis. Cancer Research, 2009; 69(2): 700-8.
45. Glazer ES, Piccirillo M, Albino V*, et al.* Phase II study of pegylated arginine deiminase for nonresectable and metastatic hepatocellular carcinoma. Journal of Clinical Oncology, 2010; 28(13): 2220-6.
46. Ascierto PA, Scala S, Castello G*, et al.* Pegylated arginine deiminase treatment of patients with metastatic melanoma: Results from phase I and II studies. Journal of Clinical Oncology, 2005; 23(30): 7660-8.
47. Shen LJ, Beloussow K, Shen WC. Accessibility of endothelial and inducible nitric oxide synthase to the intracellular citrulline-arginine regeneration pathway. Biochemical Pharmacology, 2005; 69(1): 97-104.
48. Park H, Lee JB, Shim YJ*, et al.* Arginine deiminase enhances MCF-7 cell radiosensitivity by inducing changes in the expression of cell cycle-related proteins. Molecules and Cells, 2008; 25(2): 305-11.
49. Kubo M, Nishitsuji H, Kurihara K, Hayashi T, Masuda T, Kannagi M. Suppression of human immunodeficiency virus type 1 replication by arginine deiminase of *Mycoplasma arginini*. Journal of General Virology, 2006; 87: 1589-93.

50. Izzo F, Montella M, Orlando AP*, et al.* Pegylated arginine deiminase lowers hepatitis C viral titers and inhibits nitric oxide synthesis. Journal of Gastroenterology and Hepatology, 2007; 22(1): 86-91.
51. Kwan JM, Fialho AM, Kundu M*, et al.* Bacterial proteins as potential drugs in the treatment of leukemia. Leukemia Research, 2009; 33(10): 1392-9.
52. Tsai WB, Aiba I, Lee SY, Feun L, Savaraj N, Kuo MT. Resistance to arginine deiminase treatment in melanoma cells is associated with induced argininosuccinate synthetase expression involving c-Myc/HIF-1 alpha/Sp4. Molecular Cancer Therapeutics, 2009; 8(12): 3223-33.
53. Yoon CY, Shim YJ, Kim EH*, et al.* Renal cell carcinoma does not express argininosuccinate synthetase and is highly sensitive to arginine deprivation via arginine deiminase. International Journal of Cancer, 2007; 120(4): 897-905.
54. Feun L, You M, Wu CJ*, et al.* Arginine deprivation as a targeted therapy for cancer. Current Pharmaceutical Design, 2008; 14(11): 1049-57.
55. Zhu ZW, Momeu C, Zakhartsev M, Schwaneberg U. Making glucose oxidase fit for biofuel cell applications by directed protein evolution. Biosens Bioelectron, 2006; 21(11): 2046-51.
56. Panke S, Held M, Wubbolts M. Trends and innovations in industrial biocatalysis for the production of fine chemicals. Current Opinion in Biotechnology, 2004; 15(4): 272-9.
57. Patel RN. Chemo-enzymatic synthesis of pharmaceutical intermediates. Expert Opinion on Drug Discovery, 2008; 3(2): 187-245.
58. Yokobayashi Y, Weiss R, Arnold FH. Directed evolution of a genetic circuit. Proc Natl Acad Sci U S A, 2002; 99(26): 16587-91.
59. Ellington AD, Chen X, Robertson M, Syrett A. Evolutionary origins and directed evolution of RNA. International Journal of Biochemistry & Cell Biology, 2009; 41(2): 254-65.
60. Alper H, Fischer C, Nevoigt E, Stephanopoulos G. Tuning genetic control through promoter engineering. Proceedings of the National Academy of Sciences of the United States of America, 2005; 102(36): 12678-83.

61. Drummond DA, Iverson BL, Georgiou G, Arnold FH. Why high-error-rate random mutagenesis libraries are enriched in functional and improved proteins. J Mol Biol, 2005; 350(4): 806-16.
62. Wong TS, Roccatano D, Schwaneberg U. Steering directed protein evolution: strategies to manage combinatorial complexity of mutant libraries. Environmental Microbiology, 2007; 9(11): 2645-59.
63. Wong TS, Zhurina D, Schwaneberg U. The diversity challenge in directed protein evolution. Combinatorial Chemistry & High Throughput Screening, 2006; 9(4): 271-88.
64. Fasan R, Chen MM, Crook NC, Arnold FH. Engineered alkane-hydroxylating cytochrome P450(BM3) exhibiting nativelike catalytic properties. Angewandte Chemie-International Edition, 2007; 46(44): 8414-8.
65. Titus SA, Xiao L, Southall N*, et al.* Cell-based PDE4 assay in 1536-well plate format for high-throughput screening. Journal of Biomolecular Screening, 2008; 13(7): 609-18.
66. Lafferty M, Dycaico MJ. GigaMatrix^{TM}: an ultra highthroughput tool for accessing biodiversity. JALA, 2009; 9: 200-8.
67. Yang GY, Withers SG. Ultrahigh-throughput FACS-based screening for directed enzyme evolution. Chembiochem, 2009; 10(17): 2704-15.
68. Miller OJ, Hibbert EG, Ingram CU, Lye GJ, Dalby PA. Optimisation and evaluation of a generic microplate-based HPLC screen for transketolase activity. Biotechnology Letters, 2007; 29(11): 1759-70.
69. Yoshikuni Y, Ferrin TE, Keasling JD. Designed divergent evolution of enzyme function. Nature, 2006; 440(7087): 1078-82.
70. Becker S, Schmoldt HU, Adams TM, Wilhelm S, Kolmar H. Ultra-high-throughput screening based on cell-surface display and fluorescence-activated cell sorting for the identification of novel biocatalysts. Current Opinion in Biotechnology, 2004; 15(4): 323-9.
71. Farinas ET. Fluorescence activated cell sorting for enzymatic activity. Combinatorial Chemistry & High Throughput Screening, 2006; 9(4): 321-8.

72. Agresti JJ, Antipov E, Abate AR*, et al.* Ultrahigh-throughput screening in drop-based microfluidics for directed evolution. Proceedings of the National Academy of Sciences of the United States of America, 2010; 107(9): 4004-9.
73. Leemhuis H, Kelly RM, Dijkhuizen L. Directed evolution of enzymes: library screening strategies. Iubmb Life, 2009; 61(3): 222-8.
74. Chen KC, Wu CH, Chang CY*, et al.* Directed evolution of a lysosomal enzyme with enhanced activity at neutral pH by mammalian cell-surface display. Chem Biol, 2008; 15(12): 1277-86.
75. Wang Q, Xia T. Enhancement of the activity and alkaline pH stability of Thermobifida fusca xylanase A by directed evolution. Biotechnology Letters, 2008; 30(5): 937-44.
76. Colin DY, Deprez-Beauclair P, Silva N, Infantes L, Kerfelec B. Modification of pancreatic lipase properties by directed molecular evolution. Protein Engineering Design & Selection, 2010; 23(5): 365-73.
77. Bessler C, Schmitt J, Maurer KH, Schmid RD. Directed evolution of a bacterial alpha-araylase: Toward enhanced pH-performance and higher specific activity. Protein Sci, 2003; 12(10): 2141-9.
78. Liu ZQ, Sun ZH, Leng Y. Directed evolution and characterization of a novel D-pantonohydrolase from Fusarium moniliforme. Journal of Agricultural and Food Chemistry, 2006; 54(16): 5823-30.
79. Hasan Z, Renirie R, Kerkman R, Ruijssenaars HJ, Hartog AF, Wever R. Laboratory-evolved vanadium chloroperoxidase exhibits 100-fold higher halogenating activity at alkaline pH - Catalytic effects from first and second coordination sphere mutations. Journal of Biological Chemistry, 2006; 281(14): 9738-44.
80. Makde RD, Dikshit K, Kumar V. Protein engineering of class-A non-specific acid phosphatase (PhoN) of Salmonella typhimurium: Modulation of the pH-activity profile. Biomolecular Engineering, 2006; 23(5): 247-51.
81. Kim T, Mullaney EJ, Porres JM*, et al.* Shifting the pH profile of *Aspergillus niger* PhyA phytase to match the stomach pH enhances its effectiveness as an

animal feed additive. Applied and Environmental Microbiology, 2006; 72(6): 4397-403.
82. Hirata A, Adachi M, Utsumi S, Mikami B. Engineering of the pH optimum of Bacillus cereus beta-amylase: Conversion of the pH optimum from a bacterial type to a higher-plant type. Biochemistry, 2004; 43(39): 12523-31.
83. Tomschy A, Brugger R, Lehmann M*, et al.* Engineering of phytase for improved activity at low pH. Appl Environ Microbiol, 2002; 68(4): 1907-13.
84. Sakoda H, Imanaka T. Cloning and sequencing of the gene coding for alcohol dehydrogenase of Bacillus stearothermophilus and rational shift of the optimum pH. J Bacteriol, 1992; 174(4): 1397-402.
85. Yang JH, Park JY, Kim SH, Yoo YJ. Shifting pH optimum of Bacillus circulans xylanase based on molecular modeling. Journal of Biotechnology, 2008; 133(3): 294-300.
86. MacPherson IS, Rosell FI, Scofield M, Mauk AG, Murphy MEP. Directed evolution of copper nitrite reductase to a chromogenic reductant. Protein Engineering Design & Selection, 2010; 23(3): 137-45.
87. Hida K, Hanes J, Ostermeier M. Directed evolution for drug and nucleic acid delivery. Adv Drug Deliv Rev, 2007; 59(15): 1562-78.
88. Yuan L, Kurek I, English J, Keenan R. Laboratory-directed protein evolution. Microbiology and Molecular Biology Reviews, 2005; 69(3): 373-92.
89. Rautio J, Kumpulainen H, Heimbach T*, et al.* Prodrugs: design and clinical applications. Nat Rev Drug Discov, 2008; 7(3): 255-70.
90. Barak Y, Thorne SH, Ackerley DF, Lynch SV, Contag CH, Matin A. New enzyme for reductive cancer chemotherapy, YieF, and its improvement by directed evolution. Molecular Cancer Therapeutics, 2006; 5(1): 97-103.
91. Kuhn I, Harden P, Bauzon M*, et al.* Directed evolution generates a novel oncolytic virus for the treatment of colon cancer. PLoS One, 2008; 3(6): e2409.
92. Robertson DE, Steer BA. Recent progress in biocatalyst discovery and optimization. Current Opinion in Chemical Biology, 2004; 8(2): 141-9.
93. Soares AL, Guirmaraes GM, Polakiewicz B, Pitombo RND, Abrahao-Neto J. Effects of polyethylene glycol attachment on physicochemical and biological

stability of E-coli L-asparaginase. International Journal of Pharmaceutics, 2002; 237(1-2): 163-70.
94. Kotzia GA, Labrou NE. Engineering thermal stability of L-asparaginase by in vitro directed evolution. Febs Journal, 2009; 276(6): 1750-61.
95. Orlova A, Feldwisch J, Abrahmsen L, Tolmachev V. Affibody molecules for molecular imaging and therapy for cancer. Cancer Biotherapy and Radiopharmaceuticals, 2007; 22(5): 573-84.
96. Nilsson FY, Tolmachev V. Affibody (R) molecules: New protein domains for molecular imaging and targeted tumor therapy. Current Opinion in Drug Discovery & Development, 2007; 10(2): 167-75.
97. Gronwall C, Sjoberg A, Ramstrom M*, et al.* Affibody-mediated transferrin depletion for proteomics applications. Biotechnol J, 2007; 2(11): 1389-98.
98. Renberg B, Shiroyama I, Engfeldt T, Nygren PA, Karlstrom AE. Affibody protein capture microarrays: Synthesis and evaluation of random and directed immobilization of affibody molecules. Analytical Biochemistry, 2005; 341(2): 334-43.
99. Friedman M, Orlova A, Johansson E*, et al.* Directed evolution to low nanomolar affinity of a tumor-targeting epidermal growth factor receptor-binding affibody molecule. Journal of Molecular Biology, 2008; 376(5): 1388-402.
100. Chang CCJ, Chen TT, Cox BW*, et al.* Evolution of a cytokine using DNA family shuffling. Nature Biotechnology, 1999; 17(8): 793-7.
101. Zhang JH, Dawes G, Stemmer WPC. Directed evolution of a fucosidase from a galactosidase by DNA shuffling and screening. Proceedings of the National Academy of Sciences of the United States of America, 1997; 94(9): 4504-9.
102. Crameri A, Cwirla S, Stemmer WPC. Construction and evolution of antibody-phage libraries by DNA shuffling. Nature Medicine, 1996; 2(1): 100-2.
103. Patten PA, Howard RJ, Stemmer WP. Applications of DNA shuffling to pharmaceuticals and vaccines. Curr Opin Biotechnol, 1997; 8(6): 724-33.
104. Park IS, Kang SW, Shin YJ*, et al.* Arginine deiminase: a potential inhibitor of angiogenesis and tumour growth. Br J Cancer, 2003; 89(5): 907-14.

105. Izzo F, Marra P, Beneduce G*, et al.* Pegylated arginine deiminase treatment of patients with unresectable hepatocellular carcinoma: Results from phase I/II studies. J Clin Oncol, 2004; 22(10): 1815-22.
106. Gong H, Zölzer F, von Recklinghausen G, Havers W, Schweigerer L. Arginine deiminase inhibits proliferation of human leukemia cells more potently than asparaginase by inducing cell cycle arrest and apoptosis. Leukemia, 2000; 14(5): 826-9.
107. Shen LJ, Shen WC. Drug evaluation: ADI-PEG-20 - a PEGylated arginine deiminase for arginine-auxotrophic cancers. Curr Opin in Mol Ther, 2006; 8(3): 240-8.
108. Holtsberg FW, Ensor CM, Steiner MR, Bomalaski JS, Clark MA. Poly(ethylene glycol) (PEG) conjugated arginine deiminase: effects of PEG formulations on its pharmacological properties. J Controlled Release, 2002; 80(1-3): 259-71.
109. Mûller HJ, Boos J. Use of L-asparaginase in childhood all. Crit Rev Oncol Hematol, 1998; 28(2): 97-113.
110. Turunen O, Janis J, Fenel F, Leisola M. Engineering the thermotolerance and pH optimum of family 11 xylanases by site-directed mutagenesis. Methods Enzymol, 2004; 388: 156-67.
111. Fang TY, Ford C. Protein engineering of *Aspergillus awamori* glucoamylase to increase its pH optimum. Protein Eng, 1998; 11(5): 383-8.
112. Sakoda H, Imanaka T. Cloning and sequencing of the gene coding for alcohol-dehydrogenase of *Bacillus stearothermophilus* and rational shift of the optimum pH. J Bacteriol, 1992; 174(4): 1397-402.
113. Wang WY, Malcolm BA. Two-stage PCR protocol allowing introduction of multiple mutations, deletions and insertions using QuikChange™ site-directed mutagenesis. BioTechniques, 1999; 26(4): 680-2.
114. Miyazaki K, Takenouchi M. Creating random mutagenesis libraries using megaprimer PCR of whole plasmid. Biotechniques, 2002; 33(5): 1033-8.
115. Studier FW. Protein production by auto-induction in high-density shaking cultures. Protein Expression and Purification, 2005; 41(1): 207-34.

116. Archibald RM. Deternination of citrulline and allantoin and demonstration of citrulline in blood plasma. J Biol Chem, 1944; 156(1): 121-42.
117. Boyde TRC, Rahmatullah M. Optimization of conditions for the colorimetric determination of citrulline, using diacetyl monoxime. Anal Biochem, 1980; 107(2): 424-31.
118. Guex N, Peitsch MC. SWISS-MODEL and the Swiss-PdbViewer: an environment for comparative protein modeling. Electrophoresis, 1997; 18(15): 2714-23.
119. van Gunsteren WF, Billeter SR, Eising AA*, et al.* Biomolecular simulation: the gromos 96 manual and user guide ETH Zürich; 1996.
120. Mather A, Roland D. Automated thiosemicarbazide-diacetyl monoxime method for plasma urea. Clinical Chemistry, 1969; 15(5): 393-6.
121. Wong TS, Arnold FH, Schwaneberg U. Laboratory evolution of cytochrome P450BM-3 monooxygenase for organic cosolvents. Biotechnol Bioeng, 2004; 85(3): 351-8.
122. Glieder A, Farinas ET, Arnold FH. Laboratory evolution of a soluble, self-sufficient, highly active alkane hydroxylase. Nat Biotechnol, 2002; 20(11): 1135-9.
123. Galkin A, Lu X, Dunaway-Mariano D, Herzberg O. Crystal structures representing the Michaelis complex and the thiouronium reaction intermediate of Pseudomonas aeruginosa arginine deiminase. Journal of biological chemistry, 2005; 280(40): 34080-7.
124. Chuang VTG, Kragh-Hansen U, Otagiri M. Pharmaceutical strategies utilizing recombinant human serum albumin. Pharm Res, 2002; 19(5): 569-77.
125. Tee KL, Dmytrenko O, Otto K, Schmid A, Schwaneberg U. A p-nitrothiophenolate screening system for the directed evolution of a two-component epoxygenase (StyAB). J Mol Catal B: Enzym, 2008; 50(2-4): 121-7.
126. Li L, Li ZM, Wang CH*, et al.* The electrostatic driving force for nucleophilic catalysis in L-arginine deiminase: a combined experimental and theoretical study. Biochemistry (Mosc), 2008; 47(16): 4721-32.

127. Takaku H, Matsumoto M, Misawa S, Miyazaki K. Antitumor-activity of arginine deiminase from *Mycoplasma arginini* and its growth-Inhibitory mechanism. Jap J Cancer Res, 1995; 86(9): 840-6.
128. Capocaccia R, Sant M, Berrino F, Simonetti A, Santi V, Trevisani F. Hepatocellular carcinoma: trends of incidence and survival in Europe and the United States at the end of the 20th century. American Journal of Gastroenterol, 2007; 102(8): 1661-70.
129. Shen LJ, Shen WC. Drug evaluation: ADI-PEG-20 - a PEGylated arginine deiminase for arginine-auxotrophic cancers. Current Opinion in Molecular Therapeutics, 2006; 8(3): 240-8.
130. Wang WY, Malcolm BA. Two-stage PCR protocol allowing introduction of multiple mutations, deletions and insertions using QuikChange (TM) site-directed mutagenesis. Biotechniques, 1999; 26(4): 680-2.
131. Vaughn WK, Neal RA, Anderson AJ. Computer estimation of the parameters of the sigmoidal kinetic model. Computers in Biology and Medicine, 1976; 6(1): 1-7.
132. Kelley LA, Sternberg MJE. Protein structure prediction on the web: a case study using the Phyre server. Nature Protocols, 2009; 4(3): 363-71.
133. Laskowski RA, Macarthur MW, Moss DS, Thornton JM. Procheck - a program to check the stereochemical quality of protein structures. Journal of Applied Crystallography, 1993; 26: 283-91.
134. Zhou HY, Zhou YQ. Distance-scaled, finite ideal-gas reference state improves structure-derived potentials of mean force for structure selection and stability prediction. Protein Science, 2002; 11(11): 2714-26.
135. Benkert P, Tosatto SCE, Schomburg D. QMEAN: A comprehensive scoring function for model quality assessment. Proteins-Structure Function and Bioinformatics, 2008; 71(1): 261-77.
136. Berendsen HJC, Postman JPM, van Gunsteren WF, Hermans J. Interaction models for water in relation to protein hydration. Intermolecular Forces, 1981: 331-42.

137. Hess B, Bekker H, Berendsen HJC, Fraaije JGEM. LINCS: A linear constraint solver for molecular simulations. Journal of Computational Chemistry, 1997; 18(12): 1463-72.
138. Miyamoto S, Kollman PA. Settle - an analytical version of the shake and rattle algorithm for rigid water models. Journal of Computational Chemistry, 1992; 13(8): 952-62.
139. Darden T, York D, Pedersen L. Particle mesh ewald - an N.Log(N) method for ewald sums in large systems. Journal of Chemical Physics, 1993; 98(12): 10089-92.
140. Berendsen HJC, Postma JPM, Vangunsteren WF, Dinola A, Haak JR. Molecular dynamics with coupling to an external bath. Journal of Chemical Physics, 1984; 81(8): 3684-90.
141. Hess B, Kutzner C, van der Spoel D, Lindahl E. GROMACS 4: algorithms for highly efficient, load-balanced, and scalable molecular simulation. Journal of Chemical Theory and Computation, 2008; 4(3): 435-47.

Summary and outlook

Arginine depletion based on ADI is an emerging strategy for anti-tumor treatment. ADIs have been studied for the therapy of HCCs and melanomas and were approved as an orphan drug for both kinds of tumors. ADI is proved to be effective in the treatment of leukemia. The effectiveness of ADIs as anti-tumor agent depends on their enzymatic properties (such as K_m, k_{cat}, optimum pH, stability at neutral pH). Directed evolution, without rational understanding of the targeted property, allows improving all properties that can be reflected in a screening system through iterative rounds of diversity generation and screening.

In order to improve PpADI activity at physiological pH by directed evolution, a colorimetric screening assay based on citrulline detection has been developed in 96-well microtiter plate format. Single mutation H404R was identified according to PpADI homology model (based on PaADI crystal structure), introduced to PpADI wild type and eventually resulted in 1.4-fold of increase in k_{cat}. M1 (H404R) was used as template for the first round of epPCR library generation. M2 (K5T/D44E/H404R) obtained from the first round of epPCR library showed 4-fold improved k_{cat} value when compared to the PpADI wild type. Furthermore, a shift of pH optimum from pH 6.5 to pH 7.0 was observed, combined with an increased K_m value (2.5 mM) under assay conditions (0.5 M sodium phosphate buffer, pH 7.4), compared to PpADI wild type (0.7 mM).

Arginine concentration in human plasma is however relatively low (100-120 µM). Therefore the second round of epPCR library was performed to decrease K_m value and further improve k_{cat} value. The validated screening assay was modified to reflect more close physiological condition (1 mM arginine in PBS buffer, pH 7.4). Two important variants with one additional mutation, M4 (K5T/D44E/A128T/E296K/H404R) with decreased $S_{0.5}$ vaule, and M5 (K5T/D38H/D44E/A128T/H404R) with improved k_{cat} were obtained. Their two mutations were combined and resulted in variants M6

(K5T/D38H/D44E/A128T/E296K/H404R). Under physiological pH in PBS buffer, the $S_{0.5}$ value of M6 (0.81 mM) is lower than that of PpADI wild type (1.30 mM); the k_{cat} value improved from 0.18 s^{-1} (PpADI wild type) to 17.56 s^{-1} (M5, 97.6-folds) and 11.64 s^{-1} (M6, 64.7-fold).

A reamaining challenge facing PpADI's anti-tumor application is to decrease the K_m ($S_{0.5}$) value further close to arginine concentration level in human plasma. A more sensitive assay for screening has to be developed with the addition of sensitizer like thiosemicarbazide (TSC), optimized temperature and incubation time. Improved variants should be tested tested in human plasma or with human plasma composition. *In vitro* testing of ADI variants with arginine auxotrophic tumor cell lines is the first step towards *in vivo* in human.

In summary, directed evolution has been very useful algorithim for improving ADI's k_{cat} and K_m at physiological pH (pH 7.4) for its medical application. Hope that directed evolution will be become a standard method for therapeutic protein like its use in industry.

Publications

1. **Leilei Zhu**, Kang Lan Tee, Danilo Roccatano, Burcu Sonmez, Ye Ni, Zhi-Hao Sun, and Ulrich Schwaneberg. Directed evolution of an antitumor drug (Arginine Deiminase PpADI) for increased activity at physiological pH. ChemBioChem. 2010, 11, 691-697.

2. **Leilei Zhu**, Rajni Verma, Danilo Roccatano, Ye Ni, Zhi-Hao Sun, and Ulrich Schwaneberg. A potential anti-tumor drug (arginine deiminase) reengineered for efficient operation under physiological conditions. ChemBioChem. *In press*.

3. Ye Ni, Zhenwei Li, Zhihao Sun, Pu Zheng, Yongmei Liu and **Leilei Zhu**, Ulrich Schwaneberg. Expression of arginine deiminase from *Pseudomonas plecoglossicida* CGMCC2039 in *Escherichia coli* and its anti-tumor activity. Current Microbiology. 2009, 58(6):593-598.

Patent

1. Directed evolution of arginine deiminase for increased activity at physiological pH. Application number: PCT/EP2010/061884.

Curriculum vitae

Personal data

Name:	Leilei Zhu
Gender:	Female
Date of Birth:	27th April, 1982
Place of Birth:	Weifang, China
Marital Status:	Married
Nationality:	Chinese

Education

2009-	PhD fellow of biotechnology, RWTH Aachen University, Aachen, Germany
2007-2009	PhD fellow of engineering and science, Jacobs University Bremen, Bremen, Germany
2005-2007	Master of biochemical engineering, Jiangnan University (Southern Yantze University), Wuxi, China
2001-2005	Bachelor of biotechnology, Jiangnan University (Southern Yantze University), Wuxi, China

2001-1998	The first high school of Hanting, Weifang, China
1998-1994	The sixth middle school of Hanting, Weifang, China
1989-1994	Primary school of Liuhe, Weifang, China

Directed Evolution of Arginine Deiminase (ADI) for Anti-tumor Application

Von der Fakultät für Mathematik, Informatik und Naturwissenschaften der RWTH Aachen University zur Erlangung des akademischen Grades eines(r) Doktors(in) der Naturwissenschaften oder eines(r) Doktors(in) der Ingenieurwissenschaften genehmigte Dissertation

vorgelegt von

Master of Biochemistry

Leilei Zhu

Aus Weifang China

Berichter: **Universitätsprofessor Dr. Ulrich Schwaneberg**
Universitätsprofessor Dr. Lothar Elling

Tag der mündlichen Prüfung: 14.09.2010

Diese Dissertation ist auf den Internetseiten der Hochschulbibliothek online verfügbar.

Table of contents

Acknowledgement.....I
Abstract.....III
Abbreviations V
List of figures..... VI
List of tables..... IX
Chapter 1 Arginine deiminase (ADI) 1
1.1 Arginine deiminase (ADI).....1
1.2 ADI structure 5
1.3 Catalytic reaction mechanism of ADI.....10
1.4 Anti-tumor application of ADI.....11
1.5 Conclusion.....16
Chapter 2 Directed evolution 17
2.1 Introduction to directed evolution.....17
2.2 Directed enzyme evolution for pH tolerance of enzymes 22
2.3 Directed enzyme evolution for medical application.....24
2.3.1 Prodrug enzymes for tumor chemotherapy.....24
2.3.2 Oncolytic viruses for tumor chemotherapy.....25
2.3.3 Amino acid depriving enzyme for anti-tumor applications.....27
2.3.4 Affibody molecules for cancer prognosis 28
2.3.5 Interferon for anti-tumor applicaiton 29
2.4 Conclusion.....30
Chapter 3. Directed evolution of Arginine deiminase for increased activity at physiological pH.....31
3. 1 Abstract 31
3.2 Introduction.....31
3.3 Materials and methods 33
3.3.1 Materials 33
3.3.2 Methods 34

3.3.2.1 Reagents used in assays 34
3.3.2.2 Cloning of ADI into pET42b(+) 34
3.3.2.3 Site directed mutagenesis of PpADI gene at position H404 35
3.3.2.4 Site sturation mutagenesis of PpADI gene at nine amino acid position 35
3.3.2.5 Construction of PpADI error-prone library 36
3.3.2.6 Expression of PpADI in LB media with IPTG induction 37
3.3.2.7 Expression of PpADI in auto-induction media 37
3.3.2.8 Cultivation and expression of PpADI in 96-well plates 37
3.3.2.9 Screening Procedure 38
3.3.2.10 Expression of ADI in shaking flask and purification 39
3.3.2.11 Characterization of ADI wild type and mutants 40
3.3.2.12 Molecular Modeling 41
3.3.2.13 Stability of PpADI in presence of serum 41
3.3.2.14 Activity of PpADI (wild type, M1, M2) towards arginine derivative dimethylarginine 42
3.4 Results 42
3.4.1 PpADI cloning 42
3.4.2 PpADI expression in LB media with IPTG as inducer 44
3.4.3 PpADI expression in auto-induction media 44
3.4.4 PpADI assay based on citrulline detection 46
3.4.5 PpADI screening system for citrulline production in microtiter plates 47
3.4.6 Focused libraries generated by saturation mutagenesis 50
3.4.7 Validation of variant M1 (H404R) citrulline colorimetric assay in cuvette format 50
3.4.8 epPCR library generation and screening with citrulline detection assay by screening error-prone mutant libraries 50
3.4.9 Characterization of PpADI variants 53
3.4.9.1 Determination of k_{cat} and K_m of ADI wild type and the mutants 53
3.4.9.2 Relative pH profile of wild type and mutant 54
3.4.10 Stability of PpADI in the presence of human serum 55

3.4.11 Activity of PpADI (wild type, M1, M2) towards arginine derivative (N^G, N^G)-dimethylarginine 56
3.5 Discussion 56
3.6 Conclusion 59
Chapter 4. PpADI reengineered for efficient operation under physiological conditions 60
4.1 Abstract 60
4.2 Introduction 60
4.3 Materials and methods 62
4.3.1 Materials 62
4.3.2 Methods 62
4.3.2.1 Site saturation mutagenesis of *PpADI* M2 at position A128 62
4.3.2.2 Construction of PpADI error-prone library 63
4.3.2.3 Site directed mutagenesis at position D38 of *PpADI* M4 63
4.3.2.4 Site saturation mutagenesis at position D38 and E296 of *PpADI* M3 64
4.3.2.5 Cultivation and expression of PpADI in 96-well plates 64
4.3.2.6 Improved screening system in 96-well plate to identify PpADI variants with high activities at low arginine concentration 64
4.3.2.7 Expression of PpADI in shaking flask and purification 65
4.3.2.8 Characterization of PpADI variants 65
4.3.2.9 Native polyacrylamide gel electrophoresis of PpADI variants 66
4.3.2.10 Homology modeling 67
4.4 Results 67
4.4.1 Improved screening system in microtiter plates to identify PpADI variants with high activities at low arginine concentration 67
4.4.2 Genealogic tree of directed PpADI evolution 68
4.4.3 EpPCR library construction and screening for variants with high activities at low arginine concentration 69
4.4.4 Site saturation mutagenesis of *PpADI* at position D38 and E296 70

4.4.5 Determination of kinetic constants (k_{cat} and $S_{0.5}$) of PpADI wild type and variants M3, M4, M5 and M6 72
4.4.6 Native polyacrylamide gel electrophoresis of PpADI variants 73
4.5 Discussion 74
Summary and outlook 95
Publication list 97
Curriculum vitae 98

Acknowledgement

First and foremost I want to thank my supervisor Prof. Dr. Ulrich Schwaneberg for offering me the opportunity to study in Germany, his continuous support of my PhD study and research, for his patience, motivation, enthusiasm, and immense knowledge, which influence my view of science and life. His guidance helped me all the time in research and writing of paper and thesis. I could not have imagined having a better advisor and mentor for my PhD study.

Besides my supervisor, I would like to thank other two committee member Prof. Dr. Lothar Elling and Prof. Dr. Anett Kirschner. I appreciate their taking time to read this thesis and give valuable comments.

My sincere thanks also go to Kang Lan, who became a great friend of mine after I came to Bremen of Germany three years ago. She helped me a lot with my PhD project and she was a great company in my daily life. I will never forget the two months I spent on the first cloning working in my life and how Kang Lan taught me and encouraged me.

I am grateful to Prof. Dr. Danilo Roccatano for spending a lot of time discussing my results. After the first meeting with Prof. Roccatano, I started to know and learn computational tools which are really useful for my PhD study. I also thank Rajni for her contribution of homology modeling to my project.

The members of the Schwaneberg group have contributed immensely to my personal and professional time in Jacobs University Bremen and RWTH Aachen University. The group has been a source of friendships as well as good advice and collaboration. I appreciate the help from Marina, Daniela, Gisela, Wolfgang and Brigitta in lab and Marina, Monika and Anita's patient explanation of the registration regulation RWTH Aachen University. I would like to acknowledge honorary group members. I thank Liqing for her sharing apartment with me and helped me start my life in Germany and also thank Haiyan for her offering me a room later and often cooked nice food for us. Ran shared a lot of lab techniques which are very useful for my experiments. I always admire her professional and

accurate attitude towards work. I thank other labmates who I got to know in Jacobs university: Ronny, Hemu, Chaoning, Amol, Dominik and Amir for the stimulating discussions, little help in lab and all the fun we have had in the last three years; Dragana, Ljubica, Noor, Pravine and Raluca helped me move to Aachen and we finally got through the tough transition period from Bremen to Aachen. I thank our group leaders Marco, Jan and Radivoje, who are not my direct supervisor, but are always helpful when I have questions. I thank my fellow labmates who I got to know in RWTH Aachen University: Tamara, Felix, Alex, Christian, Joelle, André, Joana……, who are always helpful with all the problems (PhD registration, Germany letters from university…….) because of my poor German.

I also want to acknowledge my students, Burcu and Alice, both of whom were hard-working and smart. They were all a great help in the lab and I really enjoyed working with them.

I would like to thank my family because of their love, support and trust. They love me the most in the world. I thank for their efforts that they made over the years to make sure I have a good growth and education environment. I wish them healthy and happy life. I thank my elder sister for her love and understanding and always taking good care of my parents these years when I am not around. I thank my husband, Haifeng, who supports me all the time and always is there for me. I am lucky to have him with me.

The financial support of the Jacobs University Bremen and RWTH Aachen University is gratefully acknowledged.

Abstract

Arginine deiminase (ADI), an arginine-degrading enzyme, is involved in the first step of arginine dihydrolase pathway. It catalyzes the hydrolysis of L-arginine to form citrulline and ammonia. ADI has been studied as a potential cancer therapeutic agent for the arginine-auxotrophic tumors, such as hepatocellular carcinomas (HCC) and melanomas. Furthermore, studies also indicate that ADI is a potential anti-angiogenic agent; therefore it could become a novel anti-cancer drug targeting the neovascularization-related tumors. Studies show ADI is more potent for the treatment of leukemia than L-asparaginase. However, the anti-tumor application of ADI for therapeutic purpose faces considerable challenges, such as, microbial ADI has low activity at physiological pH (7.35~7.45), short circulating half-life (~5 h) and high antigenicity. Pegylation of ADI improved its efficacy as a clinical drug, including its half-life in serum and antigenicity. The aim of the project is to improve ADI catalytic performance at physiological pH by directed evolution.

Protein engineering by rational design and directed evolution offers opportunities to tailor ADI properties to physiological conditions. Directed protein evolution has over the last decades become a versatile and successful approach for tailoring protein properties to industrial demands and for advancing our understanding of structure-function relationships in biocatalysts. Unlike rational design relying on the gathering of extensive structure-function relationships of enzymes, directed evolution is used to reengineer enzyme properties through iterative rounds of diversity generation and function selection for improved variants.

In order to improve the ADI activity at physiological pH, we established a directed evolution protocol for this purpose. A microtiter plate (MTP) format colorimetric screening assay based on citrulline detection with diacetyl monoxime (DAM) was developed. Reaction temperature for color development and DAM concentration

were optimized to ensure sufficient sensitivity, appropriate linear range and throughput. With the optimized assay and PpADI wild type expressed in *E. coli* as a model protein, true standard deviation 12.8 % was obtained, which is appropriate for the library screening.

With the established microtiter plate assay system, for the first time, we reengineered ADI for improved activity at physiological pH (pH 7.4) with higher potency in medical application. After one site directed mutagenesis and one round of epPCR library screening, variant M2 (K5T/D44E/H404R) was obtained. M2 shows 4-fold improved k_{cat} value than the PpADI wild type, a shifted pH optimum at pH 7.0 (by 0.5 pH unit), and however an increased K_m value, 3.6-fold under assay conditions (0.5 M sodium phosphate buffer).

Low K_m ($S_{0.5}$) value for ADI is an important factor for efficient consume of arginine in plasma because of the low arginine concentration in human plasma (100-120 µM). Therefore after our proof of concept of reengineering PpADI by directed evolution, we aim to decrease the K_m value of PpADI towards arginine and improve the k_{cat} furthermore thereby improve the efficiency of arginine depletion by ADI. The established citrulline colorimetric assay in 96-well microtiter plate is improved to reflect application conditions: PBS buffer and 1 mM arginine were used in screening system. After the second round of epPCR library and site directed mutagenesis, variant M5 (K5T/D38H/D44E/A128T/H404R) and M6 (K5T/D38H/D44E/A128T/E296K/H404R) were generated: at pH 7.4 (PBS buffer), the $S_{0.5}$ value decrease from 2.01 mM (parent M3, K5T/D44E/A128T/H404R) to 1.48 mM (M5) and 0.81 mM (M6). Under physiological pH in PBS buffer, the $S_{0.5}$ value of M6 (0.81 mM) is lower than that of PpADI wild type (1.30 mM); the k_{cat} value improved from 0.18 s^{-1} (PpADI wild type) to 17.56 s^{-1} (M5, 97.6-folds) and 11.64 s^{-1} (M6, 64.7-fold).

Abbreviations

ADI	arginine deiminase
ADH	arginine degradation pathway
ASS	argininosuccinate synthetase
ASL	argininosuccinate lyase
CARD	caspase recruitment domain
PCR	polymerase chain reaction
epPCR	error prone PCR
DAM	diacetyl monoxime
Da	dalton
DNA	deoxyribonucleic acid
E. coli	*Escherichia coli*
GMSF	guanidino-group modifying enzyme superfamily
HCC	hepatocellular carcinomas
HUVEC	human umbilical vein endothelial cells
IPTG	isopropyl β-D-1-thiogalactopyranoside
iNOs	inducible nitric oxide synthase
LB	Luria-Bertani-medium
MTP	microtiter plate
OD_{600}	optical density at 600 nm
OTC	ornithine carbamoyl transferase
PEG	polyethylene glycol
PDB	protein data bank
TSC	thiosemicarbazide
WT	wild type

List of tables

Figures	Pages
Chapter 1	
Scheme 1. Arginine dihydrolase pathway. OTC, ornithine transcarbamylase; CK, carbamate kinase.	1
Figure 1. Structural of ADIs from *P. aeruginosa* and *M. arginini*.	5
Figure 2 (A). stereoscopic view of PaADI key active site residues. 2 (B). stereoscopic view of a modeled arginine substrate (green) docked in the active site of ADI. Atomic colors are red, oxygen; blue, nitrogen; yellow, sulfur; and gray, carbon. Ion pair interactions are shown as dashed lines.	7
Figure 3. Structural characteristics of the PaADI.	9
Figure 4 (A). Stereoscopic view of ADI in the unbound and bound states. 4 (B). Structural relationship between ADI (yellow) and PAD4 (cyan).	10
Figure 5. Mechanism of PaADI catalysis of arginine to citrulline and ammonia.	11
Firgure 6. Urea cycle.	13
Firgure 7. Summary of ADI effects on arginine-related cellular functions.	15
Chapter 2	
Figure 1. Procedure of a directed evolution experiment.	18
Figure 2. Overview of screening technologies.	21
Figure 3. Hermiston's "Directed Evolution" process of viruses and derivative viral pools.	26
Chapter 3	
Figure 1. DNA electrophoresis of PpADI.	43
Figure 2. PpADI sequencing results.	43
Figure 3. SDS-PAGE of PpADI expression.	44

Figures Pages

Figure 4(A). Activity of PpADI expressed in auto-induction media. 45

Figure 4(B). SDS-PAGE of ADI expressed in auto-induction media 1, LS-5052; 2, P-5052; 3, MD-5052; 4 TYM-5052; 5, TYP-5052. 45

Figure 5. Arginine conversion by ADI and detection of citrulline using DAM/TSC assay. 46

Figure 6. Citrulline colorimetric assay in cuvette format using DAM/TSC assay. 46

Figure 7. Calibration curve of cuvette format citrulline colorimetric assay. 47

Figure 8. Citrulline colorimetric assay in MTP format using DAM assay. 47

Figure 9. Calibration curve of 96-well microtiter plate format citrulline colorimetric screening assay. 48

Figure 10. Activity values in descending order of the ADI wild-type conversion of arginine to citrulline in a 96-well microtiter plate using the optimized assay protocol. 49

Figure 11. PpADI model derived from PaADI crystal structure (PDB code 2a9gD) by SWISS MODEL WORKSPACE. 49

Figure 12 (A). Electrophoresis of epPCR products. Lane 1, 0.01 mM of $MnCl_2$; Lane 2, 0.02 mM of $MnCl_2$; Lane 3, 0.05 mM of $MnCl_2$. 51

Figure 12 (B). Electrophoresis of MEGAWHOP product with epPCR products as megaprimer. 51

Figure 13. Relative activity of ADI variants towards arginine. The relative activity is the ratio of the activity at the pH of each variant relative to the activity at pH 7.4 of wild type ADI. 52

Figure 14. Elution profile of wild type PpADI and improved variants from epPCR library, generated with Protein 230 Kit using a mircofluidic device (Agilent Bioanalyzer). BSA was added as an internal standard. 53

Figure 15. Kinetic parameters of ADI and mutants for conversion of arginine to citrulline. White: ADI wild type, grey: M1 (H404R), black: M2 (K5T D44E H404R). 54

Figure 16. pH profile of wild type ADI, M1(H404R), M2(K5T/D44E /H404R. 55

Figures Pages

Figure 17. Structural alignment of mutant M1 model with corresponding residues of the crystal structures of the PaADI (in orange). 57

Figure 18. Structural alignment of mutant M2 model with corresponding residues of the crystal structures of the PaADI (in orange). 58

Chaper 4

Figure 1. Figure 1. Activity values in descending order of the PpADI variant M3 conversion of arginine to citrulline in a 96-well microtiter plate using the optimized assay protocol. 68

Figure 2. Genealogic tree of PpADI variants (M1 to M6) with generated amino acid substitutions. Novel substitutions are indicated by an asterisk. 69

Figure 3. Native polyacrylamide gel electrophoresis of PpADI variants (M3 to M6) with different dimer/tetramer distribution 73

Figure 4. Kinetic curve of PpADI wild type, M3, M5 and M6. 75

Figure 5. A). The model of WT tetramer after energy minimization in vacuum (GROMOS 43B1). B). The model of M6 tetramer after energy minimization in vacuum (GROMOS 43B1). 77

Figure 6. A). Structure model of variant M6. B). Structure alignment of PpADI WT model and M6 model with four loops 78

List of tables

Tables Page

Chapter 1

Table 1. ADI expression, enzymatic properties and medical applications. 3

Table 2. Crystal structures of ADI in protein data bank (PDB). 6

Table 3. Residues important for catalytic function of PaADI. 8

Chapter 2

Table 1. Improvement obtained from directed evolution or rational design for pH performance. 22

Chapter 3

Table 1. Primer sequences for site saturation mutagenesis. 36

Table 2. Activity of ADI variants towards arginine determined using citrulline colorimetric assay in cuvette format. 52

Table 3. Stability of PpADI variants in the presence of human serum. 55

Chapter 4

Table 1. Nucleotide and amino acid substitutions at position 38 71

Table 2. Nucleotide and amino acid substitutions at position 296 71

Table 3. Kinetic constants of wild type PpADI and variants. 72

Arginine deiminase (ADI)

1.1 Arginine deiminase (ADI)

Arginine deiminase (ADI, EC 3.5.3.6), an arginine-metabolizing hydrolase, catalyzes the hydrolysis of L-arginine to form citrulline and ammonia. This reaction is the first step in the L-arginine degradation pathway (ADH, scheme 1, (1). First, arginine is deiminated by arginine deiminase. The resulting citrulline is converted to carbamoyl phosphate and ornithine by ornithine transcarbamylase (EC 2.1.3.3), and finally the carbamoyl phosphate is used to phosphorylate ADP by carbamate kinase (EC 2.7.2.2), producing one ATP molecule. ADI is absent in humans but present in a wide range of bacterial species such as *Pseudomonas aeruginosa* (2), *Pseudomonas plecoglossicida* (3) and *Mycoplasma arginini* (4) and in parasitic protists such as *Giardia intestinalis* (5), *Trichomonas Vaginalis* (6), *Trichomonas fetus* (7), and *Hexamita inflate* (8). For pathogenic bacteria, ADI is required in arginine dehydrolase pathway for virulence and for energy production under anaerobic conditions (9, 10).

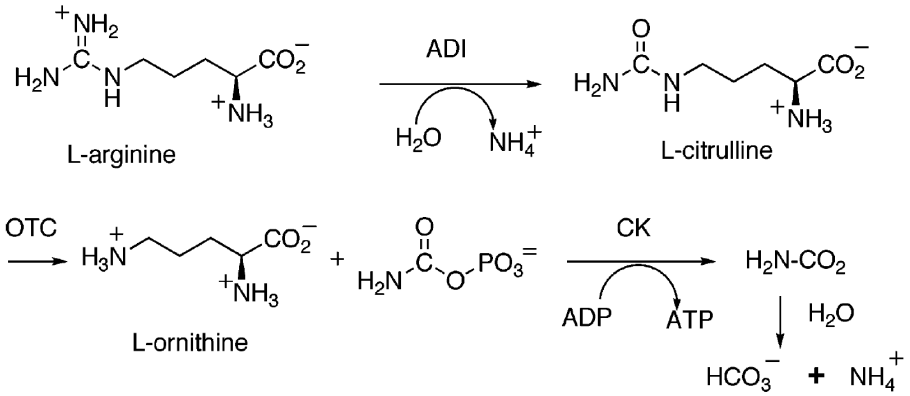

Scheme 1. Arginine dihydrolase pathway. OTC, ornithine transcarbamylase; CK, carbamate kinase.

The establishment of a high-level production system for ADI is an essential step for further research and development of this enzyme. After ADI was discovered from Mycoplasma in 1960s (11), various ADI genes have been cloned, expressed in *E. coli* strains, and the enzyme properties were also studied (Table 1).

Table 1. ADI expression, enzymatic properties and medical applications.

ADIs	Origin	Expression host/vector	Multimeric form	K_m; k_{cat}	Optimum pH	Specific activity	Medical application	References
MhADI (SYN1903)	*Mycoplasma hominis* PG21*	*E.coli* BL21 (DE3)/pET-47b	Dimer			0.618 U/mg (pH 6.5)	Human melanoma (G361), 0.036 U/ml for 50 % IC_{50}	Japan, Harasawa, 2009 (12)
MhADI	*Mycoplasma hominis* (ATCC 23114)	-	Dimer		6.0	35.5 U/mg (pH 6.0) ; 3.9 U/mg (pH 7.4)	Mouse melanoma (MH134) *in vitro*, 100 ng/ml for 50 % IC_{50}	Japan, Takaku, 1995 (13)
MhADI	*Mycoplasma hominis* (ATCC 14027)	-	Dimer	0.17 mM (pH6.6)				USA, Fenske, 1976(14)
MhADI	*Mycoplasma hominis*	*E.coli* BL21 (DE3)/pET25b		0.24 mM; 0.151 s^{-1}				China, Luo, 2007 (15)
MhADI	*Mycoplasma hominis*	*E.coli*				20 U/mg ADI (37℃). [a]	ADI-SS PEG_{20000}, human melanoma, human HCC	USA, Pheonix Pharmacologics, Inc., Clark, 2002 (16)
PaADI (PA5171)	*Pseudomonas aeruginosa* (ATCC 47085D)	*E. coli* BL21(DE3)/pET100	Tetramer	0.14±0.01 mM (pH 5.6)	5.6			USA, Dunaway-Mariano, 2005 (17)
PaADI	*Pseudomonas aeruginosa*	*E. coli* BL21 (DE3)/ pET SUMO				CARD-like domain, no catalytic activity	Human cancer cell line SKOV-3	USA, Chakrabarty, 2006 (18)
PpADI	*Pseudomonas plecoglossicida*	*E. coli* BL21 Gold-(DE3)/ pET42b		0.7 mM; 5.6 s^{-1} (pH 7.4, 0.5 M sodium phosphate buffer)	6.5	31.3 U/mg (pH 7.4, 0.5 M sodium phosphate buffer)		Germany, Schwaneberg, 2010 (3)

MaADI	*Mycoplasma arginini* (ATCC 23838D)	*E. coli* DH5α/PTTQ118				32.7 U/mg. [a]	Human umbilical vein endothelial (HUVE)	USA, Shen, 2002 (19)
MaADI	*Mycoplasma arginini* (ATCC 23838)	*E. coli* JM101/pADTc1	Dimer			33.6 U/mg (37℃, pH 6.5). [a]	Mouse hepatoma, 17 ng/ml for 50 % IC_{50}; mouse fibrosarcoma, 15 ng/ml for 50 % IC_{50}	Japan, Hayashi, 1994 (20)
MaADI	*Mycoplasma arginini* (ATCC 23838)					42 U/mg (37℃, pH 6.5); 29.9 U/mg (37℃, pH 7.4)	Mouse melanoma (MH134) *in vitro*, 10 ng/ml for 50 % IC_{50}	Japan, Takaku, 1995 (13)
MaADI	*Mycoplasma arginini* (ATCC 23838)	-					HUVE, neuroblastoma, retinoblastoma, osteosarcoma, 5~10 ng/ml for 50 % IC_{50}	Germany, Schweigerer, 1999 (21)
MaADI	*Mycoplasma arginini* (ATCC 23838)	-	Dimer	0.2 mM	6.0-7.5	50 U/mg	Mouse tumor carcinoma, fibrosarcoma and melanoma, 5~20 ng/ml for 50 % IC_{50}	Japan, Takaku, 1992 (22)
LlADI	*L. lactis* (ATCC 7962)	*E. coli* BL21Gold(DE3)/pGEM-T Easy	Trimer	8.67 mM	7.2	140.27 U/mg		Korea, Lee, 2007 (23)

[a] ADI was expressed in inclusion body and denaturation-renaturation had to be employed to get soluble protein.

1.2 ADI structure

In 1970s, Kakimoto et al. (24, 25) diffracted the first ADI crystals from *P. putida* through multiple-step chromatography followed by crystallization. Almost three decades later, the X-ray crystal structure of ADI from *P. aeruginosa* (PaADI, Figure 1A) (26) and *M. arginini* (MaADI, Figure 1B) (4) were solved to assist in understanding structure-function relationships. PaADI and MaADI share 27 % sequence identity and belong to guanidino group-modifying enzyme superfamily (GMSF). The catalytic triad (Cys-His-Glu/Asp) is conserved in members of the GMSF. Both crystal structures of PaADI and MaADI show a characteristic 5-fold pseudosymmetrical barrel with ββαβ subunits. Table 2 summarizes the crystal structures of PaADI and MaADI.

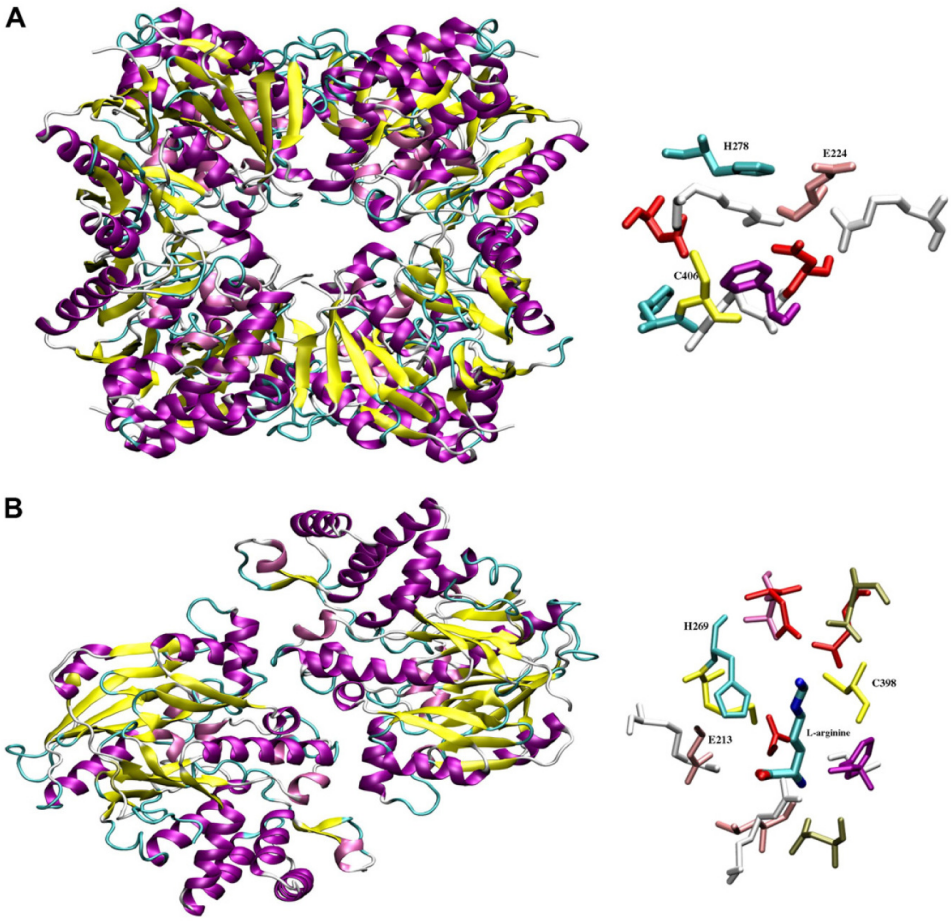

Figure 1. Structural of ADIs from *P. aeruginosa* and *M. arginini*. (A) PaADI (PDB ID: 1RXX) and stereo view of its catalytic triad (C406-H278-E224). (B) MaADI (PDB ID: 1S9R) and stereo view of its catalytic triad (C398-H269-E213) with substrate L-arginine (27).

Table 2. Crystal structures of ADI in protein data bank (PDB).

PDB code	Ligand in crystal structure	Description	Resolution (year)
2A9G	Arginine	Crystal structure of PaADI variant C406A in complex with L-arginine	2.30 Å (2005)
2AAF		Crystal structure of PaADI variant H278A forming a S-alkylthiouronium reaction intermediate	2.30 Å (2005)
2ABR		Crystal structure of PaADI variant D280A with L-arginine forming a S-alkylthiouronium reaction intermediate	2.9 Å (2005)
2ACI		Crystal structure of D166A arginine deiminase	2.50 Å (2005)
1S9R	Arginine	Crystal structure of MaADI covalently linker with a reaction in intermediate	1.60 Å (2004)
1LXY	Citrulline	Crystal Structure of MaADI covalently linked with L-citrulline	2.00 Å (2004)
1RXX		Crystal structure of MaADI	2.45 Å (2004)

MaADI was crystallized as a homodimer and its catalytic triad is formed by Cys398-His269-Glu213. MaADI has a catalytic domain and a five-helix bundle domain (Figure 3). The buried and compact substrate binding pocket is located approximately at the center of the molecule, from which a small solvent channel leads to the surface of the enzyme. The opening to the channel is located adjacent to the dimer interface region, which is at the opposite side of the 5-fold pseudosymmetric moiety of ADI. The shape and size of the channel does not permit transport of the substrate (L-arginine and end product (L-citrulline) in and out of the pocket. Substantial conformational changes in ADI are required to permit entry of the substrate and expulsion of the end product. The occurrence of "closed" and "open" form was suspected to be dependent on binding of substrate.

PaADI has a tetrametric structure with 1630 amino acid residues in total, which makes it the largest enzyme of its structural superfamily. The catalytic triad of PaADI is Cys406-His278-Glu224. Similar to MaADI, the active site of PaADI is

located in a narrow crevice formed by a network of charged residues. Ligand binding energy is derived from ion pair and hydrogen bonding interactions between active site residues and the guanidinium, carboxylate and ammonium groups of the substrate. The proposed substrate-binding model shows that the catalytic center contains abundant charged residues (e.g. Asp280, His405, Glu13 and Arg165). The ion pairing interactions between these residues contribute to the integrity and activity of ADI. In addition, Asp116, Asp227, Arg185, Arg401, His278, Glu118, and Glu224 are part of an extended charged network. The proposed catalytic mechanism suggests that the active site of PaADI is blocked by Arg401, and therefore a conformational transition is taking place upon the substrate binding. Based on the proposed reaction mechanism, Cys406 is as a key residue responsible for the nucleophilic attack on the guanidinium carbon atom of arginine. PaADI contains only one hydrophobic residue, Phe-163 and a Cys-406 with an unknown protonation state. The known functions of important residues are shown in Table 3, and the interactions between important residues and substrate arginine are shown in Figure 2.

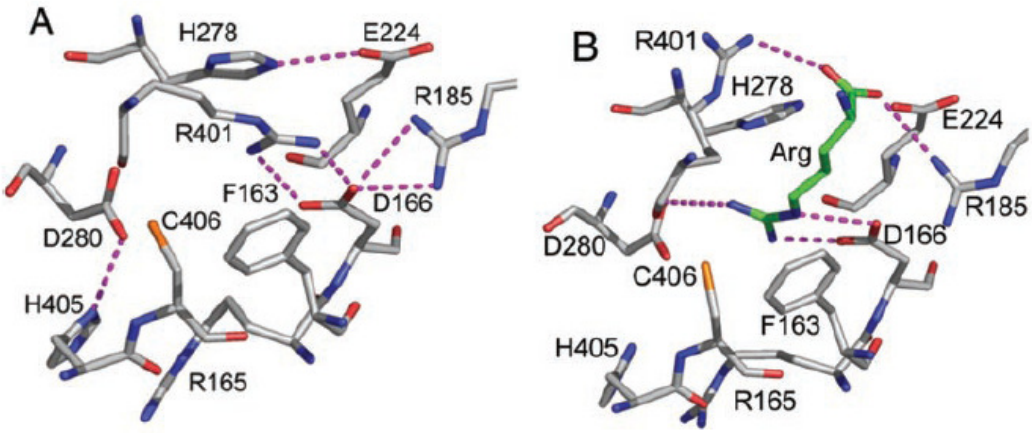

Figure 2. A. stereoscopic view of PaADI key active site residues. B. stereoscopic view of a modeled arginine substrate (green) docked in the active site of ADI. Atomic colors are red, oxygen; blue, nitrogen; yellow, sulfur; and gray, carbon. Ion pair interactions are shown as dashed lines (26).

Table 3. Residues important for catalytic function of PaADI (28, 29).	
Residues	Known/postulated function or comment
Cys406	Mounts the nucleophilic attack on the carbon atom of the guanidinium group of arginine
His278	Serves as a general base and activate the water molecule
Glu224	Modulate the ionization state of His278
Asp280	Interacts with the imidazole group of His405 F via the carboxylate group, which in turn interacts with Glu13. Invariant residue in all known ADIs
Asp280, Asp166	Fix the guanidinium group of the arginine substrate tightly by interactions with the carboxyl groups
Arg401, Arg185	Form ionic interaction with The carboxyl group of the arginine substrate
Phe163	Interacts with the hydrophobic part of arginine substrate
Glu13	Interacts His405 and is invariant in all known ADIs
His405	Sometimes is replaced by an arginine, as in the case of McADI. This may explain the low pH optimum of PaADI (5.6) in contrast to the neutral pH optimum of McADI, the enzyme that contains an arginine residue instead of His405
Arg165	Is fixed by electrostatic interactions with the main chain oxygen atoms of Thr408 and His405 and with the hydroxyl group of Thr-408
Arg401	Blocks the ADI active site via the side chain by forming an ion pair with the carboxyl group of Asp166 and occupies approximately the same position as the guanidinium group of an arginine substrate

The overall fold of MaADI and PaADI consist of five ββαβ modules in cyclical arrangement, generating a pseudo 5-fold symmetrical barrel and an additional 85-residue α-helical domain inserted between the first and the second ββαβ modules giving the typical “Clip-on-fan” moiety. The α-helical domain of PaADI mediates tetramer formation and the α-helical domain of MaADI was speculated to play a role in activating the series of reaction in arginine dehydrolysis pathway (4). Structural alignments by Chakrabarty et al. (18) demonstrated the unique 85 residue 5-α-helical bundle domain exhibiting structural similarity to the mammalian CARD (caspase recruitment domains)-containing proteins and this CARD-like domain is present only in the PaADI and MaADI but not in the other

GMSF members (Figure 3B). Furthermore, PaADI putative CARD-like domain induced apoptosis to cancer cells.

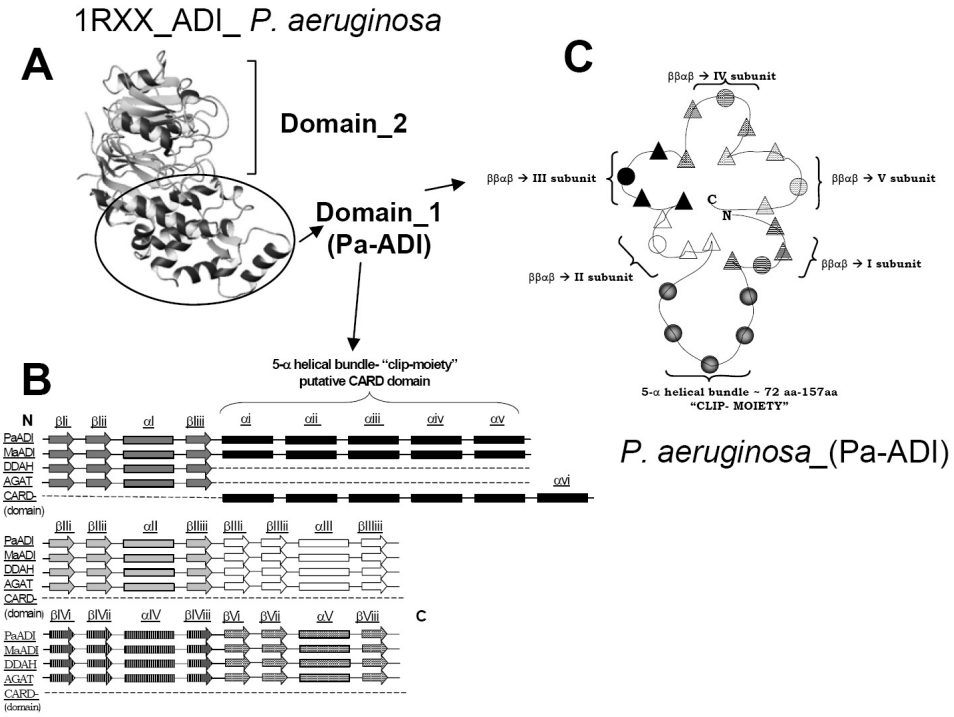

Figure 3. Structural characteristics of the PaADI. A. Ribbon drawing of PaADI (1RXX_A) highlighting the two domains. B. The presence of the CARD domain in PaADI and MaADI but its absence in other members of the GMSF (guanidino-group modifying superfamily) enzymes such as DDAH and AGAT, as shown from the structure-based sequence alignments. The CARD domain represents that of caspase-9. DDAH, dimethylarginine dimethylaminohydrolase; AGAT, arginine: glycine amidinotransferase. The β-strand and α-helices are shown as arrows and strips respectively. Roman numericals I to V are the five ββαβ subunits. The clip moiety (α-helical module) in Figure 3 is seen only in PaADI and MaADI which bears structural homology to the six-α-helical modules that form the CARD domain of the caspase-9 protein molecule. N, N-terminal; C, C-terminal. C. A schematic diagram showing the overall fold and topology of PaADI, as reported (18).

Comparison of substrate free and substrate bound structure of PaADI gives interesting insight into structure changes upon substrate binding (17). Pairwise superposition of the free wild-type PaADI (PDB code: 1rxx) and the mutant enzyme substrate complexes (PDB code: 2a9g) show that the overall fold of the structures remains similar, yet with some local changes. In particular, four loops (Figure 4) associated with the active site undergo conformational transitions not

related to crystal packing: loop 1 (residues 30-46), loop 2 (residues 178-185), loop 3 (residues 271-281, part of this loop is disordered in the apoADI structure), and loop 4 (residues 393-404). Residues adjacent to the substrate exhibit the most significant shifts. For example, the α-carbon atom of Leu41 (loop 1) shifts by 2.7Å and that of Arg185 (loop 2) by 1.8 Å; the α-carbon atom of His278 (loop 3) shifts by 0.9 Å and that of Gly400 (loop 4) by 4.4 Å. These are localized but mechanistically important conformational transitions that tighten the surrounding of the substrate. Simultaneously, substrate binding is accompanied by displacement of the side chain of Arg401 (loop 4) by more than 8 Å to enable access to the active site. The superposition of ADI and PAD4 ADI active site is shielded from the solvent by a long loop (residues 25-48 in PaADI) and the following two turns of α-helix (residues 49-56).

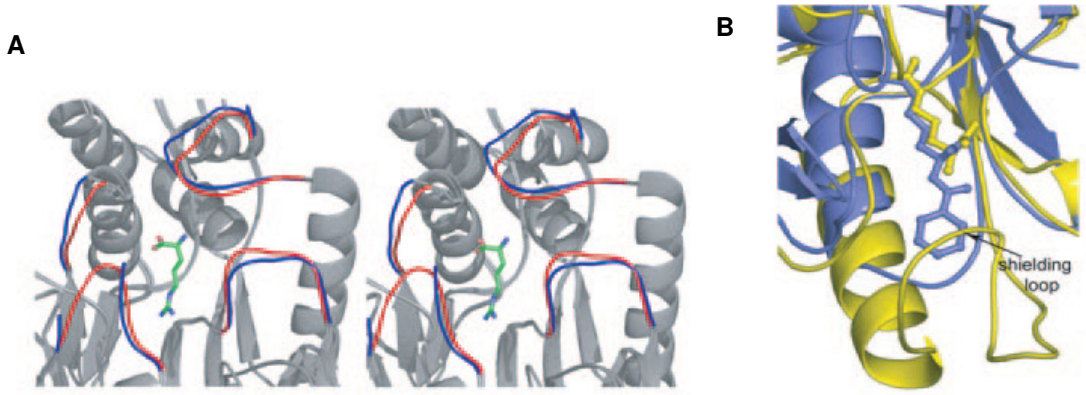

Figure 4 (A). Stereoscopic view of ADI in the unbound and bound states. Superposed molecules are colored gray where the trace of the polypeptide chain is similar in both structures. For regions exhibiting differences, loops of the apoADI structure are highlighted in blue, and loops of the ADI structure complexed with arginine are highlighted in red. 4(B). Structural relationship between ADI (yellow) and PAD4 (cyan) (17).

1.3 Catalytic reaction mechanism of ADI

The overall reaction catalyzed by ADI is the hydrolytic substitution of the ηNH_2 group from the guanidinium group Cζ of L-arginine, leading to citrulline and ammonia (Figure 5). Herzberg (17) and Arnold (4) proposed ADI catalysis mechanism for PaADI (Figure 5) and MaADI, respectively. Basically, both of the proposed mechanisms are composed of three main steps: 1) thiol group of

Cys406 mount a nucleophilic attack on the guanidinium group of arginine and a proton is transferred first to ηNH$_2$ group; 2) water molecule is activated by His278 and followed by attacking the covalent intermediate to replace and release NH$_3$; 3) the C-S covalent bond between enzyme and the resulting citrulline is cleaved and thus end product citrulline is released and free enzyme is generated for next catalytic cycle.

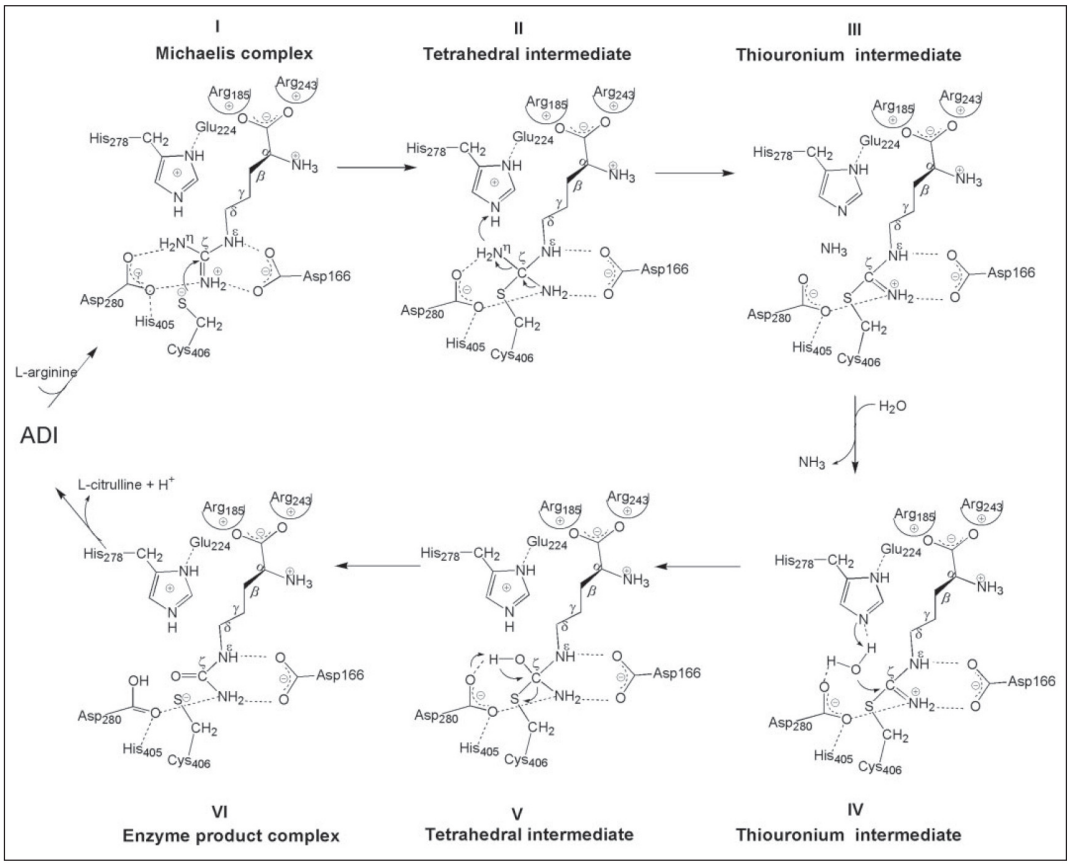

Figure 5. Mechanism of PaADI catalysis of arginine to citrulline and ammonia (17).

1.4 Anti-tumor application of ADI

Amino acids depletion is one type of targeted therapy for human cancers which are auxotrophic for a particular amino acid. Amino acids degrading enzymes, such as asparaginase (30), methioninase (31), arginase (32), arginine deiminase (27), phenylalanine ammonialyase (33) and tryptophanase (34) have been

studied for inhibition of tumor cells *in vitro*. The most representative anticancer enzyme is asparaginase, which is particularly effective in acute lymphoblastic leukaemia. PEG asparaginase is commercialized for acute lymphoblastic leukaemia treatment (Oncaspar®, pegaspargase) (35). However, asparaginase treatment is sometimes accompanied by serous side-effects including anaphylactic shock, coagulapathies as well as liver and pancreatic toxicity (36).

Arginine is an important amino acid involved in the synthesis of a wide range of peptides and proteins, production of creatine and nitric oxide, and a myriad of metabolic pathways and cellular events. It is a precursor of proline, polyamines, glutamine, glutamate, and other neurotransmitters, such as g-aminobutyric acid and also serves as a substrate for two important enzymes, arginase and nitric oxide synthetase (37). Arginine is an indispensable amino acid to children but a semi-essential amino acid in adult humans since many adult somatic cells can synthesize it from citrulline in two steps via urea cycles (Figure 6). The enzyme argininosuccinate synthetase (ASS) catalyzes the conversion of citrulline and aspartic acid to argininosuccinate which is then further converted to arginine and fumaric acid by argininosuccinate lyase (ASL). Arginine can be degraded to ornithine by the urea cycle enzyme arginase. Ornithine is then converted back to citrulline by ornithine carbamoyl transferase (OTC) and then recycles back to arginine from citrulline by ASS/ASL. Thus, the ability to regenerate arginine from citrulline depends on the amount/activity of ASS and ASL, which are tightly coupled. The sensitivity of cells to arginine deprivation depends on the ability of ASS and ASL to regenerate arginine from the alternative intermediate (ornithine, citrulline and argininosuccinate) in the urea cycle.

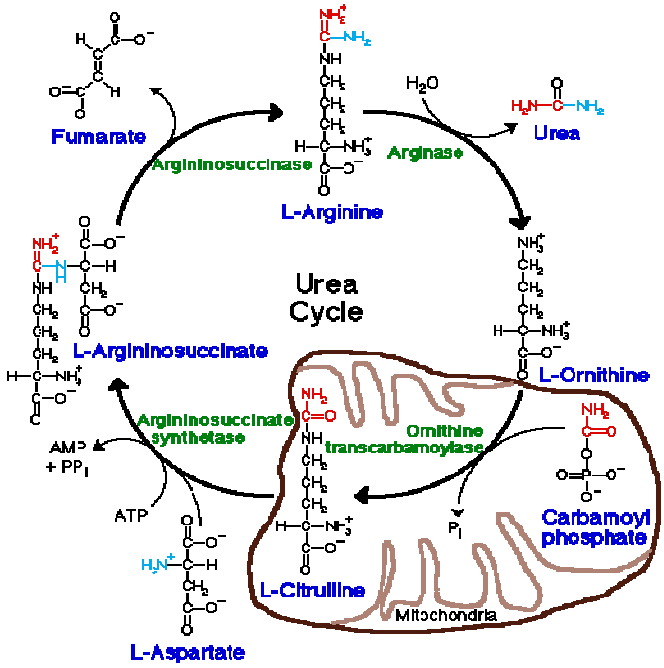

Firgure 6. Urea cycle. Argininosuccinate synthetase (ASS) catalyzes the conversion of citrulline and aspartic acid to argininosuccinate which is then further converted to arginine and fumaric acid by argininosuccinate lyase (ASL). Arginine can be degraded to ornithine by the urea cycle enzyme arginase. Ornithine is then converted back to citrulline by ornithine carbamoyl transferase (OTC) and then recycles back to arginine from citrulline by ASS/ASL.

Arginine begins to become limiting at ~10^{-4} M, whereas other amino acids can sustain growth at 10^{-5}-10^{-6} M. Wheatley et al. showed that most tumour cell lines die considerably more quickly during arginine deprivation than in the absence of any other single (or group of) essential amino acids (38). Since 1930 for the first time arginine known is essential for the growth of some forms of cancer, the potential of arginine degrading enzymes as therapeutic agents was recognized, investigated and employed for arginine auxotrophic tumor treatments. Enzymes capable of depleting arginine *in vitro* include arginase existing in human liver, arginine decarboxylase from bacterial, plant and human, and ADI from microorganism.

Arginine decarboxylase converts arginine to agmatine, which is toxic at high plasma concentration. Furthermore, arginine decarboxylase has a short half-life and it loses virtually all enzymatic activities upon pegylation though pegylation of

arginine decarboxylase is inefficient because not enough lysine residues for polyethylene glycol to attach (39).

Arginase is limited for anti-tumor application because of its low substrate affinity (K_m value 2-4 mM; plasma arginine 100-120 μM), short circulatory half-life (10-15 min) and sub-optimal enzymatic activity at physiological pH (alkaline pH optimum, pH 9.3)(40). Despite these disadvantages of arginase, Lam et al. reported remission of hepatocellular carcinoma induced by systemic release of endogenous hepatic arginase (41) and Leung et al. proved pegylated recombinant human arginase (rhArg-peg 5,000mw) can inhibit ASS-positive HCCs while ADI can not (42).

In addition, ADI, another arginine-degrading microbial enzyme, has various biological activities including anti-proliferation, anti-angiogenesis and inhibition of inducible nitric oxide synthase (iNOs). Figure 7 summarizes how ADI affect many arginine-related cellular functions. ADIs (Table 1) have been shown to have strong *in vitro* and *in vivo* inhibition for arginine auxotrophic tumors (e.g. hepatocellular carcinomas (HCCs), melanomas, retinoblastoma (43), prostate cancer(44)) and ADI from *M. hominis* (MhADI) is currently under clinical trial for HCC (phase II) (45) and melanomas (phase I/II) (46). Studies on human lymphatic leukemia cell lines confirmed ADI's anti-angiogenic activity. Among all the ADIs, MhADI and MaADI were studied most intensively (Table 1).

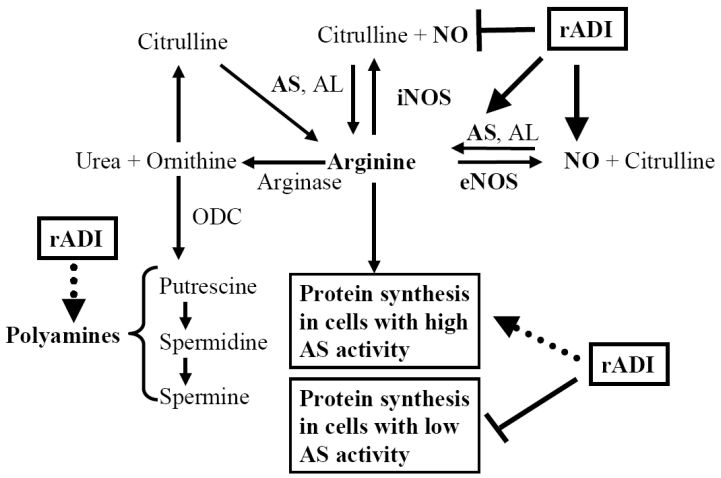

Firgure 7. Summary of ADI effects on arginine-related cellular functions. rADI inhibits NO production via iNOS, but potentiates NO production via eNOS in the cultured endothelial cell model. rADI enhances or inhibits AS activity in different cells. rADI inhibits de novo protein synthesis in cells with low AS activity, but not in cells with high AS activity. Polyamine synthesis was not significantly affected by rADI, even in cells with low AS activity. Arrow representation: solid, potentiates; blocked, inhibits; dotted, no effect (47).

In 1999, US Food and Drug Administration (FDA) designated ADI-PEG-20 orphan drug status for treating HCC and invasive malignant melanomas. In 2005, also the European Agency for the Evaluation of Medicinal Products (EMEA) also granted ADI-PEG-20 orphan drug status for HCC. Phase II trials of ADI-PEG-20 in patients with metastatic hepatocellular carcinomas have shown that the drug is safe, well tolerated, and may benefit patients with unresectable HCC. Izzo and coworker suspected that combination therapies of arginine deprivation and growth inhibition via kinase inhibitors might improve the survival rate further. Additionally, ADI enhances radio sensitivity of human mammary adenocarcinoma (MCF-7 cells) (48), exerts anti-proliferative as well as anti-angiogenic activities and inhibits the growth of viruses such as HIV-1 and hepatitis (49, 50). Current research efforts are focused on ADI's *in vivo* inhibitory effect towards leukemia, melanoma, prostate cancer, renal cell carcinoma, and human umbilical vein endothelial cells (HUVEC) (19, 44, 51-53), clinical trials for HCC (phase II) (45) and melanoma (phase I/II) (46), and tumor inhibitory mechanisms of ADI (54).

The effectiveness of ADIs as anti-tumor agent depends on their enzymatic properties (such as K_m, k_{cat}, optimum pH, stability at neutral pH), selectivity on tumor cells, stability in blood circulation and immunogenicity. Pegylation (35) has been effective in reducing their immunogenicity in animal and increase their stability to various hydrolytic enzymes in plasma. Directed evolution as powerful algorithm to design proteins allows improving all properties that can be reflected in a screening system through iterative rounds of diversity generation and screening. Small libraries of a few thousand variants are often sufficient to find improved variants (55) even without rational understanding of the targeted property. The first example of directed ADI evolution by our group (3) provides a simple and effective screening system to improve activity of PpADI at physiological pH.

1.5 Conclusion

ADI-based arginine deprivation is a novel and promising targeted approach to the treatment arginine auxotrophic tumors, in particular, melanoma, hepatocellular carcinoma and leukemia. Certain mesotheliomas and renal cell cancers were also proved to be sensitive to ADI therapy. Due to its low incidence of major side effects (myelosuppression and gastrointestinal toxicity or other major organ toxicity) arginine deprivation treatment should be combined with other anticancer treatments to increase the response rate. Reengineering of ADI by protein engineering is a promising strayegy to tailor ADI properties for demands in medical applications. Solved ADI crystal structure enables to understand structure function relationships and to guide protein engineering.

Directed evolution

2.1 Introduction to directed evolution

Enzymes are increasingly being used in the generation of products that are traditionally made using chemical synthesis and the field continues to expand its horizons, particularly as applied to the synthesis of the fine chemicals and pharmaceuticals (56, 57). Naturally occurring enzymes are often not designed for the applications of interest, since after all they are evolved in nature for a purpose other than being the catalysts of industrial processes. Directed evolution, rational design and biodiversity screening and combined approches are the main strategies to reengineer enzymes for addressing application demands. Directed evolution has emerged as a powerful enabling method for improving enzyme properties in iterative cycles of diversity generation and screening (Figure 1).

A main advantage of directed evolution compared to rational design is that it does not require structural or mechanistic information for protein optimization. Directed protein evolution has been successfully used for altering and improving protein properties (solubility, expression, enantioselectivity, stability and activity in unusual environment, allosteric interactions, tolerance to pH), as well as for regulating other molecules and systems, including RNA, DNA regulatory elements, biosynthetic pathways and genetic regulatory circuits (58-60).

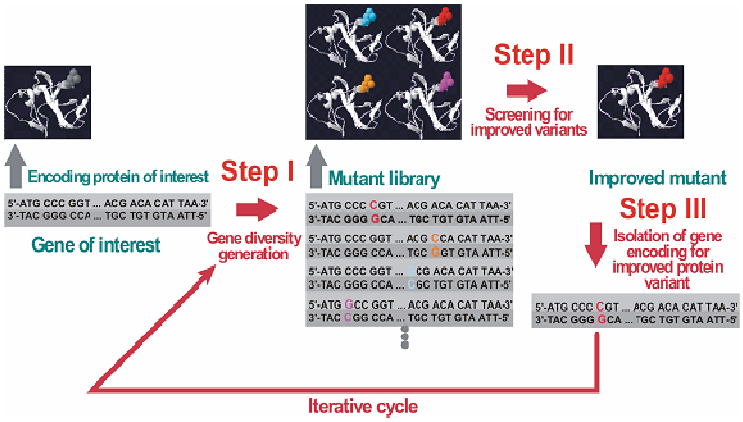

Figure 1. Procedure of a directed evolution experiment. It involves three key steps: 1) selection a good starting sequence and mutating the parent to create a library of variants; 2) identification variants with improved function and 3) isolation of gene encoding for improved variant and repeating the process until the desired function is achieved.

A parent sequence (or sequences) is chosen based on its perceived proximity to the desired function and its evolvability (the ability of a protein to adapt in response to mutation and selective pressure). A parent protein for directed evolution should exhibit enough of the desired function that small improvements can be reliably discerned in a high-throughput screen.

Variants library should be generated with high probability of finding improved variants given the screening capacity. With a high-throughput screening method, a library can be constructed to generate the large potential improvement. Arnold and coworkers(61) showed that very low mutation rates result in many functional sequences but only a small number are unique sequences, however very high mutation rates produce diverse sequences but few retain function. Schwaneberg and coworkers(62) reviewed random mutagenesis methods, focused library generation methods and computational tools for high-quality mutant libraries generation. Schwaneberg and coworkers (63) also summarized criteria for an ideal mutagenesis methods: unbiased mutational spectrum, controllable mutation frequency, consecutive nucleotide substitutions or codon-based substitutions, enable subset mutagenesis (e.g. introduction mainly positively or negatively charged amino acid), independent of gene length, technically simple and reproducible, and economical.

Screening is used to identify library members improved in the targeted property. Identification of improved variants though selection or screening is “analogous” to evolutionary pressure in natural evolution (i.e. only the fittest survive). As the word “directed” in directed evolution implies, laboratory evolutionary pressure is defined and applied by the researcher in screening system. Gradually increasing the selection pressure or evolving against a series of intermediate challenges often accumulates useful single mutations and yields desired variants (64).

Traditional methods for screening employ microtiter plate formats (96-well, 384-well, 1,536-well (65) and even 1,000,000-well (66)) or solid phase assay (agar plate, filter paper and nitrocellulose membrane), which typically enable the screening of no more than 10^6 variants by using robotic automation (67). Sometimes, fast and universal analytic methods like HPLC (68) or GC-MS (69) are utilized for performing an efficient screen of a non-natural substrate. However, the number of screened mutants is limited to 10^4-10^6. In recent years flow cytometry systems (67, 70, 71) have become increasingly attractive, especially after the development of emulsion technology offering compartmentalization and high throughput up to 10^7/h. In addition, Weitz and coworkers (72) recently reported a promising ultrahigh-throughput screening in drop-based microfluidics, by which one can screen a library of 10^8 in about 10 h. Dijkhuizen et al. compared in a review (73) six kinds of library screening strategies (Figure 2). Selection techniques rely on a direct link between cell growth and improved or acquired enzyme function and therefore it is limited to engineering detoxifying enzymes (e.g. b-lactamase) or enzymes that synthesize essential nutrients for cell growth and survival. The traditional microtiter plate screenings are medium-throughput and the most simplistic format of screening. It involves the incubation of colonies with the substrate of targeted enzyme. The crucial factor with this screening technique is that substrate conversion creates a visual signal, such as fluorescence or color, to identify colonies expressing an enzyme with desirable properties. Microtiter plate based screenings are the most commonly applied method in identifying desirable enzyme variants. Microtiter plate based

screenings enable the use of various analytical tools and in the mean while they offer a great dynamic range. Their screening capacity is usually limited to less than 10^4 variants per day. Screening based on microfluidic device and sorting device is a new screening platform for directed evolution, which offers ultra-high-throughput. It allows the discriminate between wild-type and a less active mutant and allows for the addition of substrates and quenchers at desired time thus extending the scope of directed evolution screening strategies. Cell as micro-rector, cell surface display and *in vitro* compartmentalization technology are also FACS (fluorescence-activated cell sorting system) dependent methods for high-throughput screening and allow 10^9-10^{10} screening capacity.

Once improved enzymes are identified, encoding genes are isolated and subjected to further iterative cycles of mutation and screening in order to accumulate beneficial mutations until the targeted improvement is hopefully achieved. The number of iterations required depends on the starting point, the protein fold and the selected properties which determine the possible mutational load and achievable improvement.

Four accepted requirements for successful directed evolution (http://www.che.caltech.edu/groups/fha/) are, 1) the desired function must be physically possible; 2) the function must also be biologically, or evolutionarily, feasible. In practice, this means that there exists a mutational pathway to get from here to there through ever-improving variants (see above). A good experiment will maximize the likelihood; 3) Suitable host (*E. coli* or *S. cerevisiae*) which allows functional expression of more than 10^6 variants per µg of DNA. 4) A rapid screen or selection that reflects the desired function. How rapid the screen must be depends on how rare mutations leading to the desired property are and how many must be accumulated to achieve the desired result.

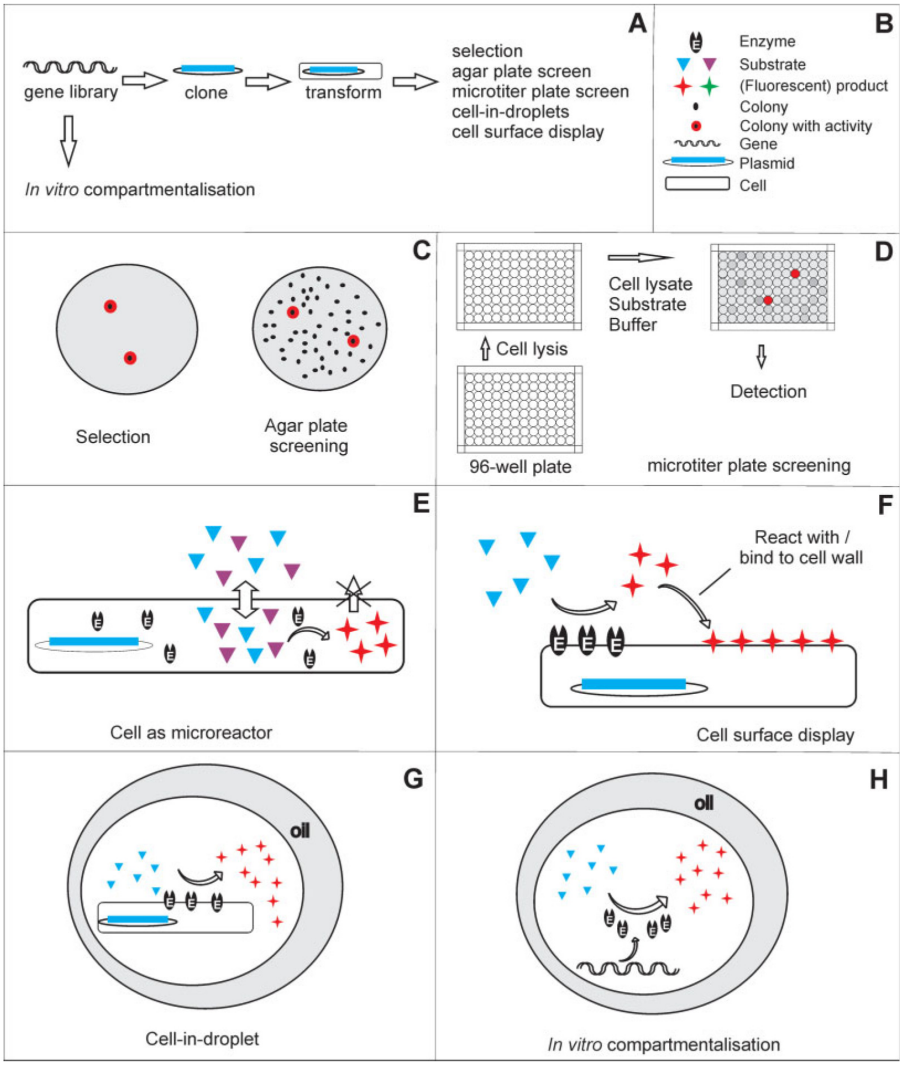

Comparison of screening and selection technologies

Strategy	Library size	Advantage	Disadvantage
Selection	$\sim 10^9$	Yields desirable variants only	Only possible if activity gives growth advantage
Agar plate screen	$\sim 10^5$	Simple to operate	Limited dynamic range
Microtiter plate screen	$\sim 10^4$	All analytical methods possible Excellent dynamic range	Relatively low screening capacity
Cell-in-droplet screen	$\sim 10^9$	Large libraries	Fluorescence detection and DNA modifying enzymes only
Cell as microreactor	$\sim 10^9$	Large libraries	Fluorescence detection only
Cell surface display	$\sim 10^9$	Large libraries	Fluorescence detection only
In vitro compartmentalization	$\sim 10^{10}$	No cloning steps Large libraries	Fluorescence detection and DNA modifying enzymes only

Figure 2. Overview of screening technologies. (A) Experimental steps from obtaining the gene library as PCR product to the actual screen. Note that cloning and transformation efficiency are often limiting library size; (B) Explanation of symbols; (C) Cell growth/survival selection and agar plate screening; (D) Microtiter plate screening; (E) Cell as micro-reactor; (F) Cell surface display; (G) Cell-in-droplet; and (H) *In vitro* compartmentalization (73).

2.2 Directed enzyme evolution for pH tolerance of enzymes

Application of enzymes in processes at a specified pH necessitates protein engineering to change their pH performance. Directed evolution and rational design method were applied to improve enzyme specific activity at certain pH or shift their pH profiles. Some representative success stories of directed protein evolution improving pH performance are summarized in Table 1.

Table 1. Improvement obtained from directed evolution or rational design for pH performance.

Enzymes	Mutagenesis methods	Screening methods	Improvements	References
Human β-glucuronidase	EpPCR and saturation mutagenesis	Flow cytometry	60-fold more active (k_{cat}/K_m) at pH 7.0 and were up to an order of magnitude more effective at catalyzing the conversion of two structurally disparate glucuronide prodrugs to anticancer agents	2008 (74)
Bacterial xylanase	DNA shuffling	Agar plate assay	About 5-fold improvement of specific activity at pH 9.0	2008 (75)
Human pancreatic lipase	EpPCR	Agar plate and microtiter plate assay	1.5-fold of activity improvement at acidic pH	2010 (76)
Bacterial arginine deiminase	EpPCR and site directed mutagenesis	Microtiter plate assay	pH optimum shifted from pH 6.5 to pH 7; 4-fold of activity improvement at pH 7.4	2010 (3)
Bacterial α-amylase	EpPCR	Microtiter plate assay	5-fold higher activity at pH 10 than wild type	2003 (77)
Eukaryote D-pantonohydrolase	EpPCR and DNA shuffling	Agar plate assay	10.5-fold higher specific activity and retain 85% of its original activity after incubation under low pH	2006 (78)
Vanadium chloroperoxidase	EpPCR, site saturation mutagenesis and site directed mutagenesis	Microtiter plate assay	About 100-fold improvement of specific activity at pH 8	2006 (79)
Bacterial class-A non-specific acid phosphatase (PhoN)	Site directed mutagenesis		1.6-fold of activity improvement over broder pH range	2006 (80)
Aspergillus niger PhyA phytase	Site directed mutagenesis		pH shifted from 5.5 to 3.8 (1.7 unit); 2.66 -fold improvement of activity at pH 3.5 than wild type.	2006 (81)
Bacillus cereus β-amylase	Site directed mutagenesis		pH optimum shifted to pH 4.2-4.8 by 2 pH units.	2004 (82)
Phytase	Site directed mutagenesis		pH optimum shifted by 0.5-1 pH unit; a slight increase in maximum specific activity	2002 (83)
Alcohol dehydrogenase	Site directed mutagenesis		pH optimum shifted from 7.8 to 9.0; about 2-fold improvement of maximum activity at pH 9.0 than that of wild type	1991 (84)

Many examples of rational reengineering of an enzyme pH optimum exist (Table 1). For shifting the pH optimum, a deep understanding of molecular dynamics is essential part of understanding enzyme flexibility. Rational design method successfully shifted enzyme pH profile. pH dependence of an enzyme is determined by the ionization of the catalytic groups, which is affected by various interactions involved in their microenvironments. In order to catalyze certain reactions, ionizable residues in active site should act as nucleophile or acid/base catalyst and they need to maintain proper ionization state for proper activities of proteins. The p*K*a value of the proton donor and the catalytic nucleophilic residue are therefore limiting the pH range at which the enzyme can function, and therefore pH-dependent activity can be differed by the p*K*a of the key residues. The p*K*a value of the residue is governed by intrinsic acidity of the functional group and other factors (electrostatic interaction from neighboring and the heterogeneous dielectric environment in the protein solution system). The electrostatic potential generated by the charged titratable residues affects the ground state of the protein, such as stability, binding to ligands and p*K*a values of ionizable groups. The electrostatic potential of proteins can be calculated by using computational procedures (Delphi, UHBD, CHARMM) and can be increased or decreased through mutations. For shifting the pH optimum of enzymes, many researchers have tried to substitute catalytic residue by site-directed mutagenesis (Table 1).

Yoo and coworkers (85) analyzed the relation between the shift of pH optimum and change in electrostatic potential due to mutation using Delphi. They identified key residues of xylanase responsible for electrostatic potential of catalytic residues but not affecting the catalysis directly. The latter hypothesis was proven by site directed mutagenesis in a later report. Wyss and coworkers (83) summarized strategies for enzyme pH profile modification, 1) replacement of ionizable groups that are directly involved in substrate or product binding and/or catalysis by nonionizable ones or by amino acids with different charge or p*K*a values; 2) replacement of residues that are in direct contact with residues

mentioned in 1) by forming hydrogen bonds and/or salt bridges; 3) alteration of longer-range (indirect) charge-charge interactions by modification of the surface charge of the enzyme.

When there is no structure-function relationship information available for an enzyme, directed evolution is the best option to tailor the pH performance of enzyme for application demands (Table 1). Directed evolution allows improving all properties that can be reflected in a screening system through iterative rounds of diversity generation and screening. Small libraries of a few thousand variants are often sufficient to find improved muteins even without rational understanding of the targeted property (76, 86). Using MTP assay, epPCR mutant libraries with a ratio of 50 % active and 50 % inactive clones have often been used successfully in directed evolution, improving enzyme properties by gradual changes (one or two amino acids changes per round of mutagenesis and screening).

2.3 Directed enzyme evolution for medical application

Directed evolution has been very useful for improving enzymes for industrial needs. In recent years, there is also growing number of enzymes applied for therapeutic purpose. For the development of protein therapeutics, directed evolution started to be used to tailor enzyme properties in medical field, for example drug delivery (87, 88) and has proven to be a useful tool for generating protein variants with enhanced therapeutic potential (88), for example, improving the effectiveness of therapeutic enzymes, antibodies, vaccines and viruses. Here, the improvements of therapeutic protein for anti-tumor application by directed evolution are discussed in more details.

2.3.1 Prodrug enzymes for tumor chemotherapy

Prodrug cancer chemotherapy has attracted considerable interest due to the possibilities it provids to overcome various barriers to drug formulation and delivery (such as poor aqueous solubility, chemical instability, insufficient oral

adsorption, rapid pre-systemic metabolism, inadequate brain penetration, toxicity and local irritation) (89). Examples of such drugs currently in use in cancer treatment include 5-fluorocytosine, cyclophosphamide, capecitabine, mitomycin C, and AQ4N (90). However, the side effects of prodrug therapy remain a serious concern which arises from the fact that noncancerous cells also possess the capacity to degrade them. This has triggered the interest to generate more effective prodrug-activating enzymes so that prodrugs can kill tumor cells at concentrations that generate little or no side effects. Further goals are to design more powerful and tumor-specific drugs, and to devise more effective methods for delivering them specifically to tumors.

By applying directed evolution through the technique of error-prone PCR, Martin and coworkers (90) indentified YieF variant exhibiting >5-fold increased capacity to kill HeLa cells. Furthermore, YieF variant was proved to be effectively delivered to tumor cells using a strain of *Salmonella typhimurium* (SL 7838).

Human β-glucuronidase, due to low intrinsic immunogenicity in humans, is an attractive enzyme for tumor-specific prodrug activation. However its utility is limited by low activity at physiological pH. Roffler and coworkers (74) developed a high-throughput screening procedure for enzymatic activity based on the stable retention of fluorescent reaction product in mammalian cells expressing properly folded glycoproteins on their surface. This procedure was utilized to screen error-prone PCR and saturation mutagenesis libraries to isolate β-glucuronidase tetramers that were up to 60-fold more active (k_{cat}/K_m) at pH 7.0 and were up to one order of magnitude more effective at catalyzing the conversion of two structurally disparate glucuronide prodrugs to anticancer agents.

2.3.2 Oncolytic viruses for tumor chemotherapy

Viral-mediated oncolysis is a novel cancer therapeutic approach with the potential to be more effective and less toxic than current therapies due to the agents' selective growth and amplification in tumor cells. To date, these agents

have been regarded as highly safe in patients but have generally fallen short of their expected therapeutic value as monotherapies.

Consequently, new approaches to generate highly potent oncolytic viruses are required. For the latter purpose, Hermiston and coworkers (91) developed a new method and termed it also ‘‘Directed Evolution’’ for creating highly potent oncolytic viruses. Viral serotypes representing Ad subgroups B-F were pooled and passaged twice on sub-confluent cultures of the target tumor cell lines at a particle-per-cell ratio of approximately 200 to invite recombination between serotypes (Figure 3). Supernatants from the second round of the high viral particle-per-cell infection of sub-confluent cultures were then used in a 10-fold dilution series to infect confluent T-75 tissue culture flasks of target tumor cell lines PC-3, HT-29, Panc-1 and MDA-231. Using this ‘‘Directed Evolution’’ methodology, the novel generated chimeric oncolytic virus ColoAd1 demonstrated ~ 2 log increase in both potency and selectivity when compared to ONYX-015 on colon cancer cells. *In vivo* and *ex vivo* studies therefore validated the innovative general approach for deriving clinically-relevant and potent anti-cancer virotherapies.

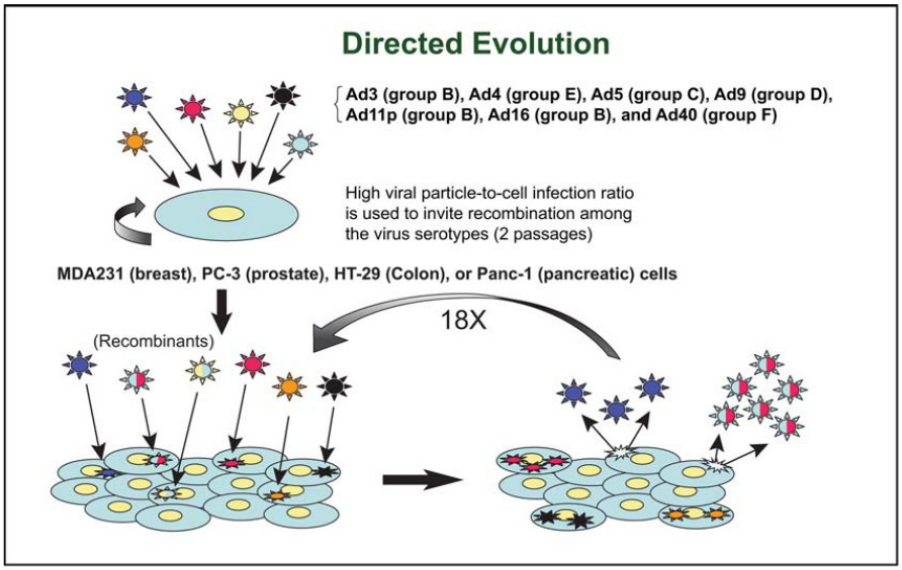

Figure 3. Hermiston’s “Directed Evolution” process of viruses and derivative viral pools (91).

2.3.3 Amino acid depriving enzyme for anti-tumor applications

Naturally available enzymes are usually not optimally suited for therapeutic purposes. This incompatibility often relates to the stability or activity of the enzymes under body conditions.

Despite many successful efforts to broaden the understanding of the structural basis of protein stability, there is still no universal strategy to stabilize protein by a limited number of rationally designed mutations. Well-known and reasonably successful types of rational engineering work include substitutions that increase rigidity (e.g. substitute amino acid Xxx with Pro or substitute Gly with other amino acid Xxx or the introduction of disulfides). These substitutions have effects on the entropy of the unfolded state, improvement of molecular packing (e.g. shortening of loops, improvement of interactions in the hydrophobic core, for example, by the removal of internal cavities), modification of surface charge networks or reinforcement of a higher oligomerization state.

Directed evolution provides a powerful approach for improving thermostability and does not need understanding of structure-function relationship. Most strategies for screening for enzyme stability rely on measuring residual enzyme activity before and after exposure to a denaturing challenge (e.g. high temperature, organic solvents, extreme pH) (92).

Bacterial L-asparaginases have been used as therapeutic agents in the treatment of lymphoblastic leukaemia. The main restrictions to the therapeutic use of L-asparaginase include its premature inactivation. As a result frequent injections are required to maintain therapeutic levels. Repeated injections and high dose can cause several types of side reactions from mild allergies and the development of immune responses to dangerous anaphylactic shocks (93). Enhancing the stability of L-asparaginase by protein engineering improves its body-residence time, and thereby minimizes immunosuppressive effects by lowering the therapeutic dose. Labrou and coworkers (94) obtained a

reengineered L-asparaginase with enhanced thermal stability. Single mutation on the surface of the protein resulted in ~10 degree increased T_m value (half-inactivation temperature). The thermostable variant has to be tested further on animals and/or humans in order to be advanced to a potent therapeutic drug.

Another example of a reengineered amino acid-deprivating enzyme is PpADI. PpADI is a promising anti-tumor enzyme however with a non-physiological optimal pH and relative high K_m value which hindering its medical application. By directed evolution and site saturation mutagenesis, PpADI variants with higher activity at physiological pH and at low arginine concentration of were obtained with improved properties to become a potent anti-tumor drug (see chapter 3 and chapter 4). *In vitro* and *in vivo* test of the improved variants are required to evaluate the anti-tumor effectiveness.

2.3.4 Affibody molecules for cancer prognosis

Affibody molecules represent a new class of affinity proteins that are based on the Z-domain scaffold derived from staphylococcal protein A (95). Among the scaffold proteins, Affibody molecules constitute the smallest non-cysteine-containing protein scaffold. The small size (~ 7 kDa), robust structure, and straightforward production procedures (either by recombinant production in bacteria or by chemical synthesis) make Affibody molecules attractive targeting agents for *in vivo* radionuclide imaging (96) as well as for various biotechnological applications (97, 98). The small size offers a convenient affinity maturation principle. Gene synthesis allows randomizing the whole gene to generate diverse mutant library. The potential use of radiolabeled Affibody molecules for high-contrast radionuclide imaging of biomarkers has been demonstrated in preclinical studies and in pilot clinical studies. Affibody molecules are non-immunoglobulin-derived affinity proteins based on a three-helical bundle protein domain.

Several of affinity proteins have been investigated for both *in vivo* diagnostics and therapy of tumor in radionuclide molecular imaging. Affinity proteins in tumor-targeted therapy can affect tumor progression by altering signal transduction or by delivering a payload of toxin, drug or radionuclide. EGFR (epidermal growth factor receptor), one of the receptor in ErbB family, has been extensively studied as biomarkers in tumor targeting and over expressed in various malignancies, associated with poor patient prognosis and are therefore interesting targets for solid tumors. High affinity and especially slow dissociation rate are important for obtaining high contrast images. Affinity in the low nanomolar range is considered as a prerequisite for successful use of peptide-based tracers.

Ståhl and coworkers (99) described the affinity maturation procedure for the generation of Affibody molecules binding with high affinity and specificity to EGFR. The library for affinity maturation was constructed using a single oligonucleotide for the rerandomization of desired positions. The new binders were selected with phage display technology and the best second-generation binders were characterized *in vitro* using real-time biospecific interaction analysis (BIA) for their binding to recombinant EGFR and with flow cytometry for their binding to native EGFR. Second-generation binders achieved an approximately 30-fold improvement in affinity (K_d = 5-10 nM) for the soluble extracellular domain of EGFR in biospecific interaction analysis using Biacore.

2.3.5 Interferon for anti-tumor applicaiton

Alpha interferons (IFN-as) are members of the diverse helical-bundle superfamily of cytokine genes, which have potent antiviral and antiproliferative activities and therefore can be used as anticancer and antiviral agents. However, doselimiting toxicity, receptor cross-reactivity, and short serum half-lives significantly reduce the clinical use of many of these cytokines.

Patten and coworkers (100) performed a family shuffling experiment with over 20 human interferon-α (Hu-IFN-α) genes. Antiviral assay and proliferation assay

were used to indentify clones with improved activity on Hu-IFN-α receptor. One clone showed 285,000-fold improved activity relative to Hu-IFN-α2a and 185-fold relative to Hu-IFN-α1 (most active native human interferon).

Selective breeding using DNA shuffling has proved to be very effective method to rapidly improve pharmaceutical proteins by which initially have low levels of the desired “activity” (101, 102). Backcrossing of evolved recommbinants with the wild type genes removes functionally neutral changes, which might reduce the immunogenicity of evolved proteins (103).

2.4 Conclusion

Proteins, especially enzymes, have gained a central role in modern chemical, biotechnological, and biopharmaceutical industries. Directed evolution has over the past proved to be a versatile and successful approach for tailoring protein properties to industrial, agricultural and medical demands and for advancing our understanding of structure-function relationships in biocatalysts. Appropriate library generation and screening methods should be employed concerning the target protein and desired property. To set up a sophisticated screening method, complex conditions in human body (pH, ion concentration, proteases, hormones etc.) should be considered. Subsequent *in vivo* or *in vitro* test of improved variants should be carried out to further validate the screening assay. Development of diversity generation and high-throughput screening method will enable evolution to solve problems efficiently. Especially, directed evolution provides a powerful strategy to rapidly advance the development of improved protein-based drugs (enzymes and antibodies, peptide and ligands). Directed evolution promises to play an increasingly important role to generate “desirable” drugs.

Chapter 3. Directed evolution of Arginine deiminase for increased activity at physiological pH

3. 1 Abstract

Arginine deiminase (ADI; EC 3.5.3.6) has been studied as a potential anti-tumor drug for the treatment of arginine-auxotrophic tumors, such as hepatocellular carcinomas (HCCs) and melanomas. Studies with human lymphatic leukemia cell lines confirmed that ADI is a potential anti-angiogenic agent effective in the treatment of leukemia. ADI from *Pseudomonas plecoglossicida* (PpADI) was cloned and expressed in *E.coli*. A main limitation of PpADI lies in its pH-dependent activity profile with a pH optimum at 6.5. A pH shift from 6.5 to 7.5 results in ~80 % activity drop (pH of human plasma is 7.35 to 7.45). For shifting PpADI pH optimum to netrual pH, a directed evolution protocol based on an adapted citrulline screening protocol in microtiter plate (MTP) format was developed and validated. Proof of concept for ADI engineering resulted in a pH optimum of pH 7.0 and increased activity under physiological conditions: at pH 7.4, variant M2 (K5T, D44E and H404R) is 4-fold more active than the wild type PpADI and retains ~30 % of its activity relative to its pH optimum, compared to ~10 % in the case of the wild type PpADI.

3.2 Introduction

Arginine deiminase (ADI) is a potential cancer therapy agent for the treatment of arginine-auxotrophic tumors (e.g. hepatocellular carcinomas and melanomas). The hepatocellular carcinoma (HCC) accounts annually for approximately 1 million new cases worldwide. In the US the incidence rate (per 100,000 persons; 1992-2002) of HCC is 8.6 with a mortality rate of 6.5 due to low responses of hepatoma to chemotherapeutic treatments (27). Current research efforts are

focused on ADI's *in vivo* inhibitory effect towards HCCs, leukemia, melanomas and human umbilical vein endothelial cells (HUVEC) (104-106), clinical trials for HCC (phase III) and melanoma (phase I/II) (105, 107), and PEG formulation of ADI to improve its efficacy as a clinical drug, including serum half-life and antigenicity (16, 108). ADI inhibited the growth of cultured leukemia cells at concentrations of 5-10 ng/ml, which were about 20-100 times lower than those of the L-asparaginase standard resulting in fewer side effects (106, 109). Arginine deprivation is speculated to be the molecular reason for ADI's inhibitory effect on human lymphatic leukemia (106). ADIs catalyze the first step of the arginine deiminase (ADI) pathway by hydrolyzing arginine to citrulline and ammonium. Several ADI genes have been identified, purified, and characterized from bacteria, archaea and some eukaryotes excluding mammalian cells and summarized in a recent review (27). None of these ADIs is from a kinetic point of view ideally suited for *in vivo* applications in humans under physiological conditions.

Protein engineering by rational design and directed evolution offers opportunities to tailor ADI properties to physiological conditions. For the proof of concept, an ADI isolated from *Pseudomonas plecoglossicida* CGMCC2039 (accession number: ABS70718) which can be functionally expressed in *E. coli* has been employed. Directed evolution approaches employ mainly *E. coli* as host due to its fast growth and high transformation efficiency which is a prerequisite for generating complex mutant libraries. Over the last decades, directed protein evolution has become a versatile and successful approach for tailoring protein properties for industrial demands (mainly in chemical synthesis) and for advancing our understanding of structure-function relationships in enzymes. A directed evolution experiment comprises iterative cycles of diversity generation and functional selection for improved variants. Only a few manuscripts for phytases (83), xylanases (110), amylases (77, 82, 111), and an alcohol deyhdrogenase (112) reported a shift of pH optima using directed evolution algorithms. None of these directed evolution campaigns targeted a medical

application and arginine deiminase has to our best knowledge not been altered in its pH activity/resistance by directed evolution.

Comparison of PaADI (*Pseudomonas aeruginosa*, pH optimum 5.6; His405) and MaADI (*Mycoplasma arginini* ADI, pH optimum 6.5, Arg397) led to the speculation that substitution of His by Arg might contribute to MaADI's increased pH optimum (17). A sequence alignment of four ADIs (MaADI, MyADI (*Mycoplasma arthritidis* ADI), PaADI and PpADI) shows that for both Pseudomonas ADIs the synonymous amino acid positions (404 & 405), contain a His whereas both Mycoplasma ADIs contain at corresponding positions an Arg. Interestingly, both Mycoplasma ADIs have an pH optimum approximately one pH unit higher than both Pseudomonas ADIs.

In this study we report the first directed ADI evolution protocol in which the pH profile of PpADI was shifted to higher pH values representing a conceptional proof that ADI properties can be tailored for demands *in vivo* treatment of arginine-auxotrophic tumors. An emphasis is given on detailed description of directed evolution conditions (mutagenic and screening).

3.3 Materials and methods

3.3.1 Materials

All chemicals were of analytical-reagent grade or higher quality and were purchased from Fluka (Neu-Ulm, Germany), Sigma-Aldrich (Steinheim, Germany) and Applichem (Darmstadt, Germany), except the resins for purification (TOSOH, Stuttgart, Germany). All enzymes were purchased from New England Biolabs (Frankfurt, Germany), Fermentas (St. Leon-Rt, Germany), and Sigma-Aldrich Chemie (Taufkirchen, Germany), unless stated otherwise.

Thermal cycler (Mastercyler gradient; Eppendorf, Hamburg, Germany) and thin-wall PCR tubes (Multi-ultra tubes; 0.2 µl; Carl Roth, Germany) were used in all PCRs. The PCR volume was always 50 µl except for Megaprimer PCR of whole

plasmid (MEGAWHOP, 20 µl); larger volumes were prepared in multiple 50-µl PCRs. The amount of DNA in cloning experiments was quantified by using a NanoDrop photometer (NanoDrop Technologies, Germany).

Pseudomonas plecoglossicida CGMCC2039 was provided by Professor Zhihao Sun (Jiangnan University, Wuxi, China).

3.3.2 Methods

3.3.2.1 Reagents used in assays

Acid-ferric solution

To dH_2O (600 ml), concentrated H_3PO_4 (70 ml, 85 %) and concentrated H_2SO_4 (160 ml, 90-91 %) were added slowly. After cooling to room temperature, $FeCl_3 \cdot 6H_2O$ (10 ml, 10 g/L) was added in the above solution, finally the total volume was adjusted to 1 liter with dH_2O.

Diacetyl monoxime -thiosemicarbazide (DAM-TSC) solution

DAM solution (10 g/L) and TSC solution (0.3 g/L) were prepared separately. The two solutions were mixed (volume ratio = 1:1) just prior to use.

3.3.2.2 Cloning of ADI into pET42b(+)

The arginine deiminase (ADI) gene was amplified from *Pseudomonas plecoglossicida* CGMCC2039 by colony PCR (94℃ for 10 min, 1 cycle; 94℃, 30 s/ 54℃, 30 s/ 72℃, 165 s, 29 cycles; 72℃ for 5 min, 1 cycle) using primer (5'-CCGCATTCCGCTGAAAAACAGAAGTACGG-3' and 5'-CTTCTCGAGTTAGTAGTTGATCGGGTCGCGCACG-3'), 1.5 U of Pfu DNA polymerase, 0.20 mM of dNTP mix and a colony of *Pseudomonas plecoglossicida* CGMCC2039. Amplification product was purified by gel extraction, digested using NdeI (20 U) and XhoI (20 U) and purified using QIAquick PCR purification kit (QIAGEN, Hilden, Germany). Cloning vector pET42b(+) was digested with NdeI (20 U) and XhoI (20 U), and purified by gel extraction kit (QIAGEN, Hilden, Germany). Digested ADI gene and pET42b(+)

were ligated using T4 DNA ligase (1 U) to give pET42b(+)-ADI and transformed into *E. coli* BL21-Gold (DE3).

3.3.2.3 Site directed mutagenesis of PpADI gene at position H404

Site directed mutagenesis of ADI gene was performed according to the published method (113) on plasmid pET42b(+)-ADI. The following oligonucleotides were used for mutagenesis of H404R: 5'-GGCCGTGGCGGCGGCCGTTGCATGACCTGCCCG-3' and 5'-CGGGCAGGTCATGCAACGGCCGCCGCCACGGCC-3' (underlining indicated the substituted nucleotide). For the mutagenic PCR (First stage: 95℃ for 30 s, 1 cycle; 95℃, 30 s/ 55℃, 1 min/ 72℃, 130 s, 3 cycles. Second stage: 95℃ for 30 s, 1 cycle; 95℃, 30 s/ 55℃, 1 min/ 72℃, 130 s, 15 cycles; 68℃ for 30 min, 1 cycle), 2 U of Phusion™ Hot Start DNA polymerase (Finnzymes, Keilaranta, Finland), 0.20 mM of dNTP mix, 25 pmol of each primer together with 100 ng of template (pET42b(+) harboring ADI gene) were used. Following the PCR, DpnI (40 U; New England Biolabs) was added, and incubated overnight at 37℃. The PCR products were purified by using a QIAquick PCR Purification Kit (Qiagen) and transformed into *E. coli* BL21-Gold (DE3) for expression.

3.3.2.4 Site sturation mutagenesis of PpADI gene at nine amino acid position

Site saturation mutagenesis of ADI gene was performed according to the published method (113) on plasmid pET42b(+)-ADI. The oligonucleotides were used for mutagenesis were listed in table 1 (underlining indicated the substituted nucleotide). For the mutagenic PCR (First stage: 95℃ for 30 s, 1 cycle; 95℃, 30 s/ 55℃, 1 min/ 72℃, 130 s, 3 cycles. Second stage: 95℃ for 30 s, 1 cycle; 95℃, 30 s/ 55℃, 1 min/ 72℃, 130 s, 15 cycles; 68℃ for 30 min, 1 cycle), 2 U of Phusion™ Hot Start DNA polymerase (Finnzymes, Keilaranta, Finland), 0.20 mM of dNTP mix, 25 pmol of each primer together with 100 ng of template (pET42b(+) harboring ADI gene) were used. Following the PCR, DpnI (40 U; New England Biolabs) was added, and incubated overnight at 37℃. The PCR products were

purified by using a QIAquick PCR Purification Kit (Qiagen) and transformed into *E. coli* BL21-Gold (DE3) for expression.

Table 1. Primer sequences for site saturation mutagenesis.

Primer name	Sequences
Leu 41 FP	AACTGCGACGAGCTGNNNTTCGACGATGTGATC
Leu 41 RP	GATCACATCG TCGAANNNCA GCTCGTCGCAGTT
Asn 360 FP	TGGGATGACGGCAACAACNNNGTGGCGCTGGAG
Asn 360 RP	CTCCAGCGCC ACCACNNNGT TGCCGTCATCCCA
Arg401 FP	GAACTGGGCCGGGGCNNNGGCGGCGGCCACTGC
Arg401 RP	GCAGTGGCCGCCGCCNNNGCCCCGGCCCAGTTC
Phe163 FP	CTGCCCAACACCCAGNNNACCCGCGACACCACC
Phe163 RP	GGTGGTGTCGCGGGTNNNCTGGGTGTTGGGCAG
Asn160 FP	CTGCCGCCGCTGCCCNNNACCCAGTTCACCCGC
Asn160 RP	GCGGGTGAACTGGGTNNNGGGCAGCGGCGGCAG
Arg185 FP	ATGTACTGGCCGGCNNNCGCCAGGAAACCCTG
Arg185 RP	CAGGGTTTCCTGGCGNNNGCCGGCCAGTACAT
Arg243 FP	ATCGGCATGGGTGAGNNNACCTCGCGCCAGGCC
Arg243 RP	GGCCTGGCGCGAGGTNNNCTCACCCATGCCGAT
His405 FP	GGCCGTGGCGGCGGCNNNTGCATGACCTGCCCG
His405 RP	CGGGCAGGTCATGCANNNGCCGCCGCCACGGCC
Gly403 FP	GCCGGGGCCGTGGCNNNGGCCACTGCATGACC
Gly403 RP	GGTCATGCAGTGGCCNNNGCCACGGCCCCGGCC

3.3.2.5 Construction of PpADI error-prone library

The library was generated by the standard error-prone PCR (epPCR) using improved variant H404R as template. For the mutagenic PCR (95℃ for 2 min, 1 cycle; 95℃, 30 s/ 55℃, 30 s/ 72℃, 30 s, 29 cycles; 72℃ for 3 min, 1 cycle), 2.5 U of Taq DNA polymerase, 0.20 mM of dNTP mix, 50 ng of template (pET42b(+) harboring ADI gene H404R), 0.01-0.1 mM of $MnCl_2$ and 10 pmol of each primer (5'-TACATATGTCCGCTGAAAAACAGAAG-3' and 5'- GTGCTCGAGTTAGTAGT TGATCGG-3') were used. The PCR products were purified by using a QIAquick PCR Purification Kit. The purified epPCR products were cloned into expression

plasmid pET42b(+) by MEGAWHOP(114). For MEGAWHOP (68℃ for 5 min, 1 cycle; 95℃ for 5 min, 1 cycle; 95℃, 1 min/ 55℃, 1 min/ 68℃, 13 min 30 s, 24 cycles; 68℃ for 30 min, 1 cycle), 1 U of Taq DNA polymerase, 0.1 U of Pfu DNA polymerase, 0.20 mM of dNTP mix together with 200 ng of template (pET42b(+) harboring ADI gene H404R) were used. Following the PCR, DpnI (40 U; New England Biolabs) was added, and incubated (4 h; 37℃). The MEGAWHOP products were transformed into *E. coli* BL21-Gold (DE3) for expression and screening.

3.3.2.6 Expression of PpADI in LB media with IPTG induction

The strain *E. coli* BL21-Gold (DE3)/ pET42b-PpADI was cultured at 37℃ in 20 ml of LB media that contained 50 μg/ml kanamycine to an absorbance of 0.6 at 578nm. Then, isopropyl β-D-thio-galactopyranoside (IPTG) was added to a final concentration 0.2 mM. The cells were harvested after 9 h induction with IPTG at 37℃. The expressed rADI was analyzed by SDS-PAGE.

3.3.2.7 Expression of PpADI in auto-induction media

A chemically defined auto-induction medium (115) containing salts and trace metals, vitamins including vitamin B12, and glucose, glycerol, and lactose were test for PpADI expression. Five kinds of auto-induction media LS-5052, P-5052, MD-5052, TYM-5052 and TYP-5052 were tested for the ADI expression, under the following conditions: 20 ml LB media in 100 ml flask, 37℃, 250 rpm, 20 h. The expressed rADI was analyzed by SDS-PAGE.

3.3.2.8 Cultivation and expression of PpADI in 96-well plates

Colonies grown on LB_{kan} agar plates were transferred, by using toothpicks, into 96-well microtiter plates (flat bottom, polystyrene plates; Greiner Bio-One GmbH, Frickenhausen, Germany), containing non-inducing medium LSG (150 μL) (115) supplemented with kanamycin (50 μg/ml). After 16 h of cultivation in a microtiter plate shaker (Multitron II, Infors GmbH, Einsbach, Germany; 37℃, 900 rpm, 70 % humidity), each well was replicated using a replicator (EnzyScreen BV, Leiden,

Netherlands) into a second series of 96-well microtiter plates containing 150 µL of auto-induction media LS-5052 (115) supplemented with kanamycin (50 µg/ml). The first set of plates was stored at -80°C after addition of glycerol. The clones in the second set of plates were cultivated for 12 h (Multitron II, Infors GmbH, 37°C, 900 rpm) and used for screening.

3.3.2.9 Screening Procedure

96-well plate format citrulline colorimetric screening assay

A modified protocol of citrulline detection based on carbamido-diacetyl reaction (116) (see Figure 1A for assay mechanism) was used for ADI activity measurement. Screening for increased activity was carried out by measuring the activity at pH 7.4 and 6.4. 20 µl of cell culture was transferred to 96-well microtiter plate. Enzyme reaction was initiated by addition of arginine solution (100 µl, 100 mM) supplemented with cetyltrimethylammoniumbromide (CTAB, 4 mM), and incubated (20 min, 37°C). Subsequently, acid-ferric solution (60 µl) and diacetyl monoxime (DAM, 20 µl, 0.5 M) were added. The reaction mixture was further incubated (15 min, 55°C). Absorbance was measured at 492 nm using a microtiter plate reader (Tecan Sunrise, Tecan Group AG, Zurich, Switzerland).

Standard deviation measurements were performed in 96-well plate format using culture from BL21-Gold (DE3) lacking ADI and in a separate experiment containing ADI. Apparent standard deviation was based on the absolute absorbance values obtained from the ADI wild type plate. The true standard deviation was calculated by subtracting the background absorbance value of the microtiter plate lacking ADI from the apparent values.

Cuvette format citrulline colorimetric assay

ADI activity was routinely measured using a modified protocol of the citrulline detection with DAM and TSC (117) (see Figure 1A for assay mechanism) in Eppendorf tubes. Enzyme reaction was initiated by addition of arginine solution (200 µl, 100 mM) to a 2-ml eppendorf tube containing crude cell lysate (50 µl), and incubated (20 min, 37°C). Subsequently, acid-ferric solution (250 µl) was

added to stop the enzyme reaction. After appropriate dilution with deionized water to ensure the concentration of produced citrulline is within linear detection range, the reaction mixture (400 µl) was mixed with acid-ferric solution (600 µl) and DAM-TSC solution (100 µl). The reaction mixture was further incubated (30 min, 70°C), followed by incubation in ice water to stop color development. Absorbance was measured at 530 nm using a Specord 200 (Analytik Jena AG, Jena, Germany).

Normalization of protein expression for wild type ADI and variants

Agilent Protein 230 Kit (Agilent Protein 230 Kit, Agilent Technologies Deutschland GmbH, Böblingen, Germany) and Agilent 2100 Bioanalyzer (Agilent 2100 Bioanalyzer, Agilent Technologies Deutschland GmbH, Böblingen, Germany) were used for normalization of protein expression in crude cell extract. The protocol used was according to Agilent protein 230 Kit Guide except BSA was used as an internal standard.

3.3.2.10 Expression of ADI in shaking flask and purification

Shaking flasks (1 liter) containing auto induction media LS-5052 (200 ml) supplemented with kanamycin (50 µg/ml) were inoculated with a 1:200 dilution of overnight culture (*E. coli* BL21-Gold(DE3) harboring pET42b-ADI) grown in non-inducing media LSG. After 12 h of expression, *E. coli* cells were harvested by centrifugation (Eppendorf 5810R 4°C, 3220 g, 30 min) and resuspended in phosphate buffer (20 ml, Na_xPO_4, 20 mM, pH 7.0). *E. coli* cells were subsequently lysed by using a high-pressure homogenizer (1500 bar, 2 cycles; Avestin Emulsiflex, Mannheim, Germany). The disrupted cells were centrifuged (Eppendorf 5417R, 4°C, 13000 g, 20 min) and the supernatant was further cleared by filtration through a low protein-binding filter (0.45 µm; Minisart RC 25 single use syringe filter; Sartorius, Hamburg, Germany). ADI wild type and mutants (H404R and K5T D44E H404R) were subsequently purified by a column chromatography procedure: (i) The filtered cell lysates were subjected to a Super-Q anion exchange column, which had been pre-equilibrated with 50 mM

phosphate buffer (Na_xPO_4, pH 7.0). 20 ml of cell lysate was loaded. ADI were eluted by a NaCl step elution in phosphate buffer (Na_xPO_4, 50 mM, pH 7.0) at a rate of 3 ml/min. (ii) The obtained ADI protein from ion exchange chromatography was subjected to a gel filtration column (Matrix: Toyoperl HW-55S, Bed volume: 33 ml, Bed height: 40 cm, Column: Omnifit).

Purified ADI was subsequently concentrated using a Amicon ultra-4 centrifugal filter device (Millipore Corporation, Billerica, U.S.A.) with a 30-kDa cut-off membrane. Total protein concentration was determined by BCA^{TM} assay kit (Pierce, Born, Germany) and homogeneity of the purified sample was controlled by SDS-page electrophoresis using standard molecular biology techniques.

3.3.2.11 Characterization of ADI wild type and mutants

Determination of k_{cat} and K_m of ADI wild type and the mutants

The k_{cat} and K_m values were determined from initial velocity data measured as a function of substrate concentration. Enzyme reaction was carried out at 37°C in a water bath. After 10 min preincubation at 37°C, the enzyme reaction was initiated by addition of purified enzyme (50 µl, 0.2-0.5 µM) to the substrate solution (200 µl, 0.2 mM to 10 mM of arginine, 0.5 M phosphate buffer, pH 7.4) in deep well plates. The reaction mixture was incubated (37°C) and every two minutes reaction mixture (30 µl) of each well was transferred to acid-ferric solution (30 µl) to stop the enzyme reaction. The color development was subsequently performed in 96-well PCR plate. Ferric-acid solution (90 µl) and DAM-TSC solution (15 µl) were added to each well. The 96-well PCR plate was then incubated (70°C, 30 min) in thermal cycler (Eppendorf Mastercyler gradient) for color development, followed by incubation in ice water to stop color development. Absorbance was measured at 530 nm using a microtiter plate reader (SPECTROstar Omega, BMG LABTECH, Offenburg, Germany). The initial velocity data obtained were fitted to the equation $v = V_{max}[S]/([S] + K_m)$ (where v is the initial velocity, V_{max} the maximum velocity, [S] the substrate concentration, and K_m the Michaelis constant) using GraphPad Prism software (GraphPad

software, San Diego, CA, USA). The k_{cat} was calculated from the ratio of V_{max} and enzyme concentration.

Determination of pH profile

Enzyme reaction was carried out at 37°C in a water bath using the following substrate solution: arginine 0.1 M, pH 5-8 phosphate/acetate buffer (0.5 M phosphate, 50 mM acetate). After 10 min preincubation at 37°C, the enzyme reaction was initiated by addition of purified enzyme (50 µl, 0.2-0.5 µM) to the substrate solution (200 µl) in deep well plates. The reaction mixture was incubated (37°C, 10 min) and acid-ferric solution (250 µl) was transferred to each well to stop the enzyme reaction. The color development was subsequently performed in 96-well PCR plate. The reaction mixture (60 µl), ferric-acid solution (90 µl) and DAM-TSC solution (15 µl) were transferred to a 96-well PCR plate. The 96-well PCR plate was then incubated (70°C, 30 min) in thermal cycler (Eppendorf Mastercyler gradient) for color development, followed by incubation in ice water to stop color development. Absorbance was measured at 530 nm using a microtiter plate reader (SPECTROstar Omega, Germany).

3.3.2.12 Molecular Modeling

Two crystal structures of PaADI (PDB codes: 1RXX, 2A9G) were used to model the mutations H405R and D44E. Only one monomeric unit of the tetrameric PaADI was used for the modeling study employing Swiss-PDB viewer (118) (www.expasy.org/spdbv). PaADI variants (H405R; D44E) were generated using the mutate command of Swiss-PDB viewer. The side chain rotamer with the best score was used for subsequent energy optimized with parameter of GROMOS96 force field for in vacuum minimization (119).

3.3.2.13 Stability of PpADI in presence of serum

Purified PpADI (wild type, M1, M2; 20 µl) was incubated (37°C, 60 min) with AB--human serum (80 ul, Invitrogen, Karlsruhe, Germany) and PBS buffer (pH7.4, 80 ul), respectively. Subsequently, the incubated ADI-serum/PBS mix (20 µl) was

added to microtiter plate containing arginine solution (100 µl, 10 mM arginine in PBS buffer, pH 7.4) and incubated (37℃, 30 min). Acid-ferric solution (120 µl) was added to stop the enzyme reaction. The produced citrulline was detected using the assay procedure employed in "Determination of kcat and Km of ADI wild type and the mutants". Before measuring absorbance at 530 nm, centrifugation (Eppendorf, 5810R 4℃, 3000 g, 10 min) was performed to remove the precipitation in the assay solution (likely proteins in serum were precipitated in acidic condition during assay procedure). Meanwhile, a serum control was test for the original citrulline concentration of serum using the same procedure mentioned above except that instead of PpADI, elution buffer of gel filtration (NaxPO4, 50 mM, pH 7.4) was used. All the absorbance values at 530 nm of ADI-serum sample were subtracted the value of serum control to get the citrulline concentration produced by PpADI. The residual activities of PpADI after incubation in serum compared to that in PBS buffer were calculated to show the stability of PpADI after incubated in human serum.

3.3.2.14 Activity of PpADI (wild type, M1, M2) towards arginine derivative dimethylarginine

Purified PpADI (wild type, M1, M2; 15 µl, ~0.2 mg/ml final concentration; >20-fold concentration used for kinetic constant determination) was incubated (37℃, 4 h) with (N^G, N^G)-dimethylarginine solution (20 mM, 100 µl). Acid-ferric solution (120 µl) was added to stop the enzyme reaction. Activity was recorded by citrulline detection using citrulline colorimetric assay (see 3.3.2.11 Characterization of ADI wild type and mutants).

3.4 Results

3.4.1 PpADI cloning

PpADI was cloned into pET42b(+) and expressed in *E.coli* BL21-Gold(DE3) using auto-induction media LS-5052 (see figure 2). The nucleotide sequence of PpADI comprises 1,254 bp nucleotide (figure 1) encoding 417 amino acids which have 85% identity to ADI from *P. aeruginosa* (PaADI). The PpADI cloned into

pET42b(+) was confirmed by nucleotide sequencing. As indicated in Figure 1, sequence analysis of ADI gene showed that there was one synonymous mutation at amino acid position D78 (GAT to GAC) compared to ADI-sequence of *P. plecoglossicida* CGMCC2039 deposited in NCBI (accession number: EU030267). The deduced ADI protein sequence has a calculated molecular weight of 46.5 kDa and shows 85% identity to ADI from *P. aeruginosa*. This clone was used for subsequent directed evolution experiments.

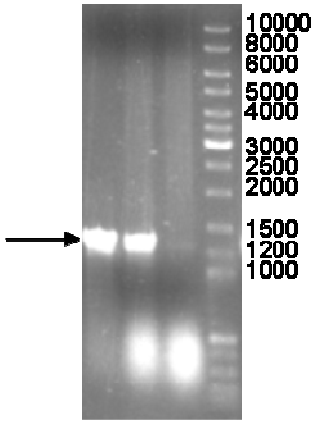

Figure 1. DNA electrophoresis of *PpADI*.

```
1       ATGTCCGCTG AAAAACAGAA GTACGGTGTC CACTCCGAAG CAGGCAAGCT GCGCAAGGTA
61      ATGGTCTGCG CTCCGGGACT GGCGCACAAG CGCCTGACCC CGAGCAACTG CGACGAGCTG
121     CTGTTCGACG ATGTGATCTG GGTCGACCAG GCCAAGCGCG ACCACTTCGA CTTCGTCACC
181     AAGATGCGCG AGCGCGGCGT GGATGTGCTG GAAATGCATA ACCTGCTCAC CGACATCGTG
241     CAGAACCCCG AGGCCCTGAA GTGGATCCTC GACCGCAAGA TCACCCCTGA CACCGTCGGG
301     GTGGGCCTGA CCAACGAAGT GCGCAGCTGG CTGGAGGGCC AGGAGCCACG CCACCTCGCC
361     GAGTTCCTGA TCGGCGGCGT GGCCGGCCAG GACCTGCCGG AGAGCGAAGG TGCCAGCGTG
421     GTCAAGATGT ACAACGACTA CCTGGGCCAC TCCAGCTTCA TCCTGCCGCC GCTGCCCAAC
481     ACCCAGTTCA CCCGCGACAC CACCTGCTGG ATCTACGGCG GCGTGACCCT CAACCCGATG
541     TACTGGCCGG CGCGACGCCA GGAAACCCTG CTGACCACCG CCATCTACAA GTTCCACCCC
601     GAGTTCACCA AGGCCGACTT CCAGGTCTGG TACGGCGACC CGGACCAAGA GCACGGCCAG
661     GCCACCCTCG AAGGCGGCGA CGTCATGCCG ATCGGCAAGG GCATCGTGCT GATCGGCATG
721     GGTGAGCGCA CCTCGCGCCA GGCCATCGGC CAACTGGCAC AGAACCTCTT CGCCAAGGGC
781     GCAGTGGAGC AAGTGATCGT CGCCGGGCTG CCGAAGTCCC GTGCGGCCAT GCACCTGGAC
841     ACCGTGTTCA GCTTCTGCGA CCGCGACCTG GTCACGGTTT TCCCGGAAGT GGTGCGCGAG
901     ATCGTGCCGT TCATCATCCG CCCGGACGAA AGCAAGCCCT ACGGCATGGA CGTACGCCGC
961     GAGAACAAGT CGTTCATCGA GGTGGTCGGC GAGCAGCTGG GCGTCAAGCT GCGTGTGGTC
1021    GAGACCGGCG GCAACAGCTT CGCCGCCGAG CGCGAGCAGT GGGATGACGG CAACAACGTG
1081    GTGGCGCTGG AGCCAGGTGT GGTCATCGGC TACGACCGCA ACACCTACAC CAATACCTTG
1141    CTGCGCAAGG CCGGGATAGA GGTCATCACC ATCAGTGCCG GCGAACTGGG CCGGGGCCGT
1201    GGCGGCGGCC ACTGCATGAC CTGCCCGATC GTGCGCGACC CGATCAACTA CTAA
```

Figure 2. PpADI sequencing results.

3.4.2 PpADI expression in LB media with IPTG as inducer

PpADI was successfully expressed in LB media with IPTG as inducer. Figure 3 (lane 4) shows the expression band of PpADI observed at ~45 kDa, which is similar to the calculated molecular weight of 46 kDa (based on http://expasy.org/tools/pi_tool.html).

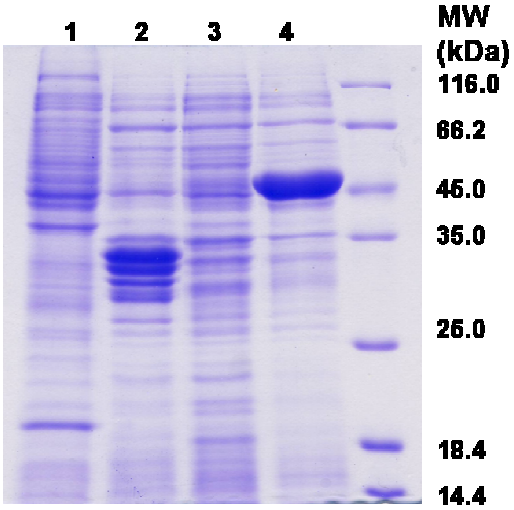

Figure 3. SDS-PAGE of PpADI expression. Lane 1: *P. plecoglossicida*; Lane 2: E. coli BL21-Gold (DE3)/ pET42b; Lane 3: E. coli BL21-Gold (DE3)/ pET42b-PpADI WT, without IPTG; Lane 4: E. coli BL21-Gold (DE3)/ pET42b- PpADI WT.

3.4.3 PpADI expression in auto-induction media

Expressing recombinant protein in auto-induction media is based upon the preferences of bacteria to selectively use different carbon sources during diauxic growth and upon the often-observed negative regulation of gene expression by catabolite repression. Auto-induction is more convenient than IPTG induction because the expression strain is simply inoculated into auto-inducing medium and grown to saturation without the need to follow culture growth and add inducer at the proper time. For high-throughput applications, the auto-induction approach has many advantages over traditional induction methods including avoidance of the strong induction and apparent toxicity associated with chemical inducers such as IPTG.

Five kinds of auto-induction media LS-5052, P-5052, MD-5052, TYM-5052 and TYP-5052 were tested for the ADI expression. Figure 4(A) and 4(B) show ADI

activity and corresponding SDS-PAGE band of the PpADI expression in different auto-induction media. The expression in auto-induction media LS-5052 is shows the highest activity and therefore LS-5052 was used for the following directed evolution experiments.

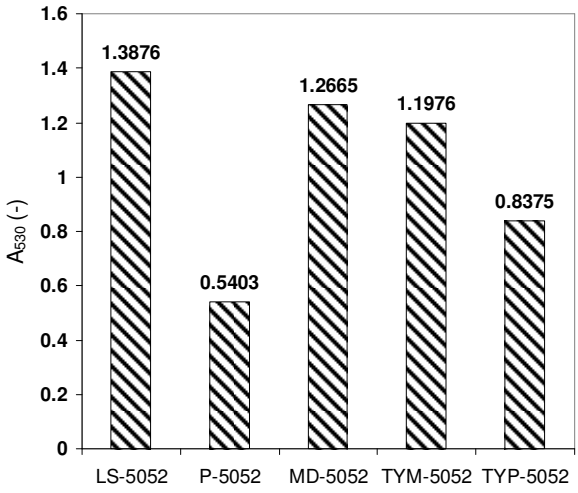

Figure 4(A). Activity of PpADI expressed in auto-induction media.

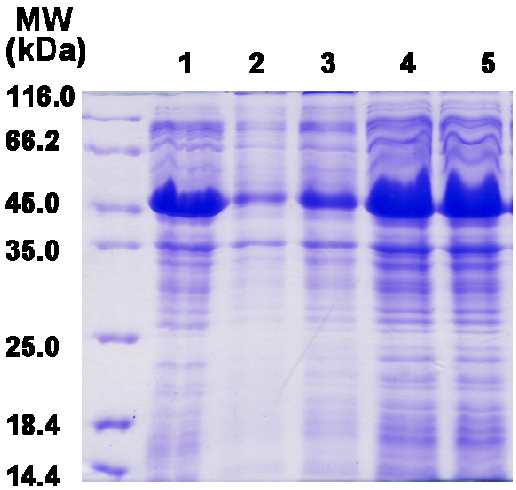

Figure 4(B). SDS-PAGE of ADI expressed in auto-induction media 1, LS-5052; 2, P-5052; 3, MD-5052; 4 TYM-5052; 5, TYP-5052.

3.4.4 PpADI assay based on citrulline detection

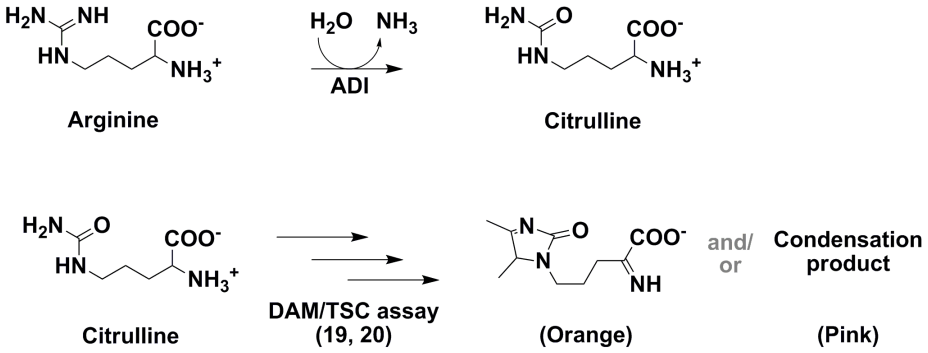

Figure 5. Arginine conversion by ADI and detection of citrulline using DAM/TSC assay.

ADI activity was measured by detecting the production of citrulline from arginine, according to carbamido diacetyl reaction (colorimetric reaction). The conditions of the carbamido diacetyl reaction is as follows： strong acid solution (H_3PO_4, H_2SO_4), oxidizing agent (Fe^{3+}), diacetyl monoxime (DAM), thiosemicarbazide (TSC), and boiling water bath. Figure 5 shows one postulated reaction mechanism for the assay which depicts the reaction between citrulline and DAM. By the addition of TSC to the reaction system, Coulombe and Favreau(120) obtained linearity of response with a more stable pink color which A_{max} was shifted from 490nm to 530nm.

Figure 6 describes the assay procedure for measuring ADI activity in 2 ml eppendorf tube. A calibration curve was prepared using citrulline standard solution (Figure 7) for determining the citrulline production during the assay.

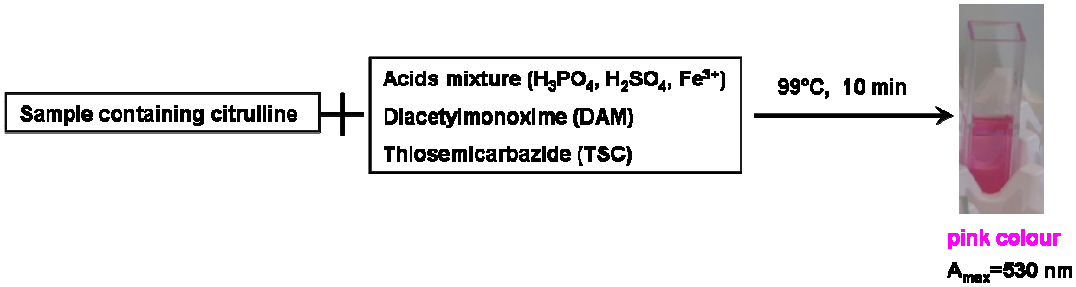

Figure 6. Citrulline colorimetric assay in cuvette format using DAM/TSC assay.

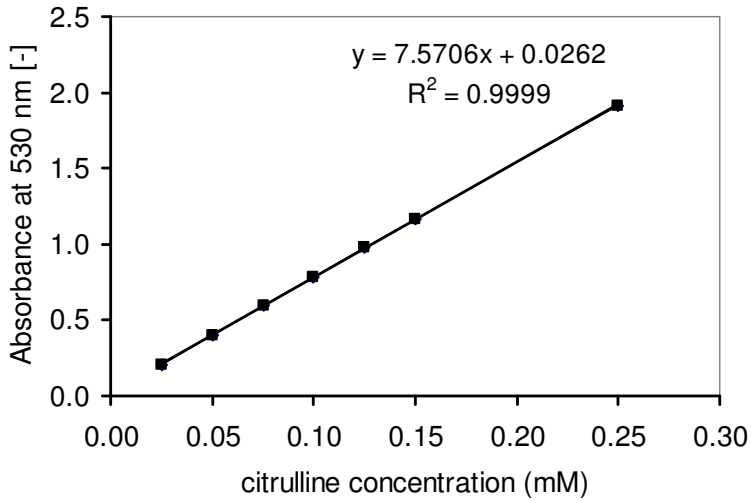

Figure 7. Calibration curve of cuvette format citrulline colorimetric assay.

3.4.5 PpADI screening system for citrulline production in microtiter plates

Two key performance parameters for identifying improved variants in microtiter plate based screening systems are the true standard variation and the linear detection range of the employed assay. Standard deviations have been reduced by optimizing expression and screening conditions (various auto-induction media and assay conditions such as amount of cell, conversion time and color development procedure). A modified version of the DAM-TSC assay for citrulline detection (Scheme 1) was selected for directed evolution of PpADI. The microtiter plate screening format was optimized for simplified handling by lowering the color development temperature (55℃ instead of 100℃), increasing the diacetylmonoxime concentration (~22-fold) and avoiding the use of the sensitizer thiosemicarbazide. Figure 8 shows the procedure of screening assay of citrulline detection.

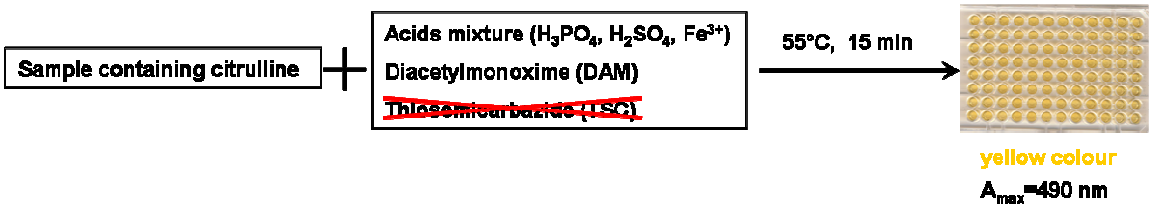

Figure 8. Citrulline colorimetric assay in MTP format using DAM assay.

Standard deviations of the modified citrulline detection assay have been reduced by optimizing expression and screening conditions (various auto-induction media and assay conditions such as amount of cell, conversion time and color development procedure). The preferred combination (150 µl LS5052 auto-induction media and 20 µl cell culture, 20 min conversion time and 15 min color develop time) resulted in a true standard deviation of 12.8 % after subtracting the background (Figure 10). Screening systems with standard deviations around 10 % have successfully been used in directed evolution experiments (121, 122). A wide linear detection window is important for identifying beneficial mutants in directed evolution experiments and screening systems for evolved mutants have to be constantly adapted for hitting the linear detection window. A linear detection range up to 6 mM citrulline could be detected (Figure 9).

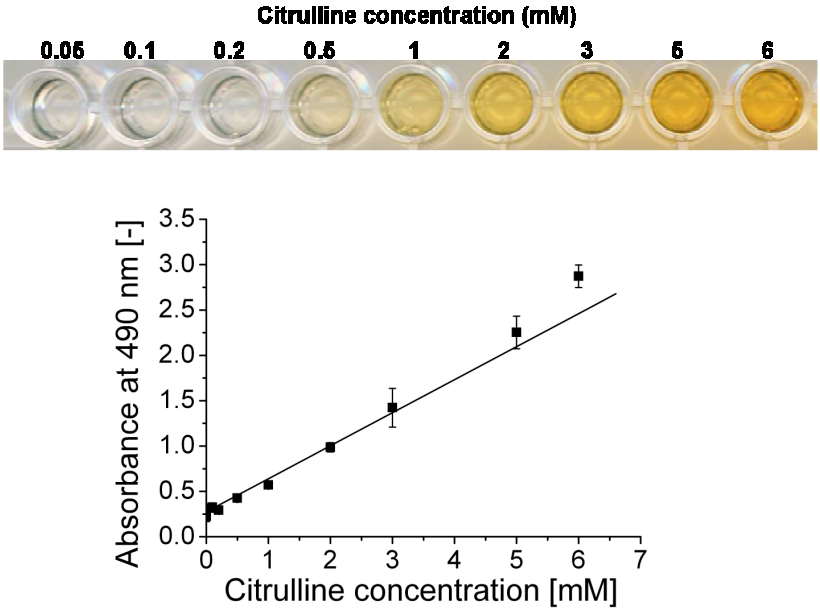

Figure 9. Calibration curve of 96-well microtiter plate format citrulline colorimetric screening assay.

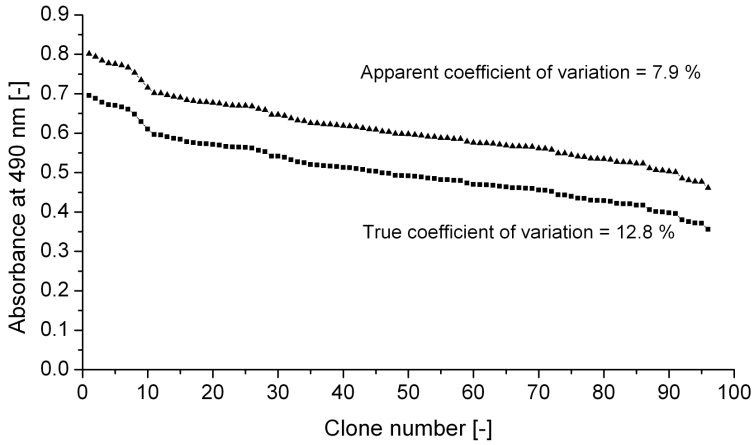

Figure 10. Activity values in descending order of the ADI wild-type conversion of arginine to citrulline in a 96-well microtiter plate using the optimized assay protocol. The apparent coefficients of variation were calculated without subtracting the background and the true coefficients of variation after background subtraction.

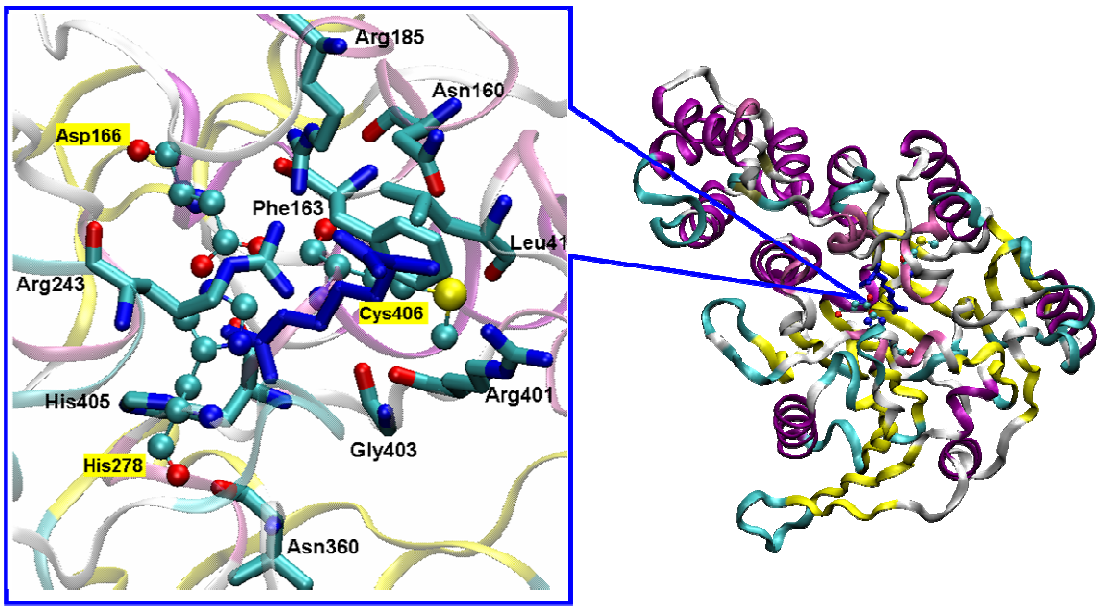

Figure 11. PpADI model derived from PaADI crystal structure (PDB code 2a9gD) by SWISS MODEL WORKSPACE.

3.4.6 Focused libraries generated by saturation mutagenesis

PpADI gene shares 83 % sequence identity with PaADI of which the crystal structure was solved (123). After submitting the ADI sequence to SWISS MODEL WORKSPACE, a proposed ADI model based on the PaADI crystal structure (PDB code 2a9gD) was obtained (Figure 11). According to this model and published literatures, 9 amino acid residues: Leu41, Asn160, Phe163, Arg185, Arg243, Asn360, Arg401, His404, Gly 403 (Figure 11) close to the active center (catalytic triad: Cys406-His278-Glu224) or known to interact with substrate arginine were selected for saturation mutagenesis.

Site saturation mutagenesis at position Leu41, Asn160, Phe163, Arg185, Arg243, Asn360, Arg401, His404 and Gly 403 were performed. 300 clones were screened for each position. However, no improved variant was identified.

3.4.7 Validation of variant M1 (H404R) citrulline colorimetric assay in cuvette format

Position H404 which was suspected to influence ADI pH profile by substitution to R404 (15). Compared to wild type PpADI, variant M1 (H404R) shows higher activity (1.8-fold) and improved activity ratio of pH 7.4 to 6.4 (4.7-fold). Therefore, M1 (H404R) was selected for directed evolution.

3.4.8 epPCR library generation and screening with citrulline detection assay by screening error-prone mutant libraries

Various concentrations of $MnCl_2$ (0.01-0.10 mM) were used in epPCR library generation to adjust the ratio of active to inactive clones. Figure 12 (A) and 12 (B) show the epPCR products and the corresponding MEGAWHOP products. Concentration of 0.01 mM $MnCl_2$ which generated 53 % inactive mutant was selected for library generation. EpPCR mutant libraries with a ratio of 50 % active and 50 % inactive clones have often been used successfully in directed evolution, improving enzyme properties by gradual changes (one or two amino acids changes per round of mutagenesis and screening). A total of 7 variants (listed in

Table 2) were identified from an epPCR library of 2400 mutants and used for further characterization. The most active variant was sequenced and two additional amino acid substitutions (K5T D44E) were identified.

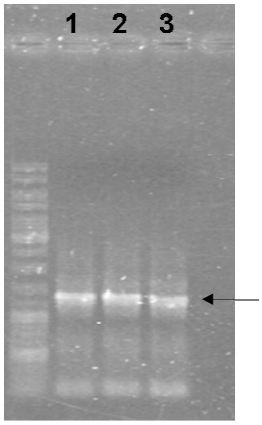

Figure 12 (A). Electrophoresis of epPCR products. Lane 1, 0.01 mM of $MnCl_2$; Lane 2, 0.02 mM of $MnCl_2$; Lane 3, 0.05 mM of $MnCl_2$.

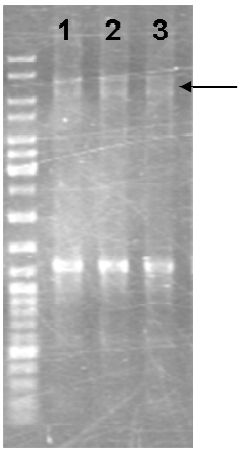

Figure 12 (B). Electrophoresis of MEGAWHOP product with epPCR products as megaprimer. Lane 1, 0.01 mM of $MnCl_2$; Lane 2, 0.02 mM of $MnCl_2$; Lane 3, 0.05 mM of $MnCl_2$.

Table 2. Activity of ADI variants towards arginine determined using citrulline colorimetric assay in cuvette format. Samples were diluted to ensure that detected citrulline concentrations are within the linear detection range of the citrulline colorimetric assay. Wild type, mutant M1 and the "best variant" M2 are in bold and prominent expression mutants (9-B3-1; 21-D5-1) are italized.

	Normalized [ADI][a]				
	Citrulline production (mM/mg)		Relative to activity at pH 7.4 of WT		Activity at pH 7.4/ activity at pH 6.4
ADI variants	pH 7.4	pH 6.4	pH 7.4	pH 6.4	
WT	9.83 (0.74)[b]	124.92 (1.98)	1.00 (0.15)	12.69 (0.01)	0.08 (0.01)
M1 (H404R)	17.80 (0.49)	45.95 (0.87)	1.81 (0.06)	4.67 (0.02)	0.39 (0.02)
M2 (K5T D44E H404R)	38.99 (0.79)	39.20 (0.31)	3.96 (0.02)	3.98 (0.02)	0.99 (0.03)
9-B3-1	24.89 (0.45)	54.50 (1.80)	2.53 (0.03)	5.54 (0.03)	0.46 (0.02)
21-D5-1	25.68 (2.68)	50.95 (2.36)	2.61 (0.07)	5.18 (0.02)	0.50 (0.01)
15-G10-2	13.11 (0.53)	47.02 (0.47)	1.33 (0.09)	4.78 (0.02)	0.28 (0.01)
2-H4-2	12.50 (0.07)	21.58 (0.09)	1.27 (0.06)	2.19 (0.04)	0.58 (0.01)
1-G11-1	24.91 (0.20)	29.12 (0.33)	2.53 (0.03)	2.96 (0.03)	0.85 (0.02)
24-E10-1	14.62 (0.62)	32.82 (0.52)	1.49 (0.08)	3.34 (0.03)	0.45 (0.02)

[a] (Based on quantification employing Agilent 2100 Bioanalyzer (Agilent Protein 230 Kit))
[b] (Standard error of triplicate measurements are given in brackets below each absolute and normalized value.)

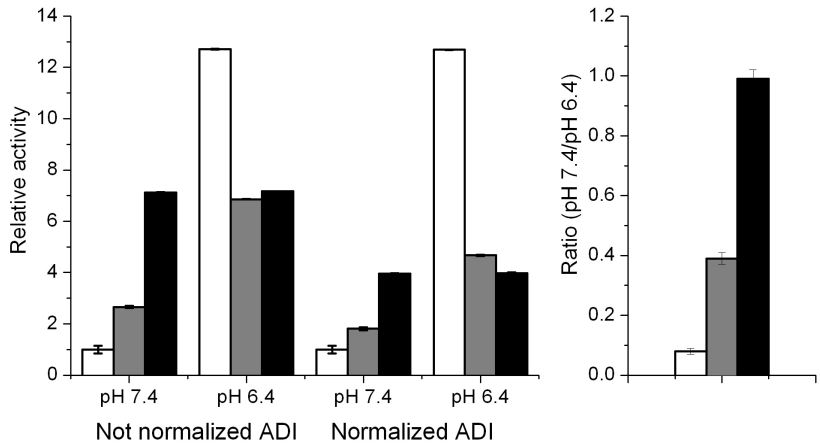

Figure 13. Relative activity of ADI variants towards arginine. The relative activity is the ratio of the activity at the pH of each variant relative to the activity at pH 7.4 of wild type ADI. White: ADI wild type, grey: M1 (H404R), black: M2 (K5T D44E H404R).

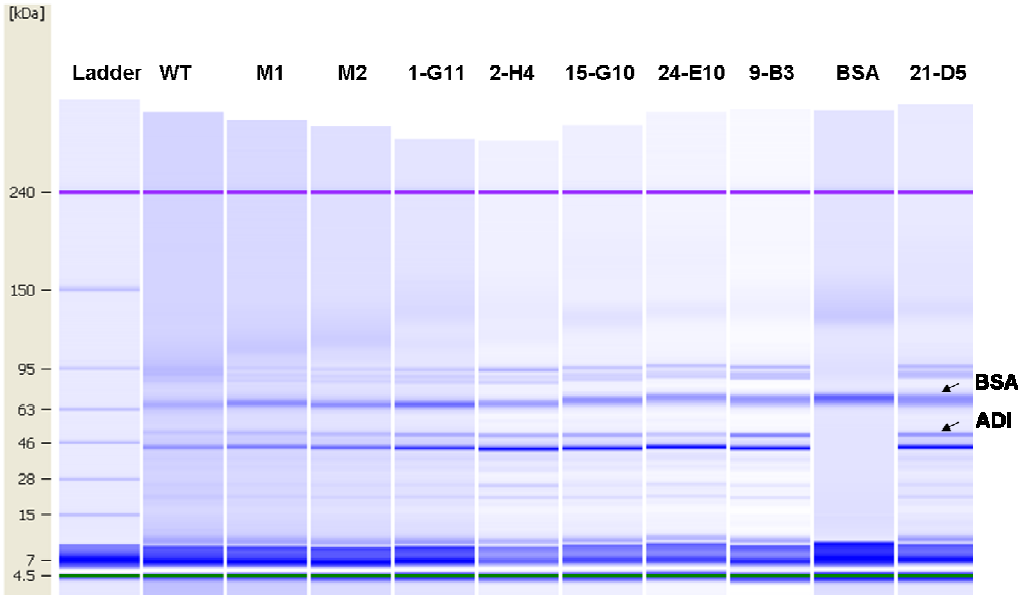

Figure 14. Elution profile of wild type PpADI and improved variants from epPCR library, generated with Protein 230 Kit using a mircofluidic device (Agilent Bioanalyzer). BSA was added as an internal standard.

3.4.9 Characterization of PpADI variants

3.4.9.1 Determination of k_{cat} and K_m of ADI wild type and the mutants

Variants selected from epPCR were first characterized using the crude cell extract to identify the most promising variants (Table 2). Using an activity ratio of pH 7.4 to 6.4 proved to be an effective method to eliminate expression mutants. Additionally ADI concentration in crude cell extract was determined using the Agilent Protein 230 Kit. Microfluidic elution profiles (Figure 14) semi-quantify differences in expression between the wild type PpADI and variants. Normalization of activities against the corresponding ADI concentrations reveals improvements in specific activities of ADI mutants (Table 2). M1, the starting variant for the directed evolution campaign, and M2 were selected for detailed characterization studies. M2 has as “best identified variants” (Figure 13) a more than 2.5-fold higher activity ratio at pH 7.4 to pH 6.4 than M1 and a 12-fold higher activity ratio than wild type in crude cell lysates.

For kinetic characterization of ADI variants the citrulline production was maintained between 0.2-0.8 mM. Calibration curve in Figure 4 shows the linear detection range in the employed 96-well PCR plate format citrulline colorimetric assay system. Figure 15 summarizes the k_{cat} and K_m values of wild type PpADI, identified variants M1 (H404) and M2 (K5T D44E H404R) which were expressed in shaking flasks cultures and purified using a two step procedure (anion exchange followed by gel filtration). Both variants M1 and M2 show an increase in k_{cat} and K_m for citrulline production at pH 7.4. Variant M2 shows a 4-fold higher k_{cat} as also obtained for specific activity in Table 2 using the crude cell extract, validating the characterization procedure with crude cell lysate. Furthermore, an increased K_m from 0.7 mM (wild type PpADI) to 1.2 mM (M1) and 2.5 mM (M2) was found.

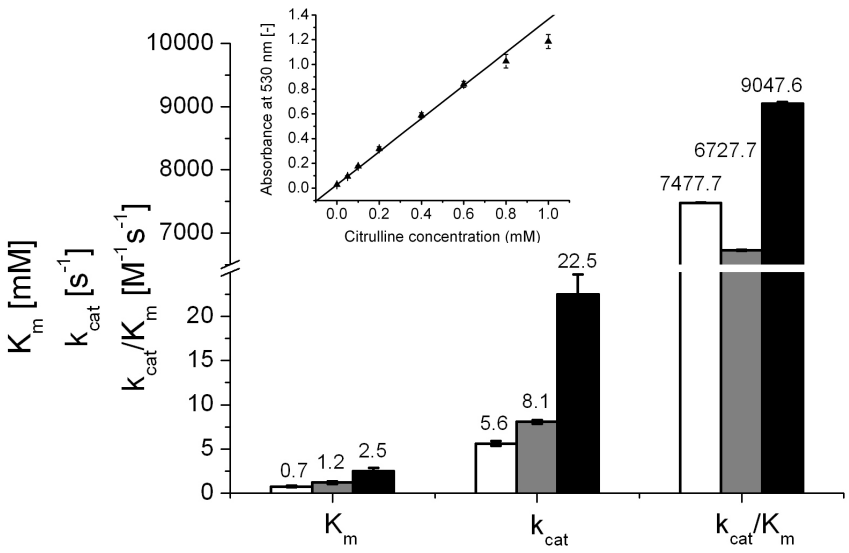

Figure 15. Kinetic parameters of ADI and mutants for conversion of arginine to citrulline. White: ADI wild type, grey: M1 (H404R), black: M2 (K5T D44E H404R). Values reported are the average of three measurements, and average deviations from the mean values are shown. Embedded calibration curve shows linearity of citrulline colorimetric assay in 96-well PCR plate format which was used to determine arginine conversions and kinetic constants.

3.4.9.2 Relative pH profile of wild type and mutant

The relative pH profile (Figure 16) of wild type PpADI and M1 (H404R) shows an identical pH optimum at pH 6.5. Compared to wild type PpADI, variant M2 (K5T

D44E H404R) shows a pH optimum at pH 7.0 which is shifted remarkably (0.5 pH units). Both M1 and M2 show decreased specific activities at pH 6.5, and increased specific activity at pH 7.5. At pH 7.0, the specific activity of M2 exceeds that of wild type PaADI (data not shown).

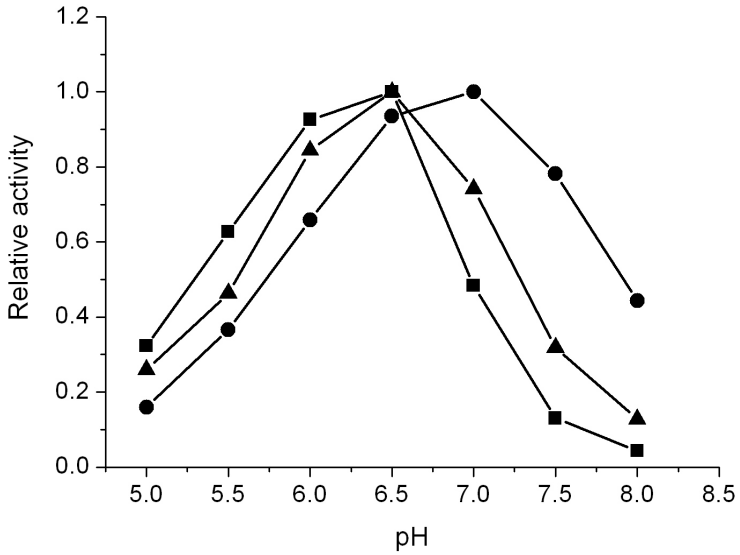

Figure 16. pH profile of wild type ADI, M1(H404R), M2(K5T/D44E/H404R). The relative activity is the ratio of the catalytic activity at the pH relative to the maximum activity of each enzyme. (■) WT, (▲) M1 (H404R), (●) M2 (K5T/D44E/H404R).

3.4.10 Stability of PpADI in the presence of human serum

Table 3 summarizes the stability of PpADI variants in serum (37℃, 60 min; standard deviation of three measurements in brackets). The mutants M1 and M2 have a similar stability in serum when compared to the wild-type PpADI wild type. The substitution D44E and H404R do not destabilize further the PpADI in serum.

Table 3. Stability of PpADI variants in the presence of human serum.

	PpADI WT	M1	M2
No incubation (A_{530})	0.08	0.27	0.98
Incubation with serum (37℃, 60 min) (A_{530})	0.05	0.15	0.69
Residual activity	60 %	55 %	70 %

3.4.11 Activity of PpADI (wild type, M1, M2) towards arginine derivative (N^G, N^G)-dimethylarginine

No detectable conversion of (N^G, N^G)-dimethylarginine could be detected with PpADI variants.

3.5 Discussion

ADI properties have to date not been engineered through directed evolution algorithms despite their often poor performances under physiological conditions and their medical importance as potential anti-tumor drug. Chemically modified of ADI (e.g. through PEGylation) (27) and fusion protein (e. g. Human serum albumin fusion, HSA) (124) have been used for addressing activity and stability demands *in vivo*. Directed evolution offers opportunities to directly improve ADI properties for *in vivo* applications and small libraries of a few thousand variants have often been sufficient to find improved muteins in directed evolution experiments (55, 125).

Our main intention in this report is to provide a validated protocol for directed ADI evolution and improving the activity at the physiological pH 7.4. *Pseudomonas plecoglossicida* CGMCC2039 (PpADI, 7.8 U/mg; pH optimum 6.5) was selected for the directed evolution studies due to its functional expression in *E. coli,* coverage of sequence space in patents and "potential" for activity improvement. PpADI is a relatively slow ADI when compared to Mycoplasma ADIs like MhADI (*Mycoplasma hominus* ADI, 35 U/mg) which would have been good alternatives for directed evolution studies (105). Reported ADI activities range from 0.115 to 140.3 IU/mg. One unit is commonly defined as the ADI amount that converts 1 µmol of L-arginine into 1 µmol of L-citrulline per minute (27).

Screening of PpADI variants yielded three amino acid positions 5, 44 and 404. Positions 44 and 404 resulted in a 4-fold higher k_{cat} at pH 7.4 and a significant shift in the pH optimum (0.5 units) when compared to wild type PpADI (Figure 17 & 8). Position 5 did not show any effect on PpADI activity.

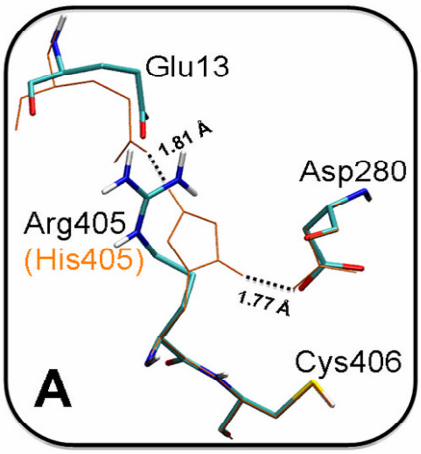

Figure 17. Structural alignment of mutant M1 model with corresponding residues of the crystal structures of the PaADI (in orange). The crystal structure of PaADI which was diffracted in absence of the substrate arginine (1RXX) was used to investigate the substitution of His405 to Arg405. The Arg405 variant shows with respect the Asp280 a different orientation of the guanidinium group when compared to side chain of His405 (in orange).

Galkin and coworkers postulated that the histidine in position 404 (corresponding position in “their” PaADI is 405) is a key residue in controlling activity at acidic and neutral pH. In protonated state of the imidazolium ring a hydrogen bonding interaction can be formed with the oxygen of Asp280 (carboxyl group). This hydrogen bond favors stabilizing interactions between Asp280 and the substrate arginine. His405 in PaADI was reported (17) to share protons with Asp280 and Glu13 and to be important for modulating electrostatic environments of closely located catalytic groups. The same report postulated that H405 is likely to be protonated when the substrate arginine binds to catalytic triad (His278, Glu224, Cys406) [(2)]. Based on these reports the His404 in PpADI was subjected to a site directed mutagenesis to Arg404 and named M1. The M1 variant (H404R) shows 40 % residual activity compared to wild type PpADI at pH 6.4 and a 1.8-fold increase in activity at pH 7.4 (see Table 1). In the M1 (H404R) mutant (see the model in Figure 17; based PaADI 1RXX; residue His404 in PpADI corresponds to His405 in PaADI), the conformational effect due to the extended side chain of Arg likely weakens the hydrogen bond to Asp280 and thus reduces the stabilizing effect on arginine binding. As a result the activity of M1 is reduced, especially at

lower pH values at which His405 is protonated. However at elevated pHs, His405 becomes increasingly deprotonated whereas Arg405 remains protonated and can therefore still stabilize Asp280 for arginine binding. The electrostatic effect suggested by theoretical and experimental studies have evidenced the importance of positively charged residues to modulate the reaction rate of PaADI (126). At pH 6.4, histidine in wild type PpADI and arginine in M1 are both positively charged. At pH 7.4, histidine is only partially positive charged and PpADI's activity is reduced (>90 %) while arginine in M1 remains positively charged preserving M1's activity (Figure 17).

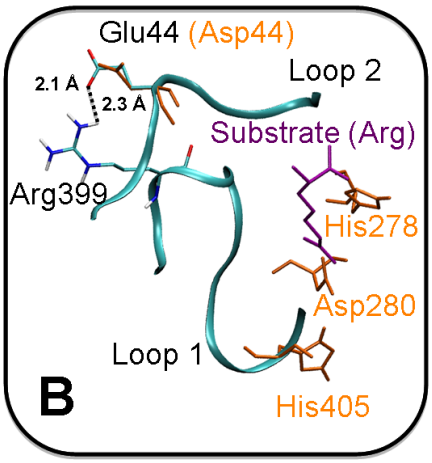

Figure 18. Structural alignment of mutant M2 model with corresponding residues of the crystal structures of the PaADI (in orange). The PaADI crystal structure in presence of substrate arginine was used (2A9G) to investigate the role of the substitution Asp44 to Glu44. The latter was solved for an inactive variant in which Cys406 was replaced by Ala406. The extended side chain of Glu44 might improve the hydrogen bond interaction with the Arg399 inducing a conformational shift of loop 1.

The PpADI H404R was used as starting variant for directed evolution. The amino acid position 44 was identified from a epPCR library (2400 variants screened) resulting in a triple mutant M2 (K5T D44E H404R). For investigating the role of each position the double mutants (K5T H404R) and (D44E H404R) were generated. Only the double mutant (D44E H404R) revealed improvements in k_{cat} (4-fold, pH 7.4; Figure 18). The rationale behind the effects of the mutation D44E on the PpADI activity is more complex to extrapolate from the available ADI crystal structures. Comparative crystallographic studies have shown that the

entrance of the active site is decorated by 4 loops that undergo conformational transitions upon arginine binding (17). The loops exhibit significant shifts that limit the access of water molecules to the active site. The Asp44 is located in loop 1 (residues 30-46) and upon binding of the substrate, Asp44 comes closer to the positively charged Arg399 located on loop 4 (residues 392 to 403). In the D44E mutant, the longer side chain reduces the distance with Arg399 favoring the formation of hydrogen bond (see model in Figure 18). The reinforced interaction between Glu44 and Arg399 might expedite conformational changes in loops, probably confining the arginine substrate in the active site and hence promote arginine conversion. In the future, we plan to further investigate the influence of H404R and D44E using molecular dynamics simulations, further boost the k_{cat} at pH 7.4 and reduce the K_m value of PpADI.

Overall site directed mutagenesis of position H404R and one round of directed evolution (2400 variants screened) resulted in a triple mutant M2 (K5T D44E H404R) with 4-fold higher k_{cat} at pH 7.4 (compared to wild type; Figure 4). The best mutant isolated, M2, has specific activity of 31.3 U/mg at pH 7.4 which is already after one round of evolution close to the specific activity of MhADI (35 U/mg) (127) at its pH optimum. The stability and specificity of improved PpADI variants are furthermore important for cancer treatment *in vivo*. First experiments in AB-human serum (Invitrogen) showed an unaltered stability of M2 compared to the wild type PpADI and (N^G, N^G)-dimethylarginine conversion could not detect with the citrulline colorimetic assay.

3.6 Conclusion

In summary, a directed evolution protocol has been developed for PpADI and validated by increasing the k_{cat} of PpADI at physiological pH (7.4). The reported screening system is the first one employed in directed ADI evolution and can likely be used for other ADIs and other properties such as temperature stability, salt/detergent stability or protease resistance.

Chapter 4. PpADI reengineered for efficient operation under physiological conditions

4.1 Abstract

The proof of concept for ADI engineering by directed evolution resulted in variant M2 (K5T/D44E/H404R). M2 has a pH optimum of pH 7.0 and 4-fold higher k_{cat} value than the wild type PpADI (pH 7.4, 0.5 M phosphate buffer) and an increased K_m value for substrate arginine. In this chapter, in order to improve the catalytic efficiency of PpADI at low concentration of arginine, variant M5 (K5T/D38H/D44E/A128T/H404R) and M6 (K5T/D38H/D44E/A128T/E296K/H404R) were generated from an epPCR library: at pH 7.4 (PBS buffer), the $S_{0.5}$ value decreased from 2.01 mM (parent M3, K5T/D44E/A128T/H404R) to 1.48 mM (M5) and 0.81 mM (M6). The $S_{0.5}$ value of M6 (0.81 mM) is lower than that of PpADI wild type (1.30 mM); the k_{cat} value improved from 0.18 s^{-1} (PpADI wild type) to 17.56 s^{-1} (M5, 97.6-folds) and 11.64 s^{-1} (M6, 64.7-fold).

4.2 Introduction

ADI-based arginine depletion is a target specific therapy for arginine-auxotrophic tumors (e.g. hepatocellular carcinomas and melanomas) and pegylated ADI is currently under clinical trials for HCC with promising results (45). HCC is the third leading cause of cancer mortality world wide with a less than 10 % 5-year survival rate (EU and USA) (128) due to low responses of hepatoma to chemotherapeutic treatments. In 1999, US Food and Drug Administration (FDA) designated ADI-PEG-20 orphan drug status for the treatment of HCC and invasive malignant melanomas, and in 2005 European Agency for the Evaluation of Medicinal Products (EMEA) also granted ADI-PEG-20 orphan drug status for the treatment of HCC. Phase II trials of ADI-PEG-20 in patients with metastatic

hepatocellular carcinomas have shown that the drug is safe, well tolerated, and may benefit patients with unresectable HCC. Izzo and coworker suspected that combination therapies of arginine deprivation and growth inhibition via kinase inhibitors might improve the survival rate further more. Additionally, ADI can enhance radio sensitivity of human mammary adenocarcinoma (MCF-7 cells) (48), exerts anti-proliferative and anti-angiogenic activities and inhibits the growth of viruses such as HIV-1 and hepatitis (49, 50). Current research efforts are focused on ADI's *in vivo* inhibitory effect towards leukemia, melanoma, prostate cancer, renal cell carcinoma, and human umbilical vein endothelial cells (HUVEC) (19, 44, 51-53), clinical trials for HCC (phase II) (45) and melanoma (phase I/II) (46), and inhibitory mechanisms of ADI to tumors (54).

Arginine deprivation is believed to be a main molecular reason for ADI's inhibitory effects on arginine auxotrophic tumors which do not express argininosuccinate synthetase (ASS). ADIs catalyze the first step of the arginine dehydrolase pathway by hydrolyzing arginine to citrulline and ammonium. ADI genes have been identified, purified, and characterized from bacteria, archaea and some eukaryotes excluding mammalian cells (see review (27)). Enzymatic properties of several recombinant ADIs have been examined, such as specific activity, functional expression level, temperature optimum, pH optimum, substrate affinity for arginine, and half-life in human plasma. Only the ADI from *Mycoplasma hominis* has so far been developed as orphan drug by Pheonix Pharmacologics Inc. for HCC and melanoma (129). From enzyme kinetic point of view, none of the ADIs is ideally suited for *in vivo* applications under physiological conditions. Protein engineering by rational design and directed evolution offers opportunities to tailor ADI properties to physiological conditions. PpADI (ADI from *Pseudomonas plecoglossicida*) was functionally expressed in *E. coli* with a simple protocol and has been engineered for the first time by directed evolution for improved activity at physiological pH (3). The variant M2 (K5T/D44E/H404R), by our group reported, showed a 4-fold higher specific activity than the wild type PpADI (0.5 M phosphate buffer, pH 7.4), but a increased K_m value (3.5-fold).

High activity at low arginine concentration is an important prerequisite for ADI's medical application, allowing low ADI dose required per treatment.
In the present work, we improved the directed evolution protocol and identified a PpADI variant with further improved activity and slightly decreased "K_m value" and PpADI variant with lowered K_m value maintaining its high catalytic activity. Those variants were characterized in respect to their kinetic constants.

4.3 Materials and methods

4.3.1 Materials

All chemicals were of analytical-reagent grade or higher quality and were purchased from Fluka (Neu-Ulm, Germany), Sigma-Aldrich (Steinheim, Germany) and Applichem (Darmstadt, Germany), except the resins for purification (TOSOH, Stuttgart, Germany). All enzymes were purchased from New England Biolabs (Frankfurt, Germany), Fermentas (St. Leon-Rt, Germany), and Sigma-Aldrich Chemie (Taufkirchen, Germany), unless stated otherwise.
Thermal cycler (Mastercyler gradient; Eppendorf, Hamburg, Germany) and thin-wall PCR tubes (Multi-ultra tubes; 0.2 µl; Carl Roth, Germany) were used in all PCRs. The PCR volume was always 50 µl except for Megaprimer PCR of whole plasmid (MEGAWHOP, 25 µl); larger volumes were prepared in multiple 50-µl PCRs. The amount of DNA in cloning experiments was quantified by using a NanoDrop photometer (NanoDrop Technologies, Germany).

4.3.2 Methods

4.3.2.1 Site saturation mutagenesis of *PpADI* M2 at position A128

Site directed mutagenesis of *PpADI* M2 (K5T/D44E/H404R) at position A128 was performed according to the published method (130). The following oligonucleotides were used for mutagenesis of A128: 5'-CTGATCGGCGGCGTGNNNGGCCAGGACCTGCCG-3' and 5'-CGGCAGGTCCTGGCCNNNCACGCCGCCGATCAG-3' (underlining indicated the substituted nucleotide). For the mutagenic PCR (First stage: 98°C for 30 s, 1 cycle; 98°C, 30 s/ 55°C, 1 min/ 72°C, 3 min, 3 cycles. Second stage: 98°C for 30

s, 1 cycle; 98℃, 30 s/ 55℃, 1 min/ 72℃, 3 min, 15 cycles; 72℃ for 3 min, 1 cycle), 2 U of PhuS DNA polymerase, 0.20 mM of dNTP mix, 25 pmol of each primer together with 100 ng of template (pET42b(+) harboring PpADI M2 gene) were used. Following the PCR, DpnI (40 U; New England Biolabs) was added, and incubated overnight at 37℃. The PCR products were purified by using a QIAquick PCR Purification Kit (Qiagen) and transformed into *E. coli* BL21-Gold (DE3) for expression.

4.3.2.2 Construction of PpADI error-prone library

EpPCR library was generated by the standard error-prone PCR (epPCR) using improved variant M3 (K5T/D44E/A128T/H404R) as template. For the mutagenic PCR (95℃ for 2 min, 1 cycle; 95℃, 30 s/ 55℃, 30 s/ 72℃, 30 s, 29 cycles; 72℃ for 3 min, 1 cycle), 2.5 U of Taq DNA polymerase, 0.20 mM of dNTP mix, 50 ng of template (pET42b(+) harboring PpADI M3 gene), 0.01-0.1 mM of $MnCl_2$ and 10 pmol of each primer (5'-TACATATGTCCGCTGAAACACAGAAG-3' and 5'-GTGCTCGAGTTAGTAGTTGATCGG-3') were used. The PCR products were purified by using a QIAquick PCR Purification Kit. The purified epPCR products were cloned into expression plasmid pET42b(+) by MEGAWHOP (114). For MEGAWHOP (72℃ for 5 min, 1 cycle; 98℃ for 1 min 30 s, 1 cycle; 98℃, 45 s/ 55℃, 45 s/72℃, 4 min, 24 cycles; 72℃ for 10 min, 1 cycle), 1.2 U of PfuS DNA polymerase, 0.20 mM of dNTP mix, 500 ng of epPCR products together with 50 ng of template (pET42b(+) harboring PpADI gene of variant M3) were used. Following the PCR, DpnI (40 U; New England Biolabs) was added, and incubated (overnight; 37℃). The MEGAWHOP products were transformed into *E. coli* BL21-Gold (DE3) for expression and screening.

4.3.2.3 Site directed mutagenesis at position D38 of *PpADI* M4

Site directed mutagenesis of *PpADI* variant M4 at position D38 was performed according to the published method on plasmid pET42b(+)-ADI-M4 (K5T/D44E/A128T/E296K/H404R). The following oligonucleotides were used for mutagenesis of D38H: 5'-ACCCCGAGCAACTGCCACGAGCTGCTGTTCGAC-3'

and 5'-GTCGAACAGCAGCTCGTGGCAGTTGCTCGGGGT-3' (underlining indicated the substituted nucleotide). Conditions for mutagenic PCR are as described in "Site saturation mutagenesis of *PpADI* M2 at position A128".The PCR products were purified by using a QIAquick PCR Purification Kit (Qiagen) and transformed into *E. coli* BL21-Gold (DE3) for expression.

4.3.2.4 Site saturation mutagenesis at position D38 and E296 of *PpADI* M3

Site saturation mutagenesis library at position D38 and E296 of *PpADI* variant M3 (K5T/D44E/A128T/H404R) were generated according to the published method on plasmid pET42b(+)-ADI-M3 using the following oligonucleotides: D38FP (5'-ACCCCGAGCAACTGCNNNGAGCTGCTGTTCGAC-3'), D38RP (5'-GTCGAACAGCAGCTCNNNGCAGTTGCTCGGGGT-3') and E296FP (5'-GTCACGGTTTTCCCGNNNGTGGTGCGCGAGATC-3'), E296RP (5'-GATCTCGCGCACCACNNNCGGGAAAACCGTGAC-3') (underlining indicated the substituted nucleotide). Conditions for mutagenic PCR are as described in "Site saturation mutagenesis of PpADI M3 gene at position A128".The PCR products were purified by using a QIAquick PCR Purification Kit (Qiagen) and transformed into *E. coli* BL21-Gold (DE3) for expression.

4.3.2.5 Cultivation and expression of PpADI in 96-well plates

Cultivation and expression in 96-well plates (flat bottom, polystyrene plates; Greiner Bio-One GmbH, Frickenhausen, Germany) were performed as previously described in 3.3.2.8.

4.3.2.6 Improved screening system in 96-well plate to identify PpADI variants with high activities at low arginine concentration

As describe previously, the modified protocol of citrulline detection based on carbamido-diacetyl reaction was used for screening for improved ADI affinity to arginine at pH 7.4. 15 µl of cell culture was transferred to 96-well microtiter plate. Enzyme reaction was initiated by addition of arginine solution (105 µl, 1mM arginine in PBS buffer, pH 7.4) supplemented with

cetyltrimethylammoniumbromide (CTAB, 4 mM), and incubated (10 min, 37°C). The following color development procedure was carried out as described previously (3).

Standard deviation measurements were performed in 96-well plate format using culture from BL21-Gold (DE3) lacking PpADI and in a separate experiment containing PpADI variant M3. Apparent standard deviation was based on the absolute absorbance values obtained from the PpADI variant M3 plate. The true standard deviation was calculated by subtracting the background absorbance value of the microtiter plate lacking ADI from the apparent values.

4.3.2.7 Expression of PpADI in shaking flask and purification

Expression of PpADI in shaking flasks and purification (by anion exchange chromatography and gel filtration) was performed as previously described in 3.3.2.10.

4.3.2.8 Characterization of PpADI variants

Preliminary determination of kinetic constants for site saturation mutagenesis variants of position 38 and 296

The k_{cat} and K_m values were determined from initial velocity data measured as a function of substrate concentration. Enzyme reaction was carried out at 37°C in incubator (Heraeus Holding GmbH, Hanau, Germany) using cell crude extract. 2 ml of expression culture was harvested by centrifugation (Eppendorf 5415R 4°C, 13,000 g, 10 min) and then freezed (-20°C, overnight). Cell lysate was prepared by resuspending the cell pellet in lysozyme (91000 U, 50 mM phosphate buffer, pH 7.4, 1.3 ml) followed by incubation (37°C, 40 min) and centrifugation (4°C, 13,000 g, 10 min). 15 µl of diluted (4 times diluted with 50 mM phosphate buffer, pH 7.4) cell lysate was transferred to 96-well microtiter plates. Enzyme reaction was initiated by addition of arginine solution (105 µl, 0.25-10 mM arginine in PBS buffer, pH 7.4) and incubated (7 min, 37°C). Subsequently, ferric-acid solution (120 µl) was added to each well to stop enzyme reaction. 60 µl of terminated

enzyme reaction mixture was transferred to 96-well PCR plate for color development. Ferric-acid solution (90 µl) and DAM-TSC solution (15 µl) were added to each well. The 96-well PCR plate was then incubated (70°C, 30 min) in thermal cycler (Eppendorf Mastercyler gradient) for color development, followed by incubation in ice water to stop color development. Absorbance was measured at 530 nm using a microtiter plate reader (Tecan Sunrise TC reader, Tecan Group AG, Zurich, Switzerland). The initial velocity data obtained were fitted to the equation $v = V_{max}[S]/([S] + K_m)$ (where v is the initial velocity, Vmax the maximum velocity, [S] the substrate concentration, and Km the Michaelis constant) using GraphPad Prism software (GraphPad software, San Diego, CA, USA). The kcat was calculated from the ratio of V_{max} and enzyme concentration.

Determination of kinetic constants of PpADI wild type and variants M3, M4, M5, M6

The k_{cat} and $S_{0.5}$ values were determined from initial velocity data measured as a function of substrate concentration. Enzyme reaction was carried out at 37°C in a water bath as described previously using purified enzyme (50 µl, 0.1-1.8 µM) to and substrate solution (200 µl, 0.5 mM to 10 mM of arginine, PBS buffer, pH 7.4) in deep well plates.

The initial velocity data obtained were fitted to the sigmoidal model of kinetics equation $v = V_{max}^{n}/(S_{0.5}^{n} + K^{n})$ (where v is the initial velocity, V_{max} is the maximum velocity, K is the substrate concentration, and $S_{0.5}$ is the ligand concentration producing half occupation (131)) using GraphPad Prism software (GraphPad software, San Diego, CA, USA). The k_{cat} was calculated from the ratio of V_{max} and enzyme concentration.

4.3.2.9 Native polyacrylamide gel electrophoresis of PpADI variants

10% of polyacrylamide native gels were used for protein electrophoresis to analyze the native form of PpADI variants. Purified protein of PpADI variants (7 µl of protein and 3 µl of loading dye) were loaded into each lane of native gel. The

molecular marker used in the gel is NativeMark™ Unstained Protein Standard (Invitrogen, Darmstadt, Germany). The electrophoresis was performed with tris/glycine buffer (pH 8.3) and electrophoresis chamber was incubated in ice-water bath. Protein bands were stained with Coomassie brilliant blue solution.

4.3.2.10 Homology modeling

Homology modeling approach was used for the structure prediction of PpADI. The model was built by using the automated structure prediction tool, Protein homology/analogy recognition engine (Phyre: http://www.sbg.bio.ic.ac.uk/~phyre/) (132). The crystal structure of PaADI (PDB ID: 2A9G) was used as template by the server and It has 84.9% sequence identity (http://blast.ncbi.nlm.nih.gov/Blast) with PpADI. Procheck program suit (http://www.ebi.ac.uk/thornton-srv/software/PROCHECK/) (133) was used to assess the stereochemical quality of the model. Ramachandran plot which represented that 84.7% residues were present in the most favoured region and 14.7% in additional allowed region (Figure 3). Dfire was used to access non bonded atomic interaction in the model (http://sparks.informatics.iupui.edu/hzhou/dfire.html/) (134), and Qmean (http://swissmodel.expasy.org/qmean/cgi/index.cgi) (135) for the estimation of global protein quality. Swiss-PdbViewer (118) was used to create the tetramer structure by fitting the monomer model on the 4 units of the 2A9G template. The variant M6 (D38H, D44E, A128T, E296K, H404R) were created by using the “mutate” tool of the Swiss-PdbViewer and by selecting rotamers with the best fitness score. All tetramers were energy minimized in vacuum using GROMOS 43B1 force field (119).

4.4 Results

4.4.1 Improved screening system in microtiter plates to identify PpADI variants with high activities at low arginine concentration

Screening assay was based on the validated citrulline colorimetric screening protocol in microtiter plate, as reported previously (3). In order to screen for variants with high activity at low arginine concentration under physiological

condition concerning pH and ion concentrations, 1 mM arginine in PBS buffer (pH 7.4) as substrate solution was employed in screening assay and enzyme reaction time was controlled accordingly (10 min). The coefficient of variation is an important performance criterion of a screening system to determine its accuracy. Optimized assay condition with 1 mM arginine (PBS buffer, pH 7.4) as substrate resulted in true coefficient of variation of 14.9 % (Figure 1). The resulting low absolute absorbance value is a main reason for the high true coefficient of variation (14.9 %). In the previous screening system, 100 mM arginine in 0.5 M sodium phosphate buffer was used and yielded higher activity variants but with higher K_m value.

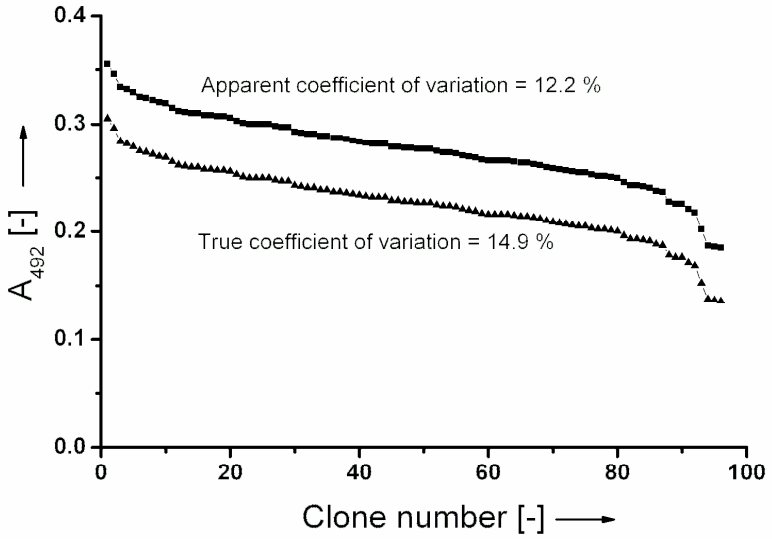

Figure 1. Activity values in descending order of the PpADI variant M3 conversion of arginine to citrulline in a 96-well microtiter plate using the optimized assay protocol. The apparent coefficients of variation were calculated without subtracting the background and the true coefficients of variation after background subtraction.

4.4.2 Genealogic tree of directed PpADI evolution

Figure 2 shows the two rounds of PpADI evolution, generation of saturation mutagenesis libraries and recombination of beneficial positions to finally obtain the PpADI variant M6 with 64.7-fold higher k_{cat} and reduced $S_{0.5}$ (1.3 mM (WT) to 0.81 mM (M6). Based on structure-function analysis of PaADI[16], M1 was generated by substitute His at position 404 with Arg. Position 404 is through

interactions with position Asp280 involved in substrate stabilization during catalysis. M1 was subject to the first round of epPCR library, from which M2 was identified showing a 4-fold improved k_{cat} value and increased K_m value (2.5 mM in 0.5 mM sodium phosphate buffer, pH 7.4)[15]. M3 was generated by a site saturation mutagenesis library at position 128 which increased in another clone the expression level (data not shown). In order to improve PpADI towards medical application demands (high activity at low arginine concentration), a second epPCR mutant library was constructed using M3 as parent. M4 with decreased $S_{0.5}$ value (0.81 mM) and M5 with increased K_{cat} value (17.56 s^{-1}) were identified after screening of ~1400 clones. In M4 the position E296 was identified to be important for lowering $S_{0.5}$ and in M5 position D38 was identified to be important for activity increase. M6 was finally constructed by combining the substations at position D38 and E296. Saturation mutagenesis of these two positions did not yield any further improved $S_{0.5}$ or activity variant.

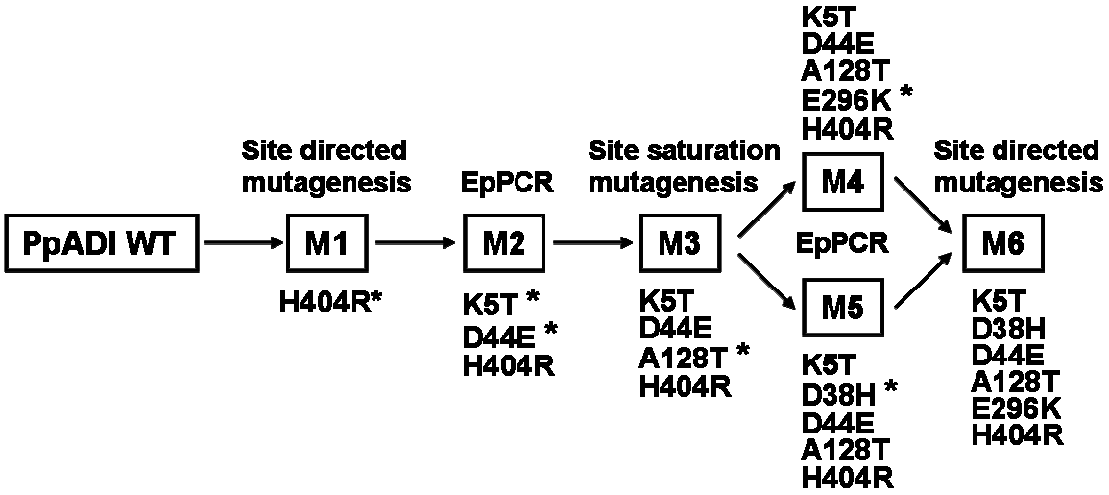

Figure 2. Genealogic tree of PpADI variants (M1 to M6) with generated amino acid substitutions. Novel substitutions are indicated by an asterisk.

4.4.3 EpPCR library construction and screening for variants with high activities at low arginine concentration

Variant M2 was used as a starting template. As described previously, M2 shifts the pH optimum from pH 6.5 to pH 7.0 and has a 4-fold faster k_{cat} than PpADI wild type. In one sequenced mutant, position A128 was identified to be

responsible for higher expression (data not shown). Site saturation mutagenesis on M2 therefore was carried out at position A128. The resulting variant M3 (K5T/D44E/A128T/H404R) showed a ~2-fold improved expression and was subsequently used as parent template for epPCR library.

Three concentrations of $MnCl_2$ (0.01-0.10 mM) were used in epPCR library generation to adjust the ratio of active to inactive clones. Instead of 0.02 mM $MnCl_2$, 0.05 mM $MnCl_2$ which generated 46 % of inactive mutant was selected for library generation. EpPCR mutant libraries with a ratio of ~50 % active and ~50 % inactive clones have often been used successfully in directed evolution, improving enzyme properties by gradual changes (one or two amino acids changes per round of mutagenesis and screening). Two variants M4 and M5 were identified from this epPCR library (~1400 clones) and further characterized. Variant M4 and M5 were sequenced and one additional amino acid substitution was identified for each variant, E296K and D38H, respectively.

4.4.4 Site saturation mutagenesis of *PpADI* at position D38 and E296

To investigate their role in improving of catalytic performance for arginine, site saturation mutagenesis library at position D38 and E296 were generated using PpADI M3 as template. For each position, ~300 clones were screened at low concentration of arginine (1 mM, PBS buffer, pH 7.4), using 96-well plate format citrulline colorimetric screening assay.

After the screening of site saturation mutagenesis libraries of position 38 and 296, variants with higher activity were chosen for preliminary kinetic investigation using crude cell extract. Beneficial mutants were identified and sequenced from both sites (Table 1). At position 38, the following beneficial substitutions were found: D38R (three times, AGA, CGG, CGT) and D38K (twice, AAG, AAA). In all cases, the negatively charged acidic amino Asp had been replaced by positively charged amino acids, Arg or His. Substitution by negatively charged Glu resulted in a clone showing a parent M3-like kinetic behavior. Hydrophobic amino acid

substitution by Pro resulted inactive clone under assay conditions. At position 296, the following substitutions were found to be beneficial: E296K (twice, AAA, AAG), E296N (once, AAC), E296T (once, ACC), E296G (once, GGA). Among these substitutions, variants with substitution to positively charged residue Lys show lowest $S_{0.5}$ value for arginine while substitution by uncharged amino acids (Asn, Thr, Gly) shows relatively marginal improvement compared to E296K. Hydrophobic amino acid substitution by Pro and Trp resulted in very low activity clones.

Table 1. Nucleotide and amino acid substitutions at position 38 in PpADI M3.

PpADI variants	Substitution at position 38	k_m (mM)
M3 (parent)	Asp (GAC)	3.74 ± 0.35
SSM-D38R	Arg (AGA, CGG, CGT)	1.16 ± 0.21
SSM-D38K	Lys (AAG, AAA)	1.01 ± 0.28
SSM-D38E	Glu (GAG)	2.95 ± 0.77
SSM-D38P	Pro (CCA)	n. d.
SSM-D38T	Thr (ACC)	n. d.
M5	His (CAC)	1.26 ± 0.12

Kinetic experiments were performed with crude cell extracts.

Table 2. Nucleotide and amino acid substitutions at position 296 in PpADI M3.

PpADI variants	Substitution at position 296	k_m (mM)
M3 (parent)	Glu (GAA)	3.74 ± 0.35
SSM-E296K	Lys (AAA, AAG)	0.20 ± 0.01
SSM-E296N	Asn (AAC)	0.53 ± 0.04
SSM-E296T	Thr (ACC)	0.61 ± 0.04
SSM-E296Q	Gln (CAA)	0.79 ± 0.06
SSM-E296G	Gly (GGA)	1.29 ± 0.12
SSM-E296W	Trp (TGG)	n. d.
SSM-E296P	Pro (CCT)	n. d.
M4	Lys (AAA)	0.27 ± 0.02

Kinetic experiments were performed with crude cell extracts.
* n. d. activity not detectable under assay conditions.

4.4.5 Determination of kinetic constants (k_{cat} and $S_{0.5}$) of PpADI wild type and variants M3, M4, M5 and M6

Table 3. Kinetic constants of wild type PpADI and variants.

	Wild type	M3 (parent)	M4	M5	M6
k_{cat} (s^{-1})	0.18 ± 0.05	10.13 ± 0.36	5.88 ± 0.09	17.56 ± 1.15	11.64 ± 0.50
$S_{0.5}$ (mM)	1.30 ± 0.25	2.01 ± 0.19	0.81 ± 0.03	1.48 ± 0.17	0.81 ± 0.09

* Kinetic contants of PpADI wild type is different from our previous report because in stead of 0.5 M phosphate buffer, PBS buffer was used for kinetic measurements. K_{cat} value of PpADI wild type dropped from 5.6 s^{-1} to 0.18 s^{-1} and k_{cat} value of M2 is reduced ~2-fold.

M3, the parent of the second round of PpADI epPCR library, M4 with decreased $S_{0.5}$, M5 with increased k_{cat} and best variant M6 with best combination of k_{cat} value and $S_{0.5}$ were selected for detailed characterization studies.

Kinetic characterization of PpADI variants was performed using PBS buffer (pH 7.4), which is commonly used in biological research. PBS buffer helps to maintain a constant pH and its osmolarity and ion concentrations usually match those of the human body. Citrulline production of PpADI variants was maintained between 0.2-0.8 mM. Table 3 summarizes the k_{cat} and $S_{0.5}$ values of parent M3 (K5T/D44E/A128T/H404R), variants M4 (K5T/D44E/A128T/E296K/H404R), M5 (K5T/D44E/A128T/D38H/H404R) and M6 (K5T/D38H/D44E/A128T/E296K/H404R), which were expressed in shaking flasks cultures and purified using a two step procedure (anion exchange follows by gel filtration). Compared to parent M3 ($S_{0.5}$ = 2.01 mM), both variants M4 and M5 have a lower $S_{0.5}$ for arginine conversion at pH 7.4, 0.81 mM and 1.48 mM, respectively. Variant M4 shows a decreased k_{cat} value, 58% of parent M3 while M5 shows a 1.7-fold higher k_{cat} compared to parent M3. Variant M6 with combined mutations (K5T/D38H/D44E/A128T/E296K/H404R) shows decreased $S_{0.5}$ value, 40 % of parent M3 (K5T/D44E/A128T/H404R), 62 % of PpADI wild type, and a 64.7-fold faster k_{cat} value than PpADI wild type. M6 is 42.3-fold faster than PpADI wild type with 0.4 mM arginine (PBS buffer, pH 7.4) as substrate.

After two rounds of epPCR libraries coupled with site directed mutagenesis, a variant M6 with 64.7-fold higher k_{cat} and lower $S_{0.5}$ value (0.81 mM) than PpADI wild type (0.31 mM). At low concentration of arginine, activity of M6 enhanced dramatically than M3 and wild type. For example, M6 is 42.3-fold faster than PpADI wild type in 0.4 mM arginine (PBS buffer, pH 7.4).

4.4.6 Native polyacrylamide gel electrophoresis of PpADI variants

Multimeric form of PpADI variants were investigated by native polyacrylamide gel electrophoresis. As shown in Figure 3, two distinct protein bands representing two multimeric forms tetramer and dimer (molecular weight of a subunit is ~ 46 kDa) were observed, but with different concentration percentage. The major multimeric form of M3 is dimer. Compared to M3, M4 with an additional mutation E296K shows a very different pattern: tetramer is the main form; while M5 with an additional mutation D38H contains more or less equal amount of dimer and tetramer. M6, with both mutations E296K and D38H, contains more tetramer than dimer.

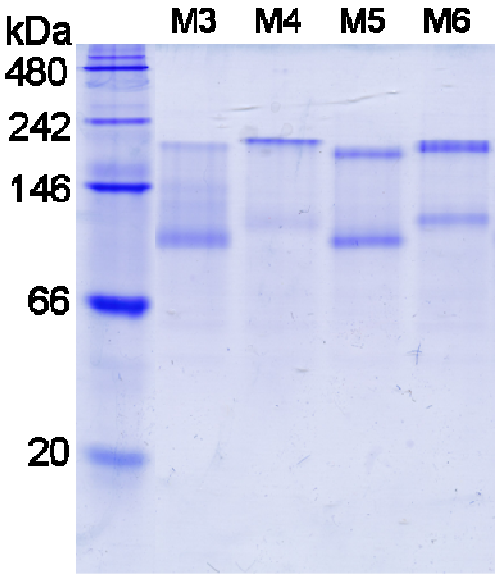

Figure 3. Native polyacrylamide gel electrophoresis of PpADI variants (M3 to M6) with different dimer/tetramer distribution. Single subunit has a molecular weight of ~46 kDa.

4.5 Discussion

Directed evolution allows improving all properties that can be reflected in a screening system through iterative rounds of diversity generation and screening. Small libraries of a few thousand variants are often sufficient to find improved variants [18] even without rational understanding of the targeted property. After establishing a first directed ADI evolution protocol yielding mutant M2, we adjusted the screening system to better reflect ADI's application conditions. Prerequisite for ADI to become an effective anti-tumor agent is that low concentrations of arginine in human plasma can effectively be converted.

Figure 2 shows the genealogic tree of PpADI evolution and before discussing the influence of each substitution individually the effect on kinetics are briefly summarized. Amino acid substitution D44E (M2) increases k_{cat} and $S_{0.5}$, substitution A128T (M3) increases the expression level, and substitution E296K (M4) decreases k_{cat} and $S_{0.5}$ and is responsible for tetramer formation. Substitution D38H (M5) increase largely k_{cat} and reduces slightly $S_{0.5}$. The combination of all mentioned residues in M6 result in a finally 64.7-fold improved PpADI activity and reduced $S_{0.5}$ (1.30 to 0.81 mM).

PpADI M3 was obtained from site saturation mutagenesis library at position A128 using M2 as template (Figure 2). M3 shows improved functional expression level of ADI (data not shown) and was used as parent for generating an epPCR library. Screening of epPCR library yielded two improved variants M4 and M5, carrying an additional mutation, E296K (M4) and D38H (M5). M4 has a decreased $S_{0.5}$ (0.81 mM) and a decreased k_{cat} value (5.88 s^{-1}; see Table 3). M5 has a decreased $S_{0.5}$ (1.48 mM) and an increased k_{cat} value (17.56 s^{-1}) when compared to parent M3 ($S_{0.5}$, 2.01 mM; k_{cat}, 10.03 s^{-1}; see Table 3). M6 which harbors both substitutions (E296K and D38H) has a decreased $S_{0.5}$ value (0.81 mM) compared to the parent M3 (1.30 mM) and the wild type (2.01 mM), and a 64.7-fold higher k_{cat} value than the PpADI wild type.

Despite further enhancing the activity of PpADI, it is crucial for an efficient conversion of the substrate arginine in human plasma (100-120 µM arginine) to reduce PpADI's "K_m" ($S_{0.5}$) value. Figure 4 shows the kinetics of PpADI WT, parent M3, and the variants M4, M5 and M6. M3 has a significantly higher k_{cat} value compared to WT, but its activity at low concentration of arginine (<1.0 mM) is very low ($S_{0.5}$ value 2.01 mM). In contrast, the most efficient variant M6 with a decreased $S_{0.5}$ value (0.81 mM) shows a remarkable activity improvement at low concentrations of arginine (<0.5 mM; see Figure 4). M6 has additional two amino acid substitutions (D38H and E296K) compared to M3 which increases k_{cat} and reduces the $S_{0.5}$ value. The combination of D38H and E296K improves especially the activity of M6 at low arginine concentrations (< 0.5 mM; see Figure 4).

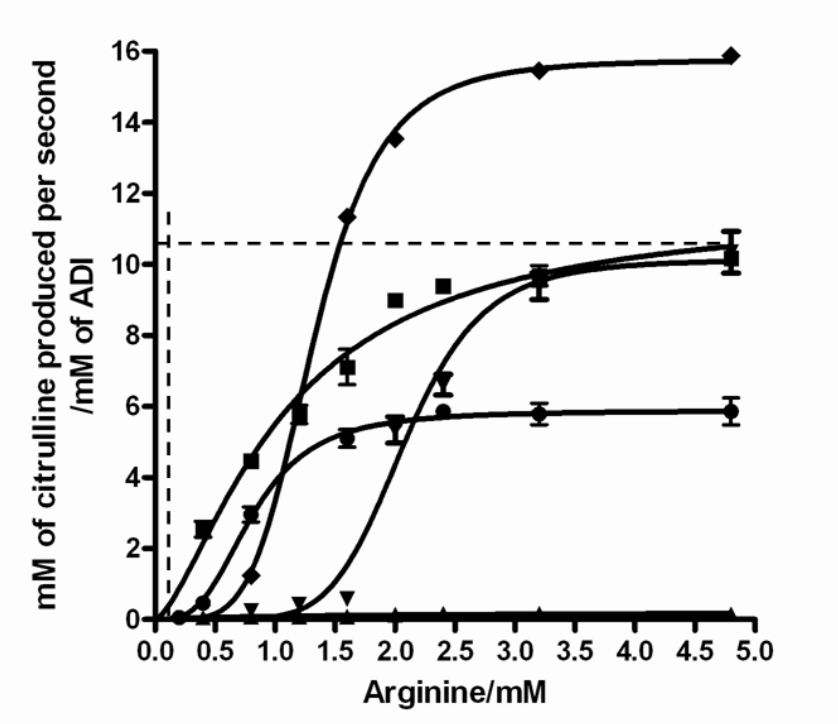

Figure 4. Kinetic curve of PpADI wild type, M3, M5 and M6. (▲) PpADI wild type, (▼) M3, (●) M4, (♦) M5 and (■) M6.

Figure 5 shows the tetrameric model (based on PaADI, PDB code 2A9G) of PpADI WT (Figure 5A) and variant M6 (Figure 5B). Monomeric units are

indicated with the letters a, b, c and d. The access channel to the active sites of each monomer is highlighted in square and faces an internal cavity generated by the assembly of four PpADI monomers. The substitutions D38H (in blue) and D44E (in green) are localized at the interface of monomer pair a-b and c-d. The substitution of Glu by Asp at position 44 provides a longer side chain in close proximity of the also negatively charged residue Asp43 (Figure 6A). The substitution E296K is localized at the border of the entrance to the internal cavity of the PpADI tetramer. E296K promotes the tetramer formation likely by introducing stabilizing interactions with other residues, for example with Thr33 (hydrogen bond). E296K inverts the charge at this position and its increased length of the side chain might promote further interactions to a neighboring monomer (Figure 6A). The combination of D44E and E296K results in a population consisting of mainly tetramers (see Figure 3; mutein M4). Interestingly with the formation of a tetramer (M4) the $S_{0.5}$ value is reduced which indicates that the tetramer complex formation promotes interactions with the substrate arginine at low concentrations. The substitution D38H together with the E296K in the mutein M6 reestablishes an almost equal population of PpADI dimers and tetramers. A hypothesis is that Lys of the E296K has an electrostatic stabilizing interaction with the Glu38 in the M4 but not to the neutral His38.

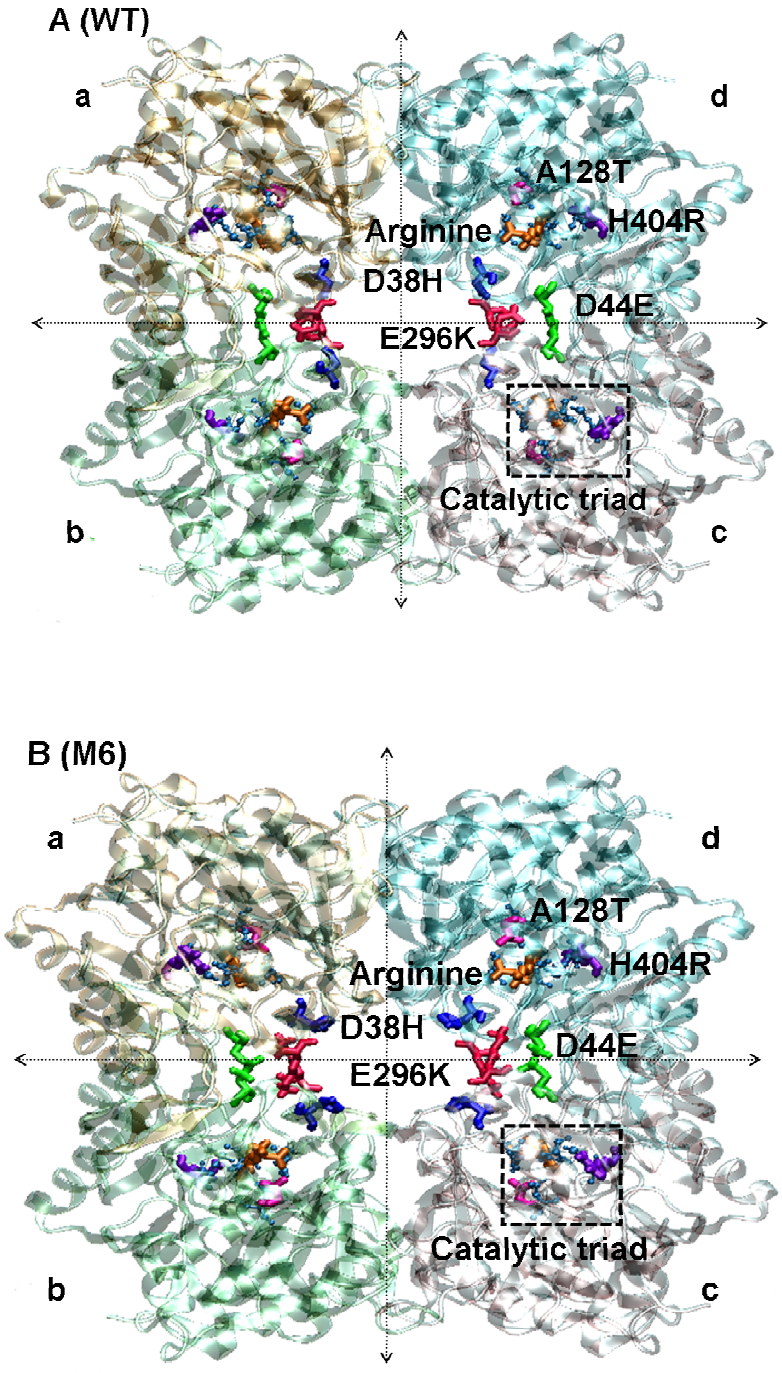

Figure 5. A). The model of WT tetramer after energy minimization in vacuum (GROMOS 43B1). B). The model of M6 tetramer after energy minimization in vacuum (GROMOS 43B1). Active site residues are represented in CRK format in a square (Blue). Mutated residues are shown in licorice format in different colors like D38H (blue), D44E (green), A128T (magenta), E296K (red) and H404R (violet). Substrate arginine is represented in orange color by licorice format.

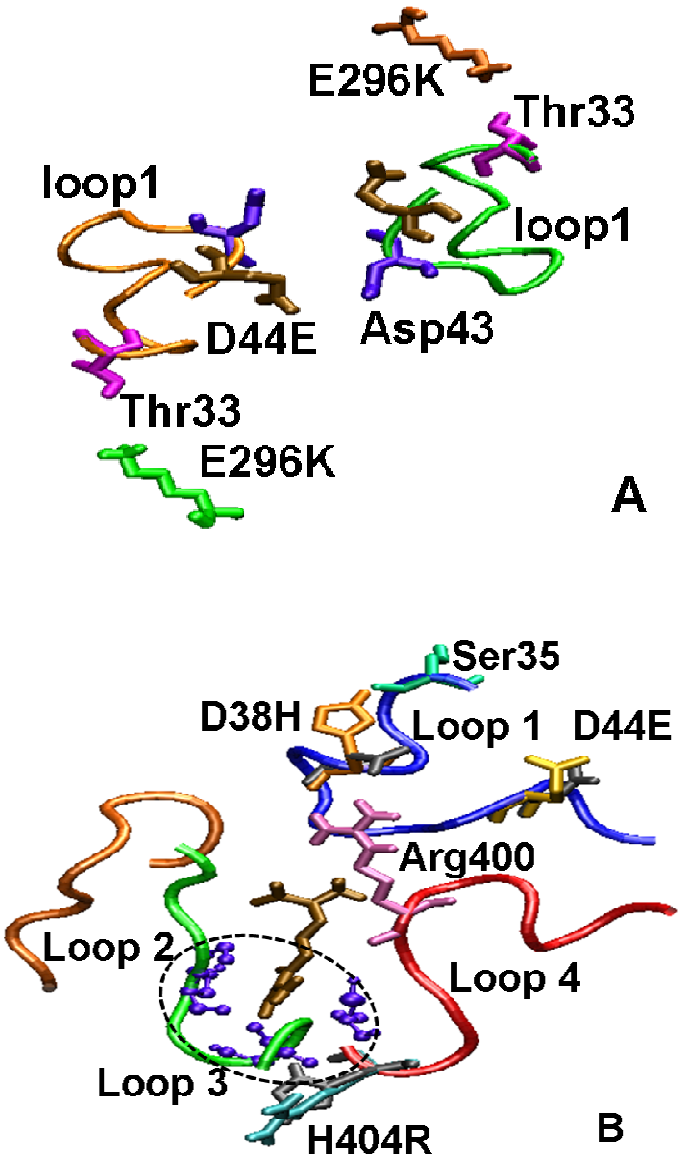

Figure 6. A). Structure model of variant M6. E296K is involved in intermonomer interaction (between chain a (orange) and b (green)) with Thr33. D44E is involved in intermonomer interaction, between chain A (orange) and B (green), with Asp43 (violet). B). Structure alignment of PpADI WT model and M6 model with four loops (loop 1:30-46, loop 2:178-175, loop 3:271-281 and loop 4: 393-404) surrounding the entrance of the active site. The substitutions in these loops and the residues involved in the interaction with those substitutions are representing: D38H (orange), D44E (yellow) and H404R (cyan, in M6; gray, in WT), Ser35 (green), Arg 400 (pink), substrate arginine (ochre), catalytic triad His278, Asp280 and Cys406 (violet, highlighted in an oval)

Figure 6B shows that the active site of the PaADI is surrounded by four loops (loop 1: 30-46, loop 2: 178-185, loop 3: 271-281, and loop 4: 393-404). These four loops undergo a conformational transition upon arginine binding and tighten

the surrounding of the arginine substrate[16]. D38 is located in loop 1 and faces towards the substrate access channel. In PpADI model (Figure 6B), the D38H mutation promotes the formation of a hydrogen bond interaction with the neighboring residues Ser35, contributing to the stability of the entropically unfavorable folded conformation of loop1. The rigidified loop 1 might be beneficial for arginine conversion. According to PaADI structure analysis, the side chain of gating residue Arg401 (Arg400 in PpADI) is located at the active site entrance and fills the substrate-binding site. The structure analysis of the C406A PaADI-L-arginine complex[16] shows that the Arg401 side chain (Arg400 in PpADI) is displaced by the substrate arginine to a position near the active site entrance that allows its hydrocarbon chain to assist shielding the catalytic site from solvent. D38 is involved in an ionic interaction and hydrogen bonding with Arg400. The substitution of Asp to His at position 38 results in a loss of ionic interactions to Arg400 due to the different lengths of the side chains. His38 can form only a hydrogen bond with active site gating residue Arg400. A weakened interaction between position 38 and Arg400 might increase the flexibility of the side chain of Arg400 which then might block less efficiently the access of arginine to the active site. As a result the variant M5 shows an improved k_{cat} value (1.7-fold compared to parent M3) due to the substitution D38H.

For elucidating further the individual role of the five identified amino acid substitutions and their influence on the active site geometry and tetramer formation crystal structures of variant M4 and M6 have to be solved.

4.6 Conclusion

In summary, with the modified screening protocol, PpADI variants with improved k_{cat} and $S_{0.5}$ were identified. The increased k_{cat} value and decreased $S_{0.5}$ value result in significant activity improvement of PpADI at low arginine concentrations. Especially the kinetic constants of PpADI variant M6 demonstrate that PpADI properties can be tailored by directed evolution. The generated PpADI variants match from their kinetic behavior therapeutic application demands much better

than the wild type PpADI. We therefore hope that by directed evolution improved PpADIs will further be investigated *in vivo* for tumor therapy.

References

1. Li L, Li ZM, Chen DQ*, et al.* Inactivation of microbial arginine deiminases by L-canavanine. Journal of the American Chemical Society, 2008; 130(6): 1918-31.

2. Lu XF, Li L, Wu R*, et al.* Kinetic analysis of *Pseudomonas aeruginosa* arginine deiminase mutants and alternate substrates provides insight into structural determinants of function. Biochemistry, 2006; 45(4): 1162-72.

3. Zhu LL, Tee KL, Roccatano D*, et al.* Directed evolution of an antitumor drug (arginine deiminase PpADI) for increased activity at physiological pH. Chembiochem, 2010; 11(5): 691-7.

4. Das K, Butler GH, Kwiatkowski V, Clark AD, Yadav P, Arnold E. Crystal structures of arginine deiminase with covalent reaction intermediates: Implications for catalytic mechanism. Structure, 2004; 12(4): 657-67.

5. Schofield PJ, Edwards MR, Matthews J, Wilson JR. The pathway of arginine catabolism in *Giardia intestinalis*. Molecular and Biochemical Parasitology, 1992; 51(1): 29-36.

6. Linstead D, Cranshaw MA. The pathway of arginine catabolism in the parasitic flagellate *Trichomonas vaginalis*. Molecular and Biochemical Parasitology, 1983; 8(3): 241-52.

7. Yarlett N, Lindmark DG, Goldberg B, Moharrami MA, Bacchi CJ. Subcellular localization of the enzymes of the arginine dihydrolase pathway in Trichomonas vaginalis and Tritrichomonas foetus. J Eukaryot Microbiol, 1994; 41(6): 554-9.

8. Biagini GA, Yarlett N, Ball GE*, et al.* Bacterial-like energy metabolism in the amitochondriate protozoon Hexamita inflata. Mol Biochem Parasitol, 2003; 128(1): 11-9.

9. Makhlin J, Kofman T, Borovok I*, et al.* Staphylococcus aureus ArcR controls expression of the arginine deiminase operon. Journal of Bacteriology, 2007; 189(16): 5976-86.

10. Seggewiss J, Becker K, Kotte O*, et al.* Reporter metabolite analysis of transcriptional profiles of a Staphylococcus aureus strain with normal phenotype

and its isogenic hemB mutant displaying the small-colony-variant phenotype. Journal of Bacteriology, 2006; 188(22): 7765-77.

11. Altucci P, Sapio V, Vitale P, de Vargas F. Mycoplasma in human pathology. Current status of the problem, with special reference to respiratory pathology. Recenti Prog Med, 1966; 41(5): 409-55.

12. Harasawa R, Koshimizu K, Kitagawa M, Asada K, Kato I. Nucleotide sequence of the arginine deiminase gene of *Mycoplasma hominis*. Microbiology and Immunology, 1992; 36(6): 661-5.

13. Takaku H, Matsumoto M, Misawa S, Miyazaki K. Antitumor activity of arginine deiminase from *Mycoplasma arginini* and its growth inhibitory mechanism. Japanese Journal of Cancer Research, 1995; 86(9): 840-6.

14. Fenske JD, Kenny GE. Role of arginine deiminase in growth of *Mycoplasma hominis*. Journal of Bacteriology, 1976; 126(1): 501-10.

15. Wei YZ, Zhou H, Sun Y, He YB, Luo YZ. Insight into the catalytic mechanism of arginine deiminase: Functional studies on the crucial sites. Proteins-Structure Function and Bioinformatics, 2007; 66(3): 740-50.

16. Ensor CM, Holtsberg FW, Bomalaski JS, Clark MA. Pegylated arginine deiminase (ADI-SS PEG(20,000) (mw)) inhibits human melanomas and hepatocellular carcinomas in vitro and in vivo. Cancer Research, 2002; 62(19): 5443-50.

17. Galkin A, Lu XF, Dunaway-Mariano D, Herzberg O. Crystal structures representing the Michaelis complex and the thiouronium reaction intermediate of Pseudomonas aeruginosa arginine deiminase. Journal of Biological Chemistry, 2005; 280(40): 34080-7.

18. Kundu M, Thomas J, Fialho AM*, et al.* The anticancer activity of the N-terminal CARD-Like domain of arginine deiminase (ADI) from *Pseudomonas aeruginosa*. Letters in Drug Design & Discovery, 2009; 6(6): 403-12.

19. Beloussow K, Wang L, Wu J, Ann D, Shen WC. Recombinant arginine deiminase as a potential anti-angiogenic agent. Cancer Letters, 2002; 183(2): 155-62.

20. Misawa S, Aoshima M, Takaku H, Matsumoto M, Hayashi H. High-Level expression of Mycoplasma arginine deiminase in *Escherichia coli* and Its efficient renaturation as an antitumor enzyme. Journal of Biotechnology, 1994; 36(2): 145-55.
21. Gong H, Zolzer F, von Recklinghausen G*, et al.* Arginine deiminase inhibits cell proliferation by arresting cell cycle and inducing apoptosis. Biochemical and Biophysical Research Communications, 1999; 261(1): 10-4.
22. Takaku H, Takase M, Abe S, Hayashi H, Miyazaki K. *In vivo* antitumor activity of arginine deiminase purified from *Mycoplasma arginini*. International Journal of Cancer, 1992; 51(2): 244-9.
23. Kim JE, Jeong DW, Lee HJ. Expression, purification, and characterization of arginine deiminase from Lactococcus lactis ssp lactis ATCC 7962 in Escherichia coli BL21. Protein Expression and Purification, 2007; 53(1): 9-15.
24. Kakimoto T, Shibatan.T, Chibata I. Crystallization of L-arginine deiminase from *Pseudomonas putida*. Febs Letters, 1971; 19(2): 166-8.
25. Shibatani T, Kakimoto T, Chibata I. Crystallization and properties of L-arginine deiminase of *Pseudomonas Putida* 2. Journal of Biological Chemistry, 1975; 250(12): 4580-3.
26. Galkin A, Kulakova L, Sarikaya E, Lim K, Howard A, Herzberg O. Structural insight into arginine degradation by arginine deiminase, an antibacterial and parasite drug target. Journal of Biological Chemistry, 2004; 279(14): 14001-8.
27. Ni Y, Schwaneberg U, Sun ZH. Arginine deiminase, a potential anti-tumor drug. Cancer Lett, 2008; 261(1): 1-11.
28. Galkin A, Kulakova L, Sarikaya E, Lim K, Howard A, Herzberg O. J Biol Chem, 2004; 279: 14001.
29. Galkin A, Lu XF, Dunaway-Mariano D, Herzberg O. J Biol Chem, 2005; 280: 34080.
30. Holle LM. Pegaspargase: an alternative? Annals of Pharmacotherapy, 1997; 31(5): 616-24.

31. Yoshioka T, Wada T, Uchida N*, et al.* Anticancer efficacy in vivo and in vitro, synergy with 5-fluorouracil, and safety of recombinant methioninase. Cancer Research, 1998; 58(12): 2583-7.
32. Lam TL, Wong GKY, Chong HC*, et al.* Recombinant human arginase inhibits proliferation of human hepatocellular carcinoma by inducing cell cycle arrest. Cancer Letters, 2009; 277(1): 91-100.
33. Shen RS, Fritz RR, Abell CW. Biochemical-Properties and Immunogenicity of L-Phenylalanine Ammonia-Lyase - Effects on Tumor-Bearing Mice. Cancer Treatment Reports, 1979; 63(6): 1063-8.
34. Yoshimoto T, Chao SG, Saito Y, Imamura I, Wada H, Inada Y. Chemical modification of tryptophanase from E. coli with polyethylene glycol to reduce its immunoreactivity towards anti-tryptophanase antibodies. Enzyme, 1986; 36(4): 261-5.
35. Feun LG, Savaraj N, Marini A*, et al.* Phase II study of pegylated arginine deiminase (ADI-PEG20), a novel targeted therapy for melanoma. Journal of Clinical Oncology, 2006; 24(18): 464s-s.
36. Gong H, Zolzer F, von Recklinghausen G, Havers W, Schweigerer L. Arginine deiminase inhibits proliferation of human leukemia cells more potently than asparaginase by inducing cell cycle arrest and apoptosis. Leukemia, 2000; 14(5): 826-9.
37. Morris SM, Jr. Regulation of enzymes of the urea cycle and arginine metabolism. Annu Rev Nutr, 2002; 22: 87-105.
38. Scott L, Lamb J, Smith S, Wheatley DN. Single amino acid (arginine) deprivation: rapid and selective death of cultured transformed and malignant cells. British Journal of Cancer, 2000; 83(6): 800-10.
39. Wheatley DN, Campbell E. Arginine catabolism, liver extracts and cancer. Pathol Oncol Res, 2002; 8(1): 18-25.
40. Thomas JB, Holtsberg FW, Ensor CM, Bomalaski JS, Clark MA. Enzymatic degradation of plasma arginine using arginine deiminase inhibits nitric oxide production and protects mice from the lethal effects of tumor necrosis factor and endotoxin. Molecular Biology of the Cell, 2001; 12: 404a-a.

41. Cheng PNM, Leung YC, Lo WH, Tsui SM, Lam KC. Remission of hepatocellular carcinoma with arginine depletion induced by systemic release of endogenous hepatic arginase due to transhepatic arterial embolisation, augmented by high-dose insulin: arginase as a potential drug candidate for hepatocellular carcinoma. Cancer Letters, 2005; 224(1): 67-80.
42. Cheng PNM, Lam TL, Lam WM*, et al.* Pegylated recombinant human arginase (rhArg-peg(5,000mw)) inhibits the in vitro and in vivo proliferation of human hepatocellular carcinoma through arginine depletion. Cancer Research, 2007; 67(1): 309-17.
43. Kim JH, Yu YS, Kim DH, Min BH, Kim KW. Anti-tumor activity of arginine deiminase via arginine deprivation in retinoblastoma. Oncol Rep, 2007; 18(6): 1373-7.
44. Kim RH, Coates JM, Bowles TL*, et al.* Arginine deiminase as a novel therapy for prostate cancer induces autophagy and caspase-independent apoptosis. Cancer Research, 2009; 69(2): 700-8.
45. Glazer ES, Piccirillo M, Albino V*, et al.* Phase II study of pegylated arginine deiminase for nonresectable and metastatic hepatocellular carcinoma. Journal of Clinical Oncology, 2010; 28(13): 2220-6.
46. Ascierto PA, Scala S, Castello G*, et al.* Pegylated arginine deiminase treatment of patients with metastatic melanoma: Results from phase I and II studies. Journal of Clinical Oncology, 2005; 23(30): 7660-8.
47. Shen LJ, Beloussow K, Shen WC. Accessibility of endothelial and inducible nitric oxide synthase to the intracellular citrulline-arginine regeneration pathway. Biochemical Pharmacology, 2005; 69(1): 97-104.
48. Park H, Lee JB, Shim YJ*, et al.* Arginine deiminase enhances MCF-7 cell radiosensitivity by inducing changes in the expression of cell cycle-related proteins. Molecules and Cells, 2008; 25(2): 305-11.
49. Kubo M, Nishitsuji H, Kurihara K, Hayashi T, Masuda T, Kannagi M. Suppression of human immunodeficiency virus type 1 replication by arginine deiminase of *Mycoplasma arginini*. Journal of General Virology, 2006; 87: 1589-93.

50. Izzo F, Montella M, Orlando AP*, et al.* Pegylated arginine deiminase lowers hepatitis C viral titers and inhibits nitric oxide synthesis. Journal of Gastroenterology and Hepatology, 2007; 22(1): 86-91.
51. Kwan JM, Fialho AM, Kundu M*, et al.* Bacterial proteins as potential drugs in the treatment of leukemia. Leukemia Research, 2009; 33(10): 1392-9.
52. Tsai WB, Aiba I, Lee SY, Feun L, Savaraj N, Kuo MT. Resistance to arginine deiminase treatment in melanoma cells is associated with induced argininosuccinate synthetase expression involving c-Myc/HIF-1 alpha/Sp4. Molecular Cancer Therapeutics, 2009; 8(12): 3223-33.
53. Yoon CY, Shim YJ, Kim EH*, et al.* Renal cell carcinoma does not express argininosuccinate synthetase and is highly sensitive to arginine deprivation via arginine deiminase. International Journal of Cancer, 2007; 120(4): 897-905.
54. Feun L, You M, Wu CJ*, et al.* Arginine deprivation as a targeted therapy for cancer. Current Pharmaceutical Design, 2008; 14(11): 1049-57.
55. Zhu ZW, Momeu C, Zakhartsev M, Schwaneberg U. Making glucose oxidase fit for biofuel cell applications by directed protein evolution. Biosens Bioelectron, 2006; 21(11): 2046-51.
56. Panke S, Held M, Wubbolts M. Trends and innovations in industrial biocatalysis for the production of fine chemicals. Current Opinion in Biotechnology, 2004; 15(4): 272-9.
57. Patel RN. Chemo-enzymatic synthesis of pharmaceutical intermediates. Expert Opinion on Drug Discovery, 2008; 3(2): 187-245.
58. Yokobayashi Y, Weiss R, Arnold FH. Directed evolution of a genetic circuit. Proc Natl Acad Sci U S A, 2002; 99(26): 16587-91.
59. Ellington AD, Chen X, Robertson M, Syrett A. Evolutionary origins and directed evolution of RNA. International Journal of Biochemistry & Cell Biology, 2009; 41(2): 254-65.
60. Alper H, Fischer C, Nevoigt E, Stephanopoulos G. Tuning genetic control through promoter engineering. Proceedings of the National Academy of Sciences of the United States of America, 2005; 102(36): 12678-83.

61. Drummond DA, Iverson BL, Georgiou G, Arnold FH. Why high-error-rate random mutagenesis libraries are enriched in functional and improved proteins. J Mol Biol, 2005; 350(4): 806-16.
62. Wong TS, Roccatano D, Schwaneberg U. Steering directed protein evolution: strategies to manage combinatorial complexity of mutant libraries. Environmental Microbiology, 2007; 9(11): 2645-59.
63. Wong TS, Zhurina D, Schwaneberg U. The diversity challenge in directed protein evolution. Combinatorial Chemistry & High Throughput Screening, 2006; 9(4): 271-88.
64. Fasan R, Chen MM, Crook NC, Arnold FH. Engineered alkane-hydroxylating cytochrome P450(BM3) exhibiting nativelike catalytic properties. Angewandte Chemie-International Edition, 2007; 46(44): 8414-8.
65. Titus SA, Xiao L, Southall N*, et al.* Cell-based PDE4 assay in 1536-well plate format for high-throughput screening. Journal of Biomolecular Screening, 2008; 13(7): 609-18.
66. Lafferty M, Dycaico MJ. GigaMatrix^{TM}: an ultra highthroughput tool for accessing biodiversity. JALA, 2009; 9: 200-8.
67. Yang GY, Withers SG. Ultrahigh-throughput FACS-based screening for directed enzyme evolution. Chembiochem, 2009; 10(17): 2704-15.
68. Miller OJ, Hibbert EG, Ingram CU, Lye GJ, Dalby PA. Optimisation and evaluation of a generic microplate-based HPLC screen for transketolase activity. Biotechnology Letters, 2007; 29(11): 1759-70.
69. Yoshikuni Y, Ferrin TE, Keasling JD. Designed divergent evolution of enzyme function. Nature, 2006; 440(7087): 1078-82.
70. Becker S, Schmoldt HU, Adams TM, Wilhelm S, Kolmar H. Ultra-high-throughput screening based on cell-surface display and fluorescence-activated cell sorting for the identification of novel biocatalysts. Current Opinion in Biotechnology, 2004; 15(4): 323-9.
71. Farinas ET. Fluorescence activated cell sorting for enzymatic activity. Combinatorial Chemistry & High Throughput Screening, 2006; 9(4): 321-8.

72. Agresti JJ, Antipov E, Abate AR*, et al.* Ultrahigh-throughput screening in drop-based microfluidics for directed evolution. Proceedings of the National Academy of Sciences of the United States of America, 2010; 107(9): 4004-9.
73. Leemhuis H, Kelly RM, Dijkhuizen L. Directed evolution of enzymes: library screening strategies. Iubmb Life, 2009; 61(3): 222-8.
74. Chen KC, Wu CH, Chang CY*, et al.* Directed evolution of a lysosomal enzyme with enhanced activity at neutral pH by mammalian cell-surface display. Chem Biol, 2008; 15(12): 1277-86.
75. Wang Q, Xia T. Enhancement of the activity and alkaline pH stability of Thermobifida fusca xylanase A by directed evolution. Biotechnology Letters, 2008; 30(5): 937-44.
76. Colin DY, Deprez-Beauclair P, Silva N, Infantes L, Kerfelec B. Modification of pancreatic lipase properties by directed molecular evolution. Protein Engineering Design & Selection, 2010; 23(5): 365-73.
77. Bessler C, Schmitt J, Maurer KH, Schmid RD. Directed evolution of a bacterial alpha-araylase: Toward enhanced pH-performance and higher specific activity. Protein Sci, 2003; 12(10): 2141-9.
78. Liu ZQ, Sun ZH, Leng Y. Directed evolution and characterization of a novel D-pantonohydrolase from Fusarium moniliforme. Journal of Agricultural and Food Chemistry, 2006; 54(16): 5823-30.
79. Hasan Z, Renirie R, Kerkman R, Ruijssenaars HJ, Hartog AF, Wever R. Laboratory-evolved vanadium chloroperoxidase exhibits 100-fold higher halogenating activity at alkaline pH - Catalytic effects from first and second coordination sphere mutations. Journal of Biological Chemistry, 2006; 281(14): 9738-44.
80. Makde RD, Dikshit K, Kumar V. Protein engineering of class-A non-specific acid phosphatase (PhoN) of Salmonella typhimurium: Modulation of the pH-activity profile. Biomolecular Engineering, 2006; 23(5): 247-51.
81. Kim T, Mullaney EJ, Porres JM*, et al.* Shifting the pH profile of *Aspergillus niger* PhyA phytase to match the stomach pH enhances its effectiveness as an

animal feed additive. Applied and Environmental Microbiology, 2006; 72(6): 4397-403.
82. Hirata A, Adachi M, Utsumi S, Mikami B. Engineering of the pH optimum of Bacillus cereus beta-amylase: Conversion of the pH optimum from a bacterial type to a higher-plant type. Biochemistry, 2004; 43(39): 12523-31.
83. Tomschy A, Brugger R, Lehmann M*, et al.* Engineering of phytase for improved activity at low pH. Appl Environ Microbiol, 2002; 68(4): 1907-13.
84. Sakoda H, Imanaka T. Cloning and sequencing of the gene coding for alcohol dehydrogenase of Bacillus stearothermophilus and rational shift of the optimum pH. J Bacteriol, 1992; 174(4): 1397-402.
85. Yang JH, Park JY, Kim SH, Yoo YJ. Shifting pH optimum of Bacillus circulans xylanase based on molecular modeling. Journal of Biotechnology, 2008; 133(3): 294-300.
86. MacPherson IS, Rosell FI, Scofield M, Mauk AG, Murphy MEP. Directed evolution of copper nitrite reductase to a chromogenic reductant. Protein Engineering Design & Selection, 2010; 23(3): 137-45.
87. Hida K, Hanes J, Ostermeier M. Directed evolution for drug and nucleic acid delivery. Adv Drug Deliv Rev, 2007; 59(15): 1562-78.
88. Yuan L, Kurek I, English J, Keenan R. Laboratory-directed protein evolution. Microbiology and Molecular Biology Reviews, 2005; 69(3): 373-92.
89. Rautio J, Kumpulainen H, Heimbach T*, et al.* Prodrugs: design and clinical applications. Nat Rev Drug Discov, 2008; 7(3): 255-70.
90. Barak Y, Thorne SH, Ackerley DF, Lynch SV, Contag CH, Matin A. New enzyme for reductive cancer chemotherapy, YieF, and its improvement by directed evolution. Molecular Cancer Therapeutics, 2006; 5(1): 97-103.
91. Kuhn I, Harden P, Bauzon M*, et al.* Directed evolution generates a novel oncolytic virus for the treatment of colon cancer. PLoS One, 2008; 3(6): e2409.
92. Robertson DE, Steer BA. Recent progress in biocatalyst discovery and optimization. Current Opinion in Chemical Biology, 2004; 8(2): 141-9.
93. Soares AL, Guirmaraes GM, Polakiewicz B, Pitombo RND, Abrahao-Neto J. Effects of polyethylene glycol attachment on physicochemical and biological

stability of E-coli L-asparaginase. International Journal of Pharmaceutics, 2002; 237(1-2): 163-70.
94. Kotzia GA, Labrou NE. Engineering thermal stability of L-asparaginase by in vitro directed evolution. Febs Journal, 2009; 276(6): 1750-61.
95. Orlova A, Feldwisch J, Abrahmsen L, Tolmachev V. Affibody molecules for molecular imaging and therapy for cancer. Cancer Biotherapy and Radiopharmaceuticals, 2007; 22(5): 573-84.
96. Nilsson FY, Tolmachev V. Affibody (R) molecules: New protein domains for molecular imaging and targeted tumor therapy. Current Opinion in Drug Discovery & Development, 2007; 10(2): 167-75.
97. Gronwall C, Sjoberg A, Ramstrom M*, et al.* Affibody-mediated transferrin depletion for proteomics applications. Biotechnol J, 2007; 2(11): 1389-98.
98. Renberg B, Shiroyama I, Engfeldt T, Nygren PA, Karlstrom AE. Affibody protein capture microarrays: Synthesis and evaluation of random and directed immobilization of affibody molecules. Analytical Biochemistry, 2005; 341(2): 334-43.
99. Friedman M, Orlova A, Johansson E*, et al.* Directed evolution to low nanomolar affinity of a tumor-targeting epidermal growth factor receptor-binding affibody molecule. Journal of Molecular Biology, 2008; 376(5): 1388-402.
100. Chang CCJ, Chen TT, Cox BW*, et al.* Evolution of a cytokine using DNA family shuffling. Nature Biotechnology, 1999; 17(8): 793-7.
101. Zhang JH, Dawes G, Stemmer WPC. Directed evolution of a fucosidase from a galactosidase by DNA shuffling and screening. Proceedings of the National Academy of Sciences of the United States of America, 1997; 94(9): 4504-9.
102. Crameri A, Cwirla S, Stemmer WPC. Construction and evolution of antibody-phage libraries by DNA shuffling. Nature Medicine, 1996; 2(1): 100-2.
103. Patten PA, Howard RJ, Stemmer WP. Applications of DNA shuffling to pharmaceuticals and vaccines. Curr Opin Biotechnol, 1997; 8(6): 724-33.
104. Park IS, Kang SW, Shin YJ*, et al.* Arginine deiminase: a potential inhibitor of angiogenesis and tumour growth. Br J Cancer, 2003; 89(5): 907-14.

105. Izzo F, Marra P, Beneduce G*, et al.* Pegylated arginine deiminase treatment of patients with unresectable hepatocellular carcinoma: Results from phase I/II studies. J Clin Oncol, 2004; 22(10): 1815-22.
106. Gong H, Zölzer F, von Recklinghausen G, Havers W, Schweigerer L. Arginine deiminase inhibits proliferation of human leukemia cells more potently than asparaginase by inducing cell cycle arrest and apoptosis. Leukemia, 2000; 14(5): 826-9.
107. Shen LJ, Shen WC. Drug evaluation: ADI-PEG-20 - a PEGylated arginine deiminase for arginine-auxotrophic cancers. Curr Opin in Mol Ther, 2006; 8(3): 240-8.
108. Holtsberg FW, Ensor CM, Steiner MR, Bomalaski JS, Clark MA. Poly(ethylene glycol) (PEG) conjugated arginine deiminase: effects of PEG formulations on its pharmacological properties. J Controlled Release, 2002; 80(1-3): 259-71.
109. Mûller HJ, Boos J. Use of L-asparaginase in childhood all. Crit Rev Oncol Hematol, 1998; 28(2): 97-113.
110. Turunen O, Janis J, Fenel F, Leisola M. Engineering the thermotolerance and pH optimum of family 11 xylanases by site-directed mutagenesis. Methods Enzymol, 2004; 388: 156-67.
111. Fang TY, Ford C. Protein engineering of *Aspergillus awamori* glucoamylase to increase its pH optimum. Protein Eng, 1998; 11(5): 383-8.
112. Sakoda H, Imanaka T. Cloning and sequencing of the gene coding for alcohol-dehydrogenase of *Bacillus stearothermophilus* and rational shift of the optimum pH. J Bacteriol, 1992; 174(4): 1397-402.
113. Wang WY, Malcolm BA. Two-stage PCR protocol allowing introduction of multiple mutations, deletions and insertions using QuikChange™ site-directed mutagenesis. BioTechniques, 1999; 26(4): 680-2.
114. Miyazaki K, Takenouchi M. Creating random mutagenesis libraries using megaprimer PCR of whole plasmid. Biotechniques, 2002; 33(5): 1033-8.
115. Studier FW. Protein production by auto-induction in high-density shaking cultures. Protein Expression and Purification, 2005; 41(1): 207-34.

116. Archibald RM. Deternination of citrulline and allantoin and demonstration of citrulline in blood plasma. J Biol Chem, 1944; 156(1): 121-42.
117. Boyde TRC, Rahmatullah M. Optimization of conditions for the colorimetric determination of citrulline, using diacetyl monoxime. Anal Biochem, 1980; 107(2): 424-31.
118. Guex N, Peitsch MC. SWISS-MODEL and the Swiss-PdbViewer: an environment for comparative protein modeling. Electrophoresis, 1997; 18(15): 2714-23.
119. van Gunsteren WF, Billeter SR, Eising AA*, et al.* Biomolecular simulation: the gromos 96 manual and user guide ETH Zürich; 1996.
120. Mather A, Roland D. Automated thiosemicarbazide-diacetyl monoxime method for plasma urea. Clinical Chemistry, 1969; 15(5): 393-6.
121. Wong TS, Arnold FH, Schwaneberg U. Laboratory evolution of cytochrome P450BM-3 monooxygenase for organic cosolvents. Biotechnol Bioeng, 2004; 85(3): 351-8.
122. Glieder A, Farinas ET, Arnold FH. Laboratory evolution of a soluble, self-sufficient, highly active alkane hydroxylase. Nat Biotechnol, 2002; 20(11): 1135-9.
123. Galkin A, Lu X, Dunaway-Mariano D, Herzberg O. Crystal structures representing the Michaelis complex and the thiouronium reaction intermediate of Pseudomonas aeruginosa arginine deiminase. Journal of biological chemistry, 2005; 280(40): 34080-7.
124. Chuang VTG, Kragh-Hansen U, Otagiri M. Pharmaceutical strategies utilizing recombinant human serum albumin. Pharm Res, 2002; 19(5): 569-77.
125. Tee KL, Dmytrenko O, Otto K, Schmid A, Schwaneberg U. A p-nitrothiophenolate screening system for the directed evolution of a two-component epoxygenase (StyAB). J Mol Catal B: Enzym, 2008; 50(2-4): 121-7.
126. Li L, Li ZM, Wang CH*, et al.* The electrostatic driving force for nucleophilic catalysis in L-arginine deiminase: a combined experimental and theoretical study. Biochemistry (Mosc), 2008; 47(16): 4721-32.

127. Takaku H, Matsumoto M, Misawa S, Miyazaki K. Antitumor-activity of arginine deiminase from *Mycoplasma arginini* and its growth-Inhibitory mechanism. Jap J Cancer Res, 1995; 86(9): 840-6.
128. Capocaccia R, Sant M, Berrino F, Simonetti A, Santi V, Trevisani F. Hepatocellular carcinoma: trends of incidence and survival in Europe and the United States at the end of the 20th century. American Journal of Gastroenterol, 2007; 102(8): 1661-70.
129. Shen LJ, Shen WC. Drug evaluation: ADI-PEG-20 - a PEGylated arginine deiminase for arginine-auxotrophic cancers. Current Opinion in Molecular Therapeutics, 2006; 8(3): 240-8.
130. Wang WY, Malcolm BA. Two-stage PCR protocol allowing introduction of multiple mutations, deletions and insertions using QuikChange (TM) site-directed mutagenesis. Biotechniques, 1999; 26(4): 680-2.
131. Vaughn WK, Neal RA, Anderson AJ. Computer estimation of the parameters of the sigmoidal kinetic model. Computers in Biology and Medicine, 1976; 6(1): 1-7.
132. Kelley LA, Sternberg MJE. Protein structure prediction on the web: a case study using the Phyre server. Nature Protocols, 2009; 4(3): 363-71.
133. Laskowski RA, Macarthur MW, Moss DS, Thornton JM. Procheck - a program to check the stereochemical quality of protein structures. Journal of Applied Crystallography, 1993; 26: 283-91.
134. Zhou HY, Zhou YQ. Distance-scaled, finite ideal-gas reference state improves structure-derived potentials of mean force for structure selection and stability prediction. Protein Science, 2002; 11(11): 2714-26.
135. Benkert P, Tosatto SCE, Schomburg D. QMEAN: A comprehensive scoring function for model quality assessment. Proteins-Structure Function and Bioinformatics, 2008; 71(1): 261-77.
136. Berendsen HJC, Postman JPM, van Gunsteren WF, Hermans J. Interaction models for water in relation to protein hydration. Intermolecular Forces, 1981: 331-42.

137. Hess B, Bekker H, Berendsen HJC, Fraaije JGEM. LINCS: A linear constraint solver for molecular simulations. Journal of Computational Chemistry, 1997; 18(12): 1463-72.
138. Miyamoto S, Kollman PA. Settle - an analytical version of the shake and rattle algorithm for rigid water models. Journal of Computational Chemistry, 1992; 13(8): 952-62.
139. Darden T, York D, Pedersen L. Particle mesh ewald - an N.Log(N) method for ewald sums in large systems. Journal of Chemical Physics, 1993; 98(12): 10089-92.
140. Berendsen HJC, Postma JPM, Vangunsteren WF, Dinola A, Haak JR. Molecular dynamics with coupling to an external bath. Journal of Chemical Physics, 1984; 81(8): 3684-90.
141. Hess B, Kutzner C, van der Spoel D, Lindahl E. GROMACS 4: algorithms for highly efficient, load-balanced, and scalable molecular simulation. Journal of Chemical Theory and Computation, 2008; 4(3): 435-47.

Summary and outlook

Arginine depletion based on ADI is an emerging strategy for anti-tumor treatment. ADIs have been studied for the therapy of HCCs and melanomas and were approved as an orphan drug for both kinds of tumors. ADI is proved to be effective in the treatment of leukemia. The effectiveness of ADIs as anti-tumor agent depends on their enzymatic properties (such as K_m, k_{cat}, optimum pH, stability at neutral pH). Directed evolution, without rational understanding of the targeted property, allows improving all properties that can be reflected in a screening system through iterative rounds of diversity generation and screening.

In order to improve PpADI activity at physiological pH by directed evolution, a colorimetric screening assay based on citrulline detection has been developed in 96-well microtiter plate format. Single mutation H404R was identified according to PpADI homology model (based on PaADI crystal structure), introduced to PpADI wild type and eventually resulted in 1.4-fold of increase in k_{cat}. M1 (H404R) was used as template for the first round of epPCR library generation. M2 (K5T/D44E/H404R) obtained from the first round of epPCR library showed 4-fold improved k_{cat} value when compared to the PpADI wild type. Furthermore, a shift of pH optimum from pH 6.5 to pH 7.0 was observed, combined with an increased K_m value (2.5 mM) under assay conditions (0.5 M sodium phosphate buffer, pH 7.4), compared to PpADI wild type (0.7 mM).

Arginine concentration in human plasma is however relatively low (100-120 µM). Therefore the second round of epPCR library was performed to decrease K_m value and further improve k_{cat} value. The validated screening assay was modified to reflect more close physiological condition (1 mM arginine in PBS buffer, pH 7.4). Two important variants with one additional mutation, M4 (K5T/D44E/A128T/E296K/H404R) with decreased $S_{0.5}$ vaule, and M5 (K5T/D38H/D44E/A128T/H404R) with improved k_{cat} were obtained. Their two mutations were combined and resulted in variants M6

(K5T/D38H/D44E/A128T/E296K/H404R). Under physiological pH in PBS buffer, the $S_{0.5}$ value of M6 (0.81 mM) is lower than that of PpADI wild type (1.30 mM); the k_{cat} value improved from 0.18 s^{-1} (PpADI wild type) to 17.56 s^{-1} (M5, 97.6-folds) and 11.64 s^{-1} (M6, 64.7-fold).

A reamaining challenge facing PpADI's anti-tumor application is to decrease the K_m ($S_{0.5}$) value further close to arginine concentration level in human plasma. A more sensitive assay for screening has to be developed with the addition of sensitizer like thiosemicarbazide (TSC), optimized temperature and incubation time. Improved variants should be tested tested in human plasma or with human plasma composition. *In vitro* testing of ADI variants with arginine auxotrophic tumor cell lines is the first step towards *in vivo* in human.

In summary, directed evolution has been very useful algorithim for improving ADI's k_{cat} and K_m at physiological pH (pH 7.4) for its medical application. Hope that directed evolution will be become a standard method for therapeutic protein like its use in industry.

Publications

1. **Leilei Zhu**, Kang Lan Tee, Danilo Roccatano, Burcu Sonmez, Ye Ni, Zhi-Hao Sun, and Ulrich Schwaneberg. Directed evolution of an antitumor drug (Arginine Deiminase PpADI) for increased activity at physiological pH. ChemBioChem. 2010, 11, 691-697.

2. **Leilei Zhu**, Rajni Verma, Danilo Roccatano, Ye Ni, Zhi-Hao Sun, and Ulrich Schwaneberg. A potential anti-tumor drug (arginine deiminase) reengineered for efficient operation under physiological conditions. ChemBioChem. *In press*.

3. Ye Ni, Zhenwei Li, Zhihao Sun, Pu Zheng, Yongmei Liu and **Leilei Zhu**, Ulrich Schwaneberg. Expression of arginine deiminase from *Pseudomonas plecoglossicida* CGMCC2039 in *Escherichia coli* and its anti-tumor activity. Current Microbiology. 2009, 58(6):593-598.

Patent

1. Directed evolution of arginine deiminase for increased activity at physiological pH. Application number: PCT/EP2010/061884.

Curriculum vitae

Personal data

Name:	Leilei Zhu
Gender:	Female
Date of Birth:	27th April, 1982
Place of Birth:	Weifang, China
Marital Status:	Married
Nationality:	Chinese

Education

2009-	PhD fellow of biotechnology, RWTH Aachen University, Aachen, Germany
2007-2009	PhD fellow of engineering and science, Jacobs University Bremen, Bremen, Germany
2005-2007	Master of biochemical engineering, Jiangnan University (Southern Yantze University), Wuxi, China
2001-2005	Bachelor of biotechnology, Jiangnan University (Southern Yantze University), Wuxi, China

2001-1998	The first high school of Hanting, Weifang, China
1998-1994	The sixth middle school of Hanting, Weifang, China
1989-1994	Primary school of Liuhe, Weifang, China